1 165262 1

165262 1

A

AGARD CONFERENCE PROCEEDINGS No. 46

AGARD CP No. 46

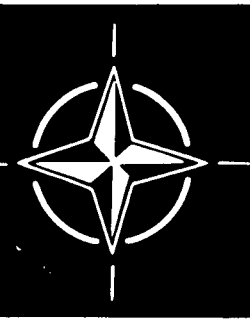
AGARD

ADVISORY GROUP FOR AEROSPACE RESEARCH & DEVELOPMENT

7 RUE ANCELLE 92 NEUILLY-SUR-SEINE FRANCE

Aeroelastic Effects from a Flight Mechanics Standpoint

NORTH ATLANTIC TREATY ORGANIZATION



DISTRIBUTION AND AVAILABILITY
ON BACK COVER

UNLIMITED

AGARD Conference Proceedings No. 46

NORTH ATLANTIC TREATY ORGANIZATION

ADVISORY GROUP FOR AEROSPACE RESEARCH AND DEVELOPMENT

(ORGANISATION DU TRAITE DE L' ATLANTIQUE NORD)

AEROELASTIC EFFECTS FROM A FLIGHT MECHANICS STANDPOINT

Papers presented at the 34th Meeting of the AGARD Flight Mechanics Panel, held in Marseille, France, 21-25 April 1969.

1969

The material in this publication has been produced
directly from copy supplied by each author.

Published March 1970

533.6.013.42

Printed by Technical Editing and Reproduction Ltd
Harford House, 7-9 Charlotte St. London. W1P 1HD

FOREWORD

As early as the beginning of the aviation industry, aeroelasticity appeared as a phenomenon which had to be well understood and fully mastered.

The magnitude of this phenomenon is still growing and has become particularly noticeable in recent years. Several factors are responsible for such a development.

1. The considerable increase of speed.
2. The thinner shapes required for transonic and supersonic flight.
3. The new airframe designs such as variable geometry.
4. The new generation of commercial aircraft: stretching of present long range liners, Jumbojets, Supersonic transports.
5. The growing interest in low level flight for military purposes.

Helicopters too are concerned: the new giant copters and aircraft using erroneously termed "rigid rotor" are more subject to the effect of aeroelasticity phenomena.

The AGARD Flight Mechanics Panel thought it would be of interest to devote one of its technical sessions, held in April 1969 in Marseilles, France, to this problem by deliberately regarding it from the flight engineer's point of view, that is forgetting as far as possible the pure structural facets such as loads, fatigue strength, flutter, etc.

The meeting set the position of the present state of the art in the field of aerodynamics and knowledge of structural properties, but the main purpose of this meeting was to study the effect of aeroelasticity on flight characteristics, on theoretical and experimental methods enabling these to be investigated, and on the inference of this situation in these various fields.

The AGARD Flight Mechanics Panel hope that this meeting was fruitful for all concerned from various countries through the ideas exchanged and will provide better understanding of the relevant problems. It is the wish of this Panel that this report gives to all persons concerned a good account on the matter discussed.

Pierre Lecomte
Chairman
Flight Mechanics Panel

AVANT-PROPOS

Déjà aux débuts de l'industrie de l'aviation, la question de l'aéroelasticité apparaissait comme un phénomène qu'il fallait bien comprendre et bien maîtriser.

L'importance de ce phénomène va toujours croissant et s'est fait particulièrement sentir au cours de ces dernières années. Une telle évolution est fonction de plusieurs éléments:

1. l'augmentation importante de la vitesse des avions;
2. les formes plus minces nécessaires au vol transsonique et supersonique;
3. les cellules de conception nouvelle, par example à géométrie variable;
4. la nouvelle génération des avions de transport commerciaux; allongement des longs-courriers actuels, Jumbojets, transports supersoniques;
5. l'intérêt toujours croissant que l'on porte, pour les besoins militaires, au vol à basse altitude.

Les hélicoptères sont également concernés: les nouveaux hélicoptères géants et les avions utilisant ce que l'on désigne par erreur des "rotors rigides" sont plus sujets a l'influence des phénomenès de l'áeroélasticité.

La Commission de la Mécanique du Vol de l'AGARD a cru intéressant de consacrer à ce problème l'une de ses sessions techniques tenue en avril 1969 à Marseille, France, en présentant délibérément le point de vue du mécanicien navigant, c'est-à-dire, en négligeant, autant que possible, les aspects purement structurels, tels que charges, résistance à la fatigue, flottement etc.

La réunion a fait le point de l'état actuel des connaissances dans le domaine de l'aérodynamique et des caractéristiques des structures, mais avait pour but principal d'étudier l'influence de l'aéroelasticité sur les qualités de vol, sur les méthodes théoriques et expérimentales permettant d'étudier celles-ci et sur la conclusion à tirer de cette situation dans ces différents domaines.

La Commission espère que tous ceux qui sont venus des différents pays pour participer à la réunion l'auront trouvée une occasion fructueuse, et que cet échange de vues conduira à une meilleure compréhension des problèmes qui se posent; la Commission désire par ce présent Rapport donner à tous ceux intéressés un compte-rendu complet des matières étudiées.

Pierre Lecomte
Président
La Commission de la Mécanique du Vol

CONTENTS

	Page
FOREWORD	iii
AVANT PROPOS	iv

SESSION I. PRELIMINARY SESSION DEVOTED TO THE STATE-OF-THE-ART

	Reference
INTRODUCTORY REMARKS* by J.J.Angelini	1
LES TECHNIQUES UTILISEES EN AEROELASTICITE POUR LA REPRESENTATION DE L'AVION EN VOL par Roland Dat et Christian Beatrix	2
PRESENT STATUS OF UNSTEADY AERODYNAMICS FOR LIFTING SURFACES by H.Bergh and R.J.Zwaan	3
PROBLEMES POSES PAR LA DETERMINATION DE FORCES AERODYNAMIQUES AGISSANT SUR L'AVION SOUPLE par L.Darovsky	4
ATMOSPHERIC TURBULENCE DESIGN CASES by J.Taylor	5
UTILISATION D'UN AVION COMME MOYEN DE MESURE DE LA DISTRIBUTION STATISTIQUE DE LA TURBULENCE par Gabriel Coupry et Guy Thomasset	6

SESSION II. FLIGHT DYNAMICS OF A FLEXIBLE VTOL ROTOR

AEROELASTIC AND STRUCTURAL DYNAMIC INFLUENCES ON V/STOL HANDLING QUALITIES by R.G.Loewy	7
AEROELASTIC PROBLEMS OF FLEXIBLE V/STOL ROTORS by D.E.Brandt	8
EFFETS AEROELASTIQUES SUR LES QUALITES DE VOL D'UN ROTOR RIGIDE par J.Gallot	9
THE INFLUENCE OF AEROELASTICITY ON STABILITY AND CONTROL OF A HELICOPTER WITH A HINGELESS ROTOR by G.Reichert	10
THE INFLUENCE OF COMPRESSIBILITY ON THE AIRLOADS ON OSCILLATING ROTOR BLADES IN HOVERING FLIGHT by W.P.Jones and B.M.Rao	11

SESSION III. FLIGHT DYNAMICS OF FLEXIBLE AIRPLANES THEORETICAL METHODS

AN ANALYTICAL METHOD FOR PREDICTING THE STABILITY AND CONTROL CHARACTERISTICS OF LARGE ELASTIC AIRPLANES AT SUBSONIC AND SUPERSONIC SPEEDS	
PART I - ANALYSIS by Arthur R.Dusto	12
PART II - APPLICATION by Howard L.Chevalier, Gerald M.Dornfeld and Robert C.Schwanz	12

* Not published.

Reference

COMMENTS, INTERPRETATION AND APPLICATION OF A METHOD FOR PREDICTING AERODYNAMIC CHARACTERISTICS OF LARGE FLEXIBLE AIRPLANES
by J.Roskam 13

AEROELASTIC RESPONSE TO UNWANTED DISTURBANCES
by J.Burnham 14

DETERMINATION DES COEFFICIENTS AERODYNAMIQUES AVION SOUPLE EN VOL SYMETRIQUE
par A.Marsan 15

COMBINED EFFECTS OF AEROELASTIC COUPLING AND AERODYNAMIC INTERFERENCE BETWEEN TWO LIFTING SURFACES (WING-TAIL, TANDEM WINGS) ON THE LONGITUDINAL STABILITY
by P.G.Hamel 16

THEORETICAL INVESTIGATIONS OF AEROELASTIC INFLUENCES ON THE LIFT DISTRIBUTION AND THE AERODYNAMIC DERIVATIVES OF SWEPT WINGS AT SYMMETRIC AND ANTISYMMETRIC STATIONARY FLIGHT CONDITIONS
by W.Schoernack and E.Hässler 17

SESSION IV. EXPERIMENTAL METHODS FOR FLIGHT DYNAMICS OF THE FLEXIBLE AIRPLANE

WIND-TUNNEL TECHNIQUES FOR THE STUDY OF AEROELASTIC EFFECTS ON AIRCRAFT STABILITY, CONTROL, AND LOADS
by A. Gerald Rainey and Irving Abel 18

FLIGHT AND GROUND LOAD MEASUREMENTS BY STRAIN GAUGES
by P.B.Hovell 19

SESSION V. STABILITY AND CONTROL AUGMENTATION DEVICES

CONSIDERATION OF STABILITY AUGMENTATION SYSTEMS FOR LARGE ELASTIC AIRCRAFT
by Clifford F.Newberry 20

INFLUENCE DES EFFETS AEROELASTIQUES SUR L'ETUDE ET LA REALISATION DE L'AMORTISSEUR DE TANGAGE ET DU PILOTE AUTOMATIQUE D'UN AVION DE TRANSPORT SUPERSONIQUE
par R.Deque 21

THE INFLUENCE OF THE ELASTIC DEGREES OF FREEDOM UPON A CONTROL SYSTEM WITH A SMALL STABILITY MARGIN
by R.Staufenbiel, H.Wald and A.Kanarachos 22

ANALYTICAL DESIGN AND FLIGHT TESTS OF A MODAL SUPPRESSION SYSTEM ON THE XB-70 AIRPLANE

PART I - DESIGN ANALYSIS
by John H.Wykes 23

PART II - FLIGHT TESTS
by Eldon E.Kordes 23

GUST ALLEVIATION TECHNIQUE ON A LARGE EXPERIMENTAL AIRPLANE
by J.A.McKillop 24

ESSAI EN VOL D'UN DISPOSITIF ABSORBEUR DE RAFALES CONFIGURATION DU SYSTEME-ANALYSE
par Jacqueline Boujot 25

APPENDIX: DISCUSSIONS OF PRESENTED PAPERS

LES TECHNIQUES UTILISEES EN AEROELASTICITE POUR LA REPRESENTATION DE L'AVION EN VOL

par Roland DAT et Christian BEATRIX

Office National d'Etudes et de Recherches Aérospatiales (ONERA)

92 Châtillon - France

R E S U M E

L'étude du comportement de l'avion déformable en vol est particulièrement complexe. On expose ici les méthodes utilisées pour la prévision des instabilités aéroélastiques et, notamment, du flottement.
La linéarisation est justifiée en admettant que l'on ne s'intéresse qu'à des mouvements de petite amplitude de part et d'autre de la position moyenne. Puis, la discrétisation est obtenue en représentant le mouvement dans une base de fonctions spatiales. La mise en équation se fait alors systématiquement en partant de l'énergie et des travaux virtuels.
On montre les avantages particuliers de la base des formes propres de vibration de l'avion au sol : convergence rapide, possibilité de déterminer les caractéristiques structurales par un essai de vibration aussi bien que par un calcul sur plans.
On expose enfin les méthodes utilisées pour l'évaluation des forces aérodynamiques instationnaires : méthode des tranches et théorie de la surface portante.
Ces techniques peuvent s'adapter à un certain nombre de problèmes de la dynamique du vol, étant donné que les mouvements d'ensemble peuvent être pris en considération sans aucune difficulté.

TECHNIQUES USED IN AEROELASTICITY FOR THE AIRCRAFT °

REPRESENTATION IN FLIGHT

S U M M A R Y

The study of the behaviour of a flexible aircraft in flight is extremely complex. The methods used for predicting aeroelastic instabilities, and in particular flutter, are discussed.
Linearization is justified, provided small amplitude motions on either side of the mean position are considered. Then, discretization is obtained by representing the motion in a space function base. It can then be systematically put in equation form, starting from energy and virtual work.
The particular advantages of the base of the natural vibration mode shapes of the aircraft on the ground are shown : rapid convergence, possibility of determining structure characteristics through vibration tests as well as design calculations.
Lastly, the methods used for evaluating unsteady aerodynamic forces are presented : "strip" theory, and lifting surface theory.
Such techniques can be adapted to a number of flight dynamics problems, because the overall motions can be taken into account without any difficulty.

CONVENTIONS

Les vecteurs et les matrices sont systématiquement désignés par des caractères gras.

Exemples : $\boldsymbol{P}(P,t)$ est un vecteur qui repère l'écart d'un point P à l'instant t, par rapport à sa position de référence.

$\boldsymbol{M}$ et $\boldsymbol{\mu}$ sont des matrices.

$\boldsymbol{S}(P)$ est une base, c'est-à-dire une ligne dont les éléments $\boldsymbol{S}_r(P)$ sont des vecteurs.

Indices : l'indice supérieure repère la ligne et l'indice inférieur la colonne.

Opération barre ($\bar{}$):

- appliquée à une matrice, la barre donne la transconjuguée : $\bar{\boldsymbol{M}}$ est la transconjuguée de $\boldsymbol{M}$.
- appliquée à un nombre complexe, l'opération barre donne le nombre complexe conjugué.
- appliquée à un vecteur elle donne l'opérateur de produit scalaire : $\bar{\boldsymbol{U}}\boldsymbol{V} = |U||V|\cos(U,V)$
- $\boldsymbol{S}$ et $\boldsymbol{T}$ étant deux bases, le produit $\bar{\boldsymbol{S}}\boldsymbol{T}$ est une matrice de nombres dont les éléments sont les produits scalaires des vecteurs de base :

$$[\bar{\boldsymbol{S}}\boldsymbol{T}]_j^{(i)} = \bar{\boldsymbol{S}}_i \boldsymbol{T}_j$$

INTRODUCTION

La dynamique du vol et l'aéroélasticité se différencient par le fait que l'une a pour objet de prévoir les mouvements d'ensemble de l'aéronef, tandis que l'autre prévoit ses déformations statiques et dynamiques.

Les spécialistes de ces deux disciplines ont appris à maitriser leurs problèmes en mettant à profit les simplifications qui sont valables dans leur domaine. C'est ainsi que les mécaniciens du vol tirent parti de l'hypothèse de l'indéformabilité et du caractère quasi-stationnaire de l'écoulement ; ils doivent, en revanche, étudier des mouvements de grande amplitude et tenir compte de phénomènes non-linéaires. Les aéroélasticiens, au contraire, se sont spécialisés dans l'étude des petits mouvements et ils ont acquis une certaine maitrise dans la prévision des vibrations ou des déformations statiques les plus complexes en vol, avec un grand nombre de degrés de liberté, pourvu que les phénomènes restent linéaires.

Mais si l'on devient plus exigeant sur la précision des calculs on doit bien admettre que la distinction entre mouvements d'ensemble et déformations établit une frontière trop schématique, car les déformations ont une répercussion sur les mouvements d'ensemble tandis que ceux-ci peuvent influencer certains phénomènes aéroélastiques. Cette interaction est d'ailleurs accentuée sur certaines structures modernes relativement souples, pour lesquelles les modes dits "d'ensemble" ont, en vol, des fréquences propres du même ordre de grandeur que les modes de vibration fondamentaux.

L'introduction des mouvements d'ensemble ne complique nullement le problème de l'aéroélasticité, pourvu que l'on puisse faire l'hypothèse que ces mouvements sont de faible amplitude.

Par contre, l'introduction des degrés de liberté de déformation dans les problèmes de la dynamique du vol risque d'imposer aux spécialistes de cette discipline une certaine harmonisation de leurs méthodes avec celles des aéroélasticiens, et cela ne saurait être réalisé que si ces méthodes leur sont connues.

Ce sont ces considérations qui motivent cet exposé à l'adresse des mécaniciens du vol.

L'auteur étant un aéroélasticien, il ne se risquera pas à analyser les problèmes de la mécanique du vol, mais il s'efforcera de faire ressortir le caractère général et systématique des méthodes employées en aéroélasticité.

D'une part, le caractère linéaire supposé des phénomènes conduit à une utilisation systématique du formalisme matriciel qui permet de condenser l'écriture et de dégager des propriétés générales valables quel que soit le nombre de degrés de liberté. D'autre part, la complexité des mouvements étudiés, lorsqu'on tient compte des déformations, impose l'emploi systématique de l'énergie et des travaux virtuels pour établir les équations du problème.

Un tel exposé se divise naturellement en 3 chapitres :

1. Un chapitre général dans lequel on établit les équations du mouvement de la structure schématisée par un système discret voisin, et où l'on montre les avantages particuliers de la représentation modale.

2. Un chapitre consacré à la détermination des caractéristiques modales où l'on distingue la méthode expérimentale (essai de vibration au sol), et les méthodes théoriques (calculs sur plans).

3. Enfin un chapitre consacré à la détermination des forces aérodynamiques généralisées, dans lequel on montre comment se fait pratiquement la mise en oeuvre de la théorie de la surface portante. Une formulation approchée, plus particulièrement adaptée aux études de dynamique du vol, est proposée.

Ce texte reste évidemment très général : il montre l'intérêt des méthodes mais ne saurait suffire à une application pratique. On trouvera une documentation plus détaillée dans les ouvrages généraux [1], [2], [3].

1. GENERALITES

1.1 - Représentation de l'avion par un système discret.

Le problème de l'avion déformable en vol est schématisé par la figure 1.

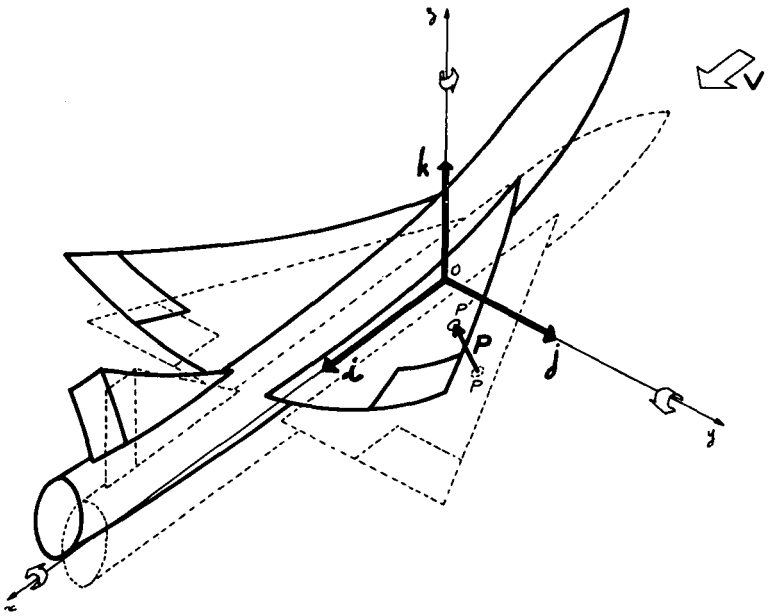


FIG. 1

Le trait plein représente l'appareil déformé à un instant donné, tandis que le pointillé le figure non déformé et en position de vol horizontal uniforme, les axes $oxyz$ étant confondus avec les axes principaux d'inertie. Cette position sert de référence pour repérer les déplacements et les déformations qui se superposent au mouvement uniforme et qui restent toujours petits.

Soit un point P de l'appareil supposé non déformé et dans la position de référence. La superposition du petit déplacement l'amène en P', et le vecteur $\overrightarrow{PP'}$ exprime l'écart à l'instant considéré. Dans la suite, on remplacera la notation $\overrightarrow{PP'}$ par $\boldsymbol{P}$, par souci de simplicité.

En considérant tous les points, on est donc conduit à définir la position du système par un champ de vecteurs qui dépend du temps : $\boldsymbol{P}(P,t)$.

Le problème ainsi posé est celui d'un système continu particulièrement complexe, et la formulation exacte conduirait à des équations aux dérivées partielles avec des conditions aux limites telles que la résolution serait pratiquement impossible.

On obtient, par contre, des approximations satisfaisantes pour l'ingénieur en limitant le nombre de degrés de liberté, c'est-à-dire en schématisant le système réel par un système discret.

Séparons d'abord les variables d'espace et la variable temps en définissant une base complète dont les éléments sont des champs de vecteurs spatiaux $\boldsymbol{S}_r(P,t)$, et qui permet de représenter n'importe quel mouvement compatible avec les liaisons par une superposition linéaire :

$$\boldsymbol{P}(P,t) = \sum_{r=1}^{\infty} \boldsymbol{S}_r(P)\, q^{(r)}(t)$$

Cette formule devient pratiquement exploitable si le nombre de vecteurs de base est limité à une valeur finie, n , ce qui revient à faire une représentation approchée du mouvement ($\boldsymbol{P} = \sum_{r=1}^{n} \boldsymbol{S}_r\, q^{(r)}$) ou à remplacer le système continu par un système discret à n degrés de liberté dont la position dépend des n paramètres $q^{(r)}$. Ces paramètres sont les coordonnées généralisées. Ce sont les inconnues du problème.

La formulation matricielle permet une écriture condensée. On la réalise en définissant la ligne $\boldsymbol{S}$, ou base, dont les éléments sont les champs de vecteurs $\boldsymbol{S}_r(P)$,

$$S = [\, S_1(P) \ldots\ldots S_n(P) \,]$$

et la colonne des coordonnées généralisées :

$$q(t) = \begin{bmatrix} q^{(1)}(t) \\ \vdots \\ q^{(n)}(t) \end{bmatrix}$$

On a :

(1) $$P(P,t) = S(P)\,q(t)$$

Cette formule est générale et permet la représentation approchée de n'importe quel mouvement comportant des déplacements d'ensemble, des déformations et des braquages de gouvernes.

Les champs de vecteurs déterminant les mouvements d'ensemble s'expriment aisément par rapport à la base orthonormée $[i\ j\ k]$ (fig. 1) liée à la position de référence.

On a :

$S_1 = k$, si $q^{(1)}$ représente la translation du c.g. suivant oz , rapporté à la longueur c .
$S_2 = -kx + iz$, si $q^{(2)}$ représente le tangage,
$S_3 = ky - jz$, si $q^{(3)}$ représente le roulis,
$S_4 = \frac{j}{c}$, si $q^{(4)}$ représente le dérapage rapporté à la longueur c ,
$S_5 = jx - iy$, si $q^{(5)}$ représente le lacet,
$S_6 = ic$, si $q^{(6)}$ représente les petits déplacements du c.g. suivant ox , rapportés à la longueur c .

La présence des gouvernes se manifeste par des discontinuités dans la répartition spatiale du mouvement. On en tient compte en introduisant des fonctions de base comportant une définition différente sur chaque gouverne et sur les autres parties de l'avion.

Ainsi, les effets de braquage pur peuvent être représentés par des fonctions simples, si l'on admet de négliger les dimensions en épaisseur devant les dimensions en plan.

$q^{(7)}$ étant la coordonnée de braquage symétrique des élevons, on a :

$$S_7 = \begin{cases} k\,[x - x_{ch}(y)] & \text{sur les élevons} \\ 0 & \text{ailleurs} \end{cases}$$

$q^{(8)}$ étant la coordonnée de braquage antisymétrique des élevons on a :

$$S_8 = \begin{cases} k\,[x - x_{ch}(y)] & \text{sur l'élevon droit} \\ -k\,[x - x_{ch}(y)] & \text{sur l'élevon gauche} \\ 0 & \text{ailleurs} \end{cases}$$

$q^{(9)}$ étant le braquage de la gouverne de direction, on a :

$$S_9 = \begin{cases} j\,[y - y_{ch}(3)] & \text{sur la gouverne de direction} \\ 0 & \text{ailleurs} \end{cases}$$

La simplification qui consiste à négliger les coordonnées en épaisseur devant les dimensions dans le plan est d'ailleurs étendue à l'ensemble de la voilure et de la dérive pour le calcul des forces aérodynamiques (hypothèse fondamentale de la théorie de la surface portante).

Le choix des vecteurs de base $S_r(P)$ est important car il détermine la rapidité de convergence de la représentation et le nombre de degrés de liberté qu'il est nécessaire d'introduire pour obtenir une précision donnée. Nous verrons tout l'intérêt que présente à cet égard la base des formes propres de vibration de l'avion au sol.

Notons dès maintenant que l'on peut mettre à profit les symétries en choisissant des vecteurs $S_r(P)$ symétriques par rapport au plan xoz , par rapport à l'axe ox et par rapport à oz . Les degrés de liberté symétriques par rapport au plan xoz ne présentent aucun couplage avec les autres et peuvent être traités séparément, ce qui permet de distinguer deux problèmes : un problème "symétrique" groupant les degrés de liberté admettant xoz comme plan de symétrie, et un problème "antisymétrique" groupant les autres degrés de liberté. La dénomination "antisymétrique" est d'ailleurs un peu impropre pour le deuxième problème, car seuls les déplacements normaux à la voilure sont antisymétriques par rapport au plan xoz .

1.2 - Equations du mouvement

On applique les équations de Lagrange après avoir exprimé l'énergie, et les travaux virtuels correspondant à une variation δq de la colonne q .

Energie cinétique : l'expression (1) détermine la vitesse en chaque point :

$$\{\, P = Sq \,\} \Rightarrow \left\{ V = \frac{dP}{dt} = S\dot{q} \right\}$$

et, dm étant l'élément de masse affecté à chaque point P , l'énergie cinétique est donnée par :

$$T = \frac{1}{2}\int_{Volume} |V|^2 dm = \frac{1}{2}\int_{Volume} \bar{V} V \, dm$$

$$= \frac{1}{2}\,\bar{\dot{q}}\int_{Volume} \bar{S} S \, dm \, \dot{q}$$

Posons :

$$M = \int_{Volume} \overline{S(P)}\, S(P)\, dm$$

Il vient :

(2) $$T = \frac{1}{2}\,\bar{\dot{q}}\, M q$$

C'est une forme définie positive, parce que la matrice M est telle que $\bar{M} = M$ et que $\bar{\dot{q}} M \dot{q} > 0 \quad \forall\, \dot{q} \neq 0$.

M est la matrice de masses généralisées. Ses éléments sont obtenus en intégrant les produits scalaires des vecteurs de base $S_i(P), S_j(P)$:

$$M_j^{(i)} = \int_{Volume} \overline{S_i(P)}\, S_j(P)\, dm$$

Energie potentielle : l'énergie potentielle associée aux déformations élastiques s'exprime également par une forme définie positive :

(3) $$U = \frac{1}{2}\,\bar{q} K q$$

où K est une matrice telle que $\bar{K} = K$ et $\bar{q} K q > 0 \quad \forall\, q \neq 0$.
K est la matrice de rigidités généralisées.

Le calcul des éléments de la matrice K est plus complexe que celui des masses généralisées. Il nécessite la connaissance des champs de contraintes ou de déformations résultant des déflexions $S_j(P)$.

Fonction de dissipation : la fonction de dissipation, D , est égale à la moitié de la puissance dissipée par les forces internes (frottements secs et dissipations par hystérésis).

Ces forces de dissipation sont assimilées à des forces de viscosité, et l'on obtient encore une forme définie positive :

(4) $$D = \frac{1}{2}\,\bar{\dot{q}} B \dot{q}$$

où B est la matrice des viscosités généralisées.

Mais le calcul de cette matrice ferait intervenir des lois de comportement visqueux qui sont d'autant plus difficiles à déterminer que les mécanismes de dissipation n'obéissent pas à des lois linéaires, et tout calcul serait illusoire.

La dissipation reste heureusement faible dans les structures aérospatiales et l'on peut, suivant les problèmes traités, négliger la matrice B ou la déduire du comportement global de la structure soumise à un test approprié.

Travaux virtuels des forces appliquées : les travaux virtuels des forces appliquées peuvent toujours s'exprimer sous la forme :

$$\delta A = \bar{Q}\, \delta q$$

où Q est la colonne des forces généralisées.

Equations de Lagrange : les equations de Lagrange s'écrivent :

$$\frac{d}{dt}\left(\frac{\overline{\partial T}}{\partial \dot{q}}\right) - \frac{\overline{\partial T}}{\partial q} + \frac{\overline{\partial D}}{\partial \dot{q}} + \frac{\overline{\partial U}}{\partial q} = Q$$

En remplaçant T , D et U par les expressions (2), (3) et (4) on obtient un système d'équations différentielles linéaires du second ordre à coefficients constants, avec second membre.

(5) $$M\ddot{q} + B\dot{q} + Kq = Q$$

Notons que le second membre est indépendant de q lorsque les forces extérieures sont imposées. Mais il peut aussi en dépendre : c'est le cas notamment des forces aérodynamiques généralisées.

1.3 - Excitation harmonique et système conservatif associé

Supposons que l'on applique à l'avion des forces d'excitation sinusoïdales à la pulsation ω . Dans ce cas, la réponse stabilisée est un mouvement harmonique, à la même pulsation.

Pour alléger l'écriture, on remplacera avantageusement les fonctions harmoniques de la forme :

$$f(t) = F\cos(\omega t + \varphi) \quad \text{par} \quad f(t) = \mathcal{R}(F e^{i\varphi} e^{i\omega t}) = \mathcal{R}(F^* e^{i\omega t})$$

(en posant $F^* = F e^{i\varphi}$)

F^* est l'affixe de $f(t)$; son module donne l'amplitude, et l'argument φ donne la phase par rapport à une référence.

Avec cette convention, si les forces appliquées sont harmoniques, la colonne $Q(t)$ se met sous la forme :

$$Q(t) = \mathcal{R}(Q^* e^{i\omega t})$$

et $q(t)$ est de la forme :

(6) $$q(t) = \mathcal{R}(q^* e^{i\omega t})$$

D'où : $$\dot{q}(t) = \mathcal{R}(i\omega q^* e^{i\omega t})$$

et $$\ddot{q}(t) = \mathcal{R}(-\omega^2 q^* e^{i\omega t})$$

On peut substituer ces expressions dans l'équation (5), en omettant l'indication $\mathcal{R}$, parce que cette équation s'applique aux affixes (parce que l'équation est linéaire).

En simplifiant par $e^{i\omega t}$, il vient :

(7) $$[-\omega^2 M + i\omega B + K]\, q^* = Q^*$$

Critère de phase : Imposons la même phase à toutes les forces d'excitation et supposons que l'on réussisse, en jouant sur la pulsation et sur la répartition de ces forces, à faire vibrer tous les points de la structure en quadrature par rapport aux forces d'excitation.

Dans ce cas, on peut prendre le mouvement comme référence de phase (puisque tous les points sont à la même phase, par hypothèse), ce qui revient à poser que q^* est réel. Le déphasage de $\pi/2$ entre forces et déplacements se manifeste alors par le fait que Q^* est imaginaire pur.

On peut alors séparer la partie réelle et la partie imaginaire de l'équation (7). Il vient :

(8-1) $$[-\omega^2 M + K]\, q^* = 0 \qquad \text{(partie réelle)}$$

(8-2) $$i\omega B q^* = Q^* \qquad \text{(partie imaginaire)}$$

L'équation (8-2) montre que les forces appliquées compensent l'effet des forces de dissipation, et l'équation (8-1) montre que l'on a isolé un mouvement propre du système conservatif associé, c'est-à-dire du système obtenu en supprimant les forces de dissipation du système réel.

ω^2 et q^* apparaissent respectivement comme valeur propre et vecteur propre de la matrice $M^{-1}K$, et on démontre qu'effectivement cette matrice admet des valeurs propres réelles et positives, et des vecteurs propres réels, à cause des propriétés des matrices M et K .

Si l'on excite la structure avec des forces harmoniques, on peut donc s'assurer que l'on a isolé un mode propre du système conservatif associé en vérifiant que les forces et les déplacements sont déphasés de $\pi/2$. C'est le critère de phase.

Cette propriété est mise à profit dans les essais de vibration au sol dont le but est précisément de déterminer les caractéristiques vibratoires, mais dans ce cas la recherche de la pulsation ω et de la répartition de forces donnée par (8-2), est délicate, parce que l'on ne connait pas à l'avance les caractéristiques du système (voir paragraphe 2.1).

La matrice $M^{-1}K$ admettant n valeurs propres et n vecteurs propres, on peut isoler n mouvements propres. Nous les distinguerons maintenant par un indice.

Soit ω_k^2 et q_k^* une valeur propre et un vecteur propre vérifiant l'équation (8-1). Alors la description du mode de vibration est obtenue en revenant aux conventions (1) et (6). On a :

$$P_k(P,t) = S(P)\, q_k^* e^{i\omega_k t}$$

(partie réelle de..... restant sous-entendu).

ou

(9) $$P_k(P,t) = \Phi_k(P)\, e^{i\omega_k t}$$

(en posant $\Phi_k(P) = S(P) q_k^*$)

$\Phi_k(P)$ représente un champ de vecteurs obtenu par combinaison linéaire des $S_r(P)$. Il est défini à un coefficient près, de même que le vecteur propre q_k^*, et il est réel. parce que q_k^* est réel. On effectue la normalisation, en levant arbitrairement l'indétermination.

Dans ces conditions, le mode propre de vibration défini par (9) est un mouvement harmonique où tous les points ont la même phase.

ω_k est la pulsation propre et $\Phi_k(P)$ la forme propre.

$\Phi_k(P)$ détermine l'amplitude et la direction du mouvement en chaque point.

Notons que parmi ces modes propres se trouvent les 6 modes d'ensemble, c'est-à-dire les 3 translations suivant les axes principaux d'inertie, et les 3 rotations autour de ces axes. Les pulsations propres correspondant à ces 6 modes seraient nulles en l'absence de forces aérodynamiques ou de suspension parasite, mais ce cas ne peut être réalisé pratiquement parce qu'il est impossible d'isoler l'avion en l'absence de forces aérodynamiques ou d'une suspension plus ou moins élastique.

1.4 - Représentation modale

Les formes propres de vibration du système conservatif associé, $\Phi_k(P)$, forment une base complète qui peut être utilisée, à la place de la base initiale $S(P)$, pour représenter le mouvement. Il suffit de poser :

$$P(P,t) = \sum_{k=1}^{n} \Phi_k(P)\, q^{(k)}(t)$$

ou :

(10) $$P(P,t) = \Phi(P)\, q(t)$$

en désignant par $\Phi(P)$ la ligne : $\Phi(P) = [\Phi_1(P) \ldots \Phi_n(P)]$

Il convient de remarquer que $q(t)$ prend une définition différente dans (10) et dans (1), puisqu'il y a eu changement de base (ou changement de variables).

Les équations du mouvement s'obtiennent comme précédemment, en substituant les $\Phi_r(P)$ aux $S_r(P)$. Elles sont du même type que (5), mais nous particulariserons les matrices correspondant à cette base remarquable en utilisant des notations différentes. Soit :

(11) $\mu\ddot{q} + \beta\dot{q} + \gamma q = Q$ le système d'équations.

Dans ce cas on bénéficie d'une importante propriété des systèmes conservatifs : l'orthogonalité des formes propres par rapport à la répartition de masses et de rigidités qui se traduit ici par le fait que les matrices de masse généralisées μ et de rigidités généralisées γ sont diagonales (voir par ex. [1], p. 70 ou chapitre 4 de [2]).

Les coefficients de ces matrices sont donnés par :

$$\mu_j^{(i)} = 0 \quad si \quad j \neq i \qquad \text{(orthogonalité)}$$

$$\mu_i^{(i)} = \int_{Volume} \overline{\Phi_i}\, \Phi_i\, dm = \int_{Volume} |\Phi_i(P)|^2\, dm$$

$$\gamma_j^{(i)} = 0 \quad si \quad j \neq i \qquad \text{(orthogonalité)}$$

$$\gamma_i^{(i)} = \omega_i^2\, \mu_i^{(i)}$$

La simplification apportée à la résolution de l'équation (11) par le caractère diagonal de μ et de γ est négligeable si β n'est pas diagonale en même temps, et c'est ailleurs qu'il faut chercher les avantages de la représentation modale.

En fait, la base des formes propres du système conservatif associé est une base naturelle déterminée par le bilan de l'énergie cinétique et de l'énergie potentielle, et elle assure une convergence rapide dans la plupart des problèmes.

Elle est particulièrement avantageuse dans les problèmes où interviennent des déformations dynamiques en vol dans le domaine des fréquences dites "de structure", parce que, dans ce cas, les forces élastiques et les forces d'inertie sont prédominantes non seulement devant les forces de dissipation, mais aussi devant les forces aérodynamiques.

C'est ainsi que dans un calcul de flottement, il suffit de considérer 2, 3 et rarement 4 formes propres de vibration, pour obtenir un résultat précis.

Mais dans les problèmes des fréquences basses (dynamique du vol) ou de déformations statiques, on peut s'attendre encore à une convergence satisfaisante en vertu du fait qu'il faut des forces de grande amplitude pour entrainer une forme de vibration en dehors de sa pulsation propre. Dans ces conditions, en effet, les formes propres de rang élevé (c'est-à-dire de fréquence propre élevée)ne peuvent pas intervenir beaucoup dans des mouvements à fréquence basse.

Le deuxième intérêt de la représentation modale réside dans le fait que les formes de vibration $\Phi_i(P)$ et les coefficients des matrices μ et γ sont accessibles à la fois au calcul et à l'expérience. On le verra dans le chapitre 2.1 consacré aux techniques de mesure des caractéristiques modales, et dans le chapitre 2.2 consacré aux méthodes de calcul.

La matrice des viscosités β , pose des problèmes de précision. Elle est toujours difficile à déterminer aussi bien par la voie théorique que par la voie expérimentale, quelle que soit la base utilisée.

Heureusement, les structures aérospatiales étant faiblement dissipatives, cette matrice intervient peu dans l'étude du comportement en vol et il n'est pas nécessaire de la déterminer avec beaucoup de précision. Dans ces conditions, on fait presque toujours les calculs en admettant que β est diagonale en même temps que μ et γ . Le problème de la mesure se trouve alors considérablement simplifié, car il suffit de faire le bilan de l'énergie dissipée dans chaque mode de vibration et de donner aux coefficients $\beta_i^{(i)}$ les valeurs qui produisent la même dissipation.

2 - DETERMINATION DES CARACTERISTIQUES MODALES DE LA STRUCTURE

2.1 - La méthode expérimentale

2.1.1 Le comportement vibratoire libre d'une structure linéaire, faiblement amortie est régi par l'équation matricielle (11) :

$$\mu\ddot{q} + \beta\dot{q} + \gamma q = 0$$

dans laquelle μ , β , γ , q , sont respectivement les matrices des masses, viscosités, raideurs généralisées et colonne des coordonnées généralisées.

Lorsque les modes propres de la structure conservative constituent la base de représentation, les matrices μ et γ sont diagonales et les valeurs à déterminer pour la prévision du comportement vibratoire de la structure sous l'action de forces extérieures généralisées Q sont :

les formes propres normalisées $\Phi_i(P)$
les pulsations propres ω_i
les masses généralisées $\mu_i^{(i)} = \int_{Volume} |\Phi_i(P)|^2 dm$
les raideurs généralisées $\gamma_i^{(i)} = \omega_i^2 \mu_i^{(i)}$
les coefficients de viscosité généralisés $\beta_i^{(i)}$

Ces différentes valeurs globales peuvent être atteintes soit par voie totalement expérimentale, soit totalement théorique, soit mixte. Le présent chapitre est consacré à l'exposé des moyens et méthodes à mettre en oeuvre dans la voie totalement expérimentale.

Cette méthode expérimentale consiste à soumettre la structure à des systèmes de forces d'excitation harmonique, en phase ou en opposition, ayant pour rôle de compenser l'énergie dissipée dans la structure. De la sorte l'équation matricielle du comportement vibratoire se trouve décomposée en un système de deux équations :

$$\mu\ddot{q} + \gamma q = 0$$
$$\beta\dot{q} = Q$$

Ce qui permet de réaliser physiquement le système conservatif associé et d'en déduire ses caractéristiques modales par l'analyse de la réponse.

Le moule mathématique représentant la structure est linéaire, à amortissement visqueux, alors que toute structure réelle présente des non linéarités plus ou moins accentuées, des frottements "secs" et des jeux. Ce moule mathématique représente par un nombre fini de masses discrètes, ressorts, dash-pot une structure continue comportant une infinité de degrés de liberté.

En outre l'essai ayant pour but de définir des caractéristiques structurales permettant la prévision du comportement vibratoire en présence d'une excitation quelconque, il importe que les conditions aux limites et les moyens introduits par l'essai soient sans influence sur ces caractéristiques; si cela n'est pas réalisable il est indispensable de pouvoir éliminer cette influence par calcul.

Le choix d'une méthode totalement expérimentale pour la constitution du schéma modal d'une structure mécanique réelle implique donc que les moyens et procédés mis en oeuvre permettent d'obtenir les valeurs absolues et les marges d'erreur des différentes caractéristiques précédemment définies ; leur détermination doit donc être effectuée au moins par deux procédés de nature différente.

Les considérations précédentes conduisent à envisager 3 phases principales dans la réalisation de l'essai global de vibration harmonique d'une structure : la préparation et l'organisation de l'essai, la détection des modes propres, et le traitement individuel des modes ; ces phases vont faire l'objet des paragraphes suivants.

2.1.2 - Préparation et organisation de l'essai

2.1.2.1 - La mise en oeuvre d'un essai de vibration exige les opérations préliminaires de préparation et d'organisation dont il est superflu de souligner l'importance. Car la qualité et la rapidité d'obtention des résultats sont en fonction de la qualité de la préparation. Ces opérations sont l'étude et la réalisation de la suspension, l'étude des plans pour le choix des points possibles d'excitation, l'établissement du programme d'essai, la préparation des documents de classement des résultats intermédiaires, du dépouillement et des résultats définitifs, la visite des lieux d'essais, la vérification des conditions matérielles nécessaires à la réalisation optimale de l'essai.

Ces opérations préliminaires ne constituent pas l'objet essentiel de ce chapitre, nous insisterons cependant sur trois points : la suspension, l'état de la structure et le traitement des informations.

2.1.2.2 - La suspension : La suspension la plus simple et la plus facile à mettre en oeuvre pour les essais industriels d'avion ou d'engin tels qu'ils sont réalisés en France est la suspension par sandows. On adopte en général dans ce cas une fréquence propre de pompage comprise entre 0,5 Hz et 1 Hz et on choisit, dans la mesure du possible, des points d'attache au voisinage des noeuds des modes fondamentaux. Dans ces conditions la suspension n'apporte que des perturbations minimales et il n'est pas nécessaire de recourir à un calcul pour connaître le comportement de la structure libre.

2.1.2.3 - L'état de la structure : Un premier examen de la structure, notamment des éléments mobiles (gouvernes principales et auxiliaires) permet de controler que cette structure n'est pas trop éloignée de la structure idéale théorique et, si tel n'est pas le cas, d'envisager les moyens propres à effectuer l'essai dans des conditions optimales.

Un essai de vibration effectué sur un avion présentant des frottements secs anormaux peut entraîner des conclusions complètement erronées sur son comportement ultérieur en vol libre, un tel état risquant de n'être pas reproductible : des modifications mineures faites avant l'essai offrent la possibilité de se rapprocher de la structure idéale, donc d'effectuer l'essai dans de meilleurs conditions et d'obtenir des informations non sujettes à caution.

2.1.2.4 - Le traitement des informations : Lors de l'essai d'une structure aéronautique on ne relève pas moins de 10^4 à 10^5 informations pour retenir dans les calculs ultérieurs de stabilité un nombre de valeurs dix fois plus faible. Il est donc indispensable d'établir un programme d'essais tel que les informations obtenues au cours d'une phase soient traitées immédiatement et disponibles pour la phase suivante. La généralisation de l'enregistrement des résultats en numérique, la miniaturisation des moyens de calcul facilitent d'ailleurs ce travail.

2.1.3 - Les procédés globaux de détection des modes propres

2.1.3.1 - La première phase de l'essai de vibration concerne l'ensemble de la structure et la totalité des modes : c'est une opération de dégrossissage ayant pour objectif la détection des modes propres dans la gamme de fréquence que l'on s'est définie.

Il est inutile d'insister sur le fait qu'au cours de cette phase on doit détecter toutes les fréquences de résonance sans omission , l'expérience montrant qu'un mode oublié au cours de cette première phase l'est à titre définitif.

2.1.3.2 - Le balayage en fréquence : Afin d'atteindre cet objectif, la structure est soumise à différentes configurations de forces d'excitation (en phase ou opposition) : dans chaque configuration la variable est la fréquence d'excitation.

Le lieu de l'affixe du vecteur réponse vitesse aux différents points de la structure est tracé dans le plan complexe. Par le double balayage en configuration de forces et en fréquences, on a la garantie que toutes les résonances de phase seront détectées. Théoriquement l'étude de la réponse en un seul point devrait être suffisante mais pratiquement l'étude de cette réponse est effectuée en une vingtaine de points. Cela d'une part accroit la sécurité dans la détection, permet une identification des modes et facilite, d'autre part, les opérations ultérieures d'isolation des modes. Par ailleurs la visualisation simultanée des courbes de Lissajou en une vingtaine de points sur oscilloscope permet à l'expérimentateur d'opérer sans voir la structure.

2.1.4. - Les procédés globaux de traitement individuel des modes

2.1.4.1 - L'appropriation des forces d'excitation : Entre les essais globaux de balayage et le traitement individuel de chaque mode se situent les procédés permettant le traitement individuel par son isolation des autres modes à savoir l'appropriation des forces d'excitation.

La structure continue ayant une infinité de degrés de liberté et ne pouvant être excitée que par un nombre fini d'excitateurs, il en résulte que cette opération d'appropriation ne peut consister qu'en une optimisation dépendant de 3 catégories de paramètres : la fréquence d'excitation, le nombre et l'emplacement des excitateurs et le dosage des forces d'excitation.

On envisage ici l'isolation du mode à sa résonance de phase, c'est-à-dire la recherche de l'appropriation des forces d'excitation permettant de vérifier au mieux le critère de phase (vitesse de la réponse de tous les points en phase ou en opposition avec les forces d'excitation). Remarquons d'ailleurs que si la matrice $\mathcal{B}$ est diagonale l'isolation du mode assurée à la résonance de phase,

l'est également à toutes les fréquences hors de la résonance.

Cette opération extrèmement importante pour la détermination ultérieure des caractéristiques modales est assez souvent longue et difficile, car on ne peut pas toujours introduire des excitations aux emplacements souhaitables ; de ce fait elle est aussi difficile à rendre automatique.

Cependant les moyens semi-automatiques réalisés à l'ONERA, en séparant les deux types d'opérations :

a) recherche de la résonance par générateur de fréquence asservi par un signal global pondéré des réponses structurales

b) appropriation, par asservissement en niveau et signe des forces d'excitation,

permettent un gain de temps appréciable dans la réalisation de cette opération.

2.1.4.2 - Le traitement individuel du mode :

1) La fréquence de résonance ayant été déterminée lors de l'isolation du mode, l'excitation est fixée à cette fréquence et le traitement individuel du mode consiste à mesurer la forme de vibration et les valeurs généralisées. Ces mesures doivent d'ailleurs être effectuées à différents niveaux d'excitation afin de contrôler la linéarité de la structure.

2) La mesure de la forme de vibration : La solution idéale consiste à répartir un nombre suffisamment grand de capteurs monodirectionnels et à enregistrer successivement par commutation les réponses. Cette solution onéreuse n'est retenue que pour les structures simples (modes de poutre engins). Pour les structures plus compliquées, comme celle des avions, on utilise un capteur manuel mobile (du type accélérométrique) que l'on met en contact, par simple pression, avec la structure. On minimise ainsi les perturbations apportées à la structure.

La vue générale de la forme propre est obtenue en reportant les amplitudes sur un plan et en faisant des rabattements (fig. 2).

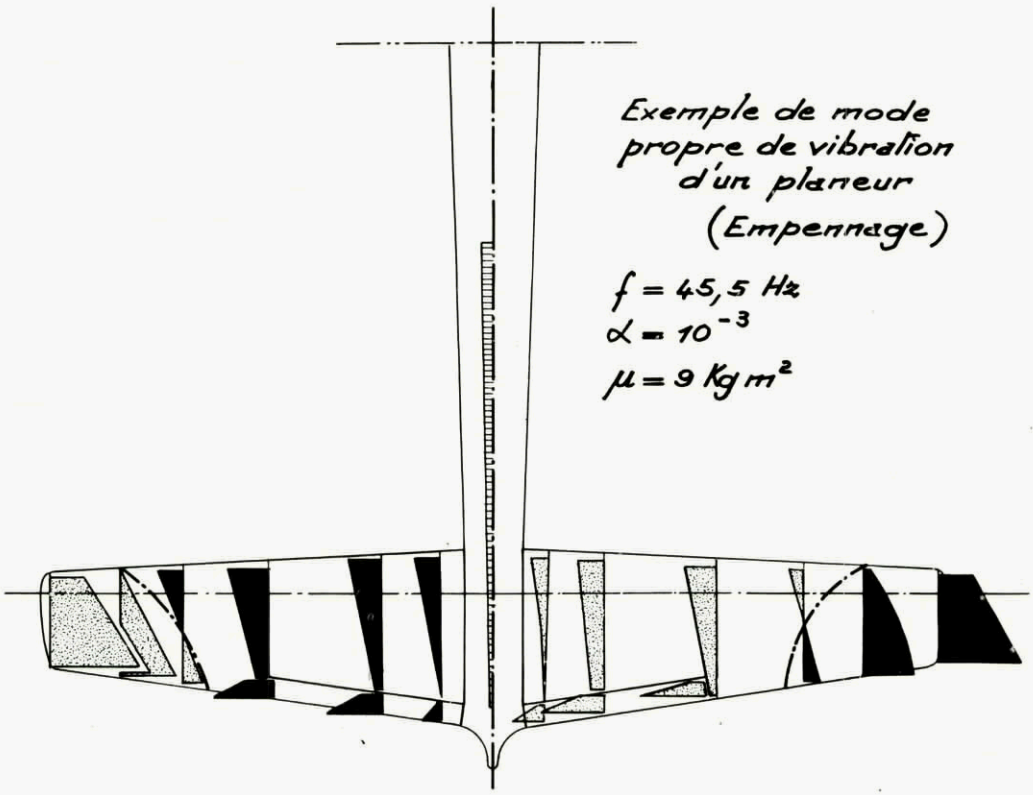


FIG. 2

3) La mesure des valeurs généralisées : Les valeurs généralisées à mesurer sont :

la masse généralisée $\mu_i^{(i)}$ ou la raideur généralisée $\gamma_i^{(i)}$ (puisqu'à la résonance de phase les deux valeurs sont liées par la relation $\mu_i^{(i)} \omega_i^2 = \gamma_i^{(i)}$),

le taux de viscosité $\alpha_i = \dfrac{\beta_i^{(i)}}{2 \mu_i^{(i)} \omega_i}$.

Nous avons indiqué précédemment que les caractéristiques modales devaient être mesurées par deux procédés de nature différente, afin de pouvoir donner la marge d'erreur sur ces valeurs, marge résultant des différences entre structures théorique et réelle.

Les catégories de procédés de nature différente sont :

1 - La catégorie des procédés fondés sur une variation d'impédance de la structure

2 - La catégorie des procédés utilisant l'énergie introduite dans la structure.

Dans la première catégorie nous citerons le procédé des masses ou raideurs additionnelles et des forces en quadrature. Ces procédés, fondés sur une faible variation d'impédance de la structure sont sensibles à la qualité de l'appropriation avant variation et par voie de conséquence exigent une réappropriation de l'excitation après variation. Ils permettent les mesures respectives de $\mu_i^{(i)}$, $\gamma_i^{(i)}$, et α_i .

Dans la deuxième catégorie nous citerons : "le travail introduit" qui donne le produit et le procédé de la "puissance complexe" d'application plus récente : par un micro-balayage autour de la fréquence de résonance , il donne la possibilité de déterminer $\mu_i^{(i)}$ et α_i . Par rapport aux autres procédés il offre l'avantage d'être moins sensible à la qualité de l'appropriation et aux faibles non linéarités structurales. Il est actuellement utilisé de façon systématique dans les essais industriels de l'ONERA.

A titre d'exemple, sur un avion léger de construction bois, son application parallèlement avec les procédés des masses addtionnelles et des forces en quadrature a montré que, dans la gamme de fréquences 0 - 100 Hz, pour la quasi-totalité des modes la marge d'incertitude sur les masses généralisées était inférieure à $\pm$ 5 %, un seul mode présentait une marge d'incertitude plus élevée mais néanmoins inférieure à $\pm$ 12 %.

2.1.5 - Application pratique

Ce bref exposé sur la méthode expérimentale de détermination des caractéristiques modales dont on pourra trouver un développement plus complet dans la référence [4] montre que cette méthode offre toutes les garanties pour la prévision de la stabilité aéroélastique des structures. Les informations qu'elle fournit peuvent aussi être utilisées avec profit dans l'étude de la stabilité des systèmes asservis [5].

En France, on considère généralement que cette méthode offre plus de garanties que les méthodes théoriques, et tous les prototypes sont soumis à l'essai de vibration au sol.

A cet effet, plusieurs installations ont été développées et portées à un haut degré d'automaticité. La figure 3 montre un avion à l'essai, suspendu par des sandows.

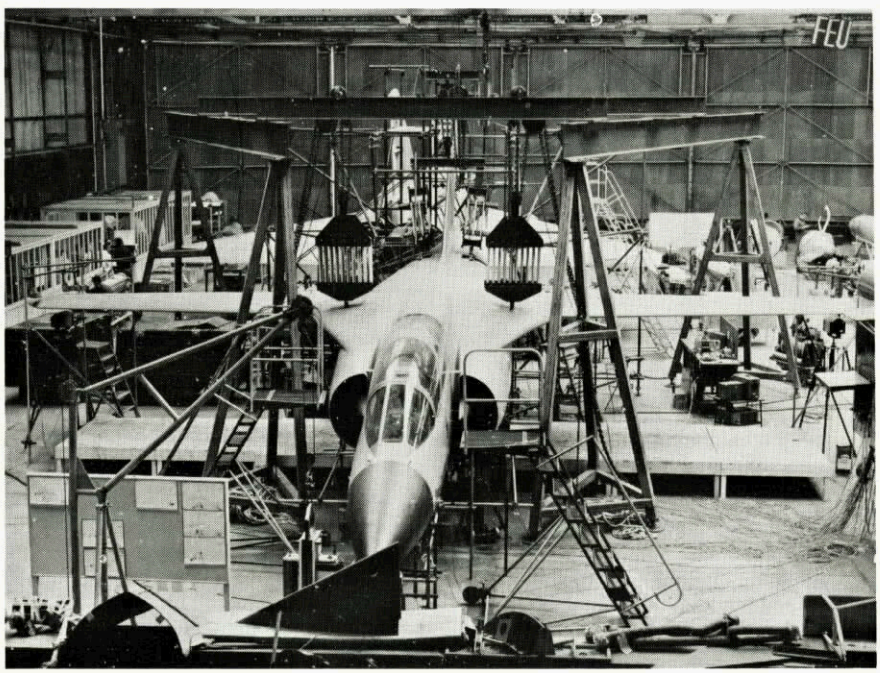


FIG. 3 - AVION SUSPENDU SOUMIS A UN ESSAI DE VIBRATION

2.2 - Méthodes théoriques - Calculs sur plans

La détermination des caractéristiques modales de la structure se fait aussi par des calculs sur plans qui permettent de commencer l'analyse des problèmes d'aéroélasticité au stade du projet, sans attendre la construction du prototype.

2.2.1 - Matrice des coefficients d'influence élastiques

Dans le paragraphe (1), on a discrétisé la structure déformable en représentant son mouvement par une superposition de déflexions $S_r(P)$.

Un autre moyen de réaliser un système discret approximativement équivalent au système réel consiste à remplacer la répartition de masses réelles par des masses ponctuelles $m_i^{(i)}$.

Considérons par exemple une voilure mince dont les déplacements se font suivant l'axe oz (fig.4).

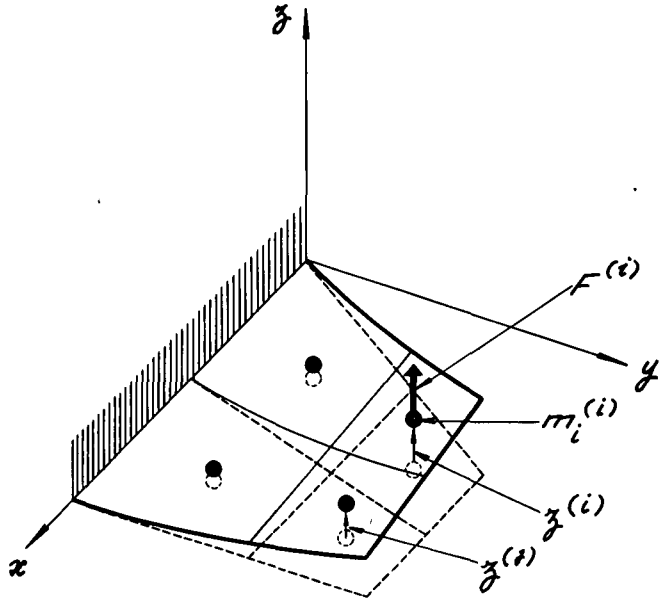


FIG. 4 - SCHEMATISATION PAR MASSES PONCTUELLES

Les degrés de liberté du système sont les variables de position $z^{(i)}$ des masses ponctuelles et les caractéristiques massiques sont définies par la matrice diagonale des $m_i^{(i)}$, qui détermine la colonne des forces d'inertie en fonction de la colonne des accélérations :

$$F^{(i)} = - m_i^{(i)} \ddot{z}^{(i)}$$

ou

$$F = - m \ddot{z} \tag{12}$$

en posant : F : colonne des forces d'inertie
m : matrice diagonale des masses
z : colonne des variables de position.

De même, les caractéristiques élastiques sont définies par la relation entre la colonne des forces et la colonne des variables de position. On peut introduire soit la matrice des coefficients d'influence élastiques, ou matrice de souplesse, soit la matrice de rigidité ou de raideur.

La première exprime les flèches connaissant les forces :

$$z^{(i)} = \sum_{j=1}^{n} E_j^{(i)} F^{(j)}$$

ou

$$z = E F \tag{13}$$

en désignant par E la matrice des coefficients de proportionnalité $E_j^{(i)}$.

La deuxième exprime les forces si les flèches sont données :

$$F^{(i)} = \sum_{j=1}^{n} K_j^{(i)} z^{(j)}$$

ou

$$F = K z \tag{14}$$

en désignant par K la matrice des coefficients $K_j^{(i)}$.

La matrice K est régulière, sauf si la structure est en equilibre indifférent, circonstance que

l'on pourra éviter en mettant une liaison appropriée, et dans ce cas on a :

(15) $$K = E^{-1} .$$

De plus, ces deux matrices sont symétriques, définies positives et permettent d'exprimer l'énergie sous la forme :

$$U = \frac{1}{2} \bar{F} E F = \frac{1}{2} \bar{z} K z$$

Mais les équations du mouvement du système conservatif peuvent s'écrire directement sans passer par l'énergie. Il suffit de remplacer la colonne F de l'équation (14) par la colonne des forces d'inertie donnée par (12). Il vient :

$$m\ddot{z} + Kz = 0$$

On se ramène à un problème de valeurs propres et de vecteurs propres en posant :

$$z = Z e^{i\omega t}$$

Il vient :

$$[-\omega^2 m + K]Z = 0$$

puis

$$[1/\omega^2 - Em]Z = 0 .$$

$1/\omega^2$ apparait comme valeur propre de Em . On aurait aussi bien pu faire apparaître ω^2 comme valeur propre de $m^{-1}K$.

Mais il convient de noter que la schématisation par masses discrètes ne permet pas de déterminer tous les modes propres de vibration avec la même précision. En effet, les erreurs croissent avec le rang du mode considéré c'est-à-dire avec la fréquence propre, parce que la complexité des déformées croit en même temps. Le sachant, on se limitera au calcul d'un nombre de valeurs propres et de vecteurs propres nettement inférieur au nombre de masses ponctuelles. C'est la raison pour laquelle il est avantageux de faire apparaître $1/\omega^2$ au lieu de ω^2 comme valeur propre. En procédant ainsi, en effet, on est conduit à extraire les valeurs propres dominantes de la matrice Em .

Il y a quelques années, on déterminait la matrice de souplesse par un essai statique dont il est facile d'imaginer le déroulement. Aujourd'hui, cet essai est supplanté par l'essai de vibration, pour la détermination des caractéristiques modales, mais il est encore pratiqué pour le contrôle des calculs d'élasticité.

Par contre, lorsque les modes propres sont déterminés par la voie théorique, on passe le plus souvent par la matrice des coefficients d'influence élastiques, qui constitue l'aboutissement du calcul d'élasticité, avant d'aborder le calcul des modes propres. Nous verrons (paragraphe 2.2.3) que cela n'est pourtant pas indispensable.

Il est évident que pour représenter les propriétés élastiques d'un avion complet, ces matrices doivent avoir un ordre élevé.

En fait, il n'est pas nécessaire de traiter tout l'avion en bloc. Il est beaucoup plus économique de traiter d'abord séparément les différentes parties : voilure, fuselage, empennage et dérive, et de les raccorder ensuite en représentant le mouvement de chacune d'elles dans sa base modale propre. C'est la méthode des "branch modes". En procédant ainsi, la convergence rapide de la base modale permet de réduire le nombre de degrés de liberté à une valeur acceptable.

2.2.2 - Méthode des éléments finis

Le calcul de la matrice de souplesse ou de la matrice de raideur se fait le plus souvent en décomposant la structure en éléments finis dont on détermine séparément les caractéristiques élastiques, et que l'on assemble ensuite en respectant les conditions de compatibilité ou d'équilibre.

Cette méthode est désignée souvent par "méthode d'Argyris" parce que cet auteur a apporté une contribution majeure à la systématisation des calculs.

Pour obtenir une bonne précision, il faut en général faire un découpage fin de la structure, ce qui conduit couramment à des problèmes avec plusieurs centaines d'inconnues. Le volume de données qu'il faut manipuler devient alors extrèmement important et les calculs restent lourds en dépit du fait que certaines matrices sont multidiagonales.

On distingue en général la méthode des forces et la méthode des déplacements, selon que l'on considère les forces ou les déplacements comme inconnus dans le problème. L'une aboutit à la matrice de souplesse et l'autre à la matrice de raideur.

La division en éléments est délicate. Dans les structures d'avions on trouve des éléments de barres travaillant en effort longitudinal, des éléments de poutres travaillant en flexion ou en torsion, et enfin des éléments de plaques en état de contrainte plan.

Les figures 5-a et 5-b montrent la décomposition d'un caisson dans le cas, simplifié à l'extrême,

où l'on admet les hypothèses suivantes :

a) les tôles travaillent en cisaillement pur,
b) les raidisseurs travaillent en traction-compression,
c) la contrainte normale varie linéairement le long de ces raidisseurs.

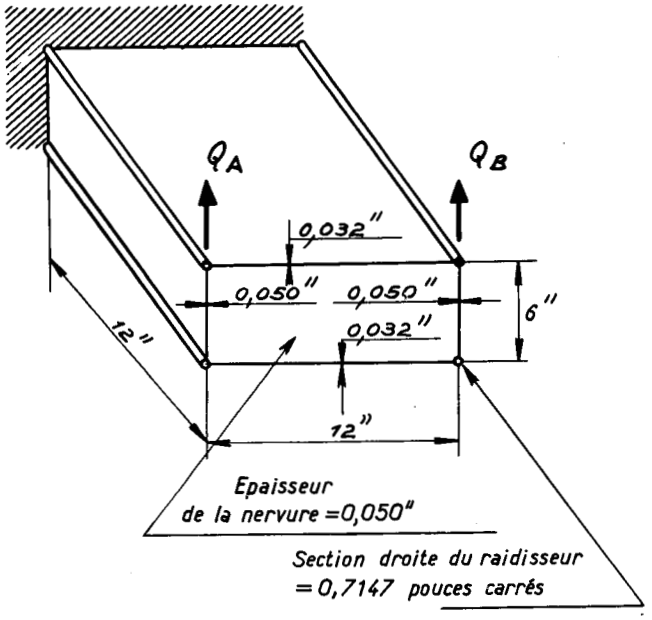


FIG. 5-a - CAISSON METALLIQUE SIMPLIFIE

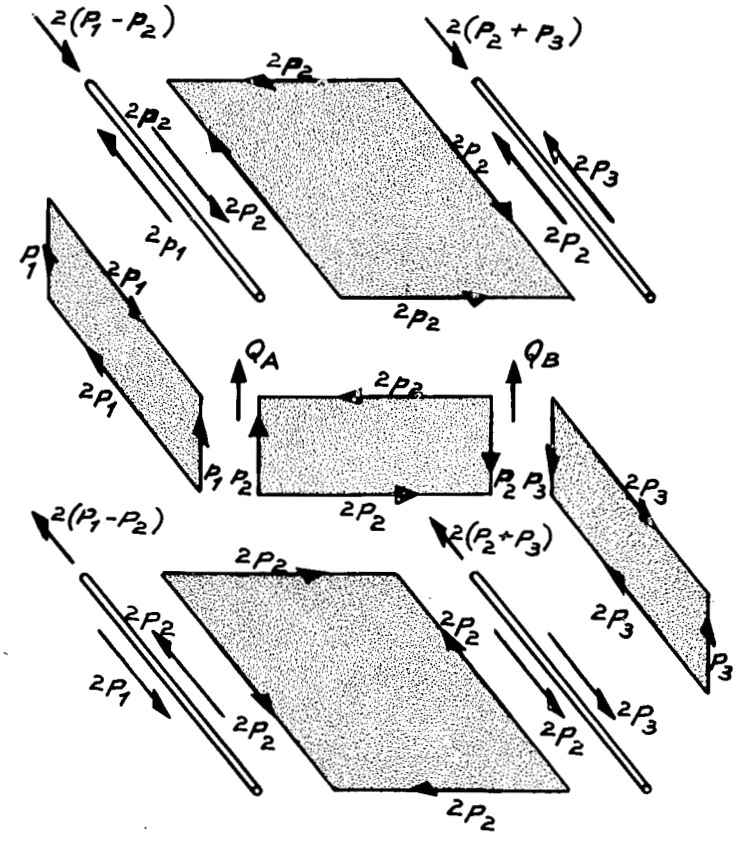


FIG. 5-b - CAISSON SIMPLIFIE ECLATE

Mais dans des cas pratiques complexes, les tôles elles-mêmes doivent être décomposées en éléments en forme de parallélogrammes ou de triangles assemblés en des noeuds, comme le montre la figure 6.

Chaque élément séparé est caractérisé lui-même par une matrice de souplesse ou de raideur qui

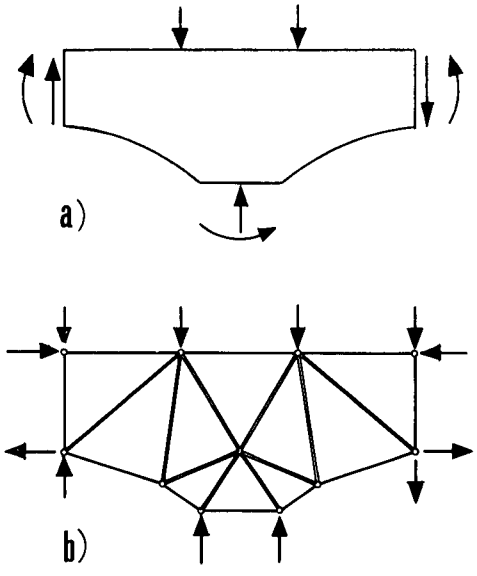


FIG. 6 - a) SYSTEME REEL
b) IDEALISATION

relie les composantes des déplacements des noeuds aux composantes des forces en ces mêmes noeuds.

Pour des éléments de plaques en état de contrainte plan, la détermination de ces matrices est déjà assez délicate. On est conduit, en général à faire des hypothèses sur le champ de contraintes ou de déformations que l'on représente par une combinaison de fonctions. Ainsi, la figure 7 illustre le cas d'un élément de plaque rectangulaire dans laquelle on admet un cisaillement constant et des contraintes normales réparties linéairement. Ce champ de contrainte est obtenu par une superposition linéaire des 5 champs élémentaires représentés sur la partie gauche de la figure. A droite on indique les déflexions correspondantes.

L'énergie potentielle de l'élément peut s'exprimer d'abord en fonction des paramètres de superposition $\beta_1 \ldots \beta_5$, puis en fonction des paramètres de déplacement des sommets qui sont reliés eux-mêmes aux β_i par une relation matricielle facile à établir. On aboutit ainsi à une forme définie positive dans laquelle apparait une matrice qui n'est autre que la matrice de raideur de l'élément.

La liaison des éléments de plaques par des noeuds est évidemment différente du cas réel, et le défaut de liaison sur les côtés devrait normalement se traduire par une augmentation considérable de la souplesse de la structure. En fait, ce défaut est compensé en grande partie par les hypothèses restrictives sur la répartition des contraintes ou des déformations dans chaque élément.

Pour obtenir les caractéristiques de la structure assemblée, qui est en général hyperstatique, il faut compléter les équations matricielles des éléments non assemblés par des équations supplémentaires, qui sont des relations d'équilibre, dans la méthode des forces, et des relations cinématiques,

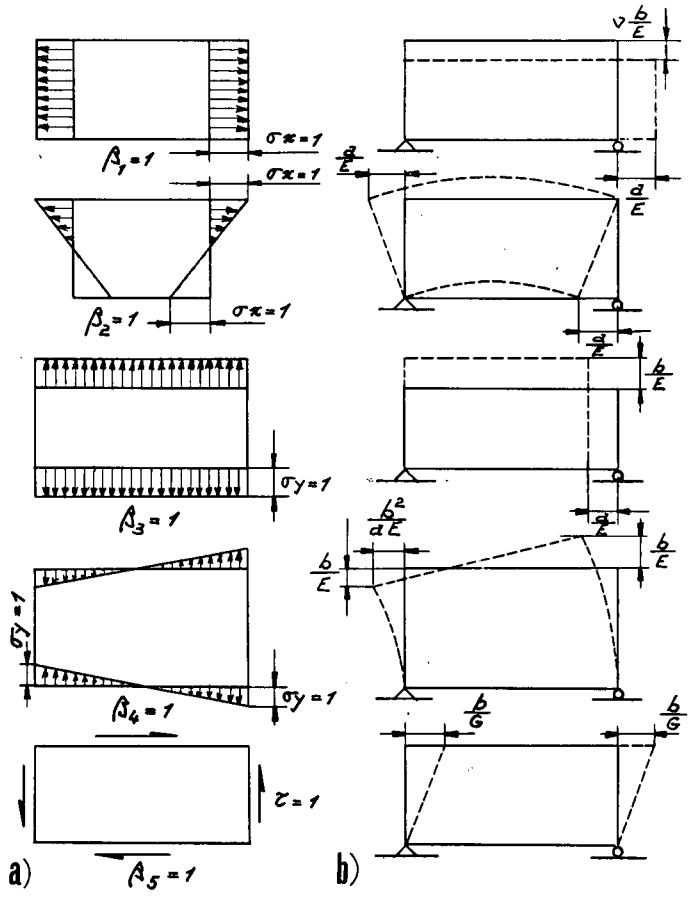


FIG. 7 - a) DIAGRAMMES DE CONTRAINTE
b) DEFORMATIONS ASSOCIEES

dans la méthode des déplacements. Nous n'entrerons pas dans le détail de la formulation matricielle qui est exposée par ailleurs, [6] à [9].

2.2.3 - Méthode de Rayleigh-Ritz

La méthode de Rayleigh-Ritz consiste à représenter le mouvement dans une base artificielle assurant la convergence. C'est pratiquement ce qui a été fait dans le paragraphe (1) en posant :

$$P(P,t) = \sum_{r=1}^{n} S_r(P)\, q^{(r)}(t)$$

S'agissant du calcul des modes propres du système conservatif, on évalue l'énergie cinétique et l'énergie potentielle et on aboutit à l'équation aux valeurs propres et aux vecteurs propres :

$$[-\omega^2 M + K]\, q^* = 0$$

L'évaluation de l'énergie cinétique et de la matrice M ne nécessite pas une définition très précise des déflexions de base $S_r(P)$. C'est ainsi que pour une aile mince, il suffit de connaître la composante de la vitesse normale à son plan, ce qui conduit à définir seulement la composante normale de la déflexion par une fonction $z(x,y,t)$. Dans ces conditions, les déflexions de base $S_r(P)$ sont des fonctions $Z_r(x,y)$, et l'on a :

$$z(x,y,t) = \sum_{r=1}^{n} Z_r(x,y)\, q^{(r)}(t)$$

Le calcul de l'énergie potentielle, par contre, suppose que la position des points est connue avec beaucoup de précision, puisqu'il fait intervenir les champs de contrainte ou de déformation liés aux déflexions de base $S_r(P)$.

Or, ces champs de contrainte ne peuvent en général être définis qu'en faisant des hypothèses. Dans le cas de l'aile mince, par exemple, on aurait une formulation relativement simple en admettant l'existence d'une surface neutre où les contraintes restent nulles, puis en supposant que la fonction $Z_r(x,y)$ représente la déflexion de cette surface suivant oz, et que les points situés de part et d'autre se sont déplacés en restant sur la même normale (fig. 8).

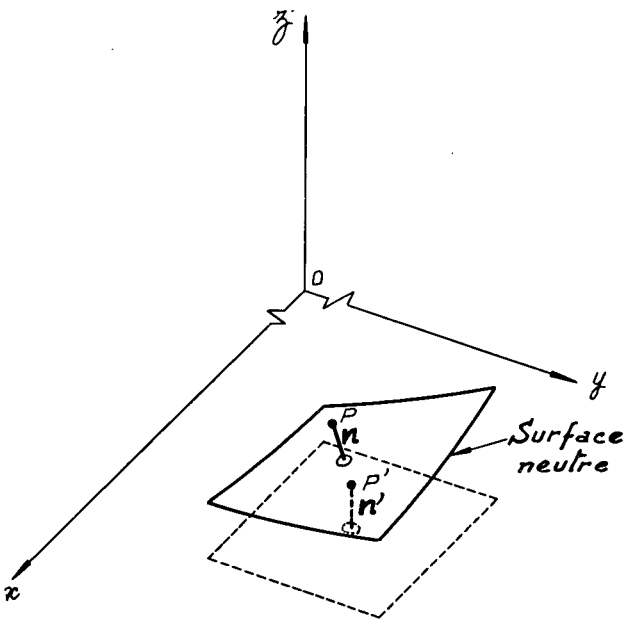


FIG. 8 - DEFORMATION

D'UN ELEMENT DE PLAQUE

Dans ces conditions, le déplacement des points et le champ de déformations correspondant à une fonction de base $S_r(P)$ sont parfaitement déterminés, et le calcul de la matrice K devient possible.

Cette façon de procéder revient à assimiler le comportement interne de l'aile à celui d'une plaque, et à négliger des déformations de cisaillement qui sont souvent importantes. Il peut en résulter une surestimation sensible de la rigidité.

Les fonctions de base $Z_r(x,y)$ peuvent être une suite limitée de polynômes ou de fonctions sinusoïdales, avec des termes particuliers pour les mouvements d'ensemble et les oscillations de gouvernes.

En définitive la méthode de Rayleigh-Ritz est particulièrement bien adaptée à certains types de structures, telles que les poutres et les plaques d'épaisseur évolutive. Dans l'application aux structures aérospatiales, elle a été supplantée par la méthode des éléments finis, mais elle semble avoir un regain de faveur depuis quelque temps, notamment pour le calcul des engins.

3 - DETERMINATION DES FORCES AERODYNAMIQUES GENERALISEES

Ce chapitre est consacré à la détermination de la colonne des forces généralisées, Q , des équations (11). Il s'agit d'un problème très complexe qui ne peut être résolu qu'en faisant appel à la fois à l'expérience et aux théories les plus élaborées.

Les possibilités de l'expérience sont cependant beaucoup plus limitées que dans le cas de l'avion rigide, parce que le nombre de paramètres nécessaires pour définir, même de façon approchée, le mouvement d'une structure déformable, est trop élevé pour que la mesure de toutes les données nécessaires soit possible.

Dans ces conditions, la détermination des forces aérodynamiques doit se fonder sur une théorie complète couvrant tous les cas. Le rôle de l'expérience n'en demeure pas moins important, indispensable même, mais il se limite à l'acquisition de données partielles qui serviront à contrôler la théorie ou à élaborer des corrections.

En dehors de quelques tentatives sporadiques, les calculs sont toujours fondés sur la théorie de l'écoulement d'un fluide parfait autour d'une surface portante animée de petits mouvements d'oscillation harmoniques au voisinage de son plan moyen. On s'intéresse ici à la mise en oeuvre pratique plutôt qu'à l'exposé de la théorie.

3.1 - Méthodes des tranches indépendantes

Pour une aile de grand allongement, ou pour des calculs de dégrossissage, la surface portante est décomposée en tranches parallèles au vent autour desquelles l'écoulement est supposé bidimensionnel.

Cette hypothèse simplifie évidemment la théorie, et, surtout, les paramètres de position et de forces d'une tranche étant relativement peu nombreux, elle permet d'utiliser des coefficients tabulés une fois pour toutes.

Pour une tranche indéformable munie d'une gouverne, ces paramètres sont définis sur la figure 9.

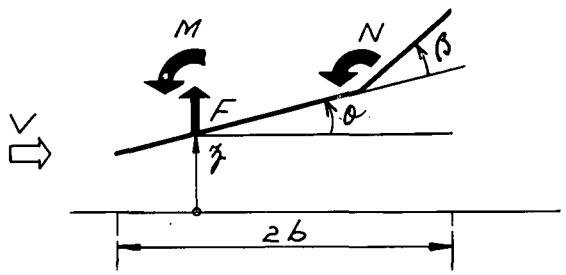


FIG. 9

La relation matricielle s'écrit :

$$\begin{bmatrix} Fb \\ M \\ N \end{bmatrix} = -\rho V^2 b^2 \Delta y \left[A' + i \frac{\omega b}{V} A'' \right] \begin{bmatrix} z/b \\ \alpha \\ \beta \end{bmatrix}$$

A' et A'' sont des matrices réelles d'ordre 3 qui dépendent du paramètre de fréquence $\frac{\omega b}{V}$, du nombre de Mach M , et de la profondeur relative de la gouverne τ .

3.2 - Théorie de l'écoulement tridimensionnel

3.2.1 - Méthode de l'équation intégrale - Matrice des coefficients aérodynamiques

La théorie bidimensionnelle s'est rapidement révélée insuffisante, et le développement des ordinateurs a permis, depuis quelques années déjà, de mettre en oeuvre la théorie de la surface portante de forme en plan quelconque, en mouvement harmonique (voir [10] à [14]).

La formulation qui permet de traiter les cas les plus généraux est obtenue en représentant l'aile par une nappe de doublets d'accélération. On aboutit ainsi à une équation intégrale exprimant la vitesse normale w en fonction de la différence de pression Δp , soit, en posant $w = w^* e^{i\omega t}$ et $\Delta p = \Delta p^* e^{i\omega t}$:

(16)
$$w^*\left(\frac{x}{L}, \frac{y}{L}\right) = V \iint_{Aile} K\left(\frac{x-\xi}{L}, \frac{y-\eta}{L}\right) \frac{\Delta p^*(\xi,\eta)}{\rho V^2} d\left(\frac{\xi}{L}\right) d\left(\frac{\eta}{L}\right)$$

où L désigne une longueur de référence, par exemple la 1/2 corde d'emplanture.

L'intérêt de cette équation réside dans le fait que le domaine d'intégration est limité à l'aile.

Le noyau dépend du paramètre de fréquence (ou fréquence réduite), $k = \frac{\omega L}{V}$, et du nombre de Mach M , et il a une expression particulièrement complexe. Il contient un pôle d'ordre 2 en $y-\eta$, et l'intégrale doit être évaluée en partie finie $(\not\int)$.

La résolution pratique se fait en représentant Δp^* par une superposition de fonctions de pression :

(17-1) $$\Delta p^*(\xi,\eta) = \rho V^2 \sum_{r=1}^{m} C_r(\xi,\eta)\, X^{(r)}$$

ou

(17-2) $$\Delta p^* = \rho V^2 \mathbf{C} \mathbf{X}$$

en désignant par $\mathbf{C}$ la base

$$\mathbf{C}(\xi,\eta) = [\, C_1(\xi,\eta) \cdots C_m(\xi,\eta)]$$

et par $\mathbf{X}$ la colonne des coefficients $X^{(r)}$.

Les fonctions de base $C_r(\xi,\eta)$ doivent contenir les singularités appropriées pour que $w^*(\xi,\eta)$ soit fini sur toute la surface portante.

On procède le plus souvent par collocation, en exprimant la vitesse normale w en fontion des coefficients $X^{(r)}$, sur un réseau de points appelés points de collocation ou de contrôle.

Il vient alors, en substituant (17-1) dans (16) :

$$w^*\left(\frac{x^{(i)}}{L}, \frac{y^{(i)}}{L}\right) = V \sum_{r=1}^{m} R_r^{(i)} X^{(r)}$$

avec

$$R_r^{(i)} = \not\iint_{Aile} K\left(\frac{x^{(i)}-\xi}{L}, \frac{y^{(i)}-\eta}{L}\right) C_r(\xi,\eta)\, d\left(\frac{\xi}{L}\right) d\left(\frac{\eta}{L}\right)$$

En désignant par $\mathbf{w}^*$ la colonne des vitesses normales aux points de collocation, $w^*\left(\frac{x^{(i)}}{L}, \frac{y^{(i)}}{L}\right)$, et par $\mathbf{R}$ la matrice des intégrales $R_r^{(i)}$, on a :

$$\mathbf{w}^* = V \mathbf{R} \mathbf{X}$$

Si le nombre de points de collocation est égal au nombre de fonctions de base, m , la matrice $\mathbf{R}$ est régulière, et l'on a :

$$\mathbf{X} = \frac{1}{V} \mathbf{A} \mathbf{w}^* \qquad \text{(en posant } \mathbf{A} = \mathbf{R}^{-1}\text{)}$$

et la pression est donnée en substituant cette expression dans (17-2) :

(18-1) $$\Delta p^*(x,y) = \rho V \mathbf{C}(x,y) \mathbf{A} \mathbf{w}^*$$

$\mathbf{A}$ est une matrice de coefficients aérodynamiques. Elle dépend de la fréquence réduite, du nombre de Mach et de la forme en plan.

Remarquons que l'on a $\mathbf{w} = \mathbf{w}^* e^{i\omega t}$ et $\Delta p = \Delta p^* e^{i\omega t}$ et que l'équation (18-1) peut aussi bien s'écrire :

(18-2) $$\Delta p(x,y,t) = \rho V \mathbf{C}(x,y) \mathbf{A} \mathbf{w}(t)$$

3.2.2 - Forces généralisées

Le travail virtuel de Δp est donné par l'intégrale.

(19) $$\delta A = \iint_{Aile} \overline{\delta z}(x,y,t)\, \Delta p(x,y,t)\, dx\, dy$$

la déflexion de l'aile, $z(x,y,t)$ est représentée dans la base modale par l'expression (10) qui devient dans ce cas :

$$z(x,y,t) = \sum_{r=1}^{n} \Phi_r(x,y)\, q^{(r)}(t)$$

ou

(20) $$z(x,y,t) = \mathbf{\Phi}(x,y)\, \mathbf{q}(t)$$

où les vecteurs de base $\Phi_r(x,y)$ qui définissent les formes propres du système conservatif se réduisent à des fonctions de x et de y , du fait que le mouvement a une direction privilégiée.

En substituant (20) et (18-2) dans (19), il vient :

$$\delta A = \rho V \, \overline{\delta q} \iint_{Aile} \overline{\Phi}(x,y) C(x,y) \, dx \, dy \, A \, w(t)$$

C'est une expression de la forme $\overline{\delta q} \, Q$, et on identifie la colonne des forces généralisées :

$$Q = \rho V L^2 \left[\iint_{Aile} \overline{\Phi}(x,y) C(x,y) \, d\left(\frac{x}{L}\right) d\left(\frac{y}{L}\right) \right] A \, w(t)$$

L'intégrale entre crochets est évaluée en général par la methode de Gauss en faisant apparaître des points d'intégration et des poids. Il vient :

$$\iint_{Aile} \overline{\Phi}(x,y) \, C(x,y) \, d\left(\frac{x}{L}\right) d\left(\frac{y}{L}\right) = \sum_{i=1}^{N} \overline{\Phi(P^{(i)})} \, H_i^{(i)} \, C(P^{(i)})$$

(en désignant par $P^{(i)}$ les points d'intégration et par $H_i^{(i)}$ les poids ou éléments de surface affectés à ces points).

Cette sommation devient un produit matriciel, à condition de définir :

- une matrice $\Phi_{(i)}$ qui définit les formes propres Φ_r aux points d'intégration ($\Phi_{(i)\,r}^{(i)} = \Phi_r(P^{(i)})$)
- une matrice $C_{(i)}$ qui définit les fonctions de pression aux mêmes points ($C_{(i)\,r}^{(i)} = C_r(P^{(i)})$)
- et la matrice diagonale des poids, H .

Il vient :

$$\iint_{Aile} \overline{\Phi} \, C \, d\left(\frac{x}{L}\right) d\left(\frac{y}{L}\right) = \overline{\Phi}_{(j)} \, H \, C_{(j)}$$

D'où :

$$Q = \rho V L^2 \, \overline{\Phi}_{(j)} H C_{(j)} A \, w(t) \tag{21}$$

Le produit matriciel $H C_{(j)} A$ est une matrice de coefficients d'influence aérodynamiques qui rappelle la matrice de coefficients d'influence élastiques ou la matrice de raideur.

Pour justifier cette interprétation, on remarque d'abord que le produit $C_{(j)} A \, w$ donne les valeurs de Δp aux points d'intégration lorsque w est connu aux points de collocation. En prémultipliant ensuite par la matrice diagonale H , dont les coefficients représentent les éléments de surface affectés à chaque point d'intégration (au coefficient L^2 près), on obtient les forces affectées à chaque point d'intégration dans l'intégration numérique.

Ce produit matriciel dépend de la fréquence réduite, du Mach, de la forme en plan, et du nombre de points d'intégration et de collocation.

Or, il est nécessaire de prendre un assez grand nombre de points pour obtenir une bonne précision. Les calculs se font couramment, en France, avec 25 points de contrôle par 1/2 aile, et certains constructeurs américains sont allés jusqu'à près de 100 points. Dans ces conditions, la matrice de coefficients d'influence n'est obtenue qu'après un volume considérable de calculs.

La vitesse normale w est donnée par la condition de non décollement :

$$w(x,y,t) = V \frac{\partial z}{\partial x} + \frac{\partial z}{\partial t} = V \Phi_x' q + \Phi \dot{q} \qquad \text{(d'après (20))}$$

et la colonne w qui donne les valeurs de w aux points de contrôle est définie par :

$$w = V \Phi_{(c)}' q + \Phi_{(c)} \dot{q}$$

(en désignant par $\Phi_{(c)}$ la matrice définissant les formes propres $\Phi_r(x,y)$ aux points de contrôle, et par $\Phi_{(c)}'$ la matrice donnant les pentes $\partial \Phi_r / \partial x$ aux mêmes points).

En régime harmonique, $\dot{q} = i\omega q$ entraine :

$$w = V \left[\Phi_{(c)}' + i \frac{\omega}{V} \Phi_{(c)} \right] q$$

d'où, en substituant dans (21) :

$$Q = \rho V^2 L^3 \left[\frac{1}{L} \overline{\Phi}_{(j)} H C_{(j)} \left(\Phi_{(c)}' + i \frac{\omega}{V} \Phi_{(c)} \right) \right] q$$

ou

$$Q = -\rho V^2 L^3 \, G(ik) \, q \tag{22}$$

avec $k = \frac{\omega L}{V}$, et en posant :

$$G(ik) = \frac{1}{L} \overline{\Phi}_{(j)} H C_{(j)} A(ik) \left[\Phi_{(c)}' + ik \Phi_{(c)} \right] \tag{23}$$

Les formes propres $\Phi_r(x,y)$ ont en général les dimensions d'une longueur et la matrice G est sans dimensions.

La formule (22) permet de compléter l'équation du mouvement (11). En tenant compte du mouvement harmonique, on a :

$$[-\omega^2\mu + i\omega\beta + \gamma + \rho V^2 L^3 G(ik)]q = 0 \qquad (25)$$

Pratiquement, la matrice $G(ik)$ est évaluée numériquement pour des valeurs discrètes et réelles de k . .

Ce calcul est d'ailleurs très volumineux et ne peut être effectué dans des conditions économiques convenables que s'il est bien organisé.

Il est indiqué notamment de calculer la matrice A et le produit matriciel $HC_{(j)}A$ (ou matrice de coefficients d'influence aérodynamiques), pour les valeurs intéressantes de la fréquence et du Mach, et de stocker les coefficients en mémoire. Ce calcul peut être lancé dès qu'une nouvelle forme en plan est mise à l'étude, sans qu'il soit nécessaire de connaître les formes propres de vibration dont dépendent les matrices Φ et Φ' de la formule (23).

L'équation (25) n'admet de solution $q \neq 0$ que pour les valeurs de ω qui annulent le déterminant caractéristique, c'est-à-dire qui vérifient l'équation :

$$\text{dét}\left(-\omega^2\mu + i\omega\beta + \gamma + \rho V^2 L^3 G\left(i\frac{\omega L}{V}\right)\right) = 0 \qquad (26)$$

Mais ces racines sont en général complexes, ce qui est en contradiction avec le fait que G n'est évaluée que pour des valeurs réelles de ω . Cette restriction n'est pas grave dans la recherche des instabilités (et en particulier du flottement) car dans ce cas il suffit de connaître les valeurs critiques de ρ et de V pour lesquelles il existe une solution harmonique. Ces valeurs critiques définissent en effet la frontière du domaine d'instabilité : d'un côté toutes les racines $p = i\omega$ ont leur partie réelle négative et de l'autre, l'une d'elles a une partie réelle positive.

Ces solutions harmoniques peuvent s'obtenir par un balayage systématique en ρ , V et ω , avec des valeurs réelles.

Le balayage est d'ailleurs considérablement simplifié si l'on néglige les forces de dissipation de structure car dans ce cas, l'équation (25) peut s'écrire :

$$\left[-1/\omega^2 - \gamma^{-1}\mu - \frac{\rho L}{k}\gamma^{-1}G(ik)\right]q = 0$$

et $1/\omega^2$ apparaît comme valeur propre d'une matrice complexe qui ne dépend que de ρ et de k .

En faisant un balayage en k on finit par trouver un couple k , ω , avec ω réel. Ce couple que nous désignons par k_{cr} , ω_{cr} , détermine alors la vitesse critique qui est donnée, d'après la définition de k , par :

$$\frac{V}{cr} = \frac{k_{cr}}{\omega_{cr} L}$$

En dehors de ce cas de calcul, les valeurs propres complexes obtenues dans ces conditions n'ont pas de signification physique. Si la partie imaginaire de ω est petite devant la partie réelle, on peut cependant justifier une interprétation qui permet de déduire des valeurs approchées des pulsations et des amortissements en fonction de la vitesse.

3.2.3 - Formulation approchée

L'explicitation donnée aux forces aérodynamiques généralisées (22) est suffisante pour les études de flottement parce qu'il s'agit avant tout de déterminer les solutions harmoniques.

Mais les conditions sont nettement différentes dans le problème de la dynamique du vol, et il vaut mieux, dans ce cas, remplacer l'équation (25) par une équation différentielle du second ordre à coefficients constants, même s'il est nécessaire pour cela de faire une approximation.

Remarquons d'abord que l'hypothèse de la linéarité doit conduire normalement à un système d'équations différentielles linéaires, puisqu'elle signifie que les forces dépendent linéairement de la colonne de coordonnées généralisées q et de ses dérivées $\dot{q}$, $\ddot{q}$ ... . Il existe donc des matrices réelles et constantes G_0 , G_1 ... qui permettent d'exprimer les forces aérodynamiques généralisées sous la forme :

$$Q = -\rho V^2 L^3 \left[G_0 q + \frac{L}{V} G_1 \dot{q} + \frac{L^2}{V^2} G_2 \ddot{q} + \cdots\right] \qquad (27)$$

où les coefficients $\frac{L}{V}$, $\frac{L^2}{V^2}$ ... sont introduits pour que G_0 , G_1 ... soient sans dimensions.

Cette expression doit être équivalente à (22) dans le cas du mouvement harmonique.

Or, $G(ik)$ peut se développer en fonction de ik avec des matrices réelles, et (22) devient :

$$Q = -\rho V^2 L^3 \left[G_0 + ik\,G_1 - k^2 G_2 - \cdots\right]q$$

et l'on a :

$$ikq = \frac{L}{V}\dot{q} \quad , \quad -k^2 q = \frac{L^2}{V^2}\ddot{q} \quad , \ \cdots$$

Dans ces conditions on peut donc identifier les matrices G_o , G_1 ... de (27), avec les termes du développement de $G(ik)$ en fonction de ik .

On obtient une formulation approchée, particulièrement bien adaptée aux problèmes de la mécanique du vol, en ne retenant que les 3 premiers termes de ce développement, soit G_o , G_1 et G_2 .

Cette approximation revient à exprimer Q en fonction des paramètres de position, des vitesses et des accélérations.

Le calcul de la matrice $G(ik)$, tel qu'il est conduit pour des raisons pratiques, ne donne pas les termes du développement; mais on peut les obtenir facilement à partir d'un calcul fait en stationnaire $(k=o)$ et d'un calcul fait à une valeur finie mais petite de k .

Considérons la matrice aérodynamique A qui intervient dans la formule (23) et qui ne dépend que de k , du Mach, et de la forme en plan.

Elle admet un développement en ik de la forme :

$$A(ik) = A_o + ikA_1 - k^2A_2 - ik^3A_3 + \dots$$

Les 3 premiers termes sont donnés par :

$$A_o = A(o)$$

$$A_1 = \lim_{k\to o} \frac{\mathcal{J}(A(ik))}{ik}$$

$$A_2 = \lim_{k\to o} \frac{A(o) - \mathcal{R}(A(ik))}{k^2}$$

En considérant une valeur finie mais petite de k , il vient :

$$A_o = A(o)$$

$$A_1 \cong \frac{\mathcal{J}(A(ik))}{ik}$$

$$A_2 \cong \frac{A(o) - \mathcal{R}(A(ik))}{k^2}$$

Ces 3 matrices qui ne dépendent que du Mach et de la forme en plan, étant calculées, on substitue

$$A = A_o + ikA_1 - k^2A_2$$

dans (23), et il vient :

$$G(ik) = G_o + ikG_1 - k^2G_2$$

avec

$$G_o = \frac{1}{L}\bar{\Phi}_{(i)} H C_{(i)} A_o \Phi'_{(c)}$$

$$G_1 = \frac{1}{L}\bar{\Phi}_{(i)} H C_{(i)} \left[\frac{1}{L}A_o\Phi_{(c)} + A_1\Phi'_{(c)}\right]$$

$$G_2 = \frac{1}{L}\bar{\Phi}_{(i)} H C_{(i)} \left[\frac{1}{L}A_1\Phi_{(c)} + A_2\Phi'_{(c)}\right]$$

et dans ces conditions, on a :

$$Q = -\rho V^2 L^3 \left[G_o q + G_1 \dot{q} + G_2 \ddot{q} \right]$$

Cette expression doit être substituée dans les équations du mouvement (11) qui deviennent :

(28) $$\left[\mu + \rho L^5 G_2\right]\ddot{q} + \left[\beta + \rho V L^4 G_1\right]\dot{q} + \left[\gamma + \rho V^2 L^3 G_o\right] q = 0$$

Le terme $\rho L^5 G_2 \ddot{q}$ mérite une attention particulière. Il traduit un effet de pseudo-inertie indépendant de la vitesse et qui se manifeste déjà dans les essais de vibration au sol. Dans ces conditions, il est inclus dans la matrice μ lorsque celle-ci est obtenue expérimentalement, et dans ce cas on évitera de l'introduire une deuxième fois.

L'équation (28) détermine le comportement de l'avion libre, tout au moins tant que l'on ne considère que des mouvements à fréquence relativement basse comme on le fait dans l'étude de la mécanique du vol.

D'autres effets peuvent être introduits de façon toujours aussi systématique, notamment l'effet d'un servo-mécanisme ou des perturbations atmosphériques.

Ces perturbations, en particulier, se manifestent par la composante de la vitesse atmosphérique normale au plan de l'aile w_{at} , qui se retranche de la vitesse normale due au mouvement propre de l'aile, et la colonne des forces généralisées correspondant à cet effet est obtenue en remplaçant w par $-w_{at}$ dans la formule (21).

3.2.4 - Gouvernes

La formulation de l'équation intégrale est remarquablement adaptée au problème de l'aile mince et lisse, c'est-à-dire sans gouvernes.

Le braquage d'une gouverne introduit une discontinuité dans la répartition de la vitesse normale, et des singularités logarithmiques sur la charnière et les bords latéraux.

Jusqu'ici, on avait renoncé à introduire ces singularités dans les fonctions de pression On se contentait d'y faire figurer les singularités de bord d'attaque, de bord de fuite et de bords latéraux qui rendent w fini et continu sur l'aile. On devait alors remplacer la répartition réelle de w par une répartition continue "équivalente" au sens d'une norme appropriée. Cette méthode conduit à des répartitions de pression érronées et à des forces généralisées peu précises, surtout en ce qui concerne les moments de charnière induits par le braquage d'une gouverne.

Un certain nombre d'auteurs ont maintenant entrepris d'introduire des singularités logarithmiques dans des programmes de calcul pour obtenir des valeurs plus significatives. Il en résulte une complication sensible des calculs.

3.2.5 - Validité pratique de la théorie

La théorie de la surface portante est maintenant exploitée depuis plusieurs années et elle a déjà fait l'objet de nombreux contrôles expérimentaux. Les résultats sont en général excellents en subsonique ($M \leqslant 0,8$) pour l'aile lisse. Dans ces cas, les effets globaux sont obtenus avec une précision surabondante pour les calculs de flottement.

Mais les résultats se détériorent avec les gouvernes, non seulement parce que les calculs numériques sont moins précis mais aussi parce que la couche limite et les fentes jouent un rôle important que la théorie ignore.

Dans ces conditions on doit admettre la nécessité d'introduire des corrections fondées sur des résultats mesurés en soufflerie.

La façon la plus appropriée d'établir ces corrections est evidemment difficile à établir. H. Bergh [15] a proposé une méthode systématique en admettant que le rapport entre la pression mesurée en un point et la pression calculée dépend peu de la forme de vibration. Cette méthode fait l'objet d'un exposé dans le même panel.

3.2.6 - Méthode des boîtes

Un exposé sur le calcul des forces aérodynamiques ne saurait être complet si l'on ne mentionnait pas une formulation établie à partir du potentiel d'une source pulsante, souvent utilisée en supersonique.

Il s'agit de l'équation qui exprime le potentiel des vitesses en fonction de sa dérivée normale sur l'aile :

$$\varphi(x,y) = \iint_{(A)} G(x-\xi, y-\eta)\, \varphi_3(\xi,\eta)\, d\xi\, d\eta$$

Le domaine d'intégration est délimité par des lignes de Mach et englobe, dans le cas où les bords ne sont pas supersoniques, une région appartenant à l'aile, où φ_3 est connu, et une région extérieure où la pression est nulle $\left(\varphi_x + i\frac{\omega L}{V}\varphi = 0\right)$.

Cette équation est particulièrement intéressante pour les ailes à bords supersoniques, mais elle reste avantageuse également dans les autres cas, à condition que le domaine d'intégration extérieur à l'aile ne soit pas trop étendu, c'est-à-dire que le nombre de Mach soit suffisamment élevé.

Pour l'exploitation pratique, on prolonge la forme en plan par des lignes de Mach pour délimiter une surface portante à bords soniques, et on couvre cette surface par un maillage.

4 - CONCLUSIONS

Cet exposé montre le caractère systématique des méthodes théoriques utilisées en aéroélasticité, aussi bien pour la prévision des propriétés élastiques que pour celle des forces aérodynamiques.

La formulation matricielle est particulièrement efficace parce qu'elle permet de manipuler un grand nombre d'inconnues en conservant une écriture simple. Les expressions donnant l'énergie, les travaux virtuels ou l'équilibre des forces gardent une forme concise particulièrement remarquable.

La notion de coordonnées généralisées est rendue indispensable par la complexité des mouvements étudiés. Elle permet d'englober tous les degrés de liberté, y compris les mouvements d'ensemble. De même, la notion de forces généralisées englobe ce que l'on désigne habituellement par portance, moment de tangage, de roulis,.. moment de charnière.

Enfin, la représentation modale constitue une particularité intéressante du point de vue pratique, à cause des propriétés d'orthogonalité, de la convergence rapide, et aussi parce qu'elle fait

intervenir des grandeurs accessibles aussi bien à l'expérience qu'à l'analyse.

Les méthodes expérimentales n'ont pas été couvertes entièrement. Il resterait à faire le bilan des mesures susceptibles de fournir des données aérodynamiques utiles pour la correction des calculs. Les maquettes aéroélastiques, véritables calculateurs analogiques, mériteraient également un long chapitre.

REFERENCES

[1] R.L. BISPLINGHOFF, H. ASHLEY, R.L. HALFMAN
Aeroelasticity - Addison-Wesley Publishing Company Inc.
Cambridge 42, Mass. (1955)

[2] R. MAZET
Mécanique vibratoire - Dunod
Paris (1966)

[3] AGARD Manual on Aeroelasticity
Vol. 1 - Aspects structuraux
Vol. 2 - Aspects aérodynamiques

[4] DE VRIES et BEATRIX
Les procédés généraux de mesure des caractéristiques vibratoires des structures linéaires faiblement amorties
Progress in Aeronautical Sciences, vol. 9
Pergamon Press - Oxford & New York (1969)

[5] C. BEATRIX et R. LABOURDETTE
L'étude d'une servo-commande par le schéma modal
La Recherche Aérospatiale n° 127 - (Novembre-décembre 1968)

[6] R.H. GALLAGHER
A correlation study of methods of matrix structural analysis
AGARDograph 69 - Pergamon Press (1964)

[7] F. DE VEUBEKE
Matrix methods of structural analysis
AGARDograph 72 - Pergamon Press (1964)

[8] J.H. ARGYRIS
Recent advances in matrix methods of structural analysis
Pergamon Press (1964)

[9] A. CORNELIS, G. DEPREZ, G. FONDER, CH. MASSONNET, R. MAQUOI et R. MULLER
Application des ordinateurs au calcul des structures
Eyrolles Masson et Cie Editeur (1968)

[10] C.E. WATKINS et al.
On the Kernel function of the integral equation relating the lift and downwash distribution of oscillating finite wings in subsonic flow
NACA Report 1234 (1955)

[11] C.E. WATKINS, J.M. BERMAN
On the Kernel function of the integral equation relating lift and downwash distribution of oscillating wings in supersonic flow
NACA Report 1257 (1956)

[12] C.E. WATKINS et al.
A systematic Kernel function procedure for determining aerodynamic forces on oscillating or steady finite wings at subsonic speeds
NACA TR.R. 48 (1959)

[13] D.E. WILLIAMS
Three dimensional subsonic theory
AGARD Manual on Aeroelasticity, vol. 2, chap. 3

[14] C.E. WATKINS
Three dimensional supersonic theory
AGARD Manual on Aeroelasticity, vol. 2, chap. 5

[15] H. BERGH et R.J. ZWAAN
A method for estimating unsteady pressure distributions for arbitrary vibration modes from theory and from measured distributions for one single mode
TR.F. 250 (1966).

Present status of unsteady aerodynamics for lifting surfaces.

by

H. Bergh[x] and R.J. Zwaan[xx]

National Aerospace Laboratory NLR, Amsterdam, Netherlands

x) Head Fluid Dynamics Division

xx) Senior Research Engineer, Fluid Dynamics Division

Summary

A survey is given of existing theoretical and experimental routine methods for determining pressure distributions or generalised forces on oscillating lifting surfaces. Some comparisons between results of theory and experiment are shown. Techniques are indicated to apply measured data in development work. Tunnelwall influence on measurements is discussed.

Notations

a_{mn}	coefficients in pressure loading series
C_{h_δ}	hinge moment due to control surface deflection
C_{n_ψ}	yawing moment due to yawing motion
ΔC_p	unsteady pressure distribution
g, h	pressure loading functions
i,j	number of vibration mode
k	reduced frequency
K_1, K_2	kernel-function
M	Mach number
Q	generalised aerodynamic force
U	free stream velocity
w	normal velocity
x,y	cartesian coordinates
z	amplitude distribution
ω	radial frequency

1 Introduction.

For a long time flight dynamics and aeroelasticity were considered as separate problem areas, studied by different people. However, for modern aircraft with increased structural flexibility, like for instance the large supersonic transports, this distinction looses sense. In fact the flight dynamicist and the aeroelasticity specialist are both trying to solve the same problem, namely that of the behaviour of a flexible aircraft under various flight conditions. Because of this common problem a close co-operation between the two groups should be very fruitful.

The occurrence of structural deformations in flight dynamics has a rather drastic effect on the aerodynamics as the use of stability derivatives becomes questionable; each derivative becomes dependent on a particular vibration mode, thus compromising the simplicity of the stability derivatives of rigid bodies.

For large aspect-ratio wings with negligible chordwise bending some relief may be obtained by using a strip analysis, assuming the aerodynamic forces on a streamwise strip to be dependent only on the motion of the strip considered. In such cases existing two-dimensional aerodynamic derivatives, with or without spanwise weighting factors, can be applied (1,2).

However, if three-dimensional aspects dominate or if chordwise deformations occur, it is necessary to use in the equations of motion the so-called generalised aerodynamic forces, defined by the integrals

$$Q_{i,j} = \iint_{\substack{\text{lifting}\\ \text{surface}}} \Delta C_p^{(i)} z^{(j)} dS$$

where $\Delta C_p^{(i)}$ is the pressure distribution generated by the i-th vibration mode and $z^{(j)}$ is the j-th vibration mode.

In the last decennium flutter specialists have been confronted with the same difficulties, because their favourite strip analysis could no longer be applied to the more complex configurations of modern airplanes. Therefore they had to develop theoretical and experimental means to determine either generalised aerodynamic forces or pressure distributions on a wide variety of aircraft configurations. As some of these means have grown to routine methods, being equally applicable to problems of flight dynamics and aeroelasticity, we recommend their use in both cases.

In the following survey we hope to give an idea of the possibilities of the existing routine methods. For shortness sake we will concentrate on harmonically oscillating lifting-surfaces. However, forces due to arbitrary motions can be composed by means of Fourier integral superposition.

2 Means for determining pressure distributions or generalised forces.

2.1 Theoretical methods.

At present, several routine methods exist for calculating generalised forces or pressure distributions on a harmonically oscillating lifting-surface. These methods cover the frequency ranges of interest to flight dynamicists. They are based on the following assumptions.

The fluid is idealised so that potential flow may be assumed. Therefore, effects of boundary layers, shock waves of finite strength and separated flows have not been included. Furthermore, the flow disturbances generated by the oscillating surface are considered to be small. Then the basic equations and boundary conditions may be linearised, leading to unsteady aerodynamical forces which are not affected by wing thickness and steady angle of incidence. These assumptions lead to the theoretical model of a plate-like wing of general planform, oscillating with small amplitudes about zero mean incidence in a uniform flow.

It will be clear that these assumptions are violated in the transonic speed range or near stall conditions. In these cases the non-uniform steady flow field may strongly affect the unsteady aerodynamic forces. Then the only way out is to linearise around the steady mean flow induced by the thickness distribution or by incidence.

As recently Landahl and Stark (3) gave an excellent review of lifting-surface theories, we will here only present the main characteristics of the most important approaches.[x)]

The kernel function method, developed for subsonic and supersonic speeds, begins with an integral equation, relating the unknown pressure distribution ΔC_p to the normal velocity w at the lifting surface, prescribed by the motion of the surface (fig.1):

---

x) For detailed information the reader is referred to 4 and 5. The subsequent references given in this section pertain only to recent work.

$$\frac{w(x,y)}{U} = \iint \Delta C_p(x',y') . K_1(x-x',y-y')dx'dy' .$$

As the pressure distribution appears implicitely in the equation, it is expressed in a series of preselected loading functions, reducing the problem to the determination of the unknown coefficients in the series expansion. Some types of loading function have been indicated in the figure. A solution is obtained by satisfying the tangency condition exactly in just as many points on the wing as there are unknown coefficients (collocation procedure), or by satisfying it approximately with a least-squares procedure in a larger set of points or with some variational technique. Appreciable gain in accuracy is achieved by choosing functions that allow an adequate loading representation especially near the edges.

In the doublet-lattice method, developed recently for subsonic flow, the pressure distribution is thought to be generated by lifting elements, distributed over a large number of panels (fig.2). An integral relation analogous to that in the kernel-function method is applied to determine the strength of each element. In the version known to us, the strengths are being calculated by collocation.

At supersonic speeds it is possible to express the pressure distribution explicitely into the downwash by means of the surface integral:

$$\Delta C_p(x,y) = \left(\frac{1}{U}\frac{\partial}{\partial x} + ik\right)\iint \frac{w}{U}(x',z') . K_2(x-x', y-y')dx'dy' .$$

In the existing box methods the integral is evaluated by dividing the wing planform into a large number of boxes in which the downwash is assumed to be constant (fig.3). Consequently the integrations over the separate boxes have to be performed only once for all for a number of vibration modes. In case of subsonic wing edges, the wing planform is extended with artificial diaphragms within the Mach cone where the pressure jump has to be zero.

Various versions of these methods are now being used for application to simple and more complicated configurations. To give an idea, fig.4 shows configurations that have been calculated with the means discussed.

For a wing with flaps the downwash becomes discontinuous along the flap leading edge and side edges and consequently large pressure gradients occur. The doublet-lattice and box methods can still be used without adaptation; in the case of the kernel-function methods the accuracy is considerably improved by introducing special loading functions with coefficients, known from local solutions (6,7,8).

The remaining examples, shown in fig.4, concern configurations when aerodynamic interference effects between two or more surfaces are involved. These interference effects can be evaluated by extending the integrals over all surfaces of interest (9).

The methods are still being improved to enlarge the accuracy and to achieve shorter computation times (10, 11). Specific problems at the moment are the choice of the loading functions, the schematisation of panels or boxes, numerical integration procedures and the best approximation of the tangency condition. In this respect we may refer to the meritorious project of the AGARD Structures and Materials Panel, with the objective to compare methods in use on the basis of calculated generalised forces for a number of defined oscillating wings. A report with contributions from several NATO countries is expected in the course of this year.

2.2 Pressure measuring techniques.

In the last decennium also considerable progress has been made in the development of methods for measuring pressure distributions on oscillating models. At present several techniques are available which are based either on the direct method or on the indirect method. In the former case a number of small pressure transducers is mounted in the model at the desired positions (refs. 12,13,14). With the indirect method pressure tubes connect the model orifices to scanning valves with pressure transducers outside the model (refs. 15,16,17). A suitable correction procedure is then needed to convert the measured pressures into the required pressures at the model surface. Leaving the details aside, we may conclude that several measuring techniques of both types have shown their capability for routine tests, covering speed and frequency ranges of practical interests.

3 Examples of application.

To illustrate the applicability of the methods discussed we will show some examples. The choice made was guided by our preference for comparisons between measured and calculated results.

Starting with subsonic flow, the first example (fig.5) shows the pressure distribution on a swept wing oscillating in an elastic mode at M= 0.85. The unsteady pressures are presented as real and imaginary parts being respectively in phase and in quadrature with the wing motion. The experimental distribution, measured recently at NLR with the indirect method, shows similar agreement with calculation as was known to exist for plain wings at low speeds (see 18,19). In 20 which was published just before completing this paper, extensive comparisons between theory and experiment for high subsonic and transonic flow are presented.

For a rectangular wing with oscillating control surface at low speeds, measured hinge moments are compared with those predicted by two different calculation methods in fig.6. Also in this case the agreement is satisfactory.

Results obtained for two T-tails are used to demonstrate the ability to calculate interference effects for more complicated configurations. In fig. 7 the yawing moment measured on a simple T-tail oscillating in yaw is presented together with results of various theoretical methods. These methods also account for the effect of the tunnelwall at the fin root. A more detailed result is shown in fig.8, comparing measured and calculated pressures for a yawing swept T-tail. In both cases, the agreement is reasonable.

To illustrate the agreement at supersonic speeds fig.9 shows the stiffness- and damping-in-pitch of an ogee wing as a function of Mach number.

At lower transonic speeds the linearised methods for subsonic flow fail to describe the detailed aerodynamics. This is clearly demonstrated in fig.10 showing pressure distributions for the same wing as in fig.5, but now at the slightly supercritical Mach number $M = 0.92$ ($M_{crit} \approx 0.89$).

The main reason for these large discrepancies is that the basic flow field has velocity gradients along and normal to the wing surface, which strongly affect the propagation of disturbances from one point to another. This is clearly illustrated in fig.11 comparing the wave patterns propagated upstream by a source at 75 per cent chord in uniform and non-uniform two-dimensional flow (28).

In recent years promising attempts have been made to incorporate the non-uniform character of the basic flow field into theory (29). A recent NLR result is given in fig.12, showing for high subsonic flow the pressure distribution on a two-dimensional wing with a control surface oscillating at low reduced frequencies. The essential effects of the non-uniformities are represented rather well. As the attempts have not yet resulted in routine methods, we still have to rely on experiments in the transonic speed range.

4 Application of measured aerodynamic results in development work.

If we want to use the experiment in development work as a means to provide the required aerodynamic data for a flexible aircraft, we are still faced with problems. Already in an early stage of design we need pressure distributions for a number of modes at various Mach numbers. The obvious solution to measure the distributions directly for all the desired modes and Mach numbers is hardly possible in practice, as it requires either a dynamically similar model or for each mode a different model.

So the question arises whether it is possible to derive the data from a restricted programme of measurements on one model, oscillating in rather arbitrary modes.

For large aspect-ratio wings with negligible chordwise deformation a solution is offered by the strip method that assumes the aerodynamic forces on streamwise strips to be dependent only on the motion of the strip considered. Then pressure distributions measured on a model oscillating in two simplified modes are sufficient, as from these tests local force and moment derivatives can be derived, that can be applied to other vibration modes.

Another possibility for large aspect-ratio wings in subsonic flow is to use a semi-empirical approach like that of Destuynder (13), who suggests to adjust the formula of Reissner's approximation for finite span with empirical factors, derived from a limited number of measured unsteady pressures.

For arbitrary wings the present authors proposed in 20 an extension of the weighting procedure of Rodden and Revell[x] (30). It is based on the assumption that the ratios between corresponding measured and calculated unsteady pressures are independent of the mode shape. Then pressure measurements and calculations for one single mode are sufficient to derive a correction matrix that may be applied to adjust the calculated values for other modes. Its usefulness has already been demonstrated for swept wings and a T-tail at low subsonic speeds (20, 32). Recently experience has been gained with applications to swept wings at high subsonic and transonic speeds. Fig.13 shows that at $M = 0.80$ predicted and measured pressure distributions agree much better than the theoretical and measured distributions. Even at the supercritical Mach number 0.95 the correction procedure gives an appreciable improvement (fig.14), although near the shock differences are still present.

Notwithstanding these promising results we still advice to check the empirical procedure in each case for two different modes. As the role of the correction matrix is to close the gap between theory and experiment it is of course recommended to use the best theory available.

5 Tunnelwall interference.

As the flow conditions in a windtunnel are different from those in free flight, one wants to have at least an assessment about the influence of the tunnelwalls on the aerodynamic data. However, the evidence about this subject is rather scarce and a common standpoint does not yet exist.

x) A similar methode has also been used for static forces (31).

In case of low speed windtunnel tests various theories predict the wall corrections to be small, provided the model is not unduly large relative to the tunnelsize. For tests at higher speeds, however, serious doubts were raised by Wight et al. (33,34) with respect to the value of dynamic measurements in ventilated wall test sections, since at NPL overall aerodynamic derivatives measured on the same half model either in various windtunnels or in test sections with different wall conditions showed large discrepancies. A typical example, taken from (34) is shown in fig.15. Apart from the differences between the results of both windtunnels, the most striking effect is the influence of the wall conditions for the 25x20 in. tunnel, even at the lower subsonic speeds.

Garner, Moore and Wight (35) tried to explain the phenomena on a theoretical basis, using an extension of the classical theory of lift interference. In essence it is assumed that the model is of small span and oscillates at low frequency in a subsonic flow and that the slotted walls may be replaced by open boundaries. Application to the experimental NPL results had some success, but there remained cases where the differences in the measured derivatives for various windtunnels were increased after correction. These effects have been attributed to viscous effects in the slots. Hall and Claridge (36), who measured the flow upwash ahead of an oscillating half wing model in a slotted wall and closed wall test section, demonstrated the importance of the viscous effects by fitting screens behind the wall slots. This resulted in a reduced upwash pattern between that of slotted and closed wall conditions.

Recent investigations of Tijdeman et al. at NLR give a more optimistic picture. A number of steady and unsteady pressure distributions over half wing models were measured in the small pilottunnel (PT 0.42 x 0.55 m^2) and in the larger high speed tunnel (HST 1.60 x 2.00 m^2), both tunnels having test sections with longitudinally slotted top and floor.

As is illustrated in the figs. 16 and 17 the results at subcritical and supercritical Mach numbers agree well, even near the side wall. Similar agreement was obtained for a half wing model with partial span control surface, notwithstanding the high blockage percentage of 2.1 % in the smaller tunnel.

Since in the HST the two models are very small compared with the size of the test section, it seems reasonable to consider these data as practically interference free. This implies that the wall corrections in the PT are bound to be small too.

To investigate the influence of the wall conditions, the half wing was also measured in the PT with closed walls. As shown in fig. 17 the change in wall condition has no perceptible influence at $M_\infty = 0.5$, but at the higher Mach number the presence of the solid walls causes a change in the unsteady pressure distributions. However, for $M_\infty = 0.85$ also the mean Mach number distribution on the wing becomes different. This indicates that the differences in unsteady aerodynamic results are caused primarily by changes in the mean flow around the models, notwithstanding the fact that the tests were performed at the same free stream Mach number. Obviously the model blockage in the closed test section disturbs the stationary flow field at the higher speeds. As the theory of (35) still assumes a uniform mean flow field around the wing, this blockage effect is not included there. It may be remarked that the mean Mach number distributions corresponding to figs. 16 and 17 were in close agreement.

From the NLR investigations the conclusions may be drawn that in comparative experiments with oscillating models in various windtunnels or in test sections with different wall conditions it is necessary to check the static behaviour of the considered models.

6 Closing word.

At the end of this survey we like to quote Ashley who stated, when speaking about simulation and graphical display in dynamic aeroelasticity (37): "Aeroelastic effects are no longer being considered as an afterthought by an isolated group of rather misunderstood specialists". Belonging to this group of people, we hope this paper has given the impression that unsteady aerodynamics may be a common tool in tackling the problems of flexible aircrafts in flight.

7 References.

1 Manual of aeroelasticity, Vol. VI. AGARD (rev. October 1968).

2 Küssner, H.G.; Wille, F. Theorie des schwingenden Streckenprofils bei kompressibeler Unterschallströmung. Teil IV: Tabellen der aerodynamischen Derivativa des schwingenden Streckenprofils mit Knick und Stufe. AVA FB 68-61 (1968).

3 Landahl, M.T.; Stark, V.J.E. Numerical lifting-surface theory. Problems and progress. AIAA Journal 6 , 11, pp. 2049-2060 (Nov. 1968).

4 Manual of Aeroelasticity, Vol. II. AGARD (rev. October 1968).

5 Bisplinghoff, R.L.; Ashley, H. Principles of aeroelasticity. John Wiley and Sons, Inc.,New York, London (1962).

6 Berman, J.H.; Shyprykevich, P.; Smedfjeld, J.B. Unsteady aerodynamic forces for general wing/ control-surface configurations in subsonic flow. Grumman Aircr. Eng. Co. Report No. ADR 06-01-67.1 (1967).

7 Ashley, H. — Subsonic oscillatory or steady airloads on wings with control surfaces and other discontinuities. AFOSR-68-0419, SUDAAR No. 336 (1968).

8 Zwaan, R.J. — On a kernel-function method for the calculation of the pressure distribution on a two-dimensional wing with harmonically oscillating control surface in subsonic flow. NLR F.261 (1968).

9 Laschka, B. Schmid, H. — Einfluss des Flügels auf die instationäre Luftkräfte am Höhen- und Seitenleitwerk in Unterschallströmung VFW-Nr. M-51/68 (1968).

10 Dat, R. Darovsky, L. Darras, B. — Considérations sur la solution matricielle du problème portant instationnaire en subsonique, et application aux gouvernes. ONERA Note Technique No. 135 (1968).

11 Kacprzynski, J.J. — On the calculation of unsteady nonlinear three-dimensional supersonic flow past wings. AFOSR-68-0517, SUDAAR No.339 (1968).

12 Wyss, J.A. Sorensen, R.M. — An investigation of the control surface flutter derivatives of a NACA 65_1-213 airfoil in the Ames 16-foot high speed wind tunnel. NASA RM A51J10 (1951).

13 Destuynder, R. — Une méthode pour l'interpretation des mesures de pressions instationnaires. AGARD Report 498 (1964).

14 Molyneux, W.G. Ruddlesden, F. — A technique for the measurement of pressure distribution on oscillating aerofoils, with results for a rectangular wing of aspect ratio 3.3 ARC Current Paper 233 (1955).

15 Lessing, H.C. Troutman, J.L. Menees, G.P. — Experimental determinations of the pressure distribution on a rectangular wing oscillating in the first bending mode for Mach numbers from 0.24 to 1.30. NASA TN D-344 (1960).

16 Bergh, H. — Some aspects of unsteady pressure measurements. AGARD Report 498 (1964). NLR MP.224 (1964).

17 Hertrich, H. — Zur experimentellen Prüfung instationärer drei-dimensionaler Tragflächentheorien bei inkompressibeler Strömung. Mitt. Max Planck Inst. Nr. 40 (1967).

18 Laschka, B. — Die Druck-, Auftriebs- und Momentenverteilungen an einem harmonisch schwingenden Pfeilflügel kleiner Streckung im niedrigen Unterschallbereich-Vergleich zwischen Theorie und Messung. EWR-Bericht Nr. 116/63 (1963), ICAS -Paper No. 64-575(1964).

19 Bergh, H. Zwaan, R.J. — A method for estimating unsteady pressure distributions for arbitrary vibration modes from theory and from measured distributions for one single mode. NLR-TR F.250 (1966).

20 Becker, J. — Instationäre Druckverteilungen an einem gepfeilten elastischen Flügel und einem gepfeilten Flügel mit schwingendem Ruder in hohen Unterschall und im Transsonikgebiet - Vergleich Theorie und Versuch. EWR-Nr. 238-68 (1968).

21 Albano, E. Rodden W.P. — A doublet-lattice method for calculating lift distributions on oscillating surfaces in subsonic flow. AIAA Paper No. 68-73 (1968).

22 Clevenson, S.A. Leadbetter, S.A. — Measurements of aerodynamic forces and moments at subsonic speeds on a simplified T-tail oscillating in yaw about the fin midchord. NACA TN 4402 (1958).

23 Rodden, W.P. Albano, E. — The subsonic aerodynamic loads on a simplified T-tail oscillating in yaw.- Summary of calculations and comparison with experiment. Northrop Co. Rep. NOR 68-126 (1968).

24 Davies, D.E. — Generalised aerodynamic forces on a T-tail oscillating harmonically in subsonic flow. RAE Rep. Structures 295 (1964).

25 Zwaan, R.J. — Calculated results for oscillating T-tails in subsonic flow and comparison with experiments. NLR MP.253 (1967).

26 Thompson, J.S.
Fail, R.A.
Oscillatory-derivative measurements on sting-mounted wind-tunnel models: method of test and results for pitch and yaw on a cambered ogee wing at Mach numbers up to 2.6
ARC R. and M. No. 3355 (1964).

27 Harris, G.Z.
The calculation of generalised forces on oscillating wings in supersonic flow by lifting surface theory.
ARC R. and M. No. 3453 (1966).

28 Tijdeman, H.
Bergh, H.
Analysis of pressure distributions measured on a wing with oscillating control surface in two-dimensional high subsonic and transonic flow.
NLR-TR F.253 (1967).

29 Andrew, L.V.
Stenton, T.E.
Unsteady aerodynamic forces on a thin wing oscillating in transonic flow.
AIAA Paper No. 67-16 (1967).

30 Rodden, W.P.
Revell, J.D.
The status of unsteady aerodynamic influence coefficients.
SMF Fund Paper No. FF-33 (1962).

31 Hedman, S.G.
The aerodynamic influence coefficients method for wing load calculations.
Paper WGLR-Fachtagung über Aerodynamik, 1-4 Oktober 1968, Berlin.

32 Zwaan, R.J.
Application of a method for estimating pressure distributions to an oscillating T-tail.
NLR TR 68048 L (1968).

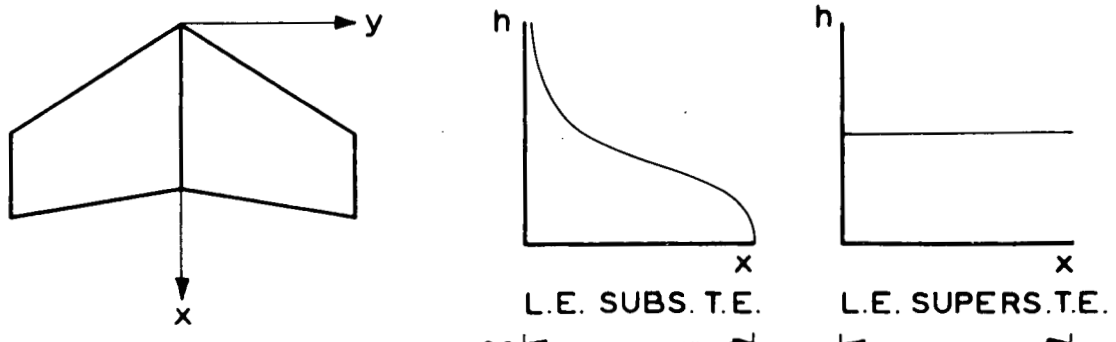
33 Wight, K.C.
A review of slotted-wall wind-tunnel interference effects on oscillating models in subsonic and transonic flow.
NPL Aero Report 1074, ARC 25 138 (1963).
Journ. Royal Aer. Soc., 68, pp. 670-674 (1964).

34 Moore, A.C.
Wight, K.C.
An experimental investigation of wall interference effects on dynamic measurements on half models in ventilated tunnels through the transonic speed range.
NPL Aero.Rep. 1243 ARC. 29 331 (1967).

35 Garner, H.C.
Moore, A.W.
Wight, K.C.
The theory of interference effects on dynamic measurements in slotted-wall tunnels at subsonic speeds and comparisons with experiment.
NPL Aero Report 1211, ARC 28 339 (1966).

36 Hall, G.Q.
Claridge, J.S.
Measurements of flow disturbances caused by an oscillating wing in a slotted wall tunnel.
Hawker Siddeley Dyn./Cov. A.R.L. Report No. 66/4 (1966).

37 Ashley, H.
Prospects for simulation and graphical display in dynamic aeroelasticity.
Prospects for simulation and simulators of dynamic systems.
Ed. by G. Shapiro and M. Rogers. Spartan Books, New York.

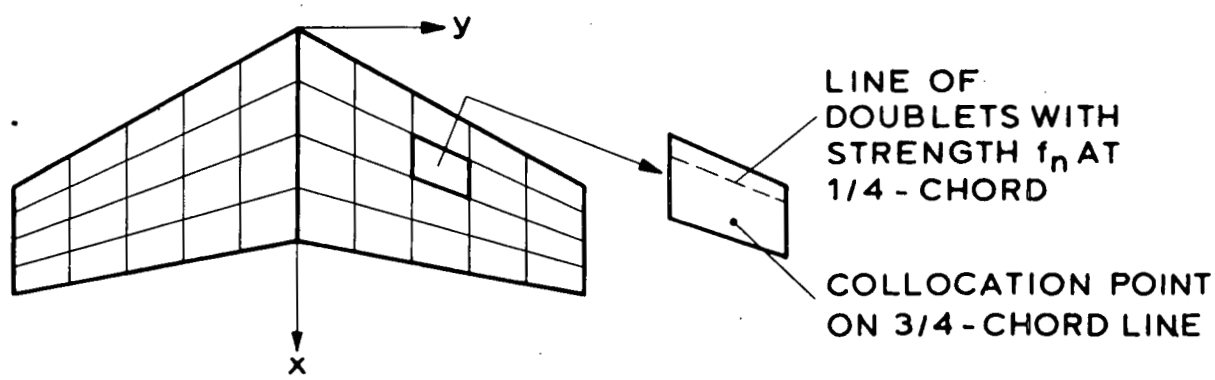


INTEGRAL EQ. : $\frac{W(x,y)}{U} = \iint_S \Delta C_p(x';y') K_1(x-x'/y-y')\, dx'\, dy'$

PRESSURE DISTR. : $\Delta C_p(x,y) = \sum_m \sum_n a_{mn}\, h(x)\, g(y)$

SOLUTION : COLLOCATION, LEAST SQUARES, VARIATIONAL PRINCIPLE.

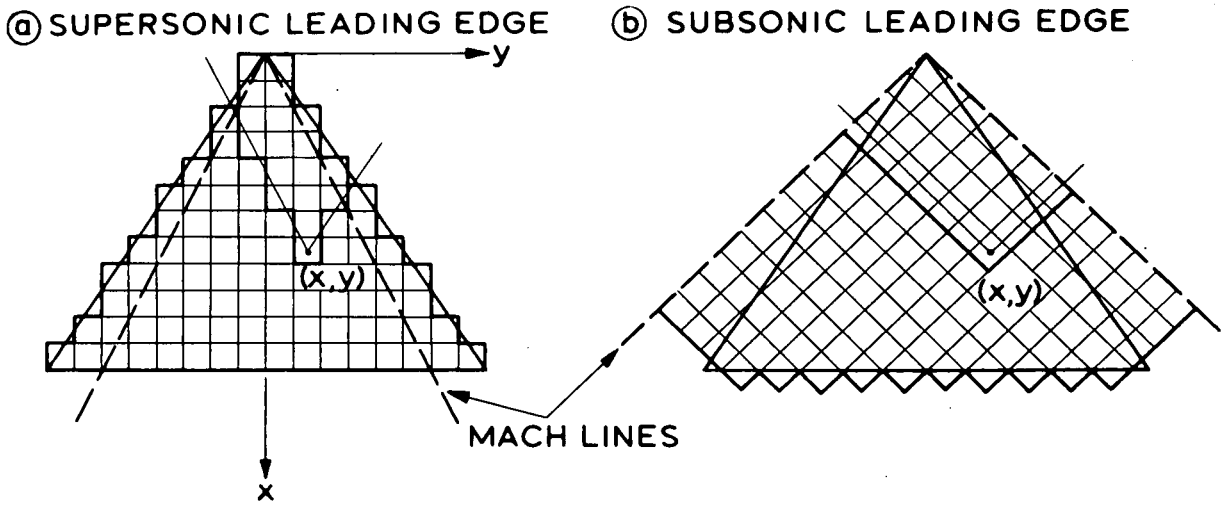
FIG. 1 KERNEL - FUNCTION METHOD, $M \gtrless 1$



INTEGRAL EQ. : $\frac{W(x,y)}{U} = \sum_n f_n \int K_1(x - x'(s), y - y'(s))\, ds$

SOLUTION : COLLOCATION

FIG. 2 DOUBLET - LATTICE METHOD, $M < 1$



$$\Delta C_p\langle x,y\rangle = \left(\frac{1}{U}\frac{\partial}{\partial x} + ik\right)\sum_n \frac{W}{U}\langle x_n, y_n\rangle \iint_{S_n} K_2\langle x';y/x';y'\rangle\, dx'dy'$$

FIG. 3 BOX METHOD, M > 1

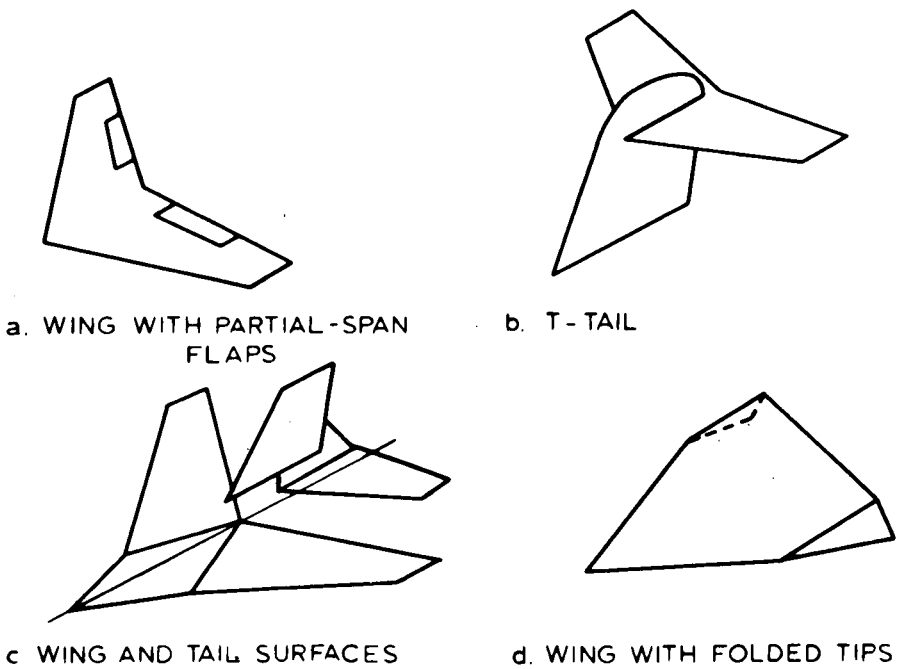


FIG. 4 CONFIGURATIONS CONSIDERED BY ROUTINE METHODS.

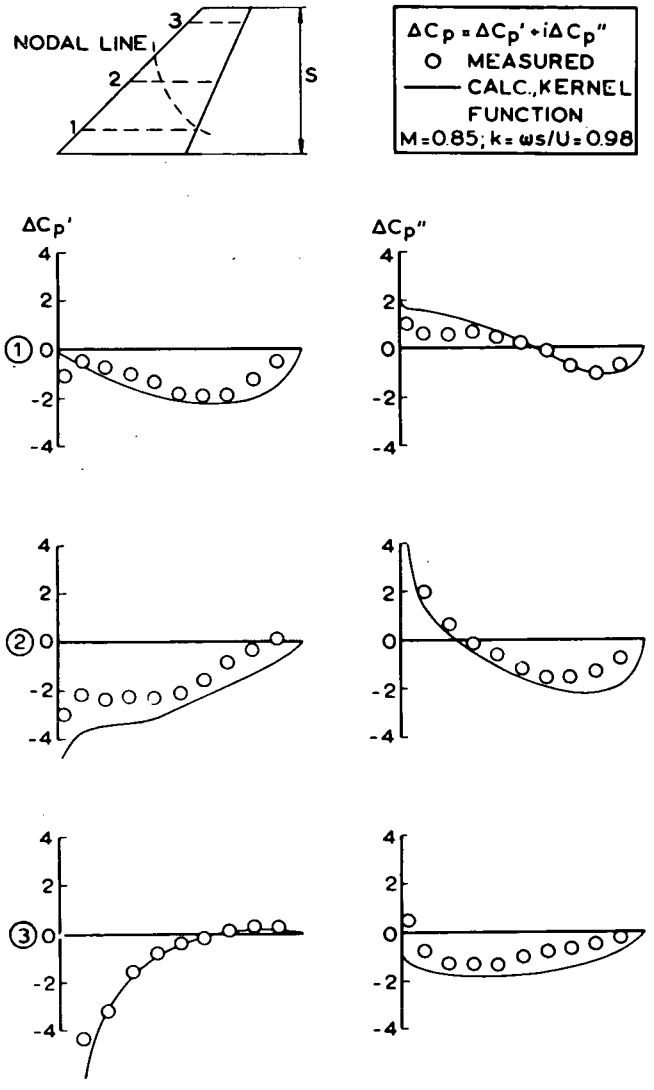


FIG. 5 PRESSURE DISTRIBUTIONS ON 6% THICK OSCILLATING SWEPT WING (RECENT NLR RESULTS).

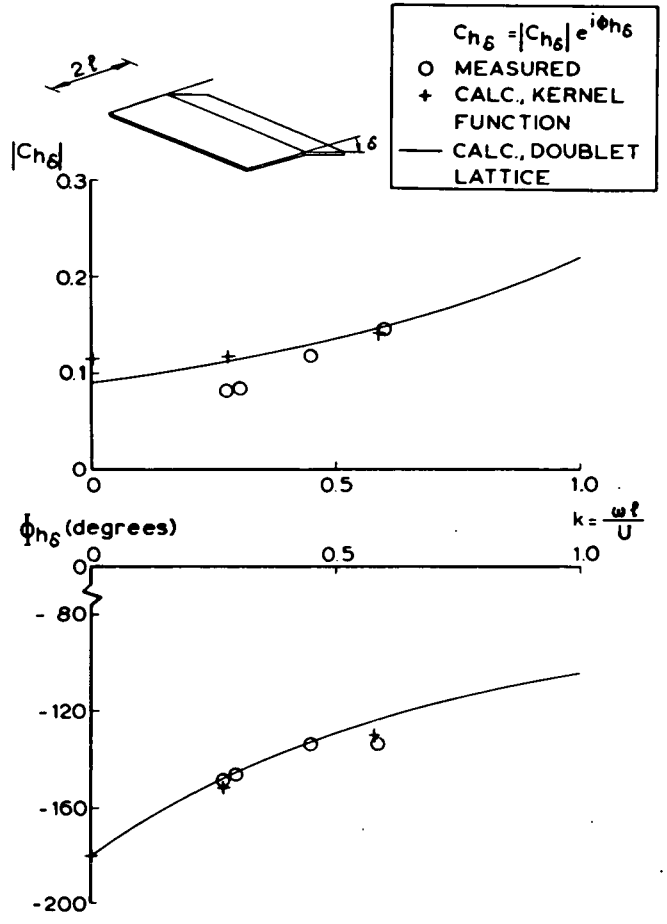


FIG. 6 HINGE MOMENT DUE TO FLAP OSCILLATING AT LOW SPEED, FOR A 40% CHORD, FULL SPAN FLAP ON RECTANGULAR WING OF A = 2 (REF. 21).

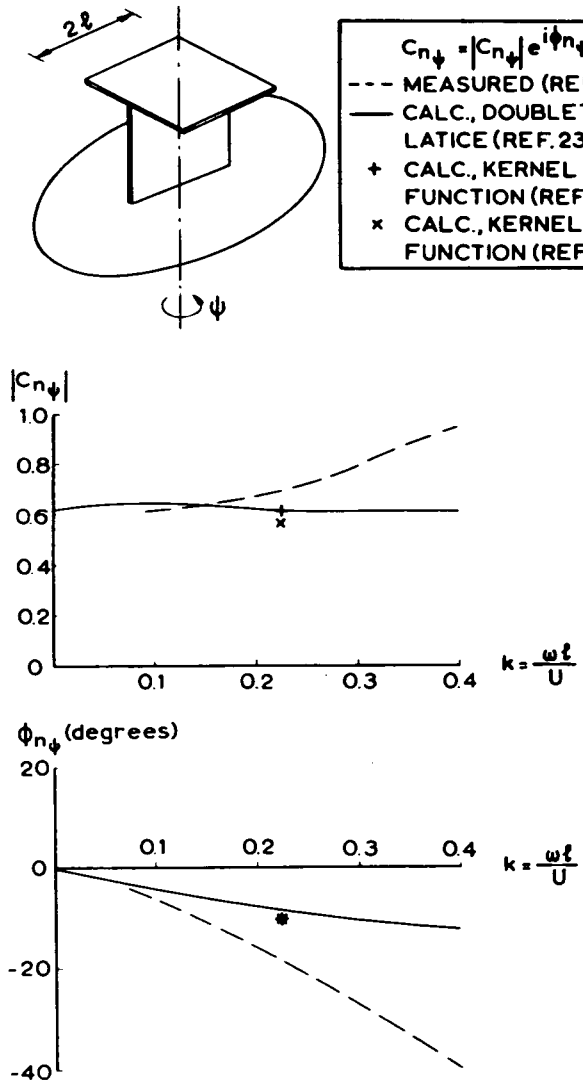


FIG. 7 YAWING MOMENT ON T-TAIL DUE TO OSCILLATION ABOUT VERTICAL AXIS AT LOW SPEEDS; REFLECTION PLATE INCLUDED.

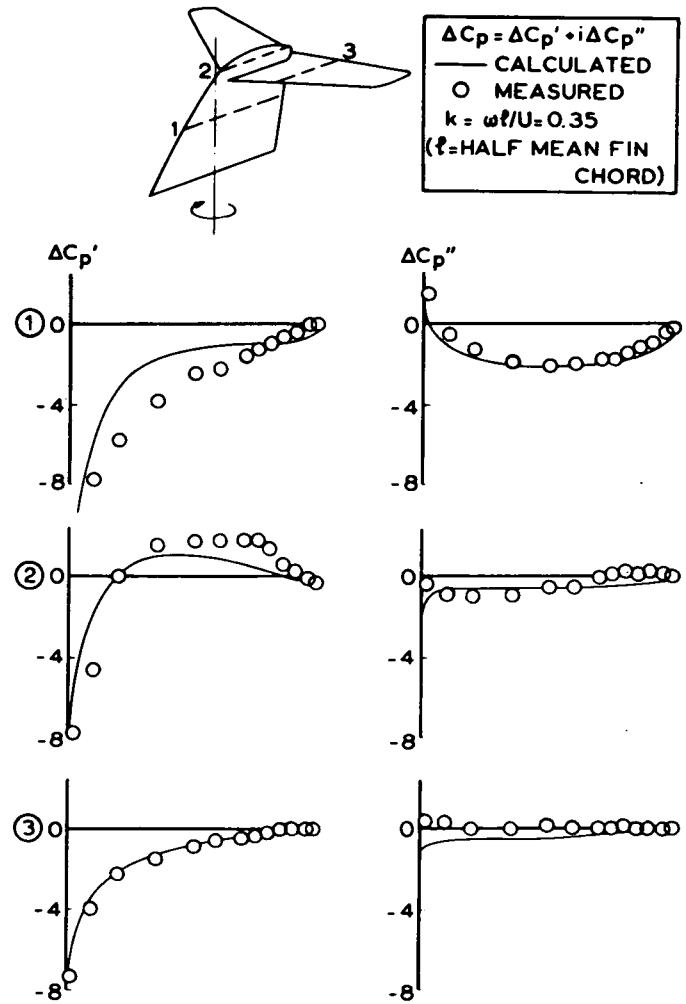


FIG. 8 PRESSURE DISTRIBUTIONS ON YAWING T-TAIL AT LOW SPEED.

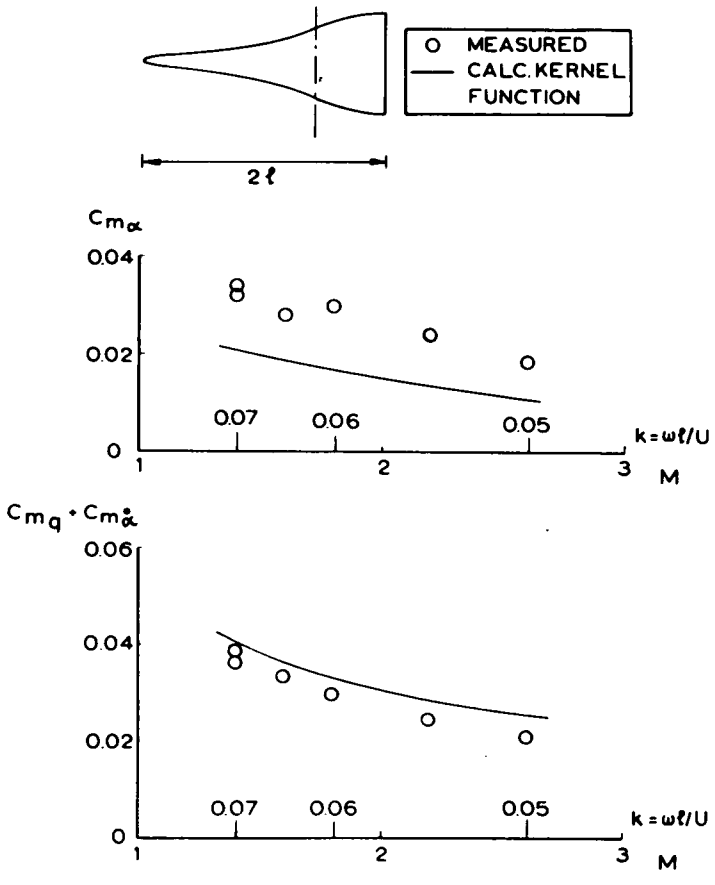


FIG. 9 PITCHING MOMENT ON OGEE WING DUE TO OSCILLATION ABOUT AXIS AT 71% OF ROOT CHORD (REF. 27).

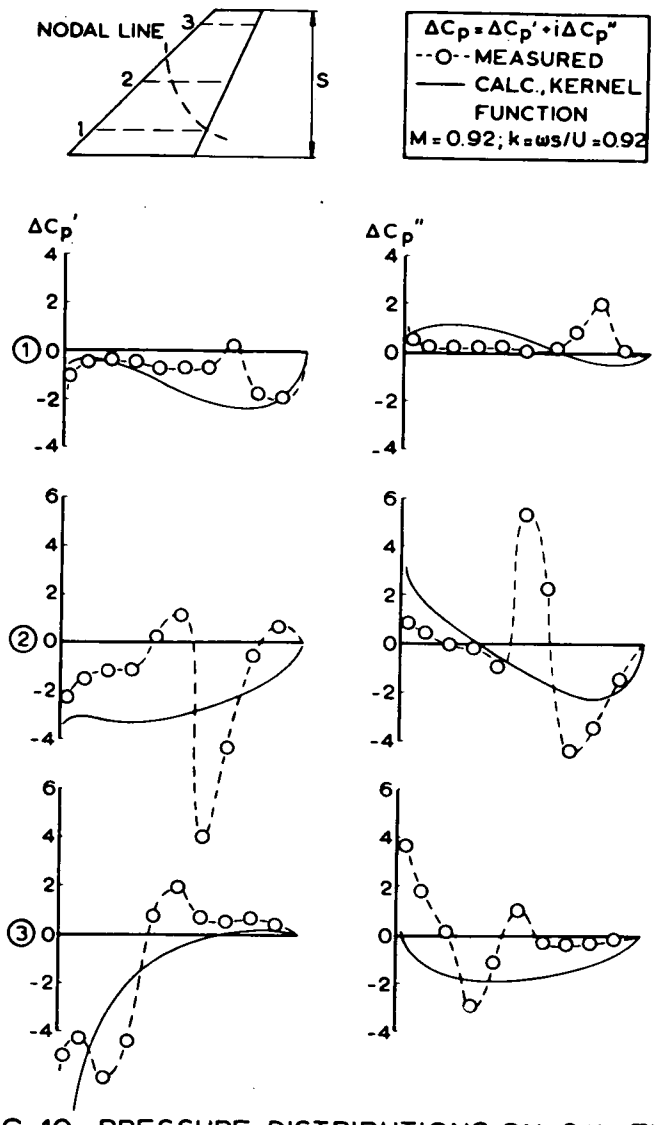


FIG. 10 PRESSURE DISTRIBUTIONS ON 6% THICK OSCILLATING SWEPT WING (RECENT NLR RESULTS).

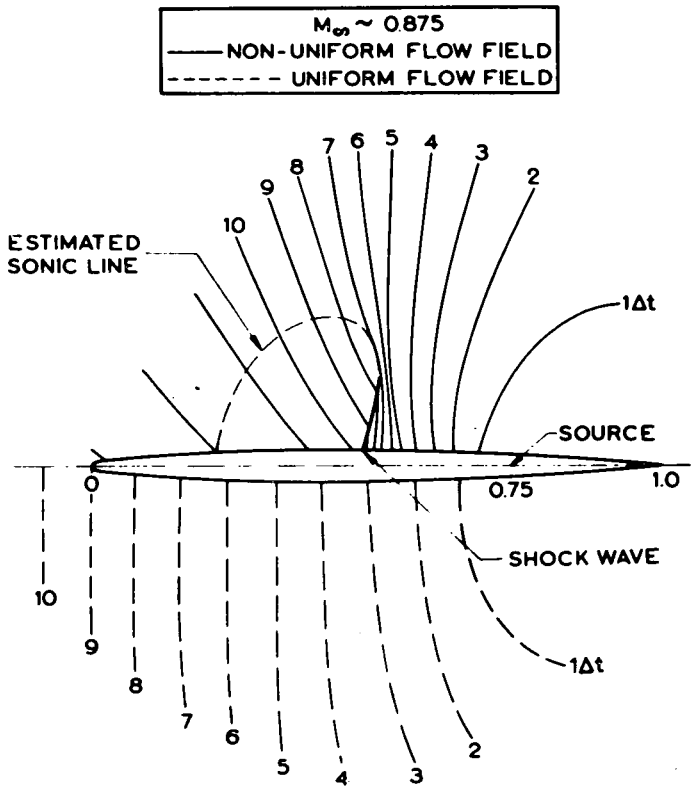


FIG. 11 UPSTREAM PROPAGATION OF DISTURBANCE WAVES GENERATED BY A SOURCE IN UNIFORM AND NON-UNIFORM FLOW.

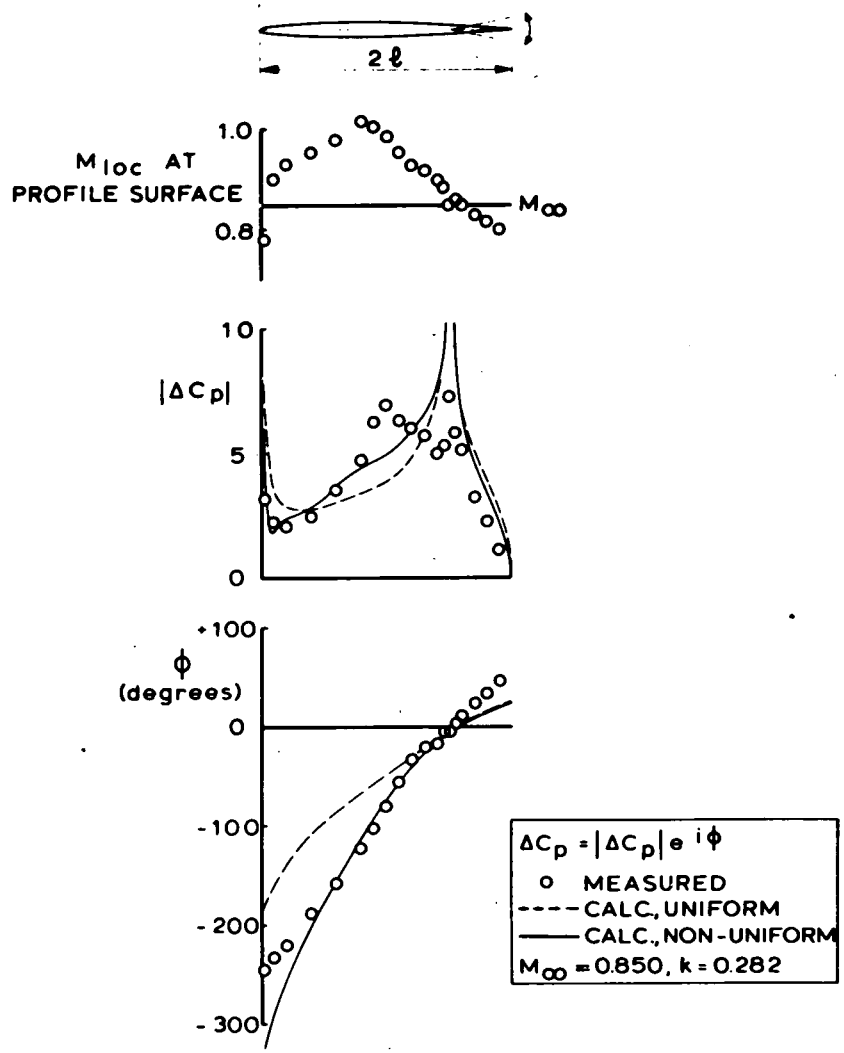


FIG. 12 PRESSURE DISTRIBUTION ON 6% THICK TWO-DIMENSIONAL WING WITH CONTROL SURFACE OSCILLATING AT LOW REDUCED FREQUENCY IN HIGH SUBSONIC FLOW (RECENT NLR RESULTS).

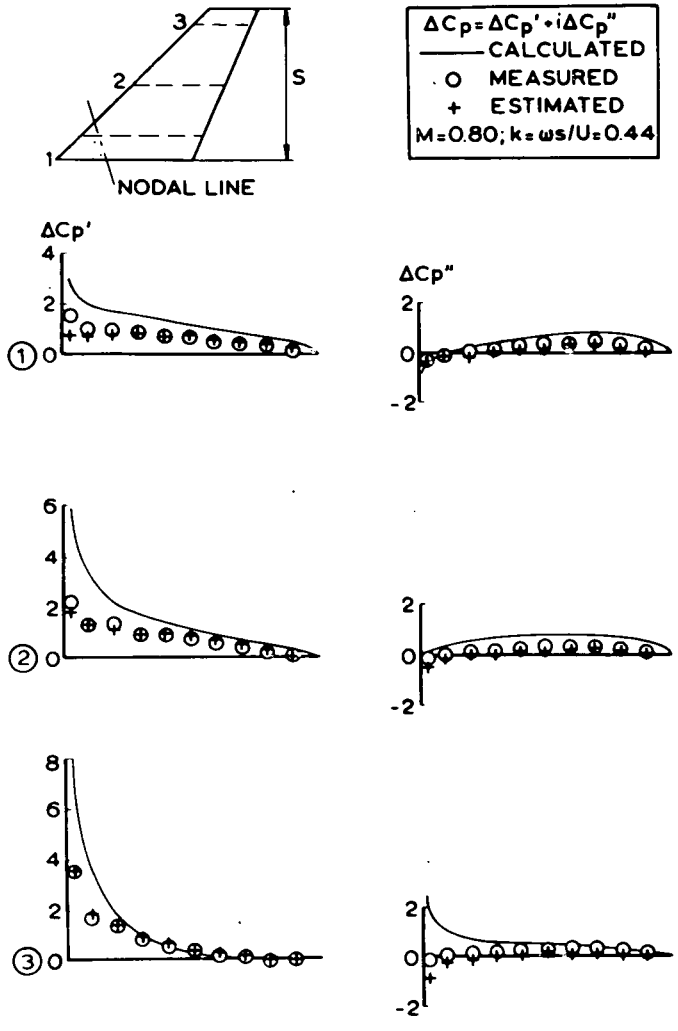


FIG. 13 APPLICATION OF CORRECTION PROCEDURE TO PREDICT PRESSURE DISTRIBUTIONS ON A SWEPT WING.

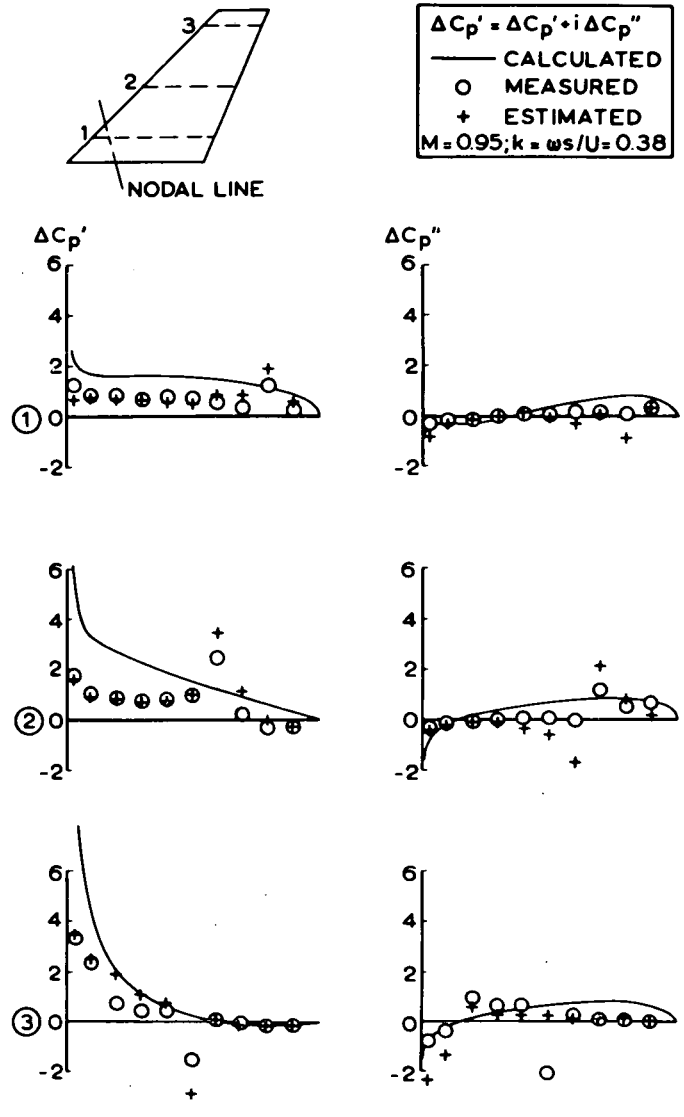


FIG. 14 APPLICATION OF CORRECTION PROCEDURE TO PREDICT PRESSURE DISTRIBUTIONS ON A SWEPT WING.

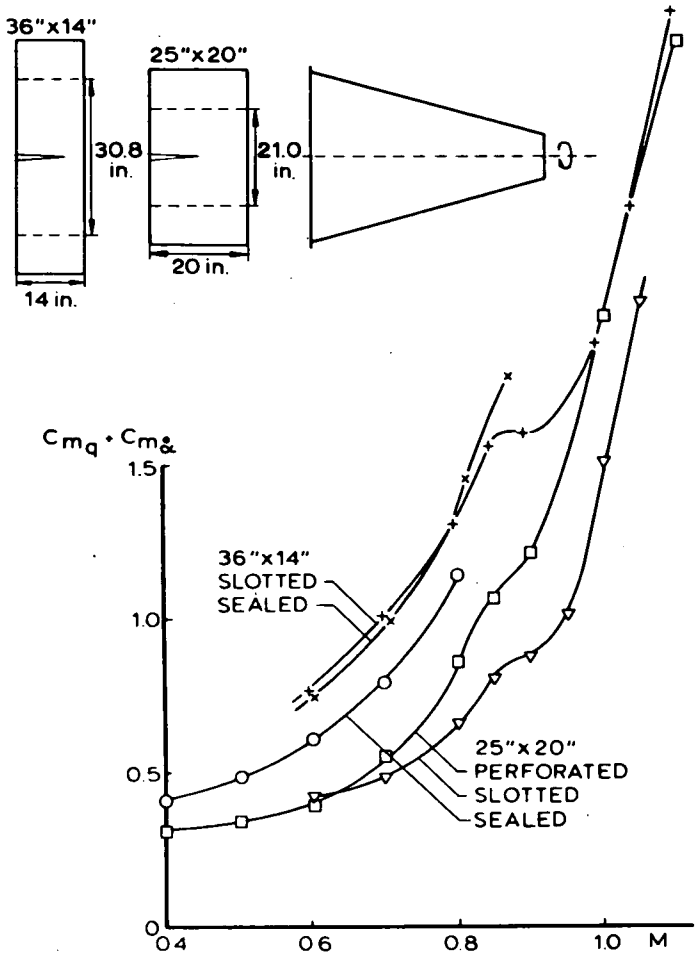


FIG. 15 VARIATION OF DERIVATIVE C_{m_α} WITH MACH NUMBER FOR TAPERED WING IN TWO VENTILATED TUNNELS (REF. 34).

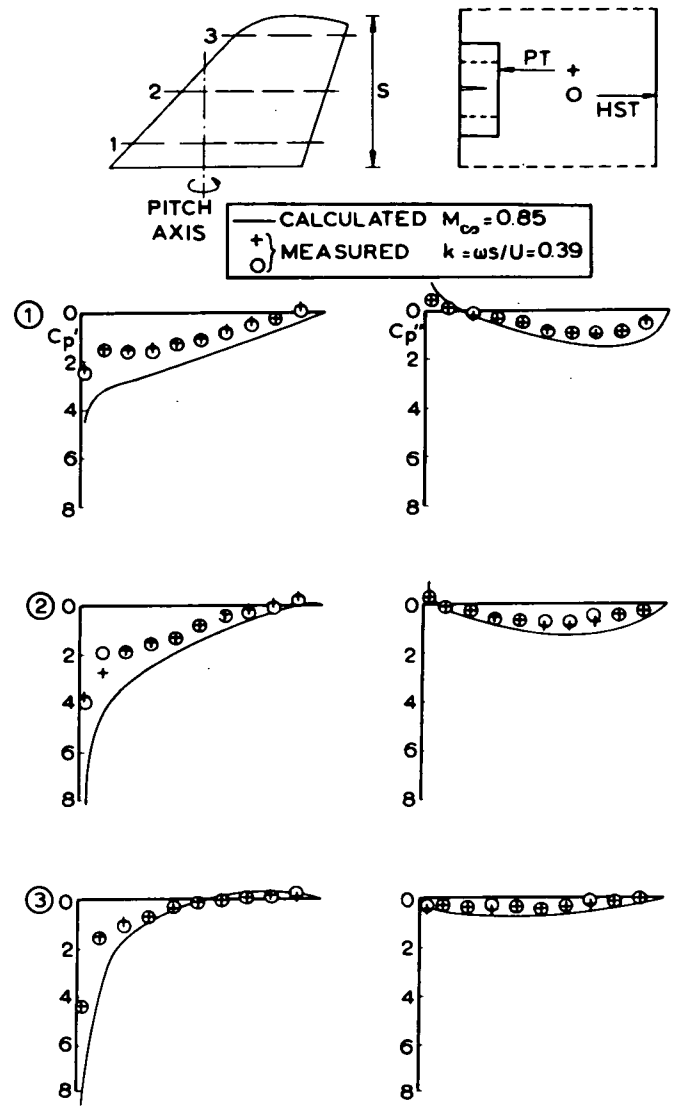


FIG. 16 TESTS ON ONE MODEL IN WIND TUNNELS OF DIFFERENT SIZE, SHOWING WALL INTERFERENCE TO BE NEGLIGIBLE.

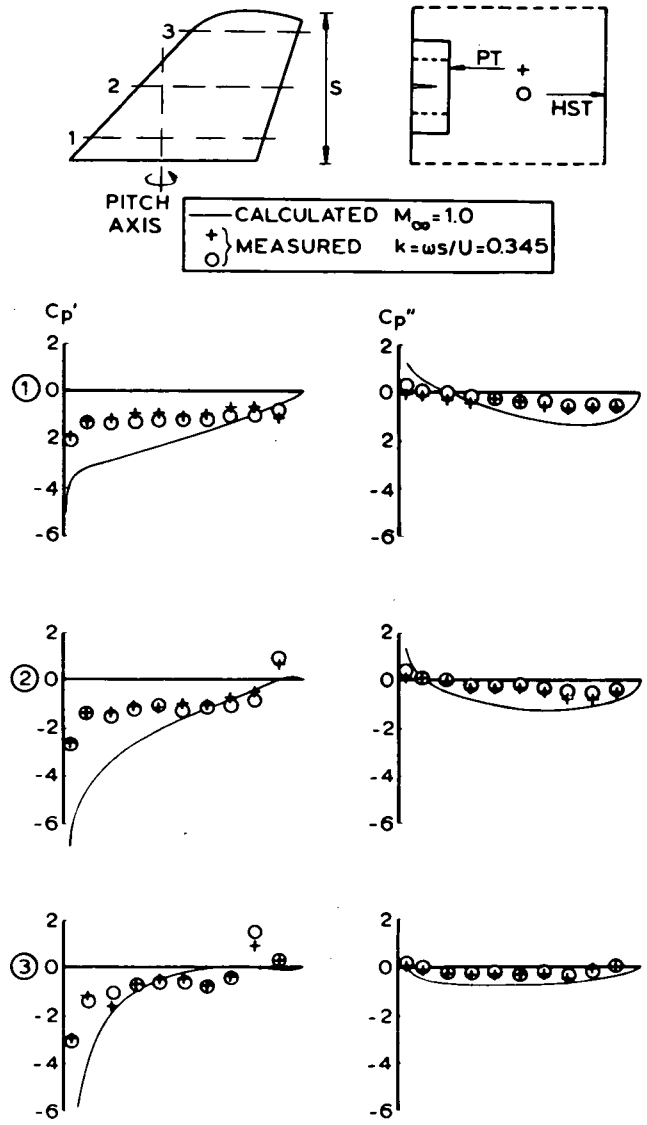


FIG. 17 TESTS ON ONE MODEL IN WIND TUNNELS OF DIFFERENT SIZE, SHOWING WALL INTERFERENCE TO BE NEGLIGIBLE.

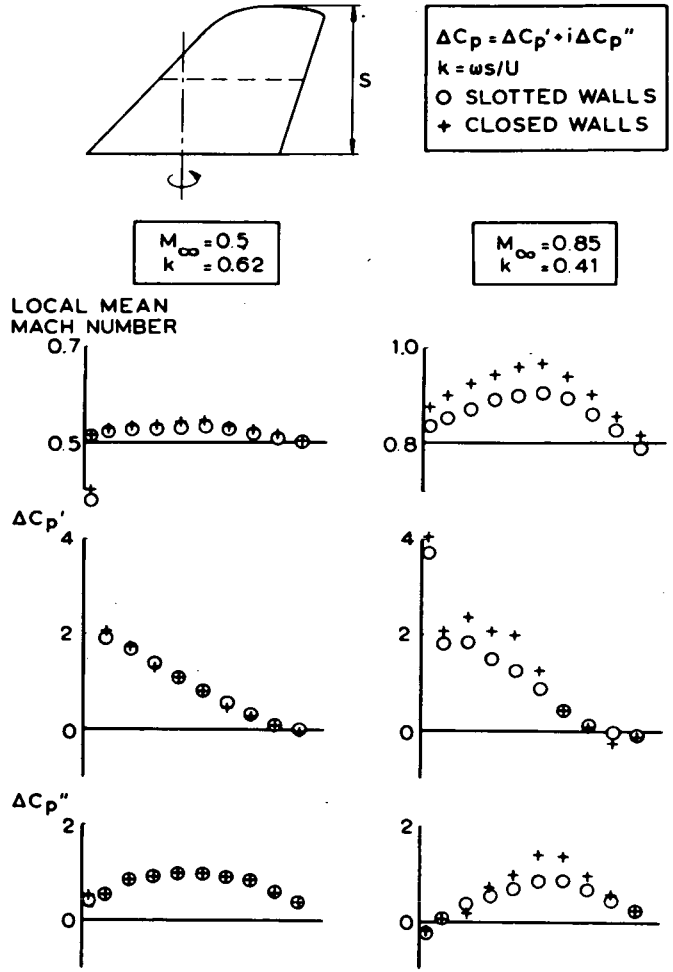


FIG. 18 INFLUENCE OF WALL CONDITIONS.

PROBLEMES POSES PAR LA DETERMINATION DE FORCES AERODYNAMIQUES AGISSANT SUR L'AVION SOUPLE

par L. DAROVSKY (SUD-AVIATION)

1. INTRODUCTION

Pendant des années les aérodynamiciens et les aéroélasticiens travaillaient dans des domaines bien séparés. Les aérodynamiciens se consacraient à la détermination de performances de l'avion idéal, supposé indéformable, tandis que les aéroélasticiens se penchaient sur la question de la sécurité de l'avion, en étudiant deux groupes de phénomènes : divergence de surfaces portantes et le couplage de modes propres, pouvant conduire au flottement.

Les exigences des avions modernes obligent pourtant les aérodynamiciens à prendre en considération les phénomènes de déformations de structure de l'avion, lentes ou relativement rapides, et d'étudier leur influence sur la manœuvrabilité et les performances des avions en vol.

D'autre part, l'augmentation de la vitesse des avions, les exigences plus sévères relatives au poids de structure, la nécessité de réduire les épaisseurs relatives de surfaces portantes, donc de diminuer les rigidités, obligent les aéroélasticiens à étudier avec plus de précision les marges de sécurité. Ainsi, progressivement, les méthodes bidimensionnelles, trop pessimistes, ont été remplacées par les méthodes tridimensionnelles, beaucoup plus proches des méthodes des aérodynamiciens.

Ce rapprochement, amorcé déjà, doit se poursuivre par une étroite collaboration entre les aérodynamiciens et les aéroélasticiens et une élaboration de méthodes de calcul plus exactes, basées sur les données de coefficients aérodynamiques théoriques et expérimentaux établis par les aérodynamiciens et adaptés à l'étude de l'avion souple.

La première question qui se pose est la suivante : par quel ensemble d'équations peut-on représenter le vol de l'avion souple ?

La réponse à cette question n'est pas simple et suivant les divers aspects d'influence de la souplesse de l'avion que l'on veut étudier, on peut proposer des moules mathématiques différents.

2. EMPLOI DE COEFFICIENTS STATIONNAIRES EQUIVALENTS

Dans tous les cas où les déformations en jeu sont lentes, par exemple, l'étude de l'efficacité de gouvernes ou l'optimisation de la voilure déformable dans le domaine de vol, on peut être tenté de conserver le système d'équations de vol de l'avion rigide, mais en considérant les dérivées aérodynamiques figurant dans ces équations comme des fonctions de la configuration massique de l'avion et de la pression dynamique, en même temps que d'autres paramètres comme le nombre de Mach, l'incidence, etc...

Cette méthode a été appliquée à Sud-Aviation et Monsieur Marsan vous fera un exposé détaillé dans quelques jours. Je ne ferai donc que quelques remarques générales sur un exemple simple.

Considérons un avion en vol horizontal à vitesse constante. Les équations du vol de l'avion rigide peuvent s'écrire :

$$C_{zo_r} + C_{zi_r} i + C_{z\beta_r} \beta = \frac{2Mg}{\rho V^2 S}$$

$$C_{mo_r} + C_{mi_r} i + C_{m\beta} \beta = 0$$

Supposons qu'aux coefficients globaux C_{zo_r}, C_{zi_r}, $C_{z\beta_r}$ correspondent les répartitions de coefficients de pression $C_{p_o}(x, y)$, $C_{p_i}(x, y)$, $C_{p_\beta}(x, y)$ et soit $C(x, y, \xi, \eta)$ la fonction de coefficients d'influence de l'avion souple. Les incidences en tous points ξ, η de la voilure de l'avion souple seront définies par l'équation intégrale.

$$\alpha(\xi,\eta) = \frac{\rho V^2}{2} \iint C(x,y,\xi,\eta)\left[C_{p_o}(x,y) + C_{p_i}(x,y) i + C_{p_\beta}(x,y)\beta + \right.$$

$$\left. + C_{p_\alpha}(x,y)\alpha(x,y) + m(x,y) g\right] dx\, dy.$$

D'autre part la condition d'équilibre des forces et des moments agissant sur l'avion souple s'exprime par deux équations :

$$C_{zo_r} + C_{zi_r} i + C_{z\beta_r}\beta + \frac{1}{S}\iint C_{p_\alpha}(x,y)\alpha(x,y)\,dx\,dy = \frac{2Mg}{\rho V^2 S}$$

$$C_{mo_r} + C_{mi_r} i + C_{m\beta_r}\beta + \frac{1}{S}\iint C_{p_\alpha}(x,y)\alpha(x,y)\,x\,dx\,dy = 0$$

L'équation intégrale de déformations permet d'exprimer $\alpha(x, y)$ en fonction linéaire de i, β et de la répartition massique $m(x, y)$. En portant cette expression de $\alpha(x, y)$ dans les équations d'équilibre, on peut les mettre sous la forme :

$$C_{zo_s} + C_{zi_s} i + C_{z\beta_s} \beta = \frac{2Mg}{\rho V^2 S}$$

$$C_{mo_s} + C_{mi_s} i + C_{m\beta_s} \beta = 0$$

Ces équations exprimant l'équilibre de l'avion souple ont la même forme que les équations du vol de l'avion rigide.

Les remarques suivantes peuvent être faites :

1°) Les "dérivées aérodynamiques" de l'avion souple dépendent de la répartition massique et de la configuration initiale de vol de l'avion rigide.

2°) Leur détermination nécessite la connaissance de la répartition des pressions aérodynamiques sur l'avion rigide.

3°) Ces coefficients ne peuvent être utilisés que dans les cas de manoeuvres et de déformations lentes et ne peuvent pas rendre compte de la réponse dynamique de l'avion souple.

Malgré les limitations précédentes cette méthode peut-être utilisée avec profit dans beaucoup de cas : étude de l'adaptation de la voilure déformable, étude de la divergence de surfaces portantes, étude des efficacités de gouvernes dans les manoeuvres lentes, etc...

Dans d'autres cas, tels que, par exemple, la réponse de l'avion souple à la turbulence atmosphérique, influence de pilote automatique, il est nécessaire de tenir compte du déphasage des forces aérodynamiques par rapport aux déformations et par rapport aux actions extérieures.

3. EQUATIONS AVEC COEFFICIENTS INSTATIONNAIRES

Depuis des années les aéroélasticiens ont étudié et ont perfectionné la théorie de forces aérodynamiques harmoniques. Les calculs tridimensionnels permettent actuellement de déterminer les forces instationnaires et, à la limite, les forces stationnaires, qui ne sont pas trop éloignées des coefficients aérodynamiques définis par les aérodynamiciens.

D'autre part, une action extérieure, telle que la turbulence, par exemple, peut être considérée comme une série d'actionsharmoniques: ce n'est qu'une application de la théorie très générale de fonctions de transfert.

On peut donc représenter (voir planche 2), le vol de l'avion souple par un système d'équations de l'avion rigide d'une part et de n équations de modes propres. Les coefficients aérodynamiques dans ces équations seront les dérivées instationnaires comprenant deux parties, l'une en phase et l'autre en quadrature avec chaque paramètre du mouvement ou de la déformation.

Le nombre de modes propres à faire intervenir dans ce système d'équations est conditionné par deux critères :

1°) D'une part la notion de la fréquence la plus élevée à mettre en jeu dans le problème donné. Si on fait abstraction du problème purement aéroélastique du couplage de modes propres, on peut indiquer, à titre d'exemple que dans la réponse de l'avion à la turbulence atmosphérique les fréquences au-delà de 8 à 10 hz peuvent être

négligées; la stabilisation ou le pilotage automatique sont encore plus limités en fréquences.

2°) D'autre part le nombre de modes doit être suffisant pour que la déformation des surfaces portantes et du fuselage soit représentée avec suffisamment de précision par l'ensemble linéaire de ces modes

Très souvent on exagère l'importance des modes supérieurs. L'étude détaillée de la participation de chaque mode dans la déformation globale, montre que dans beaucoup de cas 6, 7 modes fondamentaux donnent une précision suffisante.

Les coefficients instationnaires sont des fonctions complexes de la fréquence réduite $k = \frac{\omega}{V}$. L'utilisation des équations de vol avec les les coefficients instationnaires nécessitera des calculs assez volumineux sur la machine digitale et sera très mal adaptée à l'étude sur la calculatrice analogique.

4. EQUATIONS AVEC COEFFICIENTS QUASI-STATIONNAIRES

Dans beaucoup d'applications, sans vraiment réduire la généralité des équations précédentes, il est possible de remplacer les coefficients instationnaires par des coefficients quasi-stationnaires indépendants de la fréquence réduite (planche 3).

L'incidence locale en un point x, y de la surface portante dans le mode ξ_i peut s'écrire :

$$(\alpha_i + j\frac{\omega}{V} h_i)\xi_i = \alpha_i \xi_i + h_i \frac{\dot{\xi}_i}{V}$$

La force généralisée $F_{\xi_j \xi_i}$ définie comme travail de forces aérodynamiques du mode ξ_i dans les déplacements du mode ξ_j, peut être calculée indépendamment pour les deux termes de l'incidence $\alpha_i \xi_i$ et $h_i \frac{\dot{\xi}_i}{V}$.

$$F_{\xi_j \xi_i} = \frac{\rho V^2}{2} S \left[\bar{C}_{\xi_j \xi_i} \xi_i + \bar{C}_{\xi_j \dot{\xi}_i} \frac{\dot{\xi}_i}{V} \right] =$$

$$= \frac{\rho V^2}{2} S \left[C'_{\xi_j \xi_i} \xi_i + j\frac{\omega}{V} C'''_{\xi_j \xi_i} \xi_i + C'_{\xi_j \dot{\xi}_i} \frac{\dot{\xi}_i}{V} + j\frac{\omega}{V} C'''_{\xi_j \dot{\xi}_i} \frac{\dot{\xi}_i}{V} \right] =$$

$$= \frac{\rho V^2}{2} S \left[C'_{\xi_j \xi_i} \xi_i + (C'''_{\xi_j \xi_i} + C'_{\xi_j \dot{\xi}_i}) \frac{\dot{\xi}_i}{V} + C'''_{\xi_j \dot{\xi}_i} \frac{\ddot{\xi}_i}{V^2} \right]$$

Dans l'hypothèse de coefficients quasi-stationnaires on admettra que $C'_{\xi_j\xi_i}$, $C'''_{\xi_j\xi_i} + C'_{\xi_j\dot{\xi}_i}$, $C'''_{\xi_j\ddot{\xi}_i}$ sont des constantes indépendantes de la fréquence réduite et l'expression approchée de la force généralisée pourra s'écrire :

$$F_{\xi_j\xi_i} = \frac{\rho V^2}{2} S\left[C_{\xi_j\xi_i}\xi_i + C_{\xi_j\dot{\xi}_i}\frac{\dot{\xi}_i}{V} + C_{\xi_j\ddot{\xi}_i}\frac{\ddot{\xi}_i}{V^2}\right]$$

Les équations de vol de l'avion souple prendront maintenant la forme indiquée sur la planche 4.

La meilleure précision sera obtenue si on calcule les coefficients quasi-stationnaires correspondant au mode ξ_i à la fréquence réduite définie par la fréquence de ce mode ξ_i . Pour les coordonnées de l'avion rigide, par exemple, z et θ dans le cas de vol longitudinal, les coefficients quasi-stationnaires seront calculés pour la fréquence réduite très faible, de l'ordre de 0,02 et les termes $C_{z\dot{i}}$, $C_{m\dot{i}}$, $C_{zq}\ell + C_{z\dot{i}}$, $C_{mq}\ell + C_{m\dot{i}}$ seront remplacés par les valeurs expérimentales définies par les aérodynamiciens.

Sur les planches 5 et 6 nous donnons un exemple de calcul d'une fonction de transfert de l'accélération au droit du pilote d'un avion soumis à l'action de rafales de fréquences variables. On voit que les coefficients instationnaires et les coefficients quasi-stationnaires conduisent sensiblement aux mêmes résultats. Dans ces calculs on n'a pas tenu compte des amortissements de structure de modes propres. En introduisant cet amortissement l'écart sur les amplitudes serait encore réduit.

5. EQUATIONS AVEC FONCTIONS INDICIELLES

Enfin quelle que soit la manœuvre imposée à l'avion ou la forme de l'action extérieure, il est possible d'exprimer les équations du vol de l'avion souple à l'aide de fonctions indicielles de forces aérodynamiques.

Cette méthode est rigoureuse, elle peut être employée assez facilement sur une machine analogique ou adaptée sur une calculatrice digitale. La difficulté réside dans la détermination des fonctions indicielles que l'on détermine à partir de coefficients instationnaires harmoniques.

La relation de base consiste en une intégrale de Fourier faisant correspondre aux dérivées instationnaires harmoniques $\overline{C}(k) = C'(k) + jC''(k)$ la fonction indicielle $C^*(s)$ où $s = V.t$ (voir planche 7).

$$C^*(s) - C^*(\infty) = \frac{1}{2\pi j}\int_{-\infty}^{+\infty}\left\{\left[C'(k) - C'(0)\right] + jC''(k)\right\}\frac{e^{jks}}{k}\,dk$$

Dans cette relation les constantes $C^*(\infty)$ et $C'(0)$ sont égales : $C^*(\infty) = C'(0)$.

En remplaçant e^{jks} par :

$$e^{jks} = \cos ks + j \sin ks$$

on peut écrire :

$$C^*(s) - C^*(\infty) = (I_1 + I_2) - j(I_3 - I_4)$$

où

$$I_1 = \frac{1}{2\pi} \int_{-\infty}^{+\infty} C''(k) \frac{\cos ks}{k} dk \qquad I_2 = \frac{1}{2\pi} \int_{-\infty}^{+\infty} [C'(k) - C'(0)] \frac{\sin ks}{k} dk$$

$$I_3 = \frac{1}{2\pi} \int_{-\infty}^{+\infty} [C'(k) - C'(0)] \frac{\cos ks}{k} dk \qquad I_4 = \frac{1}{2\pi} \int_{-\infty}^{+\infty} C''(k) \frac{\sin ks}{k} dk$$

D'après les propriétés des coefficients instationnaires et des fonctions trigonomètriques, les intégrales I_1 et I_2 sont des fonctions paires de k , les intégrales I_3 et I_4 sont des fonctions impaires. On aura donc $I_3 = I_4 = 0$ et dans les intégrales I_1 et I_2 on peut remplacer les limites d'intégration $-\infty$, $+\infty$ par les limites 0 , $+\infty$.

D'autre part par la définition de la fonction indicielle $C^*(s) = 0$ pour $s < 0$, et comme I_1 est une fonction impaire de s et I_2 une fonction paire de s , on aura :

Pour $s < 0$ $\qquad -I_1 = I_2 + C^*(\infty)$

Pour $s > 0$ $\qquad I_1 = I_2 + C^*(\infty)$

Finalement, on voit que la fonction indicielle $C^*(s)$ peut se déterminer par l'une des deux relations :

$$C^*(s) = \frac{2}{\pi} \int_0^{\infty} C'(k) \frac{\sin ks}{k} dk$$

$$C^*(s) = C'(0) + \frac{2}{\pi} \int_0^{\infty} C''(k) \frac{\cos ks}{k} dk$$

Pratiquement, les valeurs de $C'(k)$ et de $C''(k)$ ne peuvent être déterminées avec précision que jusqu'à une certaine valeur finie de k. Par contre on peut déterminer $C'(\infty)$ par une méthode impulsionnelle et on sait que $C''(\infty) = 0$. Mais dans la majorité des cas on peut raccorder les courbes $C'(k)$ et $C''(k)$ à leurs valeurs asymptotiques avec suffisamment de précision.

Nous donnons quelques exemples de fonctions indicielles sur les planches 8, 9 et 10 : ce sont les fonctions de la portance, du moment et de la force généralisée d'un mode propre dans la pénétration de l'avion dans une rafale. Dans ces fonctions les valeurs initiales pour $s = 0$ sont nulles et les valeurs asymptotiques de la portance et du moment sont des coefficients expérimentaux définis par les aérodynamiciens pour l'avion rigide.

Une fois établies les fonctions indicielles, les équations du vol de l'avion souple s'écriront en fonction de paramètres de l'avion rigide et de modes propres, sous forme d'un système d'équations (planche 11) dans lequel toutes les variables sont liées aux fonctions indicielles par les intégrales de Duhamel.

6. CONCLUSIONS

Ces différentes formes d'équations montrent qu'il existe un outillage mathématique, qu'il faut peut-être approfondir et perfectionner, mais qui permettra l'étude des questions du vol de l'avion souple qui intéressent les aérodynamiciens.

Tout n'est pas fait. On remarquera que dans ces équations, celle de la traînée a été systématiquement négligée, pour une raison bien simple : les aéroélasticiens ne savent pas calculer la traînée due à une déformation élastique. Il faut donc que les aérodynamiciens se penchent sur cette question, en collaboration avec les aéroélasticiens pour pouvoir calculer les performances de l'avion souple.

Une autre remarque : depuis des années, les aéroélasticiens, en écrivant leurs équations, emploient des notations tellement différentes de celles des aérodynamiciens qu'il faut une grande expérience pour comprendre de quoi on parle. Pourtant, il s'agit toujours de la même chose : des forces aérodynamiques. Il faut donc finir par trouver un langage commun.

DETERMINATION DE DERIVEES STATIONNAIRES DE L'AVION SOUPLE

Equations du vol longitudinal de l'avion rigide

$$C_{zo_r} + C_{zi_r} + C_{z\beta_r} = \frac{2M.g}{\rho V^2 S}$$

$$C_{mo_r} + C_{mi_r} + C_{m\beta_r} = 0$$

Déformation élastique

$$\alpha(\xi,\eta) = \frac{\rho V^2}{2} \iint C(x,y,\xi,\eta)\left[C_{p_o}(x,y) + C_{p_i}(x,y)i + C_{p_\beta}(x,y)\beta + \right.$$
$$\left. + C_{p_\alpha}(x,y)\alpha(x,y) + m(x,y)g\right] dx\,dy$$

Equilibre de forces après déformation

$$C_{zo_r} + C_{zi_r}\,i + C_{z\beta_r}\beta + \frac{1}{S}\iint C_{p_\alpha}(x,y)\alpha(x,y)\,dx\,dy = \frac{2Mg}{\rho V^2 S}$$

$$C_{mo_r} + C_{mi_r}\,i + C_{m\beta_r}\beta + \frac{1}{S}\iint C_{p_\alpha}(x,y)\alpha(x,y)\,x\,dx\,dy = 0$$

Equations du vol longitudinal de l'avion souple

$$C_{zo_s} + C_{zi_s}\,i + C_{z\beta_s}\beta = \frac{2Mg}{\rho V^2 S}$$

$$C_{mo_s} + C_{mi_s}\,i + C_{m\beta_s}\beta = 0$$

EQUATIONS AVEC DERIVEES AERODYNAMIQUES INSTATIONNAIRES.

REPONSE DE L'AVION EN VOL LONGITUDINAL A LA TURBULENCE.

$$\frac{2M}{S\rho V^2}\ddot{z} + \overline{C}_{z\alpha}\left(\theta + \frac{\dot{z}}{V}\right) + \overline{C}_{zq}\ell\frac{\dot{\theta}}{V} + \sum_i \overline{C}_{z\xi_i}\xi_i = \overline{C}_{zr}e^{j\omega t}\frac{w}{V}$$

$$\frac{2I}{\ell S\rho V^2}\ddot{\theta} + \overline{C}_{m\alpha}\left(\theta + \frac{\dot{z}}{V}\right) + \overline{C}_{mq}\ell\frac{\dot{\theta}}{V} + \sum_i \overline{C}_{m\xi_i}\xi_i = \overline{C}_{mr}e^{j\omega t}\frac{w}{V}$$

— — — — — — — — — — — — —

$$\frac{2\mu_j}{S\rho V^2}\ddot{\xi}_j + \frac{2\mu_j\omega_j^2}{S\rho V^2}\xi_j + \overline{C}_{\xi_j\alpha}\left(\theta + \frac{\dot{z}}{V}\right) + \overline{C}_{\xi_j q}\ell\frac{\dot{\theta}}{V} + \sum_i \overline{C}_{\xi_j\xi_i}\xi_i = \overline{C}_{\xi_j r}e^{j\omega t}\frac{w}{V}$$

$\overline{C}_{z\alpha} = C'_{z\alpha} + j\,C''_{z\alpha}$ ... sont les dérivées aerodynamiques instationnaires dans le mouvement de l'avion, fonction de $K = \frac{\omega}{V}$.

$\overline{C}_{zr} = C'_{zr} + j\,C''_{zr}$ ... sont les dérivées aerodynamiques instationnaires dues à l'action de rafales sinusoïdales de pulsation ω.

Planche 2

DEFINITION DE DERIVEES QUASI-STATIONNAIRES

Incidence locale dans la déformation du mode ξi :

$$(\alpha_i + j\frac{\omega}{V}h_i)\xi_i = \alpha_i \xi_i + h_i \frac{\dot{\xi}_i}{V}$$

Force généralisée crée par les forces aérodynamiques du mode ξ_i dans le déplacement du mode ξ_j :

$$F_{\xi_j \xi_i} = \frac{\rho V^2}{2} S\left[\overline{C}_{\xi_j \xi_i}\, \xi_i + \overline{C}_{\xi_j \dot{\xi}_i} \frac{\dot{\xi}_i}{V}\right] =$$

$$= \frac{\rho V^2}{2} S\left[C'_{\xi_j \xi_i}\, \xi_i + j\frac{\omega}{V} C'''_{\xi_j \xi_i}\, \xi_i + C'_{\xi_j \dot{\xi}_i} \frac{\dot{\xi}_i}{V} + j\frac{\omega}{V} C'''_{\xi_j \dot{\xi}_i} \frac{\dot{\xi}_i}{V}\right] =$$

$$= \frac{\rho V^2}{2} S\left[C'_{\xi_j \xi_i}\, \xi_i + (C'''_{\xi_j \xi_i} + C'_{\xi_j \dot{\xi}_i}) \frac{\dot{\xi}_i}{V} + C'''_{\xi_j \dot{\xi}_i} \frac{\ddot{\xi}_i}{V}\right]$$

<u>Approximation quasi-stationnaire</u> : les dérivées $C'_{\xi_j \xi_i} = C_{\xi_j \xi_i}$,

$C'''_{\xi_j \xi_i} + C'_{\xi_j \dot{\xi}_i} = C_{\xi_j \dot{\xi}_i}$, $C'''_{\xi_j \dot{\xi}_i} = C_{\xi_j \ddot{\xi}_i}$ sont supposées constantes.

$$F_{\xi_j \xi_i} = \frac{\rho V^2}{2} S\left[C_{\xi_j \xi_i}\, \xi_i + C_{\xi_j \dot{\xi}_i} \frac{\dot{\xi}_i}{V} + C_{\xi_j \ddot{\xi}_i} \frac{\ddot{\xi}_i}{V}\right]$$

EQUATIONS AVEC FONCTIONS AERODYNAMIQUES QUASI-STATIONNAIRES.

REPONSE DE L'AVION EN VOL LONGITUDINAL A LA TURBULENCE.

$$\frac{1}{V^2}[A]\begin{Bmatrix}\ddot{z}\\ \ddot{\theta}\\ \ddot{\xi}_i\\ \ddot{\xi}_j\end{Bmatrix}+\frac{1}{V}[B]\begin{Bmatrix}\dot{z}\\ \dot{\theta}\\ \dot{\xi}_i\\ \dot{\xi}_j\end{Bmatrix}+[C]\begin{Bmatrix}z\\ \theta\\ \xi_i\\ \xi_j\end{Bmatrix}=\begin{Bmatrix}C_{zr}\\ \vdots\\ C_{\xi_j r}\end{Bmatrix}e^{j\omega t}\frac{w}{V}$$

$$[A]=\begin{bmatrix}\frac{2M}{S\rho}+C_{z\dot{\alpha}} & C_{z\dot{q}}\ell & C_{z\ddot{\xi}_i} & C_{z\ddot{\xi}_j}\\ C_{m\dot{\alpha}} & \frac{2I}{\ell S\rho}+C_{m\dot{q}}\ell & C_{m\ddot{\xi}_i} & C_{m\ddot{\xi}_j}\\ \hline C_{\xi_j\dot{\alpha}} & C_{\xi_j\dot{q}}\ell & C_{\xi_j\ddot{\xi}_i} & \frac{2\mu_i}{S\rho}+C_{\xi_j\ddot{\xi}_j}\end{bmatrix}\qquad [B]=\begin{bmatrix}C_{z\alpha} & C_{z\dot{\alpha}}+C_{zq}\ell & C_{z\dot{\xi}_i} & C_{z\dot{\xi}_j}\\ C_{m\alpha} & C_{m\dot{\alpha}}+C_{mq}\ell & C_{m\dot{\xi}_i} & C_{m\dot{\xi}_j}\\ \hline C_{\xi_j\alpha} & C_{\xi_j\dot{\alpha}}+C_{\xi_j q}\ell & C_{\xi_j\dot{\xi}_i} & C_{\xi_j\dot{\xi}_j}\end{bmatrix}$$

$$[C]=\begin{bmatrix}0 & C_{z\alpha} & C_{z\xi_i} & C_{z\xi_j}\\ 0 & C_{m\alpha} & C_{m\xi_i} & C_{m\xi_j}\\ \hline 0 & C_{\xi_j\alpha} & C_{\xi_j\xi_i} & \frac{2\mu_j\omega_j^2}{S\rho V^2}+C_{\xi_j\xi_j}\end{bmatrix}$$

Planche 4

REPONSE DE L AVION SOUPLE EN ACCELERATION

AU DROIT DU PILOTE

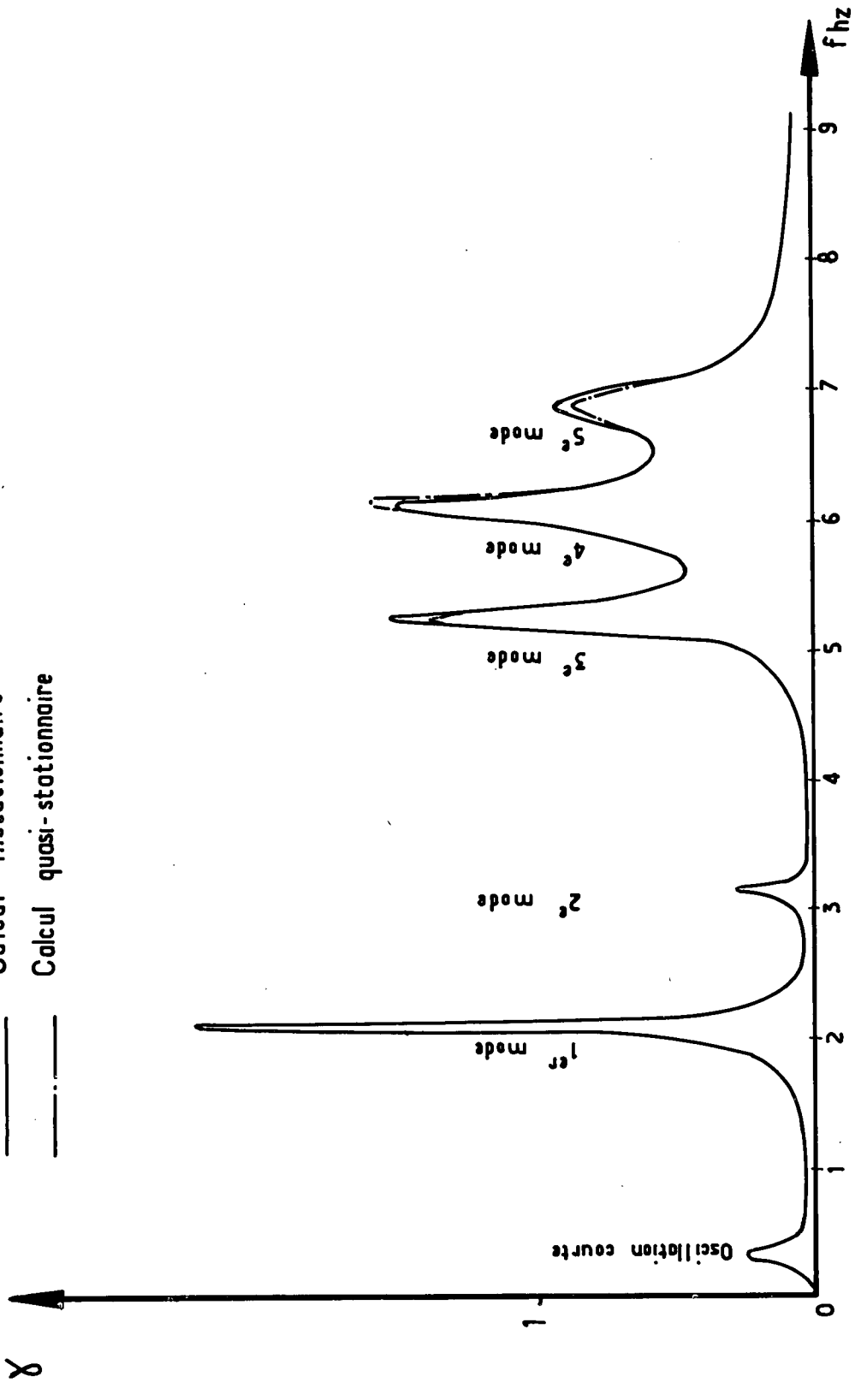
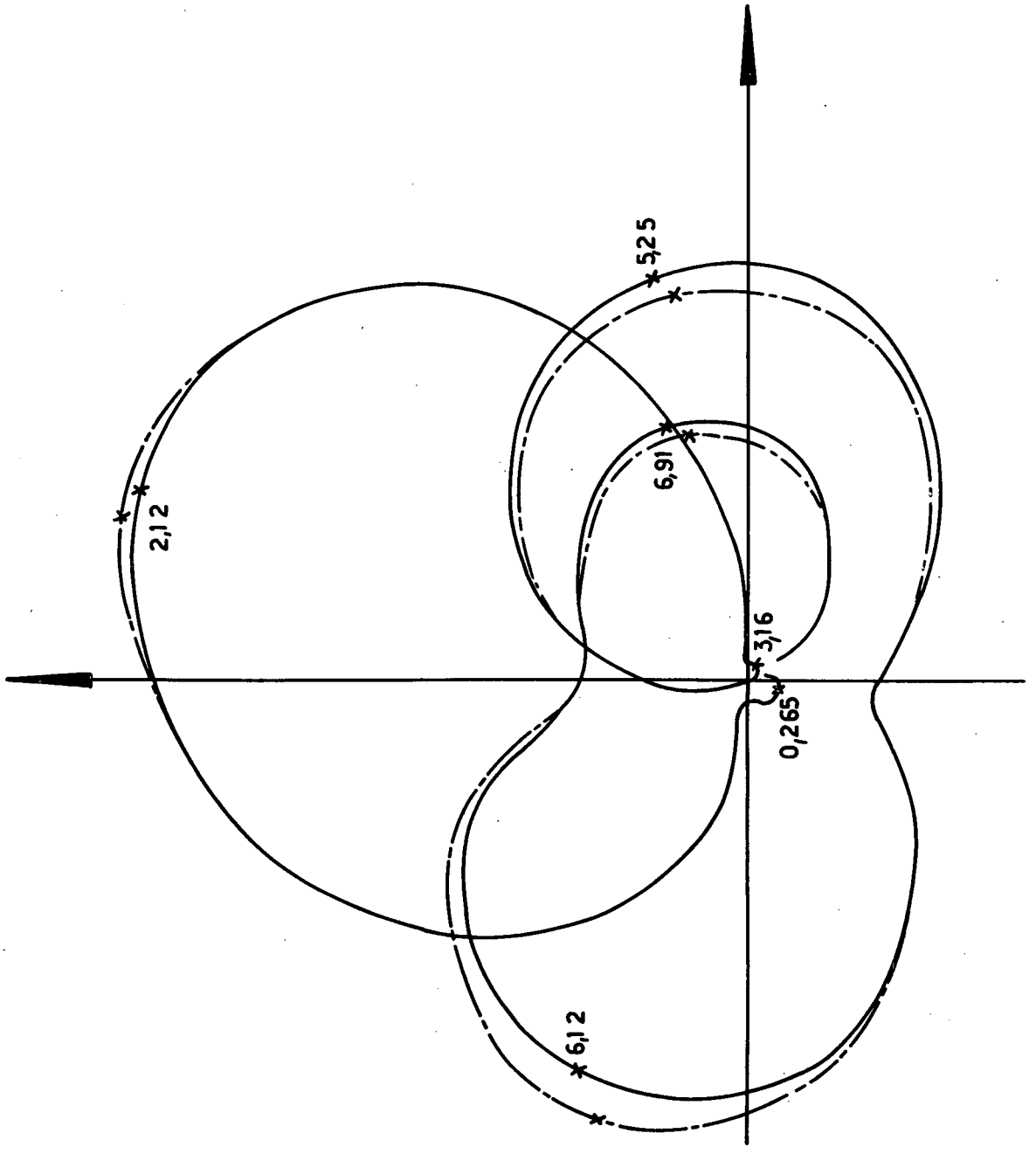


Planche 5

REPONSE DE L'AVION SOUPLE EN ACCELERATION AU DROIT DU PILOTE



——— Calcul instationnaire

—·—·— Calcul quasi-stationnaire

Planche 6

FONCTIONS INDICIELLES

Relation fondamentale entre une fonction indicielle $C^*(s)$ et les dérivées instationnaires

$$C(k) = C'(k) + jC''(k)$$

$$k = \frac{\omega}{V} \qquad s = Vt$$

$$C^*(s) - C^*(\infty) = \frac{1}{2\pi j}\int_{-\infty}^{+\infty}\left\{\left[C'(k) - C'(0)\right] + j\,C''(k)\right\}\frac{e^{jks}}{k}\,dk$$

avec la condition limite $C^*(\infty) = C'(0)$

En posant

$$C^*(s) - C^*(\infty) = (I_1 + I_2) - j(I_3 - I_4)$$

$$I_1 = \frac{1}{2\pi}\int_{-\infty}^{+\infty} C''(k)\,\frac{\cos ks}{k}\,dk \qquad I_2 = \frac{1}{2\pi}\int_{-\infty}^{+\infty}\left[C'(k) - C'(0)\right]\frac{\sin ks}{k}\,dk$$

$$I_3 = \frac{1}{2\pi}\int_{-\infty}^{+\infty}\left[C'(k) - C'(0)\right]\frac{\cos ks}{k}\,dk \qquad I_4 = \frac{1}{2\pi}\int_{-\infty}^{+\infty} C''(k)\,\frac{\sin ks}{k}\,dk$$

1°- I_1, I_2 sont des fonctions paires de K, I_3, I_4 fonctions impaires de K, donc $I_3 = I_4 = 0$

2°- Pour $s < 0$ $\quad C^*(s) = 0$ et $-I_1 = I_2 + C^*(\infty)$

3°- Pour $s > 0$ $\quad I_1 = I_2 + C^*(\infty)$

$$C^*(s) = \frac{2}{\pi}\int_0^{\infty} C'(k)\,\frac{\sin ks}{k}\,dk$$

$$C^*(s) = C'(0) + \frac{2}{\pi}\int_0^{\infty} C''(k)\,\frac{\cos ks}{k}\,dk$$

Planche 7

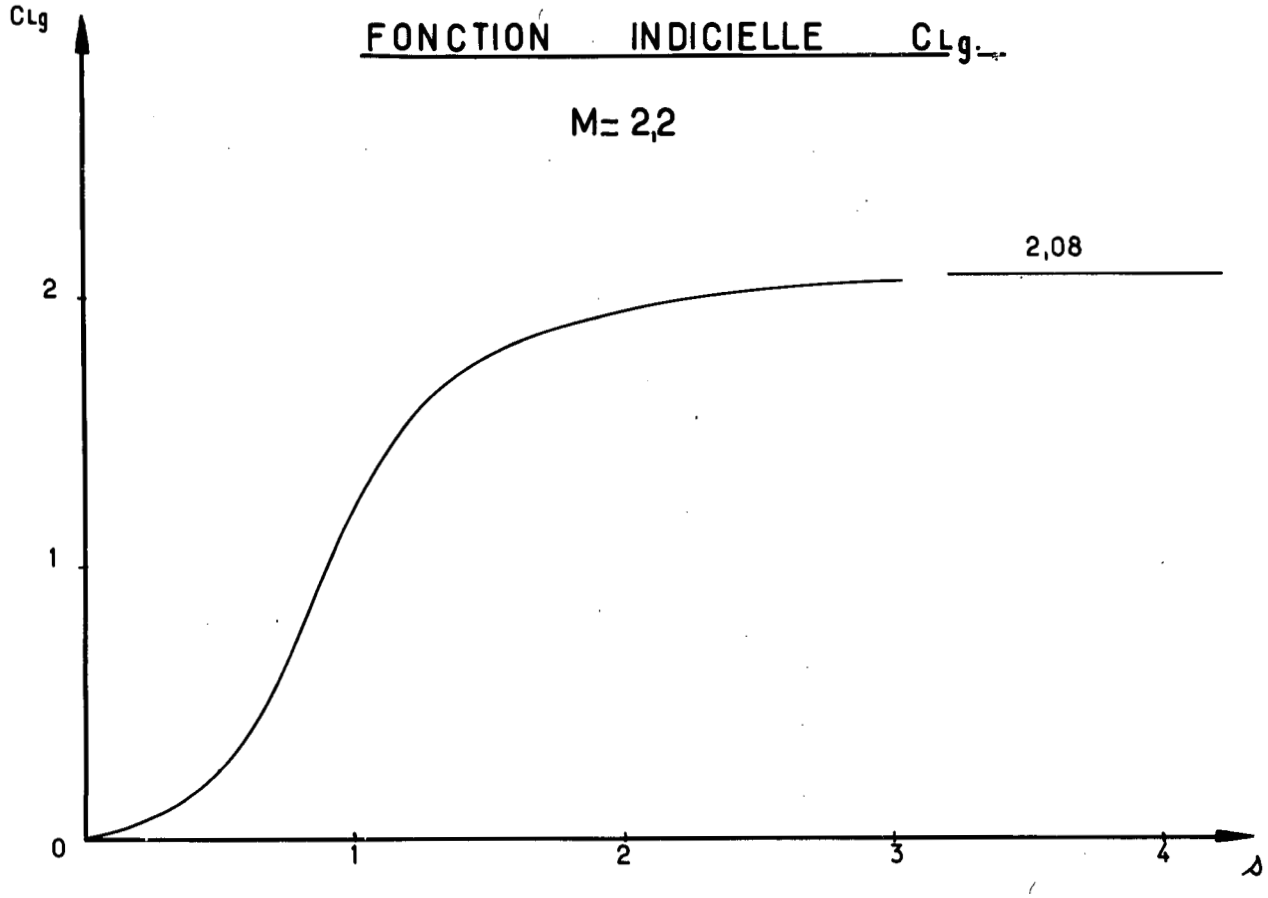


Planche 8

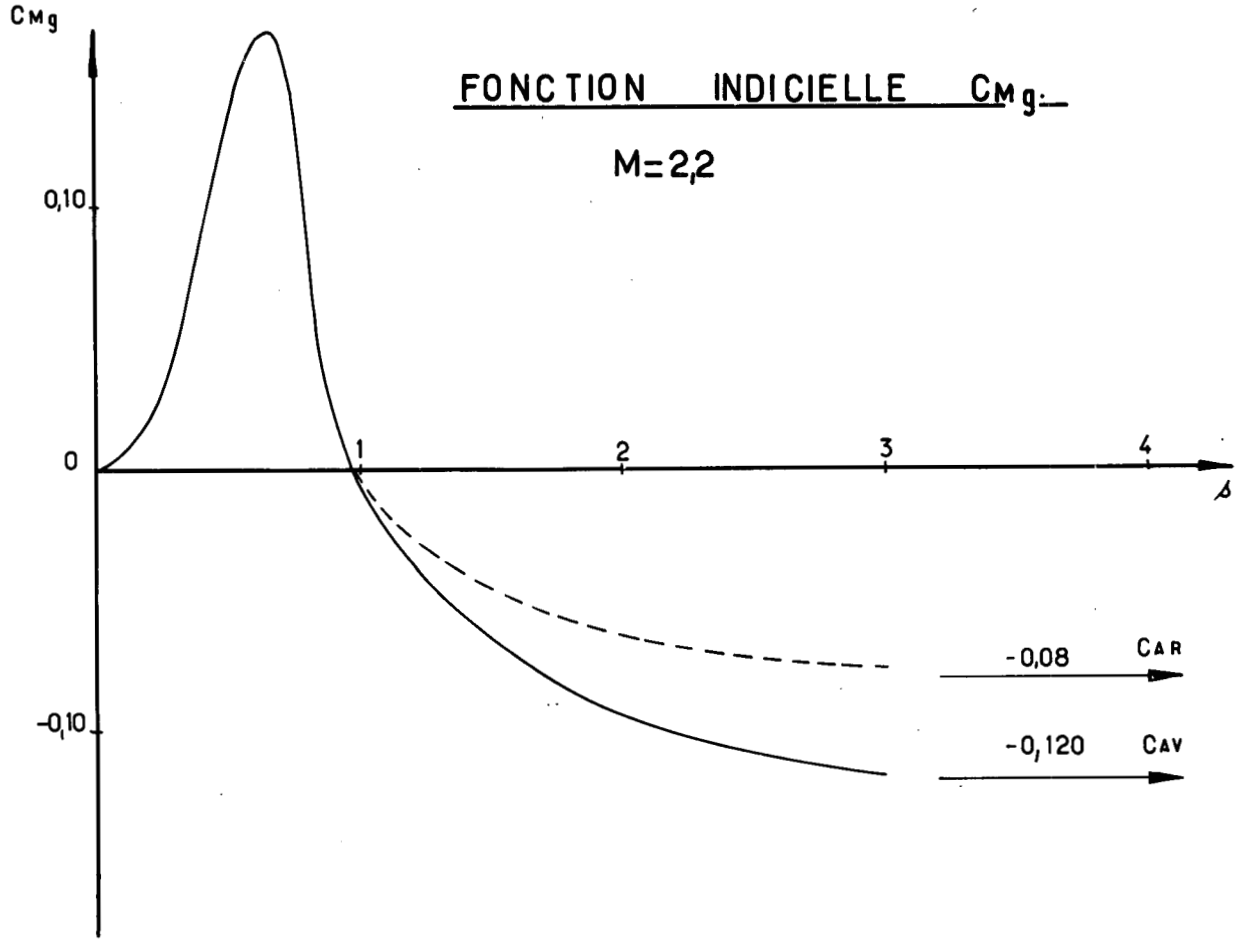


Planche 9

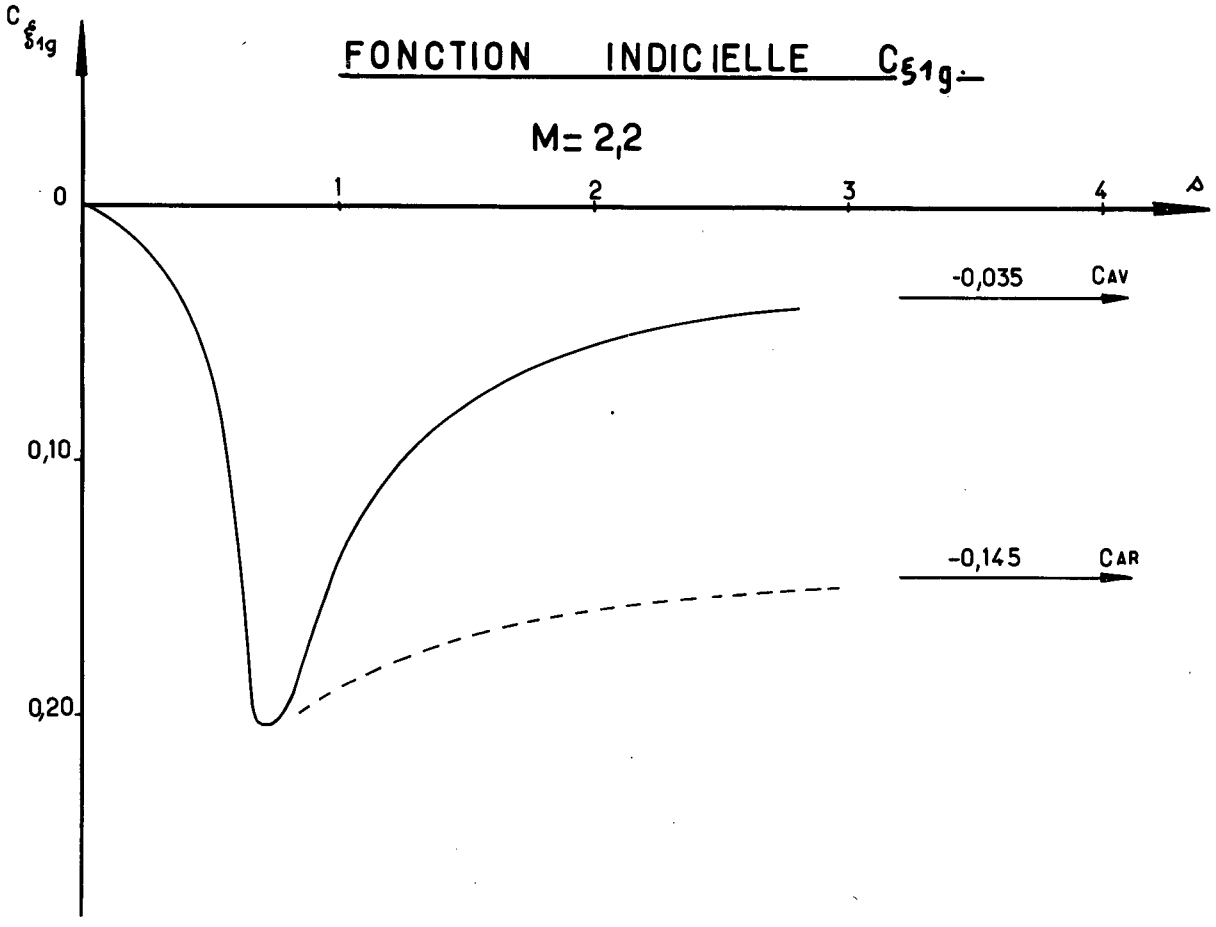

$C_{\xi_{1g}}$
FONCTION INDICIELLE $C_{\xi_{1g}}$
M= 2,2
0
1
2
3
4
Δ
-0,035
CAV
0,10
-0,145
CAR
0,20

Planche 10

EQUATIONS AVEC FONCTIONS AERODYNAMIQUES INDICIELLES.

REPONSE DE L'AVION EN VOL LONGITUDINAL AUX RAFALES ISOLEES.

$$\frac{2M}{S\rho V^2}\left(\frac{V}{2b}\right)^2\ddot{z} + \int_0^s \left(\dot{\theta} + \frac{\ddot{z}}{2b}\right) C^*_{z\alpha}(s-\sigma)d\sigma + \int_0^s \frac{\ell}{2b}\ddot{\theta}\, C^*_{zq}(s-\sigma)d\sigma + \sum_i \int_0^s \dot{\xi}_i\, C^*_{z\xi_i}(s-\sigma)d\sigma = \int_0^s \frac{d\left(\frac{u}{V}\right)}{d\sigma} C^*_{zr}(s-\sigma)d\sigma$$

$$\frac{2I}{\ell S\rho V^2}\left(\frac{V}{2b}\right)^2\ddot{\theta} + \int_0^s \left(\dot{\theta} + \frac{\ddot{z}}{2b}\right) C^*_{m\alpha}(s-\sigma)d\sigma + \int_0^s \frac{\ell}{2b}\ddot{\theta}\, C^*_{mq}(s-\sigma)d\sigma + \sum_i \int_0^s \dot{\xi}_i\, C^*_{m\xi_i}(s-\sigma)d\sigma = \int_0^s \frac{d\left(\frac{u}{V}\right)}{d\sigma} C^*_{mr}(s-\sigma)d\sigma$$

— — — — — — — — — — — — — — — — — — — —

$$\frac{2\mu_j}{S\rho V^2}\left(\frac{V}{2b}\right)^2\ddot{\xi}_j + \frac{2\mu_j\omega_j^2}{S\rho V^2}\xi_j + \int_0^s \left(\dot{\theta} + \frac{\ddot{z}}{2b}\right) C^*_{\xi_j\alpha}(s-\sigma)d\sigma + \int_0^s \frac{\ell}{2b}\ddot{\theta}\, C^*_{\xi_j q}(s-\sigma)d\sigma + \sum_i \int_0^s \dot{\xi}_i\, C^*_{\xi_j\xi_i}(s-\sigma)d\sigma =$$

$$= \int_0^s \frac{d\left(\frac{u}{V}\right)}{d\sigma} C_{\xi_j r}(s-\sigma)d\sigma$$

ATMOSPHERIC TURBULENCE DESIGN CASES

by

J. Taylor

Royal Aircraft Establishment, UK

SUMMARY

The underlying principles of the design cases for atmospheric turbulence loads on aircraft are discussed. The turbulence is considered to be made up of a number of patches each of which can be represented by a von Karman three-dimensional spectrum with a Normal distribution of crossings of different magnitudes of the turbulence velocity vector. The consequential accelerations at the aircraft centre of gravity are determined and used as a basis for comparing loads and displacements at various parts of a flexible aircraft.

RÉSUMÉ

L'auteur examine les principes qui gouvernent les cas de calcul des charges sur les avions dues à la turbulence atmosphérique. On considère que la turbulence est divisée en un certain nombre de zones qui peuvent chacune être representées par un spectre tri-dimensionnel de Von Karman où le nombre d' intersections du vecteur vitesse de turbulence pour différentes valeurs présente une distribution normale. On détermine les accélérations qui en résultent au centre de gravité de l'avion; ces accélérations sont utilisées pour comparer les charges et les déplacements à différents points d'un avion souple.

1. INTRODUCTION

The purpose of this study is to examine the design philosophy to be used in deciding on the design requirements for the loads on aircraft due to atmospheric turbulence. In discussing the philosophy that leads to the design cases it is the character rather than the magnitude of the loads that matters but it is an advantage to use measured values that can subsequently be used to define the actual values to be used for the design cases. A separate study is in hand on the frequency of occurrence of such loads but quotable numerical values will not be available for several months. One purpose of the present study is to develop a procedure that can use the large amount of data that has already been collected and also take advantage of modern theoretical methods of determining loads.

The data on turbulence loads that are most extensive are in the form of normal accelerations at a point near the aircraft centre of gravity together with height speed and weight of the aircraft at the time of their occurrence. These accelerations are almost invariably tabulated as the frequency with which various increments from 1G are exceeded. For any particular aircraft on which measurements are taken these accelerations give a good indication of the overall load on that aircraft and it is a common British practice to select the same point for a counting accelerometer, (used in conjunction with height and speed indicators) that is used for the fatigue load meter (also a counting accelerometer with a limited number of counting thresholds) that is carried regularly on practically all British Civil and Military aircraft. In this way all loads that are determined experimentally or theoretically can be related to the normal acceleration of one point on the aircraft which in turn can be used to monitor the fatigue loads and give an indication of the expected frequency of occurrence of the higher loads.

The design loads due to turbulence on any one particular aircraft can be given as the normal accelerations at the centre of gravity of the aircraft produced by the turbulence and the relationship of the loads at critical structural parts to the normal acceleration of the centre of gravity. The method of determining experimentally these relationships is discussed by P.B. Hovell in another paper at this conference. It is often convenient in the theoretical determination of loads to relate the loads to a gust velocity rather than to the centre of gravity acceleration. It might appear at first sight to be more basic but this would only be so if the operational measurements had been made of gust velocities. In fact as far as aircraft loads are concerned I have already stated that the extensive operational measurements are on normal accelerations at points near the centre of gravity and the amount of transcription to the motion of the true centre of gravity, which of course moves relative to the structure in a flexible aircraft, is much smaller than the transciption to the turbulence velocities of the air relative to the aircraft. In a linear system the transfer functions from gust velocity to normal acceleration and from either of them to the load at any point in the structure are simply related and on present knowledge of the properties of turbulence it would not be justified to contemplate anything but an equivalent linear system.

Before proceeding to discuss in more detail the motion of the centre of gravity of the aircraft it should be emphasised that in the operational research on the normal accelerations of the centre of gravity of one single type of aircraft any transcription of the information to equivalent gusts is solely for convenience of analysis as the procedure must subsequently be reversed to obtain normal accelerations from the gust velocities. However when the operational research covers normal accelerations on a number of aircraft and the data are combined to predict normal accelerations on another aircraft some common parameter, such as magnitude of equivalent gust, has to be introduced. The accuracy of the predictions to the other aircraft depends on the relative but not absolute accuracy of the relationship of normal acceleration to gust velocity although confidence in the accuracy may be good only for aircraft of similar types.

2. TURBULENCE MODEL FOR LOADS

2.1 Theoretical calculations

Current mandatory gust requirements all stipulate the magnitude and shape of a discrete gust. The number of occurrences of such equivalent gusts have been determined from normal acceleration measurements on a number of aircraft. The US shape differs slightly from the UK one but if allowance is made for this the resultant frequencies of occurrence derived from two sets of data available in 1963 are almost identical. These data form the basis for UK requirements and probably for those of other countries also.

It is considered of paramount importance that any immediate improvements in the turbulence model for aircraft loads should be such that the basic acceleration records can be used to estimate the design values that must be assigned to the model. Naturally advantage may be taken of data presented after 1963 so that changes that would have become necessary on the current model even for current aircraft can be included.

One of the principal objections to the current model is that it does not take sufficient account of the facts that in real conditions gust shapes vary considerably and that the dynamic effects due to flexibility depend considerably on the relation between the absolute dimensions of the design gust shape and those of the aircraft.

Press[1] noted in the early 1950's that an assumption of a specific shape for individual gusts could be avoided if the turbulence were represented by a Spectrum of Turbulence Energy at different wavelengths. This readily permitted the calculation of resultant spectra of normal accelerations and loads and these could include flexibility effects. As the values to be given to the turbulence model are based on the frequencies of occurrence of various levels of normal acceleration, compatibility between relative frequencies of the theoretical model and the experimental data must be achieved. This was done by Press but required the following two assumptions, which led to dubious physical concepts.

(a) The vertical velocity at any instant was assumed to be the same at every position spanwise.

(b) The frequency of crossing various levels of vertical velocity in homogeneous turbulence had to be assumed to be a normal distribution (this does not differ much from a Rayleigh distribution of velocity peaks) whereas the measured distribution of normal acceleration even in short patches of turbulence was not and appeared to be much nearer to an exponential distribution.

When the first assumption is used with any reasonably practical one dimensional spectrum of turbulence energy the calculated number of crossing of zero increment of normal acceleration of the centre of gravity becomes so large that little use could be made of it unless an arbitrary cut-off was made at some prescribed frequency.

The second assumption would be justified only if it could be assumed that a patch of turbulence had a range of RMS velocity intensities that could be represented by a normal distribution of intensity. This would not introduce doubts if the patch were very long but King[2] has found that severe storms could not be regarded as giving a Rayleigh distribution of vertical velocity peaks even when the distance traversed by the aircraft was as little as two miles.

It is now proposed to show ways in which these anomalies can be overcome and to check the accuracy of the model from normal acceleration records from aircraft in flight. The first anomaly is overcome by taking a velocity that has a spanwise variation as well as one in the line of flight. The second is overcome by taking a Rayleigh distribution of the maxima of the turbulence velocity vector rather than of the velocity component in one direction.

The model is based on the following assumptions. Each patch of turbulence has uniform properties, over the whole volume (homogeneous) and in each direction (isotropic) and can be represented by the von Karman three-dimensional spectrum of turbulence. The maxima of the turbulence velocity vector are assumed to have a Rayleigh distribution. The model is then completely defined by the intensity and the scale of the turbulence. Isotropy and the absolute magnitude of the scale of turbulence are not as important characteristics as the homogeneity and the intensity of the turbulence. Appreciable lack of isotropy could probably be tolerated where the intensity of the component in one direction is of greater significance than those in the others. The numerical value inferred for the intensity of a patch of turbulence met by an aircraft will depend markedly on the value given to the scale of turbulence but consistency between patches can be high for a wide range of scales. In order to maintain consistency in the numerical values quoted, the scale of turbulence is chosen empirically[5] to be equal to the altitude up to 1,000 ft and thereafter equal to 1,000 ft times the ratio of the air density at ground level to that at the altitude of the turbulence.

With these assumptions the total number of vertical gusts encountered per mile (zero crossings) can be determined and also the relative frequency of occurrence of gust components of different velocities. By taking the two dimensional form[5] of the vertical spectrum (slide 1) Kaynes[3] has determined the number of zero crossings without recourse to any empirical curtailing of the spectrum above certain frequencies that is essential when the one-dimensional vertical spectrum is used. Pitch is ignored but account is taken of taper and sweep-back of the wing. For consistency the gust response factors are also determined from the two-dimensional spectrum although this is not vital as the one-dimensional spectrum would give factors that are not appreciably different. The relative frequencies of occurrence of vertical gust components of various magnitudes expressed as proportions of the turbulence intensity (i.e. root mean square of the turbulence velocity over the whole patch) are calculated from the following assumptions:

(i) The frequency of occurrence of different magnitudes of the maxima of the gust velocity vector is a Rayleigh distribution.

(ii) The vector changes direction sufficiently slowly for the maxima of the components to occur at the same time as the maxima of the vector.

Slide 2 compares the distribution of occurrence of vertical gusts with the distribution of occurrence of gust vectors and gives their algebraic forms.

2.2 Experimental Normal Acceleration Records

In the theoretical predictions the numbers of gusts are the numbers of normal accelerations at the aircraft centre of gravity. In experimental investigations the accelerometer is placed on the aircraft structure and no matter how near it is to the cg in the static condition it will move relative to the cg as the structure deforms under load. The accelerations due to the high frequency structural modes are deliberately eliminated from the accelerometer records but the lower frequency ones are retained.

For most current aircraft it is likely that, when an accelerometer, as normally used in UK, is placed near the centre of gravity, it will record accelerations greater than those of the cg itself; however, it is probably justifiable to assume that the recorded total number of appreciable excursions of accelerations from 1g and back to 1g will not be significantly different from the number which actually occurs at the true centre of gravity.

For the proposed model of turbulence to be effective in predicting the normal accelerations that would occur at a particular position near the centre of gravity of one aircraft from measurements on another aircraft flying through the same patch of turbulence the relative magnitudes of the three following parameters must be known to sufficient accuracy.

(a) Gust response factor of the aircraft centre of gravity

(b) Transfer function of the acceleration at the accelerometer position relative to the centre of gravity

(c) The total number of normal accelerations at the centre of gravity for unit distance travelled (zero crossings).

The first two need to be known for both the discrete gust approach and a spectral one. For the third the isolated discrete gust approach assumes that all aircraft encounter the same number of gusts. Bullen[7] has shown, however, that if the normal accelerations at the centre of gravity are assumed to have a fixed variation with time for each gust (i.e. fixed gust shape) and they occur sufficiently frequently that they overlap, then the number of zero crossings will depend on the aircraft characteristics. His investigations indicate that atmospheric turbulence generated by solar radiation to the earth's surface tends to have the characteristics of isolated discrete gusts at low radiation but tends to have the characteristics of continuous turbulence above a certain level of radiation. The present investigation is concerned with continuous turbulence, albeit with a different representation from Bullen's. The comparison of the model for various normal acceleration measurements will show up the sum of those errors due to the model not being fully representative of continuous turbulence and those due to all the turbulence not being fully developed. The partly developed turbulence noticed by Bullen resulted in lower loads but this need not be so for all types of turbulence for all aircraft configurations. As the design gusts should be based on operational recordings these features are automatically taken account of to a large degree for similar types of aircraft and similar types of route flying. Departures from either will reduce the confidence in the deductions; this is general to the determination of most design loading conditions and not peculiar to gust loading.

There are available at the RAE normal acceleration records from several hundred flying hours below 10,000 feet on several aircraft in a form suitable for counting total acceleration crossings during the minute intervals. An analysis is in progress to check whether there is serious error in assuming that each individual minute is in homogeneous turbulence. The patch size is sufficiently small to compare the theoretical and experimental numbers of zero crossings, especially for the patches where the turbulence appears reasonably continuous.

The accuracy of the model of turbulence in predicting relative levels of normal acceleration can be checked by estimating the number of zero crossings and the intensity during each minute and determining the cumulative totals for long periods. This comparison on any one aircraft can be made on normal accelerations at the levels at which the counts were made and interpolation errors due to transferring to gust velocities before taking totals can be avoided. A comparison is made of a Rayleigh distribution of the maxima of the velocity vector with a Rayleigh distribution of the vertical component of the velocity for several aircraft. Slide 3 makes the comparison for a Viking aircraft and slide 4 shows the distances travelled at different ratios of the measured numbers of gust to the calculated values for continuous turbulence. This shows a rapid fall off above about 100%. There is a tendency for turbulence loads to be reasonably continuous fluctuations when they are present. One of the more extensive areas of turbulence encountered by the Viking is shown in Slide 5; the average of the measured number of gusts is about 87% of the calculated for continuous turbulence. An examination of an Anson flight through extensive turbulence shows similar agreement for the total number of gusts (zero crossings) as a percentage of the calculated value for turbulence. As the calculated number of zero crossings for the Anson

is about 150% of that for the Viking, this is a good indication that the number of zero crossings is dependent on the aircraft and that the calculated values given here are of the right order of magnitude. Much more work will be required to determine the relative accuracy of the calculated values.

As all the turbulence described so far does not include severe storm turbulence a check has been made of a number of patches of storm turbulence. Slide 6 gives a comparison for 36 patches of the most severe turbulence encountered by Comets and 707's in 23,000 hours of civil flying. As the individual accelerations were measured the comparison can be made on gust velocity. For this purpose it has been assumed that amplification of the accelerometer records relative to the motion of the true centre of gravity was the same for all conditions and in order to give reasonably correct numerical values[5] to the gust the amplification factor was taken to be 1.2.

3. DESIGN CONDITIONS FOR THE NORMAL ACCELERATION AT THE CENTRE OF GRAVITY

Having decided on a model of turbulence that gives an adequate representation of normal accelerations at the centre of gravity a step can be taken towards formulating design requirements by recalculating the frequency of occurrence of gust velocities from the frequency of occurrence of accelerations at the centre of gravity that were used as the basis for the current requirements.

The AGARD Loads Manual[5] gives an approximation to these data for a model of turbulence that is itself only slightly different from the present one in respect to gust response factor and has the same empirical amplification factor for the magnitude of acceleration at the accelerometer position relative to that of the true centre of gravity. These data are reproduced in slides 7, 8 and 9. In slide 7 and 8 the information is given for an aircraft with zero crossings N_0 (mean of number up and number down) given by $N_0\sqrt{\rho_0/\rho} = 9.9$ per mile. This value is the average for the aircraft used and is based on the Dryden model of turbulence with an empirical correction due to Hall to take account of the spanwise variation of the turbulence. The average value based on the von Karman model, using Kaynes's procedure, is approximately 14 per mile. Slide 9 uses an average factor to take account of changing from the Zbrozek gust alleviation factor[6] to a gust response factor based on the von Karman model of turbulence with Hall's empirical correction for the spanwise effect. This will not differ much from Kayne's procedure.

The original data from which these figures were produced are available for full re-analysis. Whilst it is not expected to show appreciable differences it will however help considerably in interpreting the meaning of the curve of frequency of occurrence in slide 9. This curve is constructed from the sum of two exponentials $\exp(-v/3.0)$ and $\exp(-v/6.0)$, where v ft/sec EAS is the gust velocity, with 1.6% of the gusts at the more severe exponential distribution. The less intense turbulence corresponds roughly to flight through cumulus and the more intense through thunderstorms. Using the relative frequency of occurrence of gusts in the model of turbulence now proposed a moderate representation of slide 9, maintaining the same proportion of severe to moderate turbulence and also the factor of 2 on intensity, can be obtained with the intensity for the two types as an RMS velocity of 5 ft/sec EAS and 10 ft/sec EAS as shown in slide 10. This greatly simplifies the representation of these basic data on accelerations at the centre of gravity for the purpose of using spectral methods of determining the normal accelerations and loads in flexible aircraft flying through turbulence.

It is considered that a simple step forward, of this or similar type, from a discrete gust procedure to a spectral procedure allows an improvement in prediction of gust loads whilst still using practically all the past experience.

If such a procedure were accepted reasonably soon experience could be built up and further refinements could be made as further loads information becomes available. Mention was made in paragraph 2.2 of one such further investigation in which the analysis of the flying is broken down into a large number of short time intervals. This will show up, in particular, where there are any systematic departures of gust pattern that produce unexpectedly large or small normal accelerations. If this occurs it should be possible to use Bullen's work to investigate the turbulence which almost certainly will lie between the extreme conditions of fully developed turbulence and an isolated discrete gust. A lot of data is now becoming available as records of individual patches of turbulence and it should be possible to isolate the more severe patches as King[2] has done.

The distribution of slide 10 is a combination of data at a wide range of heights. It seems likely[5] that the two forms of turbulence are substantially of the same intensity at all heights and it should be possible when more data become available to determine the relative frequency of occurrence of the two forms at different heights. Slides 8 and 10 could then be replaced by one curve for each type of turbulence and a table of frequency of occurrence of each at each height in cruise climb and descent instead of the total relative frequency of 98.4% and 1.6%. Until this can be done the basic data on gust loads do not warrant an elaborate mission analysis for the larger loads which depend so markedly on the changes of the above 1.6% with height. Thus for the immediate future the recommended procedure for large loads is to continue with the present design envelope but to modify the values of gust velocity so that they are related to gust response

factors instead of gust alleviation factors. Any regulating bodies making such modifications would certainly make arbitrary adjustments to the requirements were they to find appreciable reductions in design loads on certain classes of aircraft; the main danger arises in structural areas where current aircraft are much overstrength for particular design cases while future aircraft will not be.

In addition to the operational data that have been discussed there are many investigations of atmospheric conditions met by aircraft on special flights on non-operational routes and also on special flights over operational routes when normal operational flying is forbidden. Should these investigations show up "minefields" of turbulence or atmospheric conditions that might lead to serious flying hazards, flying requirements may have to be introduced. Such requirements are outside the scope of this investigation although the data obtained during the special flights can frequently be of immense value in understanding the character of loads occurring during standard operational flights.

4. DESIGN CASES FOR STRUCTURAL LOADS

The spectral form used to describe turbulence for design conditions that has been presented is suitable for direct calculation of loads without going through intermediate calculations of the acceleration at a point near the aircraft centre of gravity and taking account of all the rigid body motions of the aircraft. However for some applications this might involve excessive computing and some simplification might be attempted. The predictions have to be made for an equivalent linear system whatever method is used and it is considered that satisfactory accuracy might be obtained by calculating the normal accelerations of the centre of gravity from the aerodynamic forces with only a crude allowance for the dynamics of the motion due to the structural flexibility and then determining the structural loads that would be developed in a flexible structure whose centre of gravity moved in the manner calculated, making full allowance for structural damping but making only a crude allowance for aerodynamic damping introduced by the structural vibrations. It is thought that this procedure might be particularly appropriate to experimental verification of the transfer functions from normal acceleration at a monitoring acclerometer to loads at different parts of the structure.

5. CONCLUSIONS

A model of turbulence is proposed that is based on von Karman's turbulence energy spectrum but based on a Rayleigh distribution of the maxima of gust velocity vector instead of the commonly used vertical component of the gust velocity. By using the two dimensional spectrum the estimates of total numbers of gusts (zero crossings) are close to the measured values in continuous turbulence for two aircraft one of which has a calculated number of zero crossings 1.5 times the other. The spectrum also gives the gust response factor that converts individual gust velocities to normal acceleration at the centre of gravity.

It is concluded that the current design envelope for gusts based on the Zbrozek, or other similar, gust alleviation factor be replaced by the same envelope based on the proposed gust response factor. The total number of gusts at any particular height in current requirements may be regarded as an average for current aircraft. For a new design this number should be adjusted in the ratio of its calculated number to the average for current aircraft.

The existing data are sufficient to continue using mission analysis for design for fatigue strength but much more data are required before mission analysis can be introduced with confidence for ultimate strength.

Serious consideration must be given to the possibility that atmospheric conditions might occur in exceptionable, but predictable, circumstances in which the loads on the aircraft exceed both current and the proposed requirements. It is suggested that flying restrictions should be introduced to cater for these conditions.

REFERENCES

No.	Author	Title, etc
1	H. Press May T. Meadows and I. Hadlock	Estimates of probability distribution of root mean square gust velocity of atmospheric turbulence from operational gust load data by random process theory. NACA Tech. Note 3362.
2	G.E. King	Characteristics of severe turbulence encountered by civil aircraft. Unpublished work
3	I.W. Kaynes	Aircraft centre of gravity response to two-dimensional spectra of turbulence. Unpublished work
4	J. Taylor	Relative frequency of occurrence of different normal accelerations at the centre of gravity of aircraft in turbulence. Unpublished work
5	J. Taylor	Manual on aircraft loads. Agardograph 83, Pergamon Press 1965
6	J.K. Zbrozek	Gust alleviation factor. ARC R and M 2970 (1953)
7	N.I. Bullen	Gusts discrete and indiscrete RAE Tech. Report 69062 March 1969.

$$S(k) = \frac{\frac{220}{9}\sigma_w^2 L(2\pi ak)^4}{[1+(2\pi ak)^2]^{17/6}}$$

Three-dimensional spectrum

$$S_w(k_1,k_2) = \frac{\frac{8}{9}\sigma_w^2 (2\pi a)^4 (k_1^2+k_2^2)}{[1+(2\pi a)^2 (k_1^2+k_2^2)]^{7/3}}$$

Two-dimensional vertical spectrum

$$S_w(k) = \frac{2\sigma_w^2 L\left[1+\frac{8}{3}(2\pi ak)^2\right]}{[1+(2\pi ak)^2]^{11/6}}$$

where σ_w^2 = Mean square of vertical component of turbulence.

k = Inverse wavelength L = scale of turbulence.

$a = \left[\left(-\frac{2}{3}\right)!/\sqrt{\pi}\left(-\frac{1}{6}\right)!\right] L = 1.339\,L$

One-dimensional vertical spectrum

Fig. 1 von Kármán spectrum of turbulence

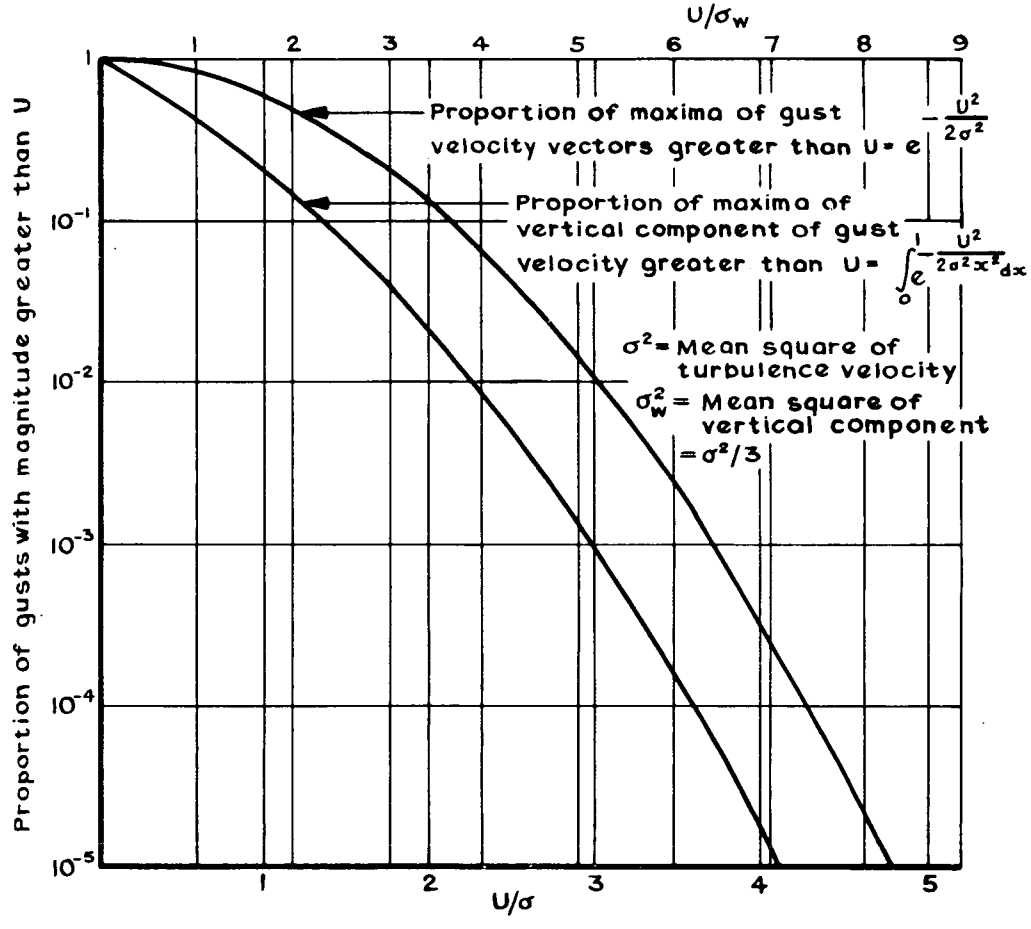


Fig. 2 Relative frequency of occurence of gusts with Rayleigh distribution of maxima of gust velocity vector

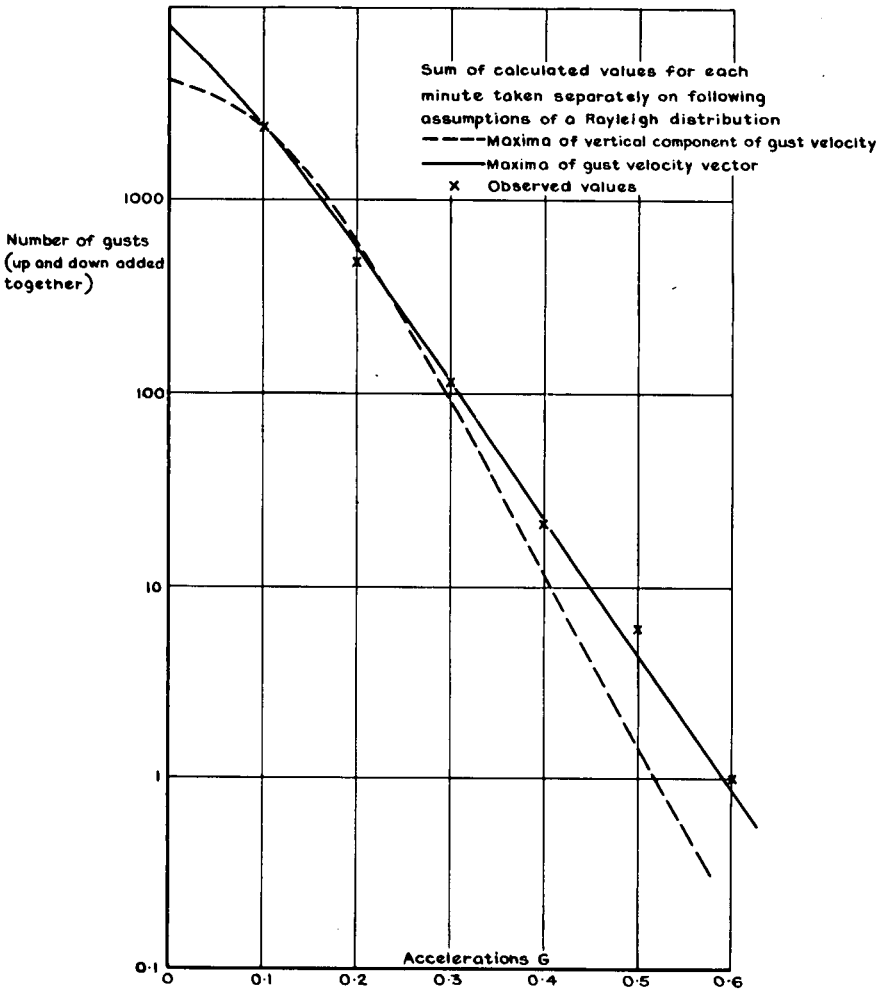


Fig. 3 Viking-frequency of occurrence of gusts in 170 minutes flying below 5000 ft

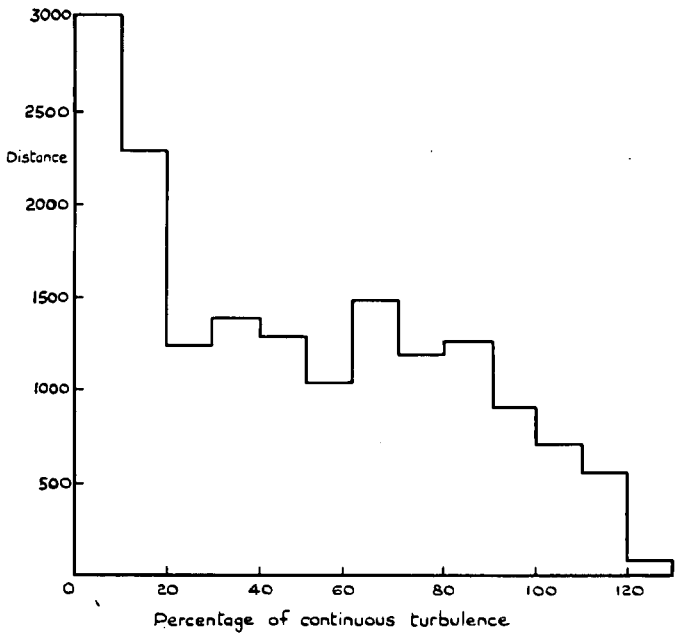


Fig. 4 Viking-distance travelled at different percentages of continuous turbulence in 170 minutes of flight. Distance as calculated number of gusts that would occur in continuous turbulence

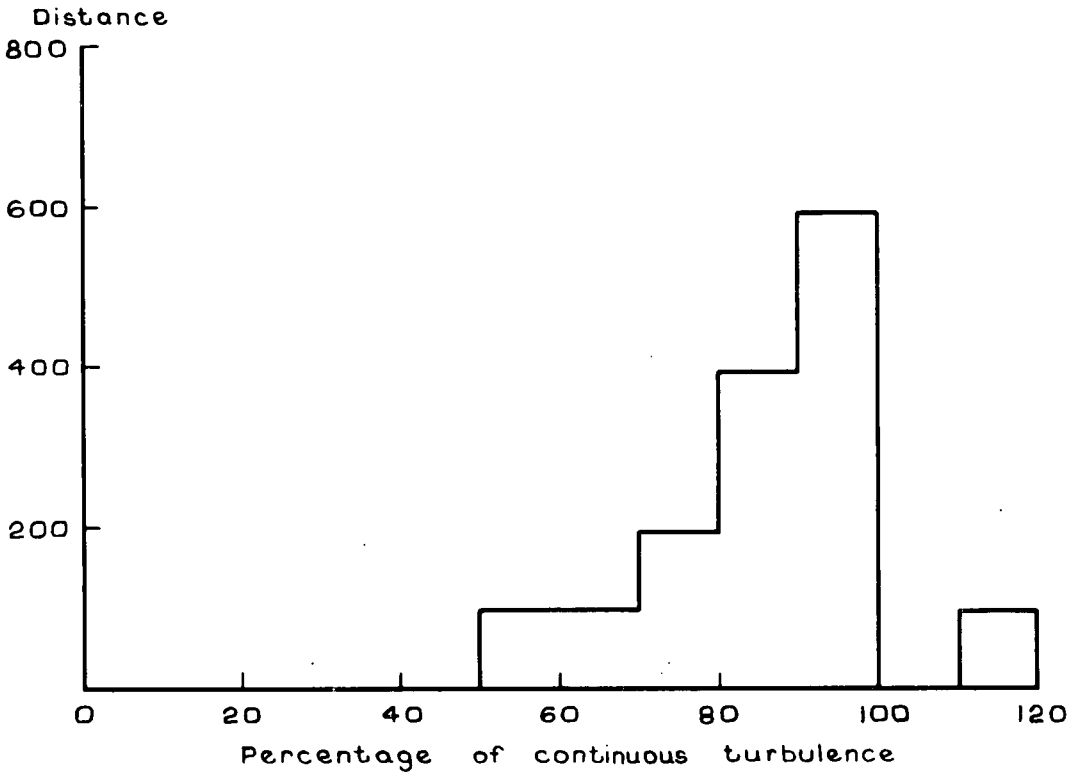


Fig.5 Viking-distance travelled at different percentages of continuous turbulence in 15 minute flight through turbulent area

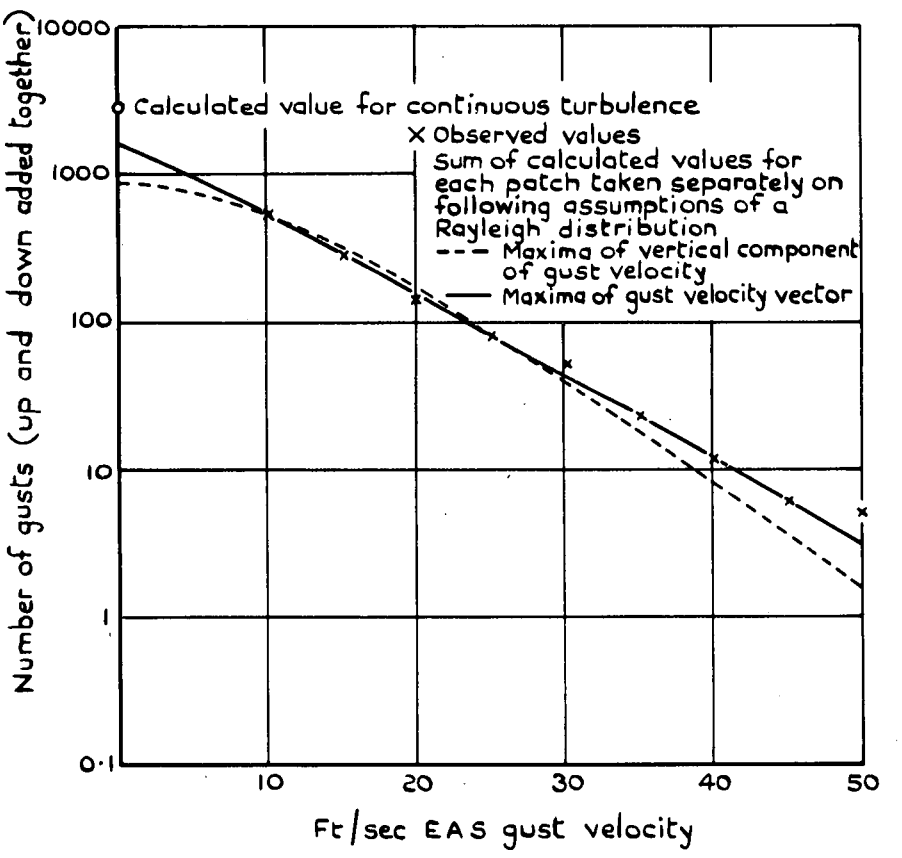


Fig.6 Comet and 707-36 patches of the most severe turbulence in 23000 hours of civil flying

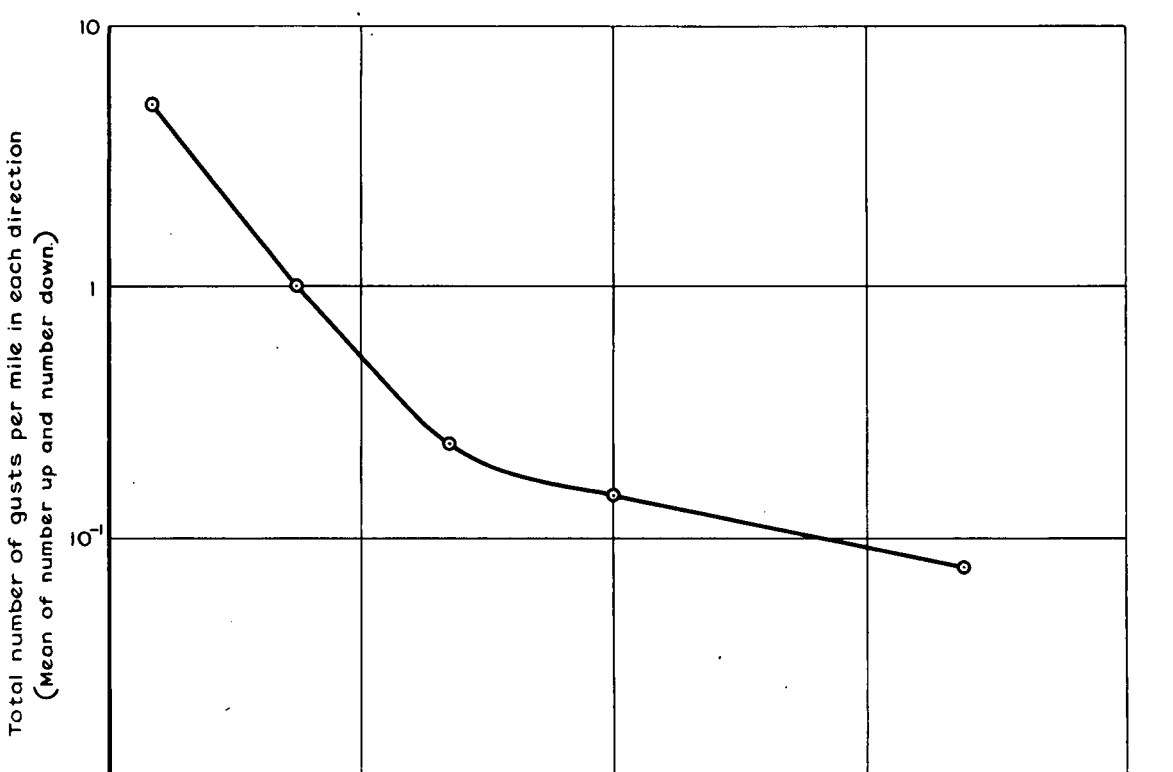


Fig.7 Variation in total number of gusts with height

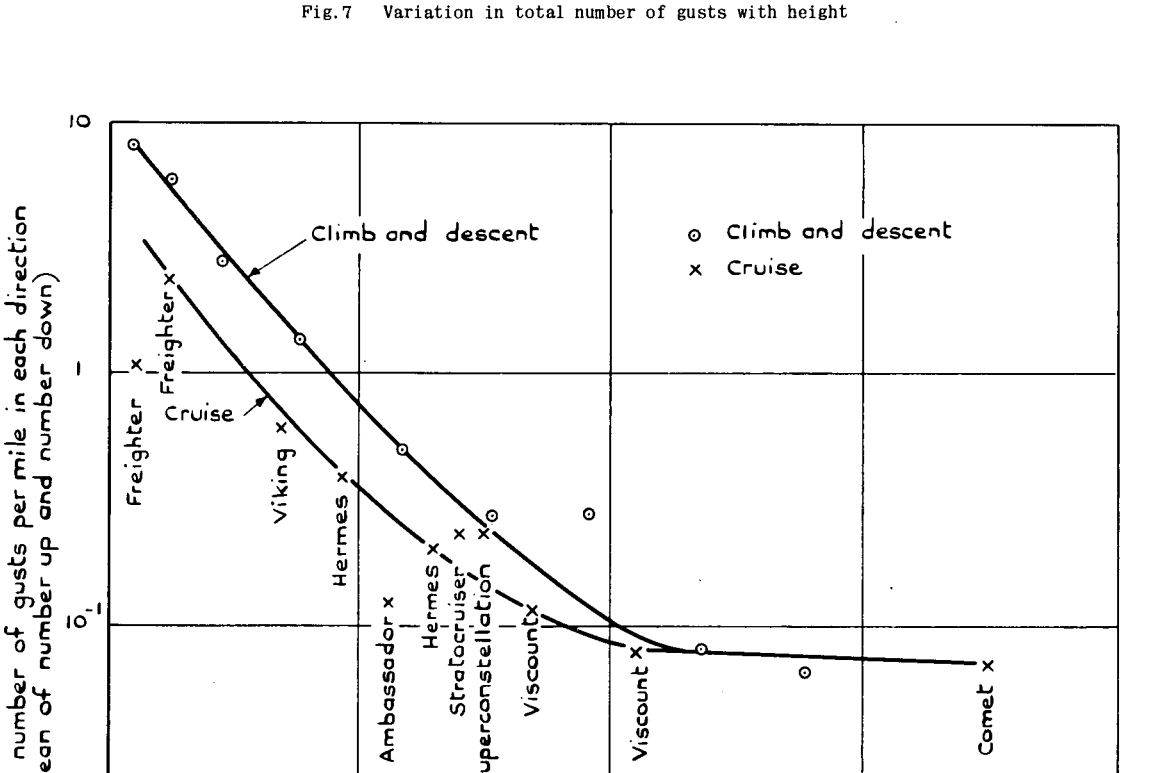


Fig.8 Comparison of total number of gusts per mile in climb and descent and in cruise

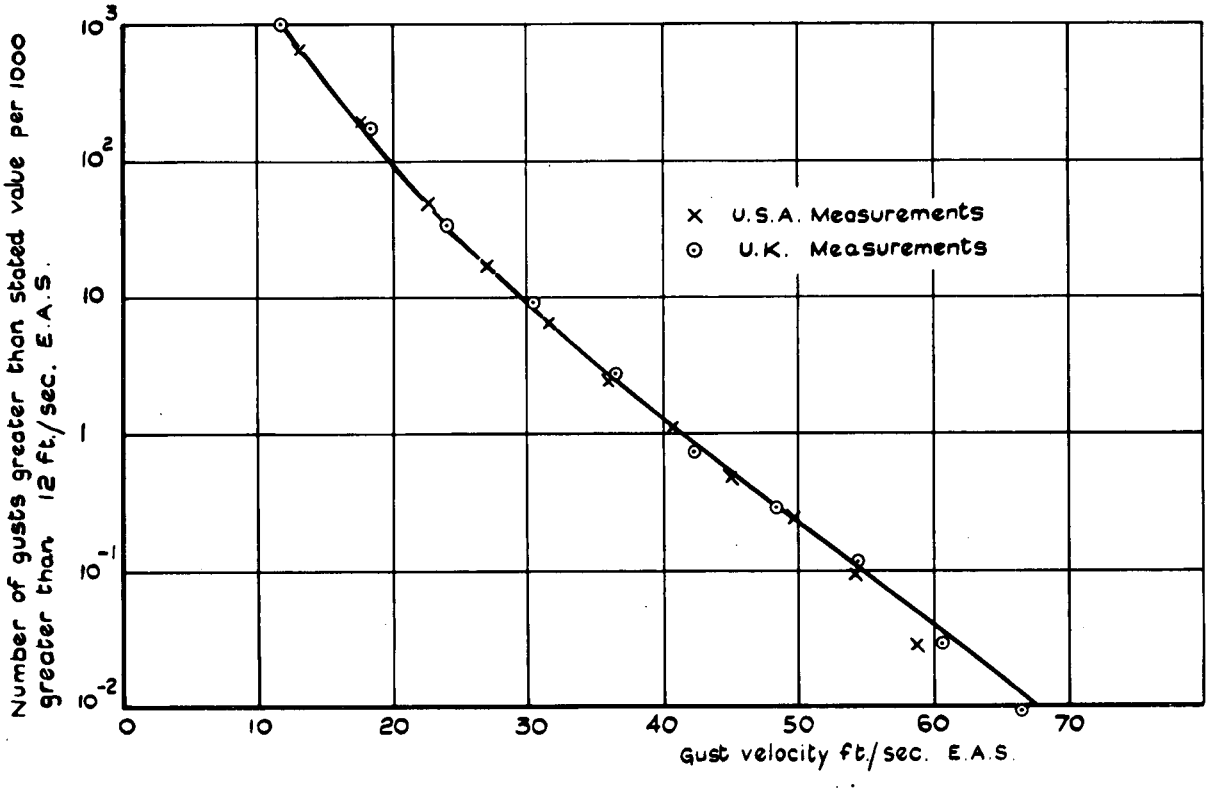


Fig. 9 Comparison of USA and UK data on relative frequency of occurrence of gusts of different magnitude

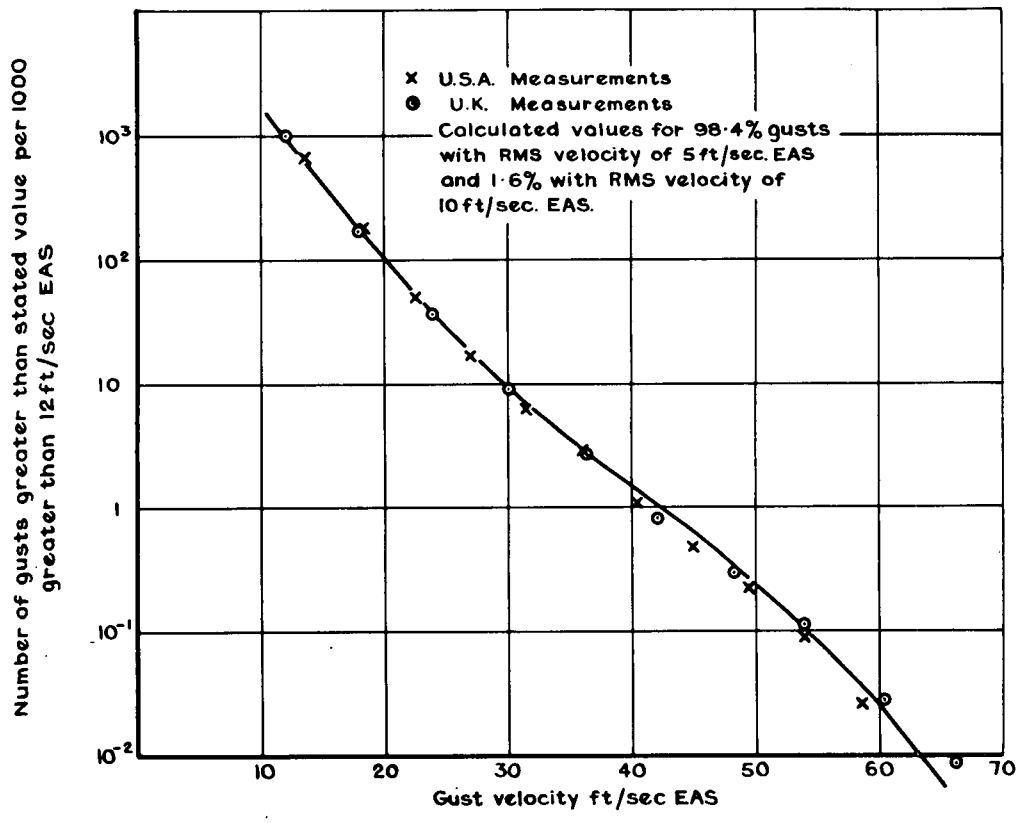


Fig. 10 Representation of the data from 10 million miles of flying by combining in the ratio of 98.4 to 1.6 uniform turbulence of one RMS velocity with another of twice the velocity

UTILISATION D'UN AVION COMME MOYEN DE MESURE DE LA DISTRIBUTION STATISTIQUE DE LA TURBULENCE

par Gabriel COUPRY et Guy THOMASSET

Office National d'Etudes et de Recherches Aérospatiales (O.N.E.R.A.)
(92 - Châtillon - France)

UTILISATION D'UN AVION COMME MOYEN DE MESURE DE LA DISTRIBUTION STATISTIQUE DE LA TURBULENCE

RESUME -

L'objet des études qui sont analysées est de présenter une méthode cohérente d'utilisation des enregistrements V.G.H. permettant la définition de "mesures de masse" de la turbulence atmosphérique.

La méthode repose sur l'étalonnage de l'avion, considéré comme instrument de mesure de la turbulence, les méthodes théoriques de prévision étant sujettes à des erreurs importantes. Il est montré qu'un étalonnage soigneux, effectué sur quelques vols, permet une excellente mesure de la distribution statistique de la turbulence à partir des accélérations du centre de gravité.

Par ailleurs, des recherches systématiques, fondées sur l'enregistrement magnétique en vol des ordres de pilotage, ont permis de dégager une technique qui soustrait, de l'accélération globale, la part due aux actions du pilote.

L'ensemble de ces travaux doit aboutir à la création d'un "compteur V.G.H." embarquable de faible encombrement.

USE OF AN AIRCRAFT FOR MEASURING THE STATISTICAL DISTRIBUTION OF TURBULENCE

ABSTRACT -

The studies presented in this paper were meant to provide a consistent method for using Velocity, Gravity and Height recordings, allowing the definition of "mass measurements" of atmospheric turbulence.

This method is based on the calibration of the aircraft regarded as a turbulence measuring instrument; the theoretical methods of prediction are being liable to considerable errors. It is shown that careful calibration, carried out on a few flights, makes it possible to measure with great accuracy the statistical distribution of turbulence, from the centre of gravity accelerations.

On the other hand, systematic research based on in-flight magnetic recording of pilot inputs has led to a technique which takes away, from the total acceleration, the part resulting from the pilot's actions.

This overall research should lead to the development of a small size airborne "velocity-gravity-height meter".

I - INTRODUCTION.-

Lors de l'étude du comportement en vol et de la prévision de la fatigue d'un avion, il est indispensable de connaître la distribution statistique des niveaux de turbulence qu'il est susceptible de rencontrer. Il est admis depuis plusieurs années qu'en dehors des recherches théoriques en cours, une méthode permettant d'avoir une connaissance approximative de cette distribution de niveaux consiste à rassembler le plus grand nombre d'informations sur les niveaux de turbulence rencontrés par les avions d'essais et surtout par les avions des lignes commerciales. Ce travail se prête particulièrement bien à une collaboration internationale.

Il est apparu très vite impossible d'obtenir suffisamment d'informations à partir de mesures directes de la turbulence et les efforts se sont orientés sur la mesure des facteurs de charge supportés par les avions. C'est dans cet esprit que la 21ème Structures and Materials Panel A.G.A.R.D. chargea Mr. Cyril G. PEICKHAM de sa mission d'information auprès des divers pays de l'OTAN, afin de définir un point de vue commun pour le classement des données V.G.H. [1].

L'expérience montre aujourd'hui que toutes les difficultés n'ont pu être encore levées. Il est encore difficile d'appliquer immédiatement à un nouvel avion les résultats globaux obtenus ; en effet, ces résultats reflètent à la fois la turbulence atmosphérique rencontrée par l'avion et sa propre fonction de transfert, d'autre part ils résultent tous de mesures effectuées dans des bandes passantes de fréquences différentes, ne conduisant en aucun cas à une bande passante universelle de longueur d'onde de la turbulence.

L'exposé ci-dessous partant des travaux de Harry PRESS et des récents résultats obtenus dans le cadre de l'A.G.A.R.D., présente une méthode de mesure de la distribution statistique de la composante verticale de la turbulence à partir de la distribution statistique de l'accélération du centre de gravité de la structure, à la suite d'un étalonnage préalable de l'avion, tout au moins en l'absence de manoeuvres du pilote. Dans le cas où de telles manoeuvres existent, une méthode est présentée qui permet de "débarrasser" les accélérations de l'avion des accélérations "parasites" dues au pilotage. Une comparaison entre les nombres de dépassements moyens par seconde des accélérations globales et des accélérations dues uniquement à la turbulence a permis de montrer que pour une bande passante donnée, caractéristique de l'avion, les comptages étaient pratiquement identiques dans les deux cas.

Dans ces conditions, moyennant un étalonnage préalable d'un avion d'une série, tous les avions de la même série deviennent de simples appareils de mesure directe de la distribution statistique de la turbulence atmosphérique.

II - UTILISATION D'UN AVION COMME INSTRUMENT DE MESURE DE LA TURBULENCE.-

2.1.- Rappel et extension de "hypothèse de Press".-

Harry PRESS considère que la turbulence atmosphérique est un processus localement stationnaire et gaussien caractérisé par une distribution statistique des écarts quadratiques moyens, $f(\sigma_w)$.

Pour chaque processus local, le nombre moyen de dépassements par seconde de l'amplitude est donné par la formule de Rice [2] :

$$N_w(x) = N_w(0) \exp\left(-\frac{x^2}{2\sigma_w^2}\right)$$

et pour l'ensemble des processus :

$$N_w(x) = \int_0^{+\infty} N_w(0,\sigma_w)\, f(\sigma_w) \exp\left(-\frac{x^2}{2\sigma_w^2}\right) d\sigma_w \qquad (1)$$

D'une manière plus générale, nous admettrons que la turbulence atmosphérique est caractérisée par une loi locale $g(\frac{x}{\sigma_w})$ supposée universelle et par une distribution des écarts quadratiques $f(\sigma_w)$; la formule (1) devant dans ce cas :

$$N_w(x) = \int_0^{+\infty} N_w(0,\sigma_w)\, f(\sigma_w)\, g(x/\sigma_w)\, d\sigma_w \qquad (2)$$

Dans la mesure où la turbulence est un processus localement stationnaire de modèle spectrale donné et d'échelle constante le nombre de passage par zéro est indépendant du σ_w, comme le montre la formule de Rice :

$$N_w(0) = \frac{1}{2\pi V} \cdot \frac{1}{\sigma_w} \left[\int_0^{+\infty} \omega^2 \, \Phi_w(\omega) \, d\omega \right]^{1/2}$$

avec

$$\Phi_w(\omega) = \sigma_w^2 \frac{L}{\pi} \cdot \frac{1 + 8/3\,(1{,}339\,\omega L/V)^2}{\left[1 + (1{,}339\,\omega L/V)^2\right]^{11/6}}$$

et la relation (2) devient :

$$N_w(x) = N_{w_0} \int_0^{+\infty} f(\sigma_w)\, g(x/\sigma_w)\, d\sigma_w \qquad (3)$$

2.2.- <u>Détermination des dépassements $N_w(x)$ à partir des dépassements $N_Y(x)$ d'un paramètre Y de réponse d'un avion.</u>

Dans la mesure où l'avion n'est soumis au cours de son vol qu'à la turbulence atmosphérique, le nombre moyen de dépassements par seconde du niveau est alors :

$$N_Y(x) = N_{Y_0} \int_0^{+\infty} f(\sigma_w)\, g(x/A_Y \sigma_w)\, d\sigma_w$$

où

$$A_Y = \frac{\sigma_Y}{\sigma_w}$$

de même, le nombre moyen de dépassement par seconde du niveau x/A_Y est :

$$N_Y(x/A_Y) = N_{Y_0} \int_0^{+\infty} f(\sigma_w)\, g\left(\frac{x/A_Y}{\sigma_w}\right) d\sigma_w \qquad (4)$$

Une comparaison entre les relations (3) et (4) montre immédiatement que :

$$N_w(x) = \frac{N_{w_0}}{N_{Y_0}} \cdot N_Y(x/A_Y) \qquad (5)$$

ou encore

$$\frac{N_{w/\sigma_w}(x)}{N_{w_0}} = \frac{N_{Y/\sigma_Y}(x)}{N_{Y_0}} \qquad (6)$$

Ces formules permettent à partir de la mesure des nombres de dépassements d'accélération de déterminer les dépassements correspondant de la turbulence, dès que l'on connait les nombres σ_Y/σ_W et N_{Wo}/N_{Yo} caractérisant l'étalonnage de l'avion.

Ces deux nombres sont calculables à partir de la fonction de transfert à la turbulence. Mais il est possible, aussi, de les obtenir à partir des densités spectralesde puissance de la turbulence et de l'accélération du centre de gravité au cours de quelques vols tests d'un avion richement équipé.

2.3.- Exploitation de la méthode.-

La méthode proposée ci-dessus suppose que les seules accélérations mesurées soient celles dues à la turbulence atmosphérique, les accélérations induites par les manoeuvres étant considérées comme négligeables. Toutes vérifications de la méthode doit donc se faire sur des tronçons de vol pour lesquels on s'est assuré que les actions du pilote avaient été pratiquement inexistantes.

Par ailleurs, si les vérifications en vol des fonctions de transfert calculées sur avions rigides, se sont avérées satisfaisantes, il n'en a pas été de même des vérifications sur avions souples, qui ont été souvent décevantes. Il a donc été décidé d'abandonner la méthode qui consistait à calculer sur plan les nombres σ_Y/σ_W et N_{Wo}/N_{Yo} .

Ces nombres ont, au contraire, été mesurés directement à la suite d'un étalonnage préalable de l'avion. On nous permettra à ce sujet de remarquer que, pour n'importe quelle mesure sur un appareil simple, le physicien juge indispensable de procéder à un étalonnage préalable.

Dans le même esprit, si l'instrument de mesure est ici l'avion, avec toute sa complexité, on peut difficilement éviter cette étape du travail.

Les contrôles expérimentaux de la relation (5) ont été effectués sur deux vols à basse altitude d'un MIRAGE III B 225 et quatre vols équivalents du TRANSALL C 160 A04.

Dans une première étape, une mesure fine de la turbulence permet de restituer la composante verticale des rafales à partir des enregistrements des réponses instantannées d'une girouette d'incidence, d'un gyromètre et d'un accéléromètre suivant une méthode couramment utilisée à l'O.N.E.R.A. [3], [4]. L'analyse spectrale des signaux obtenus a permis de vérifier que dans tous les cas la densité spectrale de la turbulence correspondait bien au modèle de Von Karman :

$$\Phi_w(f) = \frac{L}{\pi V} \cdot \frac{1 + 8/3\,(1{,}339\,\frac{2\pi f L}{V})^2}{\left[1 + (1{,}339\,2\pi f L/V)^2\right]^{11/6}}$$

Les σ_W et N_{W_o} calculés à partir de ce modèle spectral sont alors en accord avec ceux déduits des enregistrements de la turbulence.

Dans une deuxième étape les mesures des écarts quadratiques et des N_o de la réponse en accélération ont été comparées dans le cas du MIRAGE III B 225 aux résultats obtenus au cours des calculs de fonction de transfert. Les nombres d'étalonnage σ_Y/σ_W et N_{Wo}/N_{Yo} sont alors immédiatement calculables.

Les figures 1 et 2 présentent les résultats ainsi obtenus pour les deux avions.

L'étalonnage des avions effectué, la comparaison entre les nombres de dépassements de la turbulence W mesurés directement à partir des enregistrements en vol et ceux déduits à l'aide de la relation (5) des nombres de dépassements de l'accélération du centre de gravité est alors possible. Les courbes (3) et (4) montrent que la prévision des nombres de dépassements de turbulence au cours des vols tests a été très satisfaisantes.

2.4.- Influence de l'échelle et des paramètres avions.-

Les étalonnages de l'avion dépendent en fait de l'échelle de la turbulence rencontrée au cours des portions de vols sur lesquels ils ont été réalisés et qui en fait n'est pas constante, ce qui explique probablement les petites dispersions qui apparaissent sur les figures 1 et 2.

En tout état de cause cette dispersion ne peut être grande puisqu'il a été démontré [5] que le nombre $\sigma_{\ddot{z}}/\sigma_w$ variait comme la puissance un tiers de l'échelle et le nombre $N_{wo}/N_{\ddot{z}o}$ comme la puissance moins un tiers de l'échelle (fig. 5).

Ces étalonnages dépendent aussi de la fonction de transfert de l'avion qui évolue au cours du vol. Il est important de signaler que pour trois vols du TRANSALL A04 correspondant au profil de vol moyen

$$110\ m/s < V < 140\ m/s$$

$$40000\ kg < M < 44000\ kg$$

$$80\ m < z < 120\ m$$

l'ensemble des courbes réduites $N_{\ddot{z}/\sigma_{\ddot{z}}} / N_{\ddot{z}o}$, ou en tenant compte de la relation (6) $N_{w/\sigma_w}/N_{o,}$ obtenues pour quinze échantillons, d'une durée de huit minutes chacun, définit relativement bien une courbe standard (fi. 6) des nombres réduits de dépassements de la turbulence compte tenu des fluctuations de l'échelle de la turbulence et de la fonction de transfert de l'avion.

Dans ces conditions, tant que le pilote n'induit pas de facteur de charge important au cours du vol en turbulence, la prévision des nombres de dépassements de la turbulence est bonne à partir de la relation

$$N_{w(\alpha)} = \frac{N_{wo}}{N_{\ddot{z}o}} \cdot N_{\ddot{z}(\alpha/A)}$$

La courbure standard, telle qu'elle est présentée ci-dessus, se prête relativement bien à un classement condensé des masses d'informations recueillies sur les avions de ligne initialement étalonnés.

III - ELIMINATION DES EFFETS DU PILOTAGE LORS DE L'ANALYSE DES REPONSES D'UN AVION A LA TURBULENCE.-

3.1. - Pose du problème.-

Au cours des vols en turbulence d'un avion, l'accélération mesurée en un point de sa structure est la somme des réponses à deux excitations distinctes, d'une part la turbulence atmosphérique, d'autre part les ordres de braquage de la gouverne de profondeur (tout au moins tant que l'on ne s'intéresse qu'au mouvement longitudinal de l'avion) ;

Dans la mesure où il s'agit de caractériser les fonctions de transfert de l'avion relativement à la turbulence atmosphérique, il est indispensable de pouvoir éliminer de l'accélération totale mesurée en vol la partie due aux manoeuvres imposées par le pilote, et dans la mesure où ces accélérations sont collectées par des avions de ligne, l'installation permettant cette élimination doit être la plus réduite possible.

3.2.- Principe de la suppression des accélérations parasites.-

En admettant que l'avion a un comportement linéaire, et qu'il n'est excité que par la turbulence et les manoeuvres du pilote, l'accélération $\ddot{Z}_T(t)$ relevée au centre de gravité de l'avion est la somme de l'accélération $\ddot{Z}_w$ induite par la turbulence $W(t)$ et de l'accélération $\ddot{Z}_\beta$ induite par les braquages $\beta(t)$ de la gouverne de profondeur, soit :

$$\ddot{Z}_T(t) = \ddot{Z}_w(t) + \ddot{Z}_\beta(t) \qquad (7)$$

ou :

$$\ddot{Z}_T(t) = h_w(t) * W(t) + h_\beta(t) * \beta(t)$$

où $h_w(t)$ et $h_\beta(t)$ sont respectivement les réponses impulsionnelle à la turbulence et au braquage de gouverne ($*$ est le symbole du produit de convolution).

La méthode proposée consiste à enregistrer sur bande magnétique en même temps que $\ddot{Z}_T(t)$, le braquage des gouvernes $\beta(t)$, puis à fabriquer, après le vol, sur calculateur analogique, l'accélération :

$$\ddot{Z}_\beta = h_\beta * \beta$$

due aux manoeuvres et à la soustraire de l'accélération totale $\ddot{Z}_T(t)$ mesurée en vol.

Le résultat :

$$\ddot{Z}_T(t) - \ddot{Z}_\beta(t) = \ddot{Z}_w(t)$$

est bien l'accélération due à la seule turbulence, donc débarrassée des effets parasites des manoeuvres.

3.3.- Réalisation pratique.-

Dans le cadre des hypothèse faites en 3.1. et 3.2., le tangage et le déplacement vertical du centre de gravité résultent uniquement des deux équations :

$$\begin{cases} M\ddot{z} + \frac{1}{2}\rho V^2 S C_{z_i}(\theta - \dot{z}/V) = \frac{1}{2}\rho V^2 S C_{z\beta} \cdot \beta \\ I\ddot{\theta} + \frac{1}{2}\rho V^2 S l C_{mq}\dot{\theta} + \frac{1}{2}\rho V^2 S l C_{m_i}(\theta - \dot{z}/V) = \frac{1}{2}\rho V^2 S l C_{m\beta} \cdot \beta \end{cases}$$

si la seule excitation est le braquage des gouvernes de profondeur (c'est-à-dire pour $W(t) = 0$) et si on ne s'intéresse qu'aux petits mouvements de l'avion.

Un tel système différentiel est facilement réalisable sur un calculateur analogique dès que l'on connaît bien les coefficients aérodynamiques C_{z_i} , $C_{z\beta}$, C_{m_i} , C_{mq} et $C_{m\beta}$ de l'avion. La réalisation du bloc analogique de fabrication de l'accélération $\ddot{Z}_\beta$ est présentéesur la fig. 7.

Malheureusement, tous les coefficients de l'avion qui interviennent dans le calcul analogique ne sont pas connus avec la même précision et la fabrication de l'accélération de pilotage ne peut se faire sans contrôle permettant d'ajuster les coefficients aérodynamiques.

Pour ce faire, au cours d'un palier stabilisé en air calme (c'est-à-dire pour $W \approx 0$) le pilote impose des sollicitations en tangage à différentes fréquences. La turbulence étant pratiquement nulle, l'accélération $\ddot{Z}_w(t)$ qui lui est due est aussi nulle et d'après la relation (7) :

$$\ddot{Z}_T(t) = \ddot{Z}_\beta(t)$$

c'est-à-dire que l'accélération mesurée dans l'avion au cours du vol se réduit pratiquement à l'accélération; $\ddot{Z}_\beta$ induite par le pilote.

Il suffit donc de modifier légèrement les paramètres théoriques introduits dans le calcul analogique jusqu'à ce que l'on ait obtenu un minimum net pour la différence.

Le résultat de cette opération est présenté sur la fig. 8, on y trouve les ordres de braquage pour différentes fréquences, les accélérations mesurées et fabriquées ainsi que l'accélération résiduelle qui après suppression des actions du pilotage est pratiquement nulle pour un domaine important de fréquence.

3.4.- Comparaison des accélérations avant et après corrections des manoeuvres dues au pilote.-

Les coefficients du calcul analogique étant ainsi ajustés au cours de la mise au point précédente, l'opération de suppression des actions du pilote devient possible. En effet, pour des vols en turbulence où l'accélération totale $\ddot{Z}_T(t)$ mesurée au centre de gravité et les ordres $\rho(t)$ des gouvernes de profondeur sont enregistrés simultanément, l'introduction du braquage des gouvernes dans le bloc analogique simulant les équations du § 3.3.- permet la fabrication de l'accélération $\ddot{Z}_\rho(t)$ et en conséquence de l'accélération $\ddot{Z}_w(t)$ après la soustraction

$$\ddot{Z}_w = \ddot{Z}_T - \ddot{Z}_\rho$$

On peut contrôler le résultat qualitatif de cette opération et les effets importants des manoeuvres sur l'accélération au centre de gravité sur les figures 9a et 9b.

Des comptages de dépassement ont ensuite été réalisés sur $\ddot{Z}_T$ et $\ddot{Z}_w$ et les résultats ont été comparés pour différentes conditions de filtrage.

Les figures 10 et 11 présentent les résultats de cette opération. Pour deux échantillons de deux vols du TRANSALL, les comptages ont été effectués par une bande passante de filtrage variable caractérisée par une fréquence de coupure haute fixée à 10 Hz et une fréquence de coupure basse f_o variable.

La comparaison porte, pour les deux échantillons, sur quatre niveaux d'accélérations (0,1 ; 0,2 ; 0,3 et 0,4 g), pour lesquels le rapport entre les nombres moyens de comptage de $\ddot{Z}_T$ et de $\ddot{Z}_w$ est tracé en fonction de la fréquence de coupure basse f_o du filtre.

On remarque, par exemple, que pour le niveau de 0,4 g, on obtient sur l'échantillon de vol 144 :

- 2,2 fois plus de franchissement de ce niveau pour l'accélération totale que pour l'accélération due à la turbulence dans la bande 0,025 - 10 Hz
- 1,5 fois plus dans la bande 0,1 - 10 Hz
- 1,15 fois plus dans la bande 0,2 - 10 Hz
- le même nombre de franchissement dans la bande 0,25 - 10 Hz.

Dans tous les cas pour des coupures très basses, les différences de dépassements sont importantes et tendent à disparaître dès que f_o atteint 0,25 Hz, quelque soit le niveau considéré.

Il semble par conséquent que sur le TRANSALL A 04, des comptages de dépassements effectués sur l'accélération globale à travers un filtrage dans la bande (0,25 ; 10 Hz) fournissent des résultats pratiquement indépendants des manoeuvres effectuées par le pilote. Il est important de constater d'autre part que pour ce type d'avion souple, il semble que la fabrication du $\ddot{Z}_\rho(t)$ sur calculateur analogique à partir des équations de l'avion rigide soit largement suffisante compte tenu du domaine de fréquence où interviennent les manoeuvres du pilote et du domaine des fréquences de déformations de l'avion, respectivement (0-0,25 Hz et 2 - 10 Hz).

Bien entendu les résultats indiqués par les figures 10 et 11 n'ont qu'une valeur qualitative, en effet l'influence du pilotage sur les comptages dépend essentiellement de la durée des manoeuvres par rapport à la durée totale de l'échantillon. De même la fréquence 0,25 Hz citée ici comme limite des effets du pilotage est caractéristique de l'avion que nous avons utilisé et peut varier pour d'autres avions.

IV - EXPLOITATION DES DEUX METHODES.-

Il vient d'être montré qu'il était possible d'obtenir directement en vol l'accélération réellement induite sur l'avion par la turbulence, indépendamment de toute manoeuvre imposée par le pilote en cours de vol.

Il suffit pour cela de mesurer dans une bande de fréquence [f_o , f_{MAX}] l'accélération totale sur l'avion ; la fréquence f_o étant déterminée au cours de l'étalonnage préalable.

Il est clair que pour cette bande passante de fréquence l'utilisation de la méthode exposée au § II permet d'obtenir les courbes standards de la turbulence pour chaque profil de vol caractéristique. Un calcul simple permet ensuite de déterminer ce qu'auraient été ces courbes standards dans une autre bande passante de longueurs d'ondes, dès que l'on admet que la turbulence a un modèle spectral défini.

L'équipement d'un avion étalonné pourrait être alors constitué d'un accéléromètre, d'un passe bande calé sur [f_o , f_{MAX}] et d'un compteur de dépassement de niveaux du type compteur de level-crossing.

IV - CONCLUSION.-

Les deux méthodes exposées dans ce texte constituent, à notre avis, une amélioration du traitement des informations de masse recueillies de la turbulence; elles permettent de remonter aux statistiques de la turbulence rencontrée.

Actuellement les nombres caractéristiques du transfert $\sigma_{\ddot{z}}/\sigma_w$ et $N_{wo}/N_{\dot{z}_o}$ ne doivent pas être calculés, en raison des erreurs susceptibles d'entacher un tel calcul. Ces nombres doivent être "étalonnés" sur un avion richement équipé, au cours de quelques vols tests. Pendant ces vols la bande passante de fréquence, pour laquelle les accélérations induites par le pilote sont négligeables, doit être déterminée afin de définir les caractéristiques du système V.G.H. embarqué sur tous les autres avions de la même série.

REFERENCES.-

[1] Cyril G. PECKHAM — Flight-measured turbulence in the N.A.T.O. Nations - Rapport A.G.A.R.D. n° 555, (1967).

[2] J.O. RICE — Mathematical Analysis of random noise. Parts. 1 and 2. Bell Syst. Techn. Journal. Vol. XXIII N°3, July 1944 - Parts 3 and 4 Vol. XXIV N°1, January 1945.

[3] G. COUPRY — Réponse du MIRAGE III B 225 à la turbulence. Note Technique O.N.E.R.A., (1960) (non publiée).

[4] G. THOMASSET — Mesures en vol des réponses d'avions à la turbulence atmosphérique. Communication présentée aux Journées Françaises de l'Environnement, Paris 13-14 mars 1968 - Prétirage : T.P. O.N.E.R.A. n° 552.

[5] G. COUPRY — Vol en air turbulent. Note Technique O.N.E.R.A. N° 78, (1965).

[6] Harry PRESS — An approach to the predicting of the frequency distribution of gust loads on airplanes in normal operations. N.A.C.A. TN 2660, (1952).

MIRAGE III B.225

Comparaison "Prévision . Mesure"

Vol	W		Z̈ cdg				$A=\frac{\sigma_{\ddot{z}}}{\sigma_w}$	$\frac{N_{ow}}{N_{o\ddot{z}}}$
	σ^2	No	σ^2cal.	σ^2mes.	No cal.	No mes.		
80	0,174	1,21	0,464	0,500	1,68	1,45	1,64	0,72
81	0,195	1,31	0,563	0,660	1,72	1,44	1,70	0,76

Fig. 1

Transall C 160 A04

Comparaison "Prévision - Mesure"

Vol	W			Z̈ cdg			$A=\frac{\sigma''_z}{\sigma_w}$	$\frac{N_{ow}}{N_{o\ddot{z}}}$
	σ^2	N_o cal.	N_o mes.	σ^2	N_o cal.	N_o mes		
101	1,05	2,03	1,98	1,63	1,62	1,56	1,24	1,25
116	1,58	1,61	2,06	2,68	1,18	1,26	1,30	1,36
121	0,83	2,4	2,34	1,54	1,79	1,83	1,36	1,34
137	1,68	1,58	1,59	2,52	1,01	1,01	1,23	1,47

Nombre de transfert moyen

$$A = 1,28$$
$$\frac{N_{ow}}{N_{o\ddot{z}}} = 1,36$$

Fig. 2

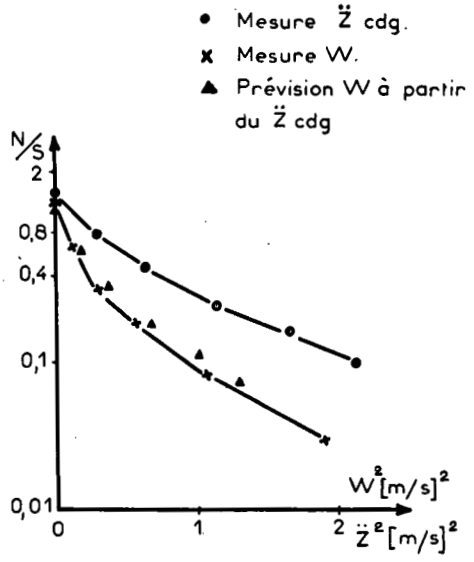


Fig. 3 MIRAGE III B

PRÉVISION DES NOMBRES DE DÉPASSEMENTS DE LA TURBULENCE

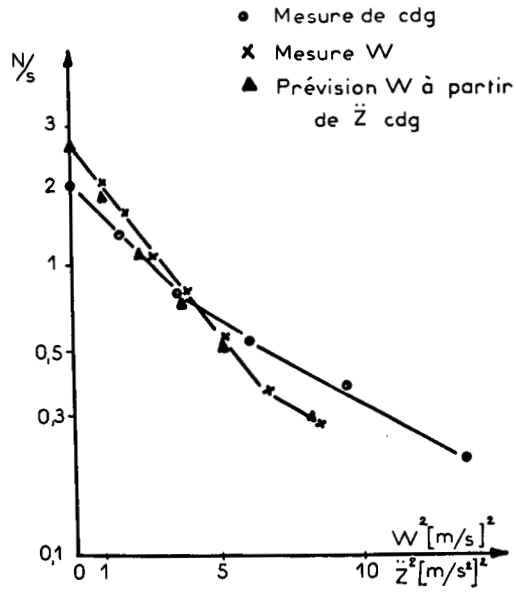


Fig. 4 TRANSALL C 160 A04
PRÉVISION DES NOMBRES DE DÉPASSEMENTS DE LA TURBULENCE

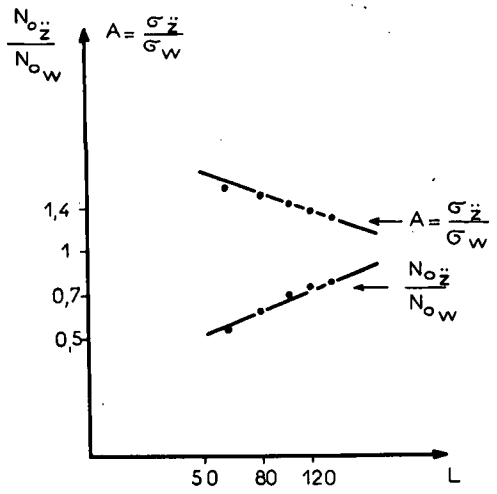


Fig. 5 VARIATION DES NOMBRES A ET $\frac{N_{o\ddot{z}}}{N_{ow}}$ AVEC L'ÉCHELLE.

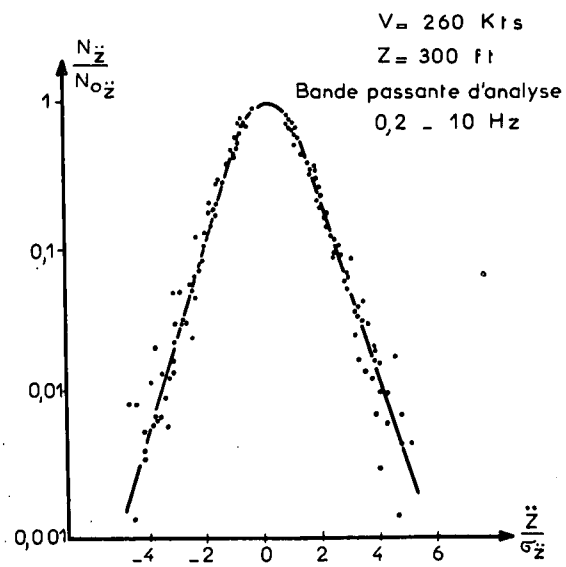


Fig. 6 TRANSALL C 160 AO4
BASSE ALTITUDE.

COURBE MOYENNE DES NOMBRES DE DÉPASSEMENTS RÉDUITS DE $\ddot{Z}$ cdg

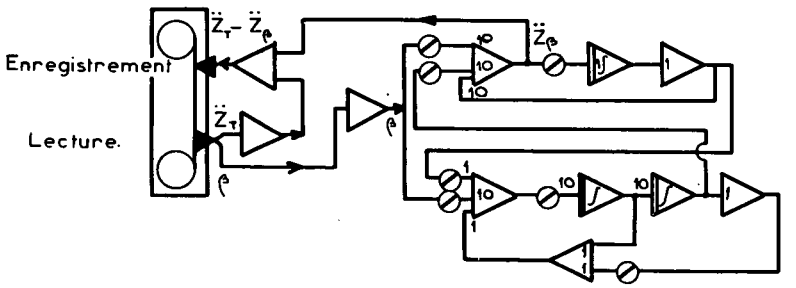
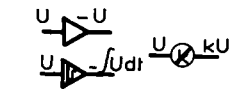


Fig. 7 Suppression des effets du pilotage longitudinal

Bloc analogique de simulation.



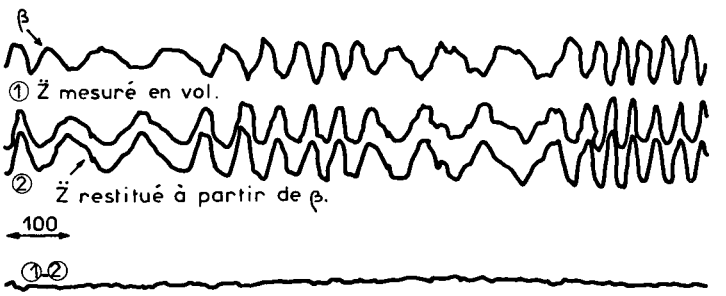
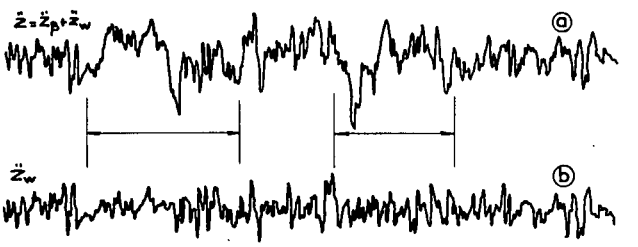


Fig. 8. SUPPRESSION DES EFFETS DU PILOTAGE.
VOL EN AIR CALME.



Fig·9 COMPARAISON ENTRE L'ACCÉLÉRATION TOTALE MESURÉE AU CENTRE DE GRAVITÉ DU TRANSALL C 160 ET L'ACCÉLÉRATION RÉELLEMENT INDUITE PAR LA TURBULENCE

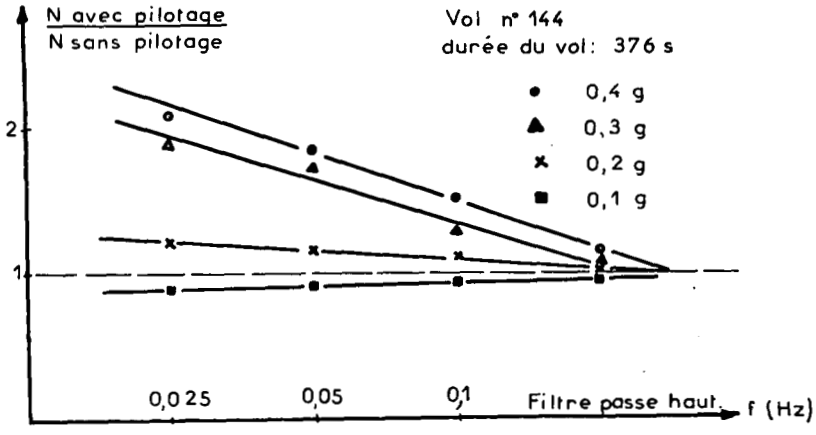


Fig. 10 COMPARAISONS DES NOMBRES DE DEPASSEMENT AVEC ET SANS PILOTAGE - (TRANSALL C 160 AO4)

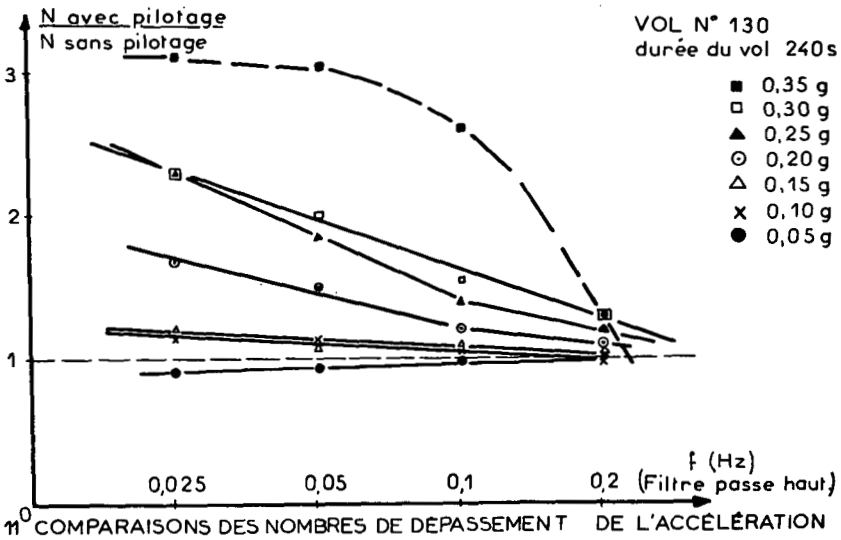


Fig. 11 COMPARAISONS DES NOMBRES DE DEPASSEMENT DE L'ACCÉLÉRATION C.d.G AVEC ET SANS PILOTAGE (TRANSALL C 160 AO4)

AEROELASTIC AND STRUCTURAL DYNAMIC INFLUENCES ON V/STOL HANDLING QUALITIES

R. G. LOEWY

University of Rochester

SUMMARY

Recent V/STOL aircraft developments--including helicopters--are reviewed as regards the influence of structural dynamic and aeroelastic characteristics on handling qualities. Parallels between problems of this kind on large fixed-wing aircraft and those of large helicopters are drawn. Some special challenges of stopped-rotor V/STOL's are considered, as are the affects of rotor isolation systems and other flexible mountings on the stability of aircraft response to control inputs and gust disturbances. A number of cases where the pilot-in-the-loop is important are also discussed.

I. Introduction

The background to the subject of structural dynamic and aeroelastic effects on V/STOL handling qualities is a rich one. There is, of course, a well-developed technology and literature on the subject of fixed-wing aircraft dynamics including the effects of static and dynamic aeroelasticity. In addition, there is an increasingly well-understood technology surrounding the stability and control of helicopters. Both areas are pertinent when rotary-wing type V/STOL aircraft are considered, so that the problems are extremely interesting and complex; but more to the point, sound starting points for their solution are available, and considerable work has been done.

A. Fixed-Wing Aircraft

When structural dynamics or aeroelastic effects must be considered in predicting the flying qualities of fixed-wing aircraft, the problems can conveniently be thought of as falling into one or more of three categories. In the first the effect of structural deformations can be accounted for by considering only their influence on the static or quasi-static aerodynamic derivatives. Local deformations on a control surface, resulting in more or less control moment than would be provided by a rigid surface (for a nominal input at the actuator attachment) is one example. A second might be reduced tail effectiveness as a result of fuselage deformations.

The second category of flexible airframe problems is one in which additional degrees of freedom must be considered. When inertia forces associated with structural deformations are important, the theoretical representation of the system must include additional equations of motion representing the flexible body motions, rather than just corrections to quasi-static aerodynamic coefficients. The third category involves auto-pilots or stability augmentation systems; here the importance of the flexible airframe deflections achieves a third kind of prominence because motion sensors will respond not just to the rigid body motions, but also to the effects of flexible body motion at their particular location.

Indicative of the material available in the literature dealing with the representation of airframe flexibility by modifying quasi-static aerodynamic coefficients are the brief discussions in Ref. 1. These include mention of the fact that at high enough speeds and with certain fixed surface-control surface characteristics, control can actually be reversed as a result of flexibility from what might ordinarily be expected, as in the case of aileron reversal. Further, structural deformations might increase aircraft sensitivity to either control or gusts as results, for example, from approaching the wing torsional divergence speed too closely.

The use of invacuo natural vibration modes as additional degrees of freedom to represent response in structural deformations, is described in more recent texts, such as Ref.2. At this point stability and control analyses differ from flutter analyses only in emphasis. In flutter analyses the flexible body motions are dominant, and while rigid body degrees of freedom are necessary, they can often be regarded only as refinements to the basic analysis. In stability and control analyses, the rigid body motions are of paramount concern so that including the flexible degrees of freedom are often considered a refinement. Clearly, as flexible body frequencies approach the rigid body frequencies and/or the couplings between them grow larger, the two analyses ultimately become indistinguishable one from the other. One parameter which acts as a powerful driving function in this direction is aircraft size. Fig. 1, summarizing the characteristics of actual fixed-wing aircraft, shows that the first symmetric bending mode frequency of the wing approaches the short period, longitudinal airplane-stability frequency at the higher gross weights. Since one of the critical flutter speeds usually involves primary wing-bending (as well as torsion) it's clear from this plot that rational flutter and stability and control analyses converge for large aircraft.

Whenever flexible body effects are accounted for by using normal vibratory modes as additional degrees of freedom, it is clear that this only approximates the infinite number of degrees of freedom required for a complete representation of continuous flexible bodies. A combination of the approaches used to handle the first and second category problems is therefore often used. That is, flexible body motions are used as additional degrees of freedom, and those higher modes not accounted for in that way are used to correct quasi-static aerodynamic coefficients. This subject is developed in Refs. 3 and 4, and the results allow minimizing the number of degrees of freedom and therefore the order of the equations to be solved while maintaining accuracy.

When auto-pilot and stability augmentation systems are involved, the placement of the sensors in a limber airframe is obviously important. This subject has been dealt with in many texts (for example Ref. 5), and reports (for example, Ref. 6). Fig. 2 is reproduced from Ref. 5 to show how the coupled rigid body, flexible body and automatic stability functions appear in a simplified block diagram. Ref. 7 and 8 are, perhaps, indicative of

the work performed with the intent of expediting the design of automatic control systems for aircraft accounting for flexible body dynamics. In the first of these, charts are provided for preliminary design purposes which account for flexible fuselage bending. The transfer function factors can be approximated for a given configuration by using these charts, compiled assuming that bending is describable by one of four standardized shapes. Required input data includes rigid airframe characteristics (e.g. airframe length, mass, and pitching moment of inertia; wing areas and locations; control types and location; and the flight envelope, that is, dynamic pressure and Mach number) and quantities typical of flexible characteristics (e.g. generalized mass, undamped natural frequencies, and structural damping, of the flexible modes; the modal deflections and slopes; and the sensor locations). In Ref. 8 it is noted that the open loop transfer function for a fuselage including elastic motion is in the same form as the open loop transfer function for the rigid body, but with corrections made up of transfer functions for flexible mode response with rigid body response as input. The method presented shows unity feedback techniques to be useful for estimating the effects of flexibility.

B. Helicopters

Turning to helicopter stability and control, one is likely to feel that this is a more recent subject. But von Karman published a paper as early as 1921 dealing with the hovering stability of a coaxial helicopter configuration (Ref. 9). Crocco also published on the same subject in 1923 (Ref. 10). These early authors, however, ignored the flexibility of rotor blades, so that except for their aerodynamic properties, the rotors in those analyses acted much like gyroscopes. In this same period, however, Juan De Cierva applied the flapping hinge to his autogyro designs, in order to reduce bending moments at the blade roots. This invention made it impossible for analysts to ignore the motion of rotor blades as flexible bodies in response to aerodynamic forces.

Although the helicopter industry still sometimes speaks of "rigid" rotors when referring to blades without hinges at the root, these hingelessrotors, so far as flying qualities are concerned, have more in common with rotors which have flapping hinges than with completely rigid rotors. This has been pointed out in Ref. 11, where the first natural flapwise frequency of rotating blades covering a wide range of practical parameters is shown to fall between 1.08 Ω and 1.50 Ω for rotors without flapping hinges. (Some supporting data for actual blades is shown in Fig. 3.) Considering that a rotating chain's first natural frequency for motions out of the plane of rotation is exactly 1.0 Ω , it's clear that hingeless rotors really do not behave very differently as regards the first out-of-plane natural frequency from a rotor with a flapping hinge.

When a present-day stability and control analyst considers a helicopter, it's quite clear from the foregoing discussion that rotor dynamics cannot be ignored. It's interesting, therefore, that the first successful helicopter stability analyses were formulated in the late 1930's without explicitly accounting for blade motions as separate degrees of freedom. Hohenemser was one of the earliest important contributors to this subject, with a paper published in 1939, Ref. 12. The basic assumptions made in these analyses were as follows:

A. Rotor blade motion is considered to take place in a plane containing the paths of the tips as they rotate, (i.e., the so-called "tip path plane"), in preference to accounting for individual blade motions.

B. Coupling between longitudinal and lateral degrees of freedom for the rotor or for the aircraft as a whole is ignored.

C. The resultant rotor force is assumed to be perpendicular to the tip path plane.

D. The rotor tip path plane is assumed to follow pitching or rolling angular velocities of the rotor shaft with a fixed angle between the rotor and shaft, this angle, however, being proportional to the pitching or rolling velocity that the rotor shaft is experiencing.

Considerations similar to those in Ref. 11 will show the first assumption to be reasonable. Both control and outside disturbances with major frequency components considerably lower than rotor speed will appear to the rotating blade as 1Ω excitation; with the blade's fundamental mode close to 1 Ω , the response of the blade tips will approximate planar motion.

The second assumption can be made with impunity in fixed-wing aircraft design because of the, usually, nearly perfect symmetry about the longitudinal centerplane of the aircraft. For a single lifting-rotor helicopter, the sense of rotation of the large lifting-rotor destroys this symmetry, and ignoring the coupling between longitudinal and lateral degrees of freedom can lead to appreciable errors for these types.

The third assumption is still more serious and almost always is unconservative as regards stability. R. H. Miller first showed in Ref. 13 that the in-plane aerodynamic force on a rotor is a destabilizing influence since it reduces the damping in roll and pitch of a rotor. Amer (Ref.14) explored this effect further and corroborated Miller's theoretical predictions in flight tests. In fact, the latter reference shows that if a rotor is operating with high enough inflow velocities, the effect of induced drag variations is so destabilizing as to overcome the positive damping in roll or pitch for a rotor without offset flapping hinges.

While they may lead to some error, the first three of the assumptions discussed above are intuitively appealing. The fourth is rather difficult to visualize and suggests a short discussion of rotor dynamics and basic rotary-wing controls. These controls are of two types; one called "collective pitch", where all blades change pitch by the same amount at the same time; the other known as "cyclic pitch", where the pitch varies sinusoidally as the blade traverses the azimuth, each blade experiencing the same pitch angle when it reaches the same place in azimuth previously occupied by the other blades. Collective pitch changes the total thrust of the rotor and its torque requirements. Cyclic pitch changes the tilt of the thrust vector without changing its magnitude or the torque required, at least to a first approximation. Both of these statements apply to the hovering condition; in forward flight, however, changes in collective will also change the thrust vector tilt and changes in cyclic will affect both the magnitude of the thrust vector and the torque required to drive the rotor. This is easily seen by picturing the differences or lack of them between aerodynamic forces on the "advancing blade" (where rotational and forward velocities add) and on the "retreating" blade (where they subtract) for cases where there is zero blade pitch and then when collective or cyclic is added.

Cyclic pitch is generally applied to rotors through a "swash-plate". This is essentially a large bearing, usually with its inner race gimballed to a non-rotating "sleeve" which slides up and down the rotor shaft. The gimbals allow it to tilt with respect to the rotor shaft and the links which change the pitch of individual blades have their lower ends attached to the outer race of the bearing or swash-plate. Thus, when the swash-plate slides up and down the shaft, the blades change their pitch collectively, and when the swash-plate tilts, the angles change cyclically. Flexibility in these members was not important in the era when cable control systems provided the fixity for the swash-plate. More recently, full-power boost actuators are mounted directly between the swash-plate and relatively rigid structure. In this situation the swash-plate often is the softest element in the control system, and because the actuators provide fixity for the swash-plate at a discreet number of points, the spring restraint in pitch experienced by the blade varies around the azimuth of rotation.

The tilt of the thrust vector which results from cyclic inputs is in general not in the same direction as the tilt of the swash-plate, because of rotor blade dynamics. This azimuthal phase angle between swash-plate tilt and thrust vector tilt is, for constant values of these angles and to the extent that blade motion can be represented by the fundamental invacuo natural vibratory modes, a function of the ratio of that natural frequency to rotational speed and the ratio of damping to critical damping in that mode. Fig. 4, reproduced from Ref. 11, illustrates these dependencies. The $\omega_1 = \Omega$ value for ϕ would be expected to be 90°, as shown, regardless of damping ratio, since a fixed swash-plate angle provides a once per revolution pitch oscillation as experienced by the blade, and if $\omega_1 = \Omega$, this is the classical case of a single degree of freedom system excited at resonance.

II. Rotors as Elements in Helicopter Control Systems

In this section differences in the dynamic response between hinged and hingeless rotors are considered, particularly as regards the response of the lifting rotor to non-steady control inputs, to check the accuracy of approximation D in the preceding section. The equation of motion for the first flapping or flap-bending mode is:

$$\ddot{\beta}_1 + A\dot{\beta}_1 + \omega_1^2\beta_1 = B\,\Theta\,\sin(\Omega t + \phi) \qquad \text{Eq. (1)}$$

This equation is the same as Equation 11 in Ref. 11, except that Θ is thought of as variable in time, and

$$A = \begin{cases} \Omega\gamma\left(\frac{1}{12} + \frac{4}{9\pi^2}\right) \\ \frac{\Omega\gamma}{8} \end{cases} \quad ; \quad B = \begin{cases} \Omega^2\gamma\frac{2}{9}\left(\frac{1}{3} + \frac{1}{\pi}\right) & \text{for cantilevered blades} \\ \frac{\Omega^2\gamma}{8} & \text{for blades hinged at the centerline of rotation.} \end{cases}$$

Where: γ = Blade Lock number = $\frac{\pi \rho C R^4}{I}$; ρ = air mass density

I = Moment of inertia of rigid blade about centerline of rotation.

R = Blade radius.

C = Blade chord.

Ω = Rotor speed (rads./sec.)

ω_1 = First flapping or flap-bending natural frequency in a vacuum.

θ = Blade pitch angle. (radians)

ϕ = Azimuthal phase angle, or control "bias".

β_1 = Deflection response at blade tip in first flap (flap-bending) mode.

These expressions assume a $\frac{1}{2}\left(1 - \cos \pi \frac{r}{R}\right)$ deflection for the cantilever blade; C and blade mass are assumed constant with the running station radius, r .

If the swash plate is assumed to be subjected to motion of the type e^{st} then the blades will be subject to the pitch angle variations $\theta_0 e^{(i\Omega + s)t}$

if $\phi = 0$, and the blade will respond with $\beta_1 = \theta_0 \Gamma e^{i(\Omega t - \Phi) + st}$

where:

$$\Gamma = \frac{B}{\Omega^2 \sqrt{\left\{\left(\frac{s}{\Omega}\right)^2 + \left(\frac{\omega_1}{\Omega}\right)^2 - 1 + \frac{A}{\Omega}\frac{s}{\Omega}\right\}^2 + 4\left\{\frac{s}{\Omega} + \frac{A}{2\Omega}\right\}^2}}$$

$$\Phi = \tan^{-1} \frac{2\left[\frac{s}{\Omega} + \frac{A}{2\Omega}\right]}{\left[\left(\frac{s}{\Omega}\right)^2 + \left(\frac{\omega_1}{\Omega}\right)^2 - 1 + \frac{A}{\Omega}\frac{s}{\Omega}\right]}$$

To achieve the desired tip path plane in steady flight, however, the control will be "biased" by the angle Φ when $s \to 0$, i.e.

$$\Phi_{s \to 0} \triangleq \phi = \tan^{-1} \frac{\frac{A}{\Omega}}{\left(\frac{\omega_1}{\Omega}\right)^2 - 1}$$

which is the expression given in Ref. 11 and plotted in Fig. 4. Hence, the control will actually be $\theta_0 e^{[(s + i\Omega)t + \phi]} \triangleq \theta_1 \cos(\Omega t + \phi) + \theta_2 i \sin(\Omega t + \phi)$

so that $\theta_1 \triangleq$ longitudinal control and $\theta_2 \triangleq$ lateral control analysis for the response in terms of longitudinal and lateral motions i.e. $\beta_1 \triangleq \beta_c \cos \Omega t + \beta_s \sin \Omega t$ yields the transfer functions

Eq. (2)
$$\begin{cases} \dfrac{\bar{\beta}_s}{\bar{\theta}_2} = \dfrac{\bar{\beta}_c}{\bar{\theta}_1} = \dfrac{B}{\Omega^2}\left[\dfrac{\left\{\left(\frac{s}{\Omega}\right)^2 + \frac{s}{\Omega}\frac{A}{\Omega} + \left(\frac{\omega_1}{\Omega}\right)^2 - 1\right\}}{\Delta}\cos\phi + \dfrac{\frac{A}{\Omega}\left(\frac{2s}{A} + 1\right)}{\Delta}\sin\phi\right] \\ -\dfrac{\bar{\beta}_s}{\bar{\theta}_1} = \dfrac{\bar{\beta}_c}{\bar{\theta}_2} = \dfrac{B}{\Omega^2}\left[\dfrac{\frac{A}{\Omega}\left(\frac{2s}{A} + 1\right)}{\Delta}\cos\phi - \dfrac{\left\{\left(\frac{s}{\Omega}\right)^2 + \frac{s}{\Omega}\frac{A}{\Omega} + \left(\frac{\omega_1}{\Omega}\right)^2 - 1\right\}}{\Delta}\sin\phi\right] \end{cases}$$

where : $$\Delta \triangleq \left[\left(\frac{s}{\Omega}\right)^2 + \left(\frac{\omega_1}{\Omega}\right)^2 - 1 + \frac{A}{\Omega}\frac{s}{\Omega}\right]^2 + 4\left[\frac{s}{\Omega} + \frac{A}{2\Omega}\right]^2$$

For the case where $\phi = 90^\circ$ and $\frac{\omega_1}{\Omega} = 1.0$, one obtains the usual transfer function for a rigid blade with a flapping hinge on the centerline of rotation. This is shown as the solid line on Fig. 5, for response to direct control, i.e. longitudinal or lateral flapping for longitudinal or lateral control, respectively. The dashed curve is for a uniform cantilever rotor with (1 − cosine) deflection shape and $\frac{\omega_1}{\Omega} = 1.5$, normalized for unity gain at $\omega = 0$.

The "centerline" curve is for the first order approximation $\frac{\bar{\beta}_s}{\bar{\theta}_2} = \frac{\bar{\beta}_c}{\bar{\theta}_1} = \frac{\gamma\Omega/16}{s + \gamma\Omega/16}$

It is seen that for frequencies up to about 10 rad/sec, which is the range of interest for aircraft stability, the frequency response characteristics are well represented by the approximation.

Now, if $\theta_{1,2}$ is considered to be a "ramp" function then the transform of $\theta_{1,2}$ equals

$$\bar{\theta}_{1,2} = \frac{\theta_t}{s^2}$$

where θ_t is the slope of the ramp; i.e. degrees of tilt per unit time.

Therefore, the tip path plane tilt* $\bar{\beta}_{1,2}$ will be given by $\bar{\beta}_{1,2} = \frac{\theta_t a}{s^2} \frac{1}{(s+a)}$

Where a equals $\frac{\gamma\Omega}{16}$. Now the lag of the tip path plane with respect to the shaft angle $\Delta\bar{\beta}_{1,2} \triangleq \bar{\theta}_{1,2} - \bar{\beta}_{1,2}$ equals $\frac{\theta_t}{s^2} - \frac{\theta_t a}{s^2(s+a)}$.

This can be rearranged as $\theta_t / s(s+a)$, which after transformation to real time yields $\Delta\beta_{1,2} = \frac{\theta_t}{a}\left(1 - e^{-at}\right)$. Therefore as t approaches infinity; that is, the steady state case, $\Delta\beta_{1,2}$, or the lag of the tip path plane with respect to the shaft, does indeed equal $16/\gamma\Omega$ times the angular rate of the shaft tilt.

If the stability of the system is in question, however, it may be necessary to represent the spectrum of the rotor response characteristics beyond 10 rads./sec. In this case Eq. (2) should be used for hingeless rotors.

Fig. 6 shows the hinged ($\frac{\omega_1}{\Omega} = 1$) and hingeless ($\frac{\omega_1}{\Omega} = 1.5$) rotor response in the plane normal to that about which the flapping or flap-bending is required. This curve for the hingeless rotor has also been normalized by the same factor which makes the direct control gain unity at $\omega = 0$. As would be expected--since the swash plate bias was specifically selected for this purpose--the cross-control response for $\omega = 0$ has zero gain. The "break points" for the curves in these figures (5 & 6), being associated with the fundamental bending frequency will, of course, occur at lower and lower frequencies as the size of rotors grow. The influence of rotor aeroelasticity and dynamics will, therefore, become more involved with aircraft flying qualities as size increases, in a manner analogous to the fixed-wing case.

A. Rotor Size Effects

Whereas Fig. 3 shows values of first flap/flap-bending natural frequencies for actual blades both hinged and hingeless, one can predict the probable dimensional natural frequencies for large rotors, by examining the relations given in Ref. 15 and assuming that rotational tip speeds, V_t, will continue to fall in the usual ranges, roughly between 600 to 800 '/sec. Cantilever natural frequencies tend to remain constant ratios of rotational speed if the design is simply scaled upward as R increases, since, as shown in Ref. 15,

$$\frac{\omega_{\beta n}}{\Omega} = \sqrt{\left(\frac{a_n}{\Omega}\right)^2 \frac{E I_o}{m_o R^4} + \left(K_o + K_1 \epsilon\right)} \neq F(R)$$

where
- I_o = root cross section moment of inertia
- m_o = root mass per length
- a_n = non-rotating natural frequency constant
- $\Omega = V_t/R$

*Actually this and the following barred quantities are Laplace transforms.

K_o, K_1 = Southwell coefficients

ϵ = blade offset from the shaft

and a_n, K_o, K_1 are functions of mass and stiffness distribution with radius. Fig. 7 uses these generalized ideas to show flap-bending natural frequencies likely to be encountered with hingeless rotors as they grow in size. The lower limit line reflects the fact that a pitch angle of 20° will lower the flap-bending frequency according to the approximation $\omega_{n\theta}^2 = \omega_n^2 - 5n^2\theta_o$. (Ref. 15).

To the extent that disc-loading (i.e. the weight carried per square foot of lifting-rotor area) tends to be constant at around 10 to 12 #/,² for large helicopters, the abscissa of this plot can easily be converted to gross weight, and thus is directly analogous to Fig. 1, for fixed-wing aircraft.

Similar arguments are valid for in-plane natural frequencies. In this case, however, the designer has more latitude in the range of frequency ratios ω_g/Ω he desires. The bending stiffness for in-plane motions is determined by the fourth power of the chordwise dimension rather than blade thickness, and centrifugal stiffening is less for bending in the plane of rotation. Minimum weight considerations will probably keep the maximum values of fundamental in-plate bending natural frequency below about 1.5Ω ; however, the lower values may go as low as 0.5Ω for hingeless rotors. This is suggested by the values of first in-plane natural frequency obtained with actual rotors shown on Fig. 7.

III. Man-machine interface problems.

Two categories of structural dynamic problems occur in which the human pilot plays a part. One is where the structural response of the aircraft or some part of it is in a range where the pilot can inadvertantly force it at a resonant frequency. The other is encountered when the pilot provides a means (or another means) of "closing the loop" between aircraft response and control input, so that unstable oscillations can result. This second category includes cases identified as P.I.O., for "pilot induced oscillations", which are specifically forbade by paragraph 2.11of Ref. 16.

A. Pilot-Forced Structural Responses

Fig. 1. is illustrative of situations in which combinations of aircraft rigid body motion and flexible airframe motions "invite" excitation by the pilot. Not only are the short-period flight stability and the first symmetric wing-bending frequencies converging as subsonic aircraft get bigger, but they are both dropping; the pilot's maximum ability to move flight controls on the other hand remains fixed.

Characterization of human pilot behavior is useful in attempting to understand such man-machine interactions. In Ref. 17 Ashkenas and McRuer point out that, in control system parlance, human behavior includes (1) "mechanization" of feedback loops, by sensing what has happened and applying corrective control inputs; (2) "mechanization" of forward loops, by anticipating what is going to be required--based on previous knowledge of the system and its mission--and applying appropriate control inputs; and (3) "adaptation" by adjusting his (and the system) gains and time constants within the ranges available to account for changes either in circumstances or in some part of the system or both.

Thinking of the human pilot as a loop-closer, the transfer function $\frac{K_p e^{-\tau s}}{T_N S + 1}$ is proposed in Ref. 18, where S is the complex Laplace-transformed time variable, and K_p is the gain, a measure of how much control output the pilot has decided to provide as a linear function of a given disturbance or aircraft response, τ = reaction time delay (.12 to .2 sec.), and T_N = a neuromuscular lag, which is somewhat adjustable but probably not below about 0.1 sec.

Since lag time constants like T_N are interpretable, for first order systems, as the time for the response to reach about 65% of the final value following a step function input, the sum of τ and T_N should be an approximation to what might be measured in flight tests as the time required for the pilot to respond substantially to step-type disturbances. Tests to determine these parameters have been conducted, are reported (for example) in Ref. 19, and form the basis for the proposed human pilot transfer functions. With this kind of frequency capability, it is clear that a pilot could, in fact, drive the first wing-bending mode of the larger aircraft at resonance, especially with the help of power-boosted controls, since the oscillatory frequency required is well within his frequency output capability. If the total of aerodynamic and structural damping in that mode is high, the

wing a very lightly stressed design, or the aircraft rigid body response sufficiently sluggish, this potential control resonance may not be important. On the other hand, none of this may be true (certainly one would hope the last is not) and the structure might still be in no danger from this loading, if significant cycling of the controls produced unpleasant motion at the pilot's station or drove an appropriate and reliable display. In this case, however, the pilot's gain-adjusting adaptation is called on to limit his control input in given frequency regimes. As has been shown in Ref. 20 and others, the magnitude of K_p which a pilot must provide, is directly correlatable with his opinion of the aircraft as a satisfactory machine. A typical plot shown in Fig. 8, reproduced from Ref. 20 data, shows this effect. Thus, if structural response requires the pilot to reduce his gain to a value viewed as a transfer function factor beyond "what pilots like", that aircraft will probably not be regarded as having satisfactory flying qualities.

Large helicopters are susceptible in this regard for two reasons. First, the helicopter is unstable in hover, requiring control inputs from a pilot, a gyro-bar, or some other stability augmentation system to maintain attitude. Typical periods of the oscillatory roll mode in hover are around 10 sec., but the rate of divergence can be so high as to double amplitudes every quarter cycle for aircraft with articulated lifting rotors. Second, the low natural frequencies in the plane of rotation, shown in Fig. 7, have no counterpart in the fixed-wing case, where chordwise stiffness is relatively much higher.

Bending normal to the chord plane has the benefit of relatively high aerodynamic damping. Bending in the chordwise direction--which is the major bending component in the plane of rotation for rotors which are neither highly twisted nor operating at high geometric pitch-has of the order of 1% of the aerodynamic damping available to flap-bending motions.

A prime criterion for structural strength has always been that stress per unit aircraft acceleration be acceptably low. The size effects on both fixed and rotary wing aircraft shown in Figs. 1 and 7 extend the interpretation of this criterion to the kind of oscillatory accelerations which the pilot, for one reason or another, may command.

There is another problem of this sort to which tail rotor helicopters are susceptible and has occurred in at least one instance on a tilt-wing V/STOL aircraft. This concerns control to a tail rotor or fan, whose function is to provide yawing or pitching moments about the aircraft C.G. Yaw control is, perhaps, most critical because it is not uncommon for the pilot of a hovering V/STOL aircraft to want to slew his aircraft rapidly from one compass heading to another. In fact, it is not unusual for a pilot to build up a rather high angular rate in yaw, in hover, and rapidly reverse the yaw rate. These kinds of control inputs, of course, will result in abrupt changes in torque on the shaft which drives the tail rotor or tail fan. On one of the early V/STOL flying test-beds, the VZ-2, there was, in fact, a tail drive-shaft failure directly attributable to pilot inputs. Fortunately, the incident occurred with the aircraft hovering close to the ground, and no damage other than the broken tail shaft was incurred. Attempts to change the natural frequency of the tail fan drive system, in this case, involved considerable weight increases. The problem was resolved by putting a fluid coupling in the shaft system, so that large impulsive torques were counteracted by more inertia relief and considerable damping was added to the system. The use of such devices, as well as a slip clutch, which was also considered, is not generally desirable, however, since they also add weight and affect maintenance and reliability. Limiting available control or how rapidly it can be applied is also most often unsatisfactory.

A simple design criterion can be proposed, however, by regarding the tail rotor-fan and shaft system as a single degree of freedom torsional system. If the effective polar moment of inertia of the tail rotor (plus close gear boxes) is called I_ψ, the equivalent tail shaft spring rate at the tail rotor, k, and the angular motion ψ, then the equation of motion is $I_\psi \ddot{\psi} + k\psi$ = applied aerodynamic torque. Since in this approximation the tail drive shaft is pictured as "fixed" at some driving point near the aircraft C.G., ψ also represents the twist angle which determines shaft stress. The aerodynamic torque can be written

$$-N\int_0^R \left[C_D + \frac{\partial C_D}{\partial \theta}\Delta\theta\right]\tfrac{1}{2}\rho(\Omega+\dot{\psi})^2 r^2 c\, dr \cong -(\Omega^2 + 2\Omega\dot{\psi})(K\Delta\theta + \bar{K})$$

where N = number of blades; C_D = section drag coefficient

$\Delta\theta$ is the change in tail-rotor (collective) pitch

$$K \triangleq N\frac{\partial C_D}{\partial \theta}\tfrac{1}{2}\rho c\frac{R^4}{4} \; ; \; \bar{K} \triangleq N C_D \tfrac{1}{2}\rho c\frac{R^4}{4}$$

and constant blade characteristics are assumed with respect to span.

The Laplace-transformed equation of motion then appears as the standard second order system

$$\left(s^2 + \frac{2\Omega[K\Delta\theta+\bar{K}]}{I_\psi}s + \frac{k}{I_\psi}\right)\bar{\psi}(s) = -\frac{K\Omega^2}{I_\psi}\frac{\Delta\theta_0}{s}$$

where $\Delta\theta_o$ is the magnitude of a step input in tail rotor pitch and the natural frequency ω_ψ and critical damping ratio ζ_ψ of the system are given by

$$\omega_\psi \triangleq \sqrt{\frac{k}{I_\psi}} \quad ; \quad \zeta_\psi \triangleq \frac{\Omega}{\sqrt{I_\psi k}}\left(K_{\Delta\theta} + \bar{K}\right)$$

For such systems the maximum amplitude occurs at a time corresponding to $\omega_\psi t \approx 3.2$, independent of $\zeta_\psi < 1.0$. Thus the maximum twist angle is approximated by

$$\psi_{MAX} \cong \left[1 - \frac{e^{-3.2\zeta_\psi}}{\sqrt{1-\zeta_\psi^2}} \sin\left(3.2\sqrt{1-\zeta_\psi^2} + \cos^{-1}\zeta_\psi\right)\right] \frac{\zeta_\psi \Omega}{I_\psi \omega_\psi}$$

Minimizing this function or, at least, constraining its value to an acceptable corresponding stress level, therefore, provides a criterion for tail rotor-fan, drive system characteristics.

Experience suggests that this is a critical design situation only when shafting is designed for low steady torques (high speed shafting), and when small diameter rotor-fans are used. If a similar problem were to become important, say, for the interconnecting shaft of a prop-rotor type V/STOL--with engines mounted inboard of the rotors or with an engine out--in the helicopter mode, it would seem to be more likely to become a design condition for a tilt-wing than a tilt-rotor type.

B. Pilot-Induced Oscillations

An interesting case of P.I.O. has been encountered in the operation of helicopters with sling loads. As described in Refs. 21 and 22, this instability is intimately tied to the "natural" control motion of the collective pitch lever. That is, by raising the lever in hover, the aircraft will move vertically upward, and vice versa. With this arrangement, if the aircraft should oscillate vertically, there is a natural tendency for the pilot to put vertical oscillatory control into collective pitch. This results from the dynamics of the pilot's body--in particular his forearm, viewed as hinged at the elbow--and from the seat suspension. A mathematical model for this situation is shown in Fig. 9 reproduced from Ref. 21, where the pilot, his seat, forearm and collective pitch lever are all lumped as one mass characteristic mounted on a spring and damper. Some of the critical parameters in this situation were identified in Ref. 21 as the ratio of slung to fuselage mass μ_m; the relative sensitivity of the collective pitch control, β_T = (vertical g's per inch of stick deflection divided by the natural frequency of the pilot-seat combination, $\omega_s)^2$; the natural frequency of the slung load (on its cable, helicopter end fixed) compared to ω_s, defined as $\beta_\ell \triangleq \left(\frac{\omega_\ell}{\omega_s}\right)^2$; the critical damping ratio of the pilot in his seat, $\zeta_s = \frac{c_s}{2\omega_s}$; and the lag in rotor force response, τ, to collective control, non-dimensionalized by the ratio of oscillation to seat frequency ratio ω/ω_s. Situations such as dealt with in Ref. 21 have, in fact, been encountered in flight, and in some cases the slung load has had to be jettisoned. One way to avoid the problem is to have a collective pitch lever which can be locked in any given position. This would destroy the feedback between fuselage oscillatory motion and the load that the rotor puts on the fuselage in response to the collective pitch stick. In one scheme, when the pilot wishes to change collective pitch, he depresses a button which disengages the lock and gives him freedom to move the collective pitch to the next position, where he may release the button and momentarily lock the collective pitch stick again.

It is not difficult to imagine a similar phenomenon being encountered in designing tilt rotor or tilt wing V/STOL aircraft. Fig. 10 attempts to show that in hover position, the symmetric wing bending mode of a V/STOL aircraft can give the kind of freedom to the prop-rotor engine Nacelle package that the slung load has from the helicopter fuselage. A comparison of Figs. 9 and 10 reveals that the only difference is in where the pilot is assumed to sit. If the comparison is drawn on the basis of where the rotor acts, then the V/STOL pilot appears to be sitting on the equivalent of the slung load. The Laplace transformed equations of motion for the helicopter case as given in and using the notation of Ref. 21 (See Fig. 9) are as follows:

$$\begin{bmatrix} s^2 + sc_s + \omega_s^2 & 0 & s^2 \\ -\omega_T^2 e^{-s\tau} & s^2 + \omega_\ell^2 \mu_m & -\omega_\ell^2 \mu_m \\ 0 & -\omega_\ell^2 & s^2 + \omega_\ell^2 \end{bmatrix} \begin{bmatrix} \bar{z}_p \\ \bar{z}_f \\ \bar{z}_\ell \end{bmatrix} = 0$$

The equivalent equations of motion for the V/STOL aircraft case using the notation in Fig. 10, are as follows:

$$\begin{bmatrix} s^2 + sC_s + \omega_s^2 & s^2 & 0 \\ -\omega_T^2 e^{-s\tau} & s^2 + sC_f + \mu_m \omega_\ell^2 & -\mu_m \omega_\ell^2 \\ 0 & -\omega_\ell^2 & s^2 + \omega_\ell^2 \end{bmatrix} \begin{bmatrix} z_p \\ z_f \\ z_\ell \end{bmatrix} = 0$$

Comparison of these equations shows that the V/STOL aircraft case is, in fact, mathematically somewhat simpler.

Several cases were run for the V/STOL aircraft with the following results; if $\beta_\ell = 0.3$, $\mu_m = 0.5$, $\eta_s = 0.25$, and $\beta_T = 0.3$ the system seems to be stable for $\omega_s\tau = 3$ and unstable for $\omega_s\tau = 0$. This analysis, like that of Ref. 21, is very conservative, in that the damping of the rotor due to aerodynamics, that due to the wing (or cable), and that in the seat system have all been neglected as regards the motion of the principle masses in the system. The results noted above are suspect since they indicate that a system with more lag in the feedback loop is more stable than one with less lag. Still, it is important that V/STOL aircraft designers take care to see that this type of P.I.O. will not occur, since the prop-rotor Nacelle package cannot be dropped like a slung load. It should be noted that some recent V/STOL aircraft are proposing to use a throttle-type lever as vertical flight control rather than a collective pitch lever. This would appear to be less natural, and it remains to be seen whether it will be satisfactory to the average pilot for the missions intended. On the other hand, a throttle type control is likely to completely avoid the kind of instability discussed here.

IV. Flexibly-Mounted Rotor-Propellers

Two V/STOL configuration and flight condition combinations can be foreseen in which rotor-propellers will operate in the helicopter state with their hubs flexibly mounted. In one of these, the hub mounting flexibility is a matter of design decision; in the other it will be largely unavoidable.

Firstly, advanced helicopters and partially unloaded compounds will use lifting rotors at high forward speeds, say between 200 and 250 knots. It is reasonable to think that the vibration levels of many of these aircraft are likely to be satisfactory only if the rotors are vibration-isolated from the fuselage. The low rotational frequencies associated with rotors require correspondingly low natural frequencies in the rotor mounting system for effective isolation. As regards handling qualities, however, this same flexibility is likely to introduce unacceptable lags in the application of control moments unless particular care is taken.

One approach to these contradictory requirements is to have an active isolation system designed to center the rotor hub with respect to the fuselage, but incapable of responding to motions above a certain frequency. In an active system this frequency can be placed relatively close to that of the lowest offending shaking frequency--normally fundamental blade-passage frequency. Such a system is described in Ref. 23.

Another approach provides an isolation system which "passes" i.e. is "soft" for only the one frequency which is most offensive and which one wishes to isolate from the fuselage. This is a "notched filter" system and is described in Ref. 24.

The second flexibly-mounted hub situation involves tilt prop-rotors at lower forward speeds. In this case the flexibility of the hub mounting is associated with fundamental wing bending-torsion, and will probably be only as stiff as weight trade-offs will allow. For the helicopter-compound with isolated rotors or tilt prop-rotor type V/STOL, the flexibility of the rotor mounting can be an important flight stability consideration, especially when stability augmentation or autopilot systems are used. One of the important modes of

motion is the combination of individual blade motion in the plane of rotation which gives rise to displacement of the rotor C.G. from the shaft center line. This is the critical motion for mechanical instability as encountered by helicopters on the ground (Ref. 25). In the flight case, however, the motions of the airframe are those of flight stability, and the accounting for the rotors must include the aerodynamic derivatives related to tip path plane tilt discussed earlier. The natural frequency of a flexibly-mounted rotor and the lowest break-point frequency of the SAS will generally be such that the corresponding degrees of freedom will enter the stability phenomenon. The damping ratio for blade lag motion and the SAS gain are generally critical parameters in this situation, and the instabilities which can be encountered generally have frequencies close to rotor speed minus or plus the fundamental rotating blade, lag frequency. The number of degrees of freedom and the fact that stability augmentation system, boost actuator, and blade motions in and out of the plane of rotation are likely to be involved tend to make analysis of this potential problem area trickier than most.

V. Gust Response

Rotary wing-type V/STOL aircraft respond in a special way to their gust environment. This problem is considerably more complex than the corresponding case for fixed-wing aircraft. For example, the detailed response of a helicopter rotor to a sharp-edge gust will depend on the azimuthal position of the first blade to enter the gust. A second complicating factor is the fact that, in contrast to fixed-wing aircraft, helicopters operating at high forward speed, where gust response is critical, may have some part of the rotor disc stalled, or at least very close to stall. Thus, the gust might change the rotor operating condition from one in which only a very small portion of the swept area is stalled to one in which a much larger portion is stalled. Ref. 26 is an excellent summary of gust response considerations in helicopter and compound helicopter design. It is shown there that the sequential entrance of a rotor into a sharp-edge gust does, in fact, reduce the maximum acceleration that the aircraft experiences; by the time the entire rotor is in the gust, the aircraft is moving upward to some degree. This overcomes the increased lift due to the rotor "flapping back" and thus increasing its angle of attack as a result of entering the gust. The rate at which the gust velocity builds up at its leading edge is shown to be of less consequence than one might think. The on-set of normal acceleration is sharper with a sharp-edge gust, but the maximum value is not very much changed whether the gust be sharp-edged or not. The most adverse distance from gust leading edge to maximum gust velocity, for 150 knots forward speed, appears to be roughly 100 ft.

When a gust is applied simultaneously to the entire rotor, the effect of nonsteady aerodynamics is to reduce maximum accelerations by about 15%. For sequential penetration, however, quasi-static aerodynamics is adequate for predicting the response. Higher modes of blade bending have little effect on the rotor thrust resulting from gust penetration, but it does, of course, affect oscillatory blade and control loads. Thus, a blade with flap hinges can be treated as a rigid hinged blade, so far as the maximum gust loads are concerned. The effect of blade Lock number, and root flapping stiffness is, however, to increase gust effectiveness, i.e. reduce gust alleviation, as blade stiffness in fundamental flapping or flap-bending motion is increased. Thus, increased flapping moment of inertia (lower Lock number), increased flapping hinge offset (in the case of hinged rotors), or increased blade root bending stiffness, in general, makes a rotary wing aircraft more g--sensitive to gusts.

One of the strongest influences on gust response is the rotor thrust coefficient usually based on hover conditions. This is a measure of the blade area and tip speed for rotary wing aircraft and is analogous to wing loading and forward speed in the case of the gust response of fixed-wing aircraft. Figs. 11 and 12, which are reproduced from Ref. 26, show this effect. In the first of these figures, the normal acceleration resulting from either a gust applied to the entire lifting rotor at once or a gust which has the shape of a sine wave squared are shown as a function of rotor thrust coefficient, at a forward speed of 200 knots. The effect of blade area loading and tip speed is very marked. The trend shown in Fig. 12 showing the difference between the normal accelerations that would be experienced by pure helicopters as compared to compound and winged helicopters in the presence of gusts, suggests that high rotor thrust coefficients at high forward speeds which result in a larger part of the rotor being stalled than when the rotor thrust coefficient is low, make a pure helicopter less gust sensitive than a compound. That is to say, the wings in unloading the rotor as it goes from hovering to high forward speed, increase the margin of the rotor from stall, so that when a gust occurs, larger lift increments are developed.

For tilt-wing and tilt-rotor aircraft, the vertical gust loadings at high forward speeds are very similar to those of an airplane with a high wing loading. The forces generated by and in the plane of the prop-rotor are, however, sensitive to advanced ratio and must be taken into account. Horizontal gusts may actually be the most severe situation for the low-disc loading tilt rotor aircraft. A calculation of this type has been reported

in Ref. 26 for a tilt-rotor aircraft flying at 350 knots and entering a 50 ft./sec. horizontal gust with a sine-squared wave front. It is noted that the response to this condition was .38 horizontal g's, and while this was noted as a reasonably moderate response for this condition, it is likely that some provisions for gust alleviation will be required for aircraft of this type.

Rotors generally provide opportunities for incorporating gust alleviation devices. Ref. 26, for example, shows that for rotors with flapping hinges, geometric coupling between the collective flapping of all blades (sometimes called "coning") and pitch angle can reduce the normal acceleration due to a gust by as much as 18%. This reduction results when the blade pitch angle is reduced $1/2^{o}$ for every 1^{o} of "coning". When faced with the combined problems of normal and horizontal acceleration, blade and control loads, and clearance between large prop-rotors and fixed airframe components, it may be necessary that advanced rotary wing V/STOL aircraft incorporate structural dynamic stability augmentation devices for gust alleviation. Techniques of this kind are being developed for fixed-wing aircraft (See Ref. 27) and should be adaptable to V/STOL types.

A. Stowed-Rotor Configurations

Two V/STOL configurational types are currently under study in which the lifting rotor is stopped, folded and "stowed" to allow flight at essentially unlimited high forward speeds. One of these, known as the "stowed-rotor compound", transfers the lift and propulsive force, respectively, to airplane type wings and turbo-prop, turbo-fan or turbo-jet propulsion at the so called "transition" speed, and then brings its helicopter-type rotor to a stop in a virtually horizontal position. Each blade is then individually rotated about a hinge located close to the rotor shaft and close to parallel to it, until all blades are lined up approximately with the aircraft longitudinal axis. In some types, all blades trail aft, in others some blades are aft, some forward. Fuselage-top fairings usually cover the "stowed" blades in these designs.

The second type is a tilt-rotor V/STOL with a propulsion package (usually turbo-fan) which relieves the prop-rotor of the propulsive function, once transition has been made to airplane flight. The prop-rotor can then be feathered and stopped, much like the propeller on a faulty engine on a conventional airplane. Once stopped, the blades are pivoted at their roots and folded aft, umbrella style, to cluster about and be faired into the nacelle. This V/STOL type is often called the "stowed tilt-rotor".

Both these configurations subject their rotors or prop-rotors to forward speed to tip speed ratios, V/V_T, much higher than rotors have ever before been exposed to in flight. As the rotational speed drops to zero, these ratios become infinite, and the blades, which because of their large radius and light-weight construction are considerably more limber than conventional propellers, lose their centrifugal stiffening. During the stopping and starting processes, forward speed, gusts and aircraft attitude thus become determining factors for blade stresses. From this viewpoint, the lowest possible forward speed at which the wing can support the aircraft weight is the best for stopping the prop-rotor. The need to keep the rotor parallel and perpendicular to the local airstream, respectively, for the stowed-rotor compound and the stowed tilt-rotor V/STOL imposes severe handling qualities criteria. Wind tunnel tests have been conducted, but to date none have carried out stop-start processes with fuselage freedoms typical of free flight. A comprehensive discussion of stowed-rotor compound testing and design considerations is given in Ref. 28.

Some of the blades of the stowed tilt-rotor V/STOL's must--in the process of being stowed or deployed--traverse regions of substantial velocity gradients, since they go from being roughly perpendicular to parallel to the chord plane of the wing. In most other respects, however, the stowed-rotor compound would seem to be more susceptible to gusts and handling qualities difficulties in its stop-start cycle. One consequence of having advance ratio, V/V_T, greater than unity for the horizontal rotor is that the entire blade span on the "retreating" side is in reverse flow; that is, the (geometric) trailing edge becomes the (aerodynamic) leading edge. Thus, if the blade elastic torsion axis were at 25% chord, on the advancing side it would be coincident with the center of pressure, and on the retreating side it would be one-half chord length behind it. This has major implications for the torsional aeroelastic divergence speed of the blade and hence on gust sensitivity. Even more important is the "swept-forward" condition that at least one of the blades being deployed to its "stowed" position will traverse. As shown in Fig. 13, sweep effects couple bending with torsion so as to raise the torsional divergence speed with sweepback and lower it with forward sweep. The combination of forward sweep, trailing edge forward, and limber bending stiffness all serve to make gust sensitivity in transition a difficult design problem for the stowed-rotor compound. This follows not only because of blade stresses, but because the hub moments resulting from stopped, forward-pointing (i.e. $180 \leq \psi \leq 270^{o}$) blades, as they are acted on by gusts and other disturbances, impose additional control requirements on the airframe.

VI. Summary and Conclusions.

The aeroelastic characteristics of rotors or rotor-propellers of rotary-wing V/STOL aircraft will influence the handling qualities of these aircraft at least by their approximate first order lag representation and more often by their higher order dynamics, whether the rotors are hinged or not. As rotors grow in size, the restriction which keeps rotor tip speeds below critical Mach number results in blade natural frequency characteristics low enough not only to couple with aircraft rigid-body response, but also to become susceptible to pilot-forced resonance and/or pilot-coupled instabilities. The combination of (1) the low damping inherent for rotor blade motion in the plane of rotation and (2) the low-natural frequencies associated with flexibly-mounted prop-rotors is so potentially important as to always require airframe-control system (including S.A.S. and autopilot) stability to be examined with due cognizance taken of these factors. Gust response of compound helicopters at high forward speed will probably be more severe, as regards the fixed airframe normal accelerations, that that of pure helicopters, although the concomitant blade and control system stress problems are likely to be less serious. For stopped-stowed rotor V/STOL's, the gust problem is most severe in transition, and seems particularly difficult for the configuration which stops and stows the lifting rotor in a horizontal position.

VII. References

1. Duncan, W. T., CONTROL AND STABILITY OF AIRCRAFT, Cambridge New Series, 1952.

2. Etkin, B., DYNAMICS OF FLIGHT, J. Wiley & Sons, 1959.

3. Schwendler, R. G. and MacNeal, R. H., OPTIMUM STRUCTURAL REPRESENTATION IN AEROELASTIC ANALYSIS, ASD-TR-61-680, January, 1962.

4. Pearce, B. F., RESIDUAL STIFFNESS EFFECTS IN TRUNCATED MODAL ANALYSES, ASD-TDR-63-334 Part II, July, 1963.

5. Kolk, W. R., MODERN FLIGHT DYNAMICS, Prentice-Hall, 1961.

6. Cannon, R. H., ROUTE-LOCUS ANALYSIS OF STRUCTURAL COUPLING IN CONTROL SYSTEMS, ASME paper N58-A-65, Meeting Nov. 30 - Dec. 5, 1958.

7. Fonda, A. G. and Frueh, F. J., FLEXIBLE FLIGHT VEHICLE TRANSFER FUNCTION FACTORS FOR USE IN AUTOPILOT PRELIMINARY DESIGN, RTD-TDR-63-4218, April, 1964.

8. Pass, H. R. and Pearce, B. F., TOPICS ON FLEXIBLE AIRPLANE DYNAMICS, PART IV COUPLING OF THE RIGID AND ELASTIC DEGREES OF FREEDOM OF AN AIRFRAME AUTOPILOT SYSTEM, ASD-TDR-63-334, Part IV, July, 1963.

9. Karman, Th. V., HELICOPTER THEORY, Zeibochrift fur Flugtechnik und Motorluftschiffahib, Vol. 12, No. 24, 1921 (Translated in "Aircraft Engineering", September, 1940).

10. Crocco, G. Arturo, INHERENT STABILITY OF HELICOPTERS, NACA TM-234, October, 1923, (From "Rendicont della R. Accademia Nazionale dei Lincei", August, 1923.)

11. Young, Maurice I., A SIMPLIFIED THEORY OF HINGELESS ROTORS WITH APPLICATION TO TANDEM HELICOPTERS, American Helicopter Society, Proceedings of the Eighteenth Annual Forum, May 2, 3, 4, 1962, Washington, D. C.

12. Hohenemser, K., DYNAMIC STABILITY OF A HELICOPTER WITH HINGED ROTOR BLADES, NACA TM-907, 1949.

13. Miller, R. H., HELICOPTER CONTROL AND STABILITY IN HOVERING FLIGHT, J.A.S., August, 1948.

14. Amer, K. B., THEORY OF HELICOPTER DAMPING IN PITCH AND ROLL AND A COMPARISON WITH FLIGHT MEASUREMENTS, NASA TN-2135, October, 1950.

15. Yntema, R. T., SIMPLIFIED PROCEDURES AND CHARTS FOR THE RAPID ESTIMATION OF BENDING FREQUENCIES OF ROTATING-BEAMS, NACA TN-3459, June, 1955.

16. Advisory Group for Aeronautical Research and Development, RECOMMENDATIONS FOR V/STOL HANDLING QUALITIES, Report 408, October, 1962.

17. Ashkenas, I. L., and McRuer, D. T., A THEORY OF HANDLING QUALITIES DERIVED FROM PILOT-VEHICLE SYSTEM CONSIDERATIONS, Aerospace Engineering, February, 1962.

18. McRuer, D. T., and Krendel, E. S., THE HUMAN OPERATOR AS A SERVO SYSTEM ELEMENT, Journal of the Franklin Institute, Vol. 267, No. 6, June, 1959.

19. Kuehnel, H. A., IN-FLIGHT MEASUREMENT OF THE TIME REQUIRED FOR A PILOT TO RESPOND TO AN AIRCRAFT DISTURBANCE, NASA TN D-221, March, 1960.

20. Hall, I. A. M., EFFECT OF CONTROLLED ELEMENT ON HUMAN PILOT, WADC TR-57-508, August, 1958.

21. Lytwyn, R. T., AN ANALYSIS OF THE DIVERGENT VERTICAL HELICOPTER OSCILLATIONS RESULTING FROM THE PHYSICAL PRESENCE OF THE PILOT IN THE COLLECTIVE CONTROL LOOP, Journal of the American Helicopter Society, January, 1967.

22. Gabel R., and Wilson, G. J., TEST APPROACHES TO EXTERNAL SLING LOAD INSTABILITIES, Journal of the American Helicopter Society, July, 1968.

23. Smollen, Leonard E., Marshall, Philip, and Gabel, Richard, ACTIVE VIBRATION ISOLATION OF HELICOPTER ROTORS., Journal of the American Helicopter Society, Vol. 7, No. 2, April, 1962.

24. Theobald, Charles E., and Jones, R., ISOLATION OF HELICOPTER ROTOR VIBRATORY FORCES FROM THE FUSELAGE, WADC TR-57-404, September, 1957.

25. Coleman, Robert P. and Feingold, Arnold M., THEORY OF SELF-EXCITED MECHANICAL OSCILLATIONS OF HELICOPTER ROTORS WITH HINGED BLADES, NACA T. N. 3844, 1957.

26. Drees, Jan M. and Harvey, Keith W., HELICOPTER GUST RESPONSE AT HIGH FORWARD SPEED, AIAA Paper No. 68-981, 5th Annual Meeting and Technical Display, October 21-24, 1968.

27. Wykes, John H., STRUCTURAL DYNAMIC STABILITY AUGMENTATION AND GUST ALLEVIATION OF FLEXIBLE AIRCRAFT, AIAA Paper No. 68-1067, 5th Annual Meeting and Technical Display, October 21-24, 1968.

28. Deckert, Wallace H. and McCloud III, John L., CONSIDERATIONS OF THE STOPPED ROTOR V/STOL CONCEPT, Journal of the American Helicopter Society, Vol. 13, No. 1, January, 1968.

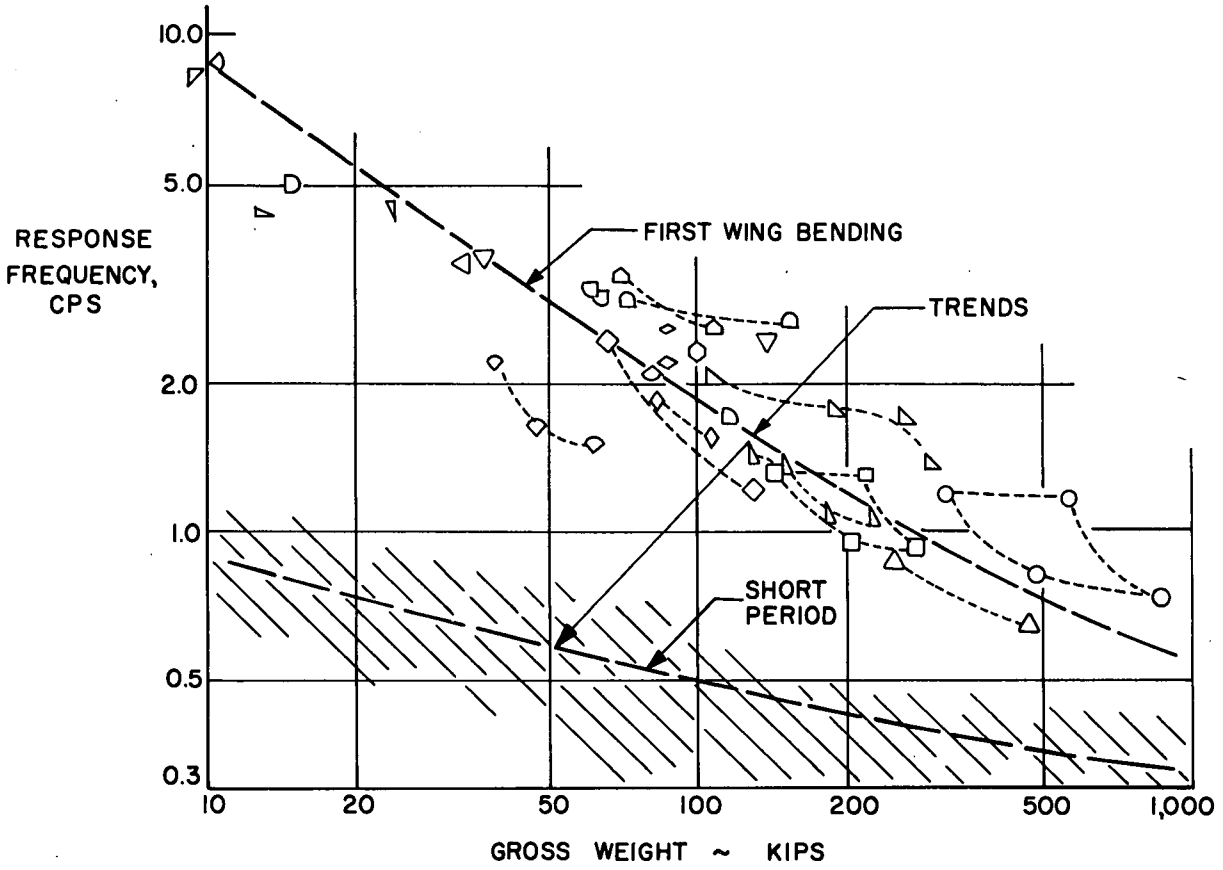


Fig. 1 Effect of gross weight on wing bending and short period response frequency

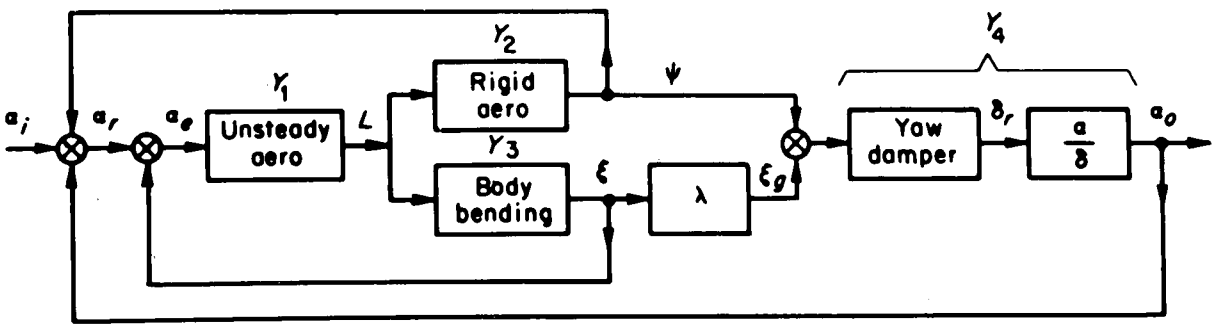


Fig. 2 Simplified block diagram of aircraft contral response including elastic modes

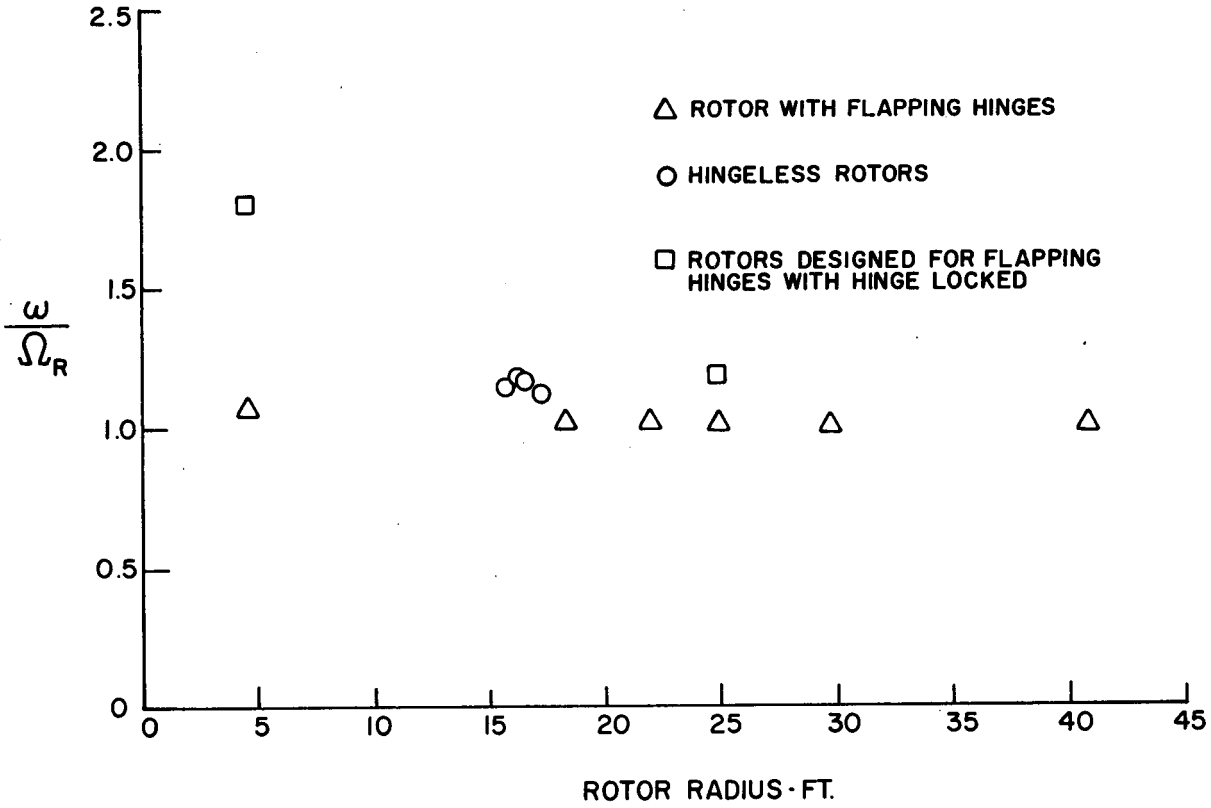


Fig.3 First flapping natural frequency as a function of radius

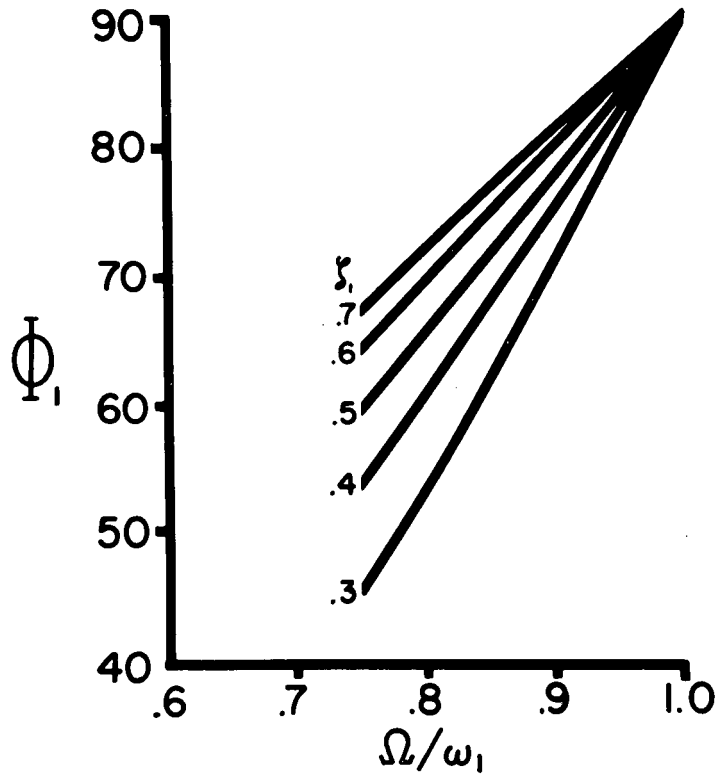


Fig.4 Phase-frequency relation for constant cyclic input

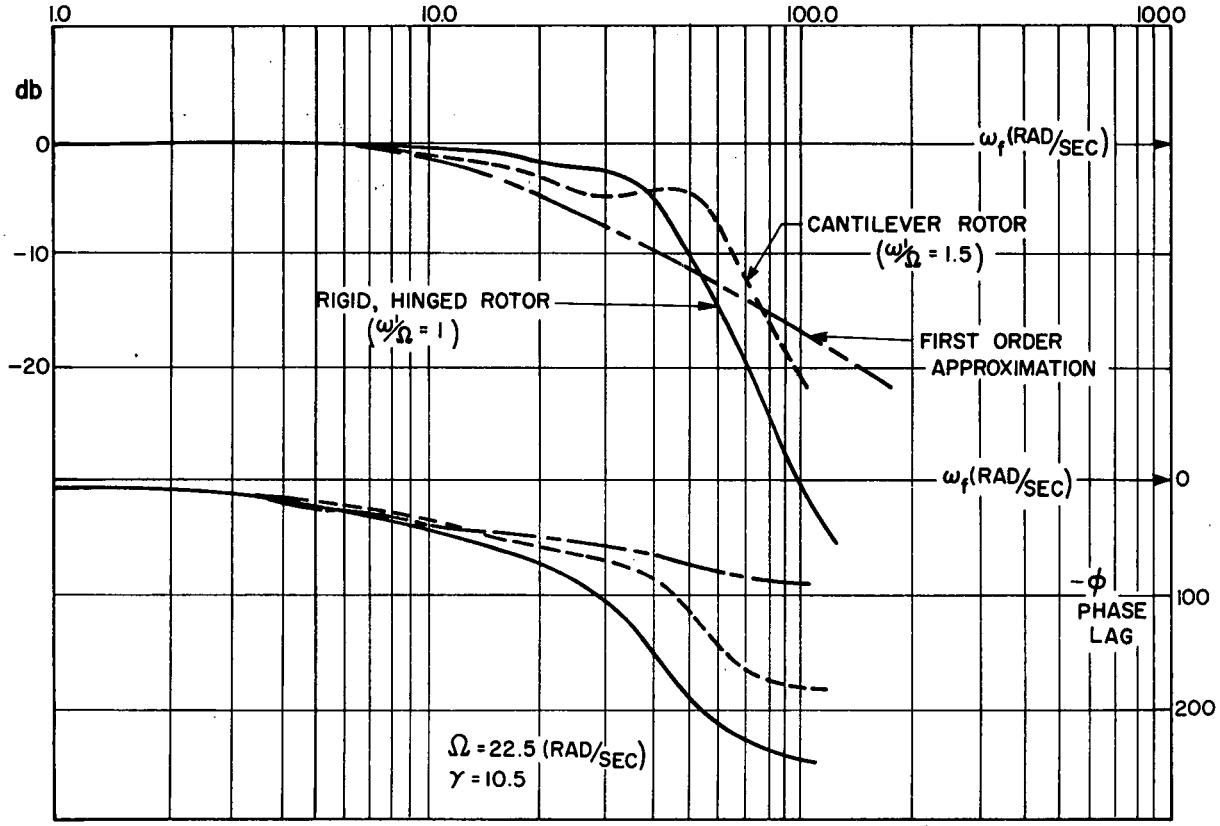


Fig.5 Direct response to cyclic control input

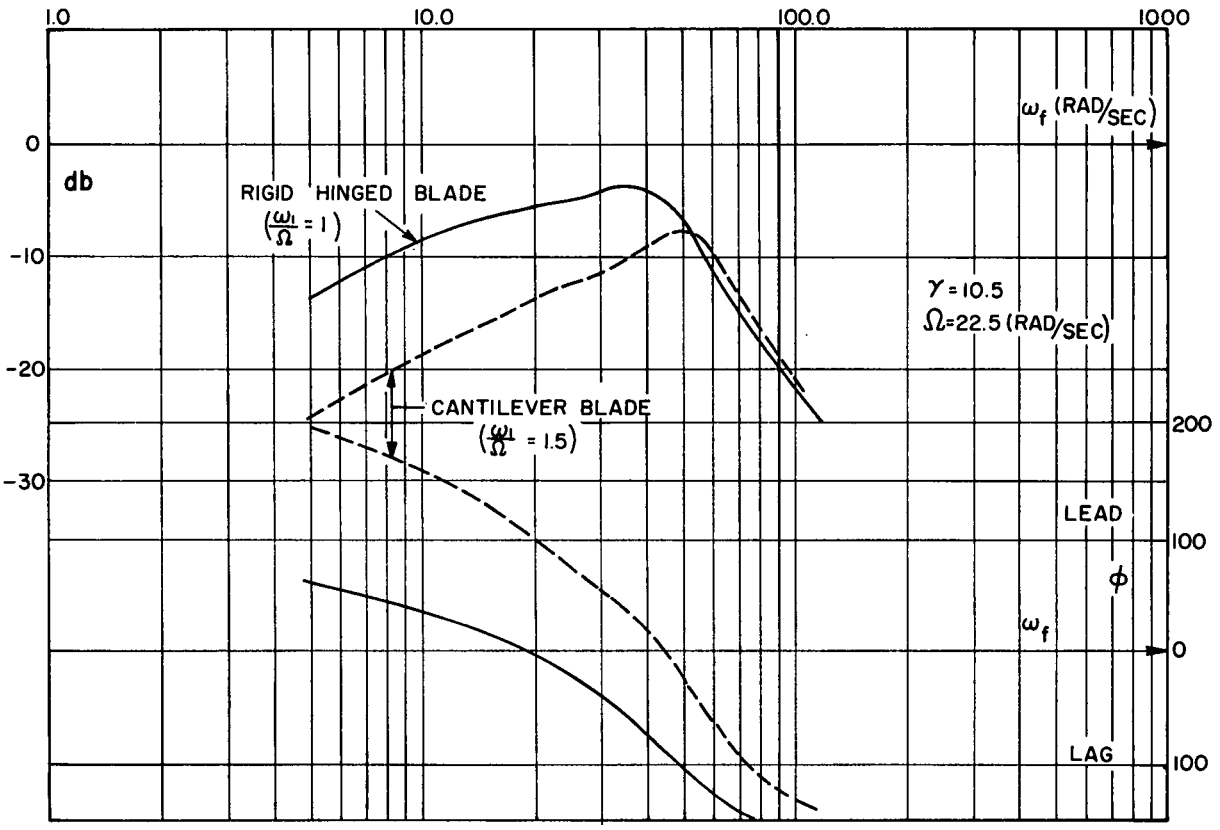


Fig.6. Cross control coupling as a function of frequency

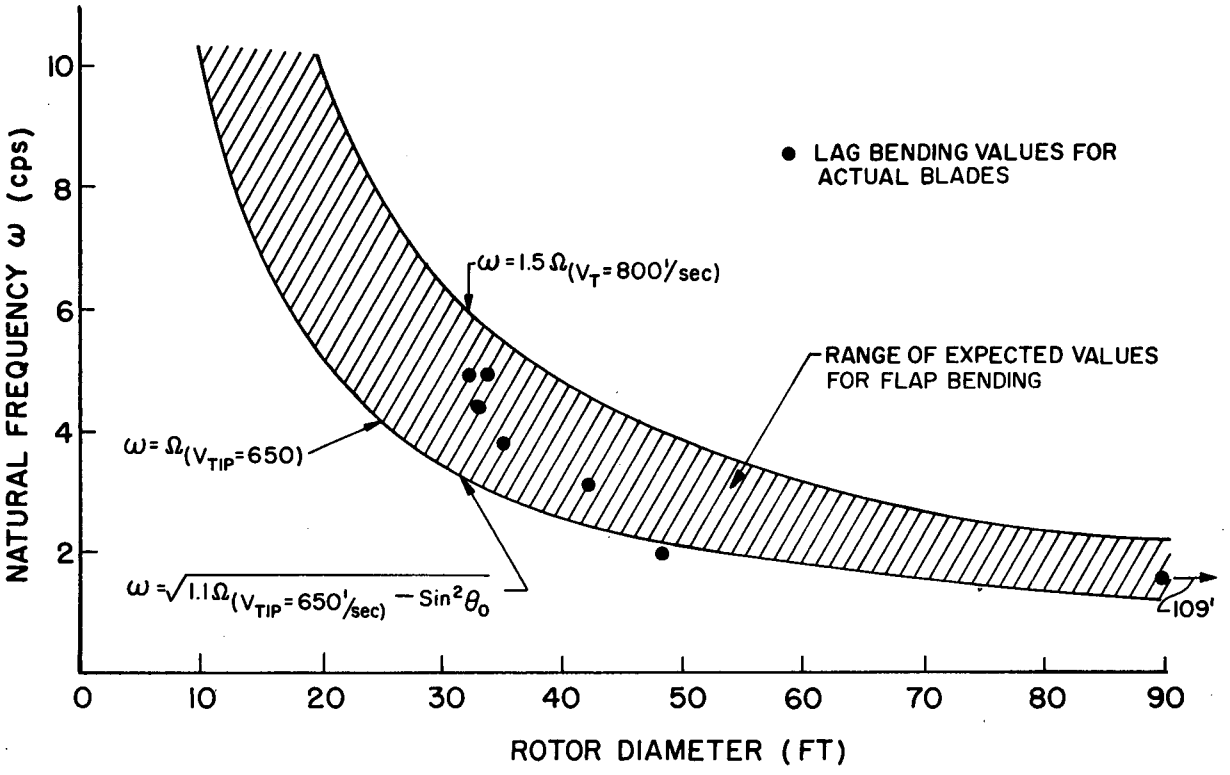


Fig.7 Fundamental natural frequency vs radius hingeless rotors

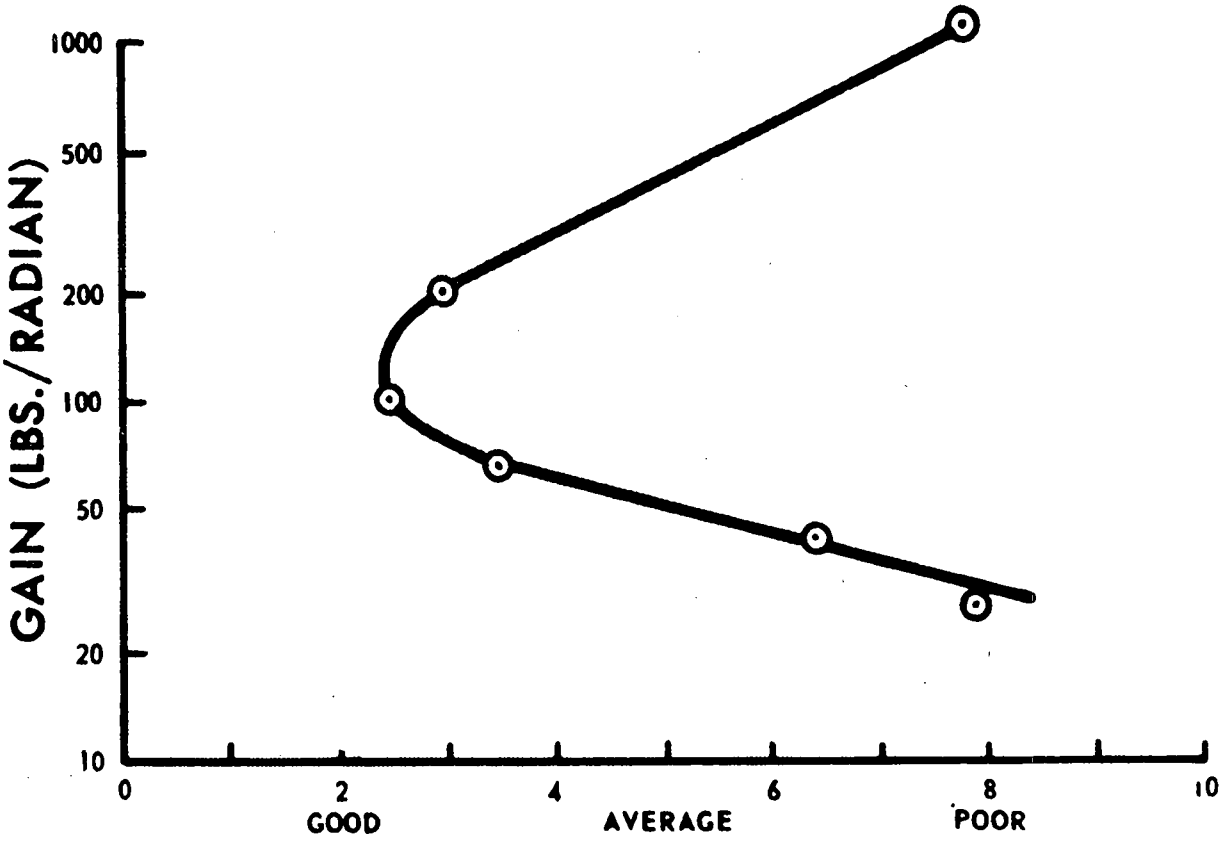


Fig.8 Pilot opinion rating

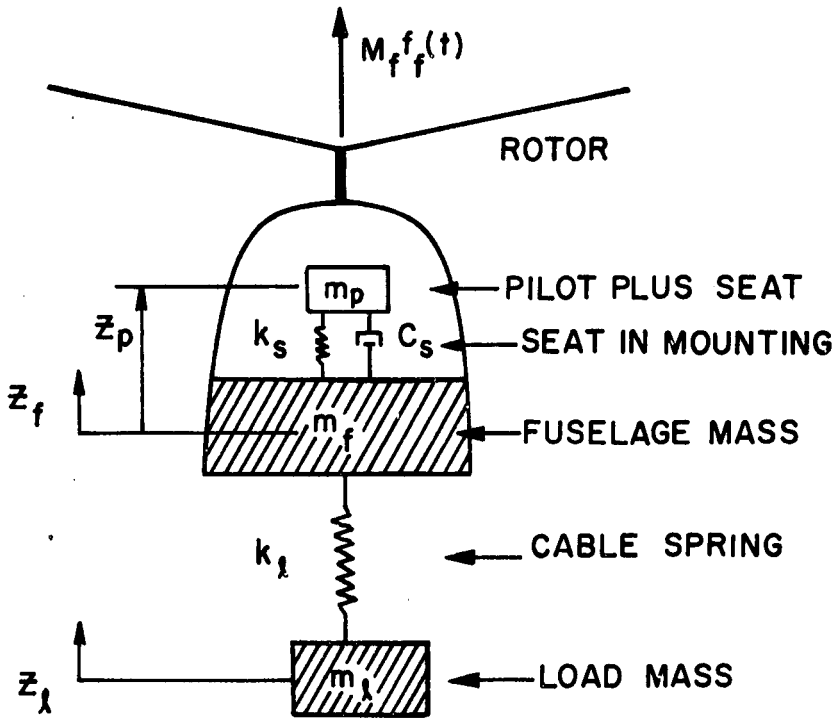


Fig. 9 Mathematical model for collective control feedback of helicopter with sling load

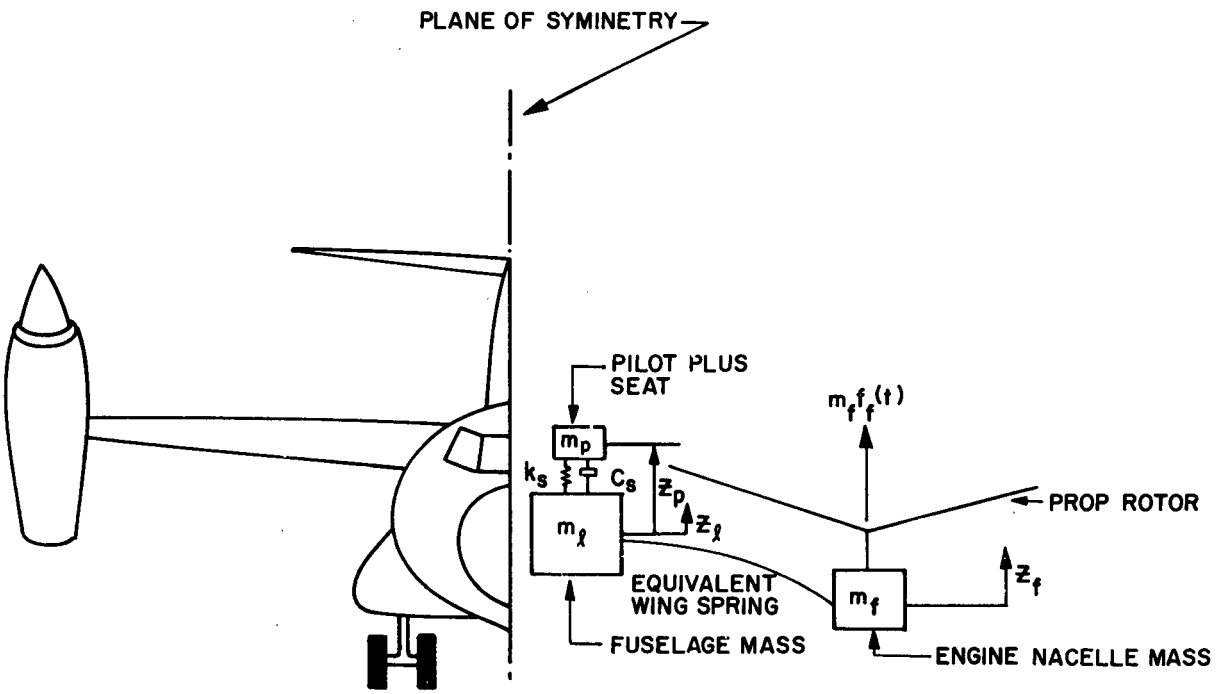


Fig. 10 Mathematical model for tilt-rotor v/stol aircraft collective control feedback

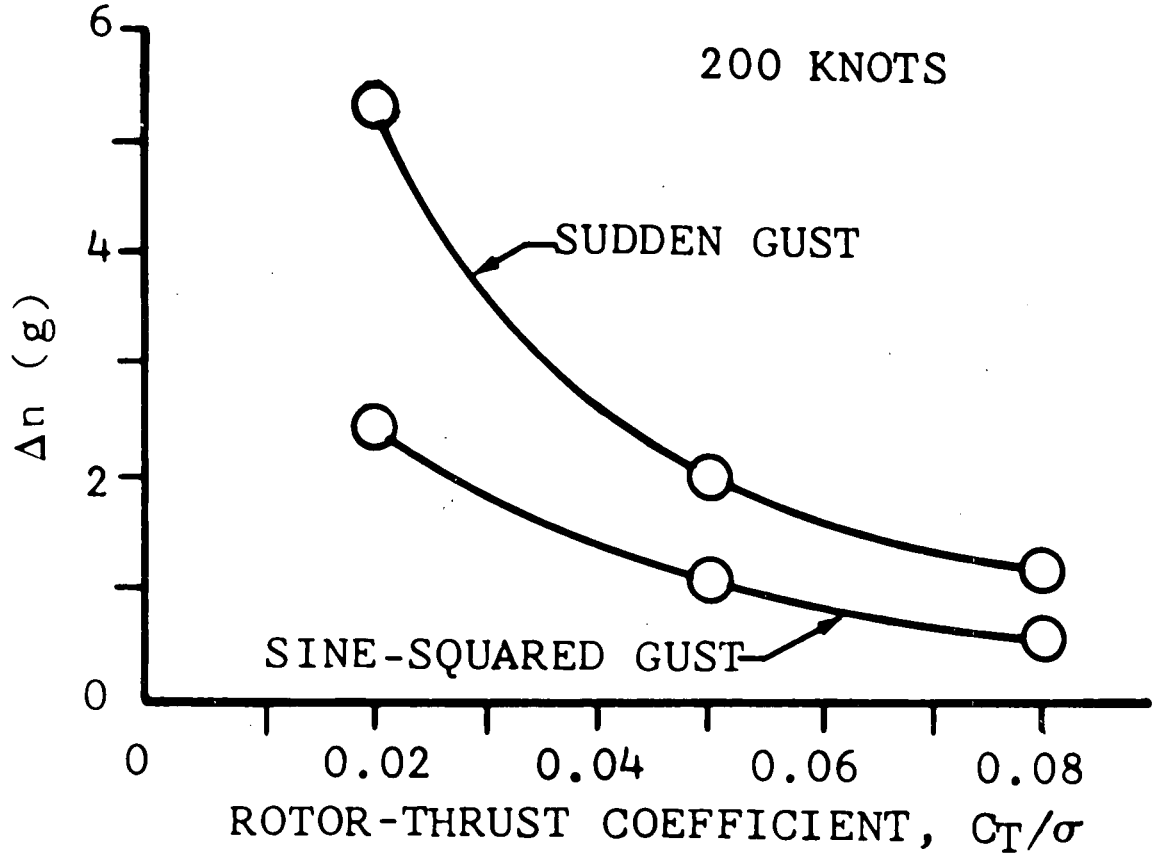


Fig. 11 Effect of Rotor-thrust coefficient on the gust load

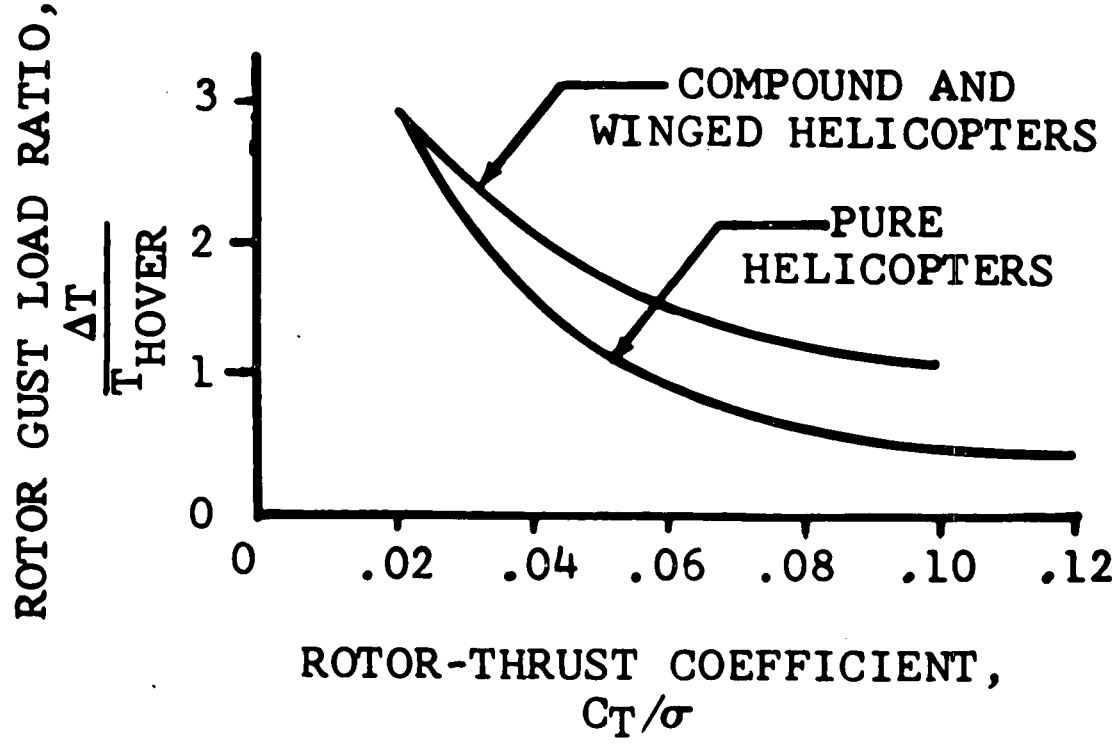


Fig. 12 Rotor gust load ratio versus C_T/σ

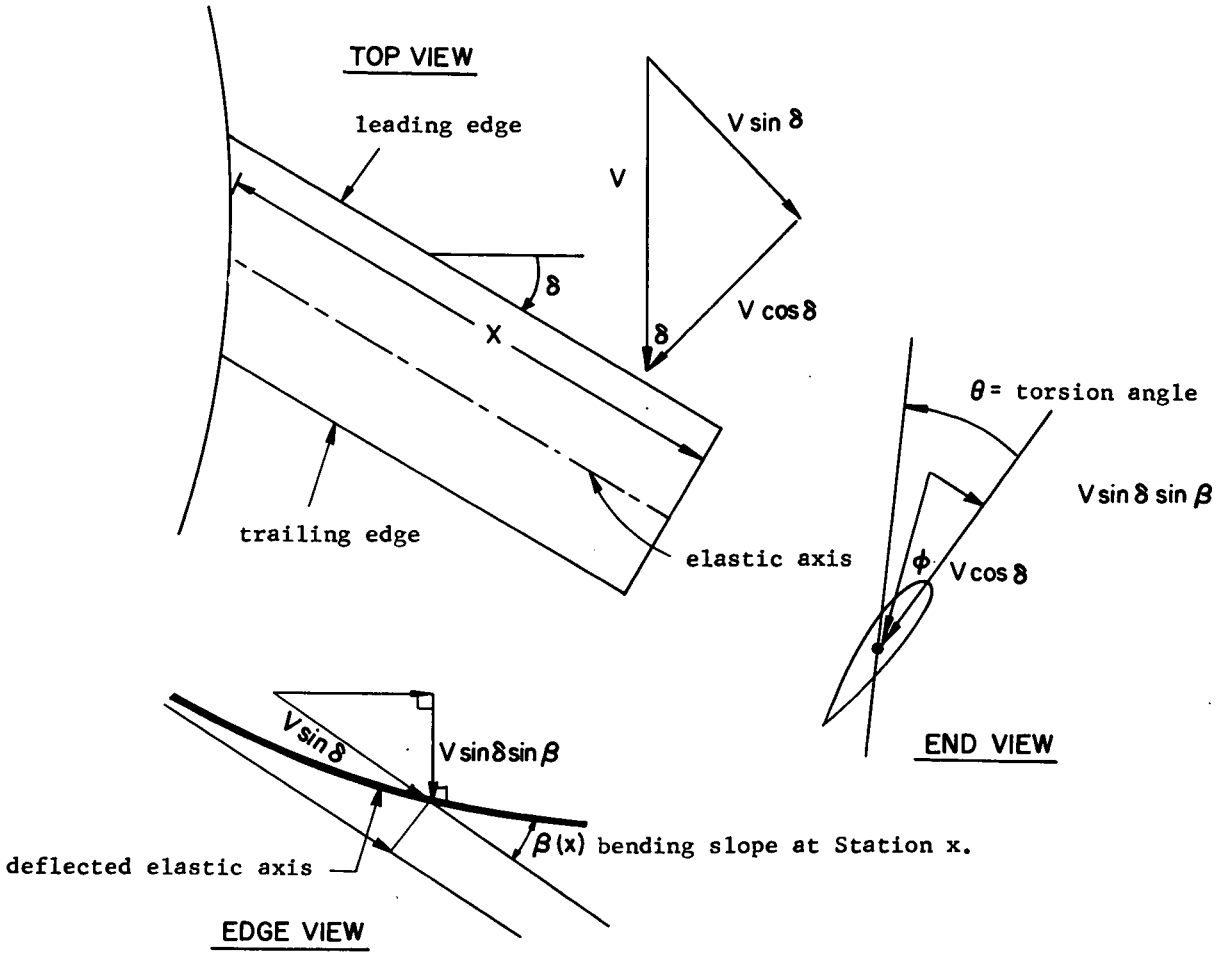


Fig. 13 Reduction in angle of attack by sweep-back and bending

AEROELASTIC PROBLEMS OF FLEXIBLE V/STOL ROTORS

by

D. E. BRANDT

Chief, V/STOL Dynamics
The Boeing Company, Vertol Division
Philadelphia, Pennsylvania

AEROELASTIC PROBLEMS OF FLEXIBLE V/STOL ROTORS

by

D. E. BRANDT

Chief, V/STOL Dynamics
The Boeing Company, Vertol Division

SUMMARY

A discussion is presented of the aeroelastic problems associated with the use of large rotors in V/STOL aircraft. These include divergence and whirl flutter of large rotors when operating in the propulsive mode, mechanical instability in the hover to ground mode, and gust response characteristics peculiar to large propulsive rotors. The mechanism of these instabilities and response phenomena are described and methods for their control using feedback concepts are examined. Some results of studies for a typical configuration are given. The value of dynamically similar models for large rotors is emphasized and some results are presented for programs involving such models.

INTRODUCTION

Requirements for aircraft which approach the helicopter's hovering efficiency as well as the high speed cruise and range characteristics of fixed wing aircraft have generated aircraft configurations which utilize the prop/rotor. Typically the prop/rotor aerodynamic characteristic must provide a good figure of merit in hover when the blades are most heavily loaded as well as a high efficiency when the blades are lightly loaded such as in cruise.

Three configurations utilizing the prop/rotor which introduce the classes of aeroelastic problems discussed herein are shown in Figure 1 through 3. The tilt wing configuration tilts the wing and propellers in the vertical position for hover. The high velocity of the slipstream stabilizes the flow over the wing and the attendent increments of lift and drag are used to advantage for excellent STOL performance.

The tilt rotor configuration is similar to the tilt wing in principle differing only in that the nacelles are tilted rather than the whole wing, and it typically has larger diameter rotors. Thus it retains hover efficiencies comparable to the helicopters and has cruise speed capabilities higher than the helicopter but somewhat less than the tilt wing.

The folding tilt rotor concept hovers and makes a transition to forward flight in the same way as the pure tilt rotor. However, when the aircraft reaches a conversion speed of between 130 to 200 knots, the rotors are feathered and stopped and the blades folded back into wing mounted nacelles. Thrust for conventional flight is then provided by convertible engines which are capable of producing either shaft power for the rotors or fan thrust. This results in forward flight efficiencies comparable to the fixed wing and higher cruise speeds than the tilt wing concept.

Virtually every such prop/rotored aircraft has design criteria based on aeroelastic problems. While most of these aeroelastic phenomena are reasonably well understood, with the current scarcity of experiences, it is not uncommon in specific cases for an aircraft to be in serious trouble because of one or more of them. Lacking historical trend and experience data, to properly account for these effects on vehicle weight and performance, it is most important in the preliminary design phase to give a detailed realistic and accurate treatment of these problems.

In this paper we will discuss a selected group of aircraft problems which are influenced by the aeroelastic aspects of the prop/rotor and which are part of the classes of problems related to structural stability and forced response. In particular the use of active feedback coupling to rotor collective or cyclic pitch will be discussed. It is emphasized that the basic philosophy guiding the design of these aircraft configurations and their feedback systems is that the aircraft should be designed with inherent stability, and the feedback systems utilized to improve the flying qualities, increase the stability margins, increase the fail-safety, and as a provisional means to incorporate solutions to marginal or unanticipated problems that might arise in the developmental flight testing program of production design aircraft.

The general class of problems are surveyed in Table I. A brief description of each follows. The more critical problems of whirl flutter, gust response, and mechanical instability will be discussed in more depth, and the extent to which test and analyses performed to date correlate or highlight important aspects of the problem will be shown.

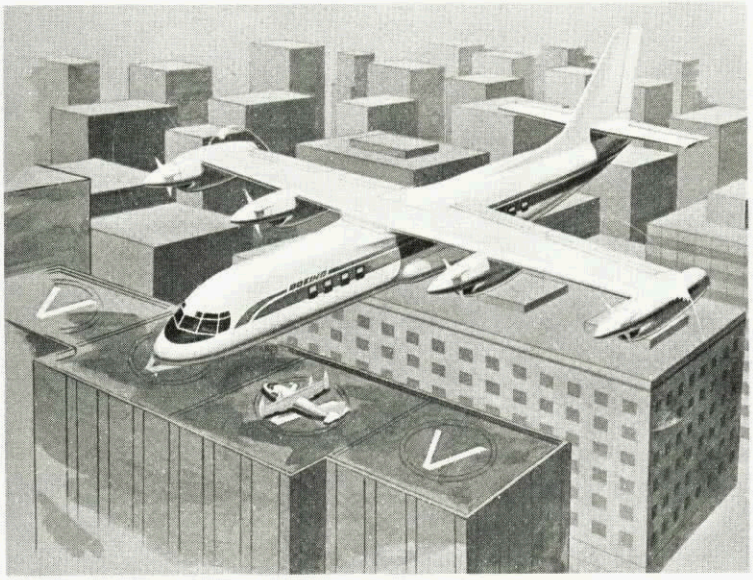


FIGURE 1 TILT WING AIRCRAFT

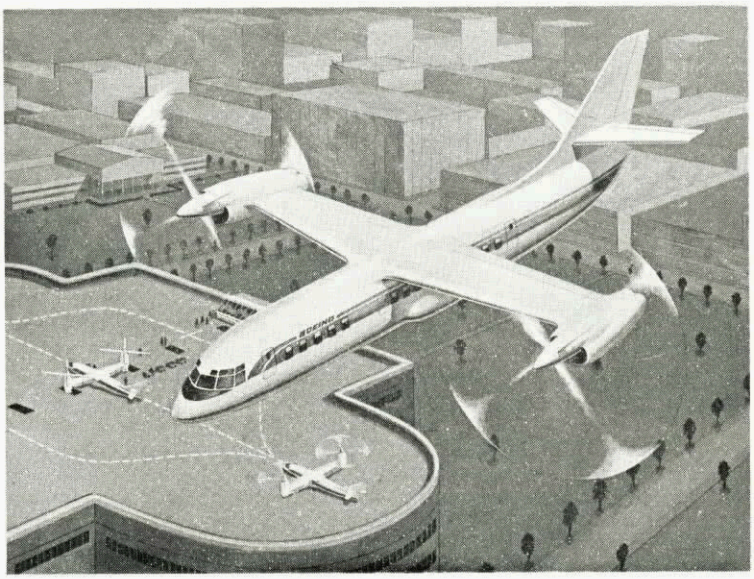


FIGURE 2 TILT ROTOR AIRCRAFT

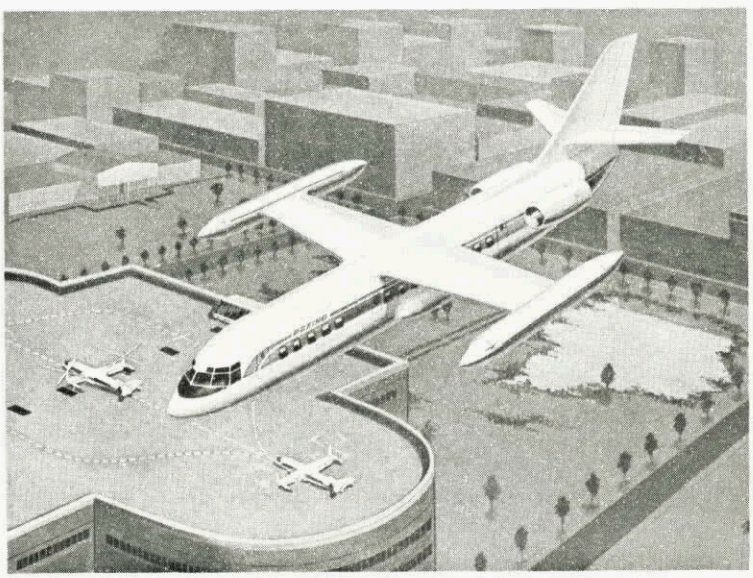


FIGURE 3 FOLDING TILT ROTOR AIRCRAFT

TABLE 1

AEROELASTIC STRUCTURAL STABILITY AND FORCED RESPONSE PROBLEMS OF PROP/ROTOR V/STOL AIRCRAFT

		CRITICAL ASPECTS	
I.	STRUCTURAL STABILITY	ROTATING PROP/ROTORS	FOLDING PROP/ROTORS
	WING/ROTOR DIVERGENCE	Large destabilizing prop/rotor normal force and moment derivatives. Derivatives may increase with angle-of-attack.	Normal force derivatives are largest valve for non-rotating blade.
	WHIRL FLUTTER	Large interaction of rotor forces with wing/nacelle motions. Reducing thrust is destabilizing. Disc tilt may be important parameter.	Large RPM variations and inflow ratios encountered.
	GROUND AND AIR MECHANICAL INSTABILITY	Applies to rotors with subcritical blade frequencies. Aircraft rigid body and multiple, variable flexible airframe modes with low effective mass are present in the important forcing frequency band.	
	PROP/ROTOR BLADE FLUTTER AND DIVERGENCE	Elastic deflections, twist, incidence of these large flexible blades result in significant coupling between the degrees of freedom.	Large variations in stiffness and equivalent sweep angles are encountered because of folding, gusts and maneuver effects.
	PITCH-LAG-FLAP INSTABILITIES	Same as flutter and divergence above	
	NON-LINEAR LIMIT CYCLE FLUTTER	Strong coupling of blade modes. Possible result of non-linear effect associated with large displacements that result from gust or control inputs.	Blade stall and large displacements at low RPMs can result from gust or maneuvers. Large RPM and inflow ratios encountered.
II.	FORCED RESPONSE		
	GUST RESPONSE	Low disc loading result in large force increments. Lateral-directional stability degraded in non-homogeneous turbulence.	
	AIRFRAME VIBRATION	Non-uniform inflow, maneuver and gust effects produce large excitation.	Transversing blade and wing natural frequencies produce large amplification of excitations.
III.	IMPORTANT RELATED EFFECTS		
	NON-UNIFORM INFLOW	Rotor-airframe steady and unsteady aerodynamic interference effects, rotor trailing vortex effects, non-axial flow conditions, gust and cross wind effects result in non-uniform inflow through the rotor disc.	

PROP ROTOR WHIRL FLUTTER AND DIVERGENCE

Propeller whirl flutter and wing-rotor divergence are problems experienced on conventional propeller driven aircraft. Prop/rotor whirl flutter was first experienced by a VTOL during the wind tunnel test of the XV-3 in 1962.

Wing-rotor divergence is a quasi-static instability of the wing and rotor which occurs at an airspeed where the combination of disturbing aerodynamic forces equals or exceeds the elastic restoring forces provided by the wing structure. This problem is particularly critical in the low-disc-loading prop/rotor configuration because of the destabilizing effect of the associated large rotor normal force and moment derivatives. That is, when the wing twists statically the rotor experiences an angle of attack and a normal force which tends to increase the twist angle, i.e. tends to produce divergence.

These destabilizing rotor aerodynamic forces are produced by a cyclic variation in angle of attack of the blade produced by non-axial flow; hence it is possible to reduce and even overcome this effect by a suitably phased application of cyclic pitch geared to the quantity causing the initial normal force. This may be envisioned in an approximate way as gearing the rotor to the wing so that its tip path plane is maintained in an unchanged orientation in space even when the wing twists. However, it should be remembered that zeroing out the normal force and maintaining the tip path plane orientation are not exactly equivalent. It should also be noted that there is evidence that the important rotor derivatives increase with tilt angle relative to the free stream so that the high speed cruise condition is not necessarily the critical divergence condition. In the stoppable rotor configuration, the condition of zero RPM where destabilizing aerodynamic forces tend to be a maximum for the axial flow case must also be addressed.

The phenomena commonly referred to as whirl flutter is a class of instability involving the wing and airframe structures modes and the gyroscopically coupled freedoms of the rotor system. It is characterized by spiraling motion of the rotor hub in an elliptical motion, rotating in the opposite direction to regular propeller rotation. Large, flexible, rotors are more likely to encounter this problem and may also introduce additional modes of instabilities.

To avoid propeller whirl flutter the normal modes of the rotor motion must prevent the transfer of energy from the airstream to the propeller/nacelle structure. This can be achieved by proper selection of mass, stiffness, and geometric characteristics (as in the classical approach for the prevention of flutter and divergence), or alternately by the use of mechanisms to apply control motions to the blades to nullify aerodynamic coupling, or by a combination of both approaches.

As in the case for divergence, it may be reasoned that since whirl flutter is caused by the large aerodynamic yaw moment produced by a pitch angle on the rotor, again caused by cyclic variation of the angle of attack around the azimuth, a cyclic pitch input to the rotor with suitable phasing and geared to wing torsion can null out the yawing moment and, therefore, the tendency to whirl.

In treating this problem we have developed stability analyses which describe the dynamic behavior of large diameter flexible rotors mounted at the tips of typical wing structures and operating at high forward speeds. These analyses also address static aeroelastic divergence.

A typical analytical model to predict flutter and divergence characteristics is shown in Figure 4. This is a 6 degree of freedom analyses which describes the coning, pitch and yaw of the disc, wing/nacelle vertical bending (vertical translation), torsion (nacelle pitch), and chordwise bending (nacelle yaw). Both the effects of structural damping and feathering feedback are included. The analysis computes the stability boundary as a function of variation in pitch and yaw natural frequencies.

Figure (5) shows a typical analytical result pertaining to a particular design where the design point lies on the boundary of a flutter region and uncomfortably close to divergence. This basic case was studied to see whether feedback of the type previously mentioned would be effective in improving the situation. It is seen from Figure 6 that feedback which makes use of the cyclic pitch phasing normally used for control and a 1:1 relation between wing twist and the cyclic pitch amplitude, reduces the torsional stiffness requirement for divergence to near zero but extends the flutter region.

This is approximately equivalent to zeroing out the normal force. Now introducing a further similar 1:1 ratio of cyclic pitch to torsion, but phased 90° in advance of that used for aircraft pitch control it is seen from Figure 7 that the flutter region disappears and comfortable margins exist for pitch and yaw divergence.

The whirl flutter behavior of large flexible rotors is an obvious area of application for model test techniques. A series of model tests have been accomplished at the Vertol Division of the Boeing Company to gain insight into the aeroelastic behavior of large flexible rotors and to provide data to correlate with analysis. Figure 8 and 9 show two models used for these purposes.

The first model was a 30 inch diameter unpowered or windmilling semi-span model generally representative of the tilt rotor configuration and was oriented toward generating parametric data to examine the flutter phenomena and substantiate the degree of validity of the analysis previously described.

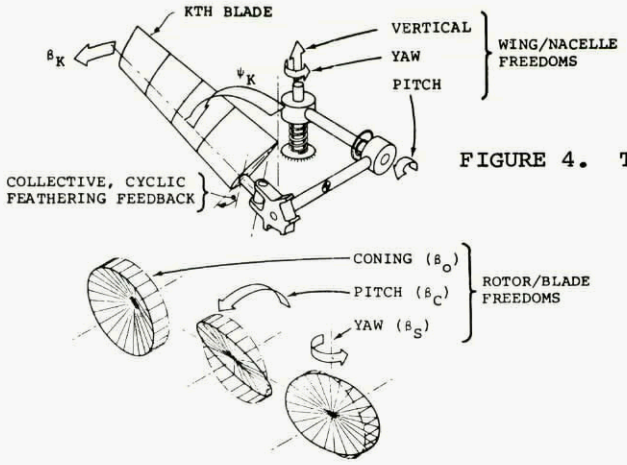


FIGURE 4. TYPICAL ANALYTICAL MODEL

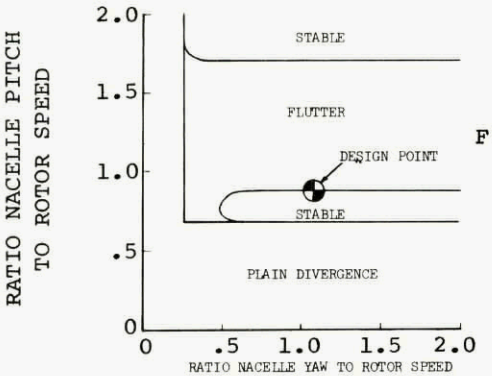


FIGURE 5. TILT ROTOR FLUTTER AND DIVERGENCE CHARACTERISTIC ZERO FEEDBACK

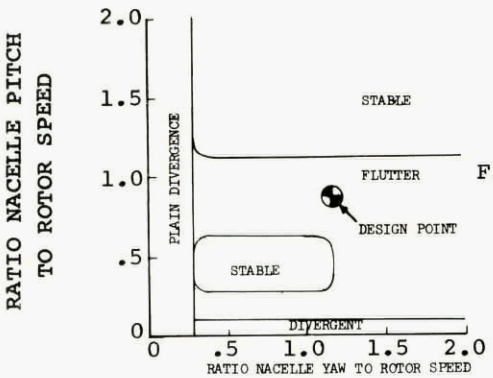


FIGURE 6. TILT ROTOR FLUTTER AND DIVERGENCE CHARACTERISTIC
+100% IN PITCH DUE TO WING TORSION

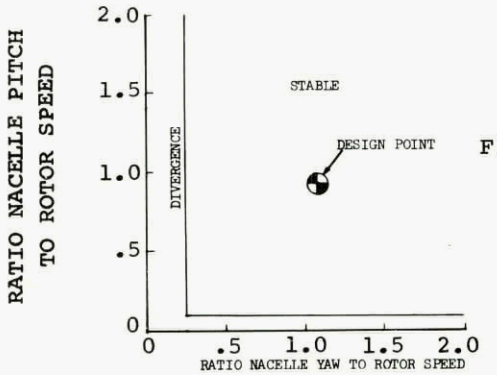


FIGURE 7. TILT ROTOR FLUTTER AND DIVERGENCE CHARACTERISTIC FEEDBACK
100% PITCH AND 100% YAW DUE TO WING TORSION

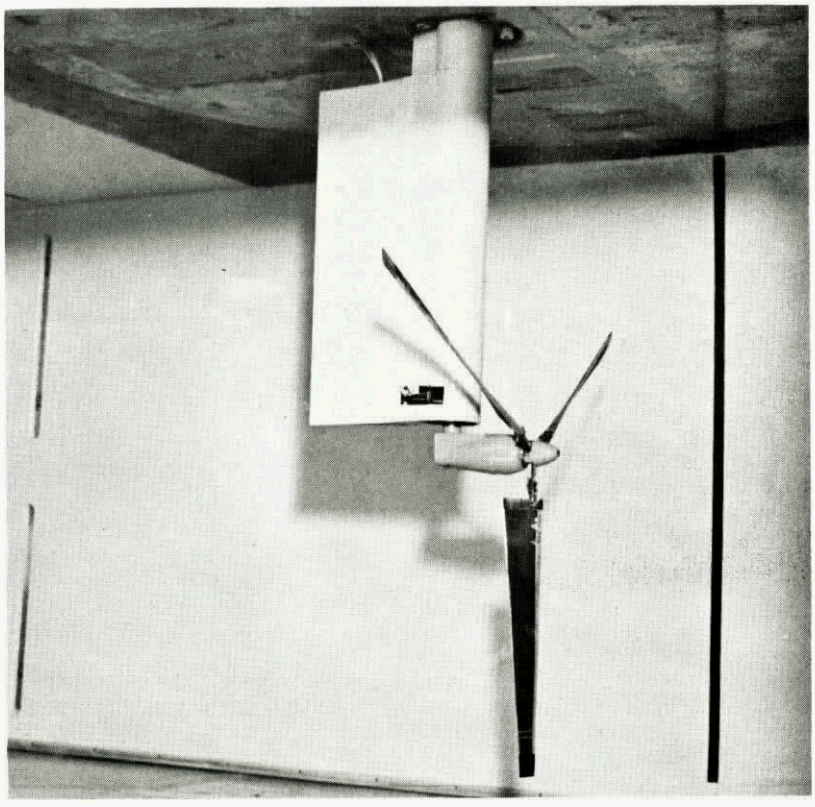


FIGURE 8 1/22 SCALE WINDMILLING DYNAMIC MODEL

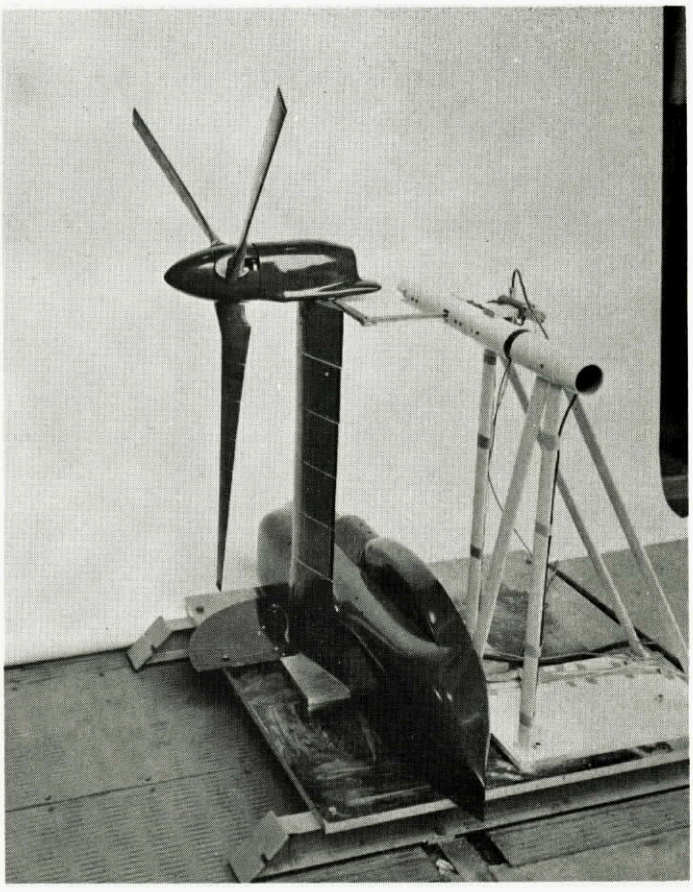


FIGURE 9 1/10 SCALE POWERED DYNAMIC MODEL

To this end, the mechanical features of the model were such that it closely simulated the mathematical model. The blades were free to flap normal to the plane of the disc only and were very stiff in the chordwise and torsional modes. Wing aerodynamic effects were excluded by shrouding the wing spar. Parametric variations of wing spar stiffness, blade hinge offset, and blade mass were investigated.

The second model was a 5 foot diameter, powered, semi-span model dynamically similar to a specific tilt rotor design. The model included remotely controlled collective and cyclic pitch, and nacelle tilt angle. The model also incorporated a variable swashplate feathering feedback. In addition to the investigation of prop whirl flutter characteristic, the model was utilized to generate blade loads data under condition of non-axial flow and cyclic pitch control.

It should be noted that the design and construction of dynamically similar model requires the same careful attention as the full scale hardware. This requires an accurate prediction of blade natural frequencies, careful balancing of the dynamic components, and the determination of and minimization of undesirable amounts of built in lateral cyclic and control free-play. Otherwise, dynamic loads, in particular 1/rev loads, will dominate the data, making needed on-site interpretations of the data difficult at best and complicating the final data reduction procedure. Even more important is the possibility of having to limit the scope of desired testing because blade loads exceed safe limits.

Typical results from the unpowered model test program are shown in Figure 10 where it can be seen that analytical flutter predictions (which neglected structural damping) are conservative and correlate well with the test data for a series of spar stiffnesses.

The flutter mode and frequency was, as predicted, essentially that of the wing fundamental coupled vertical bending mode without any significant chordwise bending of the wing (which would produce yaw of the nacelle). This is illustrated in Figure 11 where traces of blade flapping motion, and wing vertical, chordwise and torsional motions as measured by strain gages are shown. The torsion is in exact phase with the vertical wing bending as anticipated, the rotational speed plus and minus flutter frequency is clearly evident in the blade traces. This may be interpreted as the rotor tip path plane oscillating in pitch and yaw at the same frequency as the wing oscillations.

As a general comment, it should be noted that the complexity of the inter-relationship of important parameters make broad general conclusions inadvisable. The best one can say is that for the range of parameters tested for this specific model configuration, the flutter speed tended to increase with torsion stiffness, with hinge offset, and with blade weight. Typical experimental results showing the effects of blade weight, hinge offset, and beam stiffnesses are shown in Figures (12, 13, and 14 respectively). With particular reference to the stoppable rotor aircraft configurations, it can be seen from beam 3 in Figure 14 that the critical rotor RPM may be obtained as the rotor is feathered and the rotor slowed to an RPM below its normal operating RPM.

The effects of nacelle tilt relative to the free stream are illustrated in Figures 15 and 16 for two different beams. In Figure 15 the flutter speed for a fixed collective clearly increases with nacelle tilt. However, in Figure 16 which is a plot of flutter speed vs collective pitch for two discrete nacelle tilt angles, it can be seen that the flutter speed may either increase or decrease with nacelle tilt at a fixed collective depending on the collective pitch setting. It should also be observed that the most critical flutter condition is in fact at the 4.5° nacelle tilt which is more representative of cruise angles of attack. The effects of nacelle tilt on the coupled natural frequencies and mode shapes are handled in a straight forward manner and do not explain these results. Obviously the effects of non-axial flow must be carefully examined in each specific design.

Result from the powered model shown in Figure 9 are shown in Figure 17. The flutter mode in this test also involved the wing coupled vertical bending mode. Both the flutter frequency and flutter speed characteristic correlate with theory when wing aerodynamic effects are neglected. As can be seen from these data, the influence of positive thrust is stabilizing with flutter occurring near the zero or slightly negative thrust condition characteristic of a windmilling rotor. It is also noted that this flutter was limit-cycle in nature permitting long increments of time fairly deep within the flutter region without the oscillation building up to critical amplitudes. It suggests that some non-linear or wing rotor unsteady interference effects may be present.

MECHANICAL INSTABILITY

Large diameter hingeless rotors, which incorporate cyclic pitch for yaw control, such as for the tilt rotor configurations, tend to have a low inplane stiffness (i.e., the natural frequency of the first flexible mode below 1/rev) to reduce blade root stresses. These loads arise from coriolis forces which are relieved in the normal helicopter blade by the lag hinge. However, the consequence of utilizing a low inplane stiffness blade is to introduce the possibility of mechanical instability, or ground and air resonance.

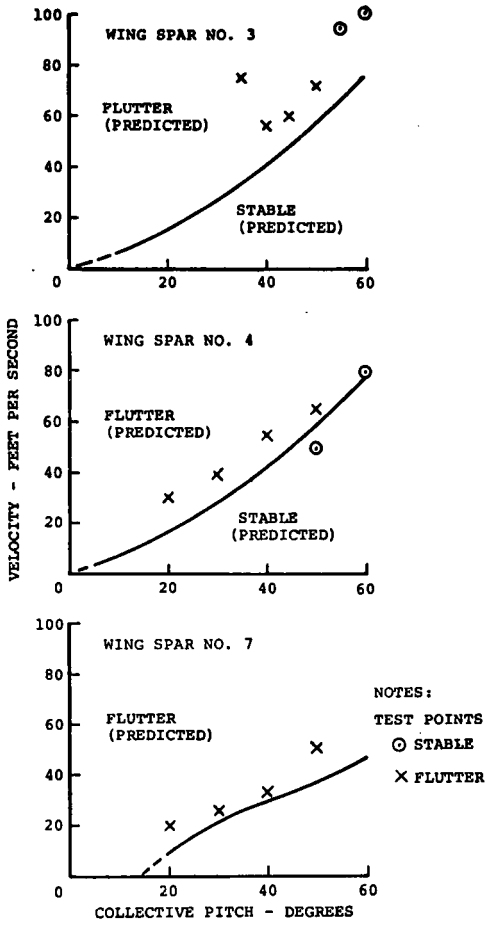


FIGURE 10. CORRELATION OF FLUTTER TEST RESULTS WITH ANALYSIS

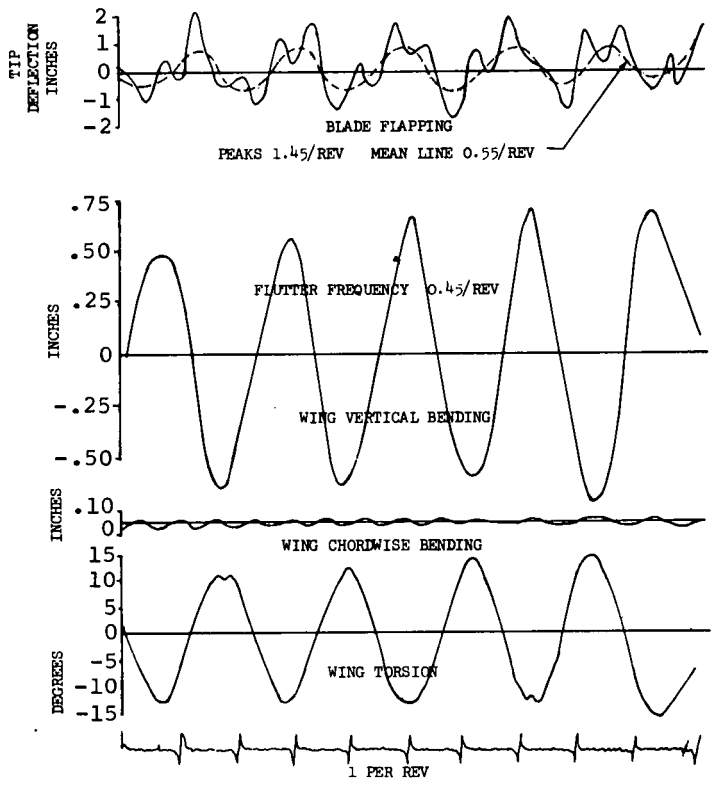
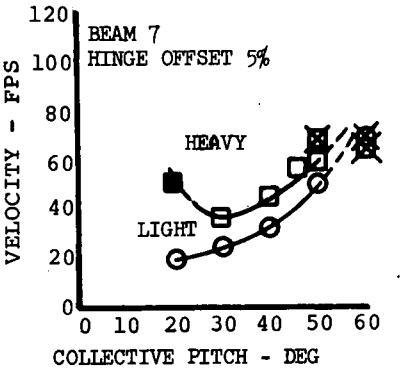
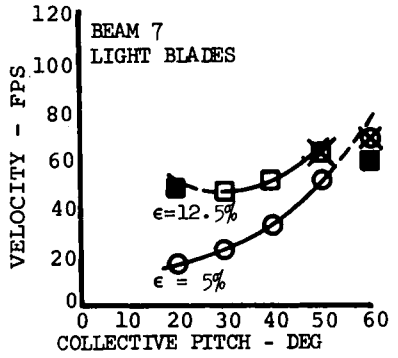


FIGURE 11. SAMPLE TRACES OF FLUTTER DATA



BLADE WT RATIO 1.58
FLAPPING MOMENT OF
INERTIA RATIO 1.90

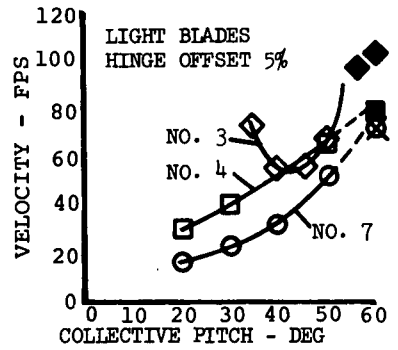
FIGURE 12. EFFECT OF BLADE WEIGHT ON FLUTTER SPEED



SYMBOLS

OPEN - FLUTTER
CLOSED - STABLE
X - DIVERGENCE

FIGURE 13. EFFECT OF HINGE OFFSET ON FLUTTER SPEED



TORSIONAL STIFFNESS
RATIO

BEAM 3 2.0
BEAM 4 1.68
BEAM 7 1.0

FIGURE 14. EFFECT OF BEAM STIFFNESS ON FLUTTER SPEED

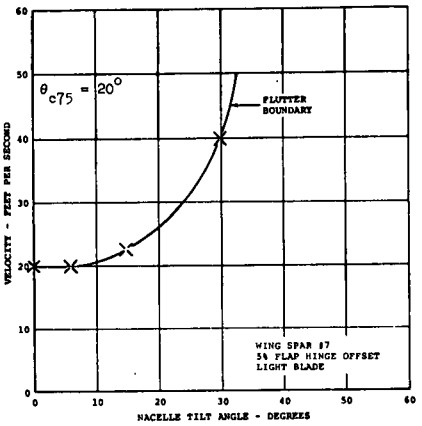


FIGURE 15. EFFECT OF NACELLE TILT ON FLUTTER SPEED

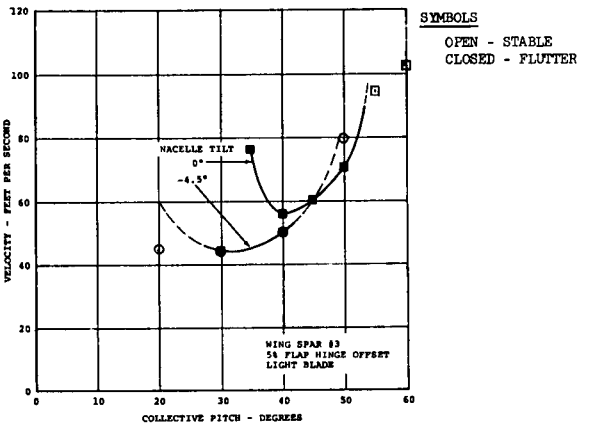


FIGURE 16. EFFECT OF NACELLE TILT ON FLUTTER SPEED

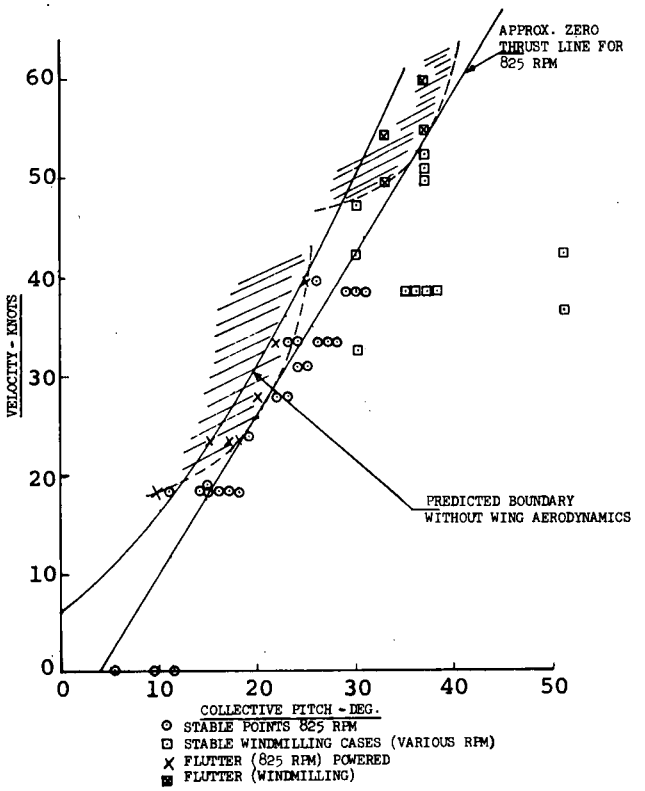


FIGURE 17. FLUTTER CHARACTERISTICS OF A 1/10 SCALED MODEL TILT ROTOR

The mechanism of mechanical instability is well understood and has been treated in helicopters on a routine basis for many years. The typical helicopter tends to be susceptible to ground resonance in a very few modes; usually coupled lateral and roll motion of the fuselage is the only mode that is significant.

V/STOL systems differ from helicopters in that the prop/rotors are mounted at the relatively flexible wing tips. Thus the rotors may have many more freedoms at the relatively low frequencies of the wing modes and low mode generalized masses. Further the natural frequencies of these wing modes vary with nacelle tilt angle. Such modes as wing symmetric or antisymmetric horizontal bending and torsion are most apt to fall within the frequency range where mechanical coupling at operating RPMs can occur.

Figure 18 is a typical frequency plot for a tilt rotor aircraft in the hover configuration indicating the increased risk of mechanical instability when structural modes are considered. Each intersection of the rotor frequency curve with the other modal frequencies is a potential point of mechanical instability. When instability occurs in a structural mode it may be more severe and more difficult to control than if associated with rigid body motion of the whole aircraft because the ratio of blade mass to modal effective mass (Λ_3 of a classical Coleman type of analysis) will be relatively larger in the structural mode than in a rigid body mode. Consequently, the damping requirement to stabilize a structural mode may be considerably larger relative to the requirement for a rigid body mode.

In either case, introducing appropriate damping to the tilt rotor configuration presents problem not found in classical helicopter technology. The body freedom modes generally found to couple significantly with the rotor usually have lateral-roll motion of the aircraft on its landing gear. In the typical helicopter with relatively small roll inertia, there are two modes involving the lateral and roll degrees of freedom each of which has a significant component of roll which exercises the oleos and provides damping in the body freedom.

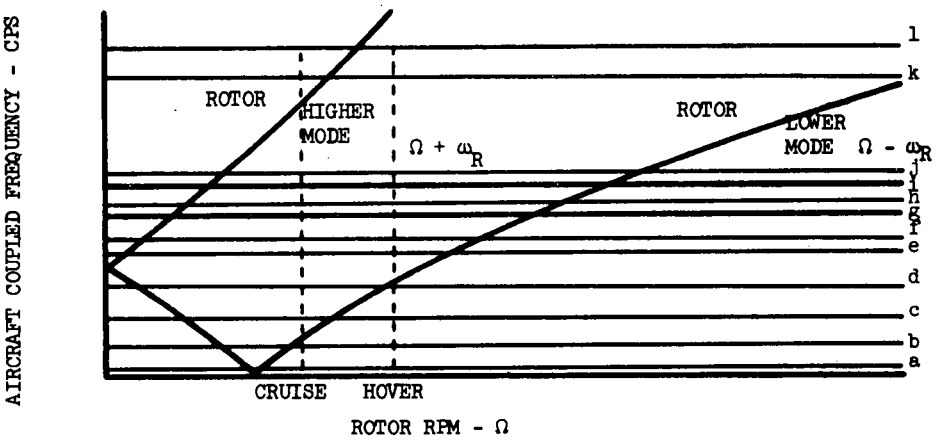
In the tilt rotor configuration, however, the rolling moment of inertia is many times larger than that of a helicopter of equivalent weight (due to the rotor location) and this effectively decouples the roll and lateral degrees of freedom so that sideways motion of the ship against the landing gear lateral stiffness can occur with practically no closure of the oleo. Thus unless a special gear is designed, only a low level of damping is available in this mode, and reliance must be placed in frequency separation to avoid ground resonance.

The hingeless rotor also presents difficulties in the provision of additional damping in the rotor modes. While it would be possible to design a hingeless rotor with devices to provide damping beyond the inherent structural damping, this adds increased cost and complexity and necessarily must be included in the design from the start. Figure 19 illustrates the potential problem for the example problem of Figure 18 in which only the critical damping of the marginal and unstable modes in or near the rotor operating RPM band are shown. For this calculation 3% critical damping has been assumed in all body modes, 1% in flexible airframe modes, and 0.5% in the blade modes. After taking account of all available damping, the system is still unstable in the horizontal wing bending mode just above operating RPMs. Given a flight reduction from design wing frequency such as might easily be found in the ground vibration survey of the first flight aircraft, the unstable region would slip into the operating band of RPM. Thus the aircraft would have a serious problem difficult to cure since damping cannot easily be added by classical methods.

However, it should be noted that these calculations have neglected the rotor aerodynamic damping. Rotor disc rolling velocity results in aerodynamic damping which is added to the body mode. The magnitude of these forces is proportional to the flapwise stiffness or equivalent hinge offset and for typical hingeless prop/rotors can be quite large relative to inherent structural damping.

Further, because these are highly twisted blades, they are also highly coupled in flap and lag motions and, therefore, there is an additional source of inplane or rotor-mode damping for most operating conditions. Kinematic coupling resulting from the rotor geometry or elastic deformations is also an important source of damping which must be carefully assessed.

Under these circumstances illustrated by the previous 2 figures, the need is apparent either for conservative design factors or the facility to bring to bear some other form of suppression. Since cyclic pitch is an essential feature of the tilt rotor design it suggests itself as the active agent of a suppression device. In this application it is envisaged that the swashplate actuator will be given an input signal from the unstable mode so that the rotor is pitched or yawed in phase with the velocity of the mode and thus provides aerodynamic damping in the mode. For example, in the case of wing horizontal bending in Figure 19 the rotor swashplate would be driven by a signal generated by fore and aft deflection of the wing. Other forms of coupling might be equally effective provided they change the properties of the system significantly. As always, with such feedback systems, care must be taken to ensure that the measures used to stabilize one system did not destablize others.



LEGEND:

a.	A/C ROLL	g.	WING SYM FWD BEND
b.	A/C YAW	h.	WING ANTI-SYM VERT BEND
c.	A/C PITCH	i.	WING ANTI-SYM FWD BEND
d.	A/C VERTICAL	j.	A/C FORE AND AFT
e.	A/C LATERAL	k.	WING SYM TORSION
f.	WING SYM. VERT. BEND.	l.	WING ANTI-SYM TORSION

FIGURE 18. AIRCRAFT FREQUENCY SPECTRUM ON GROUND WITH QUASI-NORMAL BLADE LAG MODES

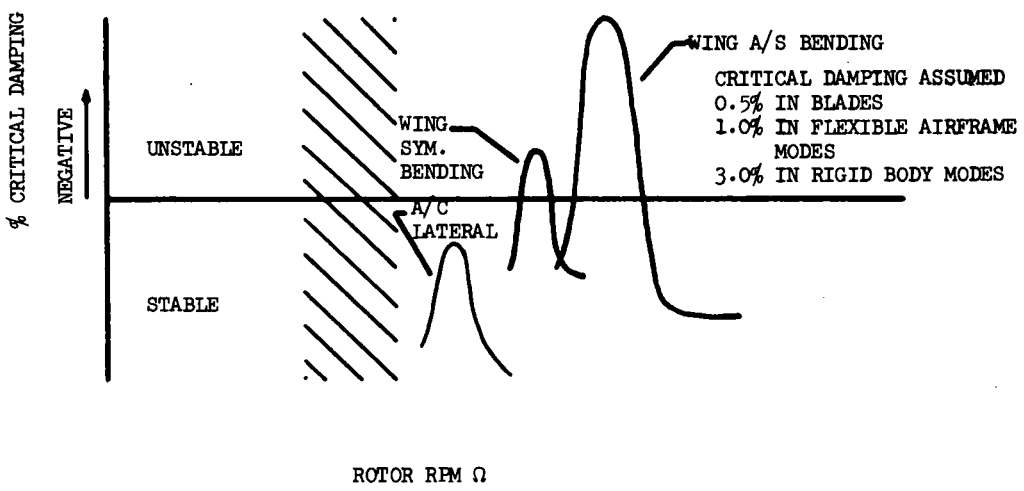


FIGURE 19. A/C DAMPING IN MARGINAL AND UNSTABLE MODES

PROP/ROTOR BLADE INSTABILITIES

Prop/rotor blades are subject to the same static and dynamic instabilities as fixed wings. The problems are more complex to deal with because the high geometric twist and incidence angles, large elastic deflection, and the rotational effect on inertia and aerodynamic forces introduce many coupling effects between the degrees of freedom. Blade deflections occur along a space curve rather than as vertical or flapwise and chordwise bending as is usually considered in helicopter or fixed wing problems.

For the rotating blade, out-of-plane and in-plane deflections in the presence of loads perpendicular to the deflections give rise to powerful torsional moments for any blade that does not have its non-rotating stiffnesses in these two directions exactly matched. The torsional natural frequency can be lowered by a factor of 4 or 5 because of the increase in feathering moment of inertia associated with these deflections. Geometric incidence required for high speed flight result in raising the natural frequencies of what are predominantly flapwise modes and lowering those which are predominantly chordwise modes.

Thus, the mechanisms are present which give rise to all of the instabilities that have been encountered in helicopter technology, such as static divergence, bending-torsion flutter, pitch-lag and flap-lag instabilities. One can anticipate the requirements for built-in geometric kinematic coupling and special treatments to control deflections to attain rotor stability throughout the required operating envelope. An excellent review of these problems can be found in Reference (1).

Slowing, stopping, and folding the rotor introduces substantial changes in stiffness because of the loss of centrifugal stiffening and, potentially, because of the inertial and folding mechanism stiffness variations associated with the folding cycle. For example, if the folding hinge is outboard of the feathering bearing, there will be a substantial change in blade torsional frequency.

The simple static torsional divergence problem encountered by sweep forward wings must be addressed for the rotor blade when it is stopped because both the effects of nacelle angle-of-attack and vertical gust will produce an effective forward sweep on at least one blade. Likewise, the classical fixed-wing bending-torsion flutter problem must be addressed as the blade is swept aft during the folding process. As in the rotating blade condition, the effects of blade deflection resulting from maneuvers and gust responses must be carefully assessed.

LIMIT CYCLE FLUTTER

In the work of Dr. M. I. Young (Reference 2) a pioneering investigation of transient flap-lag instability as a result of large displacement effect such as produced by gusts or control inputs was made for non-twisted helicopter rotors. He showed that there are normally coriolis acceleration coupling of in-plane and out-of-plane blade motions and second order non-linear effects such as time dependent perturbations in the steady lift and drag loads which could lead to limit cycle oscillations, particularly in hingeless rotors where low damping is available for inplane motions.

In the case of the prop/rotor, the relatively large twists and large blade incidence in cruising and high speed forward flight provides an inherently strong coupling in the in-plane and out-of-plane components of the blade natural oscillations. For this reason, an adequate representation of this aeroelastic phenomena requires a rigorous derivation of the motion equations. Although these unstable blade oscillations may be of limited amplitude, they can be of sufficient amplitude to degrade flying and handling qualities, and blade structural fatigue characteristics to unacceptable levels.

The stopped rotor configuration must, in addition, address the conditions of low RPM and large displacement that may arise from gust or evasive maneuvers that occur during its conversion.

GUST LOADS INDUCED ON LARGE ROTORS

The gust response behavior of large lightly loaded rotors operating in the propulsion mode presents problems not encountered in high disc loading propeller technology nor helicopter technology. Since the prop/rotor is used for hover it has the capability of delivering up to 10 times the thrust needed for propulsion in the cruise mode of operation. Hence, any change of blade section angle of attack such as that induced when the rotor meets a horizontal gust can produce large increments in thrust compared to that needed for normal cruise equilibrium. This can result in unacceptable ride qualities. It may also produce weight penalities associated with dynamic response loads in the wing which has inherently a low natural frequency in its fundamental bending modes.

Although longitudinal gust response design criteria for acceptable ride qualities are not clearly defined even in simple terms such as a cabin acceleration for a specified discrete gust (in contrast to a power spectral density criterion), our best judgment would specify a value one half the acceptable vertical acceleration of approximately 0.05 g longitudinal acceleration. A first cut qualitative assessment can be obtained by comparing the thrust increment of the V/STOL aircraft to typical high speed fixed wing propeller driven aircraft which are considered to have acceptable properties. However, one must give full recognition to the limitations of this qualitative comparison because of the significant differences that may be present in the mission spectrums.

Figure 20 illustrates the relative influence of disc loading in the cruise mode on the increment of thrust produced by a 20 ft/sec sharp edged axial gust. One can quickly conclude that the low disc loading tilt rotor aircraft are potentially 3 times as sensitive to longitudinal gust as typical fixed wing aircraft while the tilt wing aircraft are approximately 25% more sensitive.

Of course, the instantaneous effect of a sharp edge gust is equivalent to assuming constant RPM for the more rational (1-cos) gust. The effect of symmetric horizontal gusts on a relative large diameter multirotor V/STOL aircraft has been studied for a range of 1-cosine gusts of constant amplitude and varying wave length. The main study objective was to determine cabin acceleration as influenced by the RPM and flexible wing degrees of freedom and to define the requirement for gust alleviation systems. The results of this study are shown in Figures 21 through 25. The mathematical model included the A/C body freedom in the longitudinal direction, wing horizontal bending, the first rotor blade flexural mode (coning) and rotor RPM perturbations. Rotor aerodynamics are based on linearized prop/rotor aerodynamic performance characteristics.

Figure 21 illustrates the thrust increments and Figure 22 the incremental RPMs as a function of time for various gust lengths most typical of low altitudes. The thrust initially decreases due to the increased inflow velocity arising from the gust. At the same time, the dynamic system responds and an overswing effect occurs, producing positive thrust increments of almost the same magnitude as the initial negative increments. There is a progressive reduction in the magnitude of thrust increment as the gust increases in length, as there is more time for the system to overcome the rotor inertia producing a corresponding greater RPM change. This implies more of the gust energy is used in speeding up the rotor and less in changing the thrust. For comparison, the sharp edge gust or constant RPM rotor thrust levels are also shown in Figure 21. Obviously, permitting the RPM variation in the prop/rotor for these relative short time increments provides inherent gust alleviation.

The cabin acceleration is made up of two components, the response in the aircraft rigid body mode and the response in the wing horizontal free-free mode. The rigid body response (Figure 23) is merely a reflection of the thrust increment. In the bending mode, however, the initial response (Figure 24) in the cabin is opposite to that of the rigid body because of the mode shape. The net cabin acceleration is shown in Figure 25. The wing fuselage chordwise bending frequency for the aircraft considered was such that, for a forward flight velocity of 340 kts, a gust length of 300 ft was tuned to the chordwise bending frequency.

The maximum cabin acceleration response is essentially tuned to the wing fuselage chordwise bending frequency, but its magnitude is acceptably low. As can be seen, the influence of wing flexibility is to make the rebound characteristic slightly larger than the initial peak. Of course, it must be recognized that this simple analysis neglects the effects of wing aerodynamic and structural damping which will reduce the magnitude of the rebound.

The anticipated sensitivity of large rotors to gust has led naturally to the study of alleviation systems which reduce the gust loading by changes of collective pitch coupled to various aircraft or rotor responses. A form of feedback coupling found to be most effective is to gear rotor collective pitch to rotor shaft acceleration. That is to say rotor shaft acceleration is sensed and activates a collective pitch actuator which adjusts collective in such a way as to tend to maintain constant rotor thrust.

For the same tilt wing aircraft, cabin accelerations for the 250 ft gust for various gains are shown in Figure 26. For the high gain (.0009) the cabin acceleration is essentially nulled. For the system analyzed, this feedback, coupling blade collective pitch with rotor shaft acceleration, appears feasible as a means of alleviating the effects of symmetric frontal gusts. In a 20 ft/sec gust the total change of collective pitch to zero out the response is of the order of 1/2 degree. Hence, servo accuracy with respect to gain bias, threshold, etc. becomes a major engineering and design and construction consideration. Of course, the gust alleviation system's gains, rates of operations, and system thresholds must be carefully evaluated and the coupling effects between other gust direction, maneuver and pilot controls must be thoroughly investigated to support the definition of system design criteria.

In all probability, the more serious gust response problem is that of lateral-directional response in the presence of non-homogeneous turbulence. Without cross-shafting, yaw moments will be developed when one rotor experiences a gust of greater intensity than does the other. As illustrated schematically in Figure 27, when the rotors are interconnected a change in RPM on one rotor is communicated to the other rotor via the shafting. Thus in the extreme case where only one rotor experiences the gust, it will tend to speed up and develop an increment of negative thrust. The other rotor will speed up also but in doing so increases its angle of attack and develops an increment of thrust. Thus a sizeable yawing moment develops. Moreover because the rotors and shafting constitute a dynamic system, the incremental thrust on the driven rotor will tend to develop after the aircraft has developed some yawing velocity. In addition, the effects of wing flexibility and possibility of the second rotor experiencing the gust at a latter time all introduce phase lags that can seriously degrade the yaw stability of the aircraft. This may necessitate vertical fin areas larger than required by other criteria or sophistigated gust alleviation systems which involve both yaw damper as well as rotor tip path plane control.

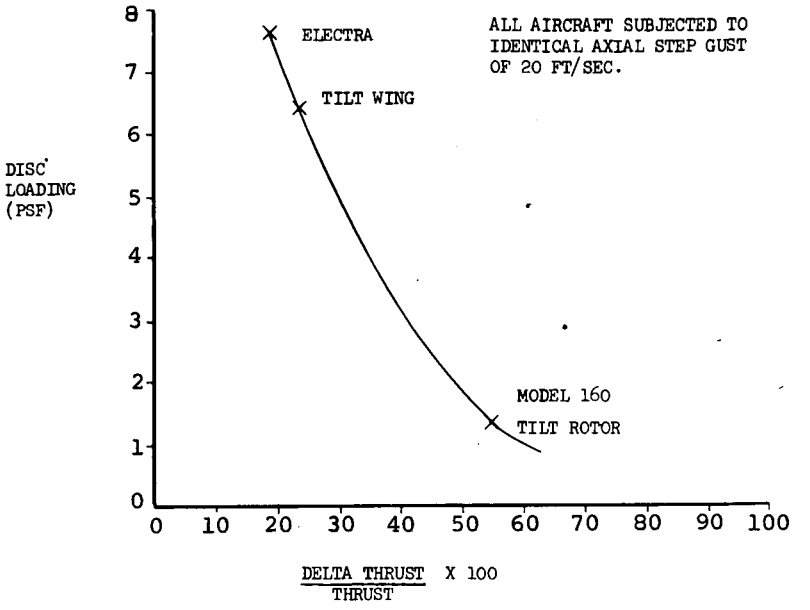


FIGURE 20. GUST SENSITIVITY AS A FUNCTION OF DISC LOADING

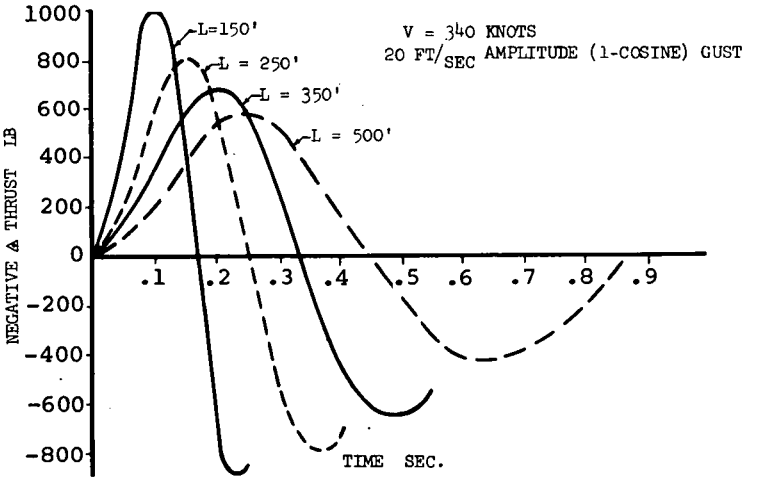


FIGURE 21. THRUST INCREMENT VS GUST LENGTH

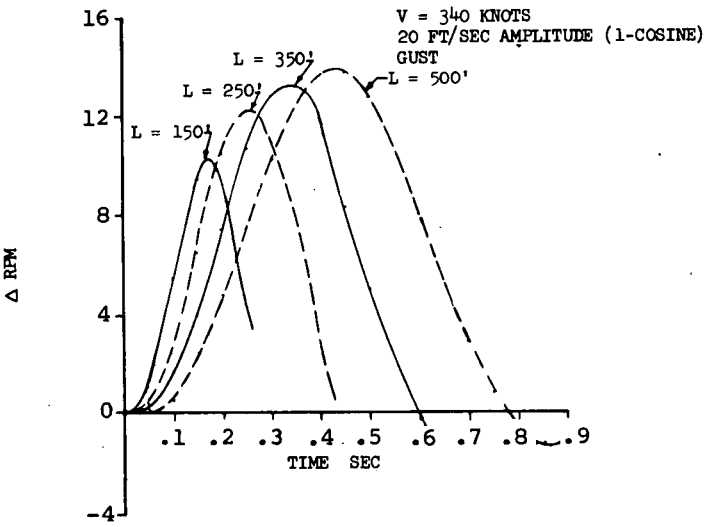


FIGURE 22. RPM INCREMENT VS GUST LENGTH

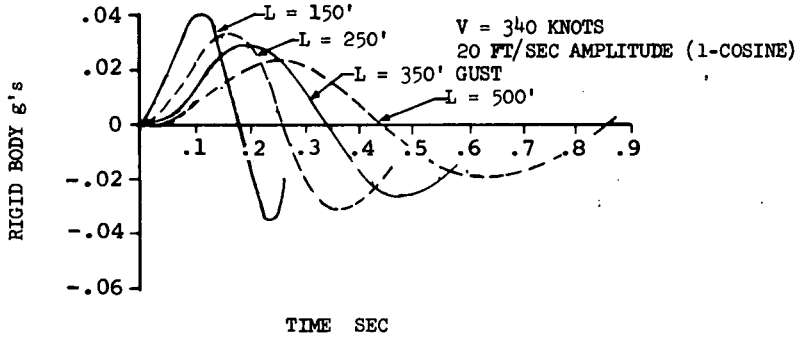


FIGURE 23. RIGID BODY ACCELERATION VS GUST LENGTH

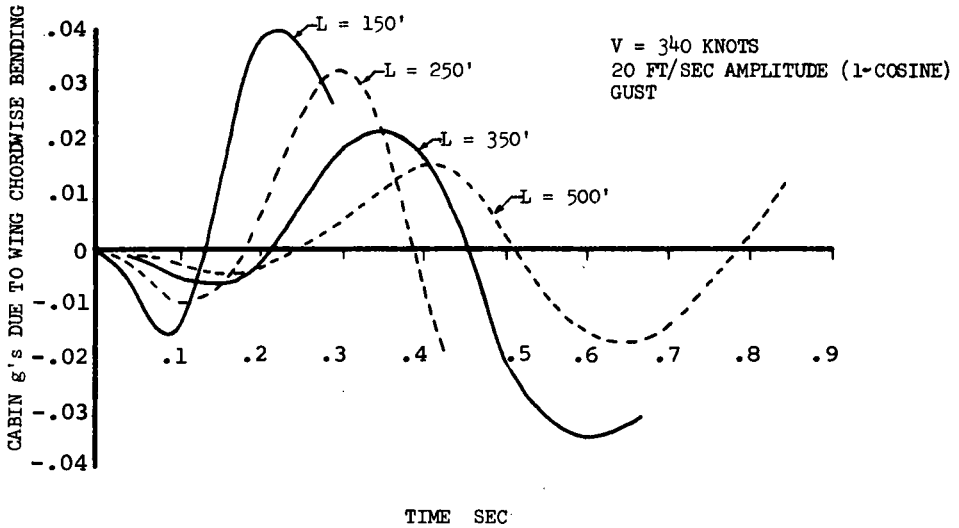


FIGURE 24. CABIN ACCELERATION RESULTING FROM CHORDWISE BENDING VS GUST LENGTH

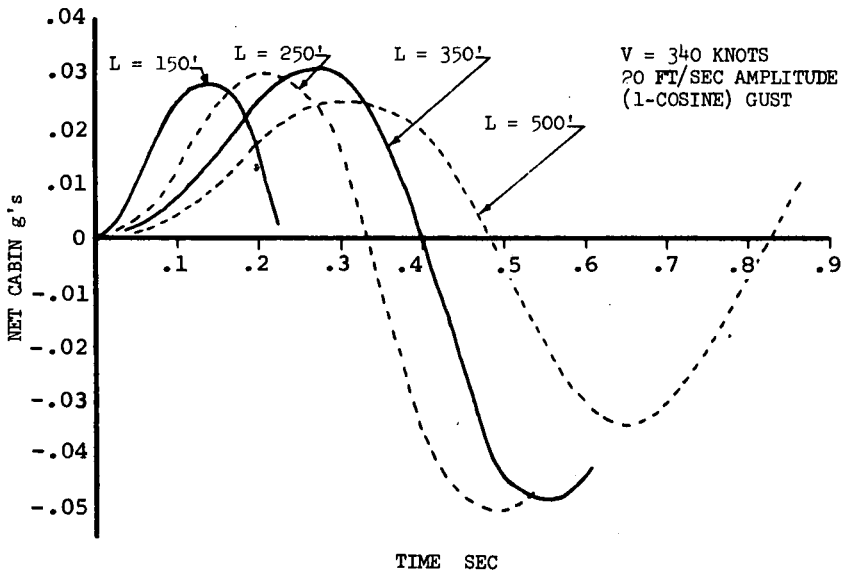


FIGURE 25. NET CABIN ACCELERATION VS GUST LENGTH

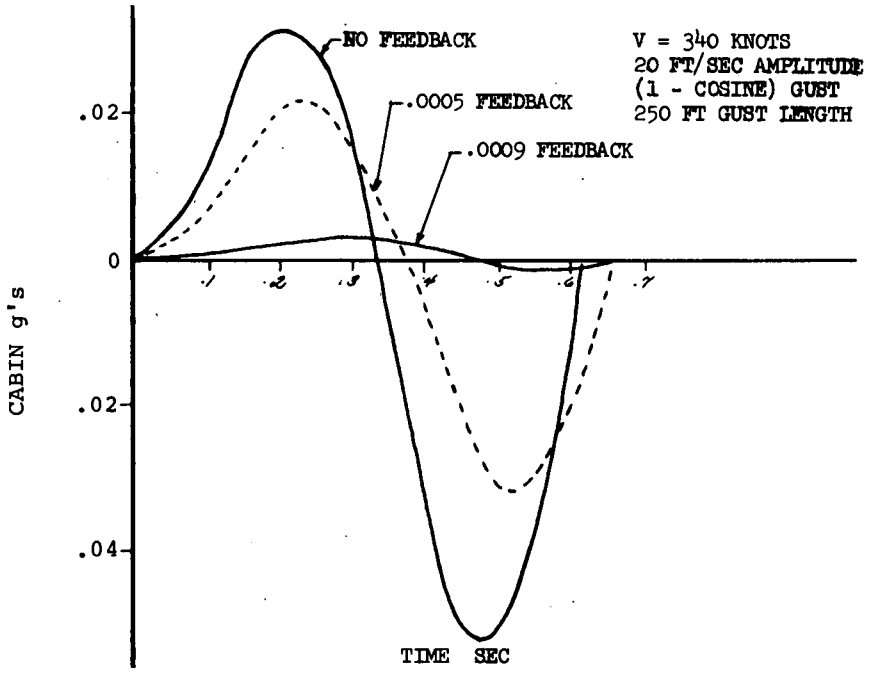
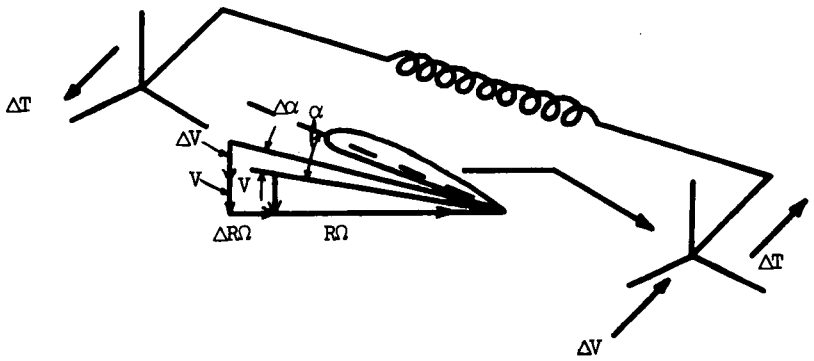


FIGURE 26. CABIN ACCELERATION WITH EFFECT OF FEEDBACK



1. ROTOR IN GUST LOSES ANGLE OF ATTACK AND SPEEDS UP. INCREMENT OF NEGATIVE THRUST.
2. ROTOR NOT IN GUST SPEEDS UP WHICH INCREASES THE EFFECTIVE BLADE ANGLE OF ATTACK. INCREMENT OF POSITIVE THRUST DEVELOPED.
3. YAW MOMENT APPLIED TO A/C
4. A/C RESPONDS
5. ROTOR THRUST INCREMENTS DEVELOP WITH PHASE LAGS SO THAT POSSIBILITY OF DEGRADATION OF YAW STABILITY EXISTS.

FIGURE 27. SCHEMATIC OF LATERAL-DIRECTIONAL RESPONSE TO ASSYMETRIC HEAD ON GUST

AIRFRAME VIBRATION

In general, the fuselage vibration characteristics require the same careful treatment currently employed in helicopter development. For the most part the technology of rotor vibratory loads and fuselage forced response predictions used in helicopter technology is directly applicable and adequate. The problem is simply more complicated because of the variable coupled natural frequencies of the airframe as previously discussed.

Within the constraints imposed by performance requirements (the number of blades, tip speed in hover and cruise, blade radius, chord, and twist) and the requirements dictated by structural loads and deflection, the rotor design should be optimized to minimize the important vibratory hub loads since the forces and moments represent a measure of the resultant aircraft forced vibration.

The low fundamental airframe coupled natural frequencies which can vary with tilt angle as previously discussed and unique loading environment which produced 1/rev loadings in particular, may necessitate effective rotor and/or powerplant isolation for structural integrity. Obviously such a requirement could have a significant effect on the whirl flutter characteristic. The high vibratory loading conditions are generally not ammenable to analytical predictions and, as such, shaking forces and moments for design must be obtained from model test data. Additionally rotor/airframe interference effects, rotor trailing vortex effects and large angles of attack at the conversion speed result in non-uniform inflow through the rotor discs, hence large aerodynamic excitations.

The stoppable rotor configuration encounters a unique transient vibration condition as rotor RPM variations necessarily transverse blade and wing natural frequencies. Because of the relative short time of duration, this problem is not likely to result in a significant human comfort problem, but could be of significance in considerations of integrity.

REFERENCES

(1) Robert G. Loewy, Review of Rotary-Wing V/STOL Dynamic and Aeroelastic Problems, AIAA Paper No. 69-202, Presented at the AIAA/AHS VTOL Research, Design, and Operations Meeting at Georgia Institute of Technology, Atlanta, Georgia, February 17 - 19 1969.

(2) M.I. Young, A Theory of Rotor Blade Motion Stability in Powered Flight, Journal of American Helicopter Society, V.9, N-3, July 1964, pp 12 - 25.

EFFETS AEROELASTIQUES sur les QUALITES de VOL d'un ROTOR RIGIDE

by

J.Gallot

Service Aerodynamique
Sud-Aviation
Marignane, France

EFFETS AEROELASTIQUES sur les QUALITES de VOL d'un ROTOR RIGIDE

par J. GALLOT, SERVICE AERODYNAMIQUE

SUD-AVIATION

MARIGNANE FRANCE

Résumé

Le rotor "rigide", à pales plastiques, est un rotor dont les pales sont relativement souples en battement et traînée, ce qui conduit à l'assimiler à un rotor articulé à forte excentricité de battement et de traînée. Cette simplification permet de représenter correctement le comportement dynamique du rotor du point de vue qualités de vol. Les résultats d'essais en vol à grande vitesse ont montré, toutefois, que le comportement de l'hélicoptère était modifié, pour les facteurs de charge élevés, par un phénomène annexe que l'on peut décrire sous le terme de couplage traînée-torsion par le statique de battement. Ce phénomène a été très bien expliqué théoriquement et une série d'essais a permis de le mettre en évidence et de trouver les paramètres permettant de le minimiser.

Notations

M_i	Gradient de moment de tangage (mN/degré)
V	Vitesse appareil (km/h)
m	Masse appareil (kg)
NR	Régime rotor (t/mn)
n	Facteur de charge
T	Période (sec)
t_D	Temps de doublement (sec)
$D\beta$	Composante en sinus du pas cyclique (en % de la course totale du manche)
βc	Préconicité du rotor
$\Delta\beta i$	Angle de cassure de la pale par rapport à l'axe de pas
$\Delta\theta$ cyclique rotor :	Variation de pas cyclique à 0,7 R due à la déformation de la pale.

Introduction

Le rotor rigide a été adopté dans le cas de l'appareil SA 340 dans le but d'utiliser une solution rotor plus simple et plus moderne à la fois. La réalisation en a été rendue possible grâce aux progrès de la technologie hélicoptère et à l'utilisation de matériaux résistant à des charges élevées, ayant de bonnes caractéristiques de fatigue.

Les avantages, pronés pour la solution rotor rigide, sont liés à la simplicité du rotor et du moyeu (fig. 1), ce qui conduit à :

- un coût de fabrication moins élevé,
- un poids et un encombrement réduits,
- une fiabilité meilleure,
- un entretien simplifié.

Par ailleurs, les qualités de vol de l'hélicoptère doivent être nettement améliorées par l'utilisation d'un rotor rigide, dont la puissance de commande et le temps de réponse rendent la maniabilité de l'appareil plus grande.

Les premiers essais ont été réalisés en Janvier 1966 sur Alouette II équipée d'un rotor tripale, en étroite collaboration avec la Société BOLKOW G.M.B.H. Le programme d'essai couvrant une endurance de 1000 heures et plus de deux années de vieillissement est achevé à l'heure actuelle. Les essais ont été poursuivis ensuite sur un appareil plus moderne et plus rapide, le SA 340, dont le premier vol eut lieu le 7 Avril 1967. L'évolution normale de l'appareil a permis de réaliser des vitesses plus élevées que sur l'Alouette Bölkow, une fois les problèmes de vibrations résolus, et de tester complètement les qualités de vol de ce rotor rigide à des vitesses élevées.

Description du rotor rigide du SA 340

L'objectif recherché (suppression des articulations de battement et de traînée) pouvait être réalisé de deux manières différentes :

- introduction d'éléments souples dans le moyeu lui-même
- ou souplesse de la pale dans la zone du col

de façon, dans les deux cas, à permettre les mouvements dynamiques de la pale en battement et en traînée.

C'est la deuxième solution qui a été retenue (fig.2). Les pales sont montées par l'intermédiaire de l'articulation de pas sur des fusées solidaires d'un moyeu très rigide (Moyeu Intégré Rigide). La pale elle-même, construite en fibre de verre, est relativement souple dans la zone du col, ce qui lui confère une première fréquence propre de battement de 1,15 Ω et une première fréquence propre de traînée de 0,82 Ω . Les caractéristiques générales des deux appareils, qui ont été utilisés par Sud-Aviation pour tester les qualités de vol de ce type de rotor, sont les suivantes :

	Alouette II Rotor rigide	SA 340
Masse maximale (kg)	1650	1600
Diamètre rotor (m)	10,20	10,5
Nombre de pales	3	3
Corde (m)	0,270	0,285
Nombre de tours rotor (t/mn)	360	378 (410)
Vitesse testée en vol (km/h)	240	280

Etude théorique du comportement dynamique d'un hélicoptère à rotor rigide

Dans le cas d'un rotor articulé classique, le comportement de l'hélicoptère est lié au mouvement de battement de la pale par rapport à l'arbre rotor.

Dans le cas du rotor rigide adopté par Sud-Aviation, ce mouvement est remplacé par une déformation en flexion de la pale que l'on peut assimiler à un battement par rapport à une articulation fictive, cette articulation étant beaucoup plus éloignée que pour un rotor articulé.

Ces considérations conduisent à un modèle de rotor simplifié : rotor équivalent à forte excentricité de battement. Du fait de l'excentrement de l'articulation de battement, le foyer du rotor rigide est très élevé, ce qui lui confère une puissance de commande et un amortissement plus élevés, mais conduit aussi à une instabilité d'assiette croissant très rapidement avec la vitesse si l'appareil est équipé d'un empennage de taille conventionnelle comme pour les rotors articulés.

La figure 3 montre, dans le cas du rotor rigide, la nécessité de contrebalancer l'instabilité statique d'assiette du rotor et du fuselage par une contribution stabilisante très importante donnée par une grande surface d'empennage, (cette nécessité pose, d'ailleurs, le problème du choix d'un emplacement optimum pour l'empennage, au point de vue aérodynamique, comme le montrèrent les résultats expérimentaux). Le fait d'augmenter la taille de l'empennage (fig.4) permet d'accroître notoirement le temps de doublement de l'oscillation à longue période, commandes bloquées, qui détermine le comportement de l'appareil après un échelon de commande ou la traversée d'une rafale.

Dans le cas d'un rotor rigide, la puissance de commande étant aussi plus élevée que pour un rotor articulé, les facteurs de charge atteints sur un échelon de cyclique sont plus importants et sont proches des limites du rotor au point de vue décrochage. Il a semblé intéressant de simuler le comportement de l'appareil dans une rafale en étudiant le facteur de charge maximum lors de la première oscillation après un échelon de cyclique de 3% à cabrer, (fig.5). L'augmentation de surface de l'empennage, théoriquement, diminue notoirement le facteur de charge atteint en ressource pour un échelon type, qui, avec l'empennage classique, aurait été prohibitif à grande vitesse, le facteur de charge atteint dépassant alors la limite de décrochage du rotor.

Résultats expérimentaux

Les premiers essais en vol, au-delà de 200 km/h, ont montré que l'appareil avait un comportement désagréable par temps turbulent avec un empennage de taille classique. Sous l'action d'une rafale ou d'un échelon de commande cyclique à cabrer, l'appareil engageait à cabrer, le facteur de charge croissant très rapidement jusqu'au décrochage du rotor, le pilote devant contrer le mouvement au pas cyclique et au pas général.

L'augmentation de la surface de l'empennage se révèla insuffisante. Un empennage, équipé de pitots, montra, par la suite, que l'efficacité de l'empennage dépend beaucoup de sa position dans le flux rotor (fig.6). Toute discontinuité dans l'alimentation de l'empennage se traduit par une variation du moment dû au fuselage et par un déplacement sensible du manche en configuration stabilisée. En ressource, ceci peut détériorer notoirement les qualités de vol de l'hélicoptère pour les oscillations de grande amplitude. Dans le cas d'un appareil à rotor rigide, la surface de l'empennage devenant importante, l'emplacement de celui-ci doit être étudié avec le plus grand soin. La stabilité longitudinale d'un appareil classique étant généralement meilleure en centrage avant, les essais à un centrage avancé de 20 cm permirent de démontrer un comportement sain jusqu'à 220 km/h environ.

Devant ces résultats plus pessimistes que les prévisions, les essais furent orientés vers l'analyse du comportement du rotor avec facteur de charge. L'allure des courbes de manche en virage à pas général et vitesse constante, altitude variable, nous est apparue significative. En effet, pour un appareil stable, ces courbes ont une pente négative (recul du manche pour une augmentation du facteur de charge), le changement de pente correspond, pour les mouvements de petite amplitude, à un mouvement apériodique divergent. Les résultats des essais montrèrent que ces courbes présentaient une inversion de pente non prévue théoriquement, pour des facteurs de charge de plus en plus faibles au fur et à mesure que le pas et la vitesse augmentent (fig.7).

Pour chaque vitesse, il existe donc un facteur de charge au-delà duquel l'hélicoptère est instable statiquement. Une série d'essais furent conduits pour montrer que le facteur de charge atteint en ressource avait une influence sur le comportement de l'appareil. Ceci fut vérifié en étudiant la réponse de l'appareil pour des échelons différents à une vitesse donnée, ce qui donna les résultats de la figure 8. Tant que le facteur de charge atteint au cours d'une évolution, suite à un échelon, restait inférieur à la limite d'instabilité déduite des courbes de cyclique en fonction du facteur de charge, l'appareil faisait une oscillation complète sans que le pilote touche aux commandes, sinon, au-delà de cette limite, l'appareil engageait à cabrer jusqu'au décrochage, ce qui nécessitait une intervention rapide du pilote au pas collectif et au cyclique.

L'examen des contraintes pales enregistrées en ressource a montré :

- l'augmentation des contraintes statiques et dynamiques de battement liée à l'accroissement du facteur de charge et au basculement du rotor en arrière,

- l'apparition de contraintes alternées de traînée sur le moyeu, correspondant à un recul dynamique pour la pale avançante,

- une augmentation de la contrainte alternée sur la biellette de pas correspondant à un moment à cabrer sur la pale en position avançante, le décrochage apparaissant finalement sur la pale reculante pour les facteurs de charge élevés.

Ces résultats ont conduit à penser que la pale se déformait en torsion lorsque le facteur de charge augmentait et que son incidence, côté pale avançante, augmentait, ce qui est équivalent à une variation cyclique de pas à cabrer au cours de la ressource (fig. 9).

Etude de la déformation de la pale en ressource

Devant ces résultats, une étude théorique simplifiée permit d'analyser le phénomène, d'essayer d'en chiffrer l'importance et de déterminer les paramètres influents. Il s'agit d'un couplage traînée-torsion par le statique de battement. En ressource, lorsque le facteur de charge augmente, la pale se déforme statiquement en battement et, pour une valeur critique de ce facteur de charge, passe au-dessus de l'axe de pas calé par rapport à l'arbre suivant l'angle de préconicité choisi. Tout effort dynamique de traînée par suite de la déformation statique de battement, produit un moment alterné de torsion, donc une torsion parasite. Compte-tenu du sens des efforts de traînée mesurés ou calculés (vers l'arrière sur la pale avançante), celà se traduit par une variation cyclique d'incidence à cabrer. La première étude supposait que la déformation était localisée dans le col de la pale, ce qui permettait de définir simplement un coefficient de couplage approché donnant la déformation de torsion pour une flèche de battement et de traînée unitaire. Ce coefficient a été mesuré sur pale au repos et il a été possible d'en déduire les valeurs de rigidité à faire intervenir dans le calcul. Une étude plus détaillée faisant intervenir la répartition de moment de torsion le long de la pale, donne des résultats semblables quantitativement. Toutefois,

la torsion est répartie sur une portion plus étendue de la pale. Cette théorie a permis de mettre en évidence l'influence des paramètres suivants sur la déformation en torsion en fonction du facteur de charge (fig. 10):

1. taux de variation de la déformée statique avec le facteur de charge,
2. angle de préconicité,
3. cassure de la pale par rapport à l'axe de pas,
4. décentrage latéral,
5. et, évidemment, les souplesses relatives en battement, traînée et torsion.

Expérimentalement, le taux de variation de la déformée statique avec le facteur de charge fut minimisé par adjonction de masses en extrêmité de pale. La pente des courbes de manche °fut nettement améliorée (fig. 11) ainsi que les qualités de vol de l'appareil. Le même effet fut atteint en augmentant le régime rotor de 378 t/mn à 410 t/mn. Le comportement de l'appareil fut amélioré de manière remarquable et le phénomène d'engagement à cabrer fut supprimé dans tout le domaine de vol, l'appareil ayant volé à 275 km/h à un facteur de charge de n = 1,7. En vol de croisière, l'appareil vole, manche bloqué pendant deux minutes, sans problème et répond normalement à des sollicitations de 2 à 3% à cabrer, les facteurs de charge maximum étant réduits de manière notable (fig. 12).

La préconicité fut augmentée sur l'Alouette Bölkow, ce qui permît d'accroître notoirement le domaine de vol de l'appareil par temps turbulent jusqu'à 210 km/h, ce qui est remarquable compte-tenu de la nature du fuselage, identique à celui de l'Alouette II série classique. Les courbes de manche sont devenues stables jusqu'à un facteur de charge de 1,6 pour un pas de 14° à 180 km/h. Le comportement de l'appareil est considéré actuellement comme comparable à celui d'un appareil équipé d'un rotor articulé.

Dans le but de vérifier plus à fond la théorie, l'influence du décentrage latéral fut testée en vol par l'adjonction d'une masse de 100 kg sur le patin du train, ce qui correspond à une variation de centrage de 6 cm. Le comportement de l'appareil fut nettement amélioré en centrage à gauche, ce qui diminue aussi les efforts sur la pale reculante.

Le phénomène de couplage traînée-torsion par le statique de battement semble, en définitive, bien établi et constitue un problème qu'il faut traiter avec le plus grand soin pour ce type de rotor.

Conclusions

L'ensemble de ces résultats expérimentaux et théoriques montre de manière significative l'importance des caractéristiques élastiques de la pale et des phénomènes aéroélastiques sur les qualités de vol d'un hélicoptère à rotor rigide.

En premier lieu, le choix de la souplesse en battement de la pale, dans une solution moyeu rigide, détermine la position de l'articulation équivalente de la pale et influe directement sur la stabilité dynamique et le contrôle de l'appareil.

Les souplesses en battement, traînée, torsion, interviennent pour déterminer le degré de couplage admissible pour un rotor de ce type. La solution optimale serait une pale ayant des rigidités en battement et en traînée très voisines et une grande rigidité en torsion.

Avec une pale dont les caractéristiques ne sont pas optimum, il est possible de minimiser cet effet pour améliorer le comportement dynamique de l'appareil en modifiant la préconicité ou le calage de la pale par rapport à l'axe de pas.

* * *

Références

1. YOUNG, M.I., A simplified theory of hingeless rotors with application to tandem helicopters,

   AHS, 18th Annual National Forum, 1962

2. HUSTON, R.J. An exploratory investigation of factors affecting the handling qualities of a rudimentary hingeless rotor helicopter,

   NASA TND-3418, 1966

3. ELBERT, A. Rade M. HUBER H. Statische und dynamische stabilität des hubschraubers SA 340 mit gelenklosem rotor in vorwärts flug

   Bölkow G.M.B.H. TND 121-1/69

4. LEGRAND, L.F. La prochaine génération des hélicoptères français

   Conférence commémorative La Cierva à la Royal Aeronautical Society - Octobre 1968.

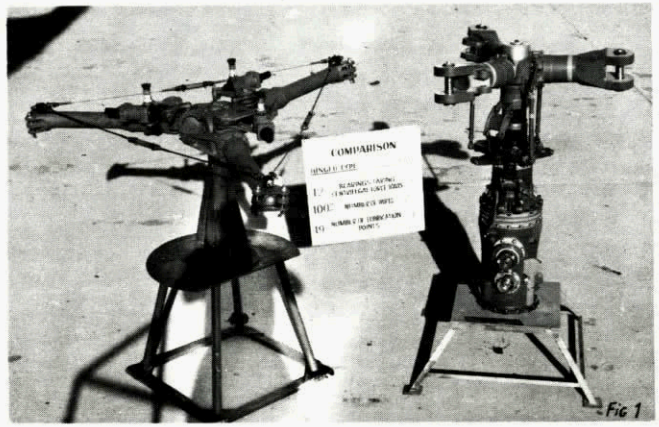


Fig 1

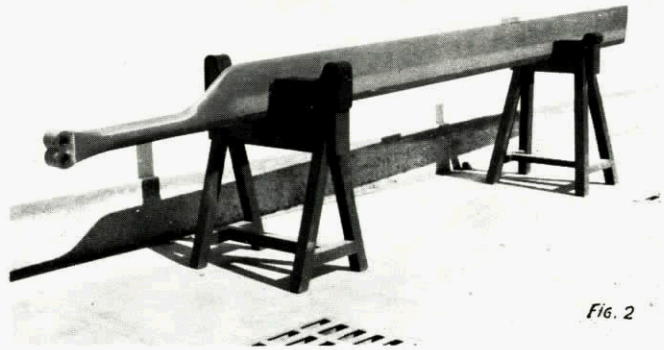


Fig. 2

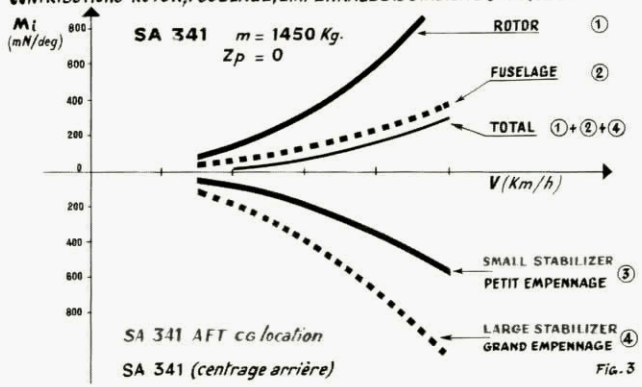


Fig. 3

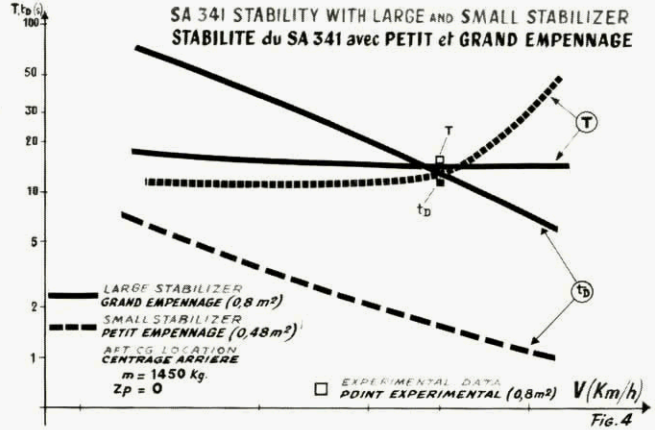


Fig. 4

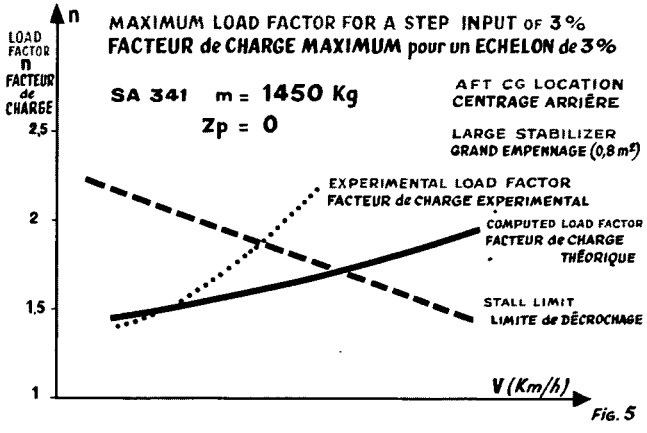


Fig. 5

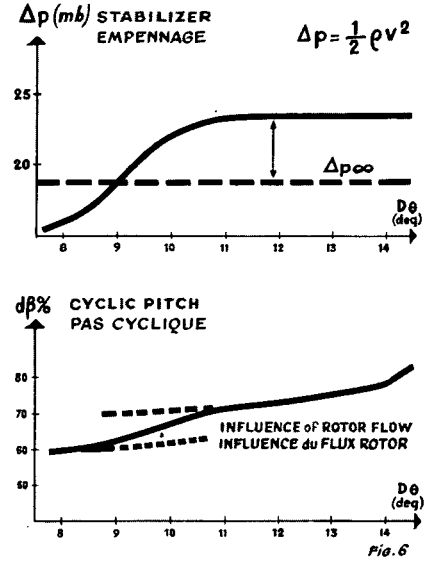


Fig. 6

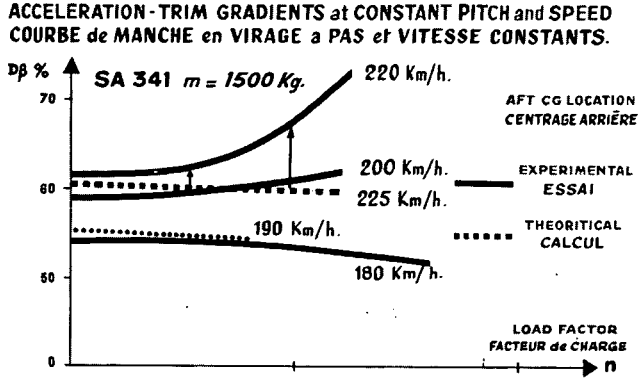


Fig. 7

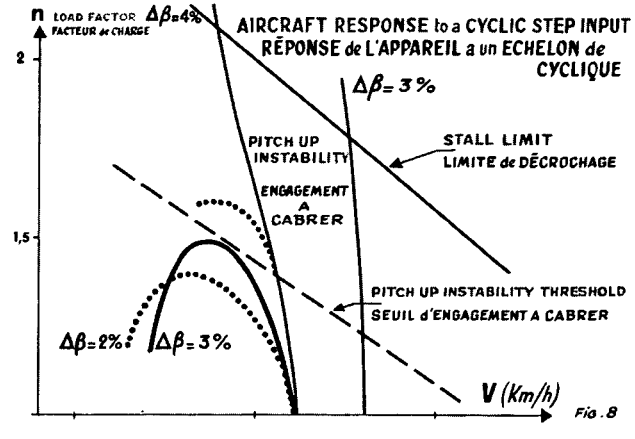


Fig. 8

COUPLING of DRAG and TWIST by the FLAPPING STATIC DEFORMATION
COUPLAGE TRAINÉE-TORSION par la STATIQUE de BATTEMENT

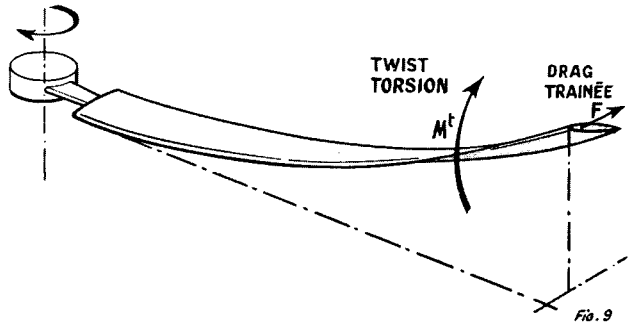


Fig. 9

INFLUENCE of LOAD FACTOR, PRE-CONICITY, BLADE ANGLE ATTACHMENT ON PARASITE CYCLIC PITCH
INFLUENCE du FACTEUR de CHARGE, de la PRÉCONICITÉ, du CALAGE de la PALE sur le PAS CYCLIQUE PARASITE

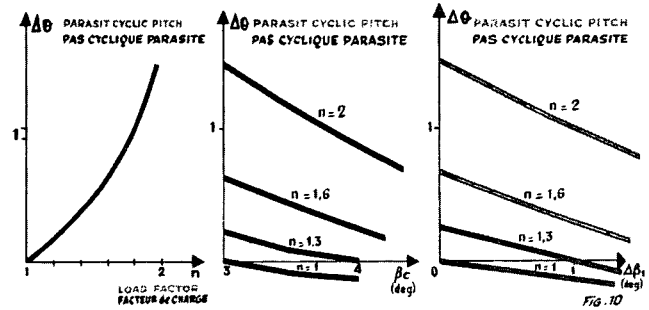


Fig. 10

INFLUENCE of BLADE TIP WEIGHTS
INFLUENCE des MASSES en BOUT de PALE.

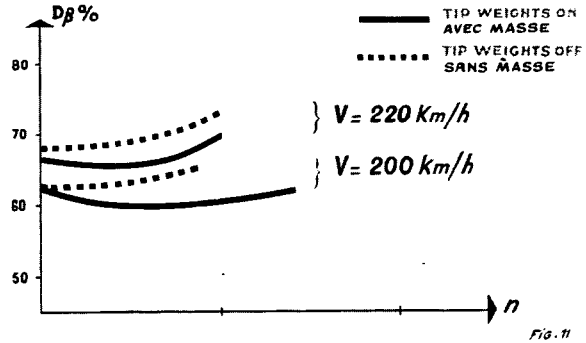


Fig. 11

INFLUENCE of ROTOR ROTATIONAL SPEED on DYNAMIC STABILITY
INFLUENCE du RÉGIME ROTOR sur la STABILITÉ DYNAMIQUE

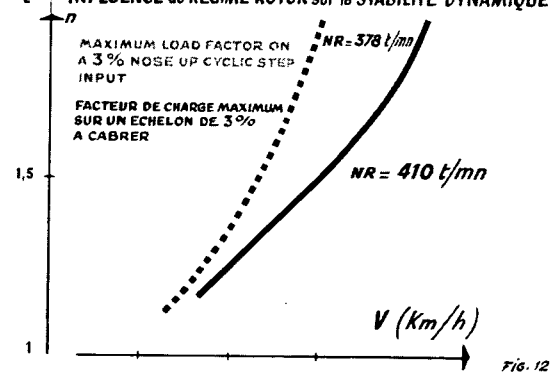


Fig. 12

THE INFLUENCE OF AEROELASTICITY ON STABILITY AND CONTROL OF A HELICOPTER WITH A HINGELESS ROTOR

by

G. Reichert

Messerschmitt-Bölkow GmbH

Ottobrunn, Germany

SUMMARY

The Bölkow rotor system features flapwise and lagwise rigid attachment of flexible fiberglass rotorblades to a very stiff hub. The flight mechanics of a helicopter with such a hingeless rotor system is mainly influenced by the aeroelastic behaviour of the rotor blades.

The paper discusses theoretical work as well as flight-test experience with the BO 105 helicopter.

The results of a parametric study showing the influence of the rotor stiffness on the stability and control characteristics in hovering and forward flight are presented. Additionally, a short discussion of some aeroelastic coupling effects and instability phenomena in flight are given.

SOMMAIRE

Dans le système de rotor de Bölkow, les pales de rotor de fibre de verre souple sont fixées de façon rigide en battement et en traînée, à un moyeu extrêmement raide. La mécanique du vol d'un hélicoptère doté d'un tel rotor rigide est essentiellement influencée par le comportement aéroélastique des pales.

L'auteur exposera les résultats des travaux théoriques et des essais en vol effectués sur l'hélicoptère BO 105.

Il présentera les résultats d'une étude paramétrique montrant l'influence de la rigidité du rotor sur les caractéristiques de stabilité et de contrôle en vol stationnaire et en translation. Il étudiera enfin brièvement certains effets du couplage aéroélastique et certains phénomènes d'instabilité en vol.

LIST OF SYMBOLS

e	hinge offset
F_θ	control stiffness
GW	gross weight
IAS	indicated airspeed
I_y	helicopter moment of inertia about y-axis
LD	logarithmic decrement
M	pitching moment
M_θ	attitude pitching moment
$M_{\dot\theta}$, $M_{\dot\theta}$	pitch damping moment
M_{η_x}	control moment, pitching
PL	pitch link load
R	rotor radius
T	period
t_D	time to double amplitude
t_H	time to half amplitude
v	airspeed
β	flapping angle
ζ	lead-lag angle
θ	blade pitch angle
θ, Θ	pitch attitude
θ_z	blade cyclic pitch
$\tau_{\dot\theta}$	time constant of pitch rate
$\tau_{\dot\phi}$	time constant of roll rate
ϕ	roll attitude
Ω	rotor frequency
$\bar\Omega$	flapping ratio to rotor frequency, ω_β/Ω
ω_E	blade natural frequency
ω_R/ω	torsional frequency ratio
ω_β	flapping frequency

INTRODUCTION

Aeroelasticity is defined as the science which studies the mutual interaction between aerodynamic forces, elastic forces and inertial forces and the influence of this interaction on airplane design. In modern high-speed fixed wing aircraft aeroelastic phenomena have profound effects mainly upon the design of the structural parts. The classical aeroelastic phenomena such as flutter define the design limits which have to be avoided. Due to elastic deformations there may be influences on control effectiveness and on the dynamic and static airplane stability, but for stability and control these effects normally are secondary.

In the case of the rotating wing airplane there exist similar aeroelastic phenomena as with fixed wing airplanes, but there are important differences due to the different airflow conditions, which induce periodic effects, and due to the high centrifugal blade loads. As a first approximation the helicopter with articulated rotor blades can be considered as a system of several rigid bodies, which are combined by inertial and aerodynamic forces. The rotation of the rotor causes a centrifugal restraint between airframe and rotor. Therefore in a helicopter with an articulated rotor there are many phenomena similar to aeroelastic phenomena without structural deflections. In the case of a helicopter with a so-called rigid or better hingeless rotor the rotorblades are flapwise and lagwise rigidly attached to the hub. Flapping and inplane movements of the rotorblades are elastic deflections. The control of the helicopter is achieved by controlling the flapping blades. Also dynamic stability is mainly influenced by the behaviour of the flapping rotor. Therefore in the case of the helicopter with a hingeless rotor all the flight dynamics are of aeroelastic origin.

In the following some problems of the hingeless rotor helicopter concerning aeroelasticity and handling qualities will be described. The analytical work and the flight test experience was done in connection with the development of a small helicopter, the BO 105 (see figure 1) which is now in final flight testing. Some of the phenomena and results have been discussed more detailed in some earlier papers (1 ÷ 4).

DESCRIPTION OF THE DYNAMIC SYSTEM

The main features of the Bölkow Rigid Rotor System are determined by its fiberglass rotorblades of high elasticity, which are rigidly attached to a very stiff hub (see figure 2). It seems therefore, to be not quite correct to use the designation "rigid rotor". The rigidity is only in the hub. There are no flapping and no lagging hinges, only the control of the rotor is done in the conventional manner using feathering bearings which allow the change of the blade pitching angle. The rotorhub, together with the mast and the gearbox is mounted rigidly to the fuselage structure.

The aeroelastic behaviour of a helicopter with this rotor system is mainly influenced by the dynamic behaviour of the elastic rotor blades. Figure 3 shows the natural frequencies of the first two uncoupled bending modes. The first flapping mode has a frequency ratio of 1.12 and the first inplane mode a ratio of .72. Primarily these two modes and the first torsional mode will fix the aeroelastic behaviour, but it is essential to avoid resonance conditions with higher modes in order to keep vibrations and blade stresses at a relatively low level. The BO 105 rotor is well tuned and there are no problems with higher modes.

For theoretical studies it is possible to use a relatively simple mathematical model. In figure 4 the main features of the equivalent system are shown. The elastically deflecting blade can be reduced to a conventional articulated blade with equivalent springs and dampers at each equivalent hinge, however with the pitch axis innermost and fixed under a precone angle to the rotorshaft. It is possible to include blade-sweep. For certain problems up to two elastic torsional hinges are used. It is possible to consider also the rotor support flexibility, which provides coupling of the various blades of the rotor.

The elastic properties of the airframe are normally of minor importance to the flight characteristics with the exception of vibration. They are of importance for the behaviour of the helicopter standing on the ground with the rotor running.

INFLUENCE OF THE FLAPWISE FLEXIBILITY ON FLIGHT DYNAMICS

Concerning handling qualities the main feature of the rigid rotor is its capability to produce very high rotor moments. This has a favorable effect on both stability and controlability of the helicopter. The main parameter is the frequency of the fundamental blade flapwise mode. It is easy to prove that the rigid rotor with elastic blades is equivalent to an articulated rotor with a certain hinge offset and a hinge restraint. Figure 5 shows the relationship. The BO 105 with the rigid rotor has a

frequency ratio of 1.12. Equivalent dynamic characteristics would be for an articulated rotor with an flapping hinge offset of about 14% and no hinge restraint, or for a rotor with zero hinge offset and a corresponding high hinge restraint. The equivalent flapping blade of the cantilevered elastic blade should correspond as accurately as possible to the dynamic as well as to the aerodynamic characteristics of the real blade. The correspondance seems to be relatively good when the difference between the first natural bending mode and its line-segment approximation by the flapping stiff blade is a minimum for the same stored energy. This normally results in an equivalent system with a higher hinge offset and a negative hinge restraint.

Using such an equivalent flapping system a stability calculation for hovering was done for different flapping frequency ratios. The results of which are shown in figure 6 for the critical mode. Helicopters normally have unstable flight characteristics. In the case of the BO 105 with a normal articulated rotor having a flapping frequency ratio near 1.0 the time to double amplitude would be below 10 seconds. The rigid rotor system does not stabilize the system but it reduces the instability. At a frequency ratio of 1.12 the time to double amplitude is about 20 seconds, which seems to be relatively stable to a helicopter pilot, who is familiar with the unstable conditions. The period of the helicopter with fixed controls is relatively long, in the special case about 15 seconds. It is nearly not influenced by the flapping stiffness.

Experience has shown that the stability values are of minor importance to the handling qualities. These are mainly influenced by the control characteristics. The capability of the rigid rotor to produce very high rotor moments will allow a more direct control of the aircraft compared to the articulated rotor. The latter produces the control moments mainly by deflection of the rotor thrust.

The effects obtainable with a certain control deflection and the corresponding time behaviour are the most important parameters in evaluating the control characteristics. Experience has shown that for a good control behaviour definite correlations must exist between control efficiency and the time behaviour. Usually the control efficiency will be expressed by the initial acceleration per unit stick deflection, which is equal to the ratio of the control moment obtainable with the stick deflection to the moment of inertia. The time behaviour is generally expressed by the damping moment which again is referred to the inertia moment. Figure 7 gives the values in pitching for the BO 105 with the rigid rotor and also with an articulated rotor of about 2% flapping hinge offset. In the diagram the established limits of satisfactory and insufficient properties by Salmirs and Tapscott are shown in comparison with military specifications and recommendations for armed helicopters. With the articulated rotor the BO 105 with a proper choice for the control ratio would be within the range of the curves of Salmirs and Tapscott. With the rigid rotor the BO 105 is within quite another range than usual for helicopters up to now. The control moment for the same stick deflection is more than three times the value of the articulated rotor. For damping a similar relation exists. The damping in the case of the rigid rotor is about four times that of the articulated rotor. This is still more important than the control moment, which can be influenced by the control ratio. The BO 105 has a very high control power due to the control ratio used, but during all tests this was no problem to the pilots. Theoretical and experimental studies have indicated that for the rigid rotor a higher control power will be beneficial for good handling in gusty weather conditions. With the control ratio, which finally has been chosen, the helicopter will be well within the recommendations for armed helicopters.

By assuming that the control primarily influences the rotary motions of the helicopter, it can be shown that the reciprocal values of the damping moment, referred to the moment of inertia, represent the time constants of the system. Figure 8 gives an impression of the different time constants with the rigid rotor and with an articulated rotor. In pitching for instance the values are about 1.2 seconds for the articulated rotor and about .2 seconds for the rigid rotor. When the time constant is short, the helicopter follows control motions more faithfully; the angular velocity and the attitude of the helicopter will be better in phase with the control displacement.

The good control characteristics, which have been expected by theoretical studies, could be proved fully during the flight tests, also under gusty weather conditions.

In forward flight there is no important change in control characteristics. Figure 9 illustrates pitching moment control derivatives versus forward speed for cyclic and collective control. The control moments for the rigid rotor are much higher than those of the articulated rotor. With forward speed the pitching moment due to cyclic control raises only slightly, but there is a very strong change for the pitching moment due to collective control. This means that at high speeds a change in collective position will have a powerful influence in changing moment. This may be very helpful for instance to stop maneuver conditions with high load-factors, because a reduction of collective angle reduces thrust and produces additionally a nose-down pitching moment.

In figure 10 the pitch damping derivative is shown. There is nearly no change with forward speed. This means that the favorable time behaviour in controlling the aircraft will be unchanged over the whole envelope.

Figure 11 shows the pitch attitude derivative of the moment, which is of main influence on the stability of the aircraft. The rigid rotor itself produces - compared to the articulated rotor - a high destabilizing moment; the moment of the fuselage is unstable too. Therefore the rigid rotor helicopter will need a larger horizontal stabilizer than is usual with normal helicopters if stable moment conditions are desired.

Just as the control characteristics, the stability behaviour of the helicopter with a rigid rotor will be influenced by its high moment capacity. The rotor is more sensitive to control inputs, but also to external disturbances. On the other hand, the higher damping moments will be advantageous. Figure 12 shows calculated stability characteristics of the BO 105 as a function of airspeed. Illustrated are the period and the time to double amplitude of the critical natural helicopter mode with fixed controls using the stabilizer area as a parameter. The period is nearly constant with speed, but for a small stabilizer area the oscillation will become more and more unstable with higher speeds. For this condition a lot of flight testing was done, but even under bad weather conditions the pilots practically did not feel this instability because of the excellent control characteristics. This is in agreement with simulation studies which showed that the pilot's judgement is mainly influenced by the control characteristics.

The diagram shows that the stabilizer area is very effective for stability. By enlarging the area significant improvements or even stable conditions can be obtained. There are some other parameters which influence stability. For instance a higher rpm or a lower disc loading are advantageous. The trend for modern aircraft is towards "hands off" stability. By a proper lay-out of the helicopter it is possible to get this without artifical stabilizing for forward flight conditions, but it seems to be questionable if it is worthwhile to do it fully with natural means and to pay for it in loadings and weight. If one wants an integrated flight control system with an autopilot, this can be used also for stabilizing. This will be the trend at least for larger helicopters.

Between the flight dynamical instability and the classical aeroelastic instabilities there is a very important difference. The pilot can overcome the instability in the flight behaviour. Because of the relative low frequency of the oscillation he is able to control and stabilize the movements of the aircraft. The controls are influencing directly this oscillation. The classical aeroelastic instabilities cannot be tolerated. The pilot has no mean to control them.

INFLUENCE OF INPLANE FLEXIBILITY

The flapwise flexibility and the corresponding aeroelastic behaviour of the rigid rotor is one of the main features of the rotor system. As shown the aeroelastics are the basis for the excellent handling characteristics. To keep blade loads at a low level also a relatively soft inplane flexibility of the blades is desired. The aforementioned inplane natural frequency ratio of about .72 may lead, according to classical "ground resonance" theory, to instabilities on the ground and in the air. It can occur when the value of rotor operational frequency minus the first inplane frequency matches, or is close to a body mode frequency. The instability is basically mechanical. It obtains driving energy from the rotating rotor and not from aerodynamic forces.

It was found by calculations and tests that for the BO 105 standing on the ground no self-excitation will occur. Even if the ground surface is such that the helicopter has a natural "rocking"-frequency close to its critical frequency the structural damping in the blades and the airframe is sufficient to prevent an instability.

Standing on the ground the body frequency is mainly influenced by the landing gear. In the air there exists the possibility of coupling between the mechanical inplane motion and the flight dynamical modes. In a theoretical study both the equations of motion of the flight dynamics and the equations for the rotor inplane degrees of freedom as used in ground resonance studies were coupled.

Figure 13 illustrates some of the typical results. There is shown the time to half amplitude respectively the time to double amplitude of the critical rotor inplane mode versus the airspeed. The lag damping of the rotorblades is used as a parameter. With nearly no damping selfexcitation will occur, but the damping has a very strong stabilizing effect. The instability is relatively smooth in a wide range compared to the more explosive instability in ground resonance with articulated rotors. It is worth to notice that the critical rotor inplane mode must be stable for all flight conditions in contrast to the flight mechanical instability, because the pilot has no means to control such oscillations.

Special tests with the fiberglass rotorblades have shown that the real damping is high enough that no instabilities will be possible. During flight tests which included special excitation it was never possible to get into an unstable region anywhere over the speed range.

For ground and air resonance phenomena the blade inplane frequency ratio is of main influence. Lowering this frequency ratio from .72 with the BO 105 to about .65 for instance would already need twice the damping to prevent instability. There will be a limit for the minimum inplane frequency ratio, if there is no possibility for artificial blade damping.

INFLUENCE OF TORSIONAL STIFFNESS

For fixed-wing aircraft the more classical aeroelastic phenomena are mainly influenced by the torsional flexibility of the lifting surfaces. Also for rotorblades torsional stiffness is an important quality. As in the case of fixed-wing torsional elasticity affects the flutter and divergence speed. In all cases, it is not the torsional stiffness of the blade alone that matters but the stiffness of the root constraint, that means of the control system, and of the blade combined in series. Figure 14 illustrates the influence of control stiffness to the torsional frequency ratio. With infinitely stiff control system the BO 105 blade would have a frequency ratio of about 4, the influence of control flexibility brings this ratio to about 3.5.

Figure 15 illustrates the stability limits for classical rotor blade flutter versus airspeed for the BO 105. The lower limit line corresponds to the stability limits of the critical advancing blade, for the upper line the stability limits are calculated with the mean air velocities at the blade during the rotation of the rotor. If pitch axis, center of gravity and aerodynamic center are at the 25% chord line, which is desirable for rotorblades, the necessary torsional frequency ratio to avoid flutter is relatively low. There is no danger of an instability.

In high speed flight the blades are subjected to an azimuthally varying aerodynamic environment that includes stall, reverse flow and compressibility. These effects may result in unstable conditions. However, the variation of the aerodynamic environment seldom allows the blade to remain in an unstable environment long enough for large divergent oscillations to occur. The blade will normally develop limit-cycle oscillations. In the case of the BO 105 there are no such problems. The advancing blade tip Mach number is rather conservative, on the other side the torsional stiffness is sufficient to prevent critical limit cycle stall flutter.

Torsional stiffness is most important because of its influence on control. At the Bölkow Rigid Rotor a substantially rigid hubarm fixes the feathering axis under a precone-angle, blade bending will be outside of this hubarm. This design will result in a coupling between feathering, inplane blade motion and flap bending. The overall lay-out has to take care that this coupling effects as well as the coupling effects in the blade itself by inertia, elastic or aerodynamic forces remain relatively small. In figure 16 measured pitch link forces are plotted over the airspeed. The forces are not higher than for helicopters of equal size with articulated blades. The control forces are not strongly changed by a change of flight condition. This allows the conclusion that the control coupling effects are relatively small which was also expected by theoretical design studies.

CONCLUSION

It may be concluded that for a helicopter with a rigid or better a hingeless rotor aeroelasticity is the basis of its characteristics. Its handling qualities, that means both stability and control, are mainly influenced by the flapwise flexibility of the rotorblades. Blade inplane flexibility and torsional stiffness have no direct influence on the flight dynamics. But they may fix design limits to avoid unacceptable instabilities. With a proper tuning of the design concerning mass distribution, elastic properties and kinematic relations it is possible also for a rigid rotor to keep coupling effects so small that they will be not of importance.

REFERENCES

1. Reichert, G.: "Flugeigenschaften bei Hubschraubern mit elastisch angeschlossenen Rotorblättern". Wissenschaftl. Gesellschaft für Luft- und Raumfahrt (WGLR), Jahrbuch 1963. (Translated by NASA: "Handling Qualities of Helicopters with Elastically Attached Rotor Blades". NASA-TT-F-11374, December 1967).

2. Reichert, G.: "Flugmechanische Besonderheiten des gelenklosen Hubschrauberrotors". Wissenschaftl. Gesellschaft für Luft- und Raumfahrt (WGLR), Jahrbuch 1965. (Translated by NASA: "Flight-Mechanical Properties of the Hingeless Helicopter Rotor". NASA-TT-F-11373, December 1967).

3. Reichert, G.; Oelker, P.: "Handling Qualities with the Bölkow Rigid Rotor System". American Helicopter Society 24th Annual National Forum 1968, Paper No. 218.

4. Woitsch, W.; Weiss, H.: "Dynamic Behaviour of a Hingeless Fiberglass Rotor". AIAA/AHS VTOL Research, Design, and Operations Meeting, Georgia Institute of Technology February 1969, AIAA Paper No. 69-204.



Fig. 1 BO 105 in Flight

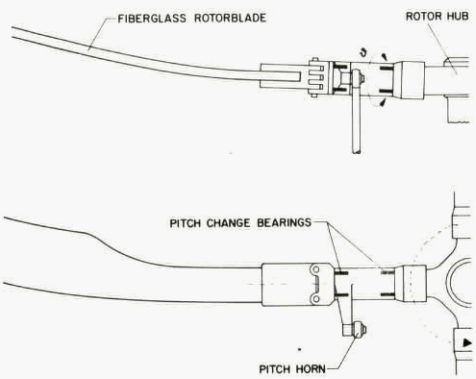


Fig. 2 The Bölkow Rigid Rotor System

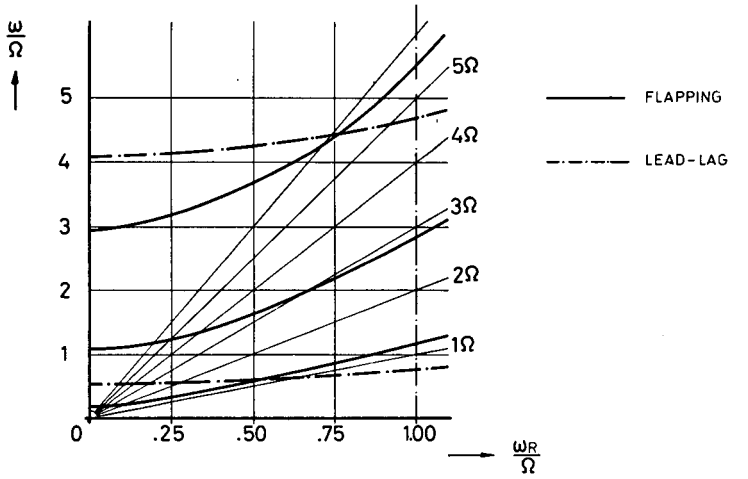


Fig. 3 Frequency Diagram of the BO 105 Rotorblade

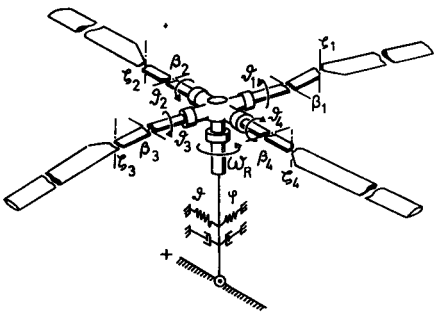


Fig. 4 Equivalent Rotorsystem for Theoretical Studies

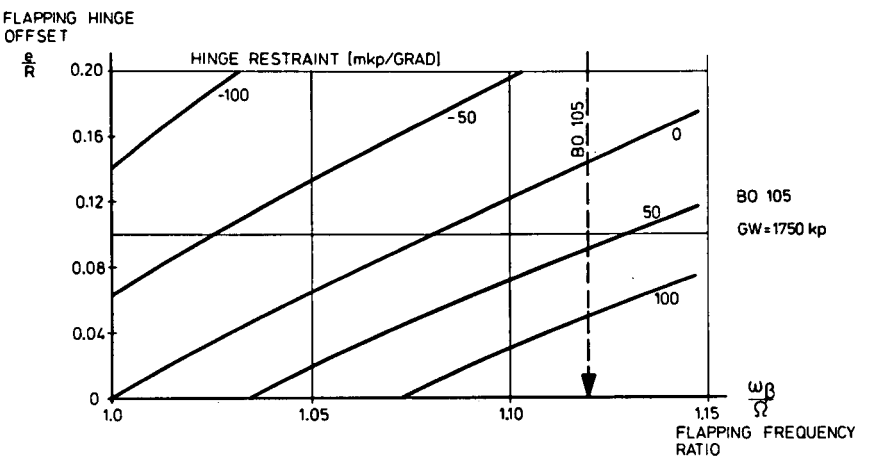


Fig. 5 Relation between Flapping Frequency, Hinge Offset and Hinge Restraint

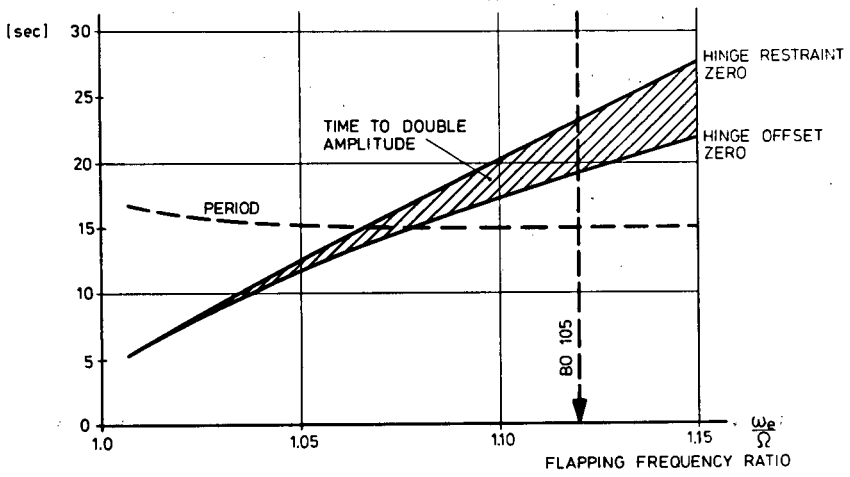


Fig. 6 Period and Time to Double Amplitude for Hovering

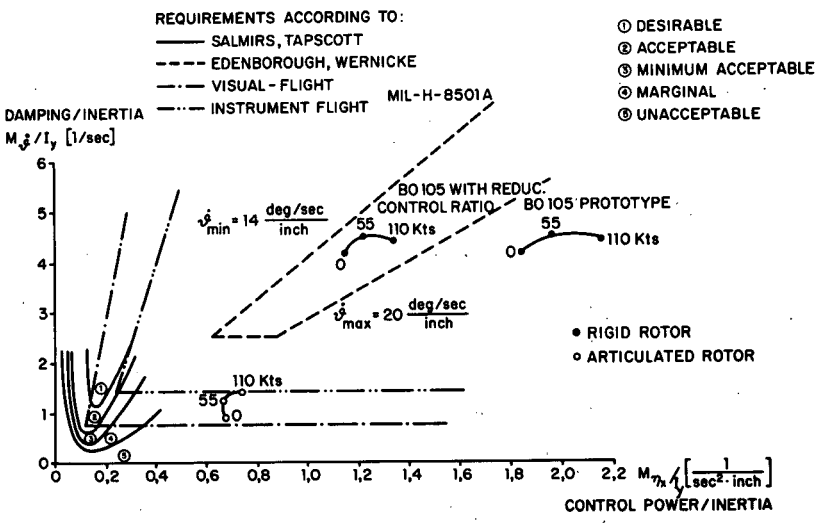


Fig. 7 Control Characteristics - Pitching

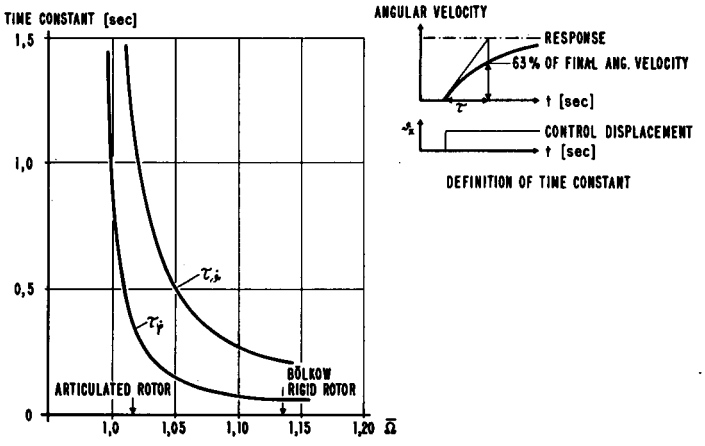


Fig. 8 Time Constants vs. Flapwise Frequency

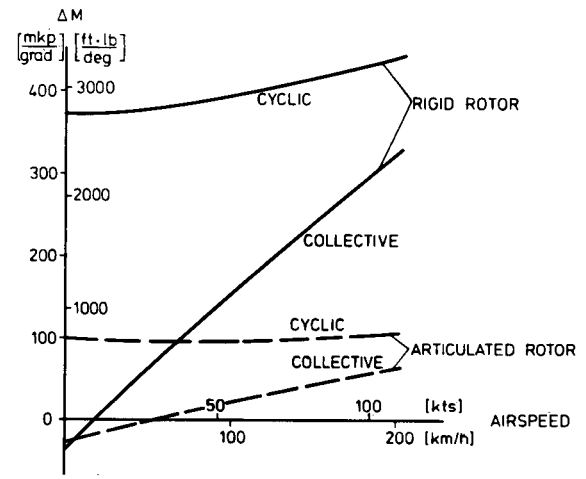


Fig. 9 Pitching Moment Control Derivatives

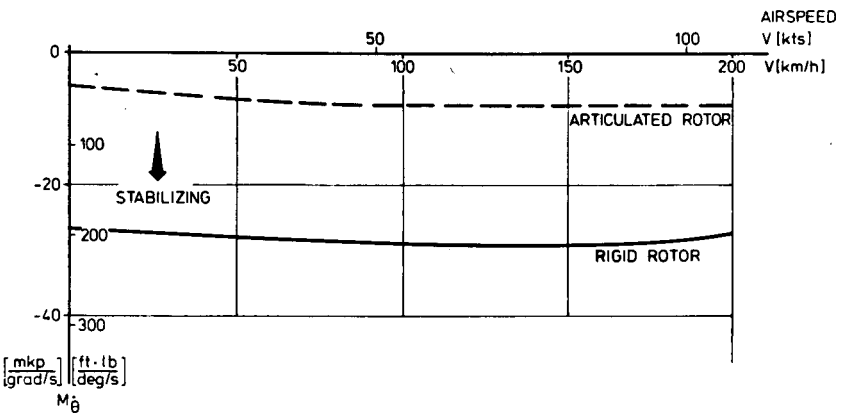


Fig. 10 Pitch Damping vs. Airspeed

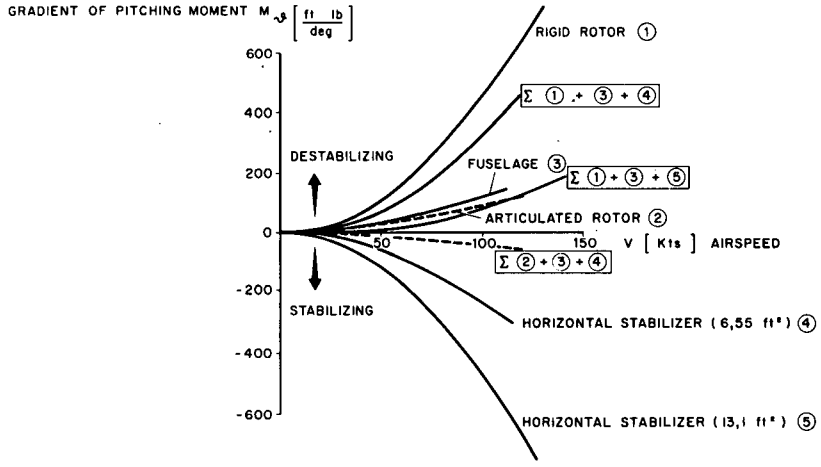


Bild 11 Attitude Pitching Moment Derivatives

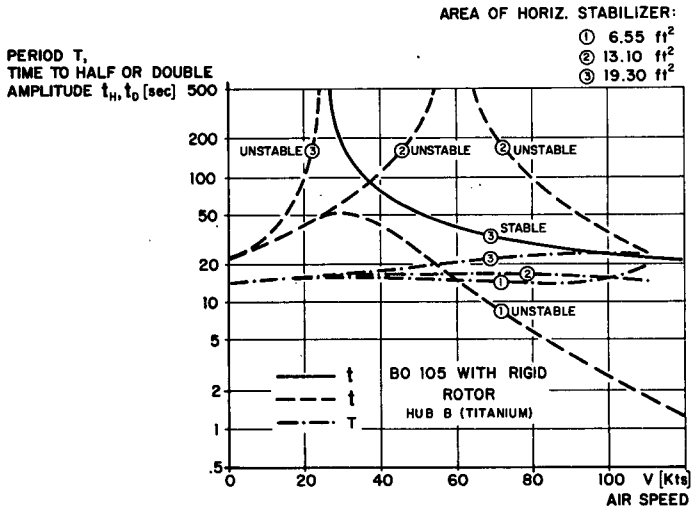


Fig. 12 Dynamic Stability in Forward Flight

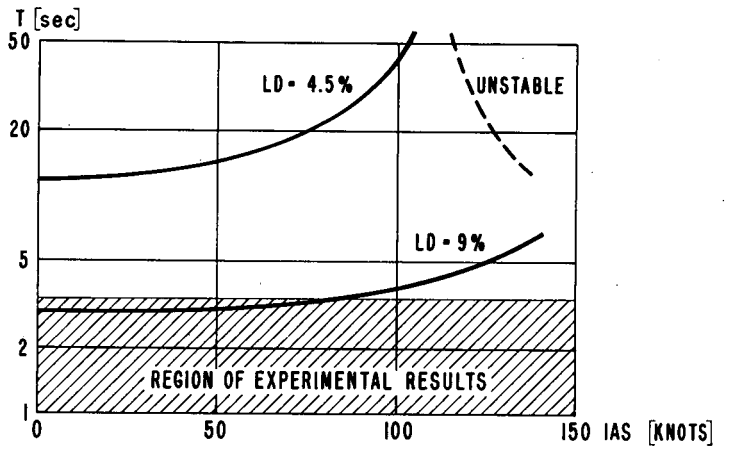


Fig. 13 Air-Resonance in Forward Flight

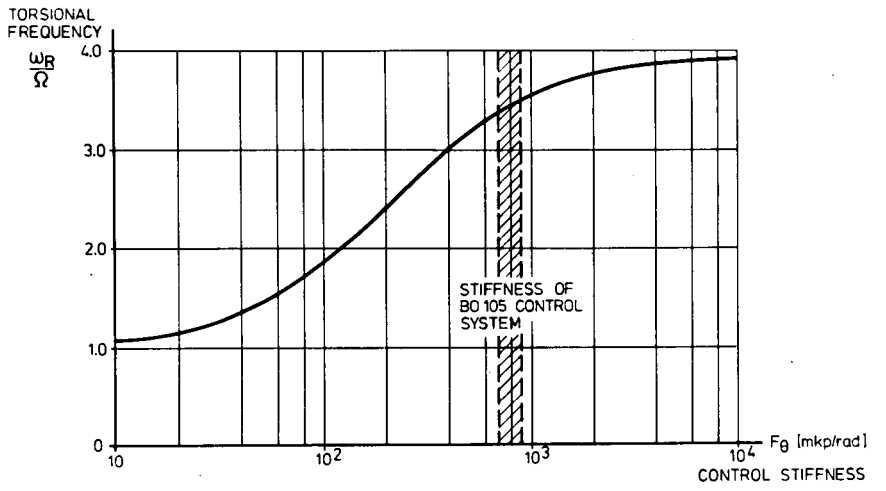


Fig. 14 Torsional Frequency as Function of Control Stiffness

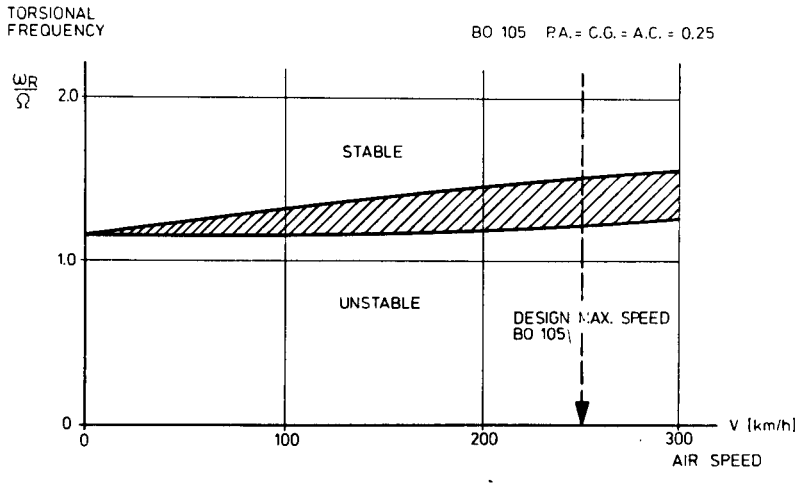


Fig. 15 Stability Limits - Classical Rotorblade Flutter

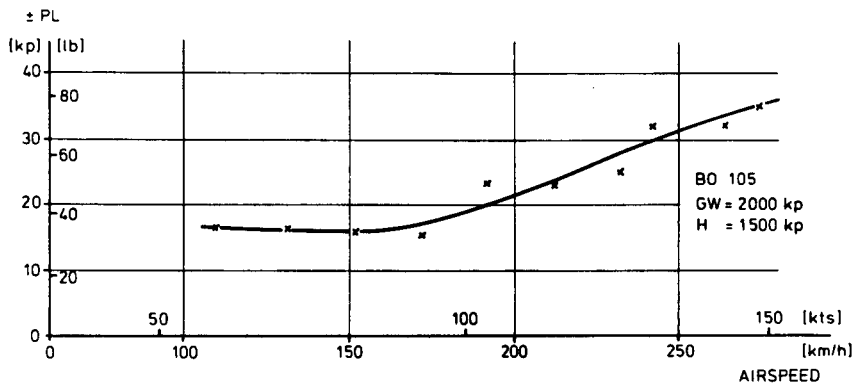


Fig. 16 Measured Alternating Pitch Link Loads

THE INFLUENCE OF COMPRESSIBILITY ON THE AIRLOADS ON OSCILLATING ROTOR BLADES IN HOVERING FLIGHT

by

W. P. Jones and B. M. Rao

Department of Aerospace Engineering
Texas A&M University
College Station, Texas, USA

THE INFLUENCE OF COMPRESSIBILITY ON THE AIRLOADS ON OSCILLATING ROTOR BLADES IN HOVERING FLIGHT

W. P. JONES* and B. M. RAO**

Department of Aerospace Engineering
Texas A&M University
College Station, Texas

1. ABSTRACT

An outline is given of a method, presented in full in an earlier paper, for determining compressibility effects on oscillating rotor blades. The theory makes use of a two-dimensional mathematical model of the flow in which a typical section of the reference blade is replaced by an airfoil with a straight wake and a system of regularly spaced infinite wakes below it, including those from other blades. This model yields the result that the downwash due to the infinite system of wakes is independent of Mach number when the blade circulation is assigned.

Aerodynamic coefficients obtained from previous work together with some additional results are given and their significance discussed from the point of view of blade instability. At the higher Mach numbers the coefficients vary considerably in value but the variation with phase difference between the wakes shows a similar trend to that for incompressible flow. The aerodynamic damping coefficients for plunging (flapping) oscillations and for pitching oscillations about the quarter-chord axis are always positive but can be small when the blade oscillates at an exact number of cycles per revolution. For pitching axis positions, forward of quarter-chord, it is shown that blade instability is possible for a wide range of axis positions and frequency parameter values.

2. INTRODUCTION

As part of a general research program† on unsteady aerodynamic problems sponsored by the U.S. Army Research Office - Durham under Project Themis, a theoretical study has been made at Texas A&M University of the compressibility effects on oscillating rotor blades for hovering flight. Some of the results of this investigation were given in a paper presented at the recent AIAA Structural Dynamics Aeroelasticity Specialist Conference held at New Orleans.(1) Since the present meeting is concerned among other subjects with aeroelasticity and its effects from the flight mechanics point of view on helicopter design, it will be appropriate to summarize the findings of our recent paper and more particularly to comment on how the results obtained would affect the helicopter's stability and flutter characteristics.

The flutter and vibration behaviour of helicopters in hovering and forward flight have been investigated extensively but most of the theoretical work has been based on the use of quasi-steady aerodynamic theory and the airloads on the rotor blades are usually estimated on the basis of incompressible flow theory.

The helical nature and distortion of the wakes of the blades introduces a serious obstacle to the development of a complete unsteady airfoil theory with frequency effects taken fully into account. However for incompressible flow, some progress has been made towards this objective, notably by J. P. Jones(2) and by R. G. Loewy(3). Both considered the case of low forward speed or hovering flight when the inflow through the rotor blades was assumed to be small. A two-dimensional mathematical model of the flow was assumed and there is evidence to support the view that, for high frequency oscillations and low inflow, this model is a reasonable approximation. The same model has also been used in our recent paper which took compressibility as well as frequency effects into account. On the basis of the analysis it would appear that the two-dimensional model used is reasonably accurate for blade sections a few chord lengths away from the tip, and that aerodynamic loads can be estimated with some confidence by strip theory when the modes of deformation of the blades and their motions are prescribed.

3. OUTLINE OF METHOD

In the paper by R. G. Loewy(3), the two-dimensional model representation of a multi-bladed rotor is discussed in detail. A similar model was used by the present authors in which the system of helical wakes from the blades is represented by a two-dimensional array of regularly spaced vortex (or doublet) sheets. Let us suppose the rotor has Q blades and that a particular blade is denoted

---

* Research Professor.

** Assistant Professor.

† Work sponsored by the U.S. Army Research Office - Durham under Project Themis Contract DAHC04-69-C-0015.

by the symbol q, where q = 0, 1, 2, 3, Q-1 in turn and q = 0 represents the reference blade. To determine the flow over a particular section of the reference rotor blade at radius r, it is assumed that the blade section can be replaced by an airfoil of the same chord moving with velocity $U(\equiv r\Omega)$ and oscillating about a mean straight line in an identical manner. The helical wakes are then replaced by a semi-infinite wake from the airfoil itself together with a system of infinite wakes as shown in Figure I.

If the rotation is such that blade q-1 follows blade q, the semi-infinite wake of the airfoil representing the reference blade section will be followed by the infinite wakes arising from blades 1, 2, 3, and Q-1, in that order, in the first revolution. The pattern repeats itself for every revolution thereafter except that the wake from the reference airfoil, q=0, also extends from $-\infty$ to ∞.

The spacing between the wakes is determined by the inflow and the rotational speed. Let us suppose that the distance between consecutive wakes is represented by $d\ell$ where 2ℓ is the chord. For low inflows, d will be small and when this is the case the two-dimensional model is believed to be fairly accurate at the higher frequencies for sections a few chord lengths inboard of the tip.

All the blades of the rotor are assumed to be oscillating with the same frequency and amplitude but not necessarily in phase. If the reference blade section is describing plunging oscillations $\mathfrak{z} = \ell z = \ell z' \exp(ipt)$ and pitching oscillations, $\alpha = \alpha' \exp(ipt)$ about its mid-chord point, taken as origin, the displacement ζ of any point P at a distance $\mathfrak{x}$ $(=\ell X)$ from mid-chord is given by

$$\zeta = \ell(z + X\alpha) = \ell(z' + X\alpha')e^{ipt} \tag{1}$$

where p is the frequency in rads/sec. The corresponding expression for the downwash distribution is

$$w(X) = U[\, i\omega z' + \alpha'(1+i\omega X)\,]e^{ipt} = w'(X)e^{ipt} \tag{2}$$

where $\omega = p\ell/U$ is the reduced frequency. The problem is then reduced to one of finding a vorticity distribution that will induce the downwash distribution w(X) in order to satisfy the tangential flow condition. This can be done with the aid of known methods and results from two-dimensional unsteady airfoil theory for compressible flow.[4]

Let the co-ordinates $\mathfrak{x}, \mathfrak{z}$ in Figure 1 be changed and assume

$$\mathfrak{x} = \ell X \ , \ \mathfrak{z} = \frac{\ell Z}{\beta} \ , \quad t = \frac{\ell T}{U} \tag{3}$$

where $\beta = \sqrt{1-M^2}$. The velocity potential ϕ of the disturbed flow due to the blade oscillations can then be expressed in terms of a modified potential Φ where

$$\phi = \ell\Phi e^{i(\lambda X+\omega T)} \tag{4}$$

and $\lambda = M^2\omega/(1-M^2)$. It can readily be proved that Φ satisfies the wave equation

$$\frac{\partial^2\Phi}{\partial X^2} + \frac{\partial^2\Phi}{\partial Z^2} + \kappa^2\Phi = 0 \tag{5}$$

where $\kappa = M\omega/(1-M^2)$. If ϕ_a and ϕ_b are the values of ϕ immediately above and below the vortex sheet, we can write

$$\phi_a - \phi_b = \ell k = \ell K(X)e^{i(\lambda X+\omega T)} \tag{6}$$

where $K(X) \equiv \phi_a - \phi_b$. It can also be readily proved that in the wake

$$i\nu K + \frac{\partial K}{\partial X} = 0 \tag{7}$$

where $\nu = \omega/(1-M^2)$ is a modified reduced frequency parameter. The corresponding boundary condition in the transformed co-ordinates is

$$W = \frac{\partial\Phi}{\partial Z} = \frac{w(X)}{\beta}\, e^{-i(\lambda X+\omega T)} = \frac{w'(X)}{\beta}\, e^{-i\lambda X} \tag{8}$$

The problem is then reduced to one of finding the solution of the equation

$$2\pi[W(X_1) - W_I(X_1)] = -\int_{-1}^{\infty} K(X) \frac{\partial^2}{\partial Z_1^2} \left[\frac{\pi i}{2} H_o^{(2)}(\kappa\sqrt{(X_1-X)^2 + Z_1^2}) \right] dX \quad , \tag{9}$$

where $W_I(X_1)$ is the modified downwash amplitude due to the system of infinite wakes and $Z_1 \to 0$. When $W_I(X_1) = 0$, the above equation corresponds to that for a single oscillating airfoil in compressible flow and its solution has been obtained.

The general equation with the W_I term included can also be solved by a method similar to that used for the single airfoil by W. P. Jones.[4] The distribution of K(X) in the immediate wake of the airfoil is of the form

$$K(X) = K(1)e^{i\nu(1-X)} \tag{10}$$

since condition (7) must be satisfied. The K(X) distribution over the first vortex sheet due to the preceding blade with a phase lead of ψ_1 is

$$K_{10} = K(1)e^{i\nu(1-X)} + i\psi_1 - \frac{2\pi i}{Q} \frac{p}{\Omega} \tag{11}$$

and that due to the q'th blade with a phase lead of ψ_q is

$$K_{qn} = K(1)e^{i\nu(1-X)} + i\psi_q - \frac{2\pi ip}{\Omega} (n + \frac{q}{Q}) \tag{12}$$

after n revolutions. When the downwash due to all the K_{qn} distributions is taken into account, it can be shown that

$$2\pi W_I(X_1) = \frac{\pi K(1)}{QD} F(Q)e^{i\nu(1-X)} \tag{13}$$

where

$$F(Q) = \frac{Q\omega d}{e^{\gamma}-1} \left[1 + \sum_{q=1}^{Q-1} e^{i\psi_q} + \frac{Q-q}{Q} \gamma \right]$$

and $\gamma = 2\pi i\, p/\Omega + Q\omega d$. This leads to the following expression for the actual downwash $w_I(X)$ due to the system of wakes, namely

$$2\pi w_I(X_1) = \frac{\pi k(1)}{Qd} e^{i\omega(1-X_1)} F(Q) \quad , \tag{14}$$

which is independent of Mach number for a given k(1). In other words when the circulation round the reference blade is assigned, the downwash due to the system of wakes is the same for compressible flow as for incompressible flow.

For a single blade F(Q) reduces to

$$F = \omega d \,/\, (e^{\gamma}-1) \tag{15}$$

where $\gamma \equiv i\psi_o + \omega d$ and $\psi_o = 2\pi\, p/\Omega = 2\pi(N+\varepsilon)$; N being the number of complete cycles of oscillation per revolution. For a single blade the variation of F with ωd for different values of ψ_o are shown in Figure 2. The function F is independent of N and depends only on the fractional part ε of $\psi_o/2\pi$ when ωd is assigned.

It should be noted that both real and imaginary parts of $F(\equiv F'+iF'')$ are very sensitive to the variations in ψ_o when ωd is small.

The solution of the basic integral equation, when W(X) is known, can be obtained as in Reference 1. When K(X) is derived the lift distribution over the section can be deduced and the total lift and pitching moment estimated.

The total lift L and nose-up pitching moment M about the mid-chord axis can then be expressed in the form

$$\frac{L}{\pi\rho\ell U^2} = (\ell_z + i\omega\ell_{\dot{z}})z + (\ell_\alpha + i\omega\ell_{\dot{\alpha}})\alpha$$

$$\frac{M}{\pi\rho\ell^2 U^2} = (m_z + i\omega m_{\dot{z}})z + (m_\alpha + i\omega m_{\dot{\alpha}})\alpha \qquad (16)$$

Values of the aerodynamic coefficients ℓ_z, $\ell_{\dot{z}}$, and so on have been calculated for a single blade and a two-bladed rotor for a range of Mach numbers for particular values of ω, d and ψ. The results were initially obtained with the reference pitching axis at mid-chord but by the use of standard transformation formulae, the coefficients for any other axis can be obtained.

4. DISCUSSION OF RESULTS

Most of the results given refer to a single oscillating rotor blade and were derived from the data given in our earlier paper. This is, however, not a severe limitation as it is known that on the basis of the two-dimensional model of the flow used, a multi-bladed rotor can often be replaced by a mathematically equivalent single blade, provided the wake spacing and the inflow have appropriate values. Further, since our interest is in blade instability, attention will be concentrated on the behaviour of the aerodynamic damping coefficients as the Mach number and other parameters are varied.

Figure 3 shows the variation of the coefficients $\ell_{\dot{z}}$ and $\ell_{\dot{\alpha}}$ with ψ_o for a range of Mach numbers when $\omega = 0.1$ and $d = 2.0$. The damping coefficient $\ell_{\dot{z}}$ decreases to a minimum at $\psi_o = 0$ and 2π for all Mach numbers. The curve for $M = 0$ agrees with that given by J. P. Jones[2] and the variation with Mach number is greatest when $\pi/4 < \psi_o < \pi/2$. In cases where the rotor blade oscillates several times per blade revolution, only the fractional part ε of the ratio p/Ω is taken into account and ψ_o is interpreted as being effectively $2\pi\varepsilon$ whatever the value of N, the number of complete cycles per revolution. For the particular M values considered the curves showing variation of $\ell_{\dot{z}}$ with ψ_o follow the same trend as in incompressible flow.

Similarly for a reference axis at quarter-chord, the curves of $\ell_{\dot{\alpha}}$ show no marked changes of shape as M is varied but the numerical values of the coefficient differ considerably. The values of $\ell_{\dot{\alpha}}$ for $M = 0.8$ range between 5.0 and -12.0 as ψ_o is varied and this result may have important consequences in blade flutter analysis.

In Figure 4 the pitching moment stiffness coefficient, $-m_\alpha$, and the damping coefficient, $-m_{\dot{\alpha}}$, are shown plotted similarly. Both coefficients correspond to a reference pitching axis at quarter-chord. At $M = 0$, the coefficient $-m_\alpha = 0$ but as M is increased its value increases slowly up to $M = 0.7$ and then increases more rapidly, particularly when $\pi/2 < \psi_o < 3\pi/2$. This corresponds to a backward movement of the aerodynamic center of the blade section. It is shown in Reference 1 that the cross damping derivative $-m_{\dot{z}}$ behaves similarly but in both cases the values of the coefficients are small being less than 0.1 for $M = 0.8$. From the stability point of view, the behaviour of the direct damping coefficient $-m_{\dot{\alpha}}$ is of more importance. At $M = 0$, its value is independent of ψ_o but as M is increased it increases in value and for $M > 0.6$ shows some variation with ψ_o. Positive values of $-m_{\dot{\alpha}}$ imply positive damping and the results indicate compressibility effects to be stabilizing for pitching oscillations about the quarter-chord axis. However, as will be shown later, this is not the case for all axis positions.

The variation of the coefficient $\ell_{\dot{z}}$ with wake spacing d may also be of interest. In Figure 5, $\ell_{\dot{z}}$ is plotted against d for $M = 0$ and $M = 0.7$ for various values of ψ_o when $\omega = 0.2$. The curves do not vary much with Mach number for this value of ω, except when d is small.

From the results given it is evident that $\ell_{\dot{z}}$ never becomes negative. While this is also true of $-m_{\dot{\alpha}}$ for pitching oscillations about quarter-chord, it is not generally the case. The value of $-m_{\dot{\alpha}}(h)$ for a pitching axis at a distance $h\ell$ forward of quarter-chord is given in terms of the values of the coefficients referred to the quarter-chord axis by the standard transformation formula

$$-m_{\dot{\alpha}}(h) = -m_{\dot{\alpha}} - h(m_{\dot{z}} - \ell_{\dot{\alpha}}) + h^2\ell_{\dot{z}} \qquad (17)$$

It was noted earlier that $\ell_{\dot{\alpha}}$ could be large and negative and it is evident that it would have a strong influence in determining the value of $-m_{\dot{\alpha}}(h)$.

For a conventional airfoil, it is known that $-m_{\dot{\alpha}}(h)$ can theoretically become negative for a small range of reference axis positions forward of quarter-chord when $M = 0$ and $\omega \leq 0.06$. For $M = 0.7$, the range of axis positions is enlarged and one degree of freedom oscillations are possible up to $\omega = 0.1$. Figure 6 shows the above instability regions together with corresponding results for hovering flight when the influence of the system of wakes is taken into account. The region of instability is then considerably increased and for $M = 0.7$, $d = 1$ and $\psi_o = 7\pi/4$ the damping coefficient $-m_{\dot{\alpha}}(h)$ is negative for a wide range of axis positions for ω values up to about $\omega = 0.2$.

Some calculations were also done for a two-bladed rotor and even larger regions of instability were obtained. The extent of the regions depend on the phase lead ψ_1 of the second blade and the values of the other parameters involved. For $M = 0.7$, $d = 1$, $\psi_o = 7\pi/4$ and $\psi_1 = 3\pi/2$ (phase lag of $\pi/2$), the coefficient $-m_{\dot{\alpha}}(h)$ is negative for an even larger range of axis positions for values of $\omega \leq 0.3$. When $\psi_1 = \pi$, instability occurs up to $\omega = 0.2$.

The implications of these results are being further studied and it may be that the instability regions mentioned can be related to those that occur in actual flight. When the amplitudes of the z and α motions are such as to produce an effective pitching axis forward of quarter-chord or when a blade torsional resonance mode has a nodal line forward of quarter-chord, the theory would predict instability.

It is realized that the mathematical model of the flow on which the theory is based is very idealised as it completely ignores tip effects, boundary layer behaviour and the helical nature of the wake. Nevertheless, the results obtained may be of some value in leading to a better understanding of instabilities at high blade-tip Mach numbers though they may be largely due to shock wave boundary layer interaction effects.

REFERENCES

1. W. P. Jones, B. M. Rao — "Compressibility Effects on Oscillating Rotor Blades in Hovering Flight". Published in proceedings of New Orleans AIAA Structural Dynamics and Aeroelasticity Specialist Conference, April 1969.

2. J. P. Jones — "The Influence of the Wake on the Flutter and Vibration of Rotor Blades". British Royal Aeronautical Society, Aeronautical Quarterly, Vol. IX, 1958.

3. R. G. Loewy — "A Two-Dimensional Approximation to the Unsteady Aerodynamics of Rotary Wings". Journal of Aerospace Sciences, Vol. 24, February 1957.

4. W. P. Jones — "The Oscillating Airfoil in Subsonic Flow". British Aeronautical Research Council, R&M 2921, 1956.

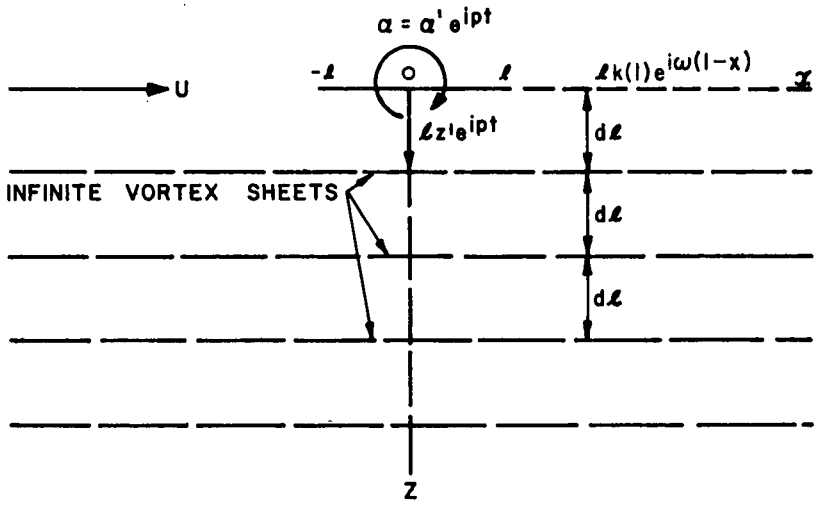


FIGURE 1: MATHEMATICAL MODEL OF AIRFOIL AND VORTEX SHEETS

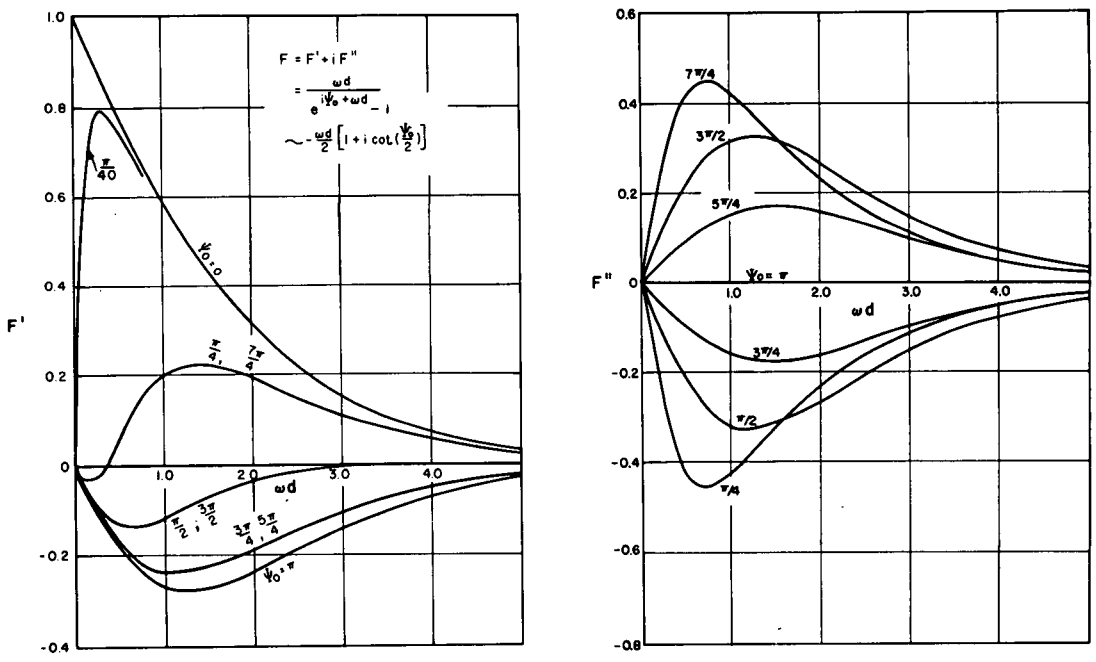


FIGURE 2: VARIATION OF F WITH ωd AND PHASE LAG FOR A SINGLE BLADE

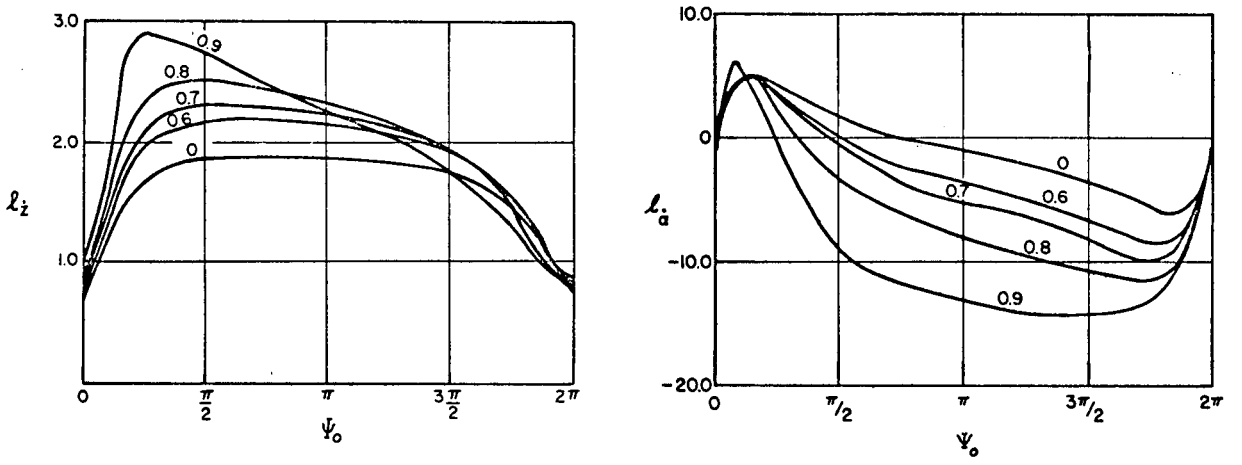


FIGURE 3: INFLUENCE OF MACH NUMBER AND PHASE ON AERODYNAMIC COEFFICIENTS (ω = 0.1; d = 2.0)

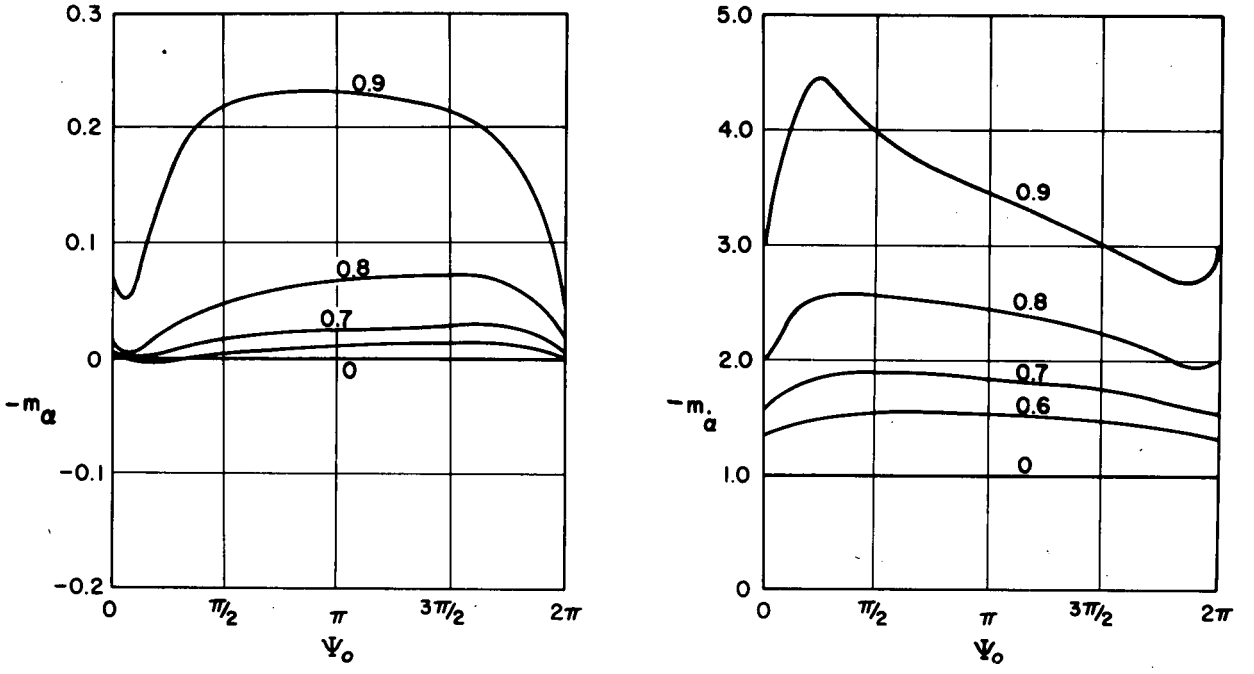


FIGURE 4: PITCHING MOMENT COEFFICIENTS REFERRED TO QUARTER-CHORD AXIS

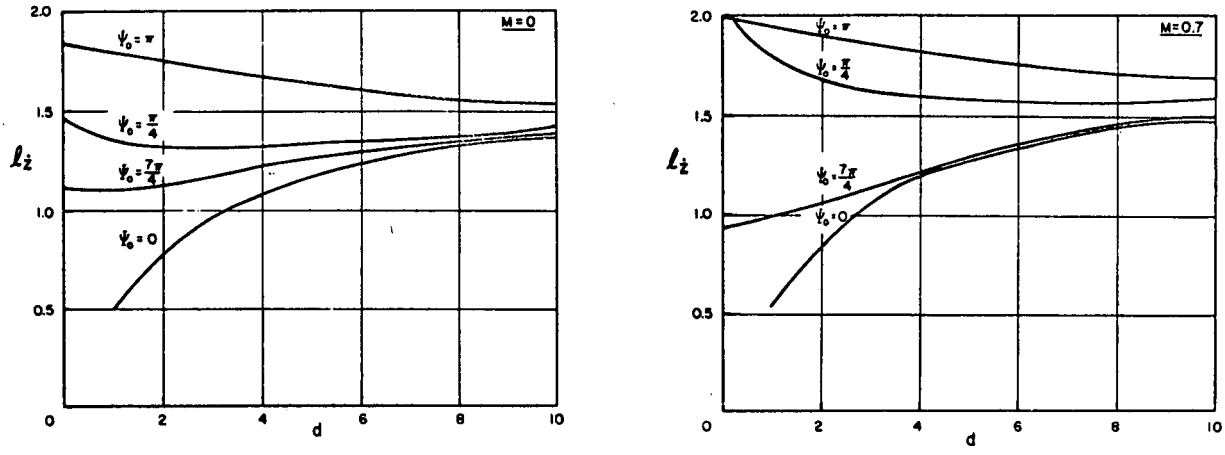


FIGURE 5: VARIATION IN $\ell_{\dot{z}}$ FOR M=0 AND M=0.7 WHEN $\omega = 0.2$

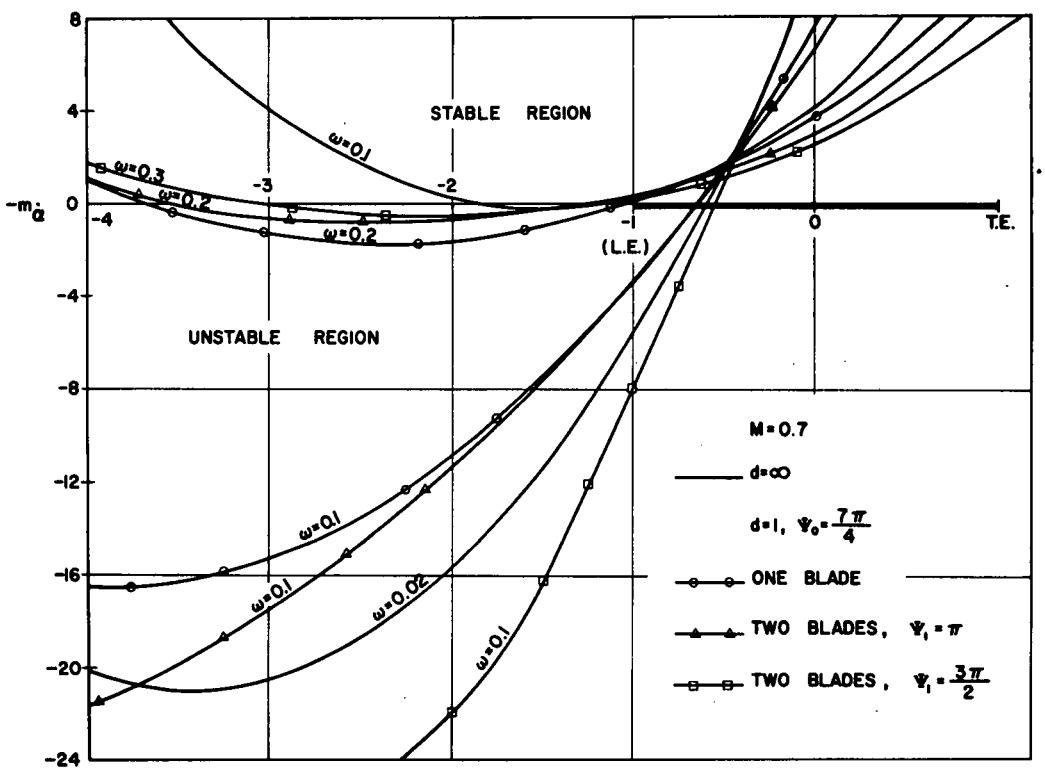


FIGURE 6: EFFECT OF REFERENCE AXIS POSITION ON PITCHING MOMENT DAMPING COEFFICIENT

AN ANALYTICAL METHOD FOR PREDICTING THE STABILITY AND CONTROL CHARACTERISTICS OF LARGE ELASTIC AIRPLANES AT SUBSONIC AND SUPERSONIC SPEEDS

PART I - ANALYSIS

by

Arthur R. Dusto

Research Specialist, Aerodynamics Staff
Commercial Airplane Division
The Boeing Company

PART II - APPLICATION

by

Howard L. Chevalier* and Gerald M. Dornfeld and Robert C. Schwanz†

*Research Scientist, Ames Research Center, National Aeronautics and Space Administration, Moffett Field, California, USA 94035

†Research Engineers, Aerodynamics Research Staff, Commercial Airplane Division
The Boeing Company, Renton, Washington, USA

An Analytical Method for Predicting the Stability and Control Characteristics of Large Elastic Airplanes at Subsonic and Supersonic Speeds, Part I - Analysis

Dr. Arthur R. Dusto

Research Specialist, Aerodynamics Staff

Commercial Airplane Division

The Boeing Company

SUMMARY

An analytical method is presented for predicting the stability characteristics of large, flexible airplanes. In this method the aerodynamic and elastic properties of the airplane are described in terms of influence coefficients. This description leads to small disturbance equations of motion for the flexible airplane which appear as two sets of matrix equations. One set governs the motion of the airplane's center of gravity and the second set governs the internal equilibrium of the airplane as an elastic body. They apply to longitudinal as well as lateral-directional motion. The formulation readily permits the use of "residual flexibility". This technique introduces the effects of the structural flexibility on the airplane's motion in an optimal manner. These effects are introduced into the small disturbance equations of motion by special modification of the stability derivatives.

The selection and development of the formulation was carried out under NASA-Ames Contract NAS 2-3662, "An Analysis of Methods for Predicting the Stability Characteristics of an Elastic Airplane". A companion paper will present validation of the principal techniques used in the formulation by comparing computer calculated stability characteristics with values measured in wind tunnel and flight areas.

1.0 INTRODUCTION

The effects of structural flexibility have been a consideration in the design of airplanes since the early days of aviation. Flutter and wing divergence as well as loss of control effectiveness have been the primary problems. The effect of flexibility on an airplane's stability has been modest and could be accounted for by small aeroelastic corrections to rigid airplane stability derivatives obtained from handbooks or wind tunnel testing.

The stability characteristics of the latest large transport type airplanes operating in the transonic and supersonic flight regimes are exceptions. The flexibility of these airplanes is considerably increased over previous transports and they are subjected to high dynamic pressures. This causes such a large aeroelastic effect on their static stability as to constitute a major consideration in configuration selection. Also, the natural frequencies of the structural motions are sufficiently reduced that aerodynamic coupling between the structural motion and the overall airplane motion is attendant. An adequate evaluation of dynamic stability must be carried out using equations of motion which accurately represent structural motion.

An influence coefficient method for evaluating stability and control characteristics of large flexible airplanes is presented which is capable of accounting for severe aeroelastic effects on static and dynamic stability. It was developed, in part, under sponsorship of the NASA-Ames Research Center, and the work was carried out under contract by The Boeing Company at Renton, Washington. Part I is a partial development of the influence coefficient method oriented toward the dynamic stability problem. Part II presents comparisons of values of stability characteristics obtained using the influence coefficients with values measured by flight testing and wind tunnel testing. The wind tunnel test values were obtained using models of the Boeing 707-320B transport and a typical supersonic transport configuration. The comparisons show the validity of the estimates based on the influence coefficients and the degree to which static and dynamic stability of these airplanes are affected by structural flexibility.

If an elastic airplane is treated as a continuous elastic body, its elastic motion is described by a time varying displacement field. For a structure as complicated as that of an airplane the continuous representation is replaced by a simplified model. The structure is divided into a large number of small segments which are elementary sub-structures. The analysis leads to structural influence coefficients which relate the deflection of the segments of the structure to the loads applied at the segments. Structural influence coefficients of this nature form the basis for describing elastic motion.

Recently an aerodynamic influence coefficient method has been developed which conforms well with the structural influence coefficient method. Each aerodynamic influence coefficient relates a change in flow incidence at one segment of the airplane's surface to the change in pressure at another surface segment.

The influence coefficient representation of both the structural and aerodynamic characteristics requires a specialized formulation of the equations of motion used in an airplane stability evaluation. The concept of a lumped parameter is used to develop equations of motion for the discrete representation required for the influence coefficients. Attention is given to the approximations involved in this representation where they effect the accuracy of predicted motions. The development leads to the residual flexibility approximation which accrues from the influence coefficient representation.

2.0 EQUATIONS OF MOTION IN LUMPED PARAMETER FORM

The equations of motion for the airplane form the mathematical model on which stability predictions are based. To utilize the influence coefficient representation of the aerodynamic and structural properties the airplane is represented by a collection of lumped masses joined together by the elastic properties of the structure. The appropriate equations of motion describe the motion of the lumped masses under the action of aerodynamic, inertia and gravity forces.

The motion of the lumped masses is treated as the motion of point masses with three translational elastic degrees of freedom relative to a body axis system. The body axis system in turn has three translational degrees of freedom and three rotational degrees of freedom relative to fixed space. The airplane has n lumped masses; and therefore, has 3n-6 elastic degrees of freedom and 6 degrees of freedom as a whole. The number of equations of motion required for a complete description of the motion is 3n.

The volume of the airplane, V, is divided into a large number, n, of volume segments, V_i, such that

$$V = \sum_{i=1}^{n} V_i \tag{2.1}$$

The lumped masses are the masses contained in the volume segments so that

$$m_i = \int_{V_i} \rho_A V_i \tag{2.2}$$

where ρ_A is the mass density of the airplane. The total mass of the airplane is therefore

$$M = \sum_{i=1}^{n} m_i \tag{2.3}$$

The position of the i^{th} lumped mass relative to a space fixed reference frame x',y',z', Fig. 1, is given by

$$\bar{r}_i' = \frac{1}{m_i} \int_{V_i} \bar{r}' \rho_A dV \tag{2.4}$$

and the position of the airplane's center of gravity is

$$\bar{r}_o' = \frac{1}{M} \int_{V} \bar{r}' \rho_A dV \tag{2.5}$$

Thus, position of the i^{th} lumped mass relative to the center of gravity is

$$\bar{r}_i = \bar{r}_i' - \bar{r}_o' \tag{2.6}$$

The position $\bar{r}_i'$ is taken to be the position of the i^{th} lumped mass when the airplane is in a state of arbitrary elastic deformation. When the airplane is free of applied forces, as it is in its fabrication jigs, the position of the ith lumped mass is denoted by $\bar{\bar{r}}_i$. The elastic displacement vector is defined by

$$\bar{d}_i = \bar{r}_i - \bar{\bar{r}}_i \tag{2.7}$$

and is the vector joining the location of the undeformed lumped mass to its deformed position. It may be computed from a continuous displacement field as

$$\bar{d}_i = \frac{1}{m_i}\int_{V_i} \bar{d}\rho_A \, dV \tag{2.8}$$

The displacement field $\bar{d}$ must be a solution to the equations of elasticity. That solution is obtained in the form of structural influence coefficients. These may be written in diadic form as

$$\begin{aligned}\bar{\bar{C}}_{ij} = {} & \bar{i}_s\left(C_{x_s x_{s_{ij}}}\bar{i}_s + C_{x_s y_{s_{ij}}}\bar{j}_s + C_{x_s z_{s_{ij}}}\bar{k}_s\right) \\ & + \bar{j}_s\left(C_{y_s x_{s_{ij}}}\bar{i}_s + C_{y_s y_{s_{ij}}}\bar{j}_s + C_{y_s z_{s_{ij}}}\bar{k}_s\right) \\ & + \bar{k}_s\left(C_{z_s x_{s_{ij}}}\bar{i}_s + C_{z_s y_{s_{ij}}}\bar{j}_s + C_{z_s z_{s_{ij}}}\bar{k}_s\right)\end{aligned} \tag{2.9}$$

where, for example, $C_{x_s y_{s_{ij}}}$ is the component of displacement, $d'_{x_{s_i}}$, of the i^{th} lumped mass in the X_s direction of a structural axis system, X_s, Y_s, Z_s, due to a unit force in the Y_s direction at the j^{th} lumped mass. Letting $\bar{Q}_j$ be a force at the j^{th} lumped mass, the resulting displacement at the i^{th} lumped mass due to forces at all the lumped masses is

$$\bar{d}'_i = \sum_{j=1}^{n} \bar{\bar{C}}_{ij} \cdot \bar{Q}_j \tag{2.10}$$

Letting the matrix [C] represent the 3n x 3n matrix of 3 x 2 sub-matrices

$$\begin{bmatrix} C_{x_s x_{s_{ij}}} & C_{x_s y_{s_{ij}}} & C_{x_s z_{s_{ij}}} \\ C_{y_s x_{s_{ij}}} & C_{y_s y_{s_{ij}}} & C_{y_s z_{s_{ij}}} \\ C_{z_s x_{s_{ij}}} & C_{z_s y_{s_{ij}}} & C_{z_s z_{s_{ij}}} \end{bmatrix},$$

letting

$$\{d'\}^T = \left\lfloor d_{x_{s_1}}, d_{y_{s_1}}, d_{z_{s_1}}, \cdots, d_{x_{s_n}}, d_{y_{s_n}}, d_{z_{s_n}} \right\rfloor \tag{2.11}$$

and letting

$$\{Q\}^T = \left\lfloor Q_{x_{s_1}}, Q_{y_{s_1}}, Q_{z_{s_1}}, \cdots, Q_{x_{s_n}}, Q_{y_{s_n}}, Q_{z_{s_n}} \right\rfloor, \tag{2.12}$$

Eq. (2.10) may be replaced by the matrix expression

$$\{d'\} = [C]\{Q\}. \tag{2.13}$$

It may be noted that a prime has been used to denote the displacement $\bar{d}'_i$ in Eq. (2.10) and to distinguish them from the displacements $\bar{d}_i$ originally introduced. The displacements $\bar{d}'_i$ join the deformed lumped masses to their undeformed positions when one point of the structure has been held fixed during the deformation. That fixed point is referred to as the structural reference point and is the origin of the structural axis system, X_s, Y_s, Z_s. For simplicity in the following let it coincide with the center of gravity of the airplane in its undeformed state.

A small translation and rotation of the structural axis system relative to the body axis system may be represented as $\bar{d}_o$ and $\bar{\theta}_o$. Then the two displacement vectors for the i^{th} lumped mass are related as

$$\bar{d}_i - \bar{d}_o - \bar{\theta}_o \times \bar{r}_i = \bar{d}'_i \tag{2.14}$$

where products of the small translation and rotation are neglected. Eq. (2.10) may now be written as

$$\vec{d}_i - \vec{d}_o - \vec{\theta}_o \times \vec{\bar{r}}_i = \sum_{j=1}^{n} \vec{\bar{C}}_{ij} \cdot \vec{Q}_j \tag{2.15}$$

Further, letting

$$\{B\}^T = \left[d_{x_o}, d_{y_o}, d_{z_o}, \theta_{x_o}, \theta_{y_o}, \theta_{z_o} \right] \tag{2.16}$$

and introducing the rigid body mode shape matrix

$$[\vec{\phi}] = \begin{bmatrix} [\vec{\phi}_1] \\ [\vec{\phi}_2] \\ \vdots \\ [\vec{\phi}_n] \end{bmatrix} \quad \text{where} \quad [\vec{\phi}_i] = \begin{bmatrix} 1 & 0 & 0 & 0 & z_i & -y_i \\ 0 & 1 & 0 & -z_i & 0 & x_i \\ 0 & 0 & 1 & y_i & -x_i & 0 \end{bmatrix}, \tag{2.17}$$

the matrix equation, Eq. (2.13), may be written as

$$\{d\} - [\vec{\phi}]\{B\} = [\bar{C}]\{Q\}. \tag{2.18}$$

The body axis system is specified as a mean axis system, (1), by requiring the elastic displacement field d to satisfy the relationships

$$\int_V \rho_A \vec{d}\, dV = 0 \tag{2.19}$$

and

$$\int_V \rho_A \vec{\bar{r}} \times \vec{d}\, dV = 0. \tag{2.20}$$

Eq. (2.19) requires that the displacement field not give rise to a change in position of the airplane's center of gravity. The requirement of Eq. (2.20) leads to dynamic uncoupling of elastic motion from rotational motion when the rotational rate is small, (2). It also satisfies the law of conservation of angular momentum when the body axis system is non-rotating and the airplane is in a state of free vibration. This is important for the purpose of introducing free-vibrational mode shapes into the analysis.

By defining the diagonal mass matrix

$$[m] = \begin{bmatrix} m_1 & & & & & \\ & m_1 & & & & \\ & & m_1 & & & \\ & & & \ddots & & \\ & & & & m_n & \\ & & & & & m_n \\ & & & & & & m_n \end{bmatrix} \tag{2.21}$$

Eq. (2.19) and (2.20) may be combined into a single matrix expression as

$$[\vec{\phi}]^T [m] \{d\} = 0. \tag{2.22}$$

Now, if Eq. (2.18) is pre-multiplied by $[\vec{\phi}]^T[m]$, Eq. (2.22) may be used to derive an expression for the vector {B} so that Eq. (2.18) may be written as

$$\{d\} = [\vec{C}]\{Q\} \tag{2.23}$$

where

$$[\vec{C}] = \left[[I] - [\vec{\phi}][M]^{-1}[\vec{\phi}]^T[m] \right][C] \quad , \tag{2.24}$$

$$[M] = [\bar{\phi}]^T [m][\bar{\phi}] , \tag{2.25}$$

and [I] is the identity matrix.

It may be shown that the elastic rotation $\bar{\theta}_0$ is of the order of magnitude of the strains in the structure. The base vectors $\bar{i}_s, \bar{j}_s, \bar{k}_s$ in the diadic form of the flexibility coefficients, Eq. (2.9), differ from base vectors $\bar{i}, \bar{j}, \bar{k}$ in the body axis system by this small rotation. Thus, the components of the flexibility coefficients in the body axis system, i.e.,

$$C_{xx_{ij}} = \bar{i} \cdot \bar{C}_{ij} \cdot \bar{i} , \quad C_{xy_{ij}} = \bar{i} \cdot \bar{C}_{ij} \cdot \bar{j} , \qquad \text{etc.,}$$

differ from the components in the structural axis system only by quantities of the order of magnitude of products of elastic strains. These differences are ignored in linear structural theory. Thus, to the order of accuracy of the analysis, components of vectors in the structural axis system are interchangeable with components in the body axis system. This interchangeability is used to represent all components in the following development in the body axis system and to disregard the subscript S involved in the preceding equations.

The forces applied to the airplane consist of inertia forces, gravity forces, and aerodynamic forces. The total force applied at each lumped mass is given by

$$\bar{Q}_i = -m_i(\bar{a}_i - \bar{g}) + \bar{F}_i \tag{2.26}$$

where the inertia force is

$$\begin{aligned} m_i \bar{a}_i = m_i \Bigg\{ & \frac{\partial}{\partial t}\left(\frac{d\bar{r}_c'}{dt}\right) + \bar{\omega} \times \frac{d\bar{r}_c'}{dt} + \frac{\partial^2 \bar{d}_i}{\partial t} \\ & + 2\bar{\omega} \times \frac{\partial \bar{d}_i}{\partial t} + \frac{\partial \bar{\omega}}{\partial t} \times (\bar{r}_i' + \bar{d}_i) \\ & + \bar{\omega} \times \left[\bar{\omega} \times (\bar{r}_i' + \bar{d}_i)\right] \Bigg\} \end{aligned} \tag{2.27}$$

with $\frac{\partial}{\partial t}$ the time rate of change apparent to an observer in the body axis system and $\bar{\omega}$ the rotation rate of the body axis system. The gravity force is given by

$$m_i \bar{g} = m_i g(-\sin\theta \bar{i} + \cos\theta \sin\phi \bar{j} + \cos\theta \cos\phi \bar{k}) \tag{2.28}$$

with θ, ϕ the Euler angles defining angle of inclination to the horizon and angle of roll. The aerodynamic forces are the result of aerodynamic surface tractions. Letting S_i be the aerodynamic surface of the i^{th} lumped mass, letting dS be a differential surface element and neglecting viscous tractions, the aerodynamic force on the i^{th} lumped mass is

$$\bar{F}_i = -\bar{q} \int_{S_i} C_p \bar{n} \, dS \tag{2.29}$$

where Cp is the surface pressure coefficient and $\bar{q}$ is the dynamic pressure.

Several approximations are now introduced regarding the inertia forces. The elastic displacements and their rates as well as the rotation rate and its rate of change are regarded as sufficiently small that products of these quantities may be neglected. This leads to

$$m_i \bar{a}_i \approx m_i \left[\dot{\bar{V}}_c + \bar{\omega} \times \bar{V}_c + \ddot{\bar{d}}_i + \dot{\bar{\omega}} \times \bar{r}_i'\right] \tag{2.30a}$$

where

$$\bar{V}_c \equiv \frac{d\bar{r}_c'}{dt} \qquad \text{and} \qquad \frac{\partial}{\partial t} \equiv \dot{(\ )} . \tag{2.30b}$$

The forces on the disturbed airplane may be separated into reference values and disturbed values. When the airplane is undergoing reference motion, the motion is a steady motion. Hence, the reference inertia force on the i^{th} lumped mass becomes

$$m_i \bar{a}_{s_i} = m_i \left[\dot{\bar{V}}_{c_p} + \bar{\omega} \times \bar{V}_{c_i} + \ddot{\bar{d}}_{p_i} + \dot{\bar{\omega}} \times \bar{r}_i'\right] . \tag{2.31}$$

The disturbance inertia force is

$$m_i \bar{a}_i = m_i \left[\dot{\bar{V}}_{cp} + \bar{\omega}_p \times V_{c_1} + \ddot{\bar{d}}_{pi} + \dot{\bar{\omega}} \times \bar{r} \right] \tag{2.32}$$

where the subscript p identifies the excess of the values to the variables over their steady, reference values. Similarly, the gravity force may be written as

$$\bar{g}_i = \bar{g}_{1i} + \bar{g}_{pi} \tag{2.33}$$

by letting $\theta = \theta_1 + \theta_p$ and $\phi = \phi_1 + \phi_p$ and using the small angle approximation in the sine and cosine functions.

The aerodynamic forces are separated as

$$\bar{F}_i = \bar{F}_{1i} + \bar{f}_i. \tag{2.34}$$

Finally, the disturbance forces acting on the lumped masses may be written as

$$\{Q_p\} = -[m]\left[\{\ddot{d}_p\} + [\bar{\phi}]\left(\{\dot{V}_p\} + [M_1]\{V_p\} + [M_2]\{r_{op}'\}\right)\right] + \{f\} \tag{2.35}$$

where

$$\{V_p\}^T = \lfloor u, v, w, p, q, r \rfloor$$

is the matrix of disturbance components of translational and rotational velocities,

$$\{r_{op}'\} = \lfloor 0, 0, 0, \phi_p, \theta_p, 0 \rfloor$$

is the matrix of orientation angles, and $[M_1]$, $[M_2]$ are suitably defined in terms of the reference motion variables to give the appropriate centrifugal and gravity disturbance forces, (3).

The disturbance forces, Eq. (2.35), may be combined with Eq. (2.23) to obtain

$$\{d_p\} = -[\bar{C}][m]\left[\{\ddot{d}_p\} + [\bar{\phi}]\left(\{\dot{V}_p\} + [M_1]\{V_p\} + [M_2]\{r_{op}'\}\right)\right] + [\bar{C}]\{f\} \tag{2.36}$$

These are the equations of motion governing the elastic motion relative to the body axis system. Also, the laws of conservation of linear and angular momentum lead to

$$[\bar{\phi}]^T\{Q_p\} = 0$$

Thus, on using Eq. (2.22), the expanded disturbance forces may be introduced to find

$$[M]\left(\{\dot{V}_p\} + [M_1]\{V_p\} + [M_2]\{r_{op}'\}\right) = [\bar{\phi}]^T\{f\} \tag{2.37}$$

Eq. (2.37) constitutes six equations of motion governing the disturbance motion of the body axis system relative to reference motion. Eq. (2.36) and (2.37) are the required disturbance equations of motion for assessing the stability of the reference motion.

The remainder of the discussion will introduce the dependence of the aerodynamic forces on the motion variables and the simplifying approximations known as quasi-static and residual flexibility, (3). The dependence of the aerodynamic forces on the disturbance motion is obtained from an aerodynamic influence coefficient method which conforms with the lumped parameter representation.

3.0 LUMPED AERODYNAMIC FORCES - AERODYNAMIC INFLUENCE COEFFICIENTS

The aerodynamic forces which act on the lumped masses and arise as a consequence of the airplane's disturbance from a reference motion may be expressed as

$$\{f\} = [A_1]\{V_p\} + [A_2]\{\dot{V}_p\} + [A_3]\{d_p\} + [A_4]\{\dot{d}_p\} + [A_5]\{\ddot{d}_p\}. \tag{3.1}$$

The aerodynamic matrices $[A_1]$, $[A_2]$, $[A_3]$, $[A_4]$, and $[A_5]$ are derived from consideration of the small disturbance formulation of the aerodynamic problem. An important intermediate step in the derivation involves the development of aerodynamic influence coefficients of the type used by Woodward, (4).

The exact inviscid fluid boundary conditions imposed by the airplane's motion through the atmosphere consist of the parallel flow requirement which can be written as

$$\left[\vec{q} - \vec{V}_c - \vec{\omega} \times \vec{r} - \dot{\vec{d}}\right] \cdot \vec{n} = 0 \tag{3.2}$$

together with the requirement of zero pressure discontinuity across the wake and the vanishing of disturbances at infinity. The small disturbance formulation arises by identifying in the boundary condition (3.2) small parameters describing the local surface inclinations (i.e., camber, thickness, and elastic deformation), the angles-of-attack and sideslip, and the rates of roll, pitch, yaw, and elastic deformation rate, and seeking an asymptotic solution in the limit as the parameters approach zero. The velocity potential is expanded in an asymptotic series involving powers of the small parameters. Substitution of this expansion into the exact flow equations and boundary conditions and equating equal order of magnitude among the small parameters leads to a sequence of simplified linear boundary value problems which individually describe the flow associated with each of the small parameters.

A velocity potential expansion particularly suited for the present analysis is of the form

$$\Phi = V_\infty \left(x + \varepsilon_0 \phi_0 + \varepsilon_1 \phi_1 + \cdots + \varepsilon_i \phi_i + \cdots \varepsilon_i \varepsilon_j \phi_i \phi_j + \cdots\right) \tag{3.3}$$

where ε_i denotes any of the small parameters. The first order potentials, $\varepsilon_i \phi_i$, are governed by the classical linear Prandtl-Glauert equations. The corresponding first order boundary conditions appear in the form of required flow incidence angles. It is convenient to combine the flow incidence angles due to camber, transverse airplane motion, structural deformation rates and airplane rotational velocities together into a single flow incidence ψ_{c_i}, satisfying the boundary condition

$$\psi_{c_i} = \left|\beta \vec{j} + \alpha \vec{k} + \frac{1}{V_\infty}\left(\vec{\omega} \times \vec{r} + \dot{\vec{d}}\right)\right| \cdot \left(\cos\gamma_i \vec{k} - \sin\gamma_i \vec{j}\right) + \theta_{c_i} \tag{3.4}$$

where

ψ_{c_i} = flow incidence at point i due to camber, transverse motion, structural deformation and airplane rotation rates.

γ_i = angular orientation of the mean surface cross section.

θ_{c_i} = local camber slope.

The remaining flow incidence due to thickness satisfies the condition

$$\psi_{t_i} = \theta_{t_i} \tag{3.5}$$

where θ_{t_i} is the local thickness slope.

In many cases the first order potentials alone are sufficient to provide a suitable approximation for the aerodynamic loads. For the particular case of sideslip, however, Rubbert (5) has shown that certain second order terms involving products of the angle of sideslip β with the other small parameters are often significant in determining a suitable approximation for the sideslip effects. These second order terms are governed by linear inhomogeneous partial differential equations whose particular solutions involve the first order flow. General forms for the particular solutions have been worked out by Rubbert (5). With these, the solutions for the second order potential can, in principle, be obtained by adding homogeneous terms to fulfill the appropriate boundary conditions, which turn out to be linear. In practice, however, it has been found that current numerical methods such as the Woodward scheme (4) do not provide suitable accuracy in the computation of the second order particular solution. The difficulty lies in the fact that these particular integrals require an accurate knowledge of various derivatives of the first order solutions which are not supplied by current numerical methods. Implementation of the second order calculations must therefore be based on improved numerical methods for solving the first order boundary value problems.

The formulation of the aerodynamic influence coefficients arises from the numerical scheme. In the Woodward scheme, for example, distributions of sources, vortices and doublets, Fig. 2, are utilized to generate the disturbance flow. Line sources are located at slender body centerlines, such as the fuselage in Fig. 2, to represent its thickness. Distributions of sources are located at middle surfaces of the segments of thin bodies such as wings and tails to represent their thicknesses. Cross flow due to camber and transverse motion of slender bodies are represented by line doublets on their centerlines. Doublet distributions (vortex distributions) including their contributions to the wake are used to represent the

wing and tail segments. Finally, interference effects on slender bodies are accounted for by surface distributions of singularities on a cylinder of mean body radius at the region of interference. The distributed source type singularities give rise to aerodynamic influence coefficients which relate the lumped pressure force at the i^{th} segment of the airplane to flow incidence due to thickness at the j^{th} segment as

$$F_i = \bar{q} A_{t_{ij}} \psi_{t_j} \tag{3.6}$$

where F_i is along the normal $\vec{n}_i$.

The distributed doublet type singularities relate the lumped pressure forces to incidence due to camber and transverse motion as

$$F_i = \bar{q} A_{c_{ij}} \psi_{c_j}. \tag{3.7}$$

These influence coefficients are applicable to quasi-steady airplane motion. The accurate calculation of sideslip effects requires an extension of this basic procedure to include the forementioned second order terms.

The approximate effects of unsteady aerodynamics are evaluated by an expansion of the solution to the unsteady flow problem in terms of reduced frequency about zero frequency. The lowest order solution yields the quasi-steady flow problem. The next higher order approximation, when combined with the lowest order approximation, yields an unsteady flow problem. The solution to this problem may be computed directly from the solution to the quasi-steady flow problem. The approach was suggested by Miles, (6), and applied to supersonic unsteady flow over wings with supersonic trailing edges. It has been shown by Brune, (7), that it is applicable to slowly oscillating wings in supersonic flow with arbitrary edges and in subsonic flow for wings of finite aspect ratio. The approximation is valid in subsonic flow for Mach numbers, M, and aspect ratios, $\mathcal{AR}$, which satisfy the requirement $\sqrt{1-M^2}\,\mathcal{AR} \ll 1$. For the Mach number aspect ratio combinations where valid, the approach leads to unsteady aerodynamic influence coefficients which are independent of the reduced frequency provided it is small by comparison with unity. The result is a relationship between the lumped aerodynamic pressure forces and the rate of change of flow incidence due to camber and transverse motion. This is expressed as

$$F_i = \bar{q} S A_{ij} \dot{\psi}_{c_j}. \tag{3.8}$$

Eq. (3.5), (3.6), and (3.7) may be combined to give

$$F_i = \bar{q} \left(A_{t_{ij}} \psi_{t_j} + A_{c_{ij}} \psi_{c_j} + S A_{ij} \dot{\psi}_{c_j} \right) \tag{3.9}$$

and it is this expression and Eq. (3.4) and (3.5) which form the basis for writing the aerodynamic equation, Eq. (3.1).

4.0 QUASI-STATIC AND RESIDUAL FLEXIBILITY APPROXIMATIONS

The preceding has led to equations of motion for the disturbance motion of an elastic airplane expressed as

$$[M]\left(\{\dot{V}_p\} + [M_1]\{V_p\} + [M_2]\{\omega_p'\} \right) = [\bar{\phi}]^T \{f\} \tag{2.37}$$

for the rigid body motion and as

$$\{\alpha_p\} = -[\bar{C}]\left[m \right]\left[\{\ddot{\alpha}_p\} + [\bar{\phi}]\left(\{\dot{V}_p\} + [M_1]\{V_p\} + [M_2]\{\omega_p'\} \right) \right] + [\bar{C}]\{f\} \tag{2.36}$$

for elastic motion, where

$$\{f\} = [A_1]\{V_p\} + [A_2]\{\dot{V}_p\} + [A_3]\{\alpha_p\} + [A_4]\{\dot{\alpha}_p\} + [A_5]\{\alpha_p\} \tag{3.1}$$

are the disturbance aerodynamic forces.

A quasi-static elastic airplane representation is one in which all inertial and damping forces associated with the elastic motion are negligible. When this assumption is valid, the elastic motion equations, Eq. (2.36), and the aerodynamic equation, Eq. (4.1), may be combined to eliminate explicit dependence of the aerodynamic forces on the elastic displacements. This results in

$$\{f\} = \left[[I] - [A_3][\bar{C}]\right]^{-1}\left[[A_1]\{V_p\} + [A_2]\{\dot{V}_p\} - [A_3][\bar{C}][m][\bar{\phi}]\left(\{\dot{V}_p\} + [M_1]\{V_p\} + [M_2]\{\omega_p'\}\right)\right] \tag{4.1}$$

When this expression is introduced into Eq. (2.37) the equations of motion may be expressed as

$$[M]\left(\{\dot{V}_p\} + [M_1]\{V_p\} + [M_2]\{\omega_p'\}\right)$$

$$= \underbrace{[\bar{\phi}]^T\left[[I] - [A_3][\bar{C}]\right]^{-1}[A_1]\{V_p\}}_{\text{steady stability derivatives}}$$

$$+ \underbrace{[\bar{\phi}]^T\left[[I] - [A_3][\bar{C}]\right]^{-1}[A_2]\{\dot{V}_p\}}_{\text{unsteady stability derivatives}} \tag{4.2}$$

$$\underbrace{-[\bar{\phi}]^T\left[[I] - [A_3][\bar{C}]\right]^{-1}[A_3][\bar{C}][m]\left(\{\dot{V}_p\} + [M_1]\{V_p\}\right)}_{\text{inertial stability derivatives}}$$

$$\underbrace{-[\bar{\phi}]^T\left[[I] - [A_3][\bar{C}]\right]^{-1}[A_3][\bar{C}][m][M_2]\{\omega_p'\}}_{\text{orientation stability derivatives}}.$$

The stability derivatives corresponding to inertial forces may be combined directly with the steady and unsteady stability derivatives. When that is done, the effect of the inertial forces on the values of the stability derivatives is referred to as inertial relief owing to the negative sign before these terms. The orientation stability derivatives are associated with the disturbance Euler angles $\emptyset$ and θ. They vanish when the flexibility goes to zero and the airplane becomes rigid. Also, it may be noted that the aerodynamic matrices contain the dynamic pressure so that the multiplier $[[I]-[A_3][\bar{C}]]^{-1}$ is dynamic pressure dependent. That dependence is the mechanism whereby phenomena such as wing divergence occur.

Eq. (2.36), (2.37), and (3.1) represent the dynamic elastic airplane and Eq. (4.1) represents the quasi-static elastic airplane. There is an airplane representation which is intermediate to these two extremes and is optimum for predicting stability characteristics of large, elastic airplanes. Its formulation is based on a free-vibration mode shape representation of the airplane's elastic deformation and is termed a residual flexibility representation, (3) and (8). This formulation includes dynamic effects of low frequency modes which are likely to couple with the rigid body motions. The effects of the higher frequency modes are included as quasi-static elastic motion.

The free-vibration modes are introduced as a transformation of the elastic displacements to generalized elastic displacements as

$$\{q_p\} = [\phi]\{u\} \tag{4.3}$$

where the columns of the transformation matrix $[\emptyset]$ are the deformation shapes associated with the modes and the quantities {u} are the generalized displacements which are functions of time alone.

The mode shapes are obtained from an eigenvalue problem which develops from the elastic motion equations when the airplane is unaccelerated, non-rotating and free of applied forces. The equations are

$$\{q_p\} = -[\bar{C}][m]\{\ddot{q}_p\}. \tag{4.4}$$

They may also be expressed in terms of stiffness as

$$[\bar{K}]\{q_p\} = -[m]\{\ddot{q}_p\} \tag{4.5}$$

where the stiffness matrix is given by

$$[\bar{K}] = [K_{11}]\left[[I] - [\bar{\phi}]\left([\bar{\phi}]^T[K_{11}][\bar{\phi}]\right)^{-1}\right][K_{11}][\bar{\phi}]$$

and $[K_{11}]$ is the inverse of the flexibility matrix [C] contained in $[\bar{C}]$.

The mode shapes are generated by assuming harmonic motion in each of the generalized displacements u_i with frequency ω_i. Under that assumption Eq. (4.5) reduces to the eigenvalue problem

$$[\bar{K}]\{\phi\}_i = \omega_i^2[m]\{\phi\}_i \tag{4.6}$$

There are 3n-6 non-zero eigenvalues. The transformation matrix has 3n-6 columns corresponding to the non-zero eigenvalues. There are six eigenvalues which are zero, and six additional eigenvectors may be constructed. They are the columns of the rigid body mode shape matrix $[\bar{\phi}]$.

The transformation matrix has the following orthogonality properties:

$$[\phi]^T[\bar{K}][\phi] = [\bar{K}] \tag{4.7}$$

where the diagonal elements of $[\bar{K}]$ are the generalized stiffness,

$$[\phi]^T[m][\phi] = [\bar{m}] \tag{4.8}$$

where the diagonal elements of $[\bar{m}]$ are the generalized masses, and

$$[\phi]^T[m][\phi] = 0. \tag{4.9}$$

When the elastic motion equations, Eq. (2.36), are expressed in terms of the stiffness matrix $[\bar{K}]$ and the transformation, Eq. (4.3), is introduced, the above orthogonality properties lead to generalized elastic equations of motion as follows:

$$[\bar{K}]\{u\} + [\bar{m}]\{\ddot{u}\} = [\phi]^T\{f\}. \tag{4.10}$$

These equations are coupled only in terms of the generalized aerodynamic forces. They are only 3n-6 in number in lieu of the original 3n equations of elastic motion. Also, the elastic deflection dependence on the inertia and gravity forces no longer appears explicity, due to the orthogonality property expressed by Eq. (4.9). It may be shown, (3), that the generalized aerodynamic forces are computed from aerodynamic forces which deviate from those which just balance the inertia and gravity forces at each lumped mass.

Equations of motion for the residual flexibility representation are obtained by partitioning the transformation such that

$$\{d_p\} = [\phi_1]\{u_1\} + [\phi_2]\{u_2\} \tag{4.11}$$

Then, letting $[\phi_2]$ contain the higher frequency mode shapes such that

$$\begin{aligned} [m][\phi_2]\{\ddot{u}_2\} &\approx 0 \\ [A_4][\phi_2]\{\ddot{u}_2\} &\approx 0 \\ [A_5][\phi_2]\{\ddot{u}_2\} &\approx 0 \end{aligned} \tag{4.12}$$

the higher frequency portion of the equations of motion, Eq. (4.10), reduce to

$$\{u_2\} = [\bar{K}_2]^{-1}[\phi_2]^T\{f\}. \tag{4.13}$$

This expression may now be used to eliminate explicit dependence of the aerodynamic forces on the generalized displacements $\{u_2\}$ The result is

$$\begin{aligned} \{f\} = \left[[I] - [A_3][\phi_2][\bar{K}_2]^{-1}[\phi_2]^T\right]^{-1} &\left[[A_1]\{\dot{V}_p\} + [A_2]\{\dot{V}_p\} + [A_3][\phi_1]\{u_1\}\right. \\ &\left. + [A_4][\phi_1]\{\dot{u}_1\} + [A_5][\phi_1]\{\ddot{u}_1\}\right]. \end{aligned} \tag{4.14}$$

Eq. (4.14) may be used to represent the aerodynamic forces in the residual flexibility formulation. The similarity of Eq. (4.14) with the aerodynamic forces in the quasi-static representation, Eq. (4.1), is readily apparent. The matrix $[\phi_2][\bar{K}_2][\phi_2]^T$ plays the role of $[\bar{C}]$ and is the residual flexibility associated with the high frequency modes. The rigid body inertial and gravity terms do not appear in Eq. (4.14) because of the orthogonality condition, Eq. (4.9), and because it is expressed entirely in terms of the free-vibration mode shapes.

The explicit dependence on the higher frequency modes may be eliminated as follows. The equations governing elastic motion, Eq. (2.36), may be expressed in terms of stiffness as

$$[\bar{K}]\{d_p\} = -[m]\{\ddot{d}_p\} + \{f\} - [m][\bar{\phi}]\{\mathcal{R}\} \tag{4.15}$$

where for simplicity of writing

$$\{\mathcal{R}\} \equiv \{\dot{V}_p\} + [M_1]\{V_p\} + [M_2]\{\kappa_p'\}. \tag{4.16}$$

The partitioned transformation, Eq. (4.11), is introduced into the left hand member of Eq. (4.15) and the entire expression is pre-multiplied by the transpose of the partitioned transformation matrix. The result may then be solved for the generalized elastic displacements to find

$$\left[\begin{array}{c}\{u_1\}\\ \hline \{u_2\}\end{array}\right] = \left[\begin{array}{c|c}[\bar{K}_1]^{-1} & [0]\\ \hline [0] & [\bar{K}_2]^{-1}\end{array}\right]\left[\begin{array}{c}[\phi_1]^T\\ \hline [\phi_2]^T\end{array}\right]\left(-[m]\{\ddot{d}_p\} + \{f\}\right). \tag{4.17}$$

Premultiplication of Eq. (4.17) by the transformation matrix leads to

$$\{d_p\} = \left([\phi_1][\bar{K}_1]^{-1}[\phi_1]^T + [\phi_2][\bar{K}_2]^{-1}[\phi_2]^T\right)\left(-[m]\{\ddot{d}_p\} + \{f\}\right) \tag{4.18}$$

and the elastic displacements of Eq. (4.18) may be equated to those of Eq. (2.36) to find

$$\begin{aligned}&[\phi_2][\bar{K}_2]^{-1}[\phi_2]^T\left(-[m]\{\ddot{d}_p\} + \{f\}\right) \\ &= \left([\bar{C}] - [\phi_1][\bar{K}_1]^{-1}[\phi_1]^T\right)\left(-[m]\{\ddot{d}_p\} + \{f\}\right) - [\bar{C}][m][\bar{\phi}]\{\mathcal{R}\}.\end{aligned} \tag{4.19}$$

The residual flexibility is now defined as

$$[\bar{C}_2] \equiv [\bar{C}] - [\phi_1][\bar{K}_1]^{-1}[\phi_1]^T \tag{4.20}$$

so that on introducing the partition transformation, Eq. (4.11); using the first of the approximations of Eq. (4.12) and the orthogonality conditions; Eq. (4.19) reduces to

$$[\phi_2][\bar{K}_2]^{-1}[\phi_2]^T\{f\} = [\bar{C}_2]\left(-[m][\phi_1]\{\ddot{u}_1\} + \{f\}\right) - [\bar{C}][m][\bar{\phi}]\{\mathcal{R}\}. \tag{4.21}$$

The explicit dependence of the aerodynamic forces on $\{u_2\}$ is eliminated in the same manner as in deriving Eq. (4.14). This time the result is left in the form

$$\begin{aligned}\{f\} = {} & [A_1]\{V_p\} + [A_2]\{\dot{V}_p\} + [A_3][\phi_1]\{u_1\} + [A_3][\phi_2][\bar{K}_2]^{-1}[\phi_2]^T\{f\} \\ & + [A_4][\phi_1]\{\dot{u}_1\} + [A_5][\phi_1]\{\ddot{u}_1\}.\end{aligned} \tag{4.22}$$

Eq. (4.21) may now be introduced to eliminate explicit dependence of Eq. (4.22) on the higher frequency mode shapes and solved for the aerodynamic forces. When that result is substituted into Eq. (2.37) the equations of motion written in terms of residual flexibility are found as

$$\begin{aligned}&[M]\left(\{\dot{V}_p\} + [M_1]\{V_p\} + [M_2]\{\kappa_p'\}\right) \\ &= \underbrace{[\bar{\phi}]^T\left[[I] - [A_3][\bar{C}_2]\right]^{-1}[A_1]\{V_p\}}_{\text{steady stability derivatives}}\end{aligned} \tag{4.23}$$

$$+\underbrace{[\bar{\phi}]^T\left[[I]-[A_3][\bar{C}_R]\right]^{-1}[A_2]\{\dot{V}_p\}}_{\text{unsteady stability derivatives}}$$

$$+\underbrace{[\bar{\phi}]^T\left[[I]-[A_3][\bar{C}_R]\right]^{-1}[A_3][\bar{C}][m][\bar{\phi}]\left(\{\dot{V}_p\}+[M_1]\{V_p\}+[M_2]\{\omega_p'\}\right)}_{\text{inertial and orientation stability derivatives}} \qquad (4.23)\ \text{cont.}$$

$$+\underbrace{[\bar{\phi}]^T\left[[I]-[A_3][\bar{C}_R]\right]^{-1}\left[\left([A_5]-[A_3][\bar{C}_R][m]\right)[\phi_1]\{\dot{u}_1\}+[A_3][\phi_1]\{u_1\}+[A_4][\phi_1]\{\dot{u}_1\}\right]}_{\text{generalized elastic displacement stability derivatives}}$$

The similarity of the above equations with the quasi-static elastic equations of motion is apparent. If all of the modes are treated as static elastic, $[\bar{C}_R]$ reduces to $[\bar{C}]$ and Eq. (4.23) becomes identical with Eq. (4.2). The residual flexibility representation reduces to the quasi-static elastic representation in the limit.

The elastic equations of motion for the residual flexibility representation of the airplane are readily obtained as

$$[\bar{m}_1]\{\ddot{u}_1\}+[\bar{K}_1]\{u_1\}=[\phi_1]^T\left[[I]-[A_3][\bar{C}_R]\right]\left[[A_1]\{V_p\}+[A_2]\{\dot{V}_p\}\right.$$
$$+[A_3][\bar{C}][m][\bar{\phi}]\left(\{\dot{V}_p\}+[M_1]\{V_p\}+[M_2]\{\omega_p'\}\right)+\left([A_5]-\qquad (4.24)$$
$$\left.[A_3][\bar{C}][m]\right)[\phi_1]\{\ddot{u}_1\}+[A_4][\phi_1]\{\dot{u}\}+[A_5][\phi_1]\{u_1\}\Big].$$

This set of equations may be made to vanish when all modes are taken as quasi-static.

The residual flexibility formulation retains only those dynamic effects of the structural motion which have important consequences on the characteristics of the rigid body motion. Whether the effect of the structural motion may be represented as quasi-static or must be represented as dynamic depends largely on the natural frequencies of the structure. The structural motion represented by motion in structural modes whose frequencies are much larger than the natural frequencies of the rigid body motion (an order of magnitude larger) will not have significant dynamic coupling with the rigid body motion.

Since aerodynamic stiffness, damping, and inertial forces on the structural modes are small by comparison with the structural inertial and stiffness forces, the free-vibration natural frequencies of the structure are close approximations to the natural frequencies of the structure of the airplane in a reference flight condition. The free-vibration frequencies of the structure and the rigid body natural frequencies based on the quasi-static airplane representation are a reasonable guide in selecting those generalized elastic freedoms which must be included in the dynamic analysis.

It has been the practice to ignore the high frequency modes such that the flexibility associated with them is completely left out of a stability analysis. This can lead to an erroneous stability evaluation. A large natural frequency for a structural mode need not imply a large generalized stiffness nor small deflections under aerodynamic loading. For example, tail surfaces on many airplanes have their section mass centers very close to the shear centers of their sections. The surface may be very flexible in torsion and its mass distribution may be quite large. But, the close proximity of the section shear and mass centers leads to the incorporation of the torsional deformation into a high frequency structural mode. The high frequency of the motion implies that the structure will respond quickly in twist under an aerodynamic couple about its shear center. The result could be a significant quasi-static effect on rigid body motion. The residual flexibility representation includes these effects without encumbering the numerical analysis of the important motion characteristics by introducing unnecessary degrees of freedom.

5.0 REFERENCES

1. Milne, R. D.: Dynamics of the Deformable Airplane, Parts I and II. Her Majesty's Stationery Office, London, 1964.

2. Hemp, W. S.: Note on the Dynamics of a Slightly Deformable Body. College of Aeronautics Report 5, England, February 1947.

3. Members of the Aerodynamics and Structures Research Organizations, Commercial Airplane Division, The Boeing Company: An Analysis of Methods for Predicting the Stability Characteristics of an Elastic Airplane, Appendix A. NASA Report CR-73274, November 1968.

4. Woodward, F.; LaRowe, R. F.; and Love, J. E.: Analysis and Design of Supersonic Wing-Body Combinations, Including Flow Properties in Near Field. Parts I and II, NASA Report CR-73107, 1967.

5. Rubbert, P. E.: Sideslip of Wing-Body Combinations. Unpublished Boeing Report on NASA-Ames Contract NAS 2-5006, 1969.

6. Miles, J. W.: The Potential Theory of Unsteady Supersonic Flow. Cambridge University Press, 1959.

7. Brune, G.: Unsteady Flow Approximation for Small Reduced Frequencies. Unpublished Boeing Report on NASA-Ames Contract NAS 2-5006, 1969.

8. Schwendler, R. G.; and MacNeal, H.: Optimum Structural Representation in Aeroelastic Analysis. ASD-TR-61-680, Computer Engineering Associates, March 1962.

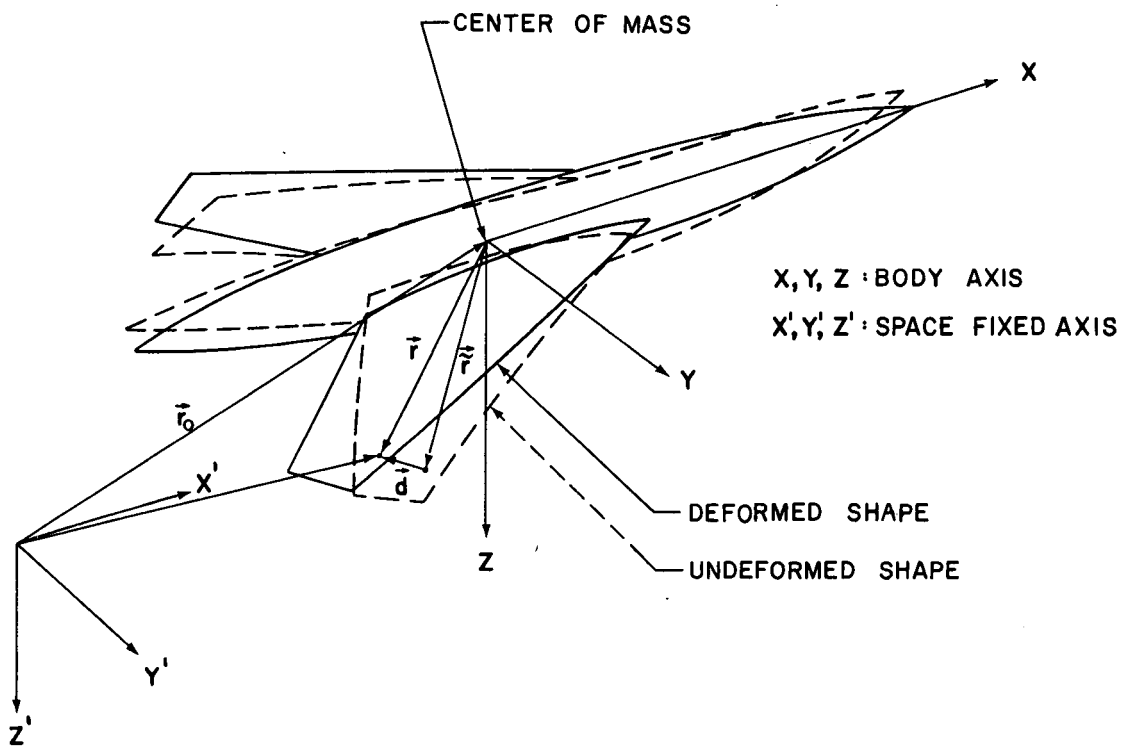


FIGURE 1 - GEOMETRIC REPRESENTATION

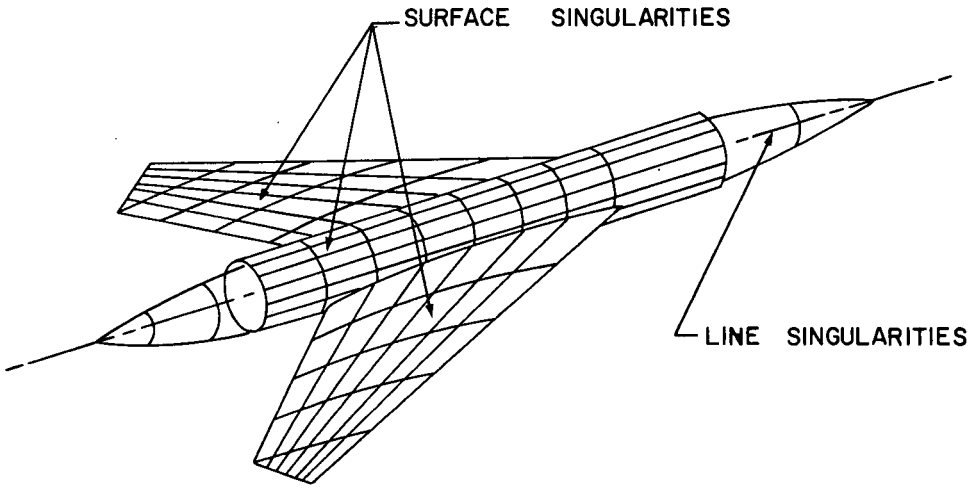


FIGURE 2 - AERODYNAMIC REPRESENTATION

AN ANALYTICAL METHOD FOR PREDICTING THE STABILITY AND CONTROL CHARACTERISTICS OF LARGE ELASTIC AIRPLANES AT SUBSONIC AND SUPERSONIC SPEEDS

PART II: APPLICATION

By

Howard L. Chevalier
Research Scientist
Ames Research Center, National Aeronautics and Space Administration
Moffett Field, California, U.S.A. 94035

Gerald M. Dornfeld and Robert C. Schwanz
Research Engineers
Aerodynamics Research Staff, Commercial Airplane Division
The Boeing Company, Renton, Washington, U.S.A.

SUMMARY

The method is applied to two aircraft representative of current design, the Boeing 707-320B and an early version of the supersonic transport. Comparisons with experimental values indicate that this purely analytical method provides reliable and useful results for estimating the longitudinal stability and control characteristics of large flexible aircraft. The effects of elasticity on the static longitudinal stability and control of the two aircraft were found to be large and unfavorable for most flight conditions. On the other hand, elasticity did not greatly affect the dynamic stability characteristics, but the results indicate that as the structural frequencies approach the frequency of motion of the airplane (ratios less than 4:1), major effects might occur.

INTRODUCTION

It is evident (1) that the analytical determination of the stability and control of an elastic airplane involves three basic considerations: (i) prediction of the aerodynamic forces, (ii) determination of the deformations in shape caused by these forces and the ensuing effects upon the forces themselves, and (iii) combination of these results to determine the dynamic motion of the airplane and its structure. Errors in the analytical results will accrue from all of these sources.

Experience has shown that the aerodynamic problem is the most difficult to treat, and the aerodynamic predictions contain large uncertainties. For these reasons an assessment of the utility of an analytic scheme for computing stability characteristics should include the validity of the aerodynamic analysis in addition to the overall accuracy of the scheme itself. Such an appraisal has already been made of the aerodynamic method of the present scheme, but is concerns only idealized wing-body shapes (2,3). The presence of nacelles, struts, hinge lines, and various other protuberances and surface discontinuities on airplanes, together with the large differences between wind tunnel and flight Reynolds number, makes it advisable to extend the appraisal to full-scale aircraft. This extension is the first objective of the present investigation.

A second, more important objective, is to determine the overall accuracy of the analytical scheme applied to elastic aircraft, thereby assessing its general usefulness in aircraft design.

To accomplish these two objectives, information concerning the effects of elasticity on the stability and control of the associated configurations is supplemented and re-examined to determine how and to what extent the principal stability and control parameters of the configurations are affected.

With but one exception all results apply only to longitudinal motion.

SYMBOLS

b	wing span, m
C_L	lift coefficient, $L/q_\infty S$
C_{L_α}	change in lift coefficient with angle of attack, $\partial C_L/\partial\alpha$, deg^{-1}
$C_{L_{\dot{\alpha}}}$	change in lift coefficient with rate of change of angle of attack, $\partial C_L/\partial(\dot{\alpha}c/2V)$, $radian^{-1}$
$C_{L_{\delta_E}}$	change in lift coefficient with elevator deflection angle, $\partial C_L/\partial\delta_E$, deg^{-1}
C_l	rolling-moment coefficient, $M_X/q_\infty Sb$

C_{l_p} change in rolling-moment coefficient with roll rate, $\partial C_l/\partial(pb/2V)$, radian^{-1}

C_m pitching-moment coefficient, $M_y/q_\infty Sc$

C_{m_q} change in pitching-moment coefficient with pitch rate, $\partial C_m/\partial(qc/2V)$, radian^{-1}

C_{m_α} change in pitching-moment coefficient with angle of attack, $\partial C_m/\partial\alpha$, deg^{-1}

$C_{m_{\dot{\alpha}}}$ change in pitching-moment coefficient with rate of change of angle of attack, $\partial C_m/\partial(\dot{\alpha}c/2V)$, radian^{-1}

$C_{m_{\delta_E}}$ change in pitching-moment coefficient with elevator deflection angle, $\partial C_m/\partial\delta_E$, deg^{-1}

c reference chord, m

h center-of-gravity location, x/c

h_m maneuver point location, x/c

h_n neutral point location, x/c

M_x rolling moment, m-N

M_y pitching moment, m-N

M Mach number

n load factor

p roll rate, radians/sec

q pitch rate, radians/sec

q_∞ dynamic pressure, N/m^2

S projected wing area, m^2

V airplane velocity, m/sec

x longitudinal distance, m

α angle of attack, deg

$\dot{\alpha}$ rate of change of angle of attack, radians/sec

δ_E elevator deflection angle, deg

ζ short-period damping ratio

ρ air density, kg/m^3

ω short-period damped natural frequency, radians/sec

Abbreviations

ALT altitude

SST supersonic transport

WT airplane weight

CONFIGURATIONS, DATA, AND COMPUTATION

Two configurations representative of current transport aircraft designs were examined in this investigation. The general arrangement of the configurations is given in Fig. 1. The Boeing 707-320B airplane is generally familiar; the supersonic transport (SST) configuration is one of the early variable-sweep designs studied. Only the fully swept configuration is considered here.

Characteristic features of the Boeing 707-320B airplane pertinent to this investigation are its relatively high aspect ratio, 6.9, and its flexible structure. For planforms of this type, good results are normally expected of aerodynamic calculations.

The aspect ratio of the supersonic transport is low, 1.25, and severely tests the range of applicability of the aerodynamic analysis. Another feature of aerodynamic interest is the shear tie between the wing and the horizontal tail, which in the fully swept condition results in a discontinuity between the slopes of these surfaces at their juncture.

The experimental data for the 707 (see (4)) were obtained from flight tests of the full-scale elastic airplane and from wind-tunnel tests of an 0.035 scale rigid model. The Reynolds number of the wind-tunnel tests, based on the reference chord length (which for the full-scale airplane is 6.92 m), ranged from 1.8 to 3.0 million.

All experimental data for the SST (4) were derived from wind-tunnel tests. Two 0.015 scale models were used - one rigid and one elastic. The elastic model was constructed so that the deflections of the wing and tail surfaces under similar loading conditions duplicated as closely as possible those calculated for the proposed full-scale airplane at cruise conditions. Body flexibility was not duplicated; the body construction was the same as that ordinarily used for rigid models. Reynolds numbers of these tests were 15 to 21 million.*

Predicted values of aerodynamic quantities were in all cases obtained by use of aerodynamic influence coefficients. With the single exception of a portion of the dynamic stability calculations for the Boeing 707-320B airplane, these aerodynamic influence coefficients were computed by a method based on lifting surface theory (2,3). The 707-320B dynamic stability calculations deviating from this procedure employed aerodynamic influence coefficients obtained from lifting line theory. All calculations neglected the effects of wing thickness and, with one exception, those of body thickness as well.

Certain shortcomings inherent in the aerodynamic analysis, even in its complete form, should also be mentioned. Two in particular are important: (i) pressure distributions near the leading edge of the wing are not well represented, and (ii) pressures over each of the panels into which the planform is divided are presumed constant for that panel. For these and other reasons, the panel arrangement used in the calculations has decisively important effects on the accuracy of the results. Fig. 2 shows the paneling used for the computations of the present investigation; the paneling was arranged in accordance with the recommendations of (2).

Structural deflections, translational and angular, were calculated by use of structural influence coefficients. The coefficients employed for the 707-320B calculations were those used in the certification of the aircraft; they had, in addition, been verified by static load and vibration tests. For the SST conputations, experimental influence coefficients determined from directly measured deflections of the statically loaded wind-tunnel models were used.

To account for the airplane weight and inertia, part of the total mass was assigned to each panel to correspond to the airplane mass distribution over its planform. Each elemental mass was concentrated at the panel centroid. The effects of aerodynamic, inertial, and gravitational forces on the elastic deflections of the structure were then handled by two different methods. The first method, termed the "quasi-static-elastic," while including for each panel the inertial forces associated with airplane center of gravity acceleration, neglected the corresponding forces arising from panel accelerations relative to the airplane center of gravity. Panel deflections and the aerodynamic forces causing them were assumed to be exactly in phase at all times. This method is also known as the "static elastic" and "equivalent elastic" procedure. The second method, the "fully elastic" representation, recognized the effects of all inertial forces as well as gravitational forces, and used the concept of normal modes to represent the shape of the structure.

The term "rigid body" indicates a single, unique configuration. The shape of this configuration is that of the loaded quasi-static-elastic airplane with its mass properly distributed for the selected total weight in the cruise condition.

RESULTS AND DISCUSSION

The data summarizing the results obtained for the two configurations of this investigation are presented in Figs. 3 through 13. These figures have been arranged to illustrate first the accuracy of the analytical method as reflected by comparisons of static stability and control parameters (Figs. 3-8); second, the effects of elasticity on static longitudinal stability and control (Figs. 3-10); and, finally, the dynamic stability characteristics (Figs. 11-13).

The basic static derivatives considered are C_{L_α}, C_{m_α}, C_{l_p}, $C_{L_{\delta_E}}$, $C_{m_{\delta_E}}$, $d\delta_E/dV$, and $d\delta_E/dn$. Although Figs. 3 through 8 illustrate many of the effects of elasticity on the aerodynamic characteristics of the configurations, discussion of these effects is deferred to the section immediately following, where the additional data of Figs. 9 and 10 are introduced. All static stability calculations for the elastic airplane are based upon its quasi-static-elastic shape.

*Full-scale reference length was 48.2 m (158 ft).

Static Stability, Evaluation of Theory

Boeing 707-320B airplane.- To evaluate the accuracy of the theoretical calculations of lift and pitching moment, the values computed for lift curve slope, C_{L_α}, and for pitching-moment derivative, C_{m_α}, of the rigid airplane are compared in Fig. 3 with the experimental data obtained from wind-tunnel tests of a rigid model. Lift curve slope computations accounting for the effects of body thickness are also included in this figure. For C_{L_α}, the agreement of predicted with experimental values is considered good, the maximum discrepancy over the Mach number range for the thin body representation being of the order of 10 percent. Calculations of C_{L_α} using the thick-body representation provided even better comparison, the maximum discrepancy being reduced to less than 5 percent.

For C_{m_α}, the error in the magnitudes of the theoretical values is somewhat greater than it is for C_{L_α}, but here also the variation with Mach number is well represented.

As was previously explained, the aerodynamic calculations (except a portion of the 707-320B dynamic stability analysis) are based upon surface theory as contrasted with the lifting line theory frequently used for planforms of the type represented by this airplane. One reason for this choice stems from the results of comparative calculations with the two theories. In all cases the results obtained with lifting surface theory were in better agreement with experimental results than those derived from lifting line analysis.

In Fig. 4 values of C_{L_α} and C_{m_α} computed for the elastic airplane are compared with measurements made in flight at the altitudes and Mach numbers indicated. To provide a basis for evaluating these results, the rigid airplane characteristics of Fig. 3 are also shown. The agreement of the elastic body calculations with the flight data for C_{L_α}, and for C_{m_α} for the 108,900 kg airplane, is noticeably better than the agreement of the rigid body calculations with the same experimental data. Thus it may be concluded that the analytical method of (1) does account for the major effects of flexibility at these subsonic Mach numbers. The two experimental points for 129,500 kg gross weight, indicating that the stability of the 707-320B airplane increases with mass, should be interpreted cautiously. The scatter of the data for 108,900 kg shows that more evidence is required before any but qualitative conclusions can be drawn. It should further be noticed that the difference between calculated and flight values for 108,900 kg gross weight approximates -0.003 and that this difference is about the same as that shown in the C_{m_α} comparison of Fig. 3.

The variation with Mach number of C_{l_p}, change in rolling-moment coefficient with rate of roll, is shown in Fig. 5. Here also the agreement of calculated with measured results is reasonably good. This conclusion is also supported by the data of Fig. 6, in which the variation of elevator angle with velocity $d\delta_E/dV$ and with load factor $d\delta_E/dn$ have been plotted. The good agreement observed in this latter figure is of more than passing significance, in that it provides an appraisal of the overall validity of the analysis. The experimental values are measured directly and with reasonable accuracy; the predicted values are determined indirectly, from calculated values of such basic derivatives as C_{L_α}, C_{m_α}, C_{m_q}, $C_{m_{\delta_E}}$, etc.

Supersonic transport.- Comparisons of predicted and experimental values of the angle-of-attack derivatives C_{L_α} and C_{m_α} for the SST configuration at Mach numbers of 1.6 and 2.7 are presented in Fig. 7. These data are plotted as functions of free-stream dynamic pressure for both rigid and elastic models. For the elastic wind-tunnel model the effects of model mass, and of mass distribution, were calculated and found to be negligible.

Predicted values of C_{L_α} for both the rigid and flexible models, when compared to the experimental data, show good agreement. The discrepancies that do occur are less than 4 percent of the experimental values.

Analytical calculations of C_{m_α} for the rigid model do not agree with the experimental values measured in the wind-tunnel tests. This result is not peculiar to this configuration nor to the thin body assumption. Experience with the aerodynamic analysis using thick body representation, while not yet extensive, indicates that the disagreement observed here both in size and direction (underestimation of the static stability) is usually encountered. The error appears to be inherent in the aerodynamic analysis as it is presently formulated. Among the possible causes may be the failure to accurately account for leading edge pressure representation and the fact that chordwise pressure distributions near the wing tip, as shown in (2) and (3), are noticeably inaccurate. These and other possibilities are currently being investigated at the NASA, Ames Research Center by wind-tunnel tests of pressure distributions models.

It should also be noted that the experimental measurements of C_{m_α} at lift coefficients of 0.02 and 0.08 shown in Fig. 7 disagree with one another. This disagreement shows that C_{m_α} is not independent of C_L; consequently, C_m varies nonlinearly with angle of attack. The formulation of the aerodynamic theory, depending as it does upon linear approximations, obviously cannot account for this nonlinear effect.

Comparisons of the predicted elevator control surface derivatives $C_{L_{\delta_E}}$ and $C_{m_{\delta_E}}$ for the SST configuration are illustrated in Fig. 8. For $C_{L_{\delta_E}}$ both rigid and elastic calculated values

generally agree well with the experimental values, except for the rigid model at 1.6 Mach number. The agreement is also good for the rigid body values of $C_{m_{\delta_E}}$. Here, however, because the elastic and experimental values disagree seriously and because calculated values of C_{m_α} are, as discussed previously, unreliable, values predicted for $C_{m_{\delta_E}}$ should be viewed with caution. It should also be observed that the predictions are unconservative.

Static Stability, Effects of Elasticity

The data used to appraise the effects of elasticity on the static stability and control of the Boeing 707-320B airplane are contained in Figs. 4-6, and in Fig. 9. For the supersonic transport configuration the relevant information appears in Figs. 7, 8, and 10. All pitching-moment data are, for the 707-320B, referred to the 25-percent chord point; and for the SST, to the 64-percent chord point.

Boeing 707-320B airplane.- The effects of elasticity on the stability derivatives C_{L_α} and C_{m_α} may be inferred by comparing the curves of Fig. 4 calculated for the rigid and elastic body shapes. For both derivatives it is clear that the changes are large and unfavorable, and that these differences increase sharply at Mach numbers above 0.4. For example, at 0.6 Mach number and 3050 m altitude the loss in C_{L_α} is 20 percent of the rigid body value, and in C_{m_α}, 50 percent. The rolling moment derivative C_{ℓ_p} also is noticeably affected (Fig. 5). For these same conditions the reduction here also approximates 50 percent.

It is interesting to examine the trend with Mach number of the magnitudes of the differences between rigid and elastic values calculated for C_{L_α}, C_{m_α}, and C_{ℓ_p}. As an example, at 0.2 Mach number the difference in the C_{L_α} curves is approximately 0.0025; at 0.4, 0.009; and at 0.8, 0.037. The loss experienced in C_{L_α} thus varies more or less quadratically with Mach number. This same result is also found for C_{m_α} and for C_{ℓ_p}. Since the dynamic pressure at constant altitude likewise varies as the square of the Mach number, the data indicate that for this airplane losses due to elasticity, at constant altitude, are primarily associated with changes in dynamic pressure.

Flight test data for C_{m_α} in Fig. 4 indicate that the effects of elasticity also change with changes in the airplane mass. The reduction in stability appears to be greater for the lighter weight airplane.

The differences between the rigid and elastic values of $d\delta_E/dn$, and of $d\delta_E/dV$ at Mach numbers below 0.3, illustrated in Fig. 6, are negligible. This result is attributed to the fact that, while changes in the basic derivatives are material, the changes neutralize each other in the process of combining these derivatives to calculate $d\delta_E/dn$ and $d\delta_E/dV$. Accordingly, the elastic effects observed here are considered to be a peculiarity of the 707-320B airplane; they may or may not be encountered in other designs. Above 0.3 Mach number the differences in $d\delta_E/dV$ increase noticeably, and in the direction of increased stability.

The effects of elasticity on the longitudinal stability of the 707 airplane are further illustrated in Fig. 9 by the comparison of calculated values of static margin and maneuver point for both rigid and elastic airplanes. The loss in stability is seen to be significant for all flight conditions. For flight near Mach number 0.6 the incremental change in static margin is 4 percent of the reference chord, amounting to approximately 20 percent of the total center-of-gravity range for this airplane. (Center-of-gravity range for the 707 is 19 percent of the reference chord.) Changes in maneuver point for the rigid and elastic airplane are approximately the same as the change that occurred in static margin.

Supersonic transport.- The effects of elasticity on the lift and pitching-moment coefficients of the SST configuration are shown in Fig. 7 for Mach numbers 1.6 and 2.7. A comparison of C_{L_α} measured for the rigid and elastic models shows that significant losses occur at both Mach numbers throughout the range of dynamic pressures investigated. The relative magnitude of these losses is approximately the same at both Mach numbers (15 percent at 1.6 and 12 percent at 2.7 Mach number). The deterioration of pitching-moment coefficient, as measured by C_{m_α}, is even more pronounced. Losses as great as 50 percent were found experimentally. These losses also persist throughout the range of dynamic pressures for both Mach numbers.

The effects of elasticity on the control derivatives $C_{L_{\delta_E}}$ and $C_{m_{\delta_E}}$ (Fig. 8) follow the same pattern. The losses are large (50 percent roughly of rigid body values) at all Mach numbers. These effects are indicated both by the experimental observations and by the theoretical predictions.

A further appreciation of the effects of elasticity on the longitudinal stability characteristics of this configuration may be obtained from examination of the shift in neutral point location. Fig. 10 presents this parameter plotted as a function of dynamic pressure for 2.7 Mach number. The variations of gross weights and dynamic pressures in Fig. 10 encompass the design operating range. Thus, 142,500 kg is the weight of the basic aircraft without fuel or payload, and 302,800 kg is the weight fully loaded with maximum fuel and payload. For the 835 m^2 (9,000 ft^2) reference wing area of this airplane the lift coefficients range from 0.073 to 0.156 at the lowest dynamic pressure, and from 0.027 to 0.057, at the highest (design cruise C_L is 0.09 to 0.12). Although, as noted in the

figure, the center of gravity (and also the moment reference point) was fixed at 64 percent of the reference chord for these calculations, the mass distribution was not constant; it was changed in each case to reflect the actual distribution expected in flight for the fuel and payload assumed.

The final design provided for a variation in the center-of-gravity location of 5 percent (0.05 reference chord). Fig. 10 shows that at 2.7 Mach number the neutral point shifts from 0.01 reference chord forward to 0.02 aft, that is, 0.03 reference chord or 60 percent of the center-of-gravity requirement itself. This shift results from changes both in dynamic pressure and in airplane load (gross weight and mass distribution), the effect of this latter quantity being greatest when the gross weight is smallest.

It is evident, of course, that at 2.7 Mach number the curves corresponding to maximum fuel and payload, and to empty weight are not realistic boundary conditions and that 0.03 total shift in neutral point would never be met in practice. It is important to remember, however, that the range of dynamic pressures considered in this figure can be encountered at Mach numbers as low as 1.0 (1100 m or 3620 ft altitude). The variation in gross weight and mass distribution for which dynamic pressures as high as 62,200 N/m^2 (1300 lb/ft^2) must be reckoned with is therefore somewhat greater than Fig. 10 implies. Whether or not the neutral point remains within the envelope of Fig. 10 throughout the Mach number range depends, among other things, on the magnitudes of the differences between C_{m_α} for the rigid airplane and C_{m_α} for the elastic airplane.

In any event, the conclusion is inescapable that this effect of elasticity confronts the designer with a major problem. To make certain that adequate longitudinal stability exists for all center-of-gravity locations and flight conditions, the elastic effects must be completely analyzed at the very beginning of the airplane design. The calculations summarized in Fig. 10 illustrate that the method presented in this paper provides the means required in early evaluations.

Dynamic Stability

While use of the quasi-static-elastic representation of the aircraft structure to analyze steady state flight characteristics is inherently a technically sound approach, the same remark cannot in general be made for dynamic stability, although this is the representation commonly used. The lower structural frequencies and the short-period frequency of the aircraft motion may be close enough to result in interchange of significant amounts of energy. To examine this possibility, and to determine the magnitude of the effects for the subject configurations, calculations were made and the results summarized in Figs. 11, 12, and 13. In the calculations the structural shape was represented (as described in (1)) by its normal modes, the number used varying from 0 (rigid body) to 20 for the SST and to 14 for the Boeing 707.

Supersonic transport.- Fig. 11 indicates that for the SST model neither damping ratio nor frequency is materially affected by elasticity at any of the three Mach numbers investigated. The fact that the damping ratios computed both from quasi-static-elastic and the fully elastic analyses (20 normal modes) are always smaller than those derived from rigid body analysis is, however, an indication that damping deteriorates with elasticity. No significance is attached to the uniformly smaller damping ratios computed using the quasi-static-elastic representation as compared to the results for 20 normal modes.

Fig. 12 shows the effects on damping ratio and frequency of varying the number of normal modes used in the fully elastic analysis. (Values shown for 0 modes in this figure differ from the rigid body values of Fig. 11 because $C_{m_{\dot\alpha}}$ and $C_{L_{\dot\alpha}}$ were not included in the normal mode calculations.) It is apparent for all three Mach numbers that the number of normal modes used had virtually no effect on either damping ratio or frequency - a result entirely consistent with the data of Fig. 11. Some clue to the reasons for this result is furnished by a comparison of structural frequencies with the frequency of motion. Values of the former quantity are 1.6 Hz for the primary mode, 2.33 Hz for the secondary, and 3.88 for the tertiary. The corresponding ratios to frequency of motion (using the value 2.8 Hz) at 2.7 Mach number are 5.7, 8.3, and 12.1. Structural and motion frequencies are therefore fairly far removed from one another, and this separation together with the damping forces present apparently nullifies any effects of coupling.

Boeing 707-320B airplane.- Consideration of similar data for the Boeing 707 airplane (Fig. 13) provides further support for this hypothesis. The first three structural fequencies of this configuration are 1.24 Hz, 2.92 Hz, and 3.39 Hz (ratios to rigid body motion: 3.5, 8.3, and 9.7). The lowest structural frequency is therefore somewhat closer to the frequency of motion than it is for the SST, and it is seen that the computed value of damped frequency for the elastic case does differ detectably from the rigid body value. The damping ratio, however, is virtually unaffected. The inference of these results, applied to other airplanes, is that further reduction in the ratio of primary structural frequency to the rigid body motion frequency below 3.5 would induce coupling between structural and rigid body motions.

In summary, while some elastic effects on the dynamic motion of both of these aircraft are apparent, the effects are nowhere large, and quasi-static-elastic or even a rigid body analysis is sufficiently accurate for most design purposes. Other designs, particularly those for which the primary structural frequencies are less than four times the frequency of rigid body motion, should be quite carefully investigated using a completely elastic representation.

CONCLUDING REMARKS

An examination of the principal longitudinal stability and control derivatives of two representative flexible airplane configurations, determined both analytically and experimentally, indicated that:

1. Except for the pitching-moment derivatives, the analytical procedure provided useful values of the principal static stability, control, and dynamic stability derivatives.

2. Discrepancies for the most part are probably attributable to errors inherent in the aerodynamic theory.

3. The fully dynamic representation of the structure based on normal mode theory would not be required for either of these two configurations. A simplified structural arrangement ("quasi-static-elastic") provided results of substantially the same accuracy.

4. The static stability characteristics of both configurations were affected strongly by elasticity and, in most cases, adversely.

5. The longitudinal control derivatives examined were also significantly and unfavorably affected.

6. Dynamic stability characteristics, as measured by damping ratio and damped frequency, were not greatly affected by elasticity. For both aircraft, however, structural frequencies were relatively far from the frequency of rigid body motion, and the data indicate that without this separation major effects might be encountered.

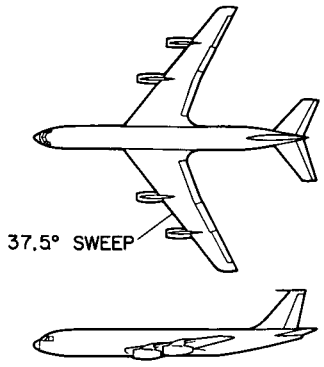
REFERENCES

1. Dusto, A. R.: An Analytical Method for Predicting the Stability and Control Characteristics of Large Elastic Airplanes at Subsonic and Supersonic Speeds, Part I - Analysis. Paper presented at the AGARD Flight Mechanics Panel Meeting on Aeroelastic Effects From a Flight Mechanics Standpoint, Marseille, France, April 1969.

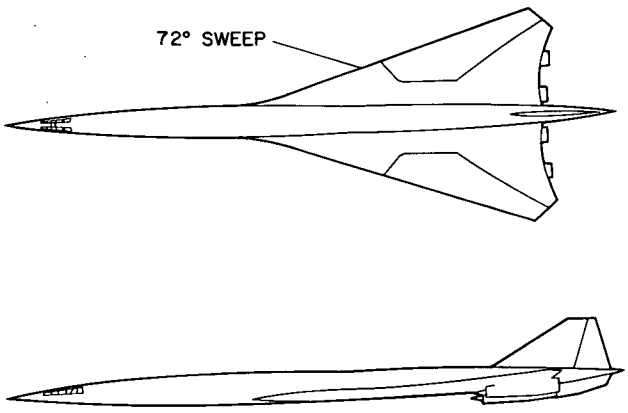
2. Woodward, F. A.; Tinoco, E. N.; and Larsen, J. W.: Analysis and Design of Supersonic Wing-Body Combinations, Including Flow Properties in the Near Field - Part I - Theory and Application. NASA CR 73106, 1967.

3. Woodward, F. A.: Analysis and Design of Wing-Body Combinations at Subsonic and Supersonic Speeds. Journal of Aircraft, vol. 5, no. 6, Nov.-Dec. 1968.

4. Members of the Aerodynamics and Structures Research Organizations, The Boeing Company, Commercial Airplane Division, Renton, Washington: An Analysis of Methods for Predicting the Stability Characteristics of an Elastic Airplane. NASA CR 73277, 1968.

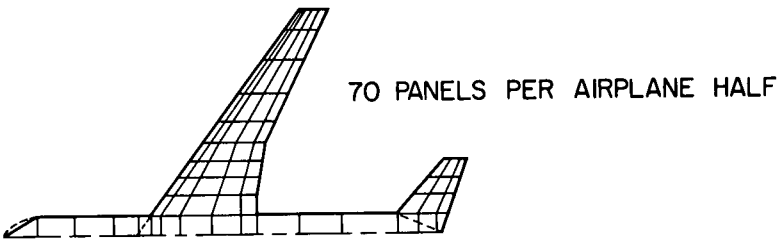


(a) BOEING 707 - 320B

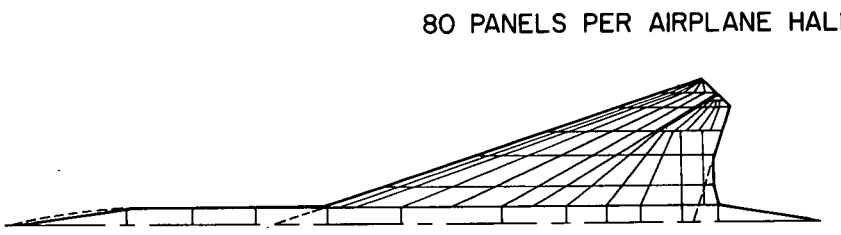


(b) REPRESENTATIVE SUPERSONIC TRANSPORT (SST)

Fig. 1.- Aircraft general arrangement.



a) BOEING 707 - 320B



b) REPRESENTATIVE SUPERSONIC TRANSPORT (SST)

Fig. 2.- Airplane paneling.

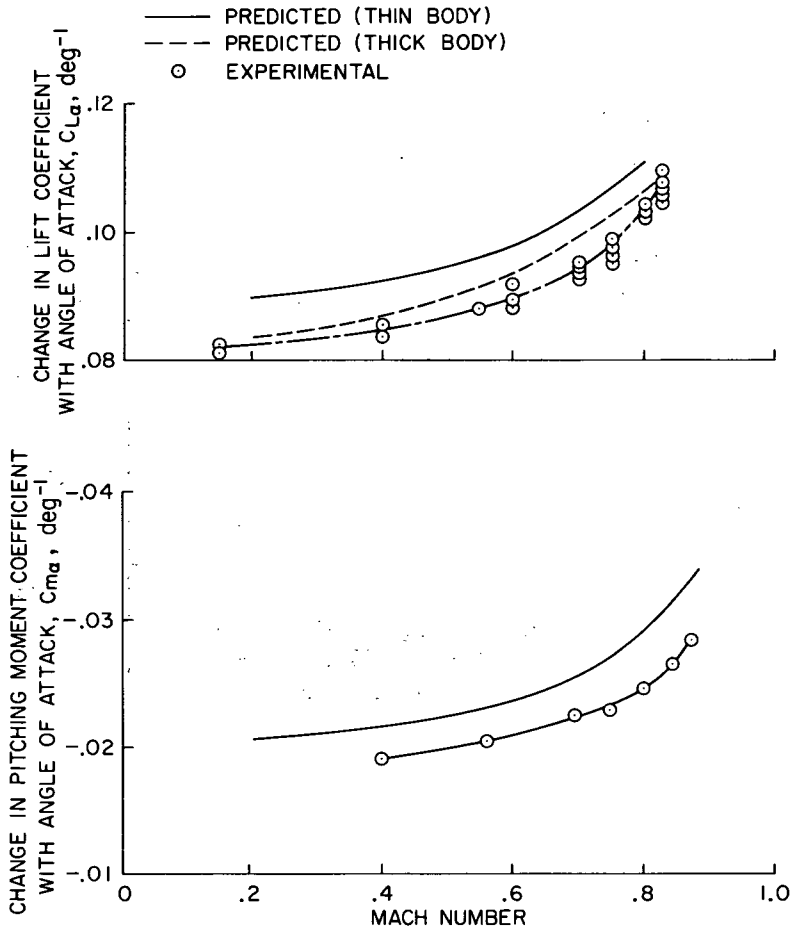


Fig. 3.- Calculated and experimental angle-of-attack derivatives, rigid body, Boeing 707-320B.

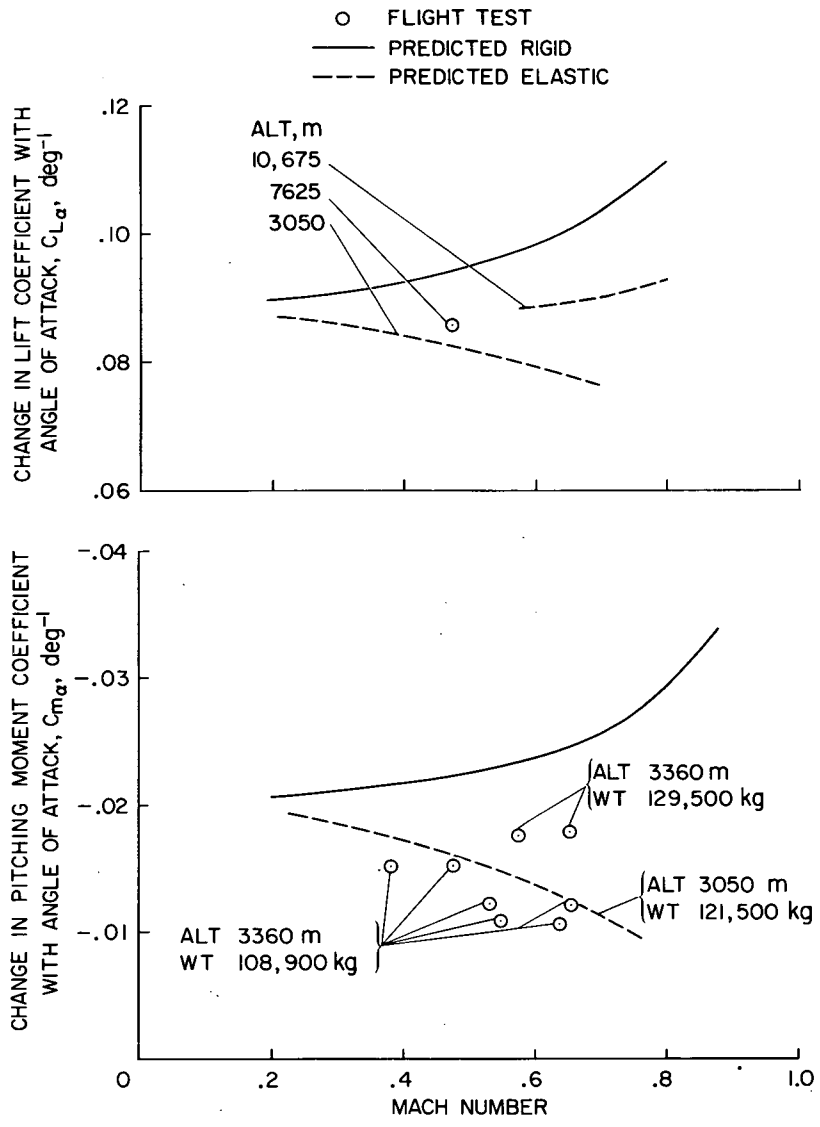


Fig. 4.- Calculated and experimental angle-of-attack derivatives, elastic body, Boeing 707-320B.

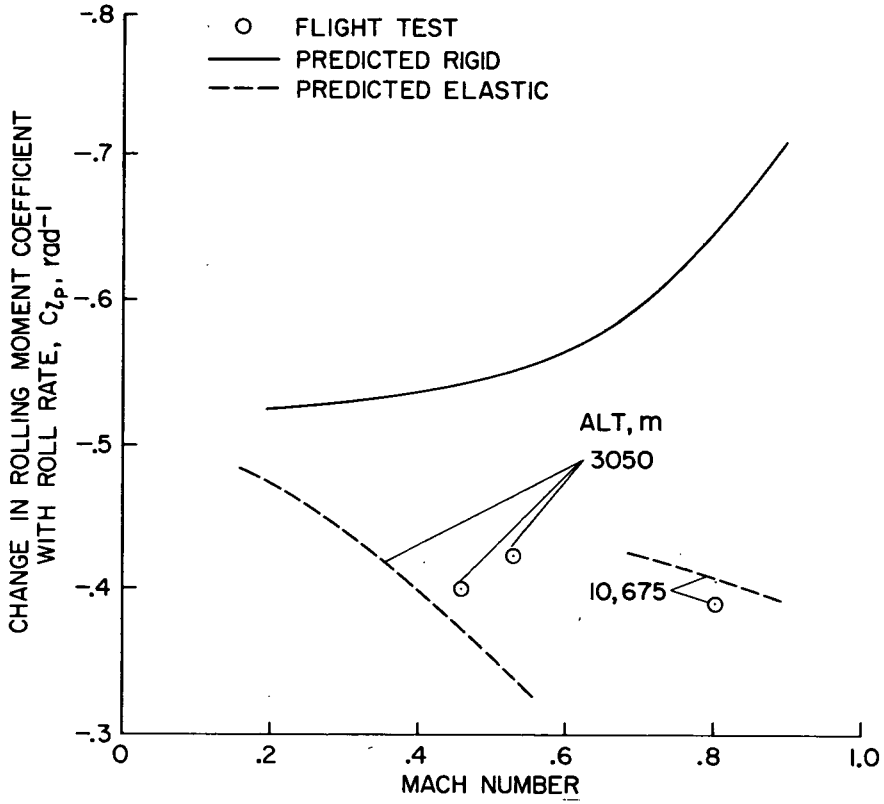


Fig. 5.- Calculated and experimental roll-rate derivative, elastic body, Boeing 707-320B.

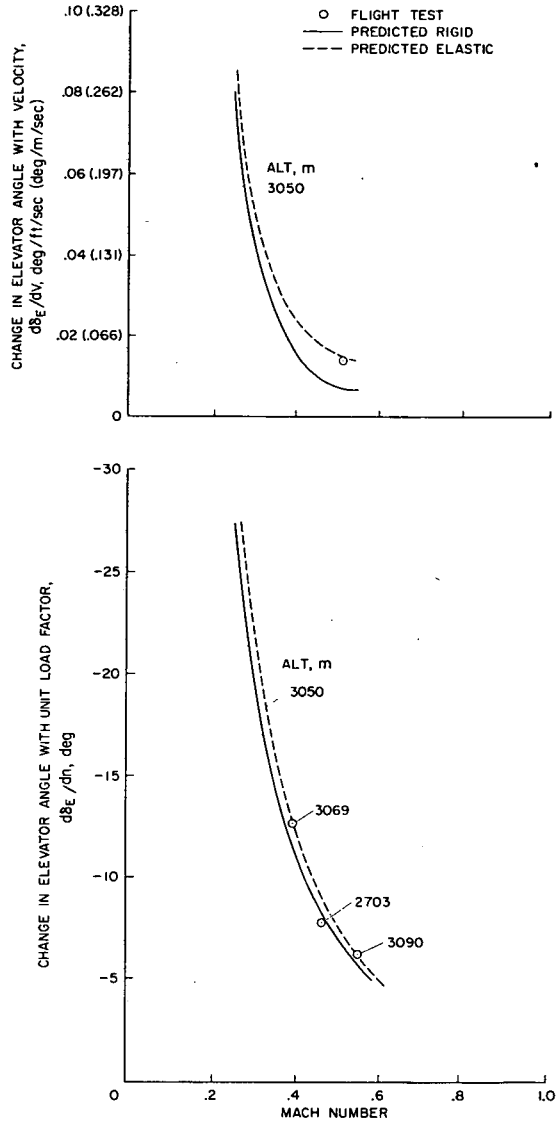


Fig. 6.- Calculated and experimental velocity and load-factor derivatives, elastic body, Boeing 707-320B.

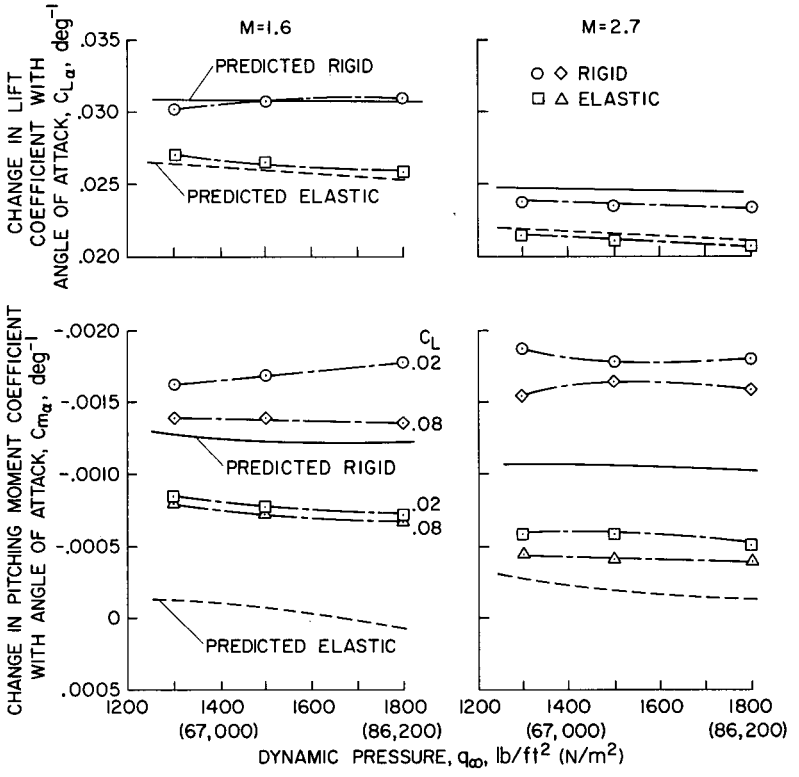


Fig. 7.- Calculated and experimental angle-of-attack derivatives, rigid body and elastic body, supersonic transport.

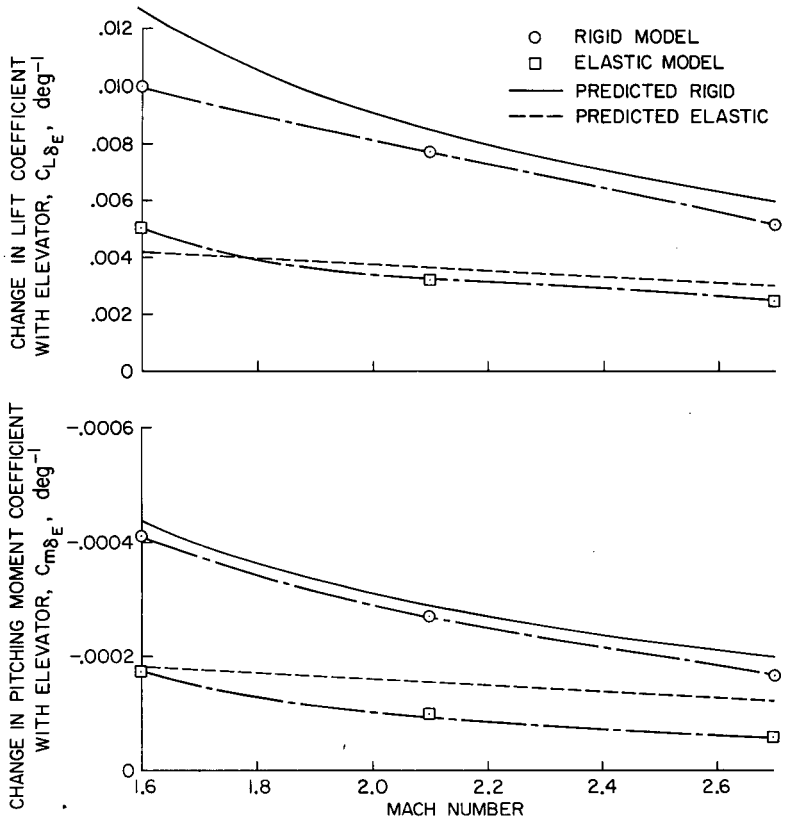


Fig. 8.- Calculated and experimental elevator deflection angle derivatives, rigid body and elastic body, supersonic transport.

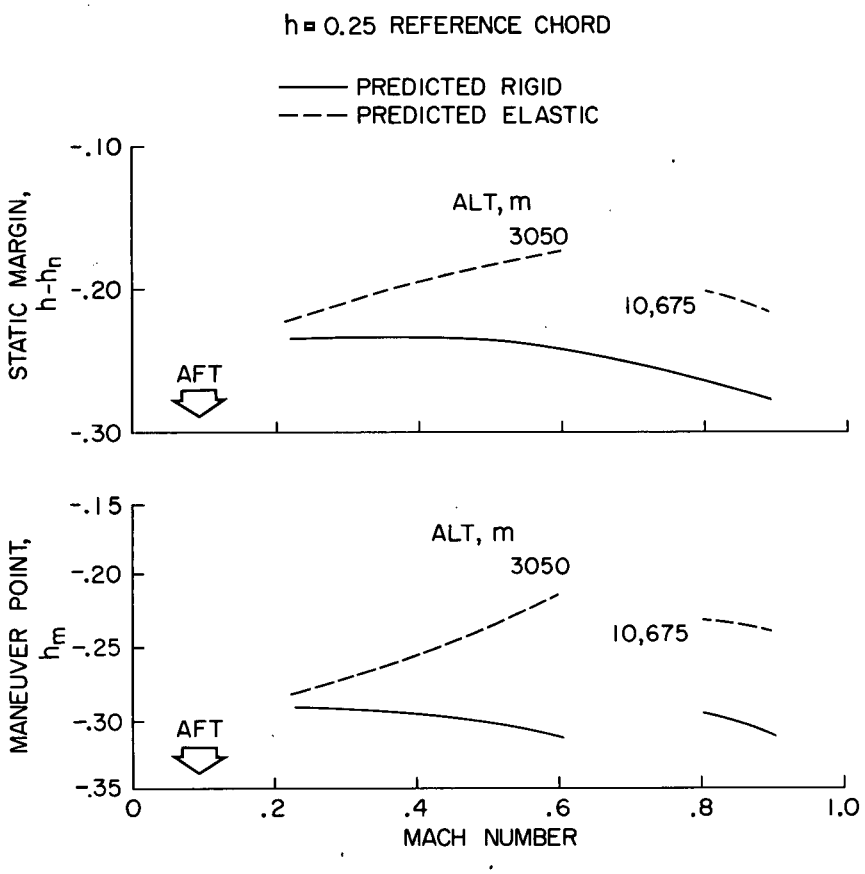


Fig. 9.- Effects of elasticity on static margin and maneuver point, Boeing 707-320B.

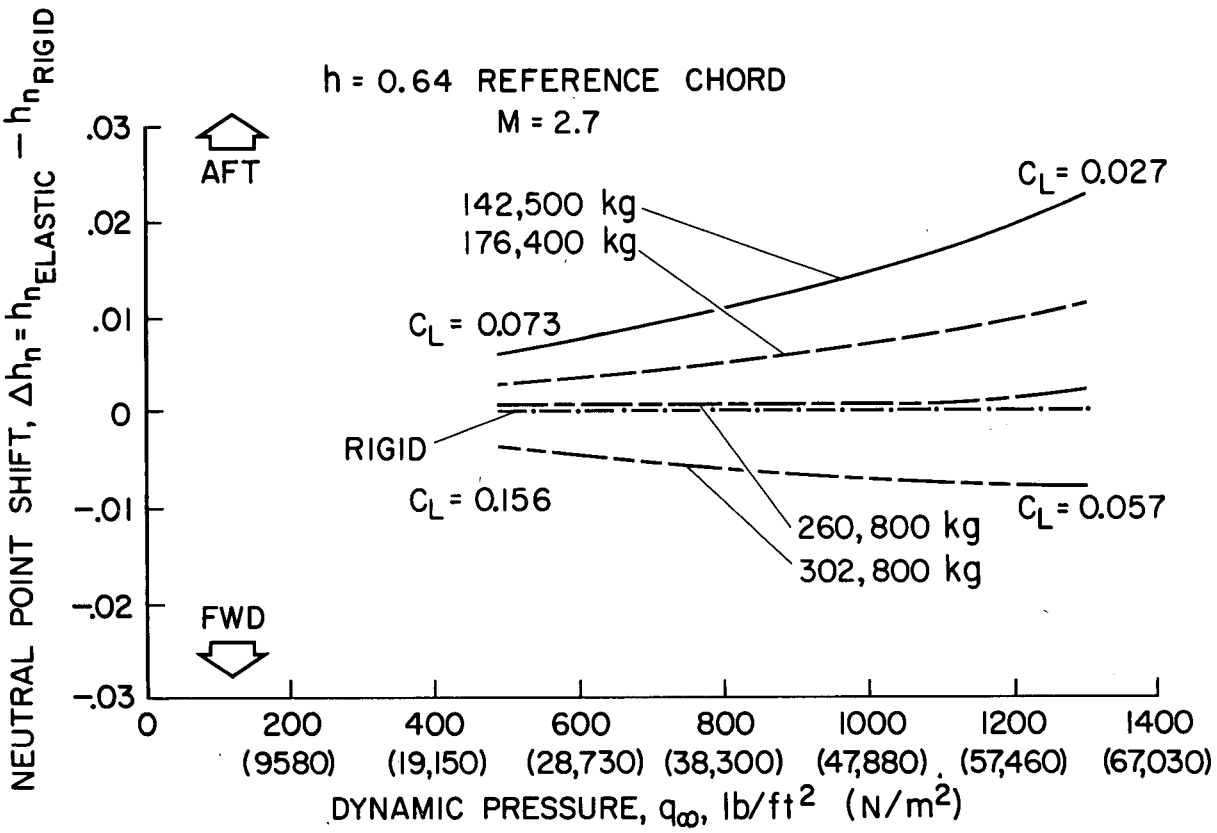


Fig. 10.- Effect of elasticity on neutral point location, supersonic transport.

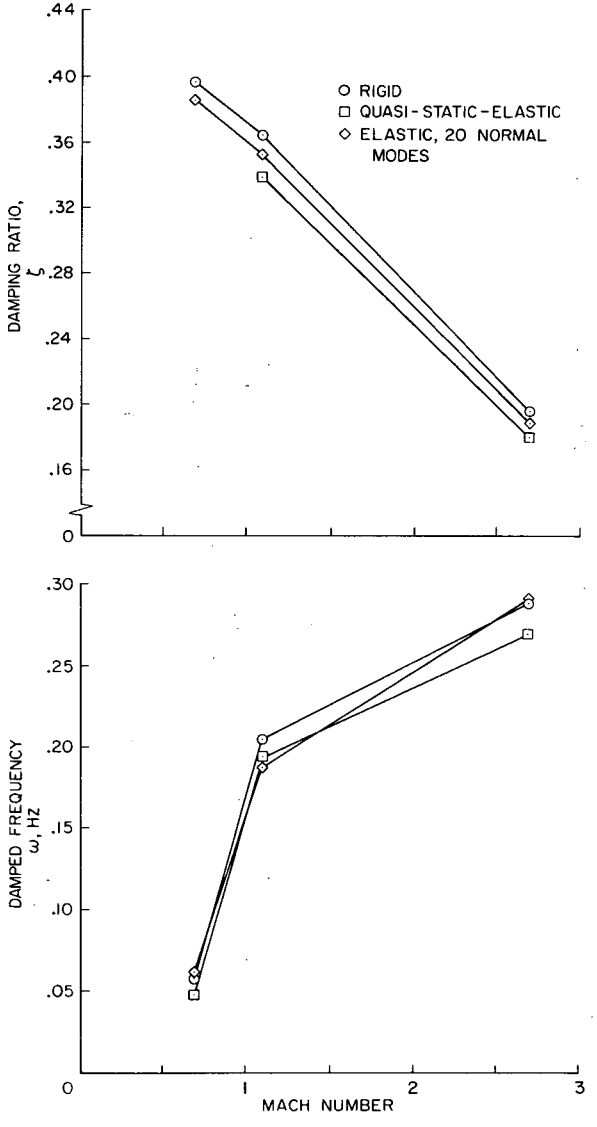


Fig. 11.- Effect of elasticity on short-period damping and frequency, supersonic transport.

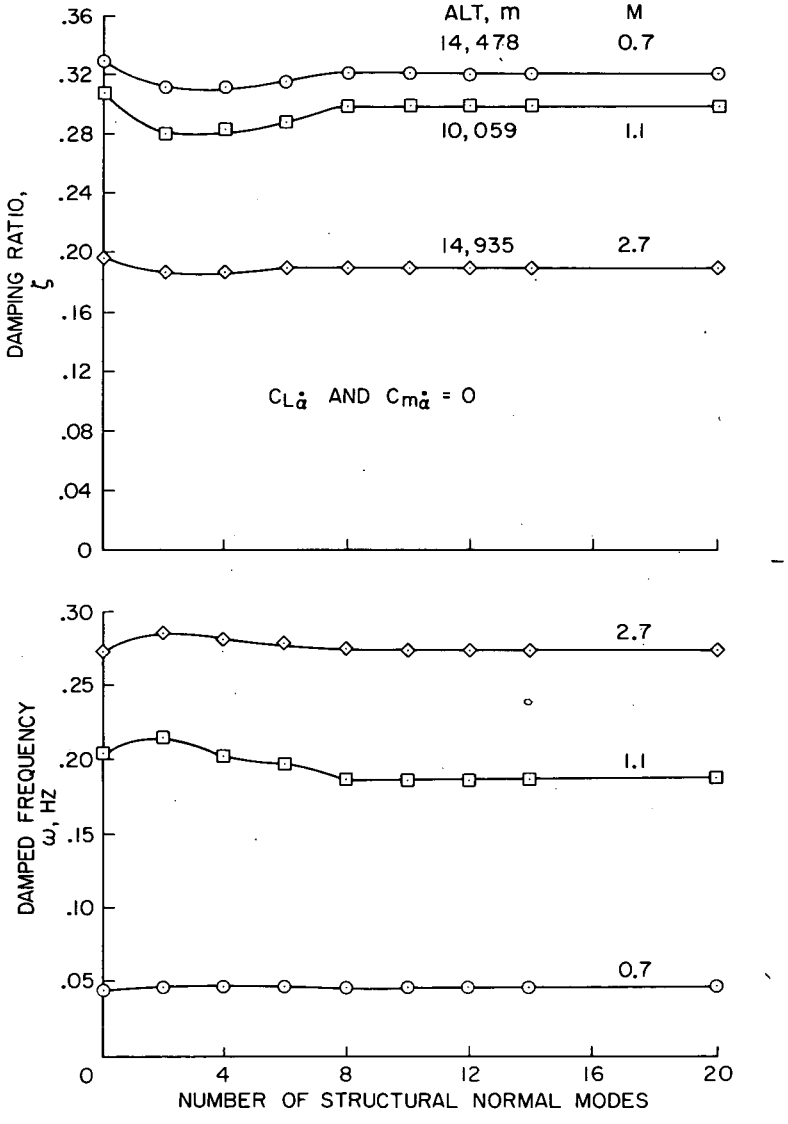


Fig. 12.- Effect of number of normal modes on short-period damping and frequency, supersonic transport.

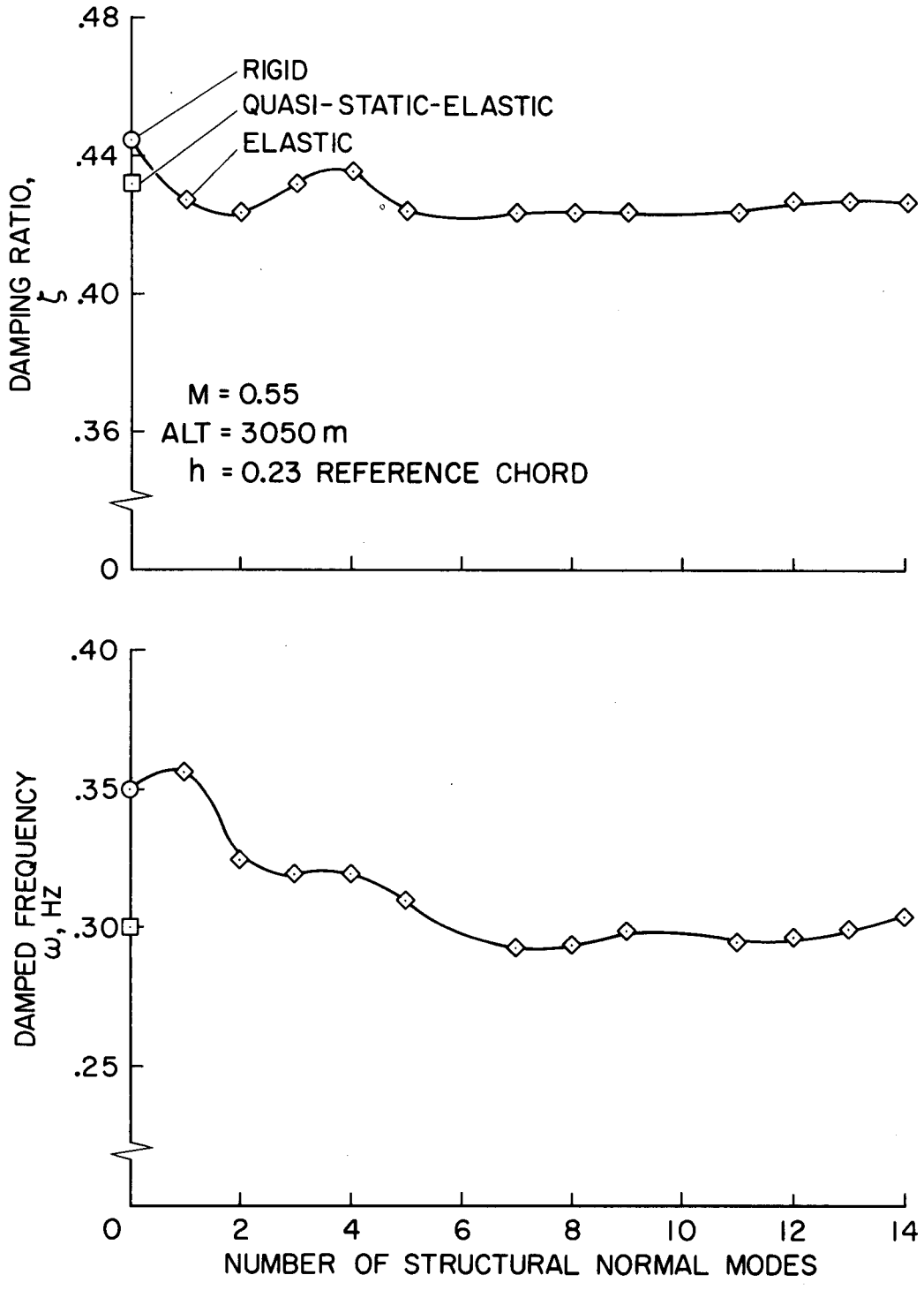


Fig. 13.- Effect of number of normal modes on short-period damping and frequency, Boeing 707-320B.

COMMENTS, INTERPRETATION AND APPLICATION OF A METHOD FOR PREDICTING AERODYNAMIC CHARACTERISTICS OF LARGE FLEXIBILE AIRPLANES

J. Roskam

Associate Professor of Aerospace Engineering and
Director of the Flight Research Laboratory, The
University of Kansas, Lawrence, Kansas

List of Symbols

Symbol	Definition	Dimension
F_{A_i}	Aerodynamic pressure force on panel i	lbs
$\bar{q}$	Dynamic pressure	lbs ft^{-2}
$[A]$	Aerodynamic influence coefficient matrix	
a_{ij}	Element of $[A]$	ft^2 rad^{-1}
α_i, α_{E_i}	Angle of attack of panel i (rigid and elastic respectively)	rad
θ_{E_i}	Elastic rotational deformation of panel i	rad
$[C_\theta]$	Structural flexibility influence coefficient matrix	
$c_{\theta_{ij}}$	Element of $[C_\theta]$	rad lbs^{-1}
m_i	Mass of panel i	slugs
g	Acceleration of gravity	ft sec^{-2}
α_1	Steady state reference angle of attack	rad
θ_{T_i}	Camber and (or) twist angle associated with panel i	rad
θ_1	Steady state attitude angle	rad
U_1	Steady state velocity	ft sec^{-1}
L	Lift	lbs
D	Drag	lbs
$C_L = \frac{L}{\bar{q}S}$	Lift coefficient	
$C_D = \frac{D}{\bar{q}S}$	Drag coefficient	
S	Reference planform area	ft^2
$\bar{c}$	Reference planform chord	ft
u	Perturbation velocity along X	ft sec^{-1}
w	Perturbation velocity along Z	ft sec^{-1}
q	Perturbation pitch rate	rad sec^{-1}
α	Perturbation angle of attack	rad
θ	Perturbation attitude angle	rad
n, n_p	Load-factor and perturbed load-factor respectively	
I_{yy}	Pitch moment of inertia	slug. ft^2
C_m	Pitching moment coefficient	
x_i	Location of panel i along X relative to the center of mass P	ft
$C_{D_u} = \frac{\partial C_D}{\partial u/U_1}$	Drag due to forward velocity	Nondimensional
$C_{L_u} = \frac{\partial C_L}{\partial u/U_1}$	Lift due to forward velocity	Nondimensional
$C_{m_u} = \frac{\partial C_m}{\partial u/U_1}$	Moment due to forward velocity	Nondimensional

Symbol	Definition	Dimension
$C_{D_\alpha} = \frac{\partial C_D}{\partial \alpha}$	Drag due to angle-of-attack	Nondimensional
$C_{L_\alpha} = \frac{\partial C_L}{\partial \alpha}$	Lift due to angle-of-attack	Nondimensional
$C_{m_\alpha} = \frac{\partial C_m}{\partial \alpha}$	Pitching moment due to angle-of-attack	Nondimensional
$C_{D_{\dot\alpha}} = \frac{\partial C_D}{\partial \dot\alpha \bar{c}/2U_1}$	Drag due to angle-of-attack rate	Nondimensional
$C_{L_{\dot\alpha}} = \frac{\partial C_L}{\partial \dot\alpha \bar{c}/2U_1}$	Lift due to angle-of-attack rate	Nondimensional
$C_{m_{\dot\alpha}} = \frac{\partial C_m}{\partial \dot\alpha \bar{c}/2U_1}$	Pitching moment due to angle-of-attack rate	Nondimensional
$C_{D_q} = \frac{\partial C_D}{\partial q \bar{c}/2U_1}$	Drag due to pitch rate	Nondimensional
$C_{L_q} = \frac{\partial C_L}{\partial q \bar{c}/2U_1}$	Lift due to pitch rate	Nondimensional
$C_{m_q} = \frac{\partial C_m}{\partial q \bar{c}/2U_1}$	Pitching moment due to pitch rate (Pitch damping)	Nondimensional
$C_{D_{\ddot\theta_I}} = \frac{\partial C_D}{\partial \ddot\theta}\Big\vert_I$	Drag due to pitch acceleration	$sec^2\ rad^{-1}$
$C_{L_{\ddot\theta_I}} = \frac{\partial C_L}{\partial \ddot\theta}\Big\vert_I$	Lift due to pitch acceleration	$sec^2\ rad^{-1}$
$C_{m_{\ddot\theta_I}} = \frac{\partial C_m}{\partial \ddot\theta}\Big\vert_I$	Pitching moment due to pitch acceleration	$sec^2\ rad^{-1}$
$C_{D_{\dot w_I}} = \frac{\partial C_D}{\partial \dot w}\Big\vert_I$	Drag due to inertial acceleration	$sec\ ft^{-1}$
$C_{L_{\dot w_I}} = \frac{\partial C_L}{\partial \dot w}\Big\vert_I$	Lift due to inertial acceleration	$sec\ ft^{-1}$
$C_{m_{\dot w_I}} = \frac{\partial C_m}{\partial \dot w}\Big\vert_I$	Pitching moment due to inertial acceleration	$sec\ ft^{-1}$
$C_{D_{\theta_I}} = \frac{\partial C_D}{\partial \theta}\Big\vert_I$	Drag due to attitude	Nondimensional
$C_{L_{\theta_I}} = \frac{\partial C_L}{\partial \theta}\Big\vert_I$	Lift due to attitude	Nondimensional
$C_{m_{\theta_I}} = \frac{\partial C_m}{\partial \theta}\Big\vert_I$	Pitching moment due to attitude	Nondimensional
$C_{L_{TRIM}}, C_{L_1}$	Trim or steady state lift coefficient	Nondimensional
$\bar{X}_{ac}$	Aerodynamic center location in fractions of $\bar{c}$	Nondimensional
$\bar{X}_{cg}$	Center of mass location in fractions of $\bar{c}$	Nondimensional
$f_{A_{X_S}}$	Perturbed force in the X_S direction	lbs
$f_{A_{Z_S}}$	Perturbed force in the Z_S direction	lbs
$m_{A_{Z_S}}$	Perturbed moment about Y_S	ft lbs
M	Airplane mass	slugs

Matrices

$[\ ]$	Square matrix (n x n)
$\{\ \}$	Column matrix (n x 1)
$\{\ \}^T$	Row matrix (1 x n)
$[\ ]$	Diagonal matrix (n x n)

Subscripts

i	Panel number
p	Perturbation quantity
x,y,z	Components along XYZ

Subscripts

s	Stability axes
E	1. Elastic
	2. Elastic including inertial effects
$\bar{E}$	Elastic for zero mass
I	Inertial
1	Steady state
n	Constant load-factor
$\bar{q}$	Constant dynamic pressure
A	Airplane
M	Model

Comments, Interpretation and Application of a Method for Predicting Aerodynamic Characteristics of Large Flexible Airplanes

J. Roskam
Associate Professor of Aerospace Engineering and
Director of the Flight Research Laboratory, The
University of Kansas, Lawrence, Kansas

Abstract

This paper discusses the potential applications to airplane design of a recently developed method to account for elastic effects on stability, control and performance characteristics of large flexible airplanes. The method lends itself well to rapid calculation of trade-off information on which to base design decisions. It is shown how the method can be used to determine the effect of changes in aerodynamic, structural and mass configuration on:

1) equilibrium and jig shape
2) lift-to-drag ratio
3) stability derivatives
4) aerodynamic center

An interpretation of elastic airplane stability derivatives is given and it is shown what format these derivatives assume if the conventional rigid airplane equations of motion are to be used.

Finally it is shown how the method should be used to 'massage' windtunnel data obtained on rigid and elastic models before these data can be applied to the full scale airplane.

1. Introduction

During the preliminary design phase (p.d.) of an airplane, its aerodynamic and structural configurations are in a continuing state of flux. Technical management is confronted with the necessity to make far reaching design decisions on the basis of rough or 'p.d.' type trade studies supplied by their technical specialists. Typical design decisions that have to be made are those relative to wing-body planform geometry, wing camber, twist and thickness distribution, nacelle location, tail size and location, mass distribution of payload and fuel, fuel sequencing requirements and general structural arrangements. In the past, when the interaction of elastic deformations with stability, control and performance of the airplane was minor or could be neglected entirely, such design decisions could often be made on the basis of accumulated design experience and design intuition. Current and future large airplanes possess a degree of structural flexibility which makes it mandatory for the designer to account accurately for its effects on aerodynamic characteristics even in the early design stage. This makes it difficult and hazardous to use an intuitive approach to the making of aerodynamic and structural configuration decisions. It is highly desirable for the designer to have available to him fast and reliable computational tools and methods that will aid him in making critical design decisions.

This paper discusses the potential applications to airplane design of a recently developed method to account for elastic effects on stability, control and performance characteristics. The method, when properly computerized, lends itself very well to quickly develop the much needed trade-off information on which to base design decisions for large flexible airplanes. A thorough derivation and substantiation of the method may be found in References 1 through 4.

Section 2 describes briefly the most essential features of the method, which applies to quite arbitrary planform configurations in subsonic and supersonic flow. In Section 3 it is pointed out how the method can be used to study systematically the effect of aerodynamic and structural configuration changes on:

1) the jig shape and equilibrium shape in cruising flight
2) the lift to drag ratio

An important consequence of flexibility is a change in the meaning and use of stability derivatives. This is discussed in Section 4, where it is also pointed out, how the conventional small perturbation equations of motion are affected. A design parameter of particular importance is the aerodynamic center. The effect of flexibility and of configuration changes on this parameter are also discussed in this section.

Another consequence of flexibility is that windtunnel data obtained from rigid (sic!) and flexible models must be massaged in a special manner before they can be considered as representative of the aerodynamic characteristics of the full scale airplane. Section 5 discusses how this may be done.

Conclusions and recommendations are presented in Section 6.

2. Essential Features and Limitations of the Method

As shown in References 1 and 2 it is possible to represent the aerodynamic pressure force distribution over an airplane as the product of a square aerodynamic influence coefficient matrix $[A]$ and a column matrix of local angles of attack $\{\alpha_i\}$:

$$\{F_{A_i}\} = \bar{q}[A]\{\alpha_i\} \tag{1}$$

Figure 1 shows the angular geometry used in relating local panel forces, F_{A_i}, to local angles of attack, α_i. The local angles of attack α_i are the sum of the overall airplane angle of attack, α_1, the local camber and twist angle, Θ_{J_i}, and the local elastic distortion angle, Θ_{E_i}. If necessary, deflection angles due to control surfaces can also be added. Each element, a_{ij}, of the matrix $[A]$ represents the pressure force* induced on panel i due to a unit angle of attack of panel j. Figure 2 shows typical examples of planform panelling that have been used. The elements of the matrix $[A]$ are a function of Mach number and of the overall geometry of the airplane which can be completely arbitrary. The matrix $[A]$ at any Mach number is computed from elementary solutions to the small perturbation flow equation in subsonic and supersonic flow. This restricts the method to situations involving attached flow (small angles of attack) and excludes transonic applications. However, it is pointed out in Reference 3 that by using an empirical approach these restrictions can be removed. Effects of thickness of wing, body and tail can also be included as pointed out in Reference 1. To simplify the discussion, the effects of thickness were neglected in Reference 2 and this approach is followed again in this paper.

The elastic properties of the structure are represented by flexibility influence coefficients, $c_{\theta_{ij}}$, which relate the elastic rotation, Θ_{E_i}, of panel i to the total force acting on panel j. This total force is made up of an aerodynamic force, F_{A_i}, and a gravitational force, $m_i g$. An inertial force, f_{I_i}, must also be considered if the airplane is allowed to rotate. Knowing the overall structural arrangement of the airplane it is possible to compute the flexibility influence coefficient matrix $[C_\theta]$ with conventional methods of matrix structural analysis. The force-deformation relationship is thus represented by:

$$\{\Theta_{E_i}\} = [C_\theta]\{F_{A_i} - m_i g\} \tag{2}$$

It is assumed in setting up Equations (1) and (2) that all angles in Figure 1 are so small that cosines are equal to one.

In this paper the airplane is also assumed to be equivalent-elastic. An equivalent elastic airplane is a designation for a particular mathematical model of an elastic airplane, where it is assumed that loads and deformations at the exterior surface of the airplane are in phase with each other and with the motions of the stability axis system. This assumption means that it is not necessary to account for structural dynamic behavior as separate degrees of freedom. The conditions of validity of this assumption are difficult to describe in a few words and the reader is, therefore, referred to Reference 4. It suffices to say that many situations exist, where this type of mathematical model is quite sufficient.

The discussion of the method will be limited to the longitudinal aerodynamic characteristics of the airplane. This is done largely because of the state-of-the-art of influence coefficient aerodynamics. From the developments discussed in References 1 and 2 it should be evident that the basic ideas behind the method can be extended to include lateral-directional aerodynamic characteristics. This is also shown in Reference 4.

3. On the Effect of Aerodynamic and Structural Configuration Changes on Airplane Shape and Lift-to-Drag Ratio

3.1 Jig Shape and Equilibrium Shape

The completely unloaded or jig shape of the airplane is represented in Figure 1 by the angles Θ_{J_i}. In a steady state flight condition the equilibrium aerodynamic pressure force distribution acting on the airplane can be expressed in a manner analogous to Equation (1) as:

$$\{F_{A_{i_1}}\} = \bar{q}_1[A]\{\alpha_1 + \Theta_{J_i} + \Theta_{E_{i_1}}\} \tag{3}$$

where the subscript 1 indicates the steady state. By analogy to Equation (2) it is possible to write the equilibrium elastic distortion of the airplane as:

$$\{\Theta_{E_{i_1}}\} = [C_\theta]\{F_{A_i} - m_i g\} \tag{4}$$

Substituting Equation (3) into Equation (4) it is possible to solve for $\{\Theta_{E_{i_1}}\}$ as follows:

$$\{\Theta_{E_{i_1}}\} = \left[[I] - \bar{q}_1[C_\theta][A]\right]^{-1}[C_\theta]\left\{\bar{q}_1[A]\{\alpha_1 + \Theta_{J_i}\} - \{m_i\}g\right\} \tag{5}$$

* Per unit dynamic pressure

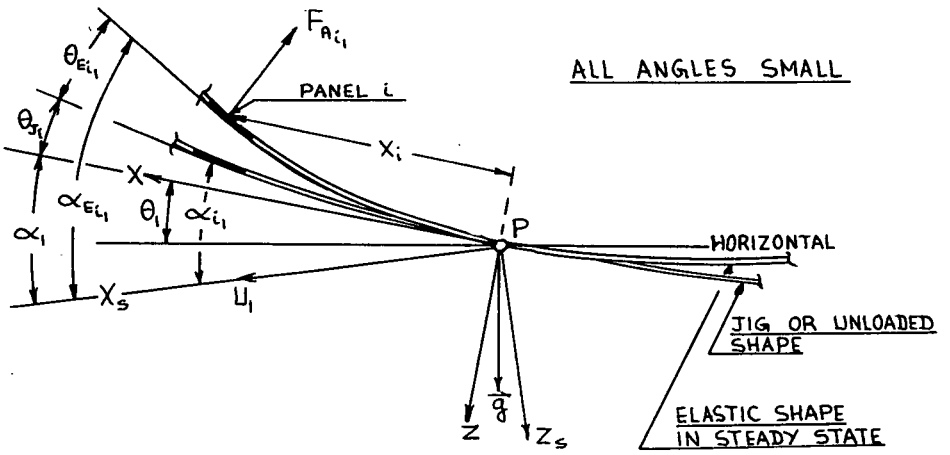


FIGURE 1 - ELASTIC AIRPLANE GEOMETRY

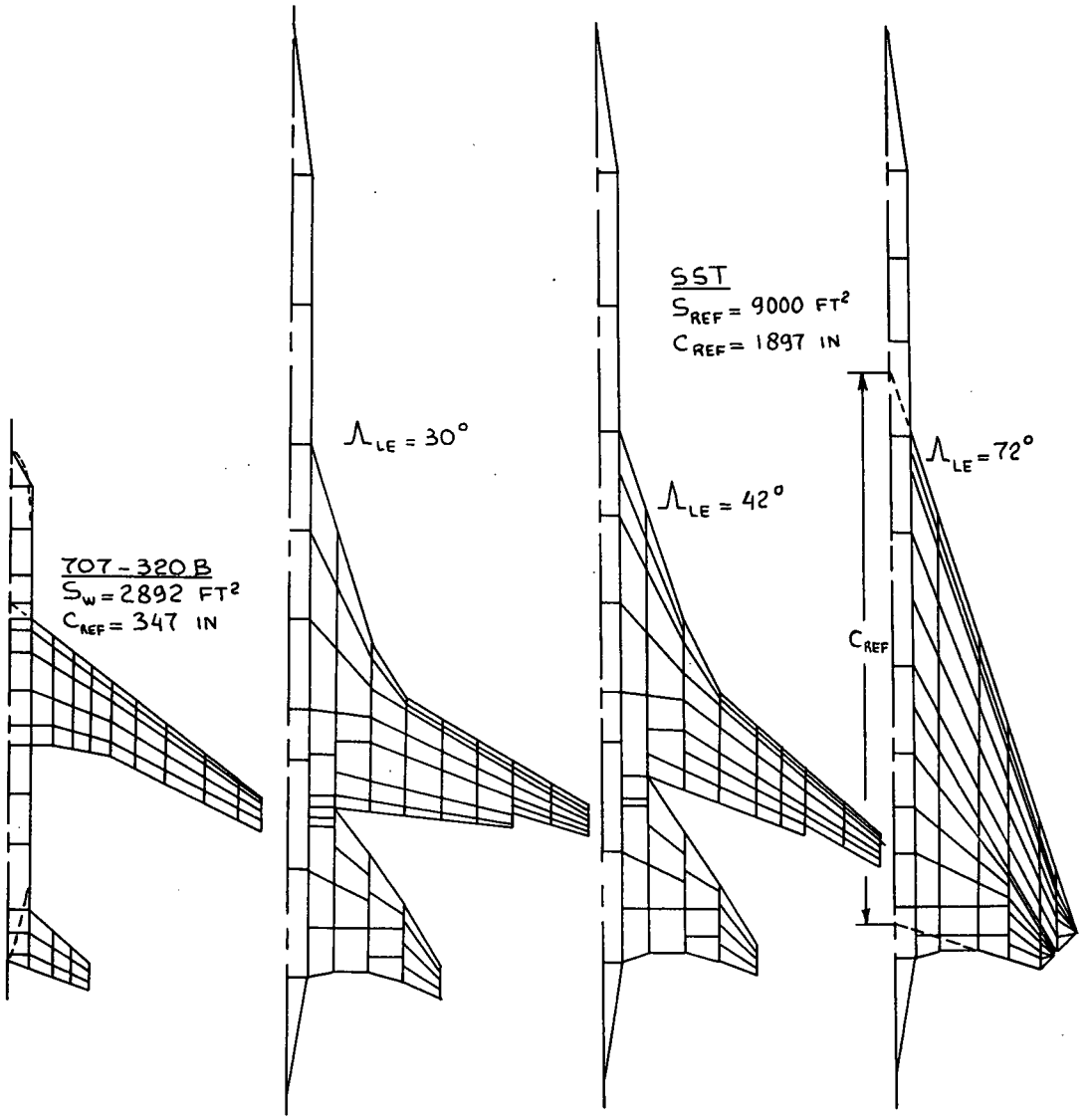


FIGURE 2 - EXAMPLES OF PANELING

The steady state dynamic pressure, $\bar{q}_1$, and the steady state reference angle of attack, α_1 , are assumed to be known. The equilibrium cruise shape of the airplane is now found by summing the jig shape $\{\theta_{J_i}\}$ and the distortion angles $\{\theta_{E_{i_1}}\}$:

$$\{\theta_i\} = \{\theta_{J_i}\} + \{\theta_{E_{i_1}}\} \qquad (6)$$

Cruise — Jig — Elastic Distortion

In most practical situations the cruise shape $\{\theta_i\}$ is prescribed by the performance aerodynamicist to assure the best possible lift-to-drag ratio, L/D , at the design cruise flight condition. Knowing the design cruise shape it is possible to use Equations (6) and (5) to find the jig shape, $\{\theta_{J_i}\}$. This jig shape is therefore interpreted as that shape to which the airplane must be assembled in the plant to yield the desired design cruise shape in the design cruise flight condition. Or, in the case of elastic windtunnel models it is the shape to which the elastic model must be machined in the shop to yield the desired design cruise shape in the design tunnel-test condition.

That large differences can indeed exist between the jig shape and the design cruise shape is illustrated in Figure 3. As shown in Figure 4, the method of Equation (4) can be used to predict such shape changes with good accuracy. By making systematic changes to the planform geometry, the structural arrangement and the mass distribution, thereby systematically changing $[A]$, $[C_\theta]$ and $\{m_i\}$ it is possible to evaluate the effect of such changes on the jig shape or cruise shape of the airplane. This is particularly valuable once the basic design of the airplane is 'frozen' and it is necessary to compute the effect of small changes in the aerodynamic, structural or mass configuration on the design cruise shape. Typical examples of systematic planform changes which can be studied efficiently with this method are illustrated in Figure 5.

3.2 Lift-to-Drag Ratio

The lift-to-drag ratio of an airplane depends on friction as well as pressure drag. It is generally assumed that the friction drag part is not dependent on the shape of the airplane but obviously the pressure drag part is. To study the effect of elastic equilibrium shape changes on the overall lift-to-drag ratio, it is proposed that it suffices to study their effect on $(L/D_{PRESSURE})$.

Substituting Equation (4) into Equation (3) and solving for $\{F_{A_{i_1}}\}$ it is found that:

$$\{F_{A_{i_1}}\} = \left[[I] - \bar{q}_1[A][C_\theta]\right]^{-1} \bar{q}_1[A]\left\{\alpha_1 + \theta_{J_i} - [C_\theta]\{m_i\}g\right\} \qquad (7)$$

From this in turn it follows that to a first order of approximation:

$$L = \{1\}^T\{F_{A_{i_1}}\}$$
$$D = \{\alpha_{E_{i_1}}\}^T\{F_{A_{i_1}}\} \qquad (8)$$

where:

$$\{\alpha_{E_{i_1}}\} = \{\alpha_1 + \theta_{J_i} + \theta_{E_{i_1}}\} \qquad (9)$$

with $\{\theta_{E_{i_1}}\}$ given by Equation (5).

The lift-to-pressure-drag ratio is thus found to be:

$$\left(\frac{L}{D}\right)_{PRESSURE} = \frac{\{1\}^T\{F_{A_{i_1}}\}}{\{\alpha_{E_{i_1}}\}^T\{F_{A_{i_1}}\}} \qquad (10)$$

Systematic variations in mass distribution $\{m_i\}$, aerodynamic configuration $[A]$ and structural configuration $[C_\theta]$ can now be carried out and their effect on $(L/D)_{PRESSURE}$ studied. Typical aerodynamic configuration changes that can be studied in this manner are illustrated in Figure 5.

It is postulated that the method can be used also to study trades between structural weight and performance parameters. This could be done by changing those elements in $[C_\theta]$ which are affected by changes in local structural configuration. By proper partitioning of $[C_\theta]$ such changes can be easily introduced in a computer program.

It should be observed that the mass matrix $\{m_i\}$ consists of two types of masses: fixed masses $\{m_{i_{FIXED}}\}$ (e.g. structure, engines, fixed equipment) and variable masses $\{m_{i_{VARIABLE}}\}$ (e.g. fuel and payload). The effect of the variable mass distribution can be studied easily by substituting suitable numbers in $\{m_{i_{VARIABLE}}\}$. Figure 6 shows a typical example of how the variable part of the mass matrix can be arranged in a practical situation.

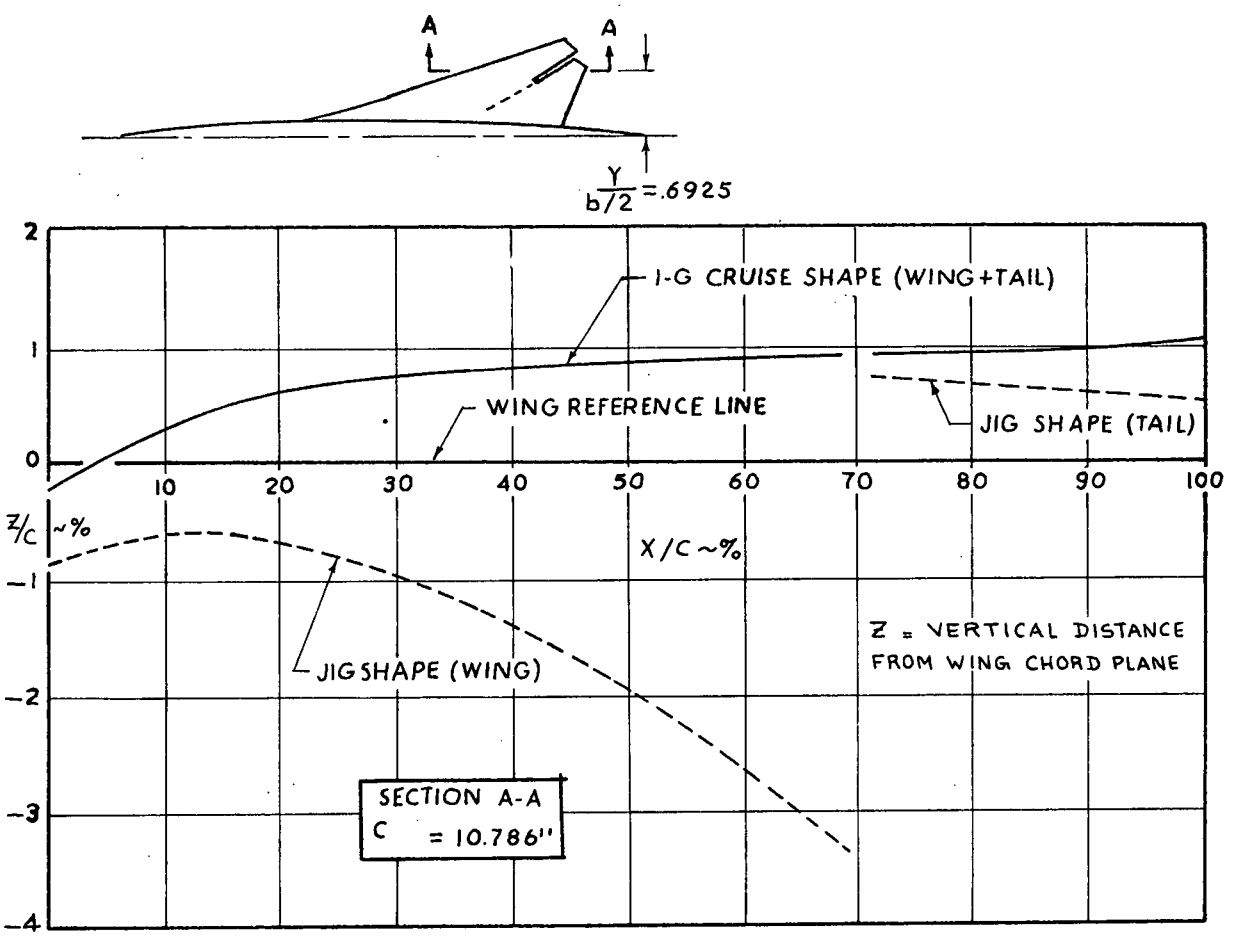


FIGURE 3 - EXAMPLE OF JIG SHAPE AND CRUISE SHAPE

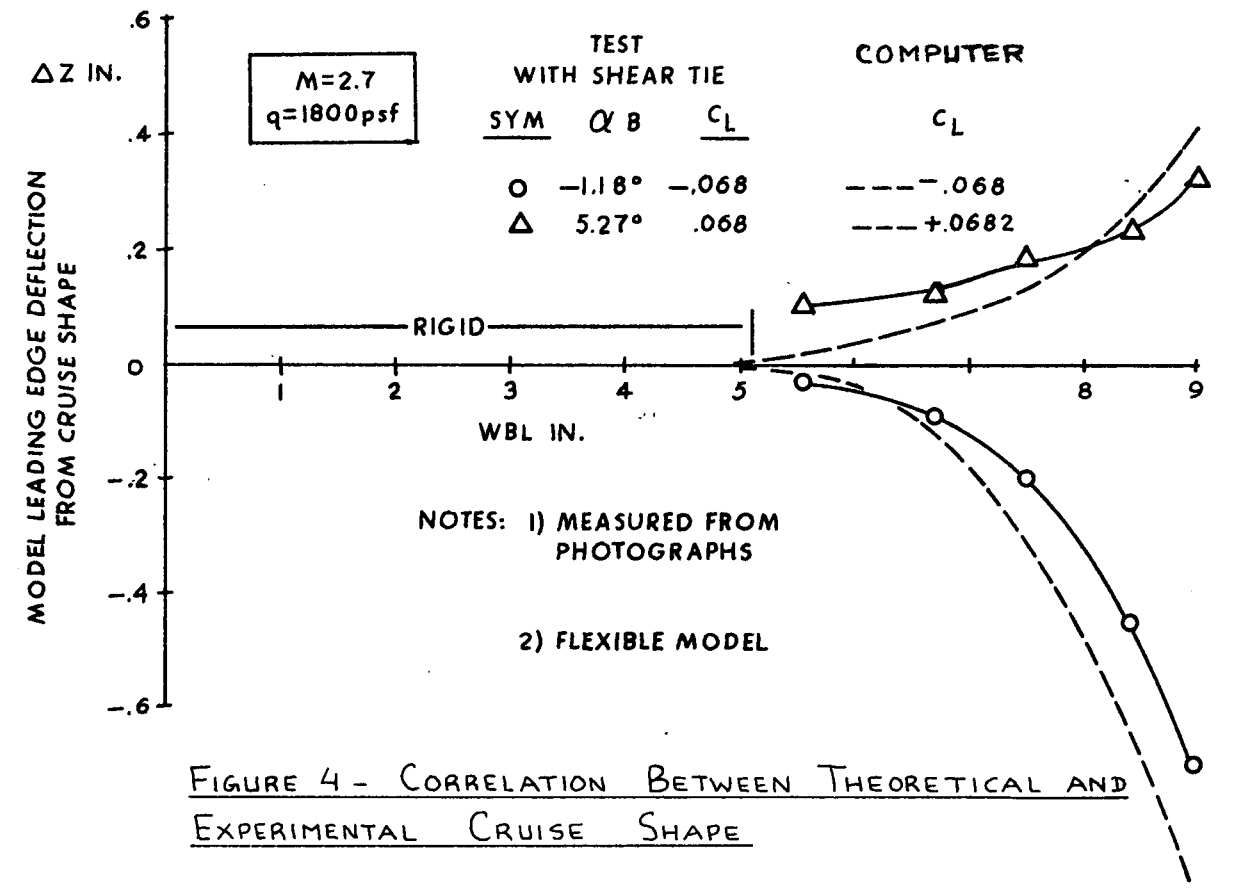


FIGURE 4 - CORRELATION BETWEEN THEORETICAL AND EXPERIMENTAL CRUISE SHAPE

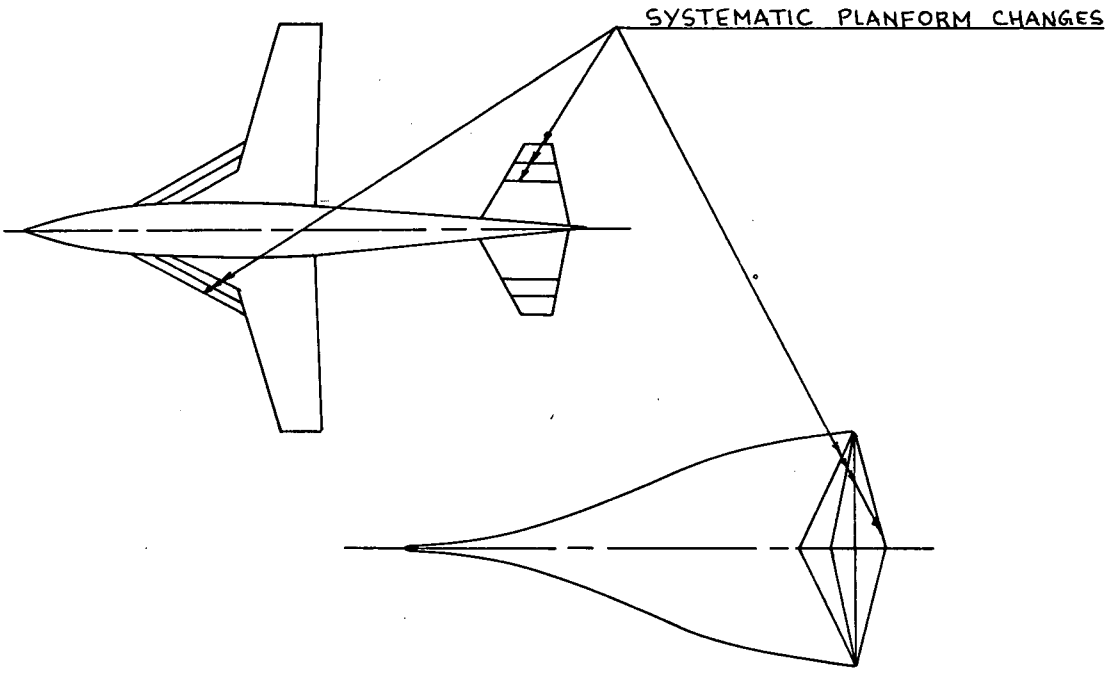
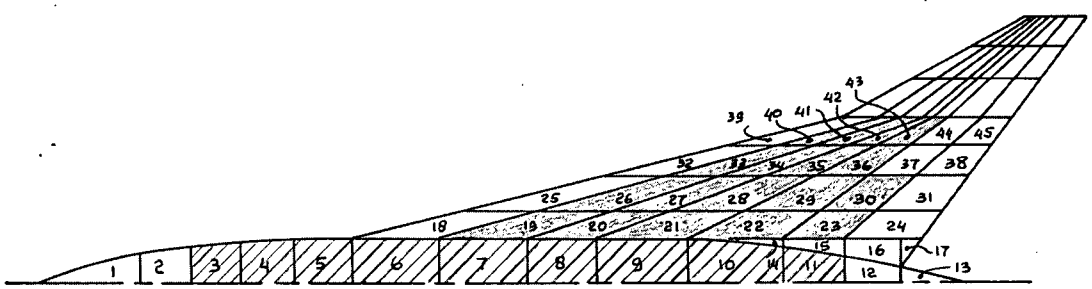


FIGURE 5 - EXAMPLES OF SYSTEMATIC CONFIGURATION CHANGES



$$\{m_{i_{VAR}}\} = \{m_{i_{FUEL}} + m_{i_{PAYLOAD}}\}$$

$m_{i_{FUEL}}$ ONLY FOR PANELS $i = 19,20,21,22,23,26,27,28,29,30,33,34,35,36,40,41,42,43$

$m_{i_{PAYLOAD}}$ ONLY FOR PANELS $i = 3-11$

FIGURE 6 - EXAMPLE OF VARIABLE MASS DISTRIBUTION

4. Interpretation and Use of Equivalent Elastic Airplane Stability Derivatives

4.1 Direct Formulation of Equivalent Elastic Stability Derivatives

It was shown in Reference 2 that, using the aerodynamic and structural influence coefficient matrices $[A]$ and $[C_\theta]$, it is possible to derive explicit formulas for the longitudinal stability derivatives of the equivalent elastic airplane. Substantiation of these formulas is presented in References 2 and 3. The formulas, arranged in a slightly different form, are presented in Table 1. It may be seen that the stability derivatives of the equivalent elastic airplane are fundamentally different from those of the rigid airplane. This is the consequence of the fact that there are two types of loads acting on an elastic airplane: aerodynamic and inertial (including gravitational). The inertial loads cause deflections of the structure which induce changes in aerodynamic loading. The aerodynamic loading itself does the same thing. In general, airplane derivatives represent the change in aerodynamic loading due to changes in the motion variables. In the formulation of Table 1 the stability derivatives are split into two categories: those due to aeroelastic effects in the absence of inertial forces (called zero mass derivatives) and those due to aeroelastic effects caused solely by inertial forces (called inertial derivatives). The following inertial effects must be accounted for:

1) those due to linear and angular accelerations and
2) those due to changes of airplane orientation with respect to the earth's gravitational field.

Thus, in addition to the regular aerodynamic stability derivatives due to α , u, q, and $\dot{\alpha}$ there can be expected to appear new inertial derivatives due to :

$\left.\begin{matrix}\dot{u}\\ \dot{w}\end{matrix}\right\}$ linear acceleration , $\quad q \Big\}$ centrifugal acceleration ,

$\dot{q} \Big\}$ angular acceleration , and $\theta \Big\}$ gravity perturbation .

Except for $\dot{u}$ all inertial perturbations are accounted for in the formulation of Table 1. Forward accelerations $\dot{u}$ are assumed to be negligible in their effect on elastic distortions.

It is now possible to formulate the complete perturbed forces and moments on an equivalent elastic airplane. This is done in Table 2 and the differences with conventional rigid airplane formulations such as used in Reference 5 are indicated.

Observe that the equations of Table 2 contain derivatives marked "zero mass" and derivatives marked 'inertial'. The physical significance of this is that zero mass derivatives are independent of the mass distribution of the equivalent elastic airplane. However, the inertial derivatives are very much dependent on the mass distribution of the equivalent elastic airplane. Observe that the inertial derivatives as used here have no relation to unsteady flow phenomena. The inertial derivatives simply occur because of elastic distortions of the airplane caused by inertial forces.

The boxed terms in Table 2 are responsible for algebraic changes in the perturbed equations of motion of the rigid airplane as presented in Reference 5. All non-boxed derivatives of Table 2 already have a 'home' in these equations. For example, the derivative $C_{m_{\ddot{\theta}_I}}$ can be pulled together with I_{yy_1} to form:

$$\left(I_{yy_1} - C_{m_{\ddot{\theta}_I}} \bar{q}_1 S\bar{c}\right)\ddot{\theta}$$

Similarly, because of the identity:

$$\dot{w} = \dot{\alpha} U_1 \tag{14}$$

it is possible to combine $\dot{w}$ inertial derivatives with the $\dot{\alpha}$ acceleration (quasi-steady) derivatives. Doing this in a consistent manner results in the small perturbation equations of motion of the equivalent elastic airplane of Table 3. The formulation of the equivalent elastic stability derivatives according to Tables 1, 2 and 3 is called the Direct Formulation.

4.2 Indirect Formulation of Equivalent Elastic Stability Derivatives

It should be pointed out that there exists another (indirect) way of accounting for inertial effects in the study of equivalent elastic airplane dynamics. This represents what has been the standard method of accounting for inertial effects or as it is frequently called, inertial relief. In this method, several acceleration terms are combined in so-called load-factor derivatives $\partial C_L/\partial n$ and $\partial C_m/\partial n$. The relationship between the load-factor derivatives and the inertial derivatives of Table 1 will now be developed.

It is possible to write the aerodynamic lift-force and pitching-moment expansion as follows:

ELASTIC AIRPLANE ZERO MASS		ELASTIC AIRPLANE INERTIAL		RIGID AIRPLANE	
$C_{D_{\alpha_{\bar{E}}}}$	$\frac{1}{S}\{\alpha_{\varepsilon_{i_1}}\}^T[B][A]\{1\}$			C_{D_α}	$\frac{1}{S}\{\alpha_{i_1}\}^T[A]\{1\}$
$C_{D_{q_{\bar{E}}}}$	$\frac{-2}{S\bar{c}}\{\alpha_{\varepsilon_{i_1}}\}^T[B][A]\{x_i\}$	$C_{D_{q_I}}$	$\frac{2}{S\bar{c}}\{\alpha_{\varepsilon_{i_1}}\}^T[B][A][C_\theta]\{m_i\}U_1^2$	C_{D_q}	$\frac{-2}{S\bar{c}}\{\alpha_{i_1}\}^T[A]\{x_i\}$
$C_{D_{u_{\bar{E}}}}$	$\frac{1}{S}\{\alpha_{\varepsilon_{i_1}}\}^T[B]\left(2[A]+M_1\left[\frac{\partial A}{\partial M}\right]\right)\{\alpha_{\varepsilon_{i_1}}\}$			C_{D_u}	$\frac{1}{S}\{\alpha_{i_1}\}^T\left(2[A]+M_1\left[\frac{\partial A}{\partial M}\right]\right)\{\alpha_{i_1}\}$
$C_{L_{\alpha_{\bar{E}}}}$	$\frac{1}{S}\{1\}^T[B][A]\{1\}$			C_{L_α}	$\frac{1}{S}\{1\}^T[A]\{1\}$
$C_{L_{q_{\bar{E}}}}$	$\frac{-2}{S\bar{c}}\{1\}^T[B][A]\{x_i\}$	$C_{L_{q_I}}$	$\frac{2}{S\bar{c}}\{1\}^T[B][A][C_\theta]\{m_i\}U_1^2$	C_{L_q}	$\frac{-2}{S\bar{c}}\{1\}^T[A]\{x_i\}$
$C_{L_{u_{\bar{E}}}}$	$\frac{1}{S}\{1\}^T[B]\left(2[A]+M_1\left[\frac{\partial A}{\partial M}\right]\right)\{\alpha_{\varepsilon_{i_1}}\}$			C_{L_u}	$\frac{1}{S}\{1\}^T\left(2[A]+M_1\left[\frac{\partial A}{\partial M}\right]\right)\{\alpha_{i_1}\}$
$C_{m_{\alpha_{\bar{E}}}}$	$\frac{1}{S\bar{c}}\{x_i\}^T[B][A]\{1\}$			C_{m_α}	$\frac{1}{S\bar{c}}\{x_i\}^T[A]\{1\}$
$C_{m_{q_{\bar{E}}}}$	$\frac{-2}{S\bar{c}^2}\{x_i\}^T[B][A]\{x_i\}$	$C_{m_{q_I}}$	$\frac{2}{S\bar{c}}\{x_i\}^T[B][A][C_\theta]\{m_i\}U_1^2$	C_{m_q}	$\frac{-2}{S\bar{c}}\{x_i\}^T[A]\{x_i\}$
$C_{m_{u_{\bar{E}}}}$	$\frac{1}{S\bar{c}}\{x_i\}^T[B]\left(2[A]+M_1\left[\frac{\partial A}{\partial M}\right]\right)\{\alpha_{\varepsilon_{i_1}}\}$			C_{m_u}	$\frac{1}{S\bar{c}}\{x_i\}^T\left(2[A]+M_1\left[\frac{\partial A}{\partial M}\right]\right)\{\alpha_{i_1}\}$
		$C_{D_{\theta_I}}$	$\frac{-1}{S}\{\alpha_{\varepsilon_{i_1}}\}^T[B][A][C_\theta]\{m_i\}g\sin\theta_1$		
		$C_{L_{\theta_I}}$	$\frac{-1}{S}\{1\}^T[B][A][C_\theta]\{m_i\}g\sin\theta_1$		
		$C_{m_{\theta_I}}$	$\frac{-1}{S\bar{c}}\{x_i\}^T[B][A][C_\theta]\{m_i\}g\sin\theta_1$		
		$C_{D_{\ddot{\theta}_I}}$	$\frac{1}{S}\{\alpha_{\varepsilon_{i_1}}\}^T[B][A][C_\theta]\{m_i x_i\}$		
		$C_{L_{\ddot{\theta}_I}}$	$\frac{1}{S}\{1\}^T[B][A][C_\theta]\{m_i x_i\}$		
		$C_{m_{\ddot{\theta}_I}}$	$\frac{1}{S\bar{c}}\{x_i\}^T[B][A][C_\theta]\{m_i x_i\}$		
		$C_{D_{\dot{w}_I}}$	$\frac{-1}{S}\{\alpha_{\varepsilon_{i_1}}\}[B][A][C_\theta]\{m_i\}$		
		$C_{L_{\dot{w}_I}}$	$\frac{-1}{S}\{1\}^T[B][A][C_\theta]\{m_i\}$		
		$C_{m_{\dot{w}_I}}$	$\frac{-1}{S\bar{c}}\{x_i\}^T[B][A][C_\theta]\{m_i\}$		

NOTE : 1) $[B]=\left[[1]-\bar{q}_1[A][C_\theta]\right]^{-1}$ 2) $\alpha_{\varepsilon_{i_1}}=\alpha_1+\theta_{s_i}+\theta_{\varepsilon_{i_1}}$ 3) $\alpha_{i_1}=\alpha_1+\theta_{s_i}$

TABLE I – LONGITUDINAL STABILITY DERIVATIVES FOR RIGID AND ELASTIC AIRPLANES

$$f_{A_{X_{S_E}}} = -\{(C_{D_{\alpha_{\bar{E}}}} - C_{L_1})\alpha + C_{D_{\dot{\alpha}_{\bar{E}}}}\frac{\dot{\alpha}\bar{c}}{2U_1} + C_{D_{u_{\bar{E}}}}\frac{u}{U_1} + C_{D_{q_{\bar{E}}}}\frac{q\bar{c}}{2U_1} +$$
$$\longleftarrow \text{ZERO MASS DERIVATIVES} \longrightarrow$$
$$+ C_{D_{\dot{w}_I}}\dot{w} + C_{D_{q_I}}\frac{q\bar{c}}{2U_1} + C_{D_{\theta_I}}\theta + \boxed{C_{D_{\ddot{\theta}_I}}\ddot{\theta}}\}\bar{q}_1 S \quad (11)$$
$$\longleftarrow \text{INERTIAL DERIVATIVES} \longrightarrow$$

$$f_{A_{Z_{S_E}}} = -\{(C_{L_{\alpha_{\bar{E}}}} + C_{D_1})\alpha + C_{L_{\dot{\alpha}_{\bar{E}}}}\frac{\dot{\alpha}\bar{c}}{2U_1} + C_{L_{u_{\bar{E}}}}\frac{u}{U_1} + C_{L_{q_{\bar{E}}}}\frac{q\bar{c}}{2U_1} +$$
$$\longleftarrow \text{ZERO MASS DERIVATIVES} \longrightarrow$$
$$+ C_{L_{\dot{w}_I}}\dot{w} + C_{L_{q_I}}\frac{q\bar{c}}{2U_1} + C_{L_{\theta_I}}\theta + \boxed{C_{L_{\ddot{\theta}_I}}\ddot{\theta}}\}\bar{q}_1 S \quad (12)$$
$$\longleftarrow \text{INERTIAL DERIVATIVES} \longrightarrow$$

$$m_{A_{Y_{S_E}}} = \{C_{m_{\alpha_{\bar{E}}}}\alpha + C_{m_{\dot{\alpha}_{\bar{E}}}}\frac{\dot{\alpha}\bar{c}}{2U_1} + C_{m_{u_{\bar{E}}}}\frac{u}{U_1} + C_{m_{q_{\bar{E}}}}\frac{q\bar{c}}{2U_1} +$$
$$\longleftarrow \text{ZERO MASS DERIVATIVES} \longrightarrow$$
$$+ C_{m_{\dot{w}_I}}\dot{w} + C_{m_{q_I}}\frac{q\bar{c}}{2U_1} + \boxed{C_{m_{\theta_I}}\theta} + C_{m_{\ddot{\theta}_I}}\ddot{\theta}\}\bar{q}_1 S\bar{c} \quad (13)$$
$$\longleftarrow \text{INERTIAL DERIVATIVES} \longrightarrow$$

TABLE 2 - PERTURBED AERODYNAMIC FORCES USING EQUIVALENT ELASTIC AIRPLANE STABILITY DERIVATIVES

$$M\dot{u} + (Mg\cos\Theta_1 + C_{D_{\theta_I}}\bar{q}_1 S)\theta + \{(C_{D_{\alpha_{\bar{E}}}} - C_{L_1})\alpha + (C_{D_{\dot{\alpha}_{\bar{E}}}} + C_{D_{\dot{w}_I}}\frac{2U_1^2}{\bar{c}})\frac{\dot{\alpha}\bar{c}}{2U_1} + \quad (15)$$
$$+ C_{D_{u_{\bar{E}}}}\frac{u}{U_1} + (C_{D_{q_{\bar{E}}}} + C_{D_{q_I}})\frac{q\bar{c}}{2U_1} + C_{D_{\ddot{\theta}_I}}\ddot{\theta}\}\bar{q}_1 S = 0$$

$$M\dot{w} - MU_1 q + (Mg\sin\Theta_1 + C_{L_{\theta_I}}\bar{q}_1 S)\theta + \{(C_{L_{\alpha_{\bar{E}}}} + C_{D_1})\alpha + (C_{L_{\dot{\alpha}_{\bar{E}}}} + C_{L_{\dot{w}_I}}\frac{2U_1^2}{\bar{c}})\frac{\dot{\alpha}\bar{c}}{2U_1} + \quad (16)$$
$$+ C_{L_{u_{\bar{E}}}}\frac{u}{U_1} + (C_{L_{q_{\bar{E}}}} + C_{L_{q_I}})\frac{q\bar{c}}{2U_1} + C_{L_{\ddot{\theta}_I}}\ddot{\theta}\}\bar{q}_1 S = 0$$

$$(I_{yy} - C_{m_{\ddot{\theta}_I}}\bar{q}_1 S\bar{c})\dot{q} - \{C_{m_{\alpha_{\bar{E}}}}\alpha + (C_{m_{\dot{\alpha}_{\bar{E}}}} + C_{m_{\dot{w}_I}}\frac{2U_1^2}{\bar{c}})\frac{\dot{\alpha}\bar{c}}{2U_1} + C_{m_{u_{\bar{E}}}}\frac{u}{U_1} + \quad (17)$$
$$+ C_{m_{\theta_I}}\theta + (C_{m_{q_{\bar{E}}}} + C_{m_{q_I}})\frac{q\bar{c}}{2U_1} + C_{m_{\ddot{\theta}_I}}\ddot{\theta}\}\bar{q}_1 S\bar{c} = 0$$

DIRECT FORMULATION

$$M\dot{u} + Mg\cos\Theta_1 + \{(C_{D_{\alpha_E}} - C_{L_1})\alpha + C_{D_{\dot{\alpha}_E}}\frac{\dot{\alpha}\bar{c}}{2U_1} + C_{D_{u_E}}\frac{u}{U_1} + \quad (40a)$$
$$+ C_{D_{q_E}}\frac{q\bar{c}}{2U_1} + C_{D_{\ddot{\theta}_E}}\ddot{\theta}\}\bar{q}_1 S = 0$$
$$\text{SMALL ?}$$

$$M\dot{w} - MU_1 q + (Mg\sin\Theta_1)\theta + \{(C_{L_{\alpha_E}} + C_{D_1})\alpha + C_{L_{\dot{\alpha}_E}}\frac{\dot{\alpha}\bar{c}}{2U_1} + C_{L_{u_E}}\frac{u}{U_1} + \quad (40b)$$
$$+ C_{L_{q_E}}\frac{q\bar{c}}{2U_1} + C_{L_{\ddot{\theta}_E}}\ddot{\theta}\}\bar{q}_1 S = 0$$
$$\text{SMALL ?}$$

$$(I_{yy} - C_{m_{\ddot{\theta}_E}}\bar{q}_1 S\bar{c})\dot{q} + \{C_{m_{\alpha_E}}\alpha + C_{m_{\dot{\alpha}_E}}\frac{\dot{\alpha}\bar{c}}{2U_1} + C_{m_{u_E}}\frac{u}{U_1} + C_{m_{q_E}}\frac{q\bar{c}}{2U_1}\}\bar{q}_1 S\bar{c} = 0 \quad (41)$$

INDIRECT FORMULATION

NOTE : EXPRESSIONS FOR $C_{D_{\alpha_E}}$ THROUGH $C_{D_{\ddot{\theta}_E}}$ ARE NOT DERIVED IN THE TEXT. HOWEVER, THEY ARE SIMILAR TO THOSE OF EQUATIONS (27-31) AND (34-38).
EXAMPLE : $C_{D_{\alpha_E}} = C_{D_{\alpha_{\bar{E}}}} + \frac{\partial C_D}{\partial n}\frac{C_{L_{\alpha_{\bar{E}}}}}{C_{L_{TRIM}} - \partial C_L/\partial n}$ WITH $\frac{\partial C_D}{\partial n} = -gC_{D_{\dot{w}_I}}$

TABLE 3 - SMALL PERTURBATION EQUATIONS OF MOTION FOR AN EQUIVALENT ELASTIC AIRPLANE

$$C_{L_{PERTURBED}} = \underbrace{C_{L_{\alpha_{\bar{E}}}}\alpha + C_{L_{\dot{\alpha}_{\bar{E}}}}\frac{\dot{\alpha}\bar{c}}{2U_1} + C_{L_{u_{\bar{E}}}}\frac{u}{U_1} + C_{L_{q_{\bar{E}}}}\frac{q\bar{c}}{2U_1}}_{\longleftarrow\ \text{ZERO MASS}\ \longrightarrow} + \underbrace{\frac{\partial C_L}{\partial n}n_{p(ERTURBED)} + C_{L_{\ddot{\theta}_I}}\ddot{\theta}}_{\longleftarrow\ \text{INERTIAL}\ \longrightarrow} \tag{18}$$

$$C_{m_{PERTURBED}} = \underbrace{C_{m_{\alpha_{\bar{E}}}}\alpha + C_{m_{\dot{\alpha}_{\bar{E}}}}\frac{\dot{\alpha}\bar{c}}{2U_1} + C_{m_{u_{\bar{E}}}}\frac{u}{U_1} + C_{m_q}\frac{q\bar{c}}{2U_1}}_{\longleftarrow\ \text{ZERO MASS}\ \longrightarrow} + \underbrace{\frac{\partial C_m}{\partial n}n_{p(ERTURBED)} + C_{m_{\ddot{\theta}_I}}\ddot{\theta}}_{\longleftarrow\ \text{INERTIAL}\ \longrightarrow} \tag{19}$$

Comparing Equations (18) and (19) with (12) and (13) shows that the inertial effects of $\dot{w}$, q and θ have been lumped together with n_p, the perturbation load factor which is defined by:

$$n = 1 + n_p = \frac{C_{L_1} + C_{L_p}}{C_{L_1}} = 1 + \frac{C_{L_p}}{C_{L_1}} \tag{20}$$

where n is the total load factor and $C_{L_1} = C_{L_{TRIM}}$, the equilibrium (steady-state) lift coefficient. It is not difficult to realize that for perturbations about rectilinear steady-state flight:

$$n_p = -\left(\frac{\dot{w}}{g} - \frac{U_1 q}{g} + \theta \sin\theta_1\right) \tag{21}$$

where U_1 = steady state speed.

θ_1 = steady-state attitude angle

This implies, therefore:

$$C_{L_{\dot{w}_I}}\dot{w} + C_{L_{q_I}}\frac{q\bar{c}}{2U_1} + C_{L_{\theta_I}}\theta \equiv \frac{\partial C_L}{\partial n}\left(-\frac{\dot{w}}{g} + \frac{U_1 q}{g} - \theta\sin\theta_1\right) \tag{22}$$

so that the following identities must be satisfied:

$$\begin{aligned} C_{L_{\dot{w}_I}} &= -\frac{1}{g}\frac{\partial C_L}{\partial n} \\ C_{L_{q_I}} &= \frac{2U_1^2}{\bar{c}g}\frac{\partial C_L}{\partial n} \\ C_{L_{\theta_I}} &= -\frac{\partial C_L}{\partial n}\sin\theta_1 \end{aligned} \tag{23}$$

Observe that the latter term vanishes for perturbations about steady level flight because then: $\sin\theta_1 = 0$. Similarly, it may be shown that:

$$C_{m_{\dot{w}_I}}\dot{w} + C_{m_{q_I}}\frac{q\bar{c}}{2U_1} + C_{m_{\theta_I}}\theta \equiv \frac{\partial C_m}{\partial n}\left(-\frac{\dot{w}}{g} + \frac{U_1 q}{g} - \theta\sin\theta_1\right) \tag{24}$$

from which:

$$\begin{aligned} C_{m_{\dot{w}_I}} &= -\frac{1}{g}\frac{\partial C_m}{\partial n} \\ C_{m_{q_I}} &= \frac{2U_1^2}{\bar{c}g}\frac{\partial C_m}{\partial n} \\ C_{m_{\theta_I}} &= -\frac{\partial C_m}{\partial n}\sin\theta_1 \end{aligned} \tag{25}$$

Observe that the latter term vanishes for perturbations about steady-state level flight because then: $\sin\Theta_1 = 0$.

Now, by substituting $n_p = \frac{C_{L_p}}{C_{L_{TRIM}}}$ from Equation (20) in Equation (18) and solving for C_{L_p} it is found that:

$$C_{L_p} = \frac{1}{1 - \frac{\partial C_L}{\partial n}\frac{1}{C_{L_{TRIM}}}} \left(C_{L_{\alpha_E}} \alpha + C_{L_{\dot{\alpha}_E}} \frac{\dot{\alpha}\bar{c}}{2U_1} + C_{L_{u_E}} \frac{u}{U_1} + C_{L_{q_E}} \frac{q\bar{c}}{2U_1} + C_{L_{\ddot{\theta}_I}} \ddot{\Theta} \right) \tag{26}$$

Or, upon defining:

$$C_{L_{\alpha_E}} = \frac{C_{L_{\alpha_E}}}{1 - \frac{\partial C_L}{\partial n}\frac{1}{C_{L_{TRIM}}}} \tag{27}$$

$$C_{L_{\dot{\alpha}_E}} = \frac{C_{L_{\dot{\alpha}_E}}}{1 - \frac{\partial C_L}{\partial n}\frac{1}{C_{L_{TRIM}}}} \tag{28}$$

$$C_{L_{u_E}} = \frac{C_{L_{u_E}}}{1 - \frac{\partial C_L}{\partial n}\frac{1}{C_{L_{TRIM}}}} \tag{29}$$

$$C_{L_{q_E}} = \frac{C_{L_{q_E}}}{1 - \frac{\partial C_L}{\partial n}\frac{1}{C_{L_{TRIM}}}} \tag{30}$$

$$C_{L_{\ddot{\theta}_E}} = \frac{C_{L_{\ddot{\theta}_E}}}{1 - \frac{\partial C_L}{\partial n}\frac{1}{C_{L_{TRIM}}}} \tag{31}$$

it is possible to write:

$$C_{L_p} = C_{L_{\alpha_E}} \alpha + C_{L_{\dot{\alpha}_E}} \frac{\dot{\alpha}\bar{c}}{2U_1} + C_{L_{u_E}} \frac{u}{U_1} + C_{L_{q_E}} \frac{q\bar{c}}{2U_1} + \boxed{C_{L_{\ddot{\theta}_E}}} \ddot{\Theta} \tag{32}$$

The boxed term, if not negligible, still causes a change in the small perturbation equations of motion as compared with the rigid case, but at least the other terms are now quite analogous to those of the conventional rigid case. By substituting $n_p = C_{L_p}/C_{L_{TRIM}}$ and Equation (32) into Equation (19) it follows that:

$$\begin{aligned} C_{m_p} = &\left\{ C_{m_{\alpha_E}} + \frac{\partial C_m}{\partial n} \frac{C_{L_{\alpha_E}}}{C_{L_{TRIM}} - \frac{\partial C_L}{\partial n}} \right\} \alpha + \left\{ C_{m_{\dot{\alpha}_E}} + \frac{\partial C_m}{\partial n} \frac{C_{L_{\dot{\alpha}_E}}}{C_{L_{TRIM}} - \frac{\partial C_L}{\partial n}} \right\} \frac{\dot{\alpha}\bar{c}}{2U_1} + \\ &+ \left\{ C_{m_{u_E}} + \frac{\partial C_m}{\partial n} \frac{C_{L_{q_E}}}{C_{L_{TRIM}} - \frac{\partial C_L}{\partial n}} \right\} \frac{u}{U_1} + \left\{ C_{m_{q_E}} + \frac{\partial C_m}{\partial n} \frac{C_{L_{q_E}}}{C_{L_{TRIM}} - \frac{\partial C_L}{\partial n}} \right\} \frac{q\bar{c}}{2U_1} + \\ &+ \left\{ C_{m_{\ddot{\theta}_I}} + \frac{\partial C_m}{\partial n} \frac{C_{L_{\ddot{\theta}_I}}}{C_{L_{TRIM}} - \frac{\partial C_L}{\partial n}} \right\} \ddot{\Theta} \end{aligned} \tag{33}$$

Or, upon defining:

$$C_{m_{\alpha_E}} = C_{m_{\alpha_E}} + \frac{\partial C_m}{\partial n} \left(\frac{C_{L_{\alpha_E}}}{C_{L_{TRIM}} - \frac{\partial C_L}{\partial n}} \right) \tag{34}$$

$$C_{m_{\dot{\alpha}_E}} = C_{m_{\dot{\alpha}_E}} + \frac{\partial C_m}{\partial n} \left(\frac{C_{L_{\dot{\alpha}_E}}}{C_{L_{TRIM}} - \frac{\partial C_L}{\partial n}} \right) \tag{35}$$

$$C_{m_{u_E}} = C_{m_{u_{\bar{E}}}} + \frac{\partial C_m}{\partial n}\left(\frac{C_{L_{u_{\bar{E}}}}}{C_{L_{TRIM}} - \frac{\partial C_L}{\partial n}}\right) \tag{36}$$

$$C_{m_{q_E}} = C_{m_{q_{\bar{E}}}} + \frac{\partial C_m}{\partial n}\left(\frac{C_{L_{q_{\bar{E}}}}}{C_{L_{TRIM}} - \frac{\partial C_L}{\partial n}}\right) \tag{37}$$

$$C_{m_{\ddot{\theta}_E}} = C_{m_{\ddot{\theta}_I}} + \frac{\partial C_m}{\partial n}\left(\frac{C_{L_{\ddot{\theta}_I}}}{C_{L_{TRIM}} - \frac{\partial C_L}{\partial n}}\right) \tag{38}$$

it is possible to write:

$$C_{m_p} = C_{m_{\alpha_E}}\alpha + C_{m_{\dot{\alpha}_E}}\frac{\dot{\alpha}\bar{c}}{2U_1} + C_{m_{u_E}}\frac{u}{U_1} + C_{m_{q_E}}\frac{q\bar{c}}{2U_1} + C_{m_{\ddot{\theta}_E}}\ddot{\theta} \tag{39}$$

With this expression, it is seen that the rigid and equivalent elastic derivative formulations for pitching moment coefficient are indeed quite similar. The $\ddot{\theta}$ term again can be pulled together with the I_{yy_1} inertia term. The formulation of equivalent elastic stability derivatives using Equations (32) and (39) is called the Indirect Formulation.

The result of using Equations (32) and (39) in the small perturbation equations of motion is indicated in Table 3 by Equations (40) and (41). Comparison with Reference 5 shows that the rigid and equivalent elastic airplane small perturbation equations are similar in algebraic format with the exception of the $C_{L_{\ddot{\theta}}}$ term which usually is negligible. It is shown in Table 4 that the derivative $C_{m_{\ddot{\theta}_I}}$ cannot always be neglected!

It is obviously advantageous to be able to use the same algebraic formulations for rigid and elastic airplane small perturbation equations of motion. In so doing however the stability derivative expressions of Equations (27)-(30) and (34)-(38) must be adhered to! It is interesting to observe the difference in interpretation between $C_{L_{\alpha_{\bar{E}}}}$ and $C_{m_{\alpha_{\bar{E}}}}$ on the one hand and $C_{L_{\alpha_E}}$ and $C_{m_{\alpha_E}}$ on the other.

The derivative $C_{L_{\alpha_{\bar{E}}}}$ is the lift curve slope of the equivalent elastic but 'zero mass' airplane. This is physically the same as saying that $C_{L_{\alpha_{\bar{E}}}}$ is the lift curve slope at constant load factor. It is pointed out in Section 5 that it is precisely this quantity which is measurable on an elastic wind-tunnel model.

On the other hand, $C_{L_{\alpha_E}}$ is the lift-curve slope of the equivalent elastic airplane for varying load factor.

Similarly, the derivative $C_{m_{\alpha_{\bar{E}}}}$ is the slope of the pitching moment versus angle of attack curve of the 'zero mass' airplane or that at constant load-factor. Again, it will be shown in Section 5 that it is $C_{m_{\alpha_{\bar{E}}}}$ which can be measured in the windtunnel.

On the other hand, $C_{m_{\alpha_E}}$ is the pitching-moment versus angle of attack slope of the equivalent elastic airplane for varying load factor.

The derivatives $C_{m_{\alpha_{\bar{E}}}}$ and $C_{m_{\alpha_E}}$ lead to different interpretations of the aerodynamic center as will be discussed in section 4.3.

4.3 Aerodynamic Center

One of the most difficult problems which arise particularly during the preliminary design phase is to predict where the aerodynamic center of the airplane moves as a consequence of changes in planform geometry. The influence coefficient method can be used to great advantage in such situations. Typical examples of planform variations that can be studied with the method are illustrated in Figure 5.

For a rigid airplane the aerodynamic center is generally found from C_{m_α} and C_{L_α} by:

$$\bar{X}_{ac} = \bar{X}_{cg} - \frac{C_{m_\alpha}}{C_{L_\alpha}} = \bar{X}_{cg} - \frac{\{x_i\}^T[A]\{1\}}{\bar{c}\{1\}^T[A]\{1\}} \tag{42}$$

In the case of the equivalent elastic airplane it was shown in Section 4.2 that a distinction must be made between angle of attack changes at constant load-factor and those at varying load factor. Similarly therefore two aerodynamic centers must be defined:

1) $\bar{X}_{ac}|_n$ = aerodynamic center location for constant load-factor
and 2) $\bar{X}_{ac}|_{\bar{q}}$ = aerodynamic center location for varying load factor.

The first definition for elastic airplane aerodynamic center should be used in trim calculations, the second for situations involving maneuvers such as steady symmetrical pull-ups and steady level turns.

In terms of these definitions and the derivatives formulated in Section 4.2 it is found that:

$$\bar{X}_{ac}|_n = \bar{X}_{cg} - \frac{C_{m_\alpha}|_n}{C_{L_\alpha}|_n} = \bar{X}_{cg} - \frac{C_{m_{\alpha_E}}}{C_{L_{\alpha_E}}} = \bar{X}_{cg} - \frac{\{x_i\}^T[B][A]\{1\}}{\bar{c}\{1\}^T[B][A]\{1\}} \tag{43}$$

while:

$$\bar{X}_{ac}|_{\bar{q}} = \bar{X}_{cg} - \frac{C_{m_\alpha}|_{\bar{q}}}{C_{L_\alpha}|_{\bar{q}}} = \bar{X}_{cg} - \frac{C_{m_{\alpha_E}}}{C_{L_{\alpha_E}}} =$$

$$= \bar{X}_{cg} - \frac{C_{m_{\alpha_E}}}{C_{L_{\alpha_E}}}\left(1 - \frac{1}{C_{L_{TRIM}}}\frac{\partial C_L}{\partial n}\right) - \frac{\partial C_m}{\partial n}\frac{1}{C_{L_{TRIM}}} =$$

$$= \bar{X}_{cg} - \frac{\{x_i\}^T[B][A]\{1\}}{\bar{c}\{1\}^T[B][A]\{1\}}\left(1 - \frac{g}{SC_{L_{TRIM}}}\{1\}^T[B][A][C_\Theta]\{m_i\}\right) + \tag{44}$$

$$- \frac{g}{SC_{L_{TRIM}}}\{x_i\}^T[B][A][C_\Theta]\{m_i\}$$

As expected, only the second type of aerodynamic center depends on the mass distribution. Equations (43) and (44) can be used to study the effect of changes in aerodynamic, structural and mass configuration on aerodynamic center. It is emphasized that even though these equations look formidable, they contain all the elements already contained in the 'direct formulation' of Table 1. For a digital computer program the addition of Equations (43) and (44) represents a negligible increment in computer time.

Reference 6 showed several examples of trends and magnitudes of mass effects on stability derivatives. More examples are presented in Reference 3. To illustrate the effect of mass on aerodynamic center some data of Reference 6 were used to compute aerodynamic centers according to Equations (43) and (44). Figure 7 presents the results. It is seen that even for the current family of subsonic jets the differences between the two types of aerodynamic center are important.

5. Prediction of Full Scale Airplane Aerodynamic Characteristics from Elastic and Rigid Model Data

A detailed discussion on the development and use of rigid and elastic wind-tunnel models in the prediction of full scale flexible airplane characteristics was presented in Reference 7. It was shown that in the case of flexible airplanes it is not possible to use the tunnel data directly. These data must be massaged using the influence coefficient method of Sections 2-4.

The purpose of this section is to discuss step-by-step the procedure that should be followed in using model data to predict the full-scale airplane variation of lift coefficient with angle of attack. In doing this, the fundamental differences that exist between an airplane in free flight and a model fixed in the tunnel are accounted for. These differences are listed in Table 5. The procedures discussed in this section apply to cases where the lift coefficient varies with angle of attack in a nonlinear manner. For extension of these procedures to the prediction of full scale $C_m - C_L$ characteristics the reader is referred to Reference 7.

It is assumed that the shape of the airplane for the design flight condition is known (cruise shape) and that a rigid model has been constructed that is a scaled duplication of this shape. It is realized that rigid models cannot be perfectly rigid, and the consequence of this is discussed also.

The idea of building rigid models of the cruise shape relies on the assumption that one particular flight condition is of major importance or that the demonstration of analytical accuracy at one flight condition is sufficient to validate estimates for other conditions. It is impractical to construct rigid models for each important flight condition. When using the word airplane, the true (elastic) airplane is meant. When using the word rigid airplane, the airplane shape that results from freezing the airplane (true, elastic) in some equilibrium flight condition is meant.

SST M	ALT. -FT.	GROSS WEIGHT -LBS.	WING SWEEP -DEG.	I_{yy_1} 10^6SLUG·FT^2 (Approx.)	$\frac{C_{m_{\delta_E}} \bar{q} S \bar{c}}{I_{yy_1}}$
.3	8,500	370,000	30	40.2	.0080
.5	9,600				.0248
.7	11,000				.0217
.5	32,500	675,000	42	47.2	.0050
.7	26,000				.0125
.9	23,500				.0198
.7	47,500	668,000	72	48.3	.0020
.9	37,000				.0031
1.1	33,000				.0097
1.3	30,000	520,000		47.6	.0425
1.5	24,000				.182
2.2	60,500				.0939
2.7	49,000				.263

707-320B M	ALT. FT.	I_{yy_1} 10^6SLUG·FT^2 (Approx.)	$\frac{C_{m_{\delta_E}} \bar{q} S \bar{c}}{I_{yy_1}}$
.255	10,000	5.025	.027
.365			.052
.548			.105
.800	35,000		.094
.850			.106
.900			.121

Table 4 - Comparison of $C_{m_{\delta_E}}$ with Pitch Inertia I_{yy_1}

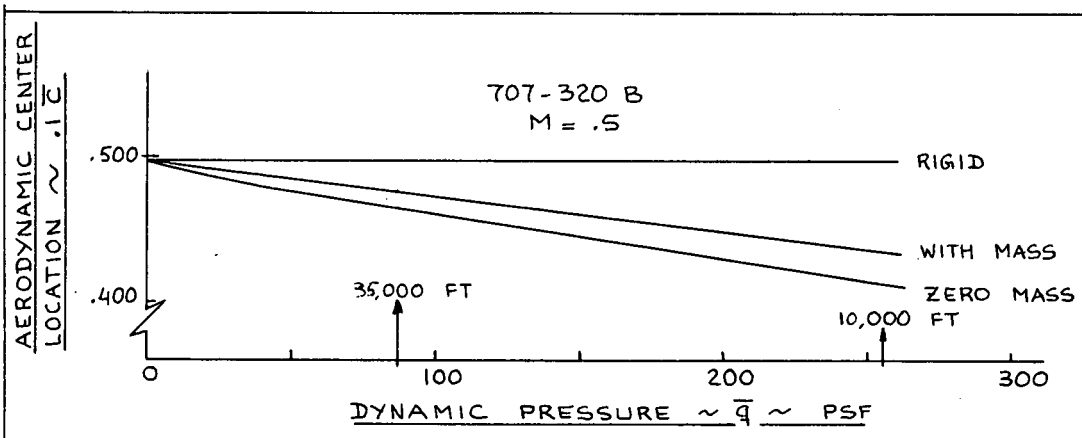


FIGURE 7 - EFFECT OF MASS DISTRIBUTION AND ELASTICITY ON AERODYNAMIC CENTER LOCATION

Airplane	Model
1. Load factor (n) varies with angle of attack.	1. Model is tested at constant load factor (n=1) when angle of attack is varied.
2. Airplane is completely flexible. Example: Wing, Tail, Body } Flexible	2. Model usually has only partial flexibility. Example: Body, Inboard wing and tail panels } Rigid; Outboard wing and tail panels } Flexible
3. Weight distribution varies for various flight conditions.	3. Weight distribution constant and not similar to any airplane distribution.
4. Airplane experiences various changes in flexiblity because of environment changes (aerodynamic heating).	4. Model experiences changes in flexibility created by wind tunnel temperatures.

Table 5 - Differences Between an Airplane and a Wind Tunnel Model

Making the assumptions that the wind tunnel model is a perfectly scaled duplication of the airplane, that Reynolds number effects and power effects are negligible, and that shock formations are properly simulated, the rigid airplane $C_{L_A}-\alpha$ curve should be identical to the measured rigid model $C_{L_M}-\alpha$ curve. This is indicated in Figure 8 by the curves marked 'rigid'

It is also assumed that an elastic model has been constructed that, when tested at cruise Mach number, cruise dynamic pressure, and cruise angle of attack, deflects to the desired cruise shape. This implies that the rigid and the elastic model have, for the design flight condition, identical values of C_L, C_m, and C_D at the design α. Figure 8 reflects this fact at point P_1. The result of wind tunnel measurements then is the establishment of $C_{L_M}-\alpha$ curves for the rigid and elastic model. This completes Step 1.

Observe that, while on the airplane, a variation of α at constant dynamic pressure implies a varying load factor; this is not so for the wind tunnel model, where the load factor is always one. Even though this fact is of no consequence to rigid airplanes and models, for the elastic airplane it has the important consequence that inertial forces participate in deforming the airplane. The different effects of gravity on airplane and model can be accounted for by introducing the concept of zero airplane and model mass. Because $n = 1$ in the tunnel, correcting to zero model mass has the effect of shifting the elastic model $C_{L_M}-\alpha$ curve (vertically) over a small amount $\Delta C_{L_{M\,m=0}}$. This amount can be computed with the influence coefficient method of Sections 2-4 (from the known model mass and stiffness distribution), but is expected to be very small. A typical value computed for the current elastic SST model is $\Delta C_{L_{M\,m=0}} = 0.00031$ at M = 2.7 and $\bar{q}$ = 456 psf. This value is indeed small, compared with the flight C_L at this Mach number and dynamic pressure, which is $C_{L_{DESIGN}} = 0.085$.

It has been assumed that the effect of model mass on model elasticity (deflection) is constant over the α range. This assumption is reasonable, particularly in view of the smallness of $\Delta C_{L_{M\,m=0}}$. The zero mass model $C_{L_M}-\alpha$ curve is now replotted on the left (i.e. airplane side of Figure 8). This completes Step 2.

For the airplane at the design angle of attack, α_{DESIGN}, it is possible to compute $\partial C_{L_A}/\partial n$, the incremental lift coefficient due to airplane mass distribution at $n = 1$. This yields point P_2. Assuming that the elastic model is perfectly scaled (dimensional and stiffness), and that local shocks and Reynolds effects are negligible, it follows that the zero-mass airplane $C_{L_A}-\alpha$ curve should be identical to the zero-mass elastic model $C_{L_M}-\alpha$ curve, but shifted vertically so that it intercepts point P_2. This provides the first anchor point for prediction of full-scale characteristics and represents Step 3.

Because the airplane in reality has mass, and because load factor varies with α, it is necessary to correct the full-scale zero mass $C_{L_A}-\alpha$ curve. Load factor is defined as:

$$n = \frac{C_{L_A}\bar{q}S}{W} \qquad (W = \text{WEIGHT}) \tag{45}$$

Notice that $n = 0$ for $C_{L_A} = 0$. Because of this it is possible to consider the line $C_{L_A} = 0$ as corresponding to a zero-gravity environment. For that reason, the airplane $C_{L_A}-\alpha$ curves for full and zero mass intersect at $C_{L_A} = 0$ (Point A_1), providing still another anchor point in the process of predicting full-scale airplane characteristics. The effect of load factor on the $C_{L_A}-\alpha$ curve is expressed by the increment:

$$\Delta C_{L_{A_n}} = \left(\frac{\partial C_{L_A}}{\partial n}\right) n \tag{46}$$

Observe that $\partial C_{L_A}/\partial n$ for the airplane is a function of its known mass and stiffness distribution, dynamic pressure, and Mach number (Equation (23) and Table 1). It is assumed that the partical derivative $\partial C_{L_A}/\partial n$ has a value independent of α. In other words, it is assumed that the incremental aerodynamic loading due to mass distribution $\Delta C_{L_{A_n}}$ is not a function of the variation of lift distribution with an angle of attack. A typical value for $\partial C_{L_A}/\partial n$ is 0.0050, which, although small compared with the design C_{L_A} at $n = 1$, is not negligible. Adding the correction $\Delta C_{L_{A_n}}$, the full-scale $C_{L_A}-\alpha$ curve of the (elastic) airplane has finally been found. Notice that both points A_1 and P_1 are on the elastic airplane $C_{L_A}-\alpha$ curve. The correction $\Delta C_{L_{A_n}}$ varies from zero at A_1 to $\partial C_{L_A}/\partial n$ at P_2, but in a linear manner. This completes Step 4.

Notes:

1. It will be observed that the process of predicting full-scale airplane $C_{L_A}-\alpha$ characteristics from elastic model data involves computer applications because it is not feasible to simulate mass and mass-distribution while at the same time testing at full-scale Mach number and dynamic pressures. This is where the influence coefficient method described in Sections 2-4 comes in.

2. The procedures indicated here depend on a number of assumptions, the essentials of which are:

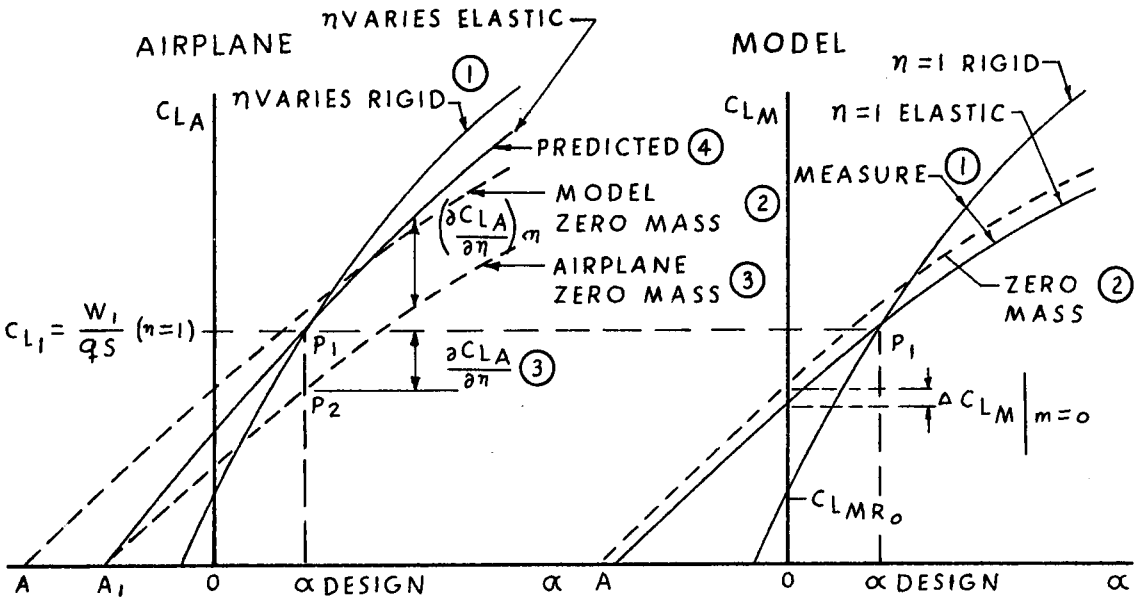


FIGURE 8 - PREDICTION OF AIRPLANE LIFT-CURVE FROM ELASTIC MODEL DATA

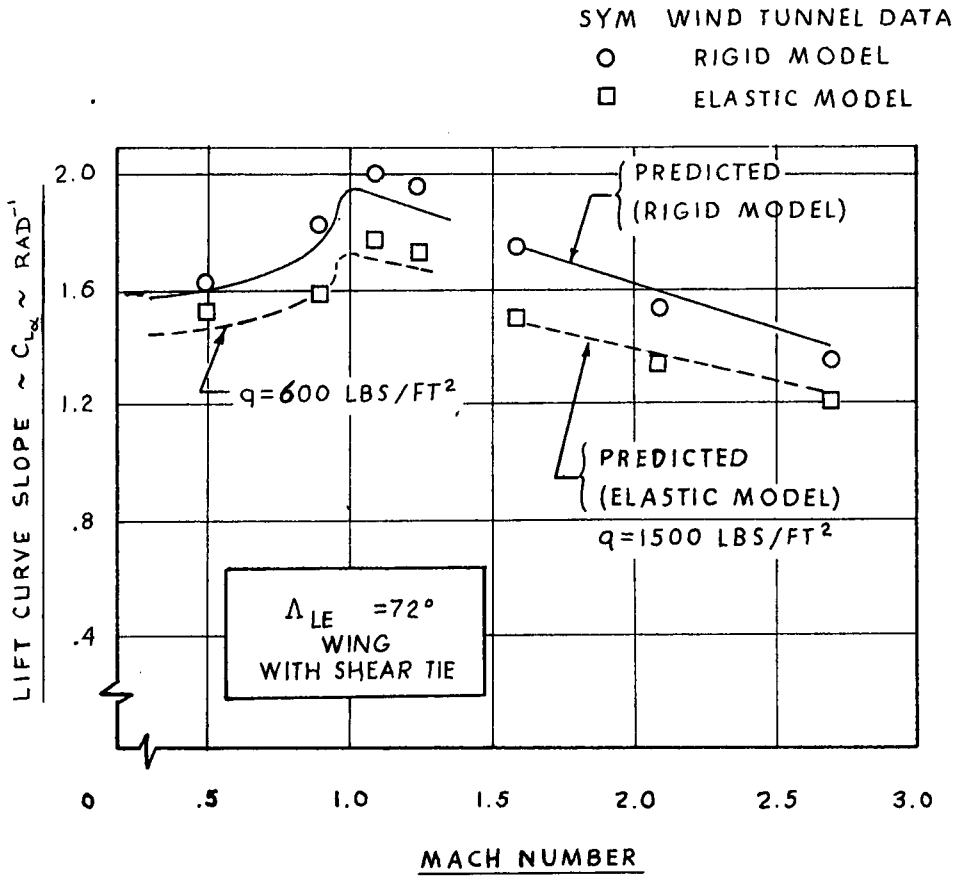


FIGURE 9 - CORRELATION OF THEORETICAL AND EXPERIMENTAL LIFT-CURVE SLOPE

a. Power, shock, and Reynolds number effects negligible (or accounted for separately)

b. $\Delta C_{L_{M_{m=0}}}$, $\partial C_{L_A}/\partial n$ are independent of α

3. The procedures indicated here can be applied at only one flight condition if, as is usually the case, only one rigid and one elastic model are available. For any other flight condition, the rigid model actually has the wrong shape. The correction procedure to be followed in that case is outlined below.

4. Notice that the (elastic) airplane lift-curve slope is made up of two components, as indicated by the following equation:

$$C_{L_{\alpha_{A_E}}} = C_{L_{\alpha_A}}\Big|_n + \frac{\partial C_{L_A}}{\partial n}\Big|_{\bar{q}} \frac{\partial n}{\partial \alpha}\Big|_{\bar{q}} = C_{L_{\alpha_{\bar{E}}}} + \frac{\partial C_{L_A}}{\partial n}\Big|_{\bar{q}} \frac{\partial n}{\partial \alpha}\Big|_{\bar{q}} \tag{47}$$

Observe the subscripts for constant n and $\bar{q}$. Now it is seen from Equation (45) that:

$$\frac{\partial n}{\partial \alpha}\Big|_{\bar{q}} = \frac{\partial n}{\partial C_{L_A}}\Big|_{\bar{q}} \frac{\partial C_{L_A}}{\partial \alpha}\Big|_{\bar{q}} = \frac{C_{L_{\alpha_E}}}{C_{L_{TRIM}}} \tag{48}$$

so by substituting into Equation (47):

$$C_{L_{\alpha_{A_E}}} = \frac{C_{L_{\alpha_{\bar{E}}}}}{1 - \frac{\partial C_{L_A}}{\partial n}\Big|_{\bar{q}} \frac{1}{C_{L_{TRIM}}}}, \text{ which agrees with Equation (27)} \tag{49}$$

This equation indicates that if the effect of mass distribution on C_L is negligible, then $C_{L_{\alpha_{A_E}}} = C_{L_{\alpha_{A_{\bar{E}}}}}$ which is to be expected. The equation also demonstrates the fact that $C_{L_{\alpha_{A_E}}}$ can be increased or decreased due to the inertial effects, depending on the sign of $\partial C_{L_A}/\partial n\,|_{\bar{q}}$. The sign of $\partial C_{L_A}/\partial n\,|_{\bar{q}}$ depends on the relative locations of center of mass loci to the elastic axis. When $\partial C_{L_A}/\partial n\,|_{\bar{q}}$ is positive (center of mass behind elastic axis) and larger than $C_{L_{TRIM}}$, the airplane lift curve slope has reversed. Observe that this reversal is different (but, of course, just as undesirable) from the reversal of the constant load factor (zero mass) lift-curve slope $C_{L_{\alpha_{\bar{E}}}}$

5. Observe that Equation (49) can account for nonlinear effects, provided $C_{L_{\alpha_{A_{\bar{E}}}}}$ is measured at the proper trim angle of attack on the elastic model.

6. In view of the smallness of $\Delta C_{L_{M_{m=0}}}$, Step 2 can be eliminated.

For arbitrary (other than cruise or design) flight conditions, the rigid model still has a shape corresponding to the cruise shape. Therefore, this shape no longer corresponds to that of the airplane if it were frozen at the new flight condition. It seems reasonable to assume that this change in shape does not affect $C_{L_{\alpha_{\bar{E}}}}$ to an appreciable extent. In other words, this shape change affects the camber and twist distribution but not $C_{L_{\alpha_{\bar{E}}}}$. Therefore, the rigid model will still give the correct lift-curve slope. The change in camber and twist distribution on the airplane can be estimated by computing the equilibrium shape of the airplane at the new flight condition. By subtracting this estimate from the known camber and twist distribution at the design flight condition, an incremental value is obtained. This incremental camber and twist distribution is responsible for an increment in lift coefficient $\Delta C_{L_{CTW}}$. This quantity can be determined from aerodynamic influence coefficient theory. The corrected rigid model (and therefore rigid airplane) $C_{L_M} - \alpha$ curve can now be obtained by shifting the measured curve vertically over $\Delta C_{L_{CTW}}$. The remaining procedures in predicting the full-scale airplane $C_{L_A} - \alpha$ curve are identical to those outlined for the design flight condition.

The question can be raised as to what should be done to correct for flexibility effects on the so-called rigid model.

In general, such corrections are expected to be small. Therefore, theoretically obtained aeroelastic model corrections should be accurate. Such corrections can be computed as soon as a flexibility matrix is obtained for the model. Such a matrix can be computed as follows:

1. Directly from the known model structure (this means an enormous amount of work and is probably not worth it)

2. Indirectly from measurement of EI and GJ distributions and applications of beam theory (this has also been done with elastic models to verify estimated stiffness properties)

3. Indirectly by measuring influence coefficients at specified control points (this could be a check on 2 to see if that approach is sufficiently accurate).

Ideally then, all model $C_{L_M}-\alpha$ data should be corrected for flexibility effects, after which the data can be used as representative of a truly rigid model in the manner described before.

The fact that the influence coefficient method of Sections 2-4 can be used with good accuracy in predicting rigid as well as elastic model behavior was illustrated by many examples in Reference 7. Figure 9 taken from Reference 7 is one such example.

6. Conclusions and Recommendations

6.1 Conclusions

It has been shown how a recently developed influence coefficient method can be used to generate the trade-off information needed in making design decisions during the p.d. phase of large flexible airplanes. Several examples were given to illustrate the use of the method in determining the effect of aerodynamic, structural and mass configuration changes on:

1) the equilibrium and jig shape
2) the lift-to-drag ratio
3) the stability derivatives
4) the aerodynamic center

It was also shown that in the case of the equivalent elastic airplane the algebraic form of the small perturbation equations of motion is the same as the one for a rigid airplane. However it is necessary to adhere to a special format for the elastic airplane derivatives and this format was derived.

Finally it was shown that wind-tunnel data obtained from rigid and elastic models must be 'massaged' in a special manner before they can be applied to the full scale airplane

6.2 Recommendations

To streamline the process of using the method in particular p.d. type applications it is desirable to mechanize the manner in which the planform changes of Figure 5 are made. It will also be necessary to develop fast methods of adjusting the structural influence coefficient matrix $[C_\theta]$ to corresponding planform changes.

An investigation should be made to determine which method of generating aerodynamic influence coefficients is best suited to p.d. applications. The current investigation employs Woodward's method of Reference 1. However several other methods can be used as indicated in Reference 8.

7. References

1. Woodward, F.A.; Analysis and Design of Wing-Body Combinations at Subsonic and Supersonic Speeds; Journal of Aircraft, Nov.-Dec. 1968.

2. Roskam, J. and Dusto, A.R.; An Influence Coefficient Method for the Prediction of Longitudinal Stability Derivatives of Rigid and Elastic Airplanes; AIAA Paper No. 69-131 presented at the 7th Aerospace Sciences Meeting, New York, January 1969.

3. Chevalier, H.D.; Dornfeld, J.M. and Schwanz, R.C.; Application of a Method for Predicting the Stability and Control Characteristics of Large Elastic Airplanes at Subsonic and Supersonic Speeds; Paper presented at the AGARD Flight Mechanics Panel Meeting on Aeroelastic Effects from a Flight Mechanics Standpoint, Marseille, France, April 1969.

4. Dusto, A.R.; An Analytical Method for Predicting the Stability and Control Characteristics of Large Elastic Airplanes at Subsonic and Supersonic Speeds; Paper presented at the AGARD Flight Mechanics Panel Meeting on Aeroelastic Effects from a Flight Mechanics Standpoint, Marseille, France, April 1969.

5. Etkin, B.; Dynamics of Flight, J. Wiley and Sons, 1959.

6. Roskam, J.; Stability Derivatives for Elastic Airplanes: Interpretation and Use; Proceedings of the Seminar on Elastic Airplane Stability, Control and Response, The University of Kansas, Lawrence, Kansas, June 1968.

7. Roskam, J.; Holgate, T. and Shimizu, G.; Elastic Wind-Tunnel Models for Predicting Longitudinal Stability Derivatives of Elastic Airplanes; Journal of Aircraft, Nov.-Dec. 1968.

8. Landahl, M.T. and Stark, V.J.E.; Numerical Lifting-Surface Theory-Problems and Progress; AIAA Journal, November 1968.

AEROELASTIC RESPONSE TO UNWANTED DISTURBANCES

by

J. Burnham

Royal Aircraft Establishment, Bedford, England

AEROELASTIC RESPONSE TO UNWANTED DISTURBANCES

by

J. Burnham

Royal Aircraft Establishment, Bedford, England

Summary

The response of aircraft to 'essentially unwanted' disturbances such as gusts and buffeting is briefly reviewed and the importance of aeroelastic effects is stressed. Mention is made of the use of automatic control systems to modify aeroelastic response to gusts and it is pointed out that similar systems can also have important handling qualities implications, thus suggesting the desireability of an integrated approach to their design.

1. INTRODUCTION

The study of flight mechanics can be looked upon as the study of the response of aircraft to two different classes of disturbance, those arising from the control system inputs made by the pilot or by some automatic device, and those arising from essentially unwanted disturbances such as gusts, buffeting and ground contacts. The object of the present paper is to consider, in fairly broad terms, the latter types of response.

A characteristic of these unwanted disturbances is that they usually contain sufficient energy at the frequencies of the aircraft elastic modes to excite them to a significant extent. The theoretical treatment of the response to these disturbances must therefore take account of these modes as well as those of the aircraft rigid body motion. The need for a unified treatment throughout the frequency range and the difficulties of providing it are discussed in Ref. 1, and will no doubt be the subject of further discussion at the present Conference, where other papers deal in greater detail with aspects which are mentioned briefly here.

2. RESPONSE TO UNWANTED DISTURBANCES

Typical spectral densities of normal acceleration measured at three points in the fuselage of a medium sized jet transport aircraft during flight through turbulence are given in Fig. 1[2] and give an indication of the sizes of the effects due to the first wing and fuselage elastic modes. As well as the importance of such effects to structural loads, it should be remembered that human sensitivity to vertical acceleration is increased as frequencies around 4 Hz and that elastic modes in this frequency range are present in most medium and large aircraft.

In the last decade, great advances have been made in theoretical methods of predicting aircraft response to turbulence, including aeroelastic effects. At least so far as the lower frequencies are concerned, covering the rigid body and first few elastic modes, present methods appear[2] to estimate response to within about 10%. Fig. 2 shows the agreement between measured and estimated spectrum shapes of the lower frequency modes. However, current theoretical methods appear to appreciably overestimate the excitation of the higher frequency modes (at higher frequencies than shown in Fig. 2). Because most structural loading occurs at the lower frequencies, it can generally be estimated[2] to within 15%. Further improvements in accuracy

are likely to imply considerable elaboration of the calculation methods, including for example the effects of variation of gust velocity over the aircraft (2 dimensional gust effects) and it is not clear that such improvements are justified for design purposes. It should also be noted that the accuracy of the flight data which has been used[2] in comparisons with theory does not appear to be much greater than that of the theory itself. If improved theories are to be developed, significantly more accurate flight results will be needed to validate them.

The theoretical techniques used in predicting the elastic response of aircraft to turbulence also lend themselves to the calculation of aircraft response to the other two important forms of unwanted disturbance, those due to buffeting and runway roughness. In these cases, however, non-linear effects may well be important. In the case of buffeting, Ref. 3 gives an account of the effects of the build-up of structural response during transient penetrations of buffet boundaries, as may occur during encounters with large gusts. It is mentioned that the possibility exists that many of the aerodynamic lags which have been 'measured' in transient buffet penetrations may have been at least partly due to lags in the structural response of the aircraft. Fig. 3 shows the magnitude of the alleviation of buffet load due to the latter when three classes of aircraft, in flight close to their buffet boundaries, encounter 1g gusts of various lengths.

The behaviour of aeroelastic models in wind tunnels provides a valuable means of predicting buffet effects. Although problems exist due to lower-than-flight Reynolds numbers and fluctuations in tunnel flow, reasonable correlations have been obtained between flight and tunnel in terms of the point of buffet onset, and at least qualitatively, in terms of the rate of increase of buffet loads with incidence[4]. An example showing a comparison between buffet boundaries measured in flight and wind tunnel is given in Fig. 4.

Loads which occur during take-off, landing and taxying often make a significant contribution to fatigue damage and the accompanying accelerations may adversely affect crew comfort and performance. Fig. 5 shows spectral densities of vertical and lateral accelerations in the cockpit and vertical acceleration at the c.g., from data measured during the take-off of a large transport aircraft (from unpublished RAE work by H. Hall), the peaks in the spectra at frequencies about about 2Hz being due to excitation of the elastic modes. As mentioned earlier, techniques developed for predicting the elastic response of aircraft to turbulence also lend themselves to studies of response to runway roughness. Probably the greatest difficulty arises from the adequate representation of nonlinearities in the undercarriage response.

3. EFFECTS OF AUTOMATIC FLIGHT CONTROL SYSTEMS

The behaviour of conventional autopilots and autostabilisers can be significantly affected by the sensors picking up response in the elastic modes, the resulting control deflections either increasing or decreasing the aircraft response, depending on phase. More complex systems, in which sensors are specifically positioned to detect the elastic modes responses and by suitable signal processing control signals are applied which

reduce them, have been designed and tested[5,6,7,8]. The performance of one such system, in terms of the improvement in fatigue damage rate, is shown in Fig. 6. These systems differ from earlier gust alleviators[9,10] in that no attempt is made to measure the gusts directly, and that they are aimed primarily at controlling the elastic mode response.

Improvements in aircraft rigid body dynamic response, due to autostabilisers, can of course lead to significant reductions in gust loads and improvements in ride qualities[11]. In general, to have a major effect on normal accelerations in the elastic modes, there seems little doubt that it would be valuable to have a control which allows the direct variation of wing lift. From a general handling qualities viewpoint, the usefulness of such 'direct lift controls' has come under increasing scrutiny. The improvement in vertical velocity response which such a control offers is shown in Fig. 7, and the effect, in terms of aircraft response to a tail gust encountered on the landing approach is illustrated in Fig. 8.

There is no doubt that an integrated approach to flight control systems, covering both handling qualities and elastic response, will be needed in future. Techniques are now available which will permit significant improvements to be made, even though problems such as 'fail safety' remain and the economic justification of such systems on a particular aircraft will need careful study. It is also worth remarking that structural response modification systems may also be valuable in reducing buffet loads and are anyway likely to be required to function adequately during penetrations beyond the aircraft's buffet boundaries.

List of References

1. A.S. Taylor, "The present status of aircraft stability problems in the aeroelastic domain". J. Roy. Aero. Soc. Spril 1959
2. C.G.B. Mitchell, "Assessment of the accuracy of gust response calculations by comparison with experiments". AIAA Paper 68-892
3. J.K. Zbrozek, J.G. Jones, "Transient buffet loads on wings" J. Sound Vib. (1967) 5 (2), 197-214
4. D.G. Mabey, "Comparison of seven wing buffet boundaries measured in wind tunnels and in flight". H.M.S.O. C.P. 840 Sept. 1964
5. J.H. Wykes, "Structural dynamic stability augmentation and gust alleviation of flexible aircraft". AIAA Paper 68-1067
6. R.P. Johannes, P.M. Burris, "Flight controls damp big aircraft bending." Control Engineering Sept. 1967
7. P.M. Burris, J.B. Dempster, "Flight testing structural performance of the LAMS flight control system". AIAA Paper 68-2
8. J.H. Wykes, A.S. Mori, "Techniques and results of an analytic investigation into controlling the structural modes of a flexible aircraft". Proceedings of the AIAA Symposium on structural dynamics and aeroelasticity, Boston, Mass. 1965 pp 419-433
9. J.K. Zbrozek, K.W. Smith, D. White, "Preliminary report on a gust alleviator investigation on a Lancaster aircraft". ARC R & M 2972 1957

10. W.H. Phillips, C.C. Craft, "Theoretical study of some methods for increasing the smoothness of flight through rough air". NACA TN 2416 1951

11. J.B. Dempster, K.L. Rogers, "Evaluation of B-52 structural response to random turbulence with various stability augmentation systems". J. of Aircraft Vol. 4 No. 6 Nov-Dec 1967

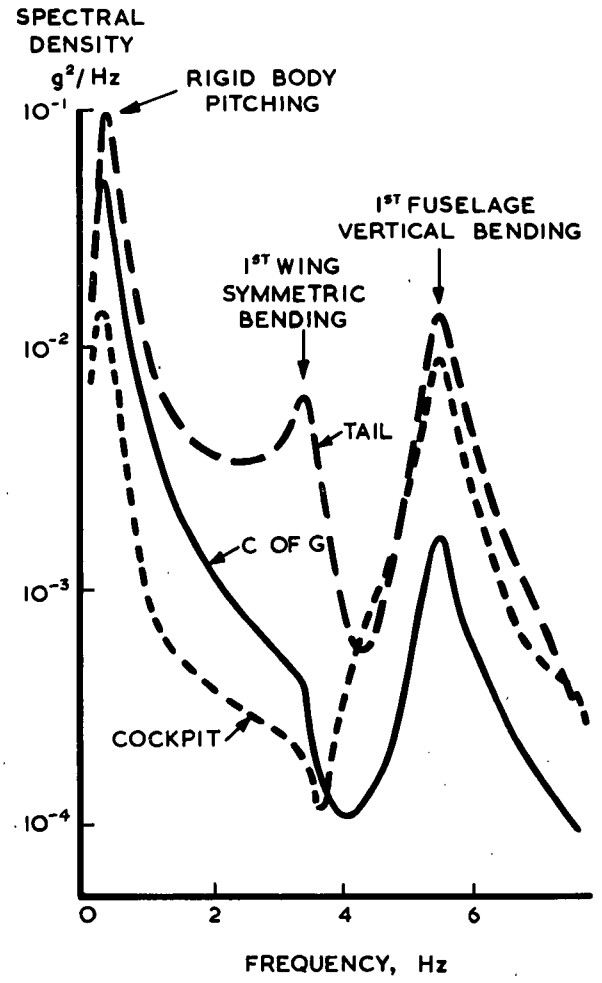


Fig. 1 Spectral densities of normal accelerations measured in flight through turbulence at the cockpit, C of G and tail of a medium sized jet transport

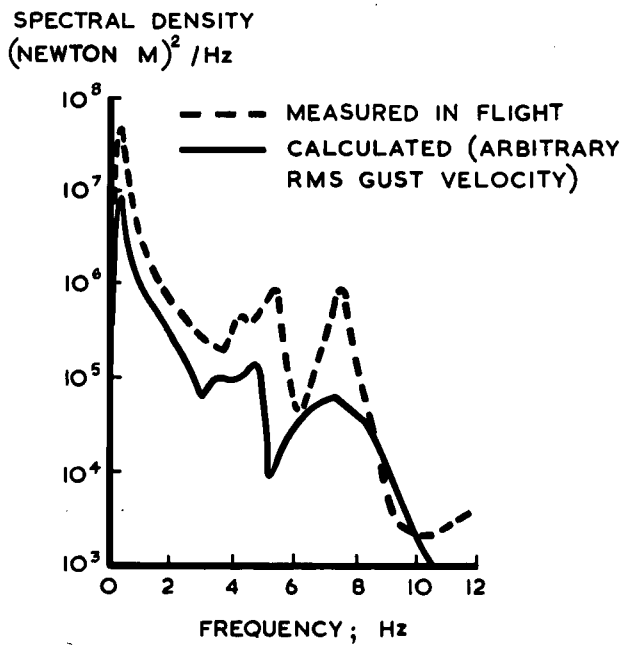


Fig. 2 Spectral density of tailplane root bending moment during flight through turbulent air in a jet transport aircraft (from ref. 2)

	WING NATURAL FREQUENCY, Hz	DAMPING RATIO
SMALL AIRCRAFT	9	0·07
LARGE AIRCRAFT	2	0·08
LARGE AND FLEXIBLE AIRCRAFT	1·5	0·06

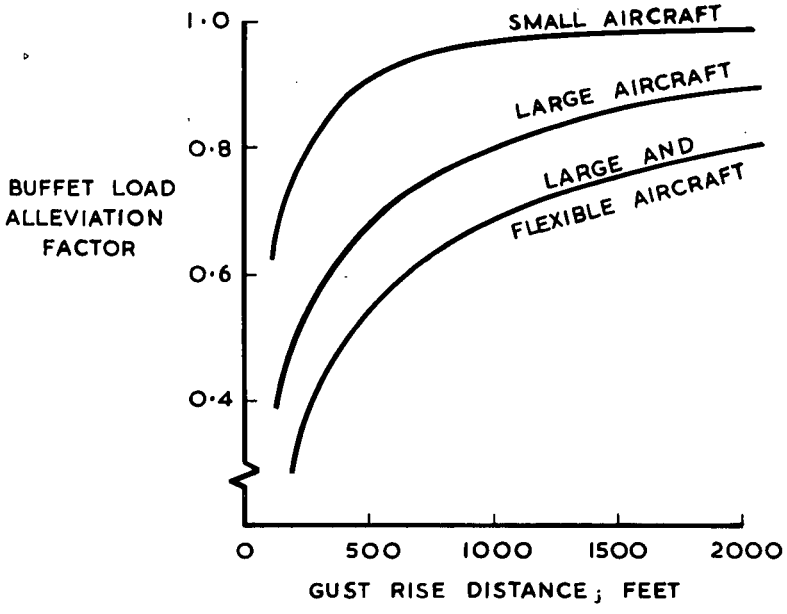


Fig.3 Effect of aircraft size and gust length on transient buffet loads (from ref.3)

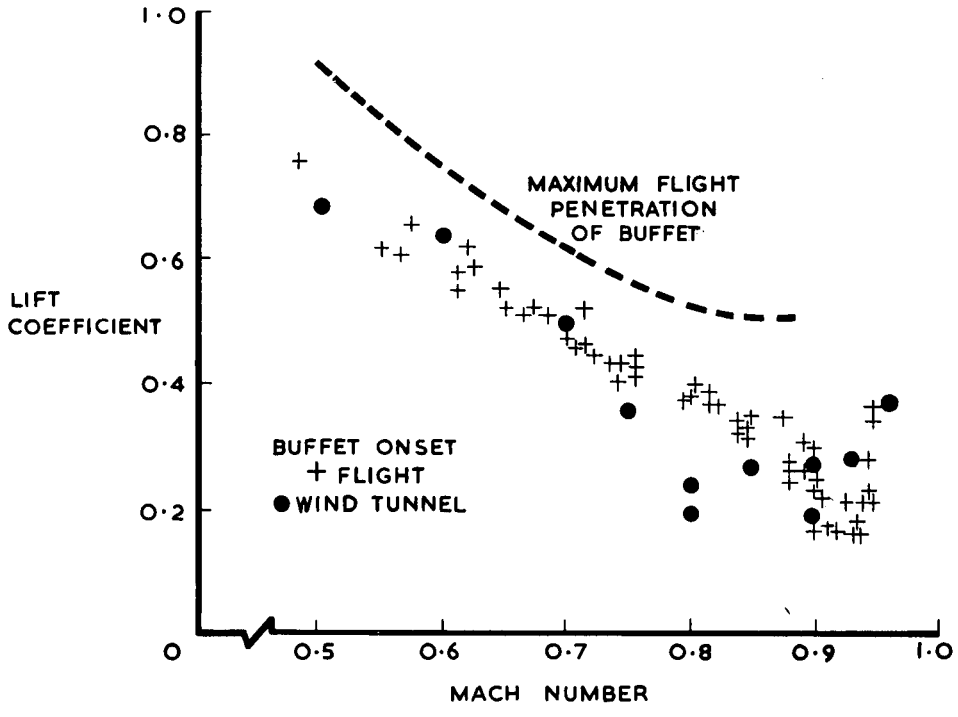


Fig.4 Comparison of flight and wind tunnel buffet boundaries (from ref.4)

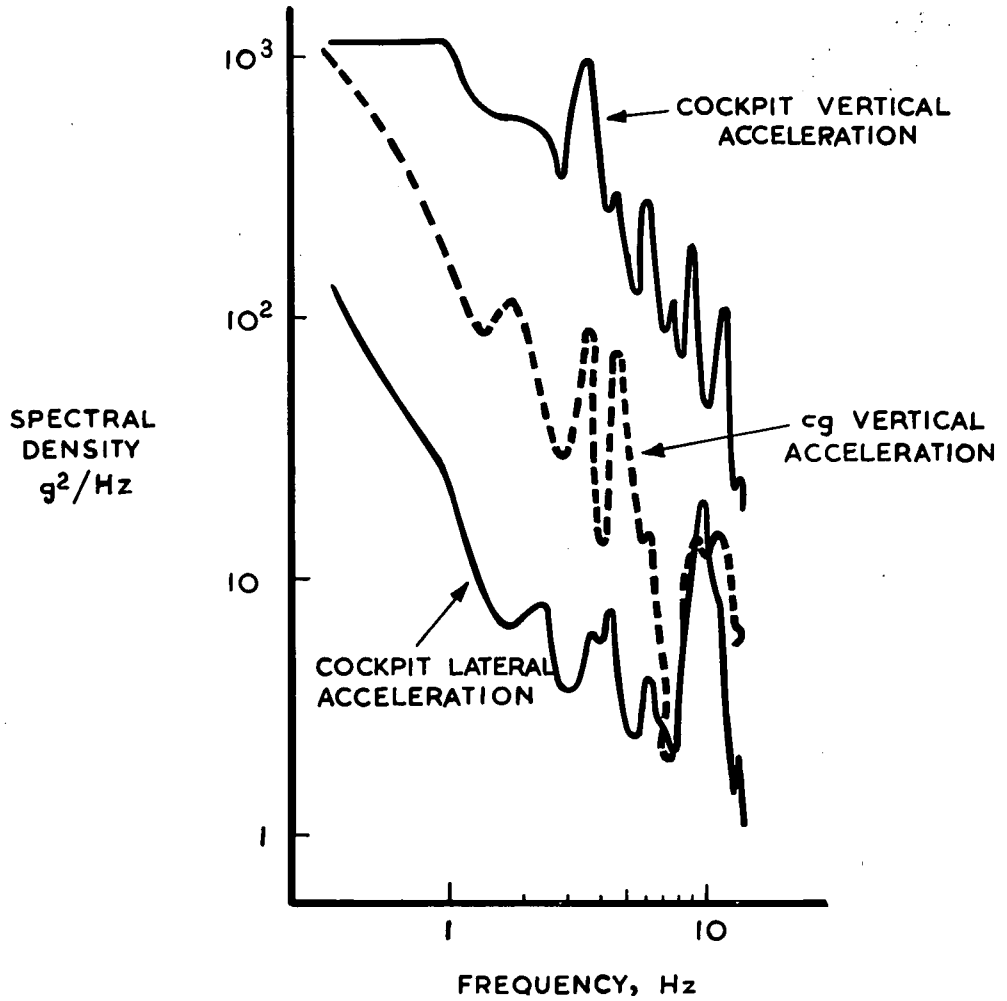
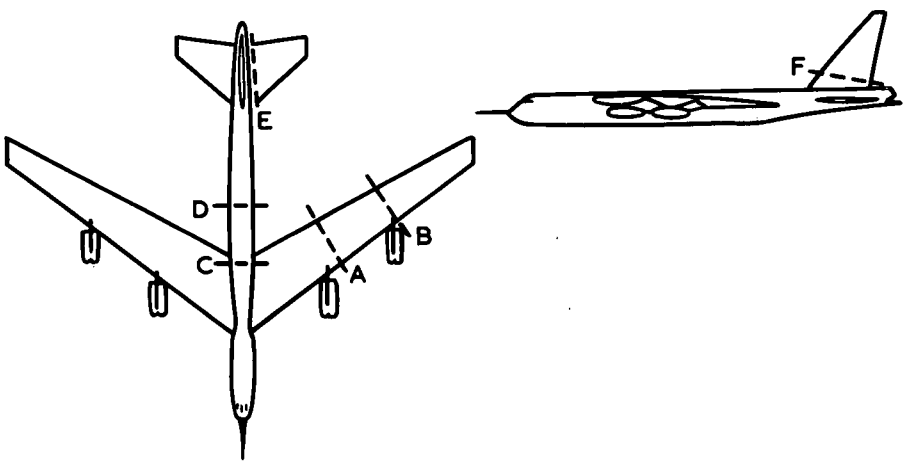


Fig.5 Spectral densities of accelerations measured during take off of a large transport aircraft



POSITION	A	B	C	D	E	F
FACTOR OF IMPROVEMENT IN FATIGUE DAMAGE RATE	5·75	1·83	6·45	3·9	2·18	5·9

Fig. 6 Theoretical values of improvements in fatigue damage rate brought about by fitting control system which modifies aeroelastic response (from ref. 6)

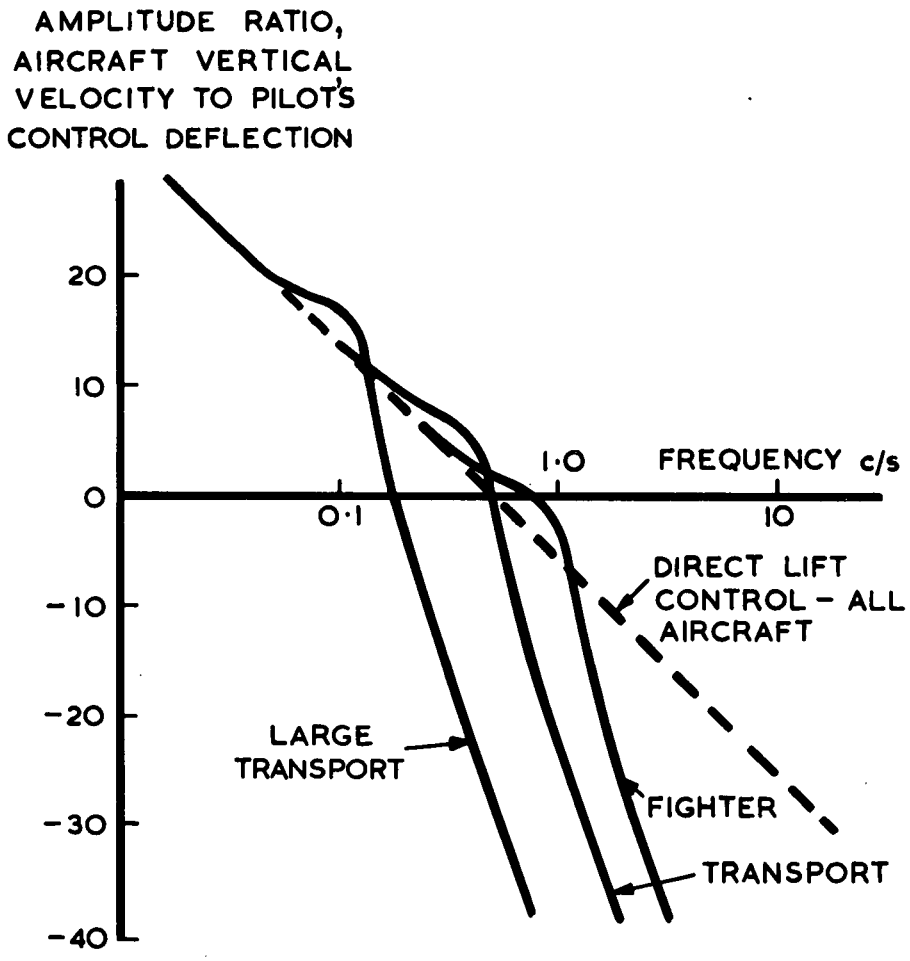


Fig.7 Effect of aircraft size on vertical velocity response to pilot's control for conventional elevators and direct lift control

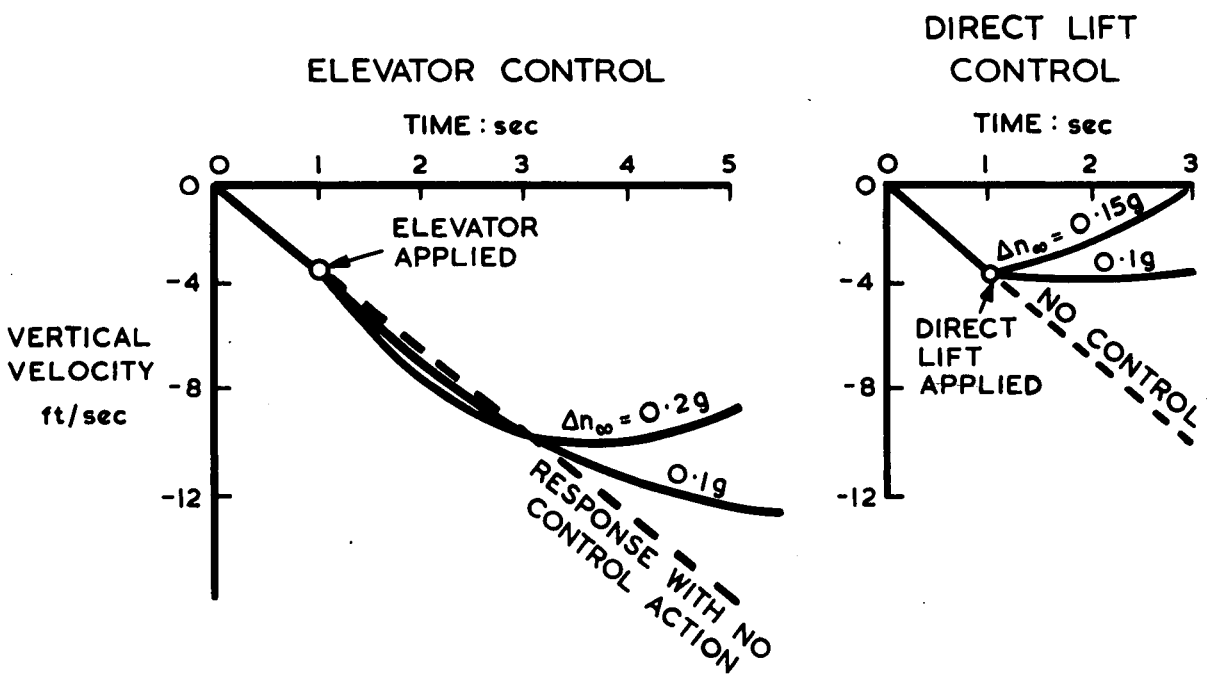


Fig.8 Effect on a large transport aircraft of a tail gust equivalent to 5% of airspeed and recovery by conventional elevator and by direct lift control

DETERMINATION DES COEFFICIENTS AERODYNAMIQUES

AVION SOUPLE EN VOL SYMETRIQUE

par A. MARSAN (SUD-AVIATION)

SOMMAIRE

L'introduction de la souplesse de l'avion dans l'étude des qualités de vol et l'affichage au simulateur a nécessité la création de nouveaux coefficients aérodynamiques qui tiennent compte de cette souplesse et conservent, pour tous les problèmes de mécanique de vol, les équations habituellement utilisées pour l'avion rigide.

Les calculs d'aéroélasticité statique ont été menés dans la mesure du possible en ayant recours aux données expérimentales plutôt qu'à la théorie pure. Ce qui explique que ces nouveaux coefficients sont en fait, des termes correctifs des coefficients mesurés en soufflerie sur maquettes rigides.

Il n'est question ici que des coefficients permettant l'étude du vol symétrique et ces coefficients sont analysés en fonction des paramètres dont ils dépendent, à savoir : mach, pression dynamique, poids et centrage.

NOTATIONS

P	Masse avion
$\bar{q}$	Pression dynamique
S	Surface de référence
ℓ	Longueur de référence
C_{zo}	Coefficient de portance à incidence nulle
C_{mo}	Coefficient de moment de tangage à incidence nulle
C_{zi}	Gradient de portance lié à l'incidence
$C_{z\beta}$	Gradient de portance lié au braquage des élevons
C_{zq}	Gradient de portance lié à la vitesse de tangage
C_{mi}	Gradient de moment de tangage lié à l'incidence
$C_{m\beta}$	Gradient de moment de tangage lié au braquage des élevons
C_{mq}	Gradient de moment de tangage lié à la vitesse de tangage
$\boxed{C}$	Matrice des coefficients d'influence structuraux
$\boxed{A}$	Matrice des coefficients d'influence aérodynamiques liant les forces sur les points d'intégration aux déformations angulaires sur les points de contrôle
$\{\Delta\alpha_j\}$	Matrice colonne des déformations angulaires aux points de contrôle j

1. INTRODUCTION

Depuis les débuts de l'aviation, les avions ne cessent d'augmenter leurs dimensions, leur allongement, leur poids et leur vitesse et on s'éloigne de plus en plus de l'avion rigide, s'il a jamais existé. Dans ces conditions, il devient impossible aujourd'hui de négliger l'aéroélasticité dans toute étude sérieuse des qualités de vol principalement pour les appareils commerciaux.

De cette aéroélasticité le flutter est la partie la plus importante et la plus étudiée ; mais il n'en demeure pas moins que certains phénomènes non vibratoires, tels la divergence et l'inversion d'ailerons, ont depuis longtemps retenu l'attention des constructeurs d'avions. Ces problèmes ne sont cependant pas les seuls à imputer à la souplesse. Tous les équilibres ou les mouvements que ce soit en vol symétrique ou en vol antisymétrique sont affectés par les déformations des différentes parties de l'avion. La seule connaissance de l'avion rigide ne suffit plus. Et une des premières études à entreprendre parce qu'elle traite du problème le plus fréquemment rencontré en vol, c'est le comportement de l'avion déformable en vol symétrique stationnaire.

2. CONSIDERATIONS PRELIMINAIRES

L'introduction de l'aéroélasticité dans les problèmes aérodynamiques fut longtemps freinée par les difficultés numériques qu'elle faisait apparaître. Maintenant, le développement des moyens mécanographiques mis à la disposition des utilisateurs, est tel qu'il met pratiquement l'aéroélasticité à la portée de tout le monde. Cependant, c'est bien souvent au prix d'une exploitation longue et laborieuse.

Ainsi, il est nécessaire, pour connaître les paramètres de vol avion souple, de résoudre le problème en avion rigide auquel on superpose un effet de souplesse, et le résultat n'est obtenu qu'après détermination de toutes les déformations. Ce processus présente l'avantage de réduire l'aéroélasticité aux petites variations autour de l'avion rigide ; une très grande part est faite aux essais de soufflerie et on ne sacrifie que très peu à toutes les théories aérodynamiques utilisées. Cependant, cette voie oblige à un double calcul et de ce fait, est difficilement maniable pour l'exploration systématique du domaine de vol. D'un autre côté, l'adaptation d'une telle méthode à un simulateur de vol est assez malaisée.

Ces considérations nous ont amenés à chercher, dans un but de simplification, à introduire les effets de souplesse avion sous forme de coefficients aérodynamiques pour conserver dans l'étude des qualités de vol, le même moule mathématique que pour l'avion rigide.

... /

3. GENERALITES SUR LA METHODE DE CALCUL

La souplesse de l'avion est parfaitement définie dès que l'on connait la relation entre les déformations et les forces induites, ce qui demande la détermination des effets structuraux et la mise au point d'une théorie aérodynamique locale.

Effets structuraux

Il nous a semblé plus commode de résoudre ces différents problèmes aéroélastiques à l'aide de coefficients d'influence plutôt qu'à l'aide de la superposition de modes propres ou élémentaires.

Les effets de flexibilité sont donc traduits par une matrice de coefficients d'influence donnant des angles de déformation dans le lit du vent en des points dits de contrôle, sous l'action de charges unitaires en des points dits d'intégration. Dans le cas du vol symétrique et d'un avion à aile delta comme CONCORDE, on ne prend en considération que les déformations de la voilure et du fuselage.

Effets aérodynamiques

La méthode employée est déduite de la théorie des surfaces portantes exposée par Hsu, Watkins, Richardson, etc ... et dont l'exploitation a déjà fait l'objet d'une conférence présentée par Mr DAROVSKY dans le cadre d'une précédente réunion de l'A.G.A.R.D.

Cette méthode permet d'obtenir une matrice de coefficients aérodynamiques liant les vitesses induites sur les points de contrôle aux coefficients du polynôme de pression choisi : elle définit donc une correspondance directe entre les déformations angulaires locales et les forces aérodynamiques qu'elles provoquent sur les points d'intégration.

Nous devons signaler que cette théorie appliquée à l'avion rigide CONCORDE donne des résultats très proches des mesures de soufflerie pour les gradients de portance et de moment de tangage, aussi bien dans le domaine subsonique que dans le domaine supersonique. (Planche 3).

4. COEFFICIENTS AERODYNAMIQUES SOUPLES

4.1 - Calcul des coefficients

Ce calcul s'applique à un avion du type CONCORDE c'est-à-dire une voilure seule avec fuselage sans empennage horizontal et se borne à l'équilibre au facteur de charge unité, uniquement pour ne pas alourdir l'exposé. L'extrapolation pour un avion classique ou pour un équilibre à un autre facteur de charge ne présente pas de difficulté majeure.

L'avion rigide en équilibre est défini par le système d'équations linéarisées et simplifiées:

$$① \begin{cases} P - \bar{q} S C'_{zi}\, i - \bar{q} S C'_{z\beta} \beta - \bar{q} S C_{zo} = 0 \\ \bar{q} S \ell C'_{mi}\, i + \bar{q} S \ell C'_{m\beta} \beta + \bar{q} S \ell C_{mo} = 0 \end{cases}$$

.../

C_{zo} et C_{mo} désignant la portance et le moment de tangage par rapport au centre de gravité, pour une incidence nulle.

La composante de la poussée est négligée car nous supposons que les incidences sont très faibles.

La souplesse de l'avion placé dans les mêmes conditions (mach, altitude, poids, centrage) ne modifie pas la résultante des forces aérodynamiques mais entraîne une variation des angles d'équilibre : Δi pour l'incidence, $\Delta\beta$ pour le braquage des élevons. Ainsi les forces dues à l'aéroélasticité et induites par :

- la variation d'incidence Δi
- la variation de braquage $\Delta\beta$
- la déformation angulaire locale $\{\Delta\alpha_j\}$

forment un système nul qui s'écrit :

$$② \quad \bar{q} S C_{z_i} \Delta i + \bar{q} S C_{z_\beta} \Delta\beta + \bar{q} \{1\}' [A] \{\Delta\alpha_j\} = 0$$

Quant à la déformation angulaire locale $\{\Delta\alpha_j\}$, elle résulte de l'action de toutes ces forces, plus de l'action des forces d'équilibre de l'avion rigide, ceci dans le cas où la maquette de soufflerie est semblable à la forme de construction à n = 0. Mais cette forme à n = 0 ne correspond à aucune configuration de vol et on construit généralement une maquette semblable à la forme de vol la plus probable, par exemple la forme optimisée pour la croisière.

Dans ces conditions, toutes les déformations angulaires sont calculées par rapport à cette forme de croisière et les forces avion rigide à prendre en considération sont les forces d'équilibre $\{F\}$ au Mach de calcul moins les forces $\{F_A\}$ permettant de passer de la forme bâti à la forme croisière.

En résumé, la déformation angulaire s'écrit :

$$③ \quad \{\Delta\alpha_j\} = [C] \left[\bar{q} \{F_\beta\} \Delta\beta + \bar{q} [A] \{1\} \Delta i + \bar{q} [A] \{\Delta\alpha_j\} + \{F\} - \{F_A\} \right]$$

$[C]$ désignant la matrice de coefficients d'influence structuraux

$[A]$ désignant la matrice de coefficients aérodynamiques

$\{F_\beta\}$ répartition des forces de braquage unitaire des élevons

En supposant que nous restions dans le domaine linéaire, nous pouvons remplacer la répartition $\{F\}$ par une répartition $\bar{q}\{F_o\}$ correspondant à $i = 0$, une répartition de forces d'incidence $\bar{q}[A]\{1\} i$, une répartition de forces de braquage $\bar{q}\{F_\beta\}\beta$ et une répartition massique $\{P\}$ de telle sorte que l'équilibre de l'avion souple se traduit par l'égalité des forces :

$$④ \quad \begin{aligned} P = {} & \bar{q} S C'_{z_i} (i + \Delta i) + \bar{q} S C'_{z_\beta} (\beta + \Delta\beta) + \bar{q} S C_{z_o} \\ & + \bar{q}^2 \{1\}' [A] [\bar{B}]^{-1} [C] [A] \{1\} (i + \Delta i) + \bar{q}^2 \{1\}' [A] [\bar{B}]^{-1} [C] \{F_\beta\} (\beta + \Delta\beta) \\ & + \bar{q} \{1\}' [A] [\bar{B}]^{-1} [C] (\bar{q}\{F_o\} - \{F_A\}) + \bar{q} \{1\}' [A] [\bar{B}]^{-1} [C] \{P\} \end{aligned}$$

.../

avec $[B]^{-1} = \left([1] - \bar{q}\,[C][A]\right)^{-1}$

$(i + \Delta i), (\beta + \Delta\beta)$ représentent respectivement l'incidence et le braquage d'équilibre de l'avion souple.

Il apparait dans l'équation (4) des termes liés à la souplesse qui ne sont en fait que des termes correctifs des gradients de portance et de C_{z_0} . Le dernier terme est à rapprocher du poids mais peut être assimilé à un gradient de portance lié au facteur de charge.

Ainsi, l'équation des forces de l'avion souple en équilibre s'écrit simplement :

⑤ $$P = \bar{q}\,S\,C'_{z_{is}}\,i_s + \bar{q}\,S\,C'_{z_{\beta s}}\,\beta_s + \bar{q}\,S\,C_{z_{os}} + \bar{q}\,S\,C'_{z_{ns}}\,n_s$$

Expression dans laquelle chacun des coefficients comprend un terme de soufflerie plus une partie due à la souplesse (exception faite du dernier qui n'a pas d'équivalent en avion rigide).

$$C'_{z_{is}} = C'_{z_{iR}} + \frac{1}{S}\,\bar{q}\,\{1\}'\,[A]\,[B]^{-1}\,[C]\,[A]\,\{1\}$$

$$C'_{z_{\beta s}} = C'_{z_{\beta R}} + \frac{1}{S}\,\bar{q}\,\{1\}'\,[A]\,[B]^{-1}\,[C]\,\{F_\beta\}$$

$$C_{z_{os}} = C_{z_{oR}} + \frac{1}{S}\,\{1\}'\,[A]\,[B]^{-1}\,[C]\,\left(\bar{q}\,\{F_0\} - \{F_\lambda\}\right)$$

$$C'_{z_{ns}} = \frac{1}{S}\,\{1\}'\,[A]\,[B]^{-1}\,[C]\,\{P\}$$

Ce sont ces nouveaux coefficients que nous désignons sous le vocable de coefficients aérodynamiques souples.

Le raisonnement fait sur les forces peut se conduire de la même manière sur les moments de tangage pour compléter le jeu de coefficients souples statiques.

Une étude de ressource équilibrée nous amènerait à définir des coefficients souples attachés à la vitesse de tangage.

Nous devons aussi envisager pour certains problèmes qui le nécessitent (la limitation de centrage par exemple), la création de coefficients de moments de charnière des élevons par l'introduction de termes correcteurs de b_o , b_1 , b_2 , b_n , b_q de sorte que le moment de charnière reste calculable par une expression telle que :

$$M_c = \bar{q}\,v\left(b_{os} + b_{1s}\,i_s + b_{2s}\,\beta_s + b_{ns}\,n_s + b_{qs}\,q\frac{l}{V}s\right)$$

V volume de référence de l'élevon.

(Le terme b_{qs} n'apportant cependant pas de grosses modifications sur le moment de charnière).

Tous les problèmes statiques ou quasi statiques de l'avion souple peuvent dès lors se traiter à l'aide des équations classiques de la mécanique de vol de l'avion rigide.

4.2 - Présentation des coefficients souples

Si cette manière de représenter la souplesse de l'avion offre de nombreux avantages pour la résolution et l'exploration du domaine de vol, elle conserve tout de même quelques inconvénients, ne serait-ce qu'à cause du nombre de paramètres dont dépendent les coefficients.

.../

Les études avion rigide ont habitué les aérodynamiciens à une interpolation en Mach ou en Mach et centrage : mais en avion souple, il faut maintenant envisager des interpolations en Mach, pression dynamique , poids et centrage. C'est pourquoi, nous séparerons ces coefficients souples en deux groupes suivant qu'ils sont fonction du Mach et de la pression dynamique ou qu'ils dépendent des quatre paramètres précités.

5. EVOLUTION DES COEFFICIENTS EN FONCTION DES DIFFERENTS PARAMETRES

5.1 - Coefficients fonction du Mach et de la pression dynamique

Pour certains, le terme correctif dû à la souplesse est purement théorique et ne varie qu'en fonction de la géométrie de la voilure. Ce sont les gradients de portance et de moment liés à l'incidence et à la vitesse de tangage, c'est-à-dire : $C'_{zis}, C'_{mis}, C'_{zqs}, C'_{mqs}$. Le coefficient b_{1s} de moment de charnière est à classer lui aussi dans cette catégorie.

Par contre, *tous les coefficients liés au braquage des élevons* ($C_{z\beta s}, C_{m\beta s}, b_{2s}$) sont créés à partir de mesures de soufflerie.

L'ensemble de ces termes correctifs est représentable par des courbes en tapis où l'on remarque que l'évolution en pression dynamique a une allure plus ou moins parabolique tandis que l'évolution en Mach rappelle celles des coefficients rigides homologues.

A noter aussi que la correction due à la souplesse sur les coefficients liés au braquage est plus importante que sur les coefficients liés à l'incidence du fait même de la répartition très arrière des forces entraînant les déformations.

Des deux termes C_{zos} et C_{mos}, c'est indéniablement le deuxième qui a la plus grande influence sur le comportement de l'avion. La correction apportée sur le terme rigide C_{mos} , fortement influencée par le Mach, évolue entre -3.10^{-3} et -5.10^{-3}, pour les maxima se rencontrant dans la zone transsonique.

5.2 - Coefficients fonction du Mach, de la pression dynamique, du poids et du centrage

Il s'agit essentiellement des termes $C'_{zns}, C'_{mns}, b_{ns}$.

Les coefficients $C'_{zns}, C'_{mns}, b_{ns}$, liés aux répartitions massiques, peuvent être considérés comme linéaires en pression dynamique et en première approximation linéaires aussi en poids, surtout si les réservoirs de combustible se situent à proximité du centre de gravité avion. Quant à l'évolution en centrage, assez faible dans la plage des centrages de vol admissibles, elle semble pour CONCORDE sensible aux remplissages des réservoirs de transfert qui se trouvent respectivement au niveau de l'onglet avant de la voilure et dans le fuselage arrière.

La variation des coefficients, tout en restant linéaire, présente deux pentes et la cassure correspond au centrage pour lequel les deux réservoirs sont vides. Pour être plus près de la vérité, il faudrait donc scinder ces coefficients en séparant l'effet de la masse structure et l'effet du remplissage de chacun des réservoirs. Cependant, ce processus compliquerait de manière notable, l'introduction de ces termes dans les équations de vol.

.../

Le coefficient C'_{mns} pour ne parler que du plus important, joue en fait le même rôle que le C_{mos}. En conséquence, nous avons tracé sur une même planche, pour donner une idée de l'ordre de grandeur, l'évolution du C_{mos} rigide, du terme correctif souple de ce C_{mos} et du C'_{mns} le long de la montée d'une mission type. (Planche 4).

5.3 - Remarques

5.3.1 - Les coefficients liés au braquage des gouvernes sont utilisés sour forme d'efficacité pour permettre l'extrapolation dans la région non linéaire des coefficients rigides. Cette représentation est alors préférable aux termes correctifs additifs qui entraîneraient une valeur trop pessimiste. (Planche 5).

Notons qu'il serait cependant possible de tenir compte des non-linéarités en introduisant des répartitions de forces de braquage, fonction du braquage lui-même, mais aux prix de calculs fastidieux et d'une exploitation complexe.

L'efficacité indépendante du braquage est donc un palliatif très acceptable.

5.3.2 - Signalons enfin pour terminer, que d'une manière générale, le terme correctif dû à la souplesse, s'oppose au terme correspondant de l'avion rigide.

6. CONCLUSION

Cette présentation n'est certainement pas une panacée, mais elle nous a semblé apporter une grande simplification dans l'étude de l'avion souple.

L'évolution et l'importance relative des différents coefficients n'ont trait qu'à l'avion CONCORDE et il n'est pas possible d'en extraire une loi générale et définitive. On peut cependant penser que les corrections faites sur les gradients de moment et en particulier sur le gradient lié au braquage des gouvernes, seront prédominantes dans tous les problèmes de qualité de vol. La seule constatation indéniable, c'est l'importance de plus en plus grande de l'aéroélasticité.

EQUATIONS D'EQUILIBRE
PL.1

1 _ Avion rigide:

$$\textcircled{1}\begin{cases} P - \bar{q}S C'_{zi}\, i - \bar{q}S C'_{z\beta}\beta - \bar{q}S C_{zo} = 0 \\ \bar{q}S\ell C'_{mi}\, i + \bar{q}S\ell C'_{m\beta}\beta + \bar{q}S\ell C_{mo} = 0 \end{cases}$$

2 _ Variations dues à la souplesse :

$$\textcircled{2}\begin{cases} \bar{q}S C'_{zi}\Delta i + \bar{q}S C'_{z\beta}\Delta\beta + \bar{q}\{1\}'[A]\{\Delta\alpha_j\} = 0 \\ \bar{q}S\ell C'_{mi}\Delta i + \bar{q}S\ell C'_{m\beta}\Delta\beta + \bar{q}\{d\}'[A]\{\Delta\alpha_j\} = 0 \end{cases}$$

3 _ Déformations :

$$\textcircled{3}\ \{\Delta\alpha_j\} = [C]\left[\bar{q}\{F_\beta\}\Delta\beta + \bar{q}[A]\{1\}\Delta i + \bar{q}[A]\{\Delta\alpha_j\} + \{F\} - \{F_A\}\right]$$

4 _ Equilibre avion souple :

$$\textcircled{4}\begin{cases} P = \bar{q}S C'_{zi}(i+\Delta i) + \bar{q}S C'_{z\beta}(\beta+\Delta\beta) + \bar{q}S C_{zo} \\ \quad + \bar{q}^2\{1\}'[A][B]^{-1}[C][A]\{1\}(i+\Delta i) + \bar{q}^2\{1\}'[A][B]^{-1}[C]\{F_\beta\}(\beta+\Delta\beta) \\ \quad + \bar{q}\{1\}'[A][B]^{-1}[C](\bar{q}\{F_o\} - \{F_A\}) + \bar{q}\{1\}'[A][B]^{-1}[C]\{P\} \\ \bar{q}S\ell C'_{mi}(i+\Delta i) + \bar{q}S\ell C'_{m\beta}(\beta+\Delta\beta) + \bar{q}S\ell C_{mo} \\ + \bar{q}^2\{d\}'[A][B]^{-1}[C][A]\{1\}(i+\Delta i) + \bar{q}^2\{d\}'[A][B]^{-1}[C]\{F_\beta\}(\beta+\Delta\beta) \\ + \bar{q}\{d\}'[A][B]^{-1}[C](\bar{q}\{F_o\} - \{F_A\}) + \bar{q}\{d\}'[A][B]^{-1}[C]\{P\} = 0 \end{cases}$$

COEFFICIENTS AERODYNAMIQUES SOUPLES

PL. 2

5_ Equations d'équilibre avion souple :

$$⑤ \begin{cases} P = \bar{q} S C'_{zis} i_s + \bar{q} S C'_{z\beta s} \beta_s + \bar{q} S C_{zos} + \bar{q} S C'_{zns} n_s \\ \bar{q} S \ell C'_{mis} i_s + \bar{q} S \ell C'_{m\beta s} \beta_s + \bar{q} S \ell C_{mos} + \bar{q} S \ell C'_{mns} n_s = 0 \end{cases}$$

avec :

$$C'_{zis} = C'_{ziR} + \frac{1}{S} \bar{q} \{1\}' \boxed{A} \boxed{B}^{-1} \boxed{C} \boxed{A} \{1\}$$

$$C'_{mis} = C'_{miR} + \frac{1}{S\ell} \bar{q} \{d\}' \boxed{A} \boxed{B}^{-1} \boxed{C} \boxed{A} \{1\}$$

$$C'_{z\beta s} = C'_{z\beta R} + \frac{1}{S} \bar{q} \{1\}' \boxed{A} \boxed{B}^{-1} \boxed{C} \{F_\beta\}$$

$$C'_{m\beta s} = C'_{m\beta R} + \frac{1}{S\ell} \bar{q} \{d\}' \boxed{A} \boxed{B}^{-1} \boxed{C} \{F_\beta\}$$

$$C'_{zns} = \frac{1}{S} \{1\}' \boxed{A} \boxed{B}^{-1} \boxed{C} \{P\}$$

$$C'_{mns} = \frac{1}{S\ell} \{d\}' \boxed{A} \boxed{B}^{-1} \boxed{C} \{P\}$$

$$C_{zos} = C_{zoR} + \frac{1}{S} \{1\}' \boxed{A} \boxed{B}^{-1} \boxed{C} \left(\bar{q} \{F_o\} - \{F_A\} \right)$$

$$C_{mos} = C_{moR} + \frac{1}{S\ell} \{d\}' \boxed{A} \boxed{B}^{-1} \boxed{C} \left(\bar{q} \{F_o\} - \{F_A\} \right)$$

$\boxed{B} = \boxed{1} - \bar{q} \boxed{C} \boxed{A}$

$\boxed{C}$: Coefficients d'influence structuraux

$\boxed{A}$: " " aérodynamiques

$\{F_\beta\}$: Forces de braquage

$\{d\}'$: Distances de la référence aux points d'intégration

Indices : s pour avion souple R pour avion rigide

EQUATIONS D'EQUILIBRE

1 _ Avion rigide:

$$(1)\begin{cases} P - \bar{q}SC'_{zi}\,i - \bar{q}SC'_{z\beta}\beta - \bar{q}SC_{zo} = 0 \\ \bar{q}S\ell C'_{mi}\,i + \bar{q}S\ell C'_{m\beta}\beta + \bar{q}S\ell C_{mo} = 0 \end{cases}$$

2 _ Variations dues à la souplesse :

$$(2)\begin{cases} \bar{q}SC'_{zi}\,\Delta i + \bar{q}SC'_{z\beta}\,\Delta\beta + \bar{q}\{1\}'\boxed{A}\{\Delta\alpha_j\} = 0 \\ \bar{q}S\ell C'_{mi}\,\Delta i + \bar{q}S\ell C'_{m\beta}\Delta\beta + \bar{q}\{d\}'\boxed{A}\{\Delta\alpha_j\} = 0 \end{cases}$$

3 _ Déformations :

$$(3)\ \{\Delta\alpha_j\} = \boxed{C}\left[\bar{q}\{F_\beta\}\Delta\beta + \bar{q}\boxed{A}\{1\}\Delta i + \bar{q}\boxed{A}\{\Delta\alpha_j\} + \{F\} - \{F_A\}\right]$$

4 _ Equilibre avion souple :

$$(4)\begin{cases} P = \bar{q}SC'_{zi}(i+\Delta i) + \bar{q}SC'_{z\beta}(\beta+\Delta\beta) + \bar{q}SC_{zo} \\ \quad + \bar{q}^2\{1\}'\boxed{A}\boxed{B}^{-1}\boxed{C}\boxed{A}\{1\}(i+\Delta i) + \bar{q}^2\{1\}'\boxed{A}\boxed{B}^{-1}\boxed{C}\{F_\beta\}(\beta+\Delta\beta) \\ \quad + \bar{q}\{1\}'\boxed{A}\boxed{B}^{-1}\boxed{C}\left(\bar{q}\{F_o\} - \{F_A\}\right) + \bar{q}\{1\}'\boxed{A}\boxed{B}^{-1}\boxed{C}\{P\} \\ \bar{q}S\ell C'_{mi}(i+\Delta i) + \bar{q}S\ell C'_{m\beta}(\beta+\Delta\beta) + \bar{q}S\ell C_{mo} \\ + \bar{q}^2\{d\}'\boxed{A}\boxed{B}^{-1}\boxed{C}\boxed{A}\{1\}(i+\Delta i) + \bar{q}^2\{d\}'\boxed{A}\boxed{B}^{-1}\boxed{C}\{F_\beta\}(\beta+\Delta\beta) \\ + \bar{q}\{d\}'\boxed{A}\boxed{B}^{-1}\boxed{C}\left(\bar{q}\{F_o\} - \{F_A\}\right) + \bar{q}\{d\}'\boxed{A}\boxed{B}^{-1}\boxed{C}\{P\} = 0 \end{cases}$$

Planche 1

COEFFICIENTS AERODYNAMIQUES SOUPLES

5 _ Equations d'équilibre avion souple

$$(5)\begin{cases} P = \bar{q}\,S\,C'_{zis}\,i_s + \bar{q}\,S\,C'_{z\beta s}\,\beta_s + \bar{q}\,SC_{zos} + \bar{q}\,SC'_{zns}\,n_s \\ \bar{q}\,S\ell C'_{mis}\,i_s + \bar{q}\,S\ell C'_{m\beta s}\,\beta_s + \bar{q}\,S\ell\,C_{mos} + \bar{q}\,S\ell\,C'_{mns}\,n_s = 0 \end{cases}$$

avec :

$$C'_{zis} = C'_{ziR} + \frac{1}{S}\bar{q}\{1\}'\boxed{A}\boxed{B}^{-1}\boxed{C}\boxed{A}\{1\}$$

$$C'_{mis} = C'_{miR} + \frac{1}{S\ell}\bar{q}\{d\}'\boxed{A}\boxed{B}^{-1}\boxed{C}\boxed{A}\{1\}$$

$$C'_{z\beta s} = C'_{z\beta R} + \frac{1}{S}\bar{q}\{1\}'\boxed{A}\boxed{B}^{-1}\boxed{C}\{F_\beta\}$$

$$C'_{m\beta s} = C'_{m\beta R} + \frac{1}{S\ell}\bar{q}\{d\}'\boxed{A}\boxed{B}^{-1}\boxed{C}\{F_\beta\}$$

$$C'_{zns} = \frac{1}{S}\{1\}'\boxed{A}\boxed{B}^{-1}\boxed{C}\{P\}$$

$$C'_{mns} = \frac{1}{S\ell}\{d\}'\boxed{A}\boxed{B}^{-1}\boxed{C}\{P\}$$

$$C_{zos} = C_{zoR} + \frac{1}{S}\{1\}'\boxed{A}\boxed{B}^{-1}\boxed{C}\left(\bar{q}\{F_o\} - \{F_A\}\right)$$

$$C_{mos} = C_{moR} + \frac{1}{S\ell}\{d\}'\boxed{A}\boxed{B}^{-1}\boxed{C}\left(\bar{q}\{F_o\} - \{F_A\}\right)$$

$\boxed{B} = \boxed{1} - \bar{q}\boxed{C}\boxed{A}$

$\boxed{C}$: Coefficients d'influence structuraux

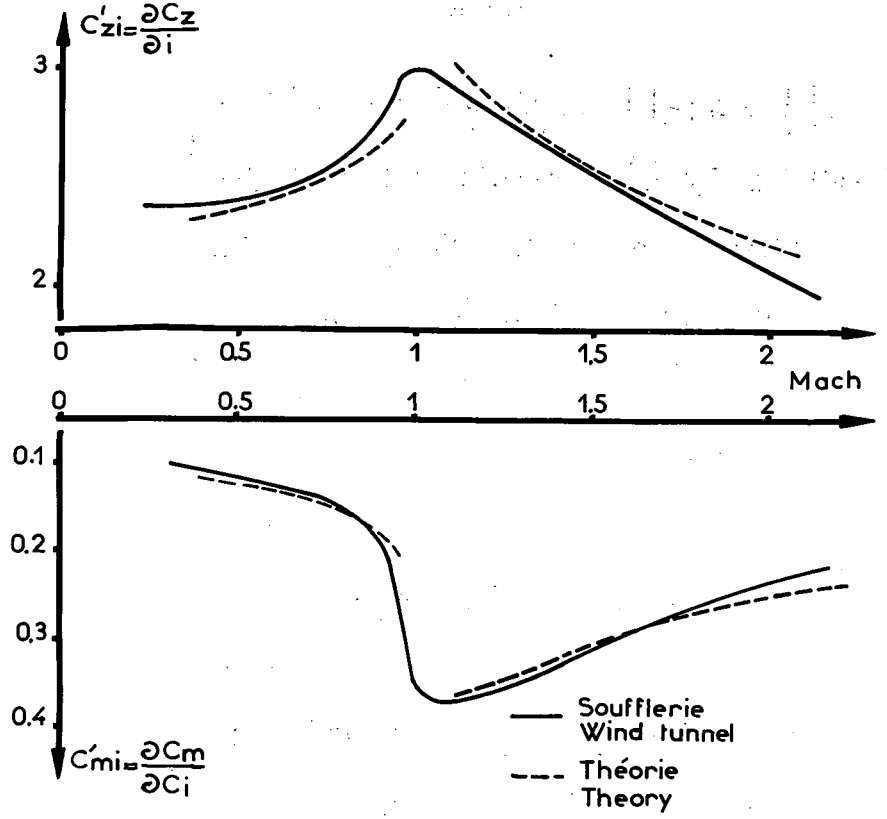
$\boxed{A}$: " " aérodynamiques

$\{F_\beta\}$: Forces de braquage

$\{d\}'$: Distances de la référence aux points d'intégration

Indices: s pour avion souple , R pour avion rigide

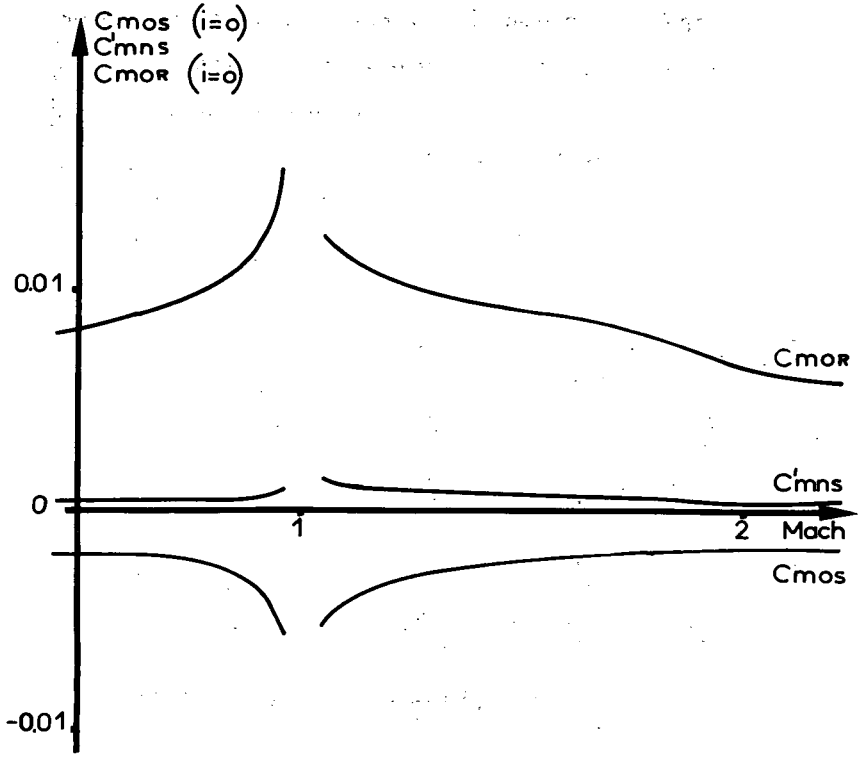
Planche 2



GRADIENTS DE PORTANCE ET DE MOMENT DE TANGAGE DE L'AVION RIGIDE

LIFT AND MOMENT DERIVATIVES OF RIGID AIRCRAFT

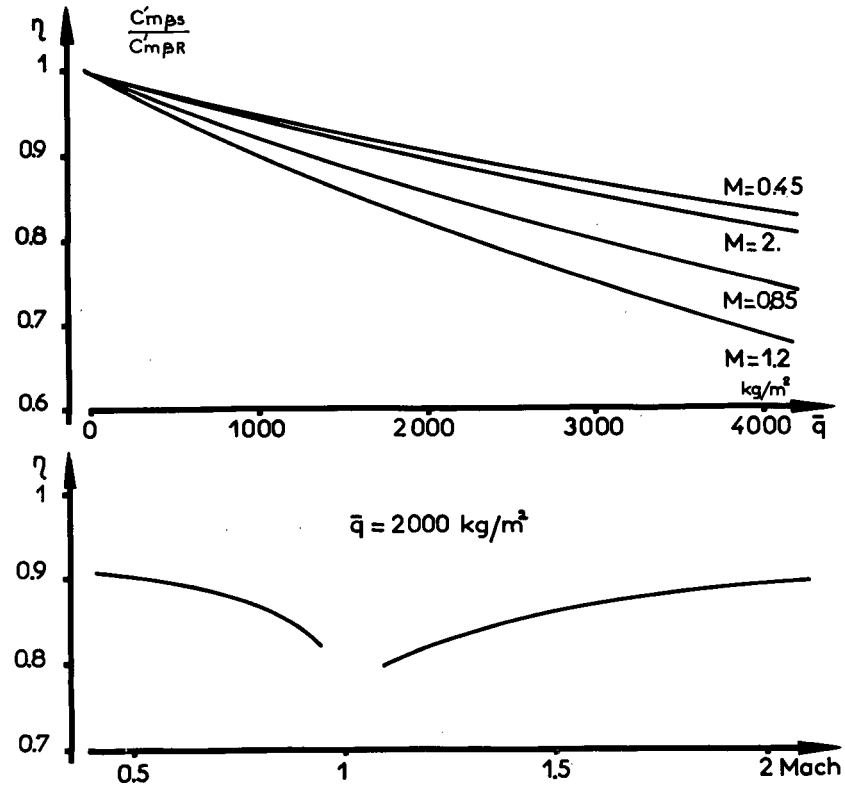
Planche 3



COEFFICIENT DE MOMENT DE TANGAGE A INCIDENCE NULLE

PITCHING-MOMENT COEFFICIENT AT ZERO INCIDENCE

Planche 4



EFFICACITE EN MOMENT DE TANGAGE
BRAQUAGE DE L'ELEVON INTERNE

PITCHING-MOMENT EFFICIENCY DUE TO
INNER ELEVON ROTATION

Planche 5

COMBINED EFFECTS OF AEROELASTIC COUPLING AND AERODYNAMIC INTERFERENCE BETWEEN TWO LIFTING SURFACES (WING-TAIL, TANDEM WINGS) ON THE LONGITUDINAL STABILITY

by

P.G. Hamel

Technische Universität Braunschweig
Lehrstuhl für Angewandte Mechanik
33 Braunschweig
Germany

SUMMARY

An analytical procedure is presented determining unsteady aerodynamic effects on the longitudinal stability of flexible flight vehicles with tandem lifting surfaces. Circulation lag effects associated with rapid changes of lift and downwash time-delay effects, due to the front wing wake that does not affect the rear wing lift instantaneously, are considered.

The root locus technique is applied to demonstrate how strongly the downwash time-delay destabilizes the first bending mode of the fuselage for certain tandem configurations. The time vector concept is being used for physical interpretation. The classical root locus method is extended to find exact critical values for downwash time-delays and to determine the behavior of the root locus in the vicinity of a critical point.

Some general results and root sensitivity investigations are given to show how structural and aerodynamic parameters and their variations influence the stability roots of the aeroelastic coupled system.

SOMMAIRE

Une méthode analytique est présentée permettant la détermination des effets non-stationnaires aérodynamiques sur la stabilité longitudinale des aéronefs flexibles à surfaces portantes en tandem. On y considère des effets de circulation retardée associés aux changements rapides des effets de portance et de temps mort à déflexion qui sont dus au sillage de l'aile avant qui n'affecte pas instantanément la portance de l'aile arrière.

La méthode de lieu de racines est appliquée pour démontrer l'influence fortement déstabilisante de la déflexion du temps mort sur la première oscillation de flexion du fuselage pour certaines configurations en tandem. Pour l'explication physique on se sert de la méthode des vecteurs de temps. On étend la méthode classique de lieu de racines de manière à ce qu'elle permet de trouver des précises valeurs critiques pour le temps mort à déflexion et de déterminer le comportement du lieu de racines au voisinage d'un point critique.

On présente quelques résultats généraux et des essais de sensibilité des racines pour démontrer l'influence des paramètres structuraux et aérodynamiques et leurs variations sur les racines de stabilité des systèmes aéroélastiques accouplés.

LIST OF SYMBOLS

$C(s)$	circulation lag function, Eq. (4)
$C_{L\alpha}$	lift curve slope
K	constant; root locus gain, Eq. (11)
l	reference length (body length)
m	mass of flight vehicle
p_j	j-th pole of the C(s)-function; j-th parameter
s	reduced complex frequency (Laplace variable) (= $\sigma \pm i\omega$) *)
S	reference surface (overall wing surface)
t^*	aerodynamic time constant (= l/U)
U	reference velocity (steady state velocity)
x	longitudinal coordinate
Δx	effective distance between tandem wings
z_j	j-th zero of the C(s)-function
$\alpha(x,s)$	local effective angle of attack, Eq. (A 4)
$\delta_{ik}^{(A)}$	damping element of the aerodynamic operator matrix, Table 1
$\delta_{ik}^{(A)I}$	interference-damping element of the aerodynamic operator matrix, Table 1
$\partial\epsilon_R/\partial\alpha$	downwash factor at the rear wing
ζ_i	damping ratio (viscous equivalent) of the i-th mode (without aerodynamics)
ζ_B	damping ratio of the first bending mode (without interference aerodynamics)
$\kappa_{ik}^{(A)}$	stiffness element of the aerodynamic operator matrix, Table 1
$\kappa_{ik}^{(A)I}$	interference-stiffness element of the aerodynamic operator matrix, Table 1
μ	flight vehicle relative density (= $2m/\rho Sl$)
μ_i	generalized mass of the i-th mode (= $\int_{(l)} \frac{d\mu}{dx}\phi_i^2(x)\,dx$)
ξ_i, ξ_k	nondimensional generalized coordinate of the i-th and k-th mode respectively (relative to the reference length l)
τ_B	reduced time constant of aerodynamic interference, Eq. (10) *)
τ_P	reduced first order Padé time constant (= $\Delta\tau/2$) *)
$\Delta\tau$	reduced aerodynamic time-delay (= $\Delta t/t^* = \Delta x/l$) *)
$\Delta\tau^*$	critical reduced time-delay, Eq. (A 12) *)
ϕ_i, ϕ_k	normalized mode deflection of the i-th and k-th mode respectively
ϕ_i', ϕ_k'	normalized mode slope of the i-th and k-th mode respectively ($\phi' = l\,d\phi/dx$)
ω_{ni}	reduced undamped natural frequency of the i-th mode (without aerodynamics) *)
ω_{nB}	reduced undamped natural frequency of the first bending mode (without interference aerodynamics) *)
ω^*	critical frequency, Eq. (A 11) *)

Suffixes

F	forward wing station
R	rear wing station
3	first bending mode (i = 3)

*) Stability roots, frequencies and times are expressed nondimensionally with the aerodynamic time constant t^*.

COMBINED EFFECTS OF AEROELASTIC COUPLING AND AERODYNAMIC INTERFERENCE BETWEEN TWO LIFTING SURFACES (WING-TAIL, TANDEM WINGS) ON THE LONGITUDINAL STABILITY

Peter G. Hamel

1. INTRODUCTION

It is well known that the stability and control analysis of large and slender flexible flight vehicles has to consider the rigid body degrees of freedom and flexible degrees of freedom. Overall surveys on this subject have been given for example in the United States by J.B. Rea (1) and in the United Kingdom by A.R. Collar (2) and A.S. Taylor (3).

In the common literature quasi-steady aerodynamics are retained since unsteady aerodynamics due to circulation lag and interference effects are usually omitted as secondary effects. Moreover, there do not exist simple relations between the classic quasi-steady stability derivatives of the general motion of the rigid body and the unsteady flutter derivatives of the harmonic elastic oscillations of the flexible flight vehicle. In the case of quasi-steady aerodynamics, the local aerodynamic lift force occurs in direct proportion to the local normal airstream velocity and is independent of other local events, for instance upstream events.

It is the purpose of this paper to present a simple analytical procedure for determining important unsteady aerodynamic effects on the longitudinal stability of flexible flight vehicles with tandem lifting surfaces. In the development of expressions for the unsteady aerodynamic effects, the growth of the forward wing lift and wake, the time-delay until the rear wing is immersed in the wake created by the forward wing and the lift build-up of the rear wing have to be considered. This aerodynamic problem has firstly been treated by R.T. Jones and L.F. Fehlner (4) for the subsonic case and by M. Tobak (5) for the supersonic case using the concept of indicial aerodynamic functions. B. Laschka (6) uses a different approach to the problem. His calculations are based on the classic Küssner integral equation reflecting the relation between the pressure distribution of a lifting surface and the induced upwash. He comes up with unsteady aerodynamic flutter derivatives for the isolated wings and additional cross derivatives which represent the main interference effect.

2. EQUATIONS OF MOTION IN GENERAL

The linearized equations of motion of the aeroelastic coupled system are represented by a matrix of coefficients multiplying a column vector of normal coordinates ξ_i

$$\left(S_i(s) + A_{ik}(s)\right) \{\xi_i\} = 0. \tag{1}$$

The matrix of coefficients is seperated into a structural operator matrix with the diagonal elements $S_i(s)$ and an aerodynamic operator matrix with the elements $A_{ik}(s)$. Appendix 1 discusses the derivation of Eq. (1) and shows that the structural operator matrix is representing the structure dynamically in its normal modes (inclusively rigid body vertical translation and pitch)

$$S_i(s) = \mu_i(s^2 + 2\zeta_i\omega_{ni}s + \omega_{ni}^2). \tag{2}$$

The aerodynamic operator matrix representing the essential nature of the unsteady airloads and providing aerodynamic coupling among the normal coordinates may be written as

$$A_{ik}(s) = \left(\delta_{ik}^{(A)} + \delta_{ik}^{(A)I}\exp(-s\Delta\tau)\right)s + \kappa_{ik}^{(A)} + \kappa_{ik}^{(A)I}\exp(-s\Delta\tau). \tag{3}$$

The single elements of Eq. (3) are summarized in Table 1. The unsteady aerodynamic effects due to circulation lag are taken into account through aerodynamic transfer functions having the general form

$$C(s) = K \frac{\prod_{j=1}^{m} (s+z_j)}{\prod_{j=1}^{n} (s+p_j)} \tag{4}$$

which can be obtained from the linear Wagner function by using the superposition integral. Compressibility and finite span effects are accounted for by modified forms of the Wagner function or, if unsteady complex flutter derivatives are in hand, by curve fitting procedures in the frequency domain.

The time-delay effect of the forward wing wake is accomplished by the exponential function $\exp(-s\Delta\tau)$ which is formed with an effective distance $\Delta\tau = \Delta x/l$ between the tandem wings. This exponential function needs a simple and suitable series approximation so that the corresponding transcendental matrix of coefficients can be transformed into a n-th order matrix polynomial, whose determinant yields the stability roots. The MacLaurin series expansion of the exponential function does not converge rapidly for large $\Delta\tau$s and both amplitude ratio and phase characteristics do not conform to that required of an ideal time-delay for a large frequency. Superior results are obtained using the linear non-minimum phase transfer function (Padé-approximation)

$$\exp(-s\Delta\tau) = \frac{f(s\Delta\tau)}{f(-s\Delta\tau)} \tag{5}$$

having the same order numerator and denominator

$$f(s\Delta\tau) = 1 - \frac{1}{2} s\Delta\tau + \ldots + \frac{(-1)^n}{(2n)!} (s\Delta\tau)^n. \tag{6}$$

In order to visualize the effect of unsteady interference between two lifting surfaces, system analysis techniques have been applied to the dynamics of the first (uncoupled) bending mode of a hypothetical flexible flight vehicle (7), assuming that the rigid body modes are not disturbed. This can be accomplished by a stability augmentation system preventing rigid body vertical translation and pitching and being insensitive to elastic oscillations by constraining the altitude and rate sensors from picking up the bending motions (8).

Within the following notations, the index "3" stands for the first bending mode, indicating that the indices "1" and "2" have been retained for rigid body translation and pitch. The Laplace variable s, time-delay $\Delta\tau$ and the stability roots are expressed nondimensionally with the body length l and the free-stream velocity V.

3. SYSTEM ANALYSIS VIEWS OF UNSTEADY INTERFERENCE EFFECTS ON THE FIRST BENDING MODE

3.1 Root Locus Method

The manupulations in this section are based on the fact that the effect of interference can be represented by a system with feedback. Thus, using Eq. (1), (2) and (3) and Table 1, the equation of motion of the first (uncoupled) bending mode (i = k = 3) can be rewritten in the root locus form (lift lag effects neglected)

$$1 + K \exp(-s\Delta\tau) \frac{s+1/\tau_B}{s^2+2\zeta_B\omega_{nB}s+\omega_{nB}^2} = 0. \tag{7}$$

The complex pole (ζ_B, ω_{nB}) embodies the first bending mode without interference effects (i.e. only the aerodynamics of the isolated wings are considered) where

$$\zeta_B \omega_{nB} = \zeta_3 \omega_{n3} + \frac{1}{2} \frac{\delta_3^{(A)}}{\mu_3} \tag{8}$$

and

$$\omega_{nB}^2 = \omega_{n3}^2 + \frac{1}{2} \frac{\kappa_3^{(A)}}{\mu_3}. \tag{9}$$

The real zero

$$1/\tau_B = \frac{\kappa_3^{(A)I}}{\delta_3^{(A)I}} = - \frac{\phi_3'(x_F)}{\phi_3(x_F)} \tag{10}$$

takes the effect of steady interference into account and is defined by the mode shape characteristics at the front wing station. The aerodynamic time-delay effect, which is mainly responsible for the unsteady interference, is represented by the exponential function $\exp(-s\Delta\tau)$. The root locus gain

$$K = - \frac{\partial \varepsilon_R}{\partial \alpha} C_{L\alpha}(x_R) \frac{\phi_3(x_F)\phi_3(x_R)}{\mu_3} \tag{11}$$

is proportional to the quasi-steady downwash factor $\partial\varepsilon_R/\partial\alpha$ at the rear wing.

The root loci of Figure 1 correspond to the hypothetical flexible flight vehicle (7) having a symmetrical mode shape $\phi_3(x)$, an effective time-delay $\Delta\tau = \Delta x/l = 0{,}6$, identical lift curve slopes of the forward and rear wing and a reduced natural frequency $\omega_{n3} = 1$. The corresponding root locus in the case of steady interference ($\exp(-s\Delta\tau) = 1$) is shown for variable gain by the dashed lines. It should be noted that the root locus branch starts at the complex pole (ζ_B, ω_{nB}) for $K = 0$ (zero downwash intensity) and terminates at the real zero ($1/\tau_B$) and at infinite for $K = \infty$ (infinite downwash intensity). In the case of unsteady interference the exponential function is represented by the first order Padé-approximation

$$\exp(-s\Delta\tau) \simeq - \frac{s - 1/\tau_P}{s + 1/\tau_P} \qquad (\omega\Delta\tau < 2) \tag{12}$$

where

$$1/\tau_P = 2/\Delta\tau \tag{13}$$

yielding an additional non-minimum phase pole/zero combination which generates a strong destabilizing phase shift of the complex root locus branch (solid line). The real root locus branch is due to the Padé-approximation and gives no physical meaning.

In Figure 2 the influence of different forward wing positions on the stability of the first bending mode is illustrated. In order to approach the problem in a reasonable manner, the simplifying assumption of a frozen mode shape was made. It is clearly evident that an increase of the effective distance between the tandem wings, characterized by increasing $\Delta\tau$, aggravates the destabilizing effect of unsteady interference.

3.2 Time Vector Method

A second attempt to visualize the unsteady interference mechanism is shown in Figure 3, where the time vector concept of K.H. Doetsch (9) has been applied. Starting again from the point where no interference effects are considered (point (O)), we obtain an isosceles triangle representing the one-degree-of-freedom oscillatory body bending mode. The triangle is characterized by the generalized mass term μ_3, damping term δ_3 and stiffness term κ_3, where the two latter terms have structural and aerodynamic components, thus,

$$\delta_3 = \delta_3^{(s)} + \delta_3^{(A)} = \mu_3 2\zeta_B \omega_{nB} \tag{14}$$

and

$$\kappa_3 = \kappa_3^{(s)} + \kappa_3^{(A)} = \mu_3 \omega_{nB}^2 . \tag{15}$$

The structural components can be seen in direct relation to Eq. (8) and (9) :

$$\delta_3^{(s)} = \mu_3 2\zeta_3 \omega_{n_3} \tag{16}$$

and

$$\kappa_3^{(s)} = \mu_3 \omega_{n_3}^2 . \tag{17}$$

For simplicity the normal coordinate of the first bending mode ξ_3 was taken to be unity.

Avoiding unnecessary details, we merely observe from Figure 3 that in the case of steady interference (point (1)) the additional interference components $\kappa_3^{(A)I}$ and $\delta_3^{(A)I}$ increase the virtual stiffness and damping of the isosceles triangle. Considering now the case of unsteady interference (point (2)), it is apparent that the time-delay effect yields a phase lag of the two interference components creating a strong reduction of the virtual damping term through the $\kappa_3^{(A)I}$-component, thus destabilizing the bending mode.

3.3 Extended Root Locus Method

This section gives a brief outline of an extended root locus method to find not only exact values for critical time-delays, but also to determine the behavior of the root locus in a neighborhood of a critical point (7).

A typical behavior of the root locus on the imaginary axis is sketched in Figure 4. In contrary to differential-difference equations with constant coefficients, like we know them from control systems with time-delay, the coefficients in our problem depend on the forward wing position and thus on the actual time-delay between the tandem wings. It is apparent from the foregoing (Eq. (7)) that the transcendental characteristic equation has the form

$$G(\Delta\tau, s) = G_1(\Delta\tau, s) - G_2(\Delta\tau, s)\, \exp(-s\Delta\tau) = 0 \tag{18}$$

where

$$G_2(\Delta\tau, s) = -K(s + 1/\tau_B) \tag{19}$$

and

$$G_1(\Delta\tau, s) = s^2 + 2\zeta_B \omega_{nB}\, s + \omega_{nB}^2 . \tag{20}$$

The critical value of $\Delta\tau$ is the value for which the characteristic equation has at least one pair of pure imaginary roots. Denoting the critical value of $\Delta\tau$ and the pure imaginary root as $\Delta\tau^*$ and $s = i\omega^*$ respectively we obtain from Eq. (18) the magnitude condition

$$\left|\frac{G_1(\Delta\tau, i\omega^*)}{G_2(\Delta\tau, i\omega^*)}\right| = 1 \qquad (21)$$

and the modified angle condition

$$\text{Arg}\left[\frac{G_1(\Delta\tau, i\omega^*)}{G_2(\Delta\tau, i\omega^*)}\right] = -\omega^* \Delta\tau^* \quad . \qquad (22)$$

The magnitude condition yields in combination with Eq. (19) and (20) the critical frequency ω^* as a function of $\Delta\tau$. From the modified angle condition in combination with Eq. (19) and (20) and the result of the magnitude condition, we obtain a critical time-delay $\Delta\tau^*$ as a function of the actual time-delay $\Delta\tau$. The complete derivation is summarized in Appendix 2.

The relief map (Figure 5) shows how in the case of the hypothetical flexible flight vehicle ($\omega_{n_3} = 0{,}5$) the computed critical time-delay depends on the actual time-delay, if the downwash intensity $\partial\varepsilon_R/\partial\alpha$ is varied. It is evident that the computed critical time-delay is only existent, if it equals the actual time-delay. This constraint is satisfied on the line of intersection of the $\Delta\tau^*$-surface and the $\Delta\tau$-plane. It is readily seen from the present example that the system is unstable, if the actual time-delay is greater than the computed critical value.

In order to determine the stability of a system with a parameter $\Delta\tau$, where the characteristic root, $s = \sigma + i\omega$, cannot be expressed explicitly in an analytical form, it is necessary to find not only critical values $\Delta\tau^*$ of the parameter, but also how a root locus intersects the imaginary axis, at a critical point, with a variation of the parameter. Thus, we need some information about the variation of the damping σ and the frequency ω at a critical point. The derivatives of σ and ω with respect to $\Delta\tau$ can be determined by differentiating the real and imaginary part of the aforeshown transcendental characteristic equation G(s) with respect to $\Delta\tau$.

For small time-delay variations $\Delta\Delta\tau$ we obtain the damping and frequency variations at a critical point from

$$\Delta\sigma^* = \left(\frac{d\sigma}{d\Delta\tau}\right)^* \Delta\Delta\tau \qquad (23)$$

and

$$\Delta\omega^* = \left(\frac{d\omega}{d\Delta\tau}\right)^* \Delta\Delta\tau \qquad (24)$$

where $(d\sigma/d\Delta\tau)^*$ and $(d\omega/d\Delta\tau)^*$ are the first order damping and frequency derivatives at a critical point. Figure 4 shows schematically how the root locus behavior can be determined at a critical point using Eq. (23) and (24) . A more detailed description of this procedure is given in Reference (7).

The final results have been plotted for the present example in Figure 6 as resultant vectors for a time-delay increment of $\Delta\Delta\tau = 0.05$. Simultaneously, Figure 6 shows a set of curves which has been computed using the first order Padé-approximation for the exponential time-delay function. It is apparent that in the critical points frequency and slope of the root loci are in very good agreement. In addition, the time-delay sensitivities given by the length of the resultant vectors go conform with the sensitivities on the set of curves.

4. NUMERICAL RESULTS IN GENERAL

Thus far, we have discussed the time-delay effect on the uncoupled first bending mode. In the next figure (Figure 7), the effect of aeroelastic coupling between the rigid body mode and the first bending mode considering the unsteady interference effects is demonstrated. The quasi-steady downwash factor was assumed to be 0.3. Again, the forward wing position, thus $\Delta\tau$, was varied along the root loci. The effect of reducing the stiffness or frequency ω_{n_3} on the stability roots is clearly evident, as the two modes approach each other. As a consequence of aeroelastic coupling, the first bending mode is throughout stabilized, where, on the contrary, the rigid body mode (short period mode) is throughout destabilized. Critical areas of the rigid body mode are apparent for medium and large tandem wing distances with the possibility of oscillatory and aperiodic instabilities, the latter being a result of reduced static stability.

Figure 8 gives an idea of the influence of the downwash intensity on the stability roots. The destabilizing effect of increasing tandem wing distances on the bending mode gives a verification of the results obtained with the system analysis methods. The rigid body mode shows a broad area of oscillatory instability.

The importance of lift lag effects is studied in Figure 9. The lift lag functions of the forward and rear wing are based on data of R.T. Jones (10) assuming incompressible aerodynamics. It is readily seen that the unsteady aerodynamics have only a small destabilizing influence on the low-frequency rigid body mode. Looking now at the first bending mode, we can notice a somewhat greater effect of lift lag. Alternatively, if finite span effects are considered, the significance of unsteady lift is attenuated. It is not the purpose of the present results to draw general conclusions about the effect of unsteady lift on the stability roots. It is merely suggested to include lift lag effects in a complete treatment of dynamic stability analysis, if frequencies of the rigid body mode and the lowest-frequency elastic modes are reasonable close.

5. ROOT SENSITIVITY TO PARAMETER VARIATIONS

In aeroelastic coupled systems, the effects of single system parameters on the stability roots are often obscure. Improvements in system characteristics obtained by modifying these parameters are therefore difficult to assess. With particular reference to the numerical results of the previous section there is the uncertainty how the variations of single aerodynamic or structural parameter affect the stability roots of the rigid body and first bending mode. Such parameter variations are of importance, for instance, if the steady reference flight condition is changed.

The characteristic equation of the aeroelastic coupled system can be written as

$$G(s,\underline{p}) = \left| S_i(s,\underline{p}^{(s)}) + A_{ik}(s,\underline{p}^{(A)}) \right| = 0 \tag{25}$$

where $\underline{p}$ is a vector with components p_j. Each such component is a variable parameter of the system. As can be seen from Eq. (25) the parameter vector $\underline{p}$ is composed of structural and aerodynamic parts $\underline{p}^{(s)}$ and $\underline{p}^{(A)}$ respectively. If s_i is a first order root of Eq. (25) the total derivative of G will be

$$dG = \frac{\partial G}{\partial s_i} ds_i + \sum_j \frac{\partial G}{\partial p_j} dp_j = 0. \tag{26}$$

Solving Eq. (26) for ds_i we obtain the differential increment in the i-th system root to the differential changes of the system parameters

$$ds_i = \sum_j S^i_{p_j} dp_j \tag{27}$$

where

$$S^i_{p_j} = -\left(\frac{\partial G}{\partial p_j}(s) \Big/ \frac{\partial G}{\partial s}(s) \right)_{s=s_i} \tag{28}$$

is defining the parameter sensitivity of the i-th system root to the j-th system parameter. In (7) the parameter sensitivities to the aerodynamic parameter vector

$$\underline{p}^{(A)} = \begin{pmatrix} C_{L\alpha}(x_F) \\ C_{L\alpha}(x_R) \\ \partial \epsilon_R / \partial \alpha \\ \rho \end{pmatrix} \tag{29}$$

and to the structural parameter vector

$$\underline{p}^{(s)} = \begin{Vmatrix} \phi_3\ (x_F) \\ \phi_3\ (x_R) \\ \phi_3'(x_F) \\ \phi_3'(x_R) \\ \omega_{n3} \end{Vmatrix} \tag{30}$$

are evaluated by employing parameter influence coefficients. These coefficients are represented by the partial derivatives of the elements standing in the system determinant (Eq. (25)) with respect to the parameters.

In the final four figures the root variations of the present hypothetical flexible flight vehicle ($\omega_{n3} = 0.5$, $\partial\varepsilon_R/\partial\alpha = 0.3$) to relative parameter variations $\Delta p_j/p_j$ are plotted vectorially. Figure 10 and Figure 11 demonstrate the effect of aerodynamic parameter variations on the rigid body and first bending mode, whereas the effect of structural parameter variation is evident from Figure 12 and Figure 13. It is readily seen from the two latter figures that only small variations from the assumed mode shape of the first bending mode may influence the stability roots of the aeroelastic coupled system quite considerably.

6. CONCLUSIONS

It was the purpose of this paper to give the analyst-designer, in the preliminary design stage, some feel and an analytical procedure for determining combined effects of aeroelastic coupling and unsteady aerodynamics on the longitudinal stability of flexible flight vehicles with tandem lifting surfaces. Some of the main conclusions which emerge from this review are as follows:

(a) Unsteady interference effects between tandem lifting surfaces must not be overlooked as secondary aerodynamic effects.

(b) System analysis methods can be used to study such aerodynamic interference effects.

(c) An increases of the effective distance between tandem wings has a strong destabilizing effect on the first bending mode.

(d) An increase of the downwash intensity aggravates the effect of point (c).

(e) As a consequence of aeroelastic coupling, the first bending mode is throughout stabilized, where on the contrary, the rigid body mode (short period mode) is throughout destabilized.

(f) Lift lag effects can be easily included in the dynamic stability analysis by introducing linear aerodynamic transfer functions.

(g) Root sensitivity investigations are attractive for inspecting the effect of structural and aerodynamic parameter variations on the stability roots.

REFERENCES

1. Rea, J.B. — Aeroelasticity in Stability and Control. Wright Air Development Center, WADC TR 55-173, 1957.

2. Collar, A.R. — Aeroelasticity-Retrosped and Prospect. J. Roy. Aeron.Soc., Vol. 63, January 1959, pp. 1-15.

3. Taylor, A.S. — The Present Status of Aircraft Stability Problems in the Aeroelastic Domain. J. Roy. Aeron. Soc., Vol. 63, April 1959, pp. 227-238.

4. Jones, R.T. Fehlner, L.F. — Transient Effects of the Wing Wake on the Horizontal Tail. NACA TN 771, August 1940.

5. Tobak, M. — On the Use of the Indicial Function Concept in the Analysis of Unsteady Motions of Wings and Wing-Tail Combinations. NACA Rep. 1188, 1954.

6. Laschka, B. Schmid, H. — Unsteady Aerodynamic Forces on Coplanar Lifting Surfaces in Subsonic Flow (Wing-Horizontal Tail Interference). Jahrbuch der WGLR, 1967, pp. 211-222.

7. Hamel, P.G. — Beiträge zum Einfluß der Tragflächen-Interferenz auf die Längsbewegung eines flexiblen Flugkörpers. To be published in Jahrbuch der WGLR, 1968.

8. Andeen, R.E. — Self-Adaptive Autopilots. Space-Aeronautics, Vol. 43, April 1965, pp. 46-52.

9. Doetsch, K.H. — The Time Vector Method for Lateral Stability Investigations. R.A.E. TR 67200, August 1967.

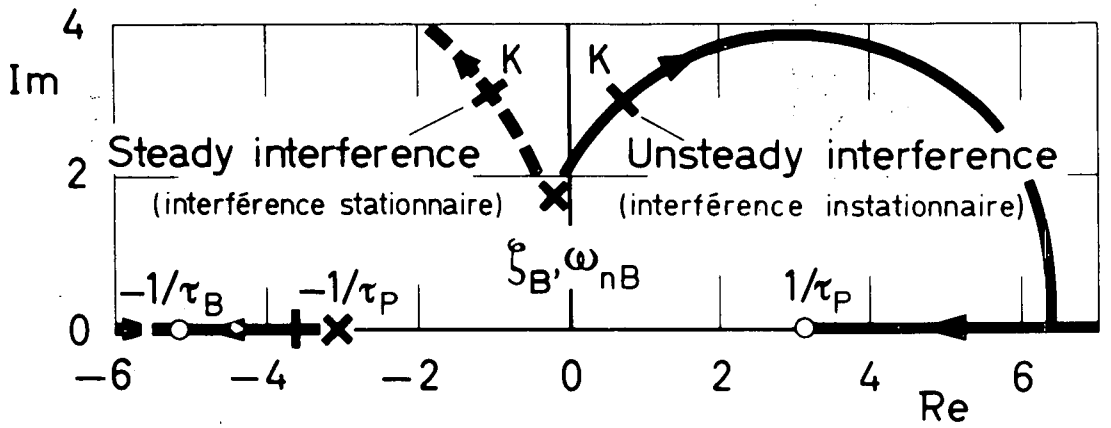
10. Fung, Y.C. — An Introduction to the Theory of Aeroelasticity. John Wiley and Sons, New York,1955, p. 344.

TABLE 1

Matrix Elements of the Aerodynamic Operator Matrix $A_{ik}(s)$

$\delta_{ik}^{(A)}$	$C_{L\alpha}(x_F)C(x_F,s)\phi_i(x_F)\phi_k(x_F) + C_{L\alpha}(x_R)C(x_R,s)\phi_i(x_R)\phi_k(x_R)$	isolated forward wing isolated rear wing	Mode deflection effect
$\kappa_{ik}^{(A)}$	$- C_{L\alpha}(x_F)C(x_F,s)\phi_i(x_F)\phi_k'(x_F) - C_{L\alpha}(x_R)C(x_R,s)\phi_i(x_R)\phi_k'(x_R)$	isolated forward wing isolated rear wing	Mode slope effect
$\delta_{ik}^{(A)I}$	$-\frac{\partial\varepsilon_R}{\partial\alpha} C(x_F,s)\phi_k(x_F)C_{L\alpha}(x_R)C(x_R,s)\phi_i(x_R)$	forward wing interference effect on rear wing	Mode deflection effect
$\kappa_{ik}^{(A)I}$	$\frac{\partial\varepsilon_R}{\partial\alpha} C(x_F,s)\phi_k'(x_F)C_{L\alpha}(x_R)C(x_R,s)\phi_i(x_R)$		Mode slope effect

$C(x_F,s) = C(x_R,s) = 1$: Lift lag effects neglected



$$K = -\frac{\partial \varepsilon_R}{\partial \alpha} C_{L\alpha}(x_R) \frac{\varphi_3(x_F)\varphi_3(x_R)}{\mu_3}$$

$$1/\tau_B = -\varphi_3'(x_F)/\varphi_3(x_F)$$

$$1/\tau_P = 2/\Delta\tau$$

$$\omega_{n3} = 1.0$$

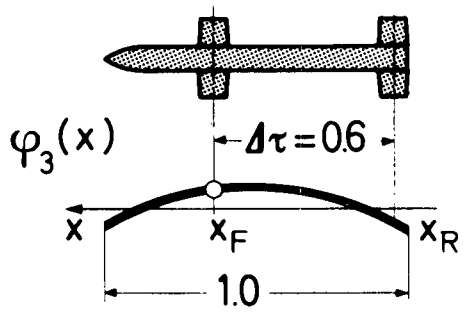
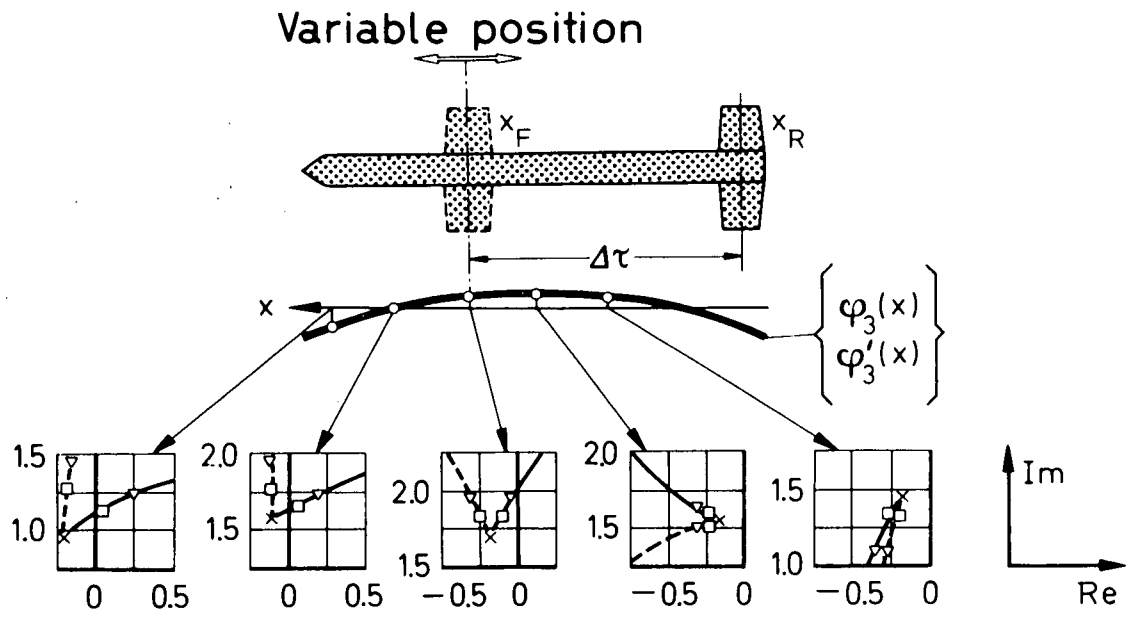


Fig. 1 Downwash effect on the first bending mode (root locus method)



---- steady interference

——— unsteady interference

$\omega_{n3} = 1.0$

	×	□	▽
$\partial\varepsilon_R/\partial\alpha$	0	1/2	1

Fig. 2 Downwash effect on the first bending mode

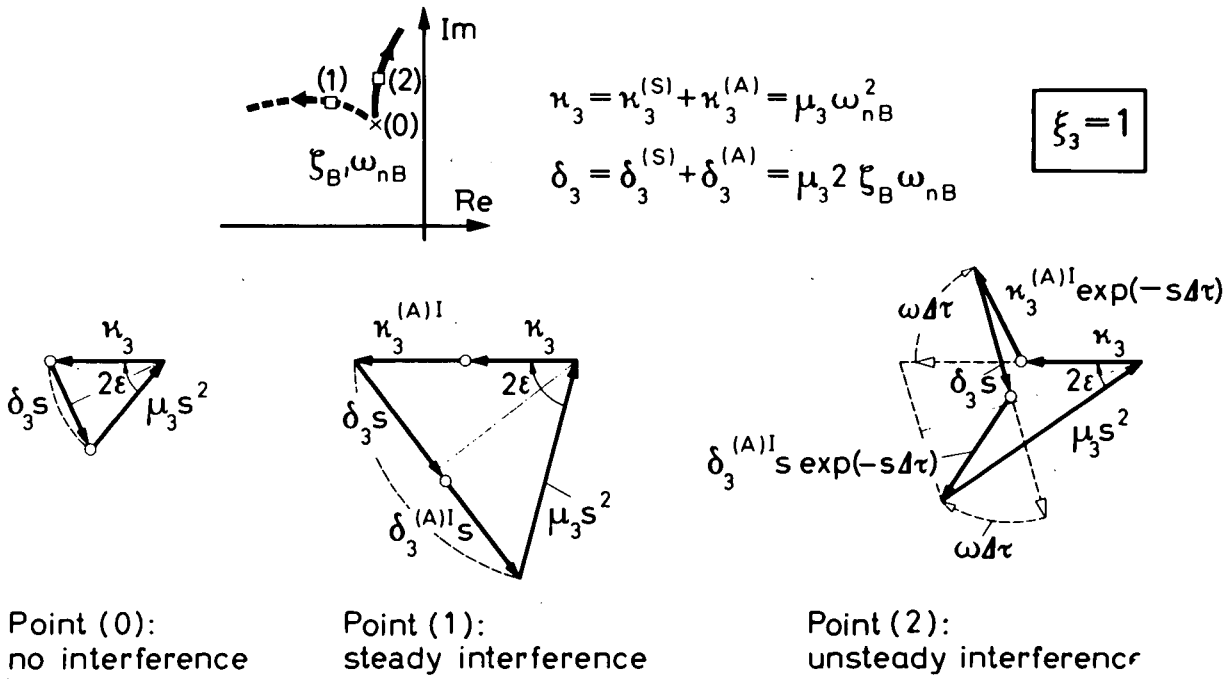


Fig. 3 Time vector diagrams of the first bending mode

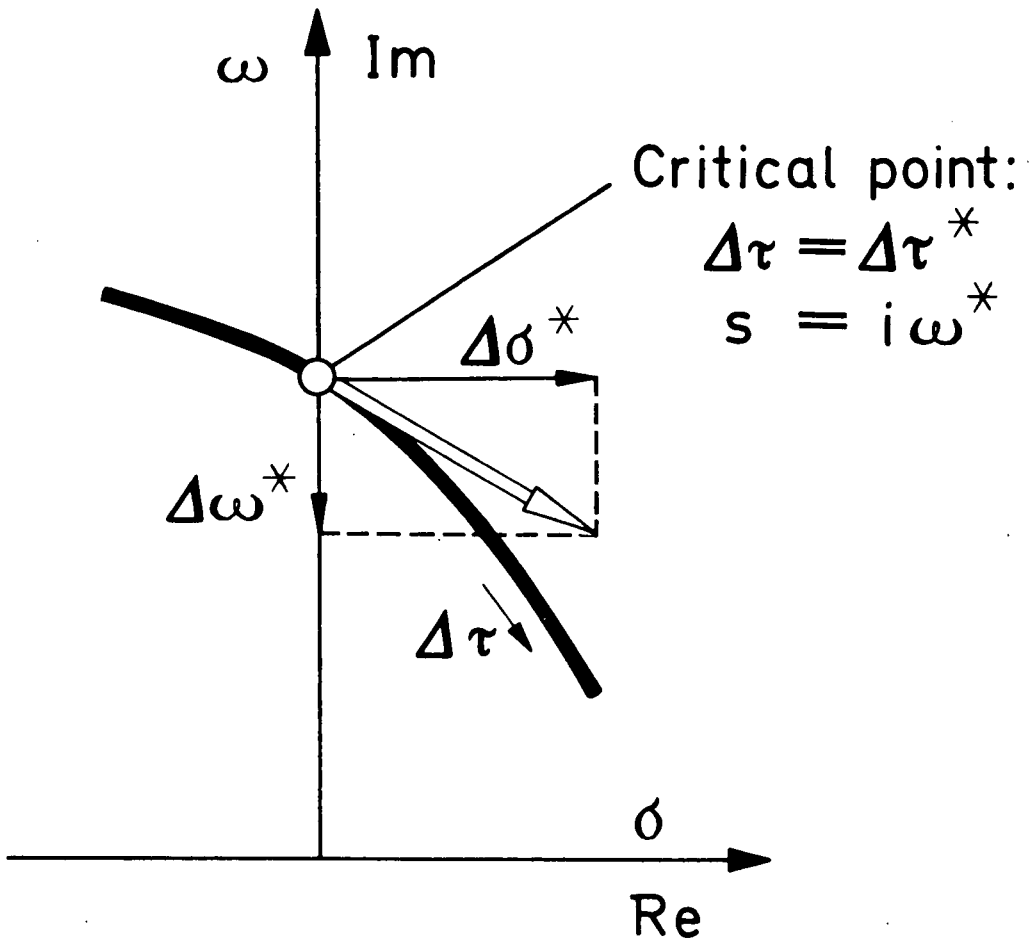


Fig. 4 Root locus behavior in the vicinity of a critical point

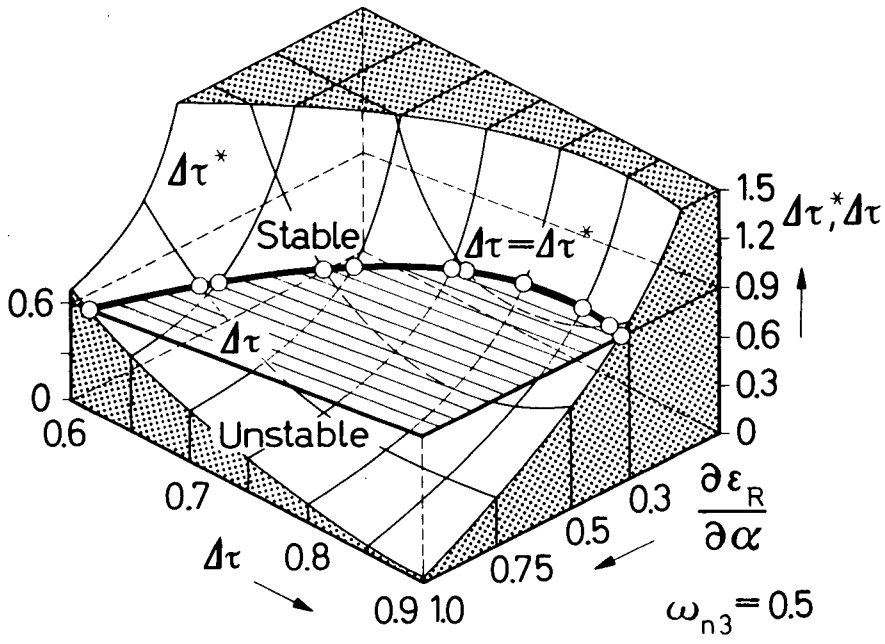


Fig. 5 Determination of critical time-delays

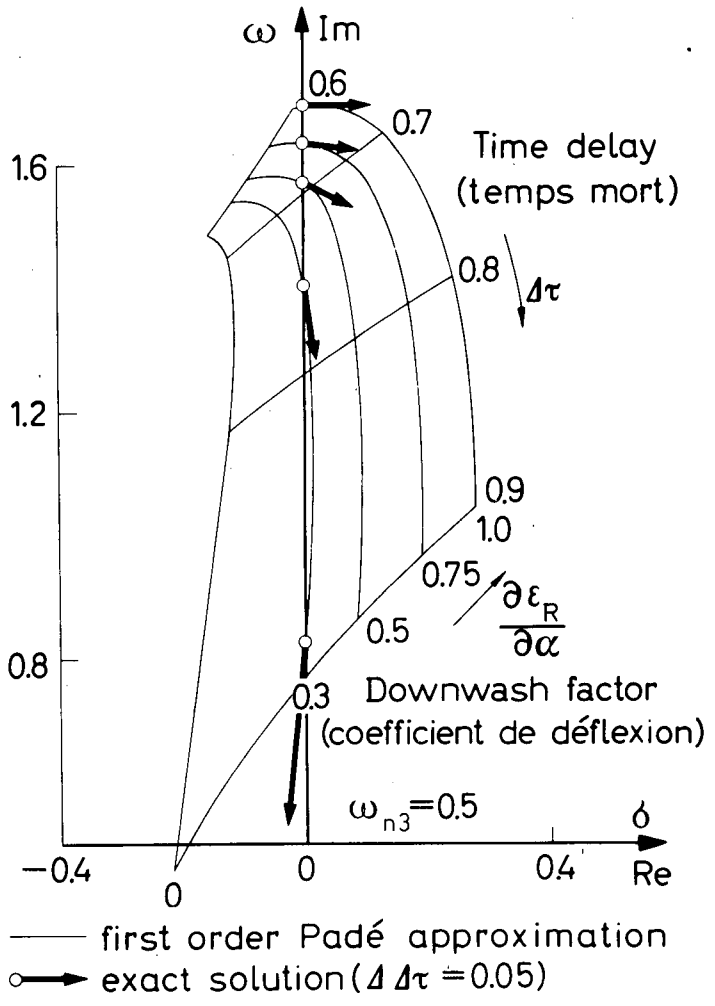


Fig. 6 Computed root loci in the vicinity of critical points

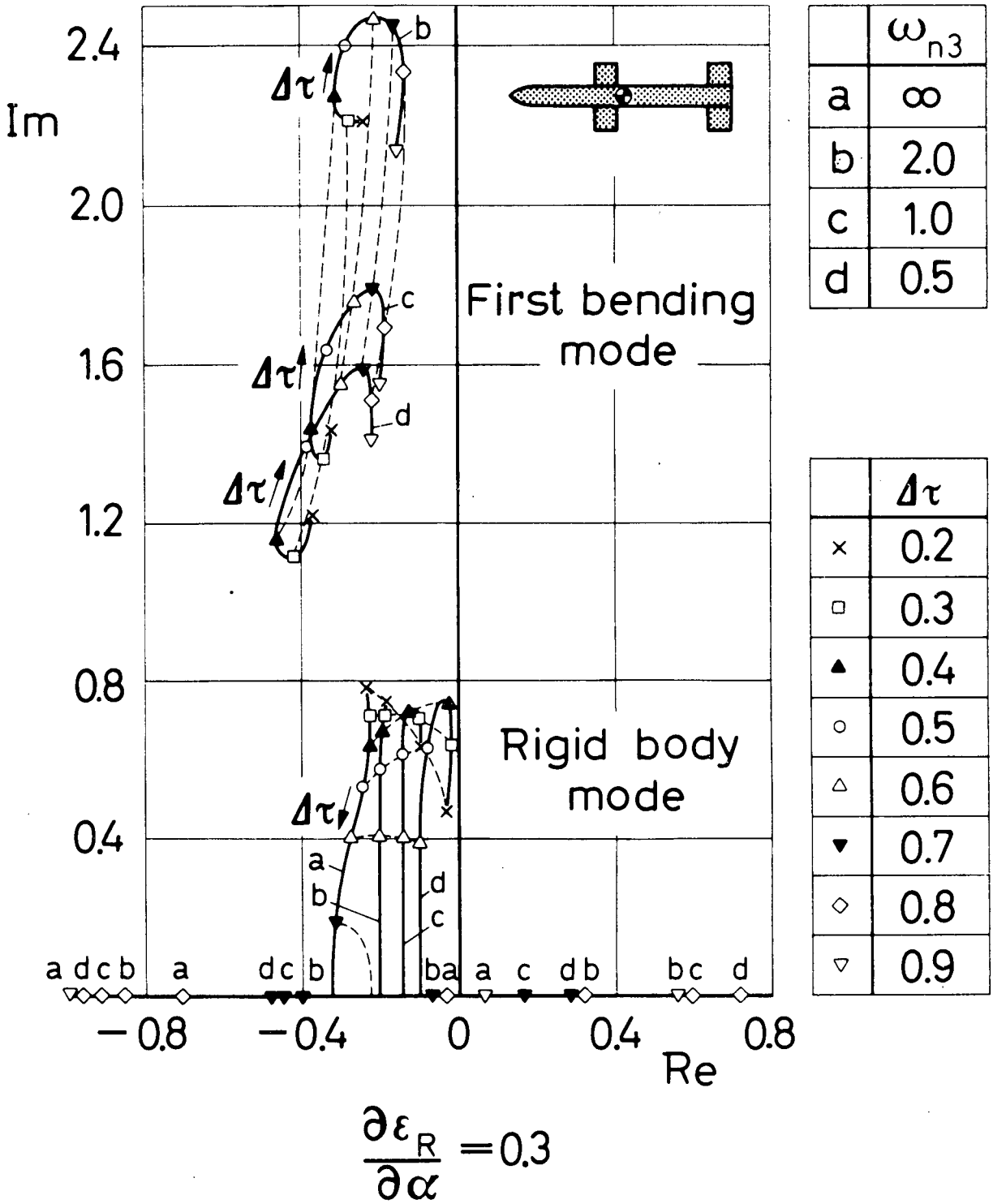


Fig. 7 Stability roots of the aeroelastic coupled system

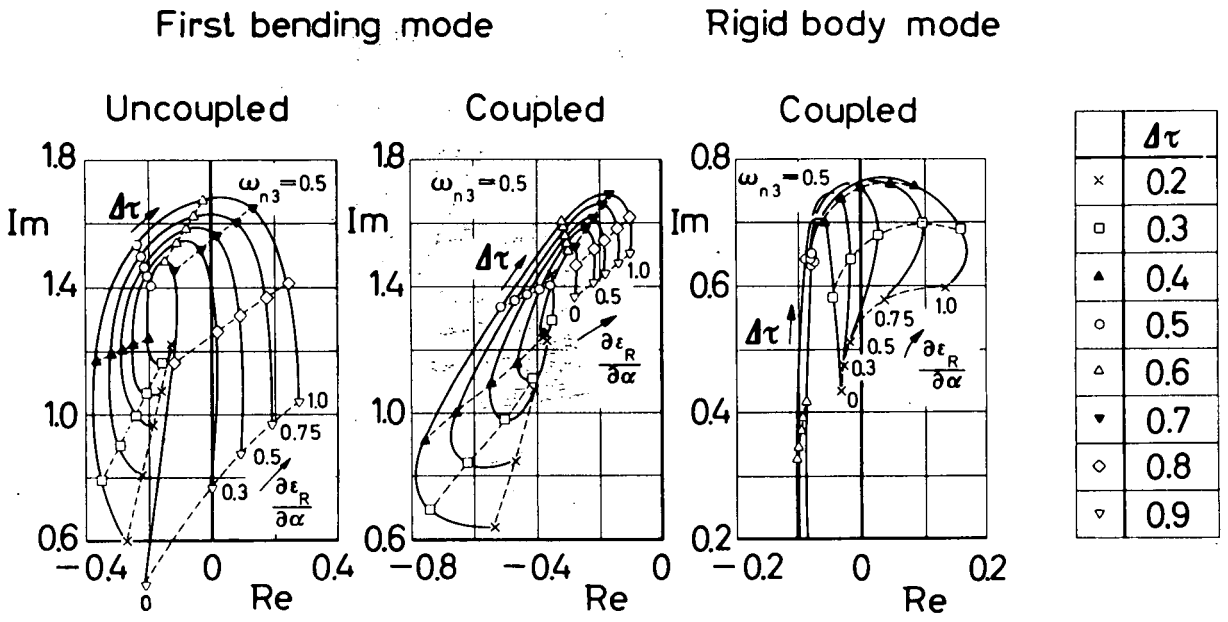


Fig. 8 Influence of downwash intensity on the stability roots

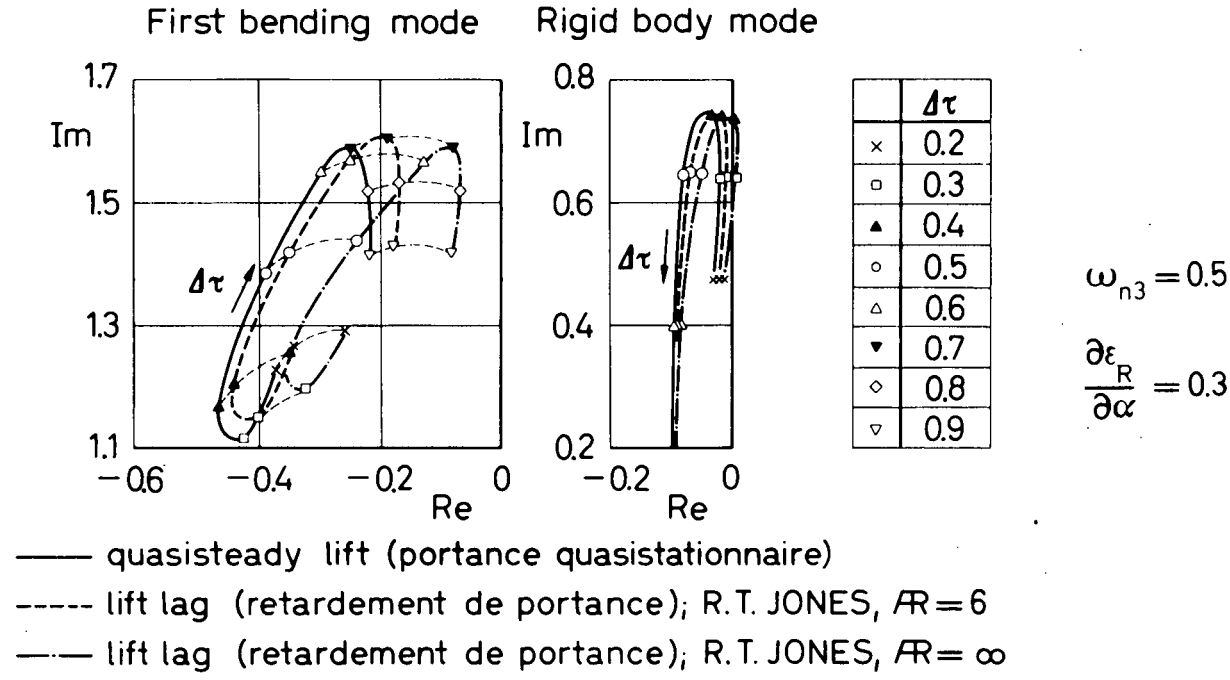


Fig. 9 Lift lag effects on the stability roots

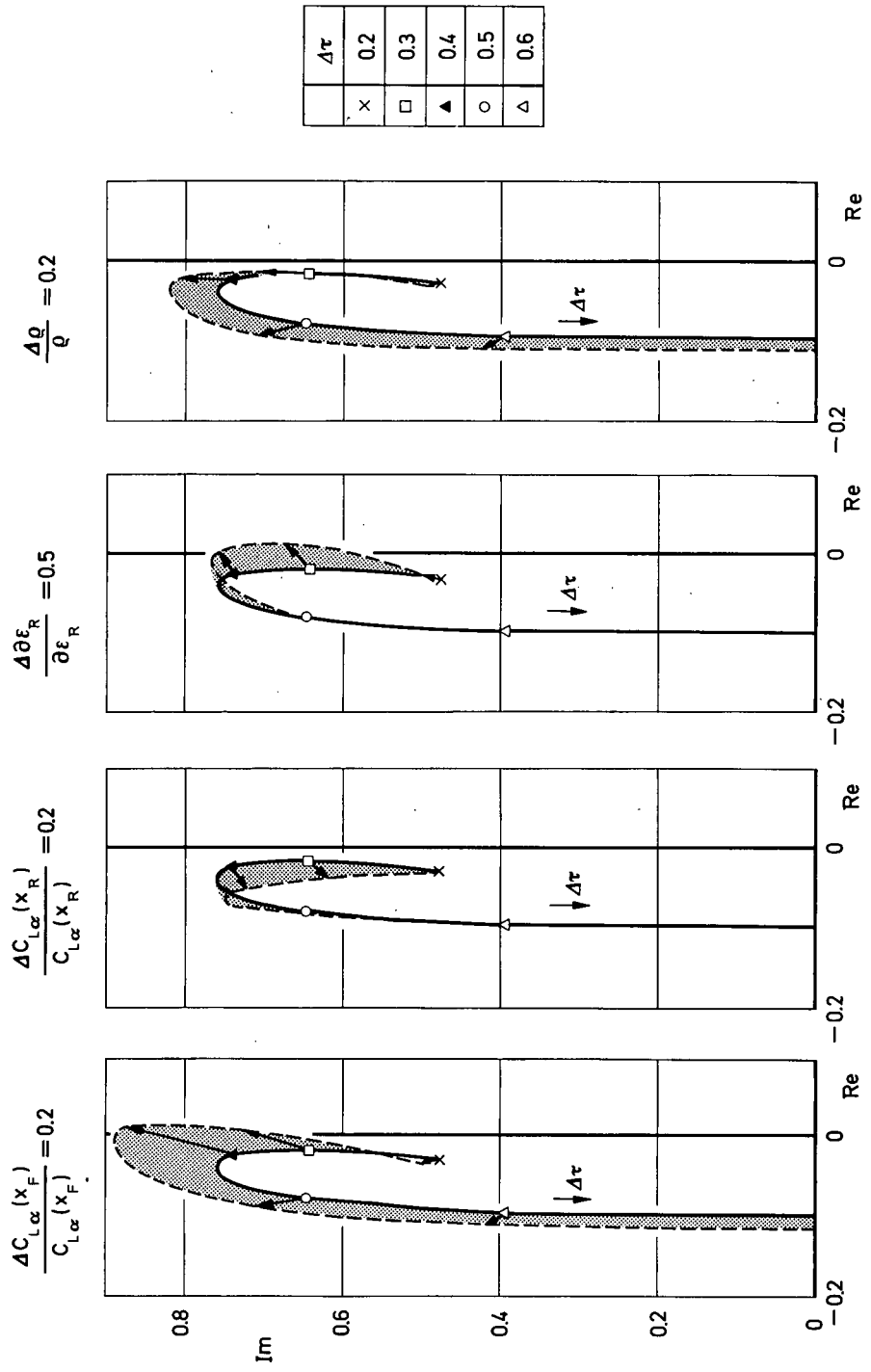


Fig. 10 Effect of aerodynamic parameter variations on the rigid body mode

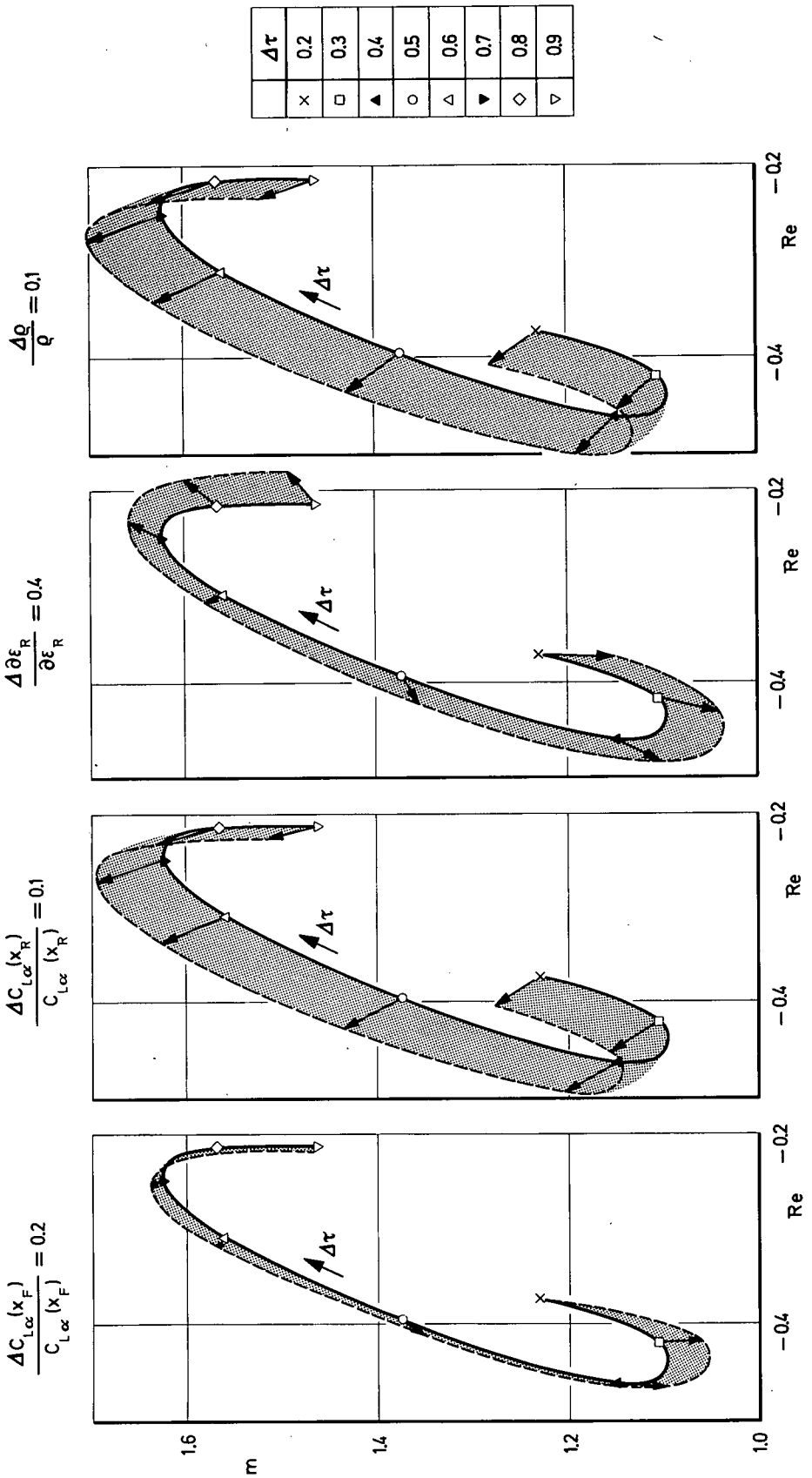


Fig. 11 Effect of aerodynamic parameter variations on the first bending mode

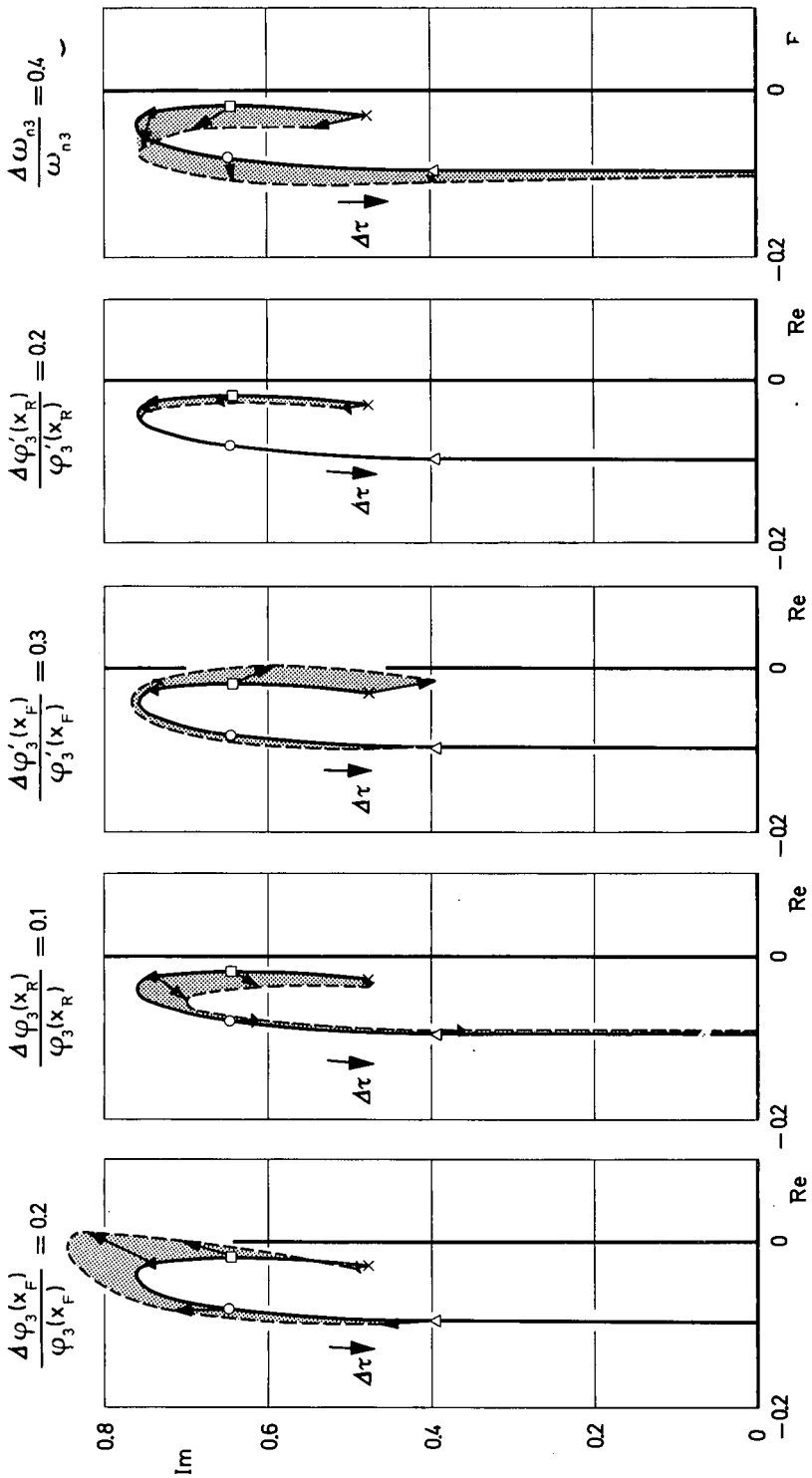


Fig. 12 Effect of structural parameter variations on the rigid body mode

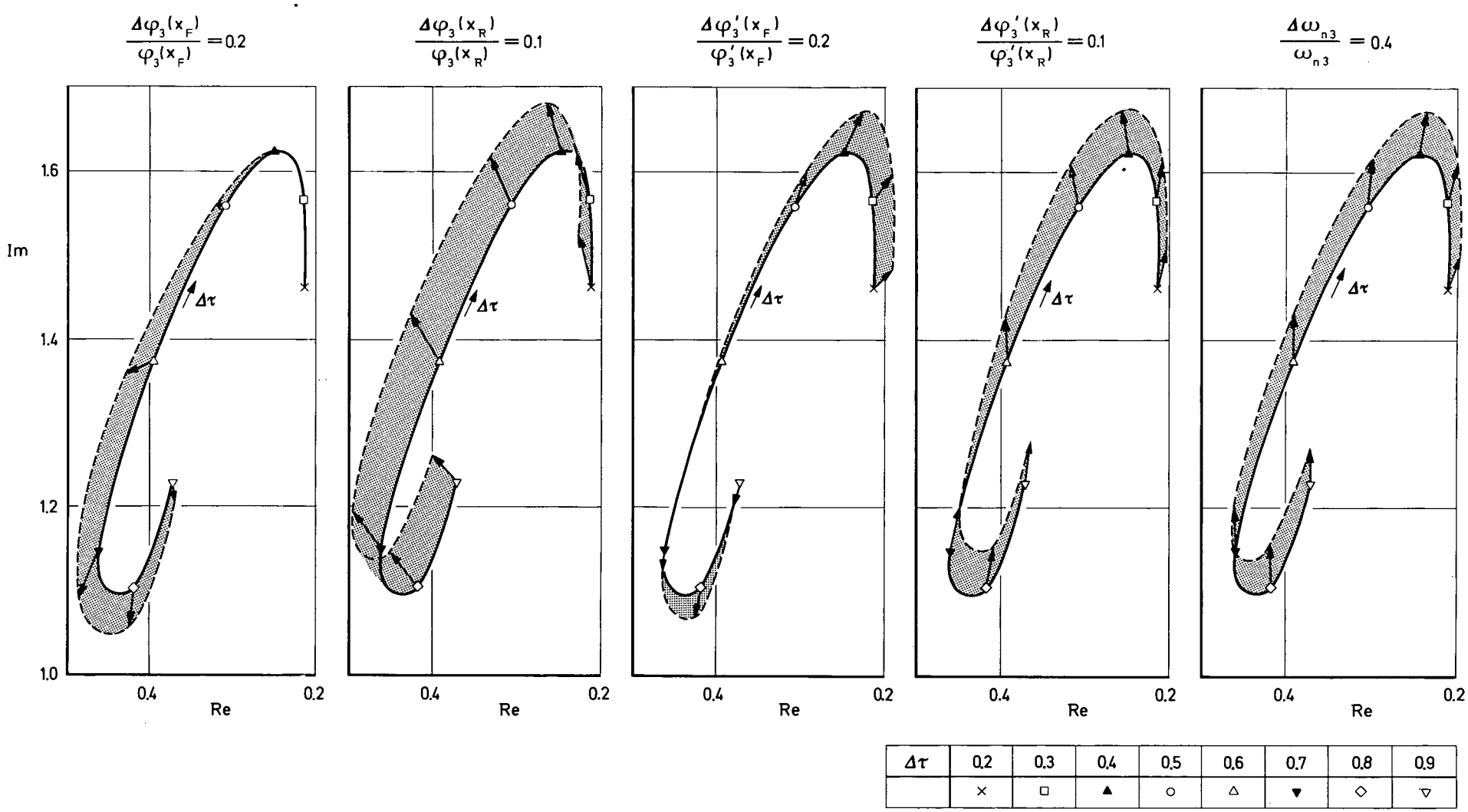


Fig. 13 Effect of structural parameter variations on the first bending mode

APPENDIX 1

Derivation of Equations of Motion

The equations defining the longitudinal motion of a flexible flight vehicle are derived from the motions of the elastic airframe taken as the summation of its rigid body motions and its motions in the natural modes of the free vibration of the structure:

$$\left(S_i(s)\right)\{\xi_i(s)\} = \{F_i(s)\} \qquad (A\ 1)$$

where $S_i(s)$ represents the structural operator of the i-th normal mode, thus,

$$S_i(s) = \mu_i(s^2+2\zeta_i\omega_{ni}s+\omega_{ni}^2).$$

Neglecting spanwise elastic effects the generalized lift force

$$F_i(s) = -\int_{(l)} \left(dC_L(s)/dx\right)\phi_i(x)\,dx \qquad (A\ 2)$$

is determined by the running airload

$$dC_L(s)/dx = d/dx\left(C_{L\alpha}(x)C(x,s)\alpha(x,s)\right) \qquad (A\ 3)$$

which provides aerodynamic coupling among the normal coordinates ξ_i as the local effective angle of attack

$$\alpha(x,s) = \sum_{k=1}^{n} \phi_k(x)s\xi_k(s) - \sum_{k=1}^{n} \phi_k'(x)\xi_k(s) \qquad (A\ 4)$$

includes contributions from all the degrees of freedom. The C(x,s)-function in Eq.(A3) takes lift lag effects into account and has the character of a linear aerodynamic transfer function.

In the case of tandem lifting surfaces a two-point-lift assumption is established for convenience and simplicity. Thus, the portion of unsteady lift at the forward wing is

$$C_L(x_F,s) = C_{L\alpha}(x_F)C(x_F,s)\alpha(x_F,s)$$

whereas the portion of unsteady lift at the rear wing is affected by the unsteady interference component of the forward wing

$$C_L(x_R,s) = C_{L\alpha}C(x_R,s)\left(\alpha(x_R,s) - \frac{\partial\varepsilon_R}{\partial\alpha}\,C(x_F,s)\alpha(x_F,s)\exp(-s\Delta\tau)\right).$$

The local effective angles of attack $\alpha(x_F,s)$ and $\alpha(x_R,s)$ are obtained from Eq.(A 4) where in the subsonic case the normalized mode deflections ϕ_k have to be taken at the 3/4 chord station in accordance with the theoretical aerodynamics (Theorem of Pistolesi).

The generalized lift force is written in accordance to Eq. (A 2) as

$$F_i(s) = -C_L(x_F,s)\phi_i(x_F) - C_L(x_R,s)\phi_i(x_R)$$

where the normalized mode deflections ϕ_i have to be taken at the 1/4 chord (subsonic case) or at the 1/2 chord station (supersonic case).

With the forgoing manipulations Eq. (A 1) can be rewritten in the form

$$\left(S_i(s) + A_{ik}(s)\right)\{\xi_i\} = 0 \qquad (A\ 5)$$

where $A_{ik}(s)$ represents the aerodynamic operator

$$A_{ik}(s) = \left(\delta_{ik}^{(A)} + \delta_{ik}^{(A)I}\exp(-s\Delta\tau)\right)s + \kappa_{ik}^{(A)} + \kappa_{ik}^{(A)I}\exp(-s\Delta\tau). \qquad (A\ 6)$$

The single terms of the aerodynamic operator are collected and defined in Table 1.

APPENDIX 2

Determination of Critical Time-Delays

The transcendental characteristic equation of the first bending mode taking unsteady interference effects into account has the form

$$G(\Delta\tau,s) = G_1(\Delta\tau,s)-G_2(\Delta\tau,s)\exp(-s\Delta\tau) = 0 \qquad (A\ 7)$$

where

$$G_1(\Delta\tau,s) = s^2+2\zeta_B\omega_{nB}s+\omega_{nB}^2 \qquad (A\ 8)$$

represents the first bending mode without interference effects and

$$G_2(\Delta\tau,s) = -K(s+1/\tau_B) \qquad (A\ 9)$$

describes the character of steady interference between the tandem wings.

A critical point corresponds to the location of a pure imaginary root $s = i\omega^*$ of the characteristic equation (A 7). Denoting the critical value of the time-delay as $\Delta\tau^*$ the following equation holds if $G_2(\Delta\tau,i\omega^*) \neq 0$:

$$\frac{G_1(\Delta\tau,i\omega^*)}{G_2(\Delta\tau,i\omega^*)} = \exp(-i\omega^*\Delta\tau^*).$$

Hence, $\Delta\tau^*$ and ω^* satisfy the two equations

$$\left|\frac{G_1(\Delta\tau,i\omega^*)}{G_2(\Delta\tau,i\omega^*)}\right| = 1 \qquad \text{(magnitude condition)}$$

and

$$\operatorname{Arg}\left(\frac{G_1(\Delta\tau,i\omega^*)}{G_2(\Delta\tau,i\omega^*)}\right) = -\omega^*\Delta\tau^*. \quad \text{(angle condition)}$$

From Eq. (A 8) and (A 9) we find the complex relation

$$\frac{G_1(\Delta\tau,i\omega^*)}{G_2(\Delta\tau,i\omega^*)} = \frac{(\omega^{*2}-\omega_{nB}^2)/\tau_B-2\zeta_B\omega_{nB}\omega^{*2}}{K(\omega^{*2}+1/\tau_B^2)} - i\omega^*\,\frac{\omega^{*2}-\omega_{nB}^2+2\zeta_B\omega_{nB}/\tau_B}{K(\omega^{*2}+1/\tau_B^2)}. \qquad (A\ 10)$$

The four coefficients ω_{nB}, ζ_B, τ_B and K depend on the mode shape characteristics at the forward wing station x_F and thus on the actual effective time-delay $\Delta\tau = (x_F - x_R)/l$ of the tandem wing system. Hence, the critical frequency ω^* which is determined from the magnitude condition of Eq. (A 10) is a function of the actual time-delay $\Delta\tau$:

$$\omega^*(\Delta\tau) = \omega_o^*\sqrt{1\pm\sqrt{1+\frac{(K/\tau_B)^2-\omega_{nB}^4}{\omega_o^{*4}}}} \qquad (A\ 11)$$

where

$$\omega_o^* = \sqrt{\frac{K^2}{2}+\omega_B^2}$$

describes the critical frequency for the limiting case, that the root locus does not intersect with the imaginary axis, but has its tangent in common with the imaginary axis at a critical point. For $K = 0$ (e.g. $\partial\varepsilon_R/\partial\alpha = 0$) the critical frequency ω^* and the critical frequency of the limiting case ω_o^* reduce to the frequency of the first bending mode without interference effects.

The angle condition of Eq. (A 10) yields the critical time-delay $\Delta\tau^*$ as a function of the actual time-delay $\Delta\tau$:

$$\Delta\tau^*(\Delta\tau) = -\frac{1}{\omega^*}\tan^{-1}\left(-\omega^*\,\frac{\omega^{*2}-\omega_{nB}^2+2\zeta_B\omega_{nB}/\tau_B}{(\omega^{*2}-\omega_{nB}^2)/\tau_R-2\zeta_B\omega_{nB}\omega^{*2}}\right) \qquad (A\ 12)$$

where ω^* is given by Eq. (A 11). The computed critical time-delay $\Delta\tau^*$ is only existant, if it equals the actual time-delay $\Delta\tau$.

THEORETICAL INVESTIGATION OF AEROELASTIC INFLUENCES ON THE LIFT DISTRIBUTION AND THE AERODYNAMIC DERIVATIVES OF SWEPT WINGS AT SYMMETRIC AND ANTISYMMETRIC STATIONARY FLIGHT CONDITIONS

by Dipl.-Ing. W. Schoernack, Dornier GmbH, Germany and
Ing.grad. E. Hässler, Dornier GmbH, Germany

Acknowledgement

We wish to acknowledge the opportunity of publishing this work granted to the authors by the DORNIER GmbH.

We have to acknowledge the permission of demonstrating the results of calculations carried out on the Airbus, which was given to us by DEUTSCHE AIRBUS GmbH.

Our special appreciation for advice, suggestions, and assistance with the theoretical problems involved is due to Mr. F. Sorg, Chief Engineer of the Loads Department of the DORNIER GmbH.

Summary

An analytic solution is given for the calculation of aeroelastic effects on the elastic wing-system. The physical problem is described by matrix-equations, using generalised coordinates.

Whilst the elastic effects are handled by a development according to Ritz, the aerodynamic forces are introduced into the calculation by using Weissinger's lifting line theory.

The analysis results in the determination of the following effects:

Deformations, changes of the angle of attack, positions of the centre of pressure, and distribution of the aerodynamic forces over the wing-span, allowing values and corrections of the total derivatives to be calculated.

Using as an example the A-300 Airbus, a big passenger aircraft just being developed, some applications of the aforementioned method are discussed, as there are:

Calculation of the aeroelastic displacement of the wing aerodynamic centre, determination of aeroelastic reductions of the wing lift gradient, and investigations pertaining to loss or reversal of control surface effectiveness - all aeroelastic influences being considered as a function of airspeed, Mach number and altitude.

Sommaire

L'auteur présentera une solution analytique au calcul des effets aéroélastiques sur un système d'aile élastique. Il décrira le problème physique à l'aide d'équations matricielles, basées sur des coordonnées généralisées.

Alors que les effets élastiques sont traités à l'aide d'un développement de Ritz, les forces aérodynamiques sont introduites dans le calcul à l'aide de la théorie de la ligne portante de Weissinger.

L'analyse permet de déterminer les effets suivants:

- déformations, modifications de l'angle d'attaque, positions du centre de poussée, et répartition des forces aérodynamiques le long de l'envergure de l'aile, permettant de calculer les valeurs et les corrections des dérivées totales.

En prenant pour exemple l'Airbus A-300, un grand avion de transport de passagers actuellement en cours de réalisation, l'auteur examinera certaines applications de la méthode mentionnée plus haut:

Calcul du déplacement aéroélastique de la position du foyer de l'aile, détermination des réductions aéroélastiques du gradient de portance de l'aile, recherches portant sur la perte ou l'inversion de l'efficacité des gouvernes, tous ces effets aéroélastiques étant considérés comme fonction de la vitesse vraie, du nombre de Mach et de l'altitude.

List of symbols

A	total airload acting at the airplane
A_w	airload acting at the wing
a. c.	aerodynamic center
α_{wE}	angle of attack of the airplane's x,y-plane
α_p	section angle of attack
α_T	twist angle of the wing elastic axis
b	span
β	angle of elevator deflection
δ	local deflection
$[E]$	matrix of the influence coefficients of deformation
$E \cdot I$	flexural stiffness of the wing structure
F	wing area
$f_A = \frac{A_w}{A}$	factor considering the wing lift relative to the total lift
f_M	compressibility factor
G	airplane gross weight
$G \cdot I_T$	torsional stiffness of the wing structure
g	acceleration due to gravity
$\gamma = \frac{c_l \cdot l}{2b}$	dimensionless airload acting at a wing segment
H	altitude
K	factor
l	wing chord length
l_a	mean aerodynamic chord of the wing
M	moment, Mach number
m	mass of a wing segment
n	load factor
p	concentrated external load acting at a wing segment
$\varphi_{i,K}$	generalised stiffness coefficient
Q	dynamic pressure
q	amplitude factor attached to the basic modes = generalised coordinate
$[S] = [E]^{-1}$	stiffness matrix
θ	moment of inertia
V	true air speed
x,y,z	system of body axes fixed to the airplane
x'	axis normal to y'
y'	swept elastic axis of the wing
ξ	aileron deflection
$\eta = \frac{y}{b/2}$	dimensionless y-coordinate

Aerodynamic coefficients

c_l	local lift coefficient
c_L	total lift coefficient
c_m	local moment coefficient
ω	angular velocity
$\dot{\omega}$	angular acceleration

Indices

α	due to an angle of attack
B	Bending
D	damping in roll
i	index of the selected basic mode (generalised coordinate) and the corresponding quantities
j	index of spanwise station, indes of the wing segment and the corresponding quantities
l	due to airloads
m	due to masses
n	number of basic modes
o	due to an angle of attack $\alpha = 0$
R	due to fuselage and tail
r	index of rigid condition
res	resultant quantity
T	torsion, refers to tailplane
v	due to aeroelastic deflection
W	refers to wing
1	refers to a unity condition
*	refers to the basic modes associated with antisymmetric conditions (only Chapter 2.2.8)

Matrix symbols

$[\ ]$	rectangular matrix
$\{\ \}$	vector, column matrix
$\widetilde{\ \ }$	row matrix
$\overline{[\ ]}$	transposed matrix
$[\ ]^{-1}$	inversed matrix
$[\diagdown]$	diagonal matrix

1. Introduction

1.1 Applicability of the method

The method to be shown here gives an analytical approximative solution to calculate the aeroelastic twist of swept wings, and the corresponding lift distribution about span.

It is possible to investigate arbitrary stationary flight load cases, namely symmetric and asymmetric cases. Furthermore the control effectiveness and the speed of control reversal as well as aerodynamic coefficients for the flexible aircraft can be determined.

1.2 Historical remarks

The reason to develop this analytical method was the necessity to get quantitative answers about aeroelastic effects for wings with considerable sweep. At the beginning there was only the tendency to calculate correct lift distributions about span. It is evident that with these lift distributions and the respective deflections further important results can be obtained by this method:

So, it is possible to calculate the control effectiveness, the speed of control reversal and divergence, and certain aerodynamic coefficients with consideration of aeroelastic effects, as the lift curve slope and the position of the wing aerodynamic center, which influence to a great extent stability and manoeuvrability.

2. Description of the method

2.1 Assumptions and conditions

2.1.1 Elastic model

In order to represent the elastomechanical properties of a wing a simplified elastic model is adopted for the load-carrying wing structure, which is represented in Fig. 1 by the spars. Instead of the swept-back spars a straight flexural torsional beam is assumed in extension of one spar, running through the whole span, (hatched in Fig. 1). This beam symbolised by its elastic axis is supported statically determined on two supports for bending loads (acting as bending moment Mx'). These supports represent the wing-fuselage joint, transmitting to the fuselage structure the loads acting on the wing. For torsional loads (acting as moment My') the spar is fixed either in the wing-fuselage attachment or in the plane of symmetry.

Because of these conditions there is no elastic coupling between flexion and torsion. As it is furthermore possible, to split up all loading cases occuring on a wing into a symmetric and an antisymmetric part, the problem can be reduced to the investigation of one half of the wing.

The most important requirement to be met by the model is:

The deflections outside the fuselage (i. e. the supports) shall represent as correctly as possible the true deformations.

At a glance, this simplified elastic model seems to be justified only for unswept wings. A swept wing, however, represented by its elastic axis, can be replaced as well by this model, provided the boundary conditions in the plane of symmetry can be satisfied. This premise guarantees the deflections of a straight beam about span, as assumed with our model, to be equal to those of a beam mirrored in the plane of symmetry.

These conditions can be met for the swept wing shown in Fig. 1 with the following assumptions, considering the basic load components separately:

1. in the case of "symmetric bending" a remaining moment My is balanced in the plane of symmetry,
2. in the case of "antisymmetric bending" the system is balanced without additional forces,

3. in the case of "symmetric torsion" the external moments are balanced by the supports; this means that there are no torsional deflections between the supports,

4. in the case of "antisymmetric torsion" a remaining moment Mx is balanced in the plane of symmetry.

Cases 2 and 3 contain no special conditions, and an explanation is to be given for cases 1 and 4:

Strictly speaking, these conditions are not formally satisfied in the above required form, since actually there does not exist a one-dimensional beam, and therefore the remaining forces are reacted in the central portion of the two spars or in the wing-fuselage attachment. It can be expected that this error affects the deflections very little and by correcting the flexural and torsional stiffnesses in the area of the central wing part and the wing-fuselage attachments the real deformations can be approximated still better.

The conditions, which characterise the usual design of an unswept central wing part, can be realised with sufficient exactness using the same means.

2.1.2 Aerodynamic model

The aerodynamic model of the wing, used to calculate the lift distributions about span, is based on Weissinger's lifting line theory. Wings of arbitrary planform and section design can be calculated with the Weissinger method. The dihedral of the wing is neglected.

2.1.3 Special arrangements for the mathematical treatment

The mathematical properties of the method require the lift and the mass distributions about the wing span to be split up into single forces and single masses, and require these lift forces and the mass loads corresponding to the concentrated masses to act at the same spanwise stations respectively. For this purpose the wing is divided into segments. The airload distribution acting on each segment is concentrated into a single force (Fig. 2a and b) which is applied to the centre of pressure of the respective wing section. The airload couple due to section camber is allowed for by removing the point of the airload application from the section a. c. by a quantity of $(c_m/c_l)_p$ in units of chord length into the centre of pressure. In order to represent the mass distribution the mass of each wing segment is concentrated into the centre of gravity (Fig. 2c), and at this point the corresponding mass loads are applied. The air and mass loads acting at the fuselage and the tail appear as supporting loads and do not affect the considerations.

In addition the following restrictions are involved in the method of calculation: From all loads acting at the system only the z-components are considered, loads acting in the z-or y-direction are neglected.

2. Mathematical derivation

2.2.1 Description of the problem

Let us use for the following considerations an arbitrary stationary flight case of an airplane with given geometric and elastic properties. The flight condition is determinded by the appropriate parameters of air speed, Mach number, gross weight, corresponding mass distribution, and load factor. It is attached to a balanced condition that is shown for the chosen model in Fig. 3.

For reasons of clearness in the graphical illustrations only the load conditions of pure bending are shown. The torsional load cases prove only slightly different from these.

For this balanced condition the airload distributions about span as well as the deflections of the wing have to be determined.

2.2.2 Description of the development according to Ritz

With the symbols δ for elastic deflection and p for external force applied at the spanwise stations mentioned above the law of elasticity gives the following relations between the deformations and the forces, representing the basis of the method:

(1a) $$\{\delta\} = [E] \cdot \{p\}$$

(1b) $$\{p\} = [S] \cdot \{\delta\}$$

with Eqs. (1a) and (1b) to be read as matrix equations.

The above symbols mean:

$\{\delta\}$ = vector of deflections

$\{p\}$ = vector of external forces

$[E]$ = matrix of influence coefficients of deformation

$[S] = [E]^{-1}$ = matrix of stiffnesses.

For the solution of the problem a development according to Ritz is carried out based on the following assumptions:

It is assumed that the elastic deformations $\{\delta\}$ of the system can be approximately represented by a linear superposition of a finite number of basic modes $\{\delta_i\}$ of deflection, the choice of these modes being arbitrary. The only restriction is that the modes have to be linearly independent.

This can be written in matrix equations:

(2a) $$\{\delta\} = \sum_{i=1}^{n} \{\delta_i^*\}$$

(2b) $$\{\delta_i^*\} = \{\delta_i\} \cdot q_i$$

(2c) $$\{\delta\} = [\delta_{j,i}] \cdot \{q_i\}$$

The symbols introduced mean:

n = number of the selected basic modes

$\{\delta_i\}$ = vector of the i^{th} basic mode

$[\delta_{j,i}]$ = matrix of the basic modes

q_i = amplitude factor (weight factor) of the i^{th} mode

$\{q_i\}$ = vector of the generalised coordinates giving the participation of the respective basic modes and the corresponding derived modes

Another fundamental condition for the mathematical treatment is the introduction of the amplitude resp. weight factors q_i of the above mentioned basic modes as generalised coordinates.

Since according to the premises there is no coupling between flexural and torsional deformations, the deflections can be split into a portion resulting from the bending of the elastic axis and a portion resulting from the twist of the elastic axis. For this reason it is possible to make independent arrangements for the basic modes of bending and torsion respectively.

These basic modes are selected in such a way, that the true deformations of the wing can be approximated by a small number of modes. Some of the involved parameters (e.g. the stiffness coefficients) being rather uncertain in most cases, it is not useful, to assume too big a number of modes on the one hand and of spanwise segments on the other hand. It is, however, of greater importance to choose the modes such that the expected boundary conditions are satisfied as much as possible.

For our computer program we selected 6 modes $\{\delta_i\}$ for both flexural and torsional deflections in such a way as to approximate by polygonal curves both the run of the curvature d^2z/dy^2 and the gradient of the twist angle $d\alpha_T/dy$ along span.

For this purpose the basic modes are introduced as triangular functions as outlined in Fig. 4. As it can be seen, these are chosen such that by superposition of these triangular functions, having varying amplitudes, a polygonal curve for each set of modes is obtained. The run of the bending line gradient dz/dy and the run of the twist angle α_T is obtained from these functions by integration. These functions

represent, save a constant factor, the distribution of the section angle of attack about span, which is used directly for the computation of the lift distributions according to Weissinger's method. This will be treated later in greater detail. Another integration of the bending line gradient finally leads to the deflections z(y) of the wing elastic axis. This sort of approximation seemed to us to be sufficiently exact, since the deflections themselves are obtained by integration of the above functions, producing an improvement of the approximation.

The basic modes are, among others, submitted to the following boundary conditions, which can be recognized in Fig. 4.

For the flexural modes:

1. The curvature of the bending line is zero at the wing tip.
2. The curvature between the supports in the fuselage is constant so far as symmetric cases are concerned.
3. The curvature between the supports proceeds linear at zero value in the plane of symmetry so far as antisymmetric cases are concerned.

For the torsional modes:

1. The twist angle α_T equals zero between the supports in all symmetric cases.
2. The gradient of the twist angle $d\alpha_T/dy$ is constant between the supports in the antisymmetric cases.

2.2.3 Introduction of the air and mass loads

The basic modes of the system, just described, represent a deflection of the wing (Eq. 2c). These deflections result in an angle of attack of the wing sections varying about span, which is composed of the respective basic modes of the section angle of attack

$$(2d) \quad \{\delta\} \longrightarrow \{\alpha_\rho\} = \sum_{i=1}^{n} \{\alpha_{\rho i}\} \cdot q_i = [\alpha_{\rho j,i}] \cdot \{q_i\}$$

The spanwise lift distributions can be calculated for these distributions of section angle of attack according to Weissinger's lifting line theory. They are transformed into concentrated single forces p_{vj} at the spanwise stations j. From the point of view of programming technique it was considered convenient to adopt the segmentation required by Weissinger's method for the forces and masses as well. Because of the linear relation between the aerodynamic loads and the angle of attack the airload distribution produced by wing deformation can be composed by matrix operation as follows:

$$(3a) \quad \{p_v\} = \sum_{i=1}^{n} \{p_i\} \cdot q_i = [p_{j,i}] \cdot \{q_i\}$$

This means consequently that each basic mode is connected with a corresponding lift distribution about span, the mode and the lift distribution being linearly dependent.

By introducing the usual dimensionless aerodynamic expressions Eq. (3a) is transformed into

$$(3b) \quad \{p_v\} = \left(\sum_{i=1}^{n} \{\gamma_i\} \cdot q_i\right) \cdot Q \cdot b^2 = Q \cdot b^2 \cdot [\gamma_{j,i}] \cdot \{q_i\}$$

$\{\alpha_\rho\}$ = vector of the total section angles of attack due to aeroelastic deformation

$\{p_v\}$ = vector of the total airloads produced by the aeroelastic deformations

$\{\alpha_{\rho i}\}$ = vector of the section angles of attack associated with the basic mode

$\{p_i\}$ = vector of the airloads associated with the i^{th} mode

$\alpha_{\rho j,i}$ = section angle of attack at the j^{th} spanwise station associated with the i^{th} mode

$p_{j,i}$ = airload at the j^{th} spanwise station associated with the i^{th} mode

Q = dynamic pressure

b = span

$\gamma_{j,i}$ = dimensionless airload at the j^{th} spanwise station associated with the i^{th} mode with

$$(3c) \qquad \gamma_j = \int_{(\Delta(\frac{2y}{b}))_j} \gamma' \cdot d(2y/b) \qquad \text{with } (3d) \quad \gamma'_{(\frac{2y}{b})} = \frac{(c_L \cdot l)_{(\frac{2y}{b})}}{2b}$$

After introducing the airloads produced by the wing deformations the airloads associated with the non-deformed airplane have to be derived. For the flexible airplane a load case can be expressed as a superposition of a basic condition "rigid airplane" with an additional condition "additional aeroelastic effects".

It has to be noted here, that the aeroelastic properties have reactions on the condition "rigid airplane". So, the angle of attack and the air loads occurring with the airplane assumed rigid in a flight case with identical parameters, except the above mentioned, do not equal the corresponding values of the basic condition "rigid airplane" of the airplane assumed flexible.

The basic condition "rigid airplane" is represented by its airload and massload distributions about the wing span $\{p_{lr}\}$ and $\{p_m\}$ respectively, and can be expressed by matrix operation:

$$(4) \qquad \{p_r\} = \{p_{lr}\} + \{p_m\}$$

the airload portion can be divided into 2 parts

$$(5) \qquad \{p_{lr}\} = \{p_o\} + \{p_\alpha\}$$

First the airloads shall be considered:

The airload distribution for an airplane assumed rigid resulting from zero angle of attack of the x,y-plane - i.e. $\alpha_{WE} = 0$ - is designated $\{p_o\}$, the airload distribution resulting from an angle of attack $\alpha_{WE} = \alpha$ is designated $\{p_\alpha\}$. According to Eq. (3b) we can write:

$$(6) \qquad \{p_o\} = \{\gamma'_o\} \cdot Q \cdot b^2$$

The dimensionless airload distribution $\{\gamma_o\}$ thus results from the incidence of the wing relative to the x,y-plane on the one hand and from the design geometric and aerodynamic twist of the wing sections about span on the other hand.

The airload distribution for an angle of attack $\alpha = \alpha_{WE}$ constant about span can be written

$$(7) \qquad \{p_\alpha\} = \{\gamma'_{\alpha=1}\} \cdot \alpha \cdot Q \cdot b$$

At last the mass forces have to be considered. They can be written without difficulties:

$$(8) \qquad \{p_m\} = \{n_j \cdot g \cdot m_j\}$$

n_j is the local load factor at the spanwise stations j. It is constant about span for all symmetric load cases and linearly variable about span for all asymmetric load cases.

2.2.4 Establishing of the system of equations

Having introduced all existing external loads these can be collected as follows:

$$(9) \qquad \{p\} = \{p_o\} + \{p_\alpha\} + \{p_m\} + \{p_v\}$$

The right hand side substituded by Eqs. (6), (7), (8) and (3b) Eq. (1b) can be changed into

$$(10)\quad \{p\} = Q \cdot b^2 \left(\{\gamma_0\} + \{\gamma_{\alpha=1}\} \cdot \alpha + [\gamma_{j,i}]\{q_i\}\right) + \{n \cdot g \cdot m\} = [S] \cdot \{\delta\}$$

The vector $\{\delta\}$ represents, as explained earlier, the wanted total deformations of the system, which have been approximated by superposition of the basic modes (s. Eq. 2c).

With this Eq. (10) can be transformed:

$$(11)\quad Q \cdot b^2 \cdot \left(\{\gamma_0\} + \{\gamma_{\alpha=1}\}\alpha + [\gamma_{j,i}]\{q_i\}\right) + \{n \cdot g \cdot m\} = [S][\delta_{j,i}]\{q_i\}$$

The system of equations written in the form of the matrix equation (11) contains beside the wanted vector $\{q_i\}$ one more wanted parameter, namely the angle of attack α_{WE} of the whole airplane. In order to include α in the equations (11) a complete reorganization of the equations would have been necessary including an additional physical condition for α. This showed to be unfavorable and for this reason an other way was chosen to eliminate α :

The system of equations (11) was split up into two systems, the one containing the portions independent of the angle of attack

$$(11a)\quad Q \cdot b^2 \cdot \left(\{\gamma_0\} + [\gamma_{j,i}] \cdot \{q_{i_0}\}\right) + \{n \cdot g \cdot m\} = [S] \cdot [\delta_{j,i}] \cdot \{q_{i_0}\}$$

the other dealing with the α-dependent portions:

$$(11b)\quad Q \cdot b \cdot \alpha \cdot \left(\{\gamma_{\alpha=1}\} + [\gamma_{j,i}] \cdot \{q_{i_{\alpha=1}}\}\right) = [S] \cdot [\delta_{j,i}] \cdot \{q_{i_{\alpha=1}}\} \cdot \alpha$$

(11a) can be transformed into

$$(12a)\quad Q \cdot b^2 \{\gamma_0\} + \{n\ g\ m\} = \left([S] \cdot [\delta_{j,i}] - Q \cdot b^2 [\gamma_{j,i}]\right) \cdot \{q_{i_0}\}$$

In the same manner (11b) into

$$(12b)\quad \alpha \cdot Q \cdot b^2 \{\gamma_{\alpha=1}\} = \left([S] \cdot [\delta_{j,i}] - Q \cdot b^2 [\gamma_{j,i}]\right) \cdot \{q_{i_{\alpha=1}}\} \cdot \alpha$$

2.2.5 Description of the stiffness coefficients

At this point it is necessary to consider more closely the representation of the elastic properties of the system by the stiffness matrix $[S]$.

The computation of this matrix is a complicated and tedious work with the possibility of mistakes and errors and accuracy problems. These disadvantages can be avoided by transforming the stiffness matrix $[S]$ into the matrix of generalised stiffnesses $[\gamma_{ik}]$ corresponding to the introduced generalised coordinates. This matrix is obtained by the following operation

$$(13)\quad [\gamma_{ik}] = \overline{[\delta_{j,i}]} \cdot [S] \cdot [\delta_{j,i}]$$

the quantity $\overline{[\delta_{j,i}]}$ representing the transposed matrix $[\delta_{j,i}]$

The coefficients γ_{ik} of this matrix can be expressed by the following integrals:

For the flexural modes:

$$(14a)\quad \gamma_{ik} = \int_{b/2} M_{\beta i} \cdot d\left(\frac{dz}{dy}\right)_k = \int_{b/2} M_{\beta i} \cdot \left(\frac{d^2 z}{dy^2}\right)_k \cdot dy$$

with $M_{\beta i} = \left(\frac{d^2 z}{dy^2}\right)_i \cdot E \cdot I$ we obtain from Eq. (14a)

(14b) $$\gamma_{ik} = \int_{b/2} E \cdot I_{(y)} \cdot \left(\frac{d^2 z}{dy^2}\right)_i \cdot \left(\frac{d^2 z}{dy^2}\right)_k \cdot dy$$

Analogous for the torsional modes:

(15a) $$\gamma_{ik} = \int_{b/2} M_{T_i} \cdot d\alpha_{T_k} = \int_{b/2} M_{T_i} \cdot \left(\frac{d\alpha_T}{dy}\right)_k \cdot dy$$

with $M_{T_i} = \left(\frac{d\alpha_T}{dy}\right)_i \cdot G \cdot I_T$ we obtain from Eq. (15a)

$$\gamma_{ik} = \int_{b/2} G \cdot I_T \cdot \left(\frac{d\alpha_T}{dy}\right)_i \cdot \left(\frac{d\alpha_T}{dy}\right)_k \cdot dy$$

With the quantities $\frac{d^2 z}{dy^2}$ and $\frac{d\alpha_T}{dy}$ respectively representing the basic modes these integrals can be determined easily, provided the flexural and the torsional stiffness about span is known.

Since the modes appearing in the integral expressions exist only about a limited spanwise segment, the matrix $[\gamma_{ik}]$ is not fully occupied. It contains values different from 0 only in the diagonal row and their neighbouring rows.

With the coefficients themselves resulting from integration no accuracy problems are to be expected. With this preparation we are able to continue in the derivation of the equation systems.

2.2.6 General solution of the system of equations

By multiplying Eqs. (12a) und (12b) from the left with the transposed matrix of deflections $[\delta_{j,i}]$ one gets

(16a) $$Q \cdot b^2 \cdot \overline{[\delta_{j,i}]} \cdot \{\gamma_{i0}\} + \overline{[\delta_{j,i}]} \cdot \{n \cdot g \cdot m\} = \left(\overline{[\delta_{j,i}]} \cdot [S] \cdot [\delta_{j,i}] - Q \cdot b^2 \cdot \overline{[\delta_{j,i}]} \cdot [\gamma_{j,i}]\right) \cdot \{q_{i_0}\}$$

(16b) $$Q \cdot b^2 \cdot \overline{[\delta_{j,i}]} \cdot \{\gamma_{\alpha=1}\} \cdot \alpha = \left(\overline{[\delta_{j,i}]} [S] [\delta_{j,i}] - Q \cdot b^2 \cdot \overline{[\delta_{j,i}]} \cdot [\gamma_{j,i}]\right) \{q_i\}_{\alpha=1} \cdot \alpha$$

According to Eq. (13) the term $\overline{[\delta_{j,i}]}\,[S]\,[\delta_{j,i}]$ can be replaced by the generalised stiffness matrix of the elastic system $[\gamma_{ik}]$.

Now (16a) und (16b) can be solved for $\{q_i\}$

(17a) $$\{q_{i_0}\} = \left([\gamma_{ik}] - Q \cdot b^2 \cdot \overline{[\delta_{j,i}]} [\gamma_{j,i}]\right)^{-1} \cdot \left(Q \cdot b^2 \cdot \overline{[\delta_{j,i}]} \{\gamma_{i0}\} + \overline{[\delta_{j,i}]} \cdot \{n \cdot g \cdot m\}\right)$$

(17b) $$\{q_{i_{\alpha=1}}\} = \left([\gamma_{ik}] - Q \cdot b^2 \cdot \overline{[\delta_{j,i}]} \cdot [\gamma_{j,i}]\right)^{-1} \cdot \left(Q \cdot b^2 \overline{[\delta_{j,i}]} \{\gamma_{\alpha=1}\}\right.$$

2.2.7 Solution for a given balanced condition

Eqs. (17a) and (17b) are coupled by the airplane angle of attack α to represent the investigated flight case:

The balanced condition of the symmetrical case is represented by

(18a) $A = n \cdot G$ and

(18b) $A_W = f_A \cdot n \cdot G$

where A = total lift

A_W = wing lift

n = total load factor

G = airplane weight

f_A = correction factor allowing for the lift acting on fuselage and tail.

A_W can be written, using the expressions for the external loads derived in Eq. 21a - c:

$$(19) \quad A_W = f_A \cdot n \cdot G = \alpha (A_{\alpha=1} + A_V \cdot (q_{\alpha=1})) + A_V (q_0) + A_0$$

Hence the angle of attack α can be determined:

$$(20) \quad \alpha = \frac{f_A \cdot n \cdot G - A_V (q_0) - A_0}{A_{\alpha=1} + A_V (q_{\alpha=1})}$$

In Eqs. (19) and (20) the symbols have the following meaning:

$A_{\alpha=1}$ = airload of the rigid wing resulting from $\alpha = 1$ [rad]

$$(21a) \quad A_{\alpha=1} = \underset{\sim}{\tilde{1}} \{\gamma_{\alpha=1}\} \cdot Q \cdot b^2$$

A_0 = airload resulting from the design geometric and aerodynamic twist of the rigid wing

$$(21b) \quad A_0 = \underset{\sim}{\tilde{1}} \{\gamma_0\} \cdot Q \cdot b^2$$

$A_{V(q)}$ = airload produced by the aeroelastic twist, composed of the given basic modes with corresponding amplitude vector $\{q\}$

$$(21c) \quad A_{V(q)} = \underset{\sim}{\tilde{1}} [\gamma_{j,i}] \cdot \{q\} \cdot Q \cdot b^2$$

After evaluating the airplane angle of attack α finally the resulting aeroelastic effects can be calculated with the introduced basic modes and the corresponding quantities:

$$(22) \quad \{q_{res}\} = \alpha \{q_{\alpha=1}\} + \{q_0\}$$

$$(23) \quad \{\delta_{res}\} = [\delta_{j,i}] \cdot \{q_{res}\}$$

likewise the airloads due to twist

$$(24) \quad \{p_{res_V}\} = Q \cdot b^2 \cdot [\gamma_{j,i}] \cdot \{q_{res}\}$$

2.2.8 Special derivation for antisymmetric conditions

With antisymmetric load cases the application of the method is similar to the treatment of symmetric cases.

Analogous to Eq. (17) the twist deformations and loads result from the basic modes - being modified in the region between the supports in the fuselage for antisymmetric cases - and the vectorial solution with the given airload distribution $\{\gamma_1\}$.

$$(25) \quad \{q_1\} = ([\gamma_{i,k}^*] - [\overline{\delta_{j,i}^*}] \cdot [\gamma_{j,i}^*] \cdot Q \cdot b^2)^{-1} \cdot [\overline{\delta_{j,i}^*}] \cdot \{\gamma_1\} \cdot Q \cdot b^2$$

In this equation $\{\gamma_1\}$ represents an airload distribution corresponding to an aileron deflection $\xi = 1$ or a damping in roll with $\omega_x \cdot b/2v = 1$.

The effects caused by the antisymmetric mass forces associated with a rolling accleration $\dot{\omega}_x = 1$ result in

$$(26) \quad \{q_{\dot{\omega}_{x=1}}\} = ([\gamma_{i,k}^*] - [\overline{\delta_{j,i}^*}] \cdot [\gamma_{j,i}^*] \cdot Q \cdot b^2)^{-1} \cdot [\overline{\delta_{j,i}^*}] \cdot [y_j] \cdot \{m_j\}$$

The diagonal matrix $[y_j]$ containing the distances of the mass elements m_j from the roll axis.

With this we obtain the following airload portions:

due to aileron deflection

$$(27) \quad \{p_\xi\} + \{p_{v_\xi}\} = Q \cdot b^2 \cdot (\{\gamma_{\xi\cdot 1}\} + [\gamma^*_{j,i}] \cdot \{q_{\xi\cdot 1}\}) \cdot \xi$$

due to damping in roll $\frac{\omega_x \cdot b}{2v}$:

$$(28) \quad \{p_D\} + \{p_{v_D}\} = Q \cdot b^2 \cdot (\{\gamma_{\frac{\omega_x \cdot b}{2v}\cdot 1}\} + [\gamma^*_{j,i}] \cdot \{q_{\frac{\omega_x \cdot b}{2v}\cdot 1}\}) \cdot \frac{\omega_x \cdot b}{2v}$$

due to mass loads:

$$(29) \quad \{p_{v_m}\} = Q \cdot b^2 \cdot [\gamma^*_{j,i}] \cdot \{q_{\dot\omega_x \cdot 1}\} \cdot \dot\omega_x$$

The rolling moments produced by the above loads are obtained by multiplying from the left hand side Eqs. (30, 31, 32) by the row vector $\widetilde{y_j}$, consisting of the distances of the segment reference points j from the roll axis.

$$(30) \quad M_\xi = \widetilde{y_j} \cdot (\{p_\xi\} + \{p_{v_\xi}\});$$

$$(31) \quad M_D = \widetilde{y_j} \cdot (\{p_D\} + \{p_{v_D}\});$$

$$(32) \quad M_{v_m} = \widetilde{y_j} \cdot (\{p_{v_m}\})$$

The total rolling moment produced by airloads results in

$$(33) \quad M_x = M_\xi + M_D + M_{v_m} = \xi \cdot M_{\xi\cdot 1} + \frac{\omega_x \cdot b}{2v} \cdot M_{D1} + \omega_x \cdot M_{v_{m1}}$$

This moment is balanced by the moment of the mass forces caused by rolling acceleration

$$(34) \quad M_x - \dot\omega_x \cdot \theta_x = 0$$

Now Eq. (33) is introduced into Eq. (34), hence

$$(35) \quad M_{\xi\cdot 1} + \frac{\omega_x \cdot b}{2v} M_{D1} + \dot\omega_x \cdot (M_{v_{m1}} - \theta_x) = 0$$

From this equation it is to be recognized that from the three quantities ξ, ω_x, $\dot\omega_x$, two have to be determined, in order to obtain the third one.

2.3 Consideration of Mach number effects

The method permits to introduce in a simple way the effects of Mach number upon the aerodynamic load distributions of the wing.

Herein the wing geometry transformed for the respective Mach number according to the Prandtl-Glauert-Ackeret rule has to be introduced into the Weissinger-calculations. Furthermore the distributions of angle of attack as well as the values of section c_{m_0} and section a. c. position have to be corrected for the considered Mach number.

3. Numerical calculations

3.1 General

The following considerations show some applications of the method just described. Using as an example a big passenger aircraft now under development, the A-300, the performance and results of numerical investigations are described. The configuration of this aircraft as used in the calculations, is shown in Fig. 5. By these investigations which were carried out on a computer, the aeroelastic influence on a number of stability- and controllability derivatives are determined.

Consideration is given to the wing as well as to the horizontal tailplane. Since the method is applicable in the same manner for large and small aspect ratios, it can be used as it is for the calculation of airload distributions on the tailplane. Certain difficulties for the calculations arise indeed from the wing-fuselage- and tailplane-fuselage interference respectively. A considerable influence of the fuselage on the amount of the derivatives exists especially at the horizontal tailplane, where at stations near the fuselage the real lift is essentially smaller than the theoretical. These difficulties can be met approximately by changing the chord lengths of the tailplane along span in an appropriate manner. However for the given problem this is a matter of secondary importance, since the elastic deformations of the wing- or tailplane structure within the fuselage region are very small compared with those at stations more outwards. Furthermore the loads acting inboard do not affect very much the deformations at all. This will mean, that in cases, where only changes of aerodynamic coefficients due to structural flexibility are considered, it is permissible to handle the fuselage-wing interference in the way just mentioned. In all numerical investigations, which follow, not the absolut amount of the derivatives is the principal matter to demonstrate but rather its differences between rigid and flexible structure. With the results of such calculations the outcomes of windtunnel tests can be corrected for aeroelastic effects.

3.2 Position of the aerodynamic center of a flexible wing

First of all the influence of dynamic pressure and Mach number on the aerodynamic center position of a flexible wing shall be discussed qualitatively. It is known, that the aerodynamic center position of a swept rigid wing is independent of the dynamic pressure and changes only little with Mach number. In order to include the effects of structural flexibility of the wing into the determination of the a. c. position, the question must first be raised, whether an aerodynamic center for the flexible wing can be defined at all. Obviously this can be affirmed because of the linear relation between the aerodynamic loads on the wing, which are proportional to the angle of attack, and the aeroelastic twist of the wing due to the loads. In other words this means that not only for the rigid wing but also for the flexible wing the shape of the lift distribution, produced by a change in angle of attack is invariable with the amount of $\Delta\alpha$.

In opposition to the rigid wing however, the shape of the spanwise lift distribution of a flexible wing changes essentially with dynamic pressure and Mach number. Hence the a. c. position, being identical with the position of the center of the lift distribution also varies with dynamic pressure and Mach number.

In the case of a conventional swept back wing configuration it will be seen that the aerodynamic center of the wing assumed to be flexible is located more forward than for the one assumed to be rigid. This follows from the fact, that by the wing bending due to the airloads, changes in angle of attack are produced. As a result considerable lift reductions are obtained especially at the outer wing stations. These effects are illustrated in Fig. 6.

For this demonstration an airspeed of 570 knots at M = 0,9 has been assumed. As a result of the modification of the lift distribution the resultant lift force moves inwards along the swept wing and thus gives a forward shift of a. c. These aeroelastic effects are particularly large at high speeds and high Mach numbers. At low speeds they are almost negligible and disappear completely at Mach number zero.

In order to evaluate with the described method the aeroelastic influence on the aerodynamic center position of the wing, separated from other effects, the following way will be used.

Assuming the a. c. positions of the local sections in parts of the chord and the local section lift gradients as function of Mach number are known, first the lift distributions are determined under the assumption that the wing is absolutely rigid. These calculations are done for different Mach numbers. They give a theoretical a. c. position of the wing as function of Mach number.

These calculations are repeated, using the same aerodynamic parameters, but now introducing the real wing stiffnesses in bending and torsion. In these series of calculations not only the Mach number but also the dynamic pressure is variable. The investigations for the flexible wing must be performed assuming the mass parameters of the wing to be zero, in order to achieve that their influence on the wing deformations and hence on the lift distribution is eliminated. From the two series of calculations "wing rigid" and "wing flexible" the shift of the aerodynamic center due to the aeroelastic effects will be found easily by integration of the corresponding lift distributions.

The results of such an investigation, carried out for the A-300-wing, are shown in Fig. 8. In this illustration, the shifts of a. c. position are plotted against Mach number for different altitudes. In order to demonstrate the dependence of the aeroelastic shift of a. c. position on the dynamic pressure, additional lines are plotted representing $\varrho/2 \cdot V^2$ = constant. From the figure it can be seen that the shifts grow largely with increasing Mach number and dynamic pressure.

The most important assumptions of the investigations, leading to the quoted results are as follows:

The local a. c. position is at 25 per cent of the local chord length.

The factor, to correct the circulation quantities according to Weissinger for compressibility effects at every station of the span is shown in Fig. 7.

The straight elastic axis is assumed in 30 per cent of the chord.

3.3 Slope of lift curve of flexible lifting surfaces

As already mentioned and pictured in Fig. 6 the total lift A obtained for a flexible swept back wing at a given angle of attack is smaller than the lift for a rigid wing at the same angle of attack. To say it once again this comes from the fact, that if the wing bends up due to the lift, an additional distribution of angles of attack which increase along span, are produced whereby a downward acting airload is developed diminishing the primary airload. Of course, this is valid only for wings with swept back geometry. If the wing is swept forward, the effect is in revers. In that case the original lift would be amplified. Since airloads and deformations are proportional to the change of the geometric angle of attack, as follows from the equations, the gradient of lift coefficient can be defined in the usual manner:

$$\frac{\partial c_{L_W}}{\partial \alpha} = \frac{A}{Q \cdot F \cdot \alpha}$$

Whilst this quantity for a rigid wing depends only on the Mach number, for a flexible wing it is dependent on dynamic pressure and additionally on the Mach number.

The method shown here allows to determine directly the relation between the lift A and the geometric angle of attack α required to produce this lift. So it is very easy to calculate the derivative $\frac{\partial c_{L_W}}{\partial \alpha}$

For the wing actually under consideration these derivatives are obtained from the same calculations, as used for the determination of the aeroelastic shifts of a. c. position. They are plotted against Mach number for different altitudes in Fig. 9. The corresponding values of the rigid wing are also plotted.

A similar investigation was carried out for the horizontal tailplane of the A-300 aircraft, the geometry of which is to be seen from Fig. 5.

In addition to the flexibilities of the tailplane itself further flexibilities herein appear which affect the aerodynamic derivatives. Due to the loads acting at the tailplane, the rear fuselage will bend. Furthermore the attachments in the rear fuselage, provided to support the loads and moments of loads acting on the tailplane, will show local deformations, which are expected to be considerable. These additional effects bring about a change in angle of attack at the tailplane as a whole, whereby the gradient of lift coefficient will be additionally decreased. By reasons of structural layout, it can be of great interest, to seperate the two influences,

flexibility of the tailplane itself on the one hand, and change of angle of attack due to fuselage bending and local deformation of the attachment members on the other hand.

This can be realized with the given method by applying two different ways of examination, and comparing the results obtained.

1. Only the flexibility of the tailplane is considered, fuselage and attachment are assumed to be rigid.

2. The whole structure, tailplane, attachment and fuselage is flexible.

The first manner of examination is identical with that one, used in determining the wing lift gradient. Therefore the tailplane lift coefficient in this case will be obtained in the way, already described.

For the determination of the derivatives in case 2, in which the whole structure is assumed flexible, a few additional relations are to be established since the elastic model, on which the method is based does not include degrees of freedom of the wing-fuselage attachment. These relations may be shortly explained.

We imagine the loads, acting on the horizontal tailplane, to be separated into a free moment and a pure load, which acts at the theoretical supporting point explained in Fig. 1. By modifying the tailplane's bending and torsional stiffnesses between the supporting point and the fuselage center line, the deformation of the attachment including fuselage bending due to the free moment on the tailplane can be simulated. The derivation of the equations, necessary for these modifications may be omitted here.

The second portion of the attachment deformation, which is due to the load, acting at the supporting point and producing fuselage bending can be considered by correction of the results, obtained from the lift distribution calculations in a manner to be explained below. Let α_{o_T} be the change of the angle of attack at the tailplane due to the load at the supporting point, having the amount A_{eff_T}. From the calculations by the given method, which not yet include the influence of α_{o_T}, the total lift A_T^* at an angle of attack α_T^* may be obtained, whereby a lift gradient $\left(\partial c_{L_T} / \partial \alpha_T\right)^*$ comes about.

We then have the expression

$$A_{eff_T} = A_T^* - \Delta A_T = \left(\frac{\partial c_{L_T}}{\partial \alpha_T}\right)^* \cdot Q \cdot F_T \cdot \left(\alpha_T^* - \alpha_{o_T}\right)$$

If we define

$$A_{eff_T} = \left(\frac{\partial c_{L_T}}{\partial \alpha_T}\right) \cdot Q \cdot F \cdot \alpha_T^*$$

it follows by taking advantage of the linear relation

$$\alpha_{o_T} = K \cdot A_{eff_T}$$

the equation

$$\left(\frac{\partial c_{L_T}}{\partial \alpha_T}\right) = \left(\frac{\partial c_{L_T}}{\partial \alpha_T}\right)^* \left(1 - K \cdot \left(\frac{\partial c_{L_T}}{\partial \alpha_T}\right) \cdot Q \cdot F_T\right)$$

By transforming this equation, the effective gradient of the lift coefficient is given by:

$$\frac{\partial c_{L_T}}{\partial \alpha_T} = \frac{\left(\frac{\partial c_{L_T}}{\partial \alpha_T}\right)^*}{1 + \left(\frac{\partial c_{L_T}}{\partial \alpha_T}\right)^* \cdot K \cdot Q \cdot F_T}$$

All calculations on the A-300 being described here are based on lift coefficient gradients for rigid structure. These quantities are for the tailplane essentially smaller than the theoretical ones because of the loss of lift in the fuselage region. In order to attain these values actually by the theoretical analysis, the tailplane geometry, given in Fig. 5 must be modified suitably in the inner region.

Considering all the corrections, just described, the derivatives $\left(\frac{\partial c_{LT}}{\partial \alpha_T}\right)$ of the horizontal tailplane as shown in the Fig. 11 and 12 are obtained. They are plotted against Mach number for different altitudes. For the purpose of comparison the corresponding values of the rigid structure are also plotted in the figures. The graphs demonstrate that the reduction of the lift coefficients due to the aeroelastic influence at high speeds is considerable. Comparing the results of the two ways of examination it follows that the portion which is due to the deformation of the attachments and the fuselage is the main portion, this being an interesting and remarkable result.

3.4 Elevator effectiveness of a flexible tailplane

In order to apply the given method for the determination of the loading conditions at the horizontal tailplane, when the elevator is deflected, the following considerations are to be made. The method does not deal directly with the elevator deflection, which is assumed to stretch over the whole span of the tailplane. However, it is possible to introduce this parameter in the way now to describe.

We replace the angle of elevator deflection ß by an equivalent angle of attack

$$\alpha_\beta = \frac{\partial \alpha}{\partial \beta} \cdot \beta$$

Herein is $\frac{\partial \alpha}{\partial \beta}$ the flap effectiveness to obtain by section aerodynamics. The local lifts, induced by this angle of attack are assumed to act at the local aerodynamic centers. The additional moment due to ß, in respect to the local a. c. is considered by introduction of a moment coefficient $c_{m\beta}$, which is proportional to ß. So we have transfered the lifting surface with the flap being deflected into another with cambered sections, the camber being proportional to the angle of attack.

In order to evaluate the total effective airload and the derivative $\frac{\partial c_{LT}}{\partial \beta}$ which can be derived from it due to the elevator deflection we proceede as follows.

By a first sequence of calculations the angles of attack necessary to produce a given total lift A at the tailplane are figured out, assuming $c_{m\beta}$ to be zero. These angles of attack, which may be called $\alpha_T^{(1)}$ are determined as function of dynamic pressure and Mach number. The calculations performed here are identical with those, carried out to find the derivatives $\frac{\partial c_{LT}}{\partial \alpha_T}$. Therefore we obtain by them these derivatives according to whether the flexibility of attachments and fuselage is considered or not in the manner above explained.

A second sequence of calculations is performed subsequently, considering an arbitrary moment coefficient $c_{m\beta}$. The same total lift A as in the first sequence herein is required. By the choice of $c_{m\beta}$, the elevator deflection, related to $c_{m\beta}$ by

$$c_{m\beta} = \frac{\partial c_{m\beta}}{\partial \beta} \cdot \beta$$

and consequently the angle of attack α_β so is established. The term $\partial c_{m\beta}/\partial \beta$ will be taken from section aerodynamics. The results obtained with this investigation are the angles of attack, necessary to produce the lift A as a function of Mach number and dynamic pressure. These angles of attack might be called $\alpha_T^{(2)}$.

The total lift, due to the elevator deflection will be obtained by subtracting from A the lift which is due to a change in angle of attack given by the relation

$$\Delta \alpha_T = \alpha_T^{(2)} - \alpha_\beta$$

$$= \alpha_T^{(2)} - \frac{\partial \alpha}{\partial \beta} \cdot \frac{\partial \beta}{\partial c_{m\beta}} \cdot c_{m\beta}$$

Developing all equations, representing these matters and doing some conversions with them the following relation, giving the lift coefficient due to a change of elevator deflection finally comes about:

$$\frac{\partial c_{LT}}{\partial \beta} = \frac{\frac{\partial c_{LT}}{\partial \alpha_T}\left(\alpha_T^{(1)} - \alpha_T^{(2)} + \frac{\partial \alpha}{\partial \beta} \cdot \frac{\partial \beta}{\partial c_{m\beta}} \cdot c_{m\beta}\right)}{\frac{\partial \beta}{\partial c_{m\beta}} \cdot c_{m\beta}}$$

The lift generated by a change of ß becomes zero, (that means the derivative disappears) if the terms in the brackets become zero. The speed at which this condition is satisfied is known as "speed of elevator reversal", because at higher speeds the produced lift would be negative.

Fig. 10 shows the results of a corresponding investigation for the A-300 horizontal tailplane, in which all flexibilities, that of the tailplane itself and those of the attachments and fuselage have been taken into account. In the graph the lifting coefficient due to a change of elevator deflection ß is plotted against Mach number at different altitudes. According to this graph elevator reversal occurs at M = 0,86 at sea level, this speed being sufficiently above V_D.

4. Conclusions

With this method the aircraft engineer is given the capability to determine with any desired exactness the aeroelastic deformations and their effects occurring on swept-back lifting surfaces, provided the elastic properties of the wing structure are available.

The advantages of this method relative to iterative methods are, in our opinion, the clearness and the possibility to overlook the participation of the individual load components.

The numerical examples presented demonstrate the essential tendencies of the aeroelastic effects.

The results of these calculations can be used to correct the stability and manoeuvrability derivatives obtained from wind tunnel tests or rigid calculations.

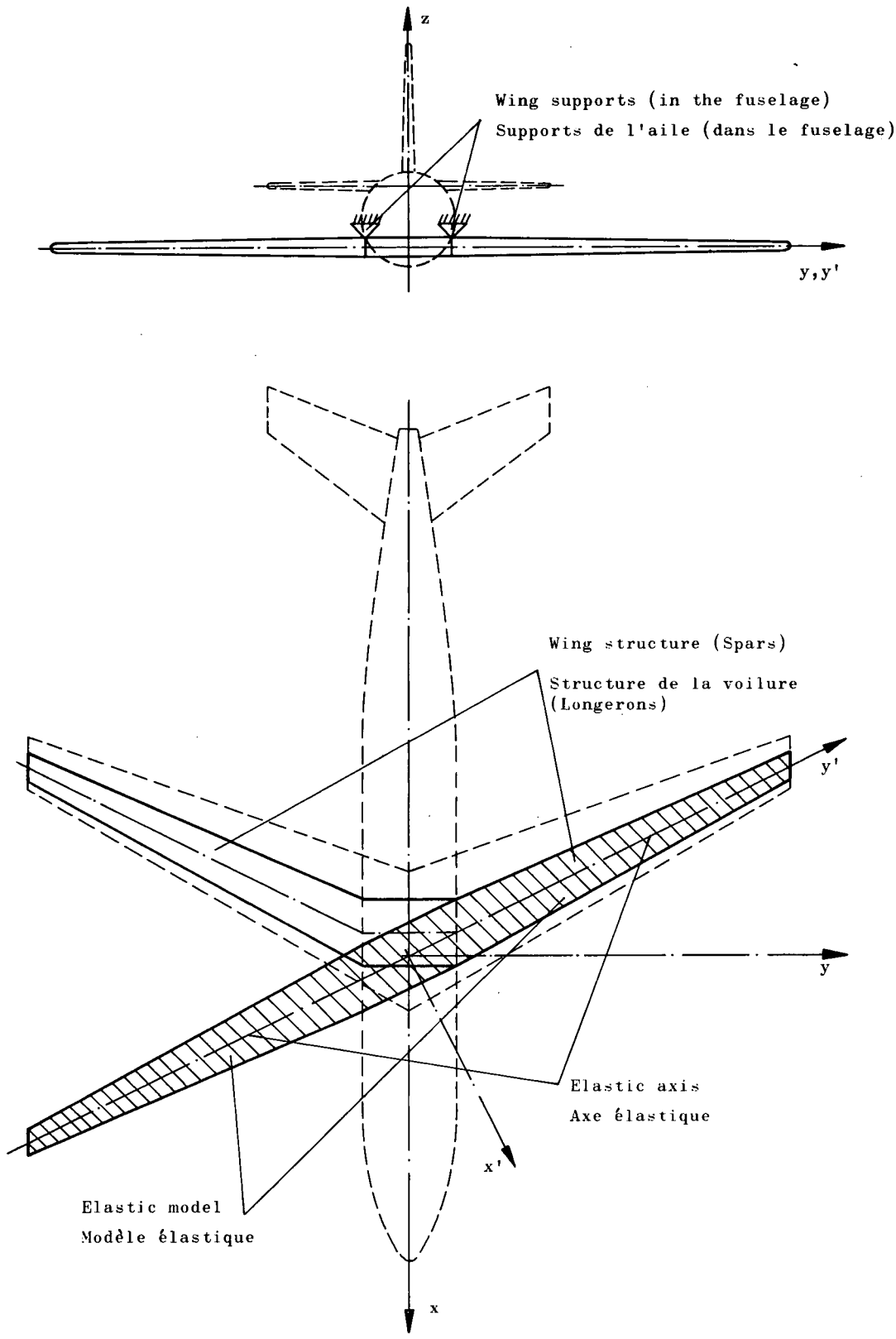


Fig. 1 Elastic model
Modèle élastique

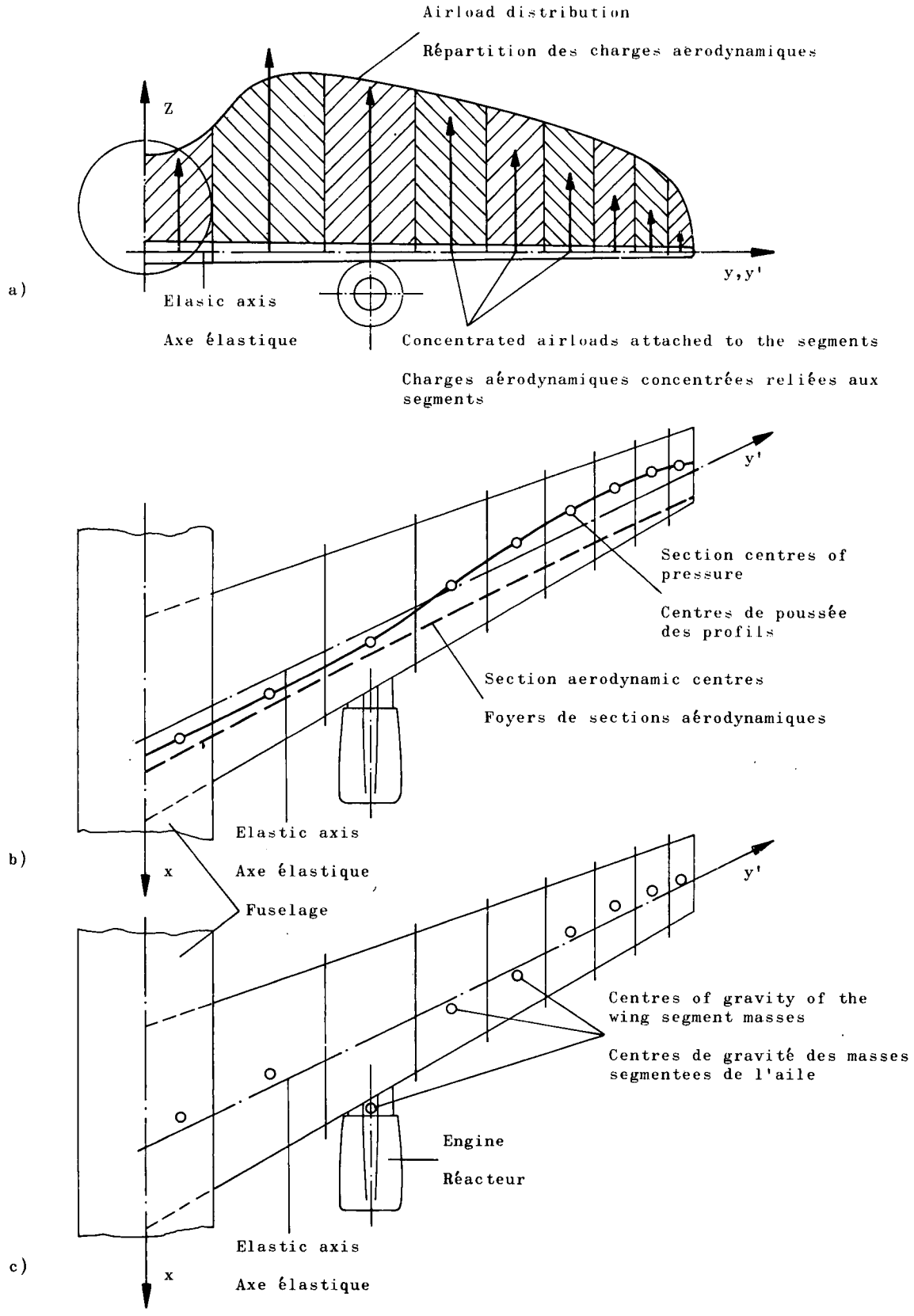
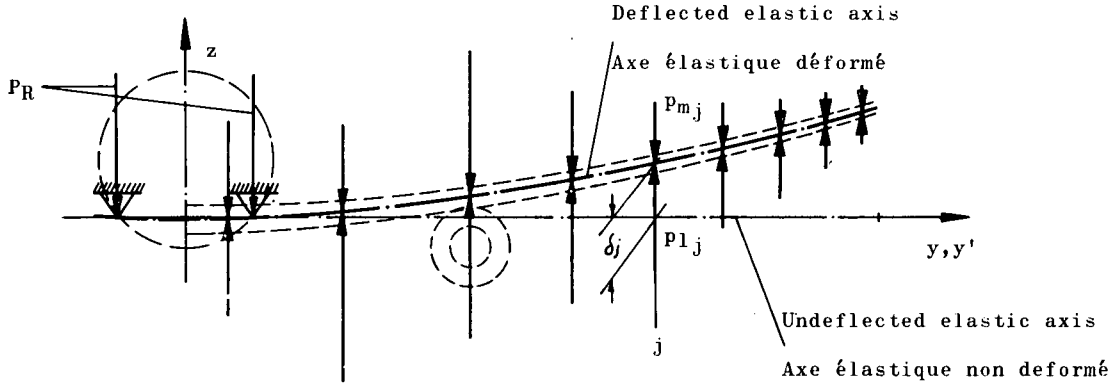


Fig. 2 Airload and mass load distributions

Répartitions des charges aérodynamiques et de masses



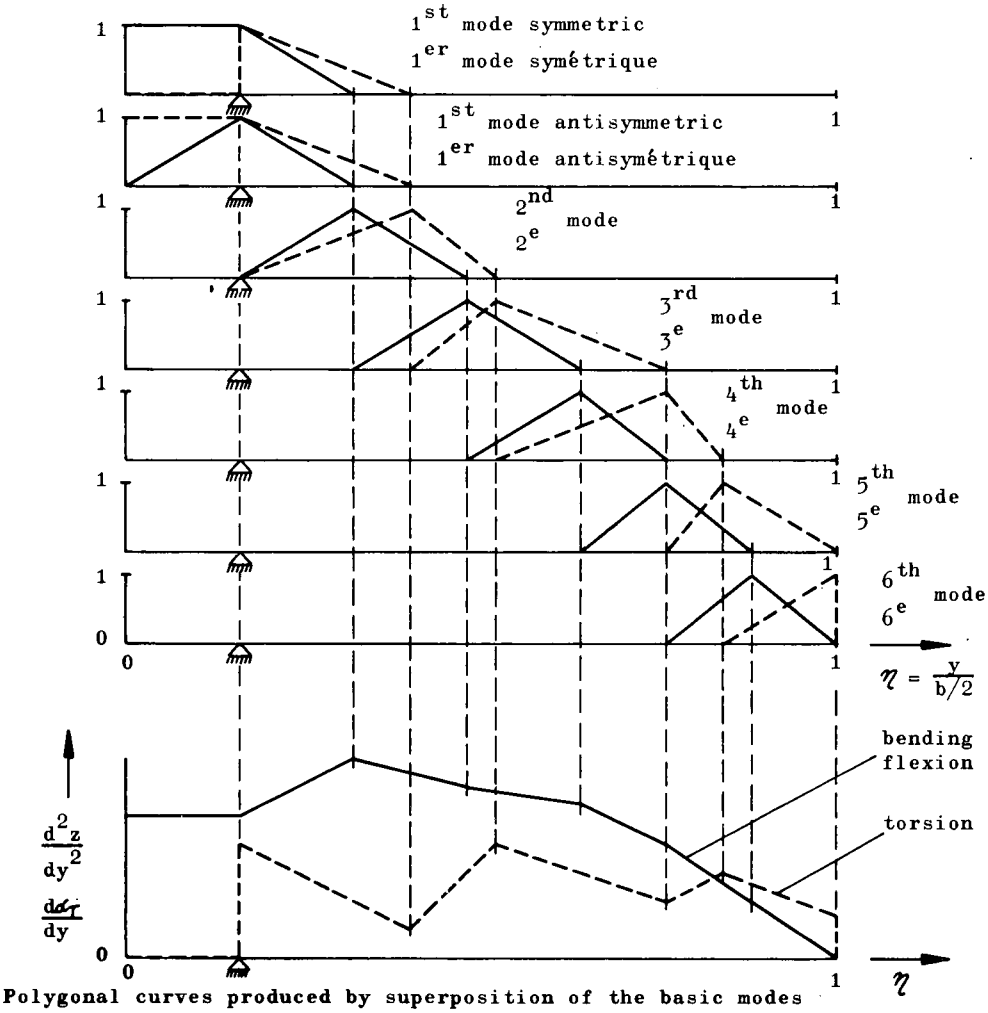
p_{m_j} mass loads
charges de masses

p_{l_j} air loads
charges aérodynamiques

δ_j displacements of the elastic axis
déformations de l'axe élastique

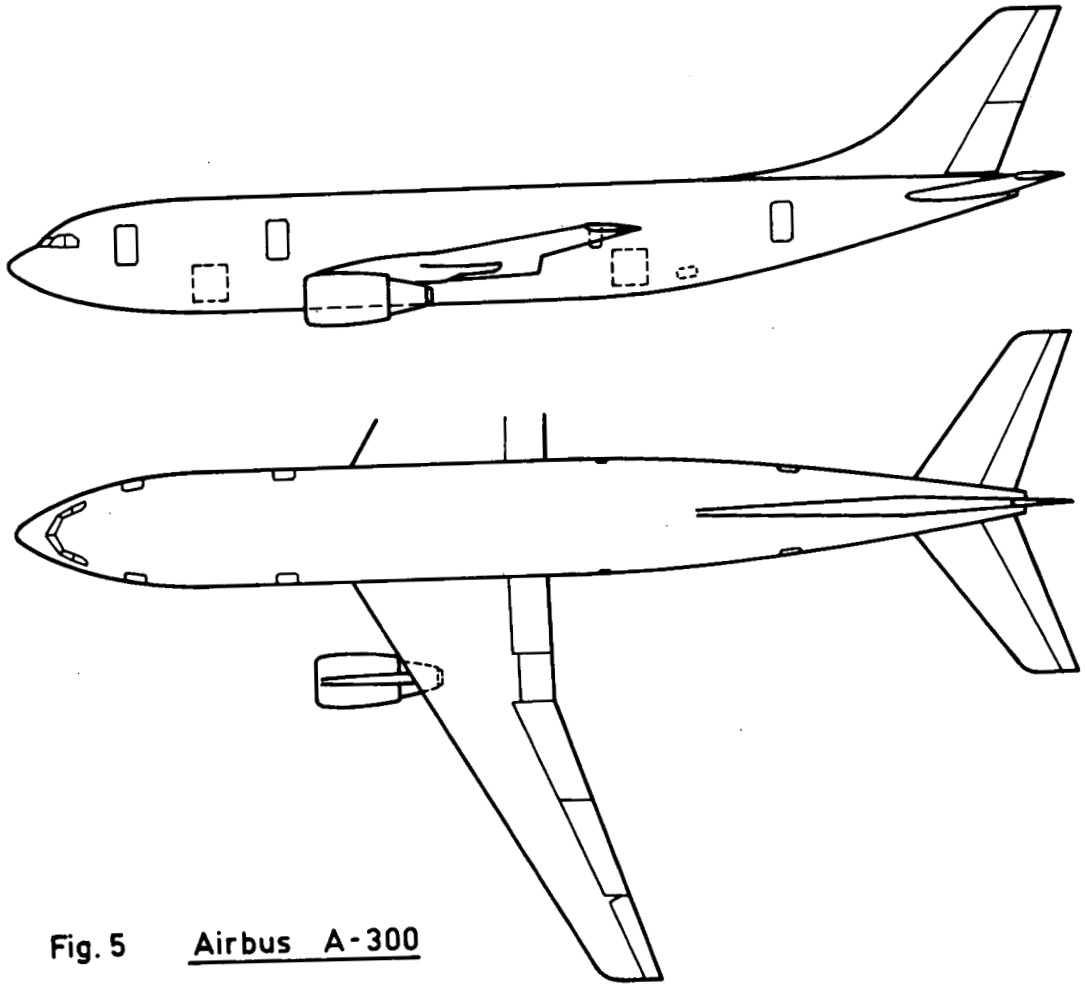
P_R resultant loads from fuselage and tail
charges résultantes de fuselage et empennage

Fig. 3 Typical load case applied to the elastic system
Application typique des charges au système élastique



Polygonal curves produced by superposition of the basic modes
Courbes polygonales produites par superposition des modes élémentaires

Fig. 4 Basic modes applied for the calculations
Modes élémentaires appliquées aux calculations



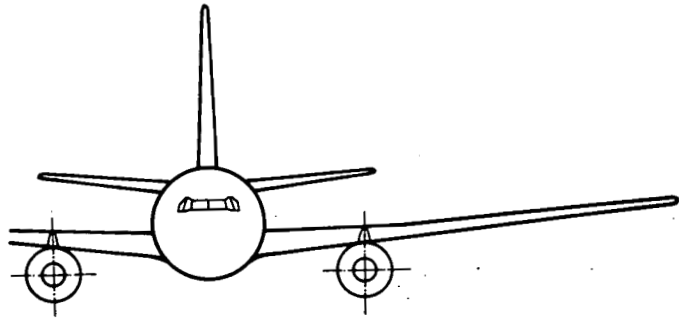


Fig. 5 Airbus A-300

	Wing Aile	Horizontal tailplane Empennage horizontal
Span Envergure	45,10 [m]	16,95 [m]
Area Surface	260 [m^2]	70 [m^2]
Aspect ratio Allongement	7,85	4,10

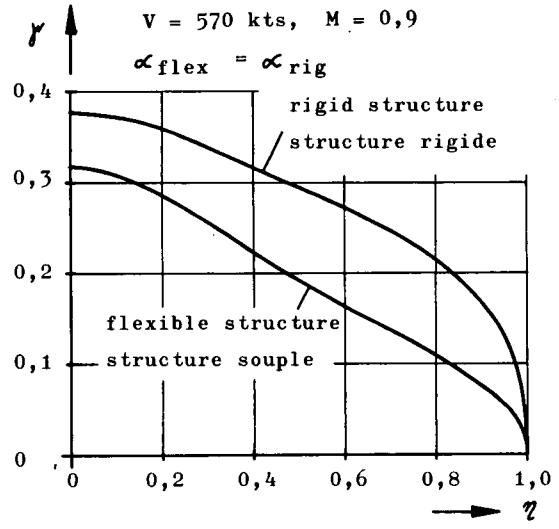


Fig. 6 Spanwise lift distribution on the wing

Répartition des charges aérodynamique sur l'envergure de l'aile

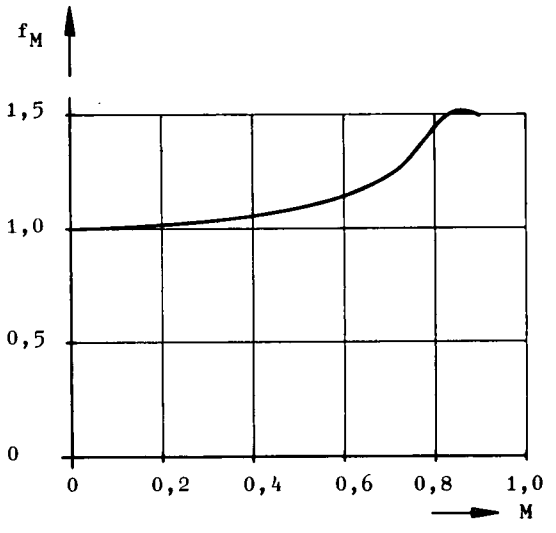


Fig. 7 Compressibility factor

Facteur de compressibilité

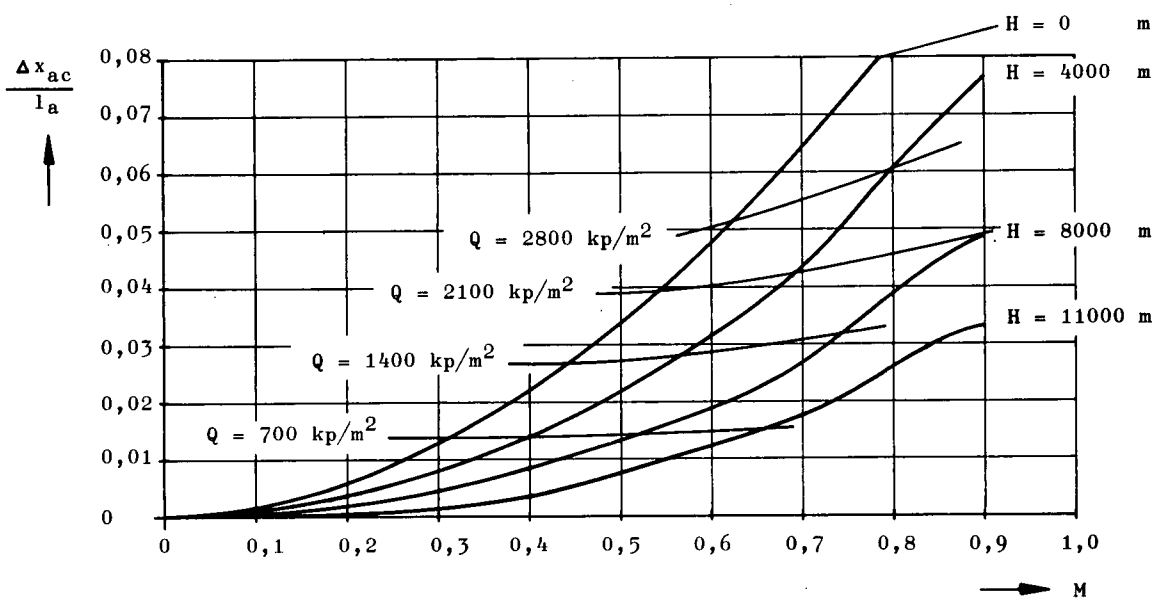


Fig. 8 Shift of the a.c. position of the wing due to aeroelastic effects

Mouvement du foyer de l'aile du aux effets aéroelastiques

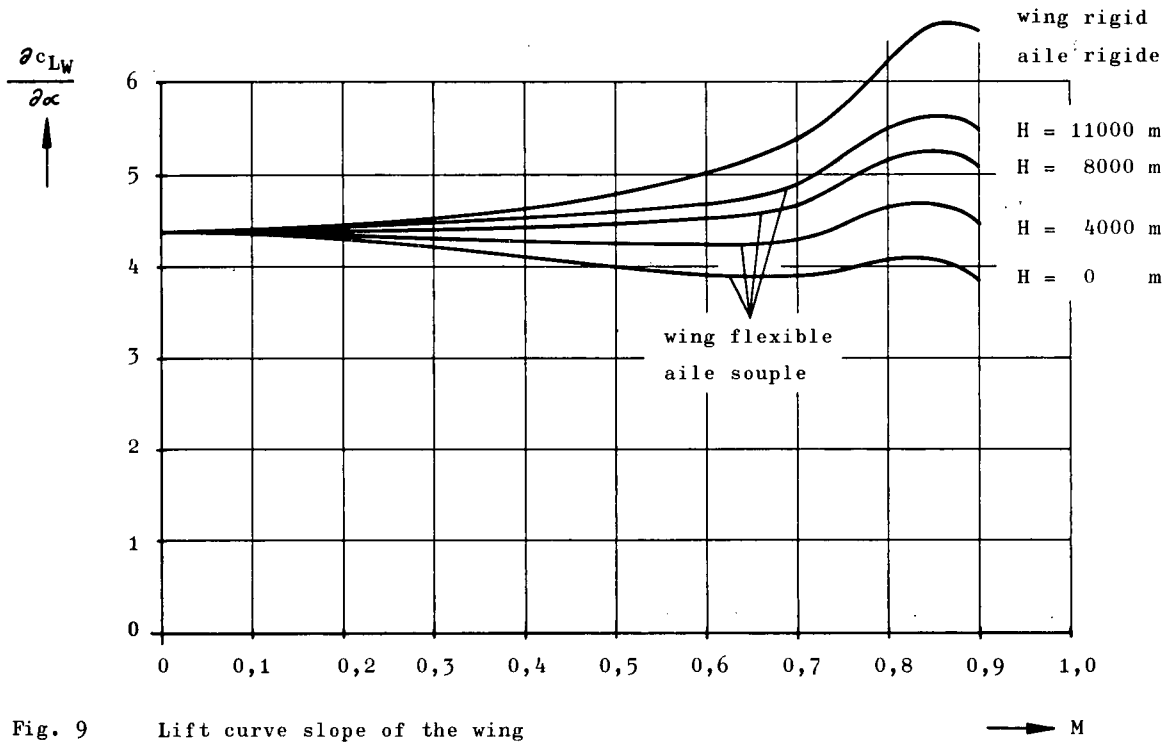


Fig. 9 Lift curve slope of the wing

Gradient de portance de l'aile

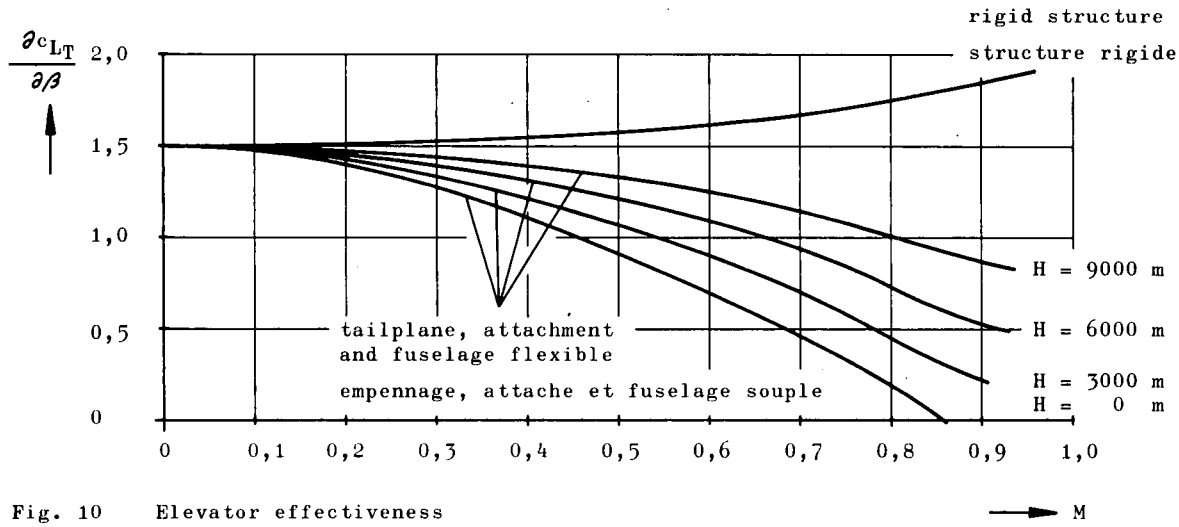


Fig. 10 Elevator effectiveness

Efficacité de la gouverne de profondeur

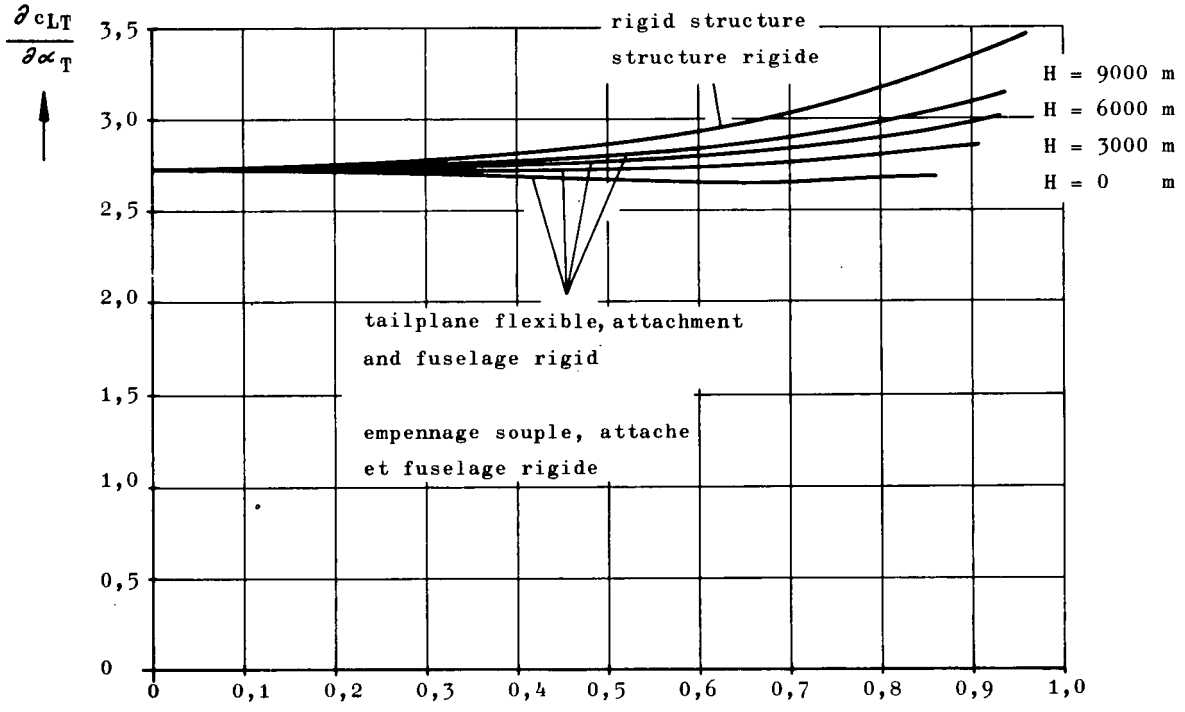


Fig. 11 Lift curve slope of the horizontal tailplane

Gradient de portance de l'empennage horizontal

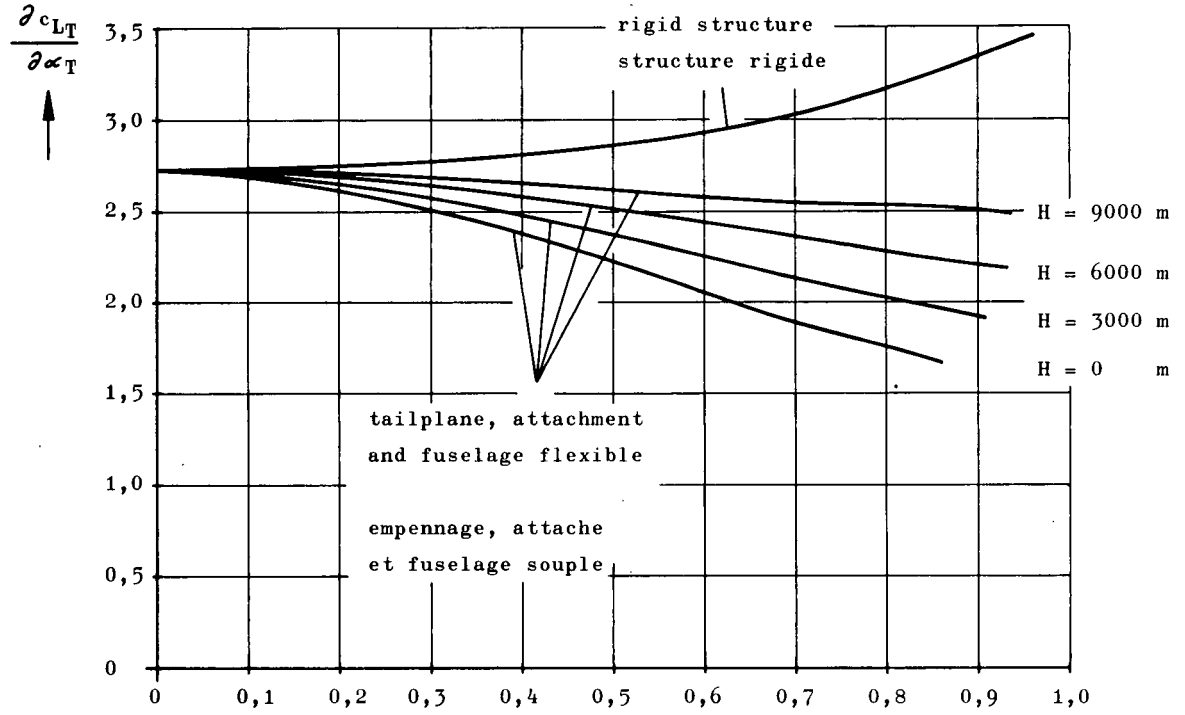


Fig. 12 Lift curve slope of the horizontal tailplane

Gradient de portance de l'empennage horizontal

WIND-TUNNEL TECHNIQUES FOR THE STUDY OF AEROELASTIC EFFECTS ON AIRCRAFT STABILITY, CONTROL, AND LOADS

By A. Gerald Rainey and Irving Abel

NASA Langley Research Center
Langley Station, Hampton, Va., USA

WIND-TUNNEL TECHNIQUES FOR THE STUDY OF AEROELASTIC EFFECTS ON AIRCRAFT STABILITY, CONTROL, AND LOADS

By A. Gerald Rainey* and Irving Abel**
NASA Langley Research Center

SUMMARY

Techniques for wind-tunnel studies of a variety of stability, control, and response characteristics of elastic aircraft which are in use at the NASA Langley transonic dynamics tunnel have been described. All of these methods employ a dynamic, aeroelastically scaled model supported on a simple two-cable mount system which provides close simulation of free-flight conditions. The mount system has proven to be very versatile and, with variations, has been successfully applied to several different problems. Both static and dynamic control effectiveness and stability derivatives have been studied using the basic approach followed in flight testing; namely, measuring the response of the model to known control inputs. Response to sinusoidal gusts have been investigated using the basic model-mount system in conjunction with a device to impart sinusoidal gusts to the wind-tunnel airstream. And, finally, problems associated with high lift such as buffeting have been studied by adding a device to the basic arrangement which compensates for the lift in excess of the model weight without sacrifice of model freedom of movement.

INTRODUCTION

The Langley transonic dynamics tunnel began operations in 1959 with the primary function of providing the United States with a suitable facility for research and development of dynamics aspects of new aircraft in the important transonic speed range. In the time since 1959, the staff of this facility has spent a large portion of its efforts in developing new or improved techniques for experimentally studying aeroelastic and dynamics problems in wind tunnels. One of the earliest technique development tasks undertaken was that of providing a suitable mount system for complete models with good simulation of free-flight dynamics. Many types of mount systems were considered and several were actually tried in the wind tunnel (without noteworthy success). Eventually, Wilmer H. Reed III conceived the mount system that is now called, simply, the two-cable mount system. Although developed and used primarily for flutter studies (about 50 percent of the work done in the tunnel is in flutter), the two-cable mount, with variations, has proven to be very versatile.

This paper is intended to provide a brief description of the two-cable mount system and several of the applications that have been made using this system in studying flight mechanics problems other than flutter. A more complete review of the subject mentioned in the title of this paper would include a description of the Model Fly program sponsored by the U.S. Air Force Flight Dynamics Laboratory, or perhaps some of the dynamic stability derivative measurement techniques developed by several aerodynamic research organizations. However, for brevity, the paper will be confined to the familiar programs conducted within the authors' own organization.

SYMBOLS

a	horizontal distance between model center of gravity and outer cable-tangency point on rear pulleys
b	wing span
C_{l_p}	roll damping, $\frac{\partial C_l}{\partial(\frac{\dot{\phi} b}{2V})}$
C_{l_δ}	aileron effectiveness, $\frac{\partial C_l}{\partial \delta_a}$

*Head, Aeroelasticity Branch, Dynamic Loads Division, NASA Langley Research Center, Langley Station, Hampton, Virginia USA

**Aero-Space Technologist, Aircraft Aeroelasticity Section, Aeroelasticity Branch, Dynamic Loads Division, NASA Langley Research Center, Langley Station, Hampton, Virginia USA

C_P	coefficient of friction for rotating pulley
C_Z, C_θ	simplified damping coefficient of mount system in vertical translation and pitch, respectively
d	horizontal distance between model plane of symmetry and outer cable-tangency point on rear pulleys
e	horizontal distance between model center of gravity and outer cable-tangency point on front pulleys
g	acceleration due to gravity
h	vertical distance between model center of gravity and outer cable-tangency point on front pulleys
I_x, I_y, I_z	roll, pitch, and yaw moment of inertia about x,y,z axes, respectively
I_{xz}	product of inertia
K_{ij}	spring constant of mount support relating a force or moment in mode $i(x,y,z,\theta,\psi,\phi)$ to a displacement in mode $j(x,y,z,\theta,\psi,\phi)$
L,M,N	roll, pitch, and yaw moments about x,y, and z axes, respectively
L_A, M_A, N_A	roll, pitch, and yaw aerodynamic moments
L_C, M_C, N_C	roll, pitch, and yaw cable mount moments
L_R, L_F	length of rear and forward cables, respectively, from wall attachment point to outer cable-tangency point on pulleys
l	a characteristic length
m	mass of model including pulleys
M_{c_0}	cable-mount pitching moment at $\theta = \theta_t$, $K_{\theta\theta}\theta_t$
M_P	pulley moment due to friction
N_P	resultant pulley force, acting through pulley bearings, due to T_F
P	roll rate, $\dot{\phi}$
q	dynamic pressure, $1/2\,\rho V^2$
r_P	pulley radius
S	wing area
T_R, T_F	support cable tension in rear and front cables, respectively
ΔT	change in cable tension due to model displacement and rotation
V	flow velocity
x,y,z	displacement coordinates of model center of gravity
X,Y,Z	external forces on model in x,y,z coordinate directions, respectively
Y_A, Z_A	side and vertical translation aerodynamic forces, respectively
Y_C, Z_C	side and vertical translation cable forces, respectively
Z_{c_0}	cable-mount vertical force at $\theta = \theta_t$, $K_{z\theta}\theta_t$
Z_P	displacement of rear cable attachment points on roll control device
α	phase angle between aileron displacement and roll
β_F	angle in vertical plane between x axis and forward cables
β_R	angle in horizontal plane between x axis and rear cables
δ_a	aileron angle, $\delta_a(t) = \delta_0 e^{i\omega t}$

θ pitch angle perturbation about trim

θ_t pitch angle for trimmed flight

μ dimensionless mass ratio

ρ mass density of wind-tunnel test medium

ϕ roll angle

ψ yaw angle

ω circular frequency

THE TWO-CABLE MOUNT SYSTEM

General Requirements and Description

As mentioned previously, an early task for the staff of the new transonic dynamics tunnel was the development of a suitable mount system for studying dynamics problems on large complete vehicle models. The view was adopted that a goal of perfect free-flight simulation would be sought as opposed to other approaches which might have been considered which would require application of correction factors for the influence of the mount. With this view in mind, the ideal system is one having no restraint or, in effect, a free-flight system. The practical system seeks to approach this ideal in at least those aspects most important to the test at hand. Some desirable features which such a mount system might have are:

1. A soft support such that the natural frequencies associated with the mount are well below those of the free-flight and elastic modes.

2. Allow freedom of movement of sufficient amplitude for normal model motion due to turbulence, trim changes, and the like.

3. Moving masses associated with the mount should be negligible relative to the important generalized masses of the model.

4. Aerodynamic interference should be low.

5. Convenient trim adjustments and safety devices.

6. Predictable static and dynamic stability under all operating conditions.

7. Simplicity.

The two-cable-mount system, described in some detail by Reed and Abbott (1) has been developed and used extensively in the Langley transonic dynamics tunnel. This system incorporates most of the desirable features listed above.

Basically it is a very simple arrangement as illustrated in figure 1. Two loops of small diameter stranded steel wire cable extend in mutually perpendicular planes from the model to the tunnel walls, one loop upstream and the other downstream. The cables pass through pulleys located within the fuselage contour and tension is applied by stretching a soft spring in the rear cable loop. The small-diameter cable causes little aerodynamic interference and the moving parts of the mount system (cable, pulleys, etc.) have small mass compared with the important generalized masses of the average model. Stability and natural frequencies of the cable-supported model are controlled by the preload tension of the soft spring in the cable loop. Low spring stiffnesses are associated with this system which result in low natural mount related frequencies while permitting large translational and rotational motions.

Remotely operable aerodynamic trim control is provided in the model to keep it centered in the tunnel throughout the test range. Usually only pitch and roll trim control are required. Normally, models can be easily trimmed by a single operator or "pilot" using a miniature airplane-type control stick which actuates on-off trim switches.

Although the mount system is basically simple, its dynamic and static stability cannot be determined intuitively. The stability problem for a model on the mount system is somewhat more complex than that of the free-flying airplane in that the mount system provides additional modes which may become unstable. The stability analysis described below has proven to be reasonably accurate. This analysis is used in the design of the system for each new model.

Stability Analysis

Consider the cable configuration shown schematically in figure 2. The x, y, and z axes form a right-hand set of space-fixed orthogonal coordinates with the origin at the center of gravity of the model in trimmed flight. The model is assumed to be rigid so that its motion in the tunnel is completely described by five degrees of freedom; namely, y and z translation of the center of gravity (fore and aft motion deleted)*, and ϕ, θ, and ψ rotations about the x, y, and z axes, respectively.

The linearized small perturbation equations of motion for the system can be written as follows:

Vertical translation:

$$Z_A + Z_C + mg = m\ddot{z}$$

Pitch:

$$M_A + M_C = I_y\ddot{\theta}$$

Side translation:

$$Y_A + Y_C = m\ddot{y}$$

Roll:

$$L_A + L_C = I_x\ddot{\phi} - I_{xy}\ddot{\psi}$$

Yaw:

$$N_A + N_C = I_z\ddot{\psi} - I_{xz}\ddot{\phi}$$

The C and A subscripts denote cable and aerodynamic terms, respectively.

Once interior properties of the model are fixed, the ability to change the characteristics of the mount system lies mainly with the mount restraint force components. The longitudinal and lateral mount restraint forces and moments can be expressed as follows:

Longitudinal:

$$Z_C = Z_{C_O} - K_{z\theta}\theta - K_{zz}z + Z(\dot{z},\dot{\theta})$$

$$M_C = M_{C_O} - K_{\theta z}z - K_{\theta\theta}\theta + M(\dot{z},\dot{\theta})$$

Lateral:

$$L_C = -K_{\phi y}y - K_{\phi\phi}\phi - K_{\phi\psi}\psi + L(\dot{y},\dot{\phi},\dot{\psi})$$

$$N_C = -K_{\psi y}y - K_{\psi\phi}\phi - K_{\psi\psi}\psi + N(\dot{y},\dot{\phi},\dot{\psi})$$

$$Y_C = -K_{yy}y - K_{y\phi}\phi - K_{y\psi}\psi + Y(\dot{y},\dot{\phi},\dot{\psi})$$

The linearized stiffness influence coefficients (K_{ij}) are obtained by determining the total forces and moments about the center of gravity from each of the cables due to a small perturbation from trim. Equations defining the stiffness influence coefficients have been derived (1) as a function of mount system geometry and cable tensions. For the particular example presented in figure 2 (vertical cables forward, horizontal cables aft) the longitudinal stiffness influence coefficients are as follows:

$$K_{zz} = 2\left[\frac{T_F}{L_F}\cos^2\beta_F + \frac{T_R}{L_R}\right]$$

*With a spring in only one of the two cables, the fore and aft motion of the model in the x direction is effectively locked out. In principle, this motion could be provided by placing another soft spring in the forward cable, however, this arrangement has not been explored experimentally.

$$K_{z\theta} = 2\left[a\frac{T_R}{L_R} - \frac{T_F}{L_F} h\cos\beta_F\sin\beta_F - \frac{T_F}{L_F} e\cos^2\beta_F \right]$$

$$K_{\theta z} = K_{z\theta}$$

$$K_{\theta\theta} = 2a^2\frac{T_R}{L_R} + 2aT_R\cos\beta_R + 2T_F\left[h\sin\beta_F + e\cos\beta_F + \frac{1}{L_F}(e\cos\beta_F + h\sin\beta_F)^2 \right]$$

The steady-state terms Z_{c_0} and M_{c_0} resulting from trim changes are

$$Z_{c_0} = -K_{z\theta}\theta_t$$

$$M_{c_0} = -K_{\theta\theta}\theta_t$$

The method of treating the damping terms $Z(\dot{z},\dot{\theta})$ and $M(\dot{z},\dot{\theta})$ has been found to be important in improving the accuracy of the analysis. Initially (1) the damping was considered to be concentrated at the center of gravity. However, instabilities were encountered which were not properly explained until a more realistic treatment of the damping terms was developed which placed the damping forces at the actual point of action on the model. These two methods of treating the damping are illustrated in fig. 3. With the damping forces acting at the pulleys, additional coupling terms are included in the analysis which can be either stabilizing or destabilizing.

Equations defining the aerodynamic terms appearing in the equations of motion are discussed in (1). Aerodynamic derivatives used in the equations are normally estimated from the best available information on the aircraft being tested. (Suitably adjusted to model conditions.)

A computer program is available by which the stability boundaries may be studied for any given model and a reasonably safe choice of design parameters selected. Some uncertainty may still exist, however, due to inaccuracies in the information used in the analysis (aerodynamic derivatives, for example).

Some Practical Considerations

As a safety precaution in case of model instability or failure, the model is attached to a quick acting snubbing cable system, normally slack, which when actuated will apply damping to any rigid body modes and sufficient force to bring the model to the tunnel center. It has been found important to analyze the model for this snubbed condition (one model was lost when the "safety" device was actuated).

It is considered good practice at the Langley transonic dynamics tunnel to study a "dummy" model prior to risking the expensive aeroelastically scaled model. The dummy model is built to match the geometry, mass, and inertia, but not the elastic properties of the aeroelastically scaled model. Such a model serves many useful purposes, not the least of which is training of the test crew immediately prior to the tests of the expensive model. Complete aeroelastically scaled models for the transonic dynamics tunnel may cost on the order of $50,000 to $500,000 to design and build, while a dummy model may cost as little as $5,000 to $10,000.

The basic mount system described above has proven to be very versatile. Variations on the basic arrangement have been developed to provide particular capabilities required by various study objectives. Some of these variations on the basic arrangement are described in subsequent sections.

THE AIRSTREAM OSCILLATOR

Some years ago a need for a wind-tunnel technique for measuring frequency-response functions for gust response research was recognized. A system for generating controlled sinusoidal gusts in a wind tunnel was developed (2) and installed in the transonic dynamics tunnel (3). A brief description of the system and some preliminary results obtained using the airstream oscillator follows.

Figure 4 is a sketch of the interior of the tunnel, viewed from the entrance section downstream toward the test section, showing schematically some of the main features of the system. Two sets of vanes, in a biplane arrangement, are located on the side walls of the tunnel entrance section. The vanes on each of the two sides are driven by a hydraulic motor and flywheel through linkages which produce nearly sinusoidal vane oscillations about the zero angle-of-attack position. Because of these heavy flywheels, the existing oscillator has only sinusoidal capability. Vane angular range is adjustable from 0° to 12°. Frequency is adjustable from 0 to 20 Hz by means of an electrical control system. Synchronization of the two sides is maintained by the electrical control system, and the phasing of the two sides may be varied from "in sync" to 180° out of synchronization.

The aerodynamic effect of the oscillating vanes on the test section flow results from cross-stream flow components induced by the trailing vortices from the vane tips. These vortices extend downstream through the test section (near the side walls) as rather discrete vortex cores. These vortices alternate in sign as the vanes oscillate, and the system passes downstream through the test section with a spacing (wave length) depending upon the frequency and the stream velocity. When the vanes are "in sync," the principal oscillating component over the middle portion of the airstream is directed vertically. If the vanes are "out of sync" both lateral and vertical components produce a kind of rolling gust about the tunnel centerline.

At present an evaluation program is underway to study the system's usefulness as a tool in the study of aircraft gust response. It was felt some time ago that results of preliminary tests with simple models (3) were sufficiently encouraging to justify an expanded program with a realistic model. The airplane selected for this expanded program is a large subsonic jet bomber for which extensive flight data are available for comparison with model results.

In order to obtain valid frequency-response measurements, the model must be supported in the wind tunnel with sufficient freedom to simulate free-flight rigid-body motions. An initial design analysis of a basic two-cable mount system indicated that the mount system produced unacceptably large deviations of the rigid body frequencies. A variation of the basic arrangement was developed which, according to the analysis, causes less than 5 percent deviation of both the frequency and damping of the short period and Dutch roll modes. This variation of the mount, again, consists of two cable loops, one of which is free to run through pulleys on the tunnel floor and ceiling upstream of the model; the other is led aft from the model to pulleys on the tunnel side wall (fig. 5). The ends of the cable loops are pinned to the model at a point near the center of gravity. This arrangement produces very low rotational stiffness about the center of gravity.

Studies have been completed of a "dummy" model to verify the performance of the mount system and some typical results are shown in fig. 6. The comparison of measured center-of-gravity response to calculated response indicates satisfactory agreement at least in the range of frequency near the short period frequency. The sharp peak in the calculated response at very low frequencies is associated with the vertical translation mode of the model on the mount system (a resonant mode which does not exist for the airplane).

CONTROL EFFECTIVENESS AND DERIVATIVE MEASUREMENTS

All modern high-speed aircraft are subject to significant aeroelastic effects on their stability and control characteristics. Aileron reversal is, perhaps, the most prominent example. Techniques for handling these problems in design have evolved over the years and are generally considered to be adequate. Nevertheless, wind-tunnel techniques for research on these problems as well as for potential application in the design process will be useful. The technique to be described below again employs a dynamic, aeroelastically scaled model supported on the two-cable mount system.

The basic approach used is, in principle, identical to the approach used in flight tests; namely, measurements are made of the response of the model to known control inputs (either static or dynamic) and the equations of motion are solved for the unknown aerodynamic coefficients. This approach has been applied in two cases in the Langley transonic dynamics tunnel; (1) measurement of static slope of the lift curve through deflection of the elevator, and (2) measurement of dynamic aileron roll effectiveness including the reversal condition. The first case was quite simple and was accomplished successfully. The second case is considerably more involved and perhaps of greater interest, and is, therefore, described further.

The equations of motion used are identical to those for a rigid airplane. However, the aerodynamic derivatives used in this manner represent the quasi-static elastic derivatives or the equivalent rigid body derivatives. Furthermore, the

deformation effects associated with gravity forces are neglected. (Some of the difficulties associated with this aspect are discussed subsequently in the section on High Lift Problems.)

Etkin (4) has shown that, for many conventional airplane configurations, the roll equation in free flight can be simplified and treated as a single degree of freedom. It was also shown by Abel (5) that by properly designing the two-cable mount system a model flown in the wind tunnel can also be forced to behave very nearly as a single degree of freedom in roll.

The problem is now greatly reduced to measuring only the dynamic response of the model in roll as shown schematically in figure 7. The single-degree-of-freedom roll equation can be written in the form

$$I_x\ddot{\phi}(t) - \frac{qSb^2}{2V} C_{l_p}\dot{\phi}(t) + K_{\phi\phi}\phi(t) = qSbC_{l_\delta}\delta_a(t)$$

where $K_{\phi\phi}\phi(t)$ is the only term associated with the mount system. For sinusoidal motion, the aileron deflection is

$$\delta_a(t) = \delta_0 e^{i\omega t}$$

The steady-state roll response becomes

$$\phi(t) = \phi_0 e^{i(\omega t+\alpha)}$$

$$\dot{\phi}(t) = i\omega\phi_0 e^{i(\omega t+\alpha)}$$

$$\ddot{\phi}(t) = -\omega^2\phi_0 e^{i(\omega t+\alpha)}$$

where α is the phase angle between aileron displacement and roll angle. Hence, the roll equation can be written as,

$$C_{l_p}\left[\frac{i\omega qSb^2}{2V}\phi_0 e^{i\alpha}\right] + C_{l_\delta}\left[qSb\delta_0\right] = (-I_x\omega^2 + K_{\phi\phi})\phi_0 e^{i\alpha} \qquad (1)$$

The dynamic roll angle ϕ_0 and the phase angle α are measured over a range of discrete aileron frequencies ω. A set of redundant algebraic equations is then generated from equation (1) which in turn can be solved for the aerodynamic derivatives C_{l_p} and C_{l_δ}. (All other terms appearing in equation (1) are known values for the particular model and test condition.)

In free flight the simplified roll equation is

$$I_x\ddot{\phi} - \frac{qSb^2}{2V} C_{l_p}\dot{\phi} = qSbC_{l_\delta}\delta_a$$

For steady-state roll $\ddot{\phi} = 0$; hence

$$\dot{\phi} = -\frac{C_{l_\delta}}{C_{l_p}} \frac{2V\delta_a}{b} \qquad (2)$$

Free-flight control effectiveness is normally expressed in terms of the wing tip helix angle $Pb/2V$, where $P = \dot{\phi}$. Therefore, equation (2) can be written as

$$\frac{Pb}{2V} = -2\left(\frac{C_{l_\delta}}{C_{l_p}}\right)\delta_a$$

The free-flight control effectiveness is determined from the measured model values of C_{l_p} and C_{l_δ} at the properly scaled flight condition. That is,

$$\left(\frac{Pb}{2V}\right)_{Airplane} = -2\left(\frac{C_{l_\delta}}{C_{l_p}}\right)_{Model} \times \left(\frac{V\delta_a}{b}\right)_{Airplane}$$

A comparison of flight measured and model predicted full-scale aileron effectiveness is given in figure 8. The data are presented in terms of helix angle (Pb/2V) versus full-scale dynamic pressure at a Mach number of 0.75. The model reversal point (Pb/2V = 0) shown in fig. 8 was experimentally determined in a somewhat different manner. The static roll angle is measured for a given static deflection of the ailerons for a static measurement of C_{l_δ}. At the reversal point C_{l_δ} will be zero. The comparison between predicted and measured flight control effectiveness shown in figure 8 is considered to be satisfactory.

By using this type of testing technique not only is the reversal boundary established, but also the aileron effectiveness of the airplane as a function of Mach number and dynamic pressure may be determined.

The measurements described above were made employing another variation of the two-cable mount system. The only control available on the model for trim in roll were the ailerons. Since reversal conditions were to be studied and because of difficulty in using the ailerons for trim while they were oscillating, an auxiliary roll control device was developed. This device for imparting a mechanical rolling moment to the model is shown in fig. 9.

The required roll control was accomplished by traversing the downstream attachment points of the rear cable in opposite directions along the tunnel walls. A differential deflection of the rear cable produces a direct rolling moment applied to the model through the mount system. The rear cable is deflected by passing each branch through a separate pulley assembly which traverses on a shaft mounted to the tunnel wall. The pulley assemblies are displaced by a remotely operated drive system actuated by the model "pilot."

HIGH LIFT PROBLEMS

There are several problems associated with high lift coefficients where aeroelastic effects are important. These include buffeting and stability and control characteristics. Complete dynamic, elastic models have not been used often in studying these problems. Some of the reasons for this and a new technique for research in this area are outlined below.

Nature of the Experimental Difficulty

Models tested on the two-cable mount system ordinarily are trimmed to be in equilibrium at the centerline of the tunnel. In this position, the vertical forces due to the mount system are zero and the lift on the model is just sufficient to support the weight of the model. This "1g" condition for the model will not, in general, properly represent 1g flight for the simulated airplane. This is because the balance of gravitational forces with aerodynamic forces, expressed as the dimensionless Froude number, is usually not scaled in a dynamic, aeroelastically-scaled, true Mach number model.

The Froude number can be written as:

$$F = \frac{mg}{\rho V^2 l^2} = \left(\frac{m}{\rho l^3}\right)\frac{gl}{V^2} = \mu\frac{gl}{V^2}$$

where μ is the dimensionless mass ratio parameter which must be scaled for dynamic similarity. Recognizing the relative invariability of the gravity constant g, the remaining terms in the Froude number indicate that gravity forces will be properly scaled only when the velocity scale factor is equal to the square root of the length scale factor. However, the requirement for equal Mach number fixes the required velocity scale factor as the ratio of the test speed of sound to the flight speed of sound. For most wind tunnels using air as a test medium, this ratio will not differ much from 1.0. In the Langley transonic dynamics tunnel where Freon-12 is used as a test medium, the speed of sound ratio is about 1/2 leading to a length scale factor of about 1/4 required for simulation of gravity forces. However, the size of the tunnel dictates length scale factors of about 1/8 for fighters and about 1/20 for large transports. Thus, the models tested on the mount system lifting their weight operate at lift coefficients much lower than those for the aircraft.

For Freon testing, the relationship between lift coefficient and length scale factor is

$$C_{L_M} \cong 4\left(\frac{l_M}{l_A}\right) C_{L_A}$$

The Lift-Balancing Device

One means of attacking this problem in a approximate manner, for studies where simulation of the flight lift coefficients is important, is to provide an external force in addition to the model weight. Again, this force must be applied without significantly altering the dynamics of the system, i.e., it must have small mass and stiffness. Such a device has been developed and installed in the transonic dynamics tunnel.

The device used can be described as a very soft pneumatic spring and it is shown schematically in figure 10. Essentially the device consists of a cylinder housing a light-weight piston, the rod of which is attached to the model through a flexible cable. The volume of air on either side of the piston provides a low spring rate, and, therefore, a minimum of restraint. Exhaust and inlet valves are operated to maintain an air pressure on the piston so that the force just equals the aerodynamic lift generated by the model in excess of the model weight. Angle of attack is changed by altering the tail incidence angle and then balancing the additional lift produced by the model with the balancing device.

An essential feature of the device is a "blow-by" piston, i.e., a piston that does not seal one side of the piston from the other. Thus, if a small incremental force generated by the model (in addition to the static force the piston in counterbalancing) causes the system to be displaced rapidly, the air tends to escape around the piston rather than being compressed. This reduces any change in piston force due to movement of the piston, and, therefore, significantly reduces the stiffness of the system. The relatively loose fit of the piston also minimizes friction in the device.

The advantages of this device in combination with the two-cable mount are as follows:

1. The system is both simple to fabricate and operate.

2. Large lift counterbalancing forces can be generated.

3. The system has low mass, stiffness, and friction.

4. The inherent restriction found in the two-cable mount which relies on the model just lifting its own weight is relaxed, allowing approximate simulation of high lift.

The simulation is only approximate because the part of the total lift which is reacted by the lift-balancing device is concentrated at or near the model center of gravity. Thus, the structural deformations associated with this simulated gravity force are not truly scaled because this force does not have the proper distribution. The proper distribution of gravity forces on the model is a formidable experimental problem. The present technique does cause the model to produce the correct total lift, however, the distribution of lift will be in error.

Applications

In preparation for a study of buffet loads and response, two different "dummy" models (described previously) have been investigated exploring the performance of the lift-balancing device. The device worked very well and did not cause any additional stability problems at modest lift coefficients. Two different limitations in maximum obtainable lift coefficient were found. In the first case, at certain conditions involving extensive regions of separated flow, the model became dynamically unstable, not unlike the airplane. The usefulness of the technique for studying stability characteristics at high lift has not been explored but shows promise.

In the second case, the aerodynamic control power was resisted by the restoring moments of the mount system at angles of attack below the desired attitude. There are several approaches available to overcome this latter limitation and one approach has been successfully demonstrated. The model of a large subsonic bomber described previously in connection with gust frequency response function measurements was successfully tested up to its maximum lift coefficient where instability occurred. It will be recalled that this model was supported on a variation of the two-cable

mount system which has very low restoring moments. Thus, the aerodynamic control power was adequate to force the model to desired attitudes.

CONCLUDING REMARKS

Techniques for wind-tunnel studies of a variety of stability, control, and response characteristics of elastic aircraft which are in use at the NASA Langley transonic dynamics tunnel have been described. All of these methods employ a dynamic, aeroelastically scaled model supported on a simple two-cable mount system which provides close simulation of free-flight conditions. The mount system has proven to be very versatile and, with variations, has been successfully applied to several different problems. Both static and dynamic control effectiveness and stability derivatives have been studied using the basic approach followed in flight testing; namely, measuring the response of the model to known control inputs. Response to sinusoidal gusts have been investigated using the basic model-mount system in conjunction with a device to impart sinusoidal gusts to the wind-tunnel airstream. And, finally, problems associated with high lift such as buffeting have been studied by adding a device to the basic arrangement which compensates for the lift in excess of the model weight without sacrifice of model freedom of movement.

REFERENCES

(1) Reed, W. H., III; and Abbott, F. T., Jr.: A New "Free-Flight" Mount System for High Speed Wind-Tunnel Flutter Models. Proceedings of the Symposium on Aeroelastic Dynamic Modeling Technology, U.S. Air Force Systems Command, RTD-TDR-63-4197, Part I, 1964.

(2) Reid, C. F., Jr.; and Wrestler, C. G., Jr.: An Investigation of a Device to Oscillate a Wind-Tunnel Airstream. NASA TN D-739, 1961.

(3) Gilman, Jr., Jr.; and Bennett, R. M.: A Wind-Tunnel Technique for Measuring Frequency-Response Functions for Gust Load Analyses. Journal of Aircraft, vol. 3, no. 6, Nov.-Dec. 1966.

(4) Etkin, B.: Dynamics of Flight, Stability, and Control. John Wiley and Sons, Inc., 1959.

(5) Abel, I.: A New Wind-Tunnel Technique for the Measurement of Various Aircraft Stability Derivatives. A thesis presented to the faculty of the Department of Engineering, University of Virginia, June 1968.

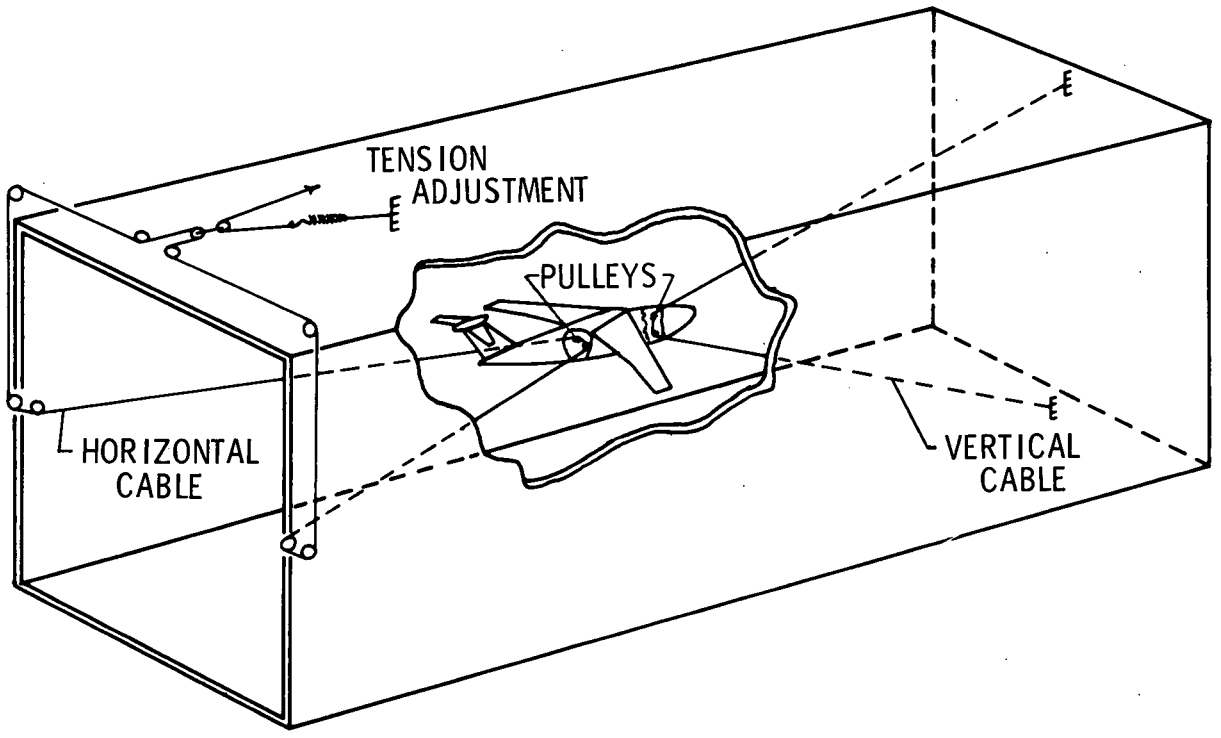


Figure 1. Two-cable-mount system.

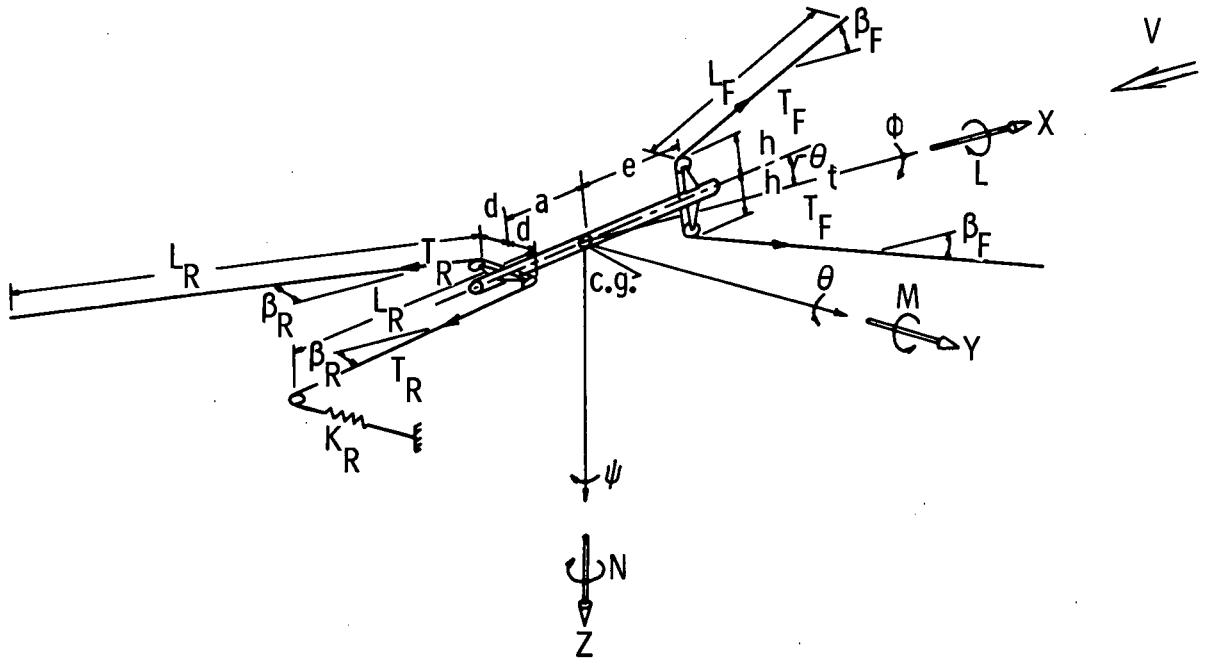


Figure 2. Two-cable-mount configuration.

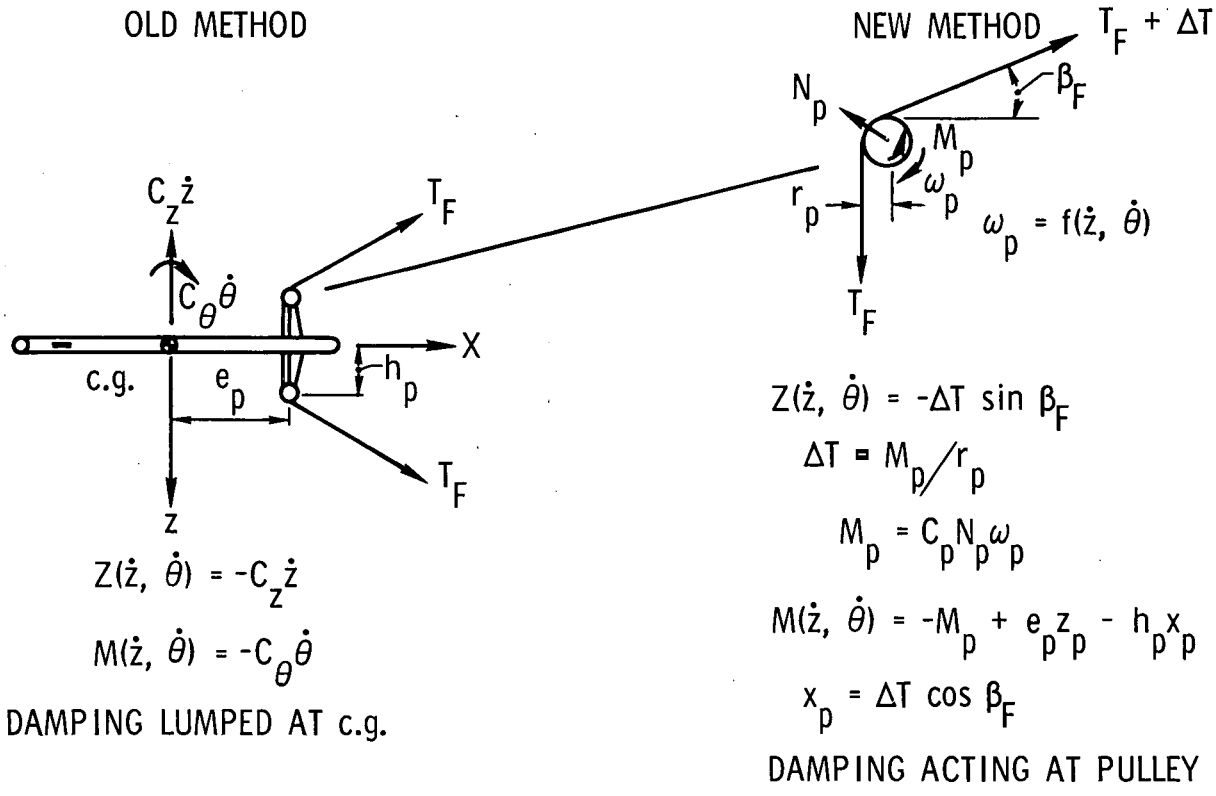


Figure 3. Mount damping.

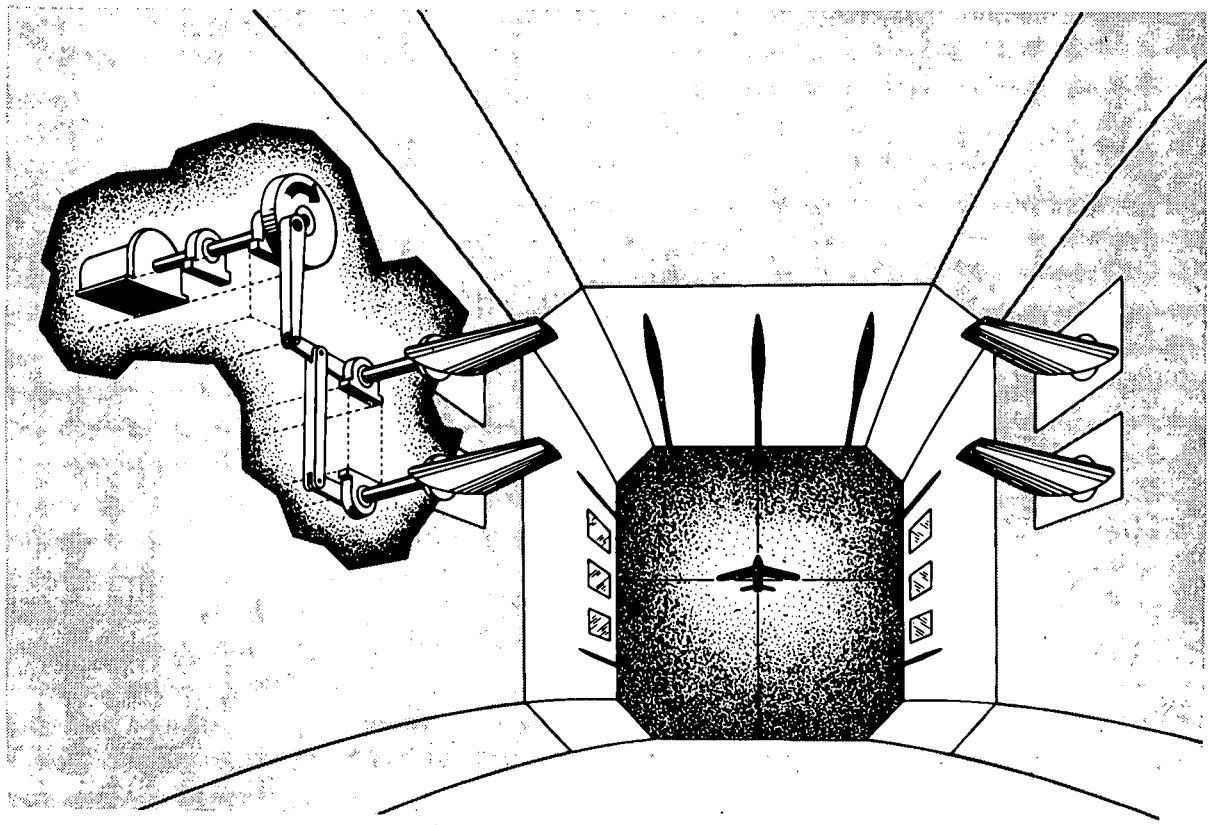


Figure 4. Langley transonic dynamics tunnel airstream oscillator. View looking downstream toward model with cutaway showing schematic of mechanism.

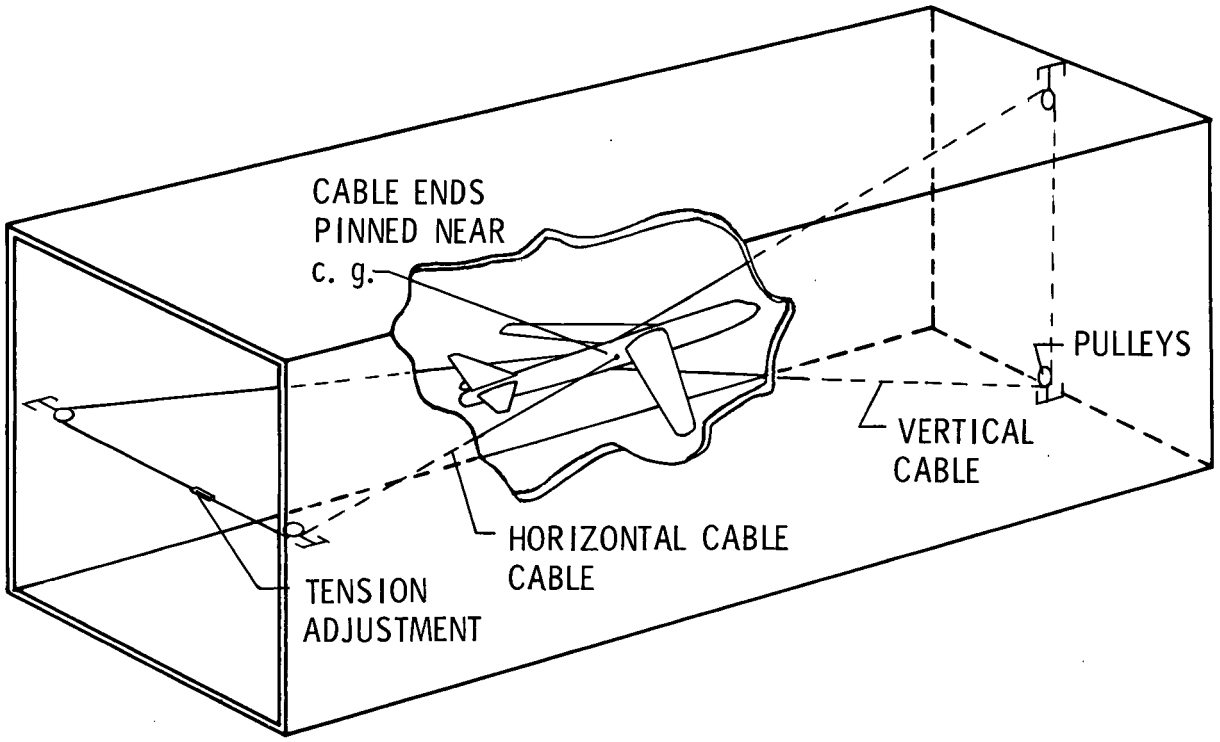


Figure 5. Modified two-cable-mount system.

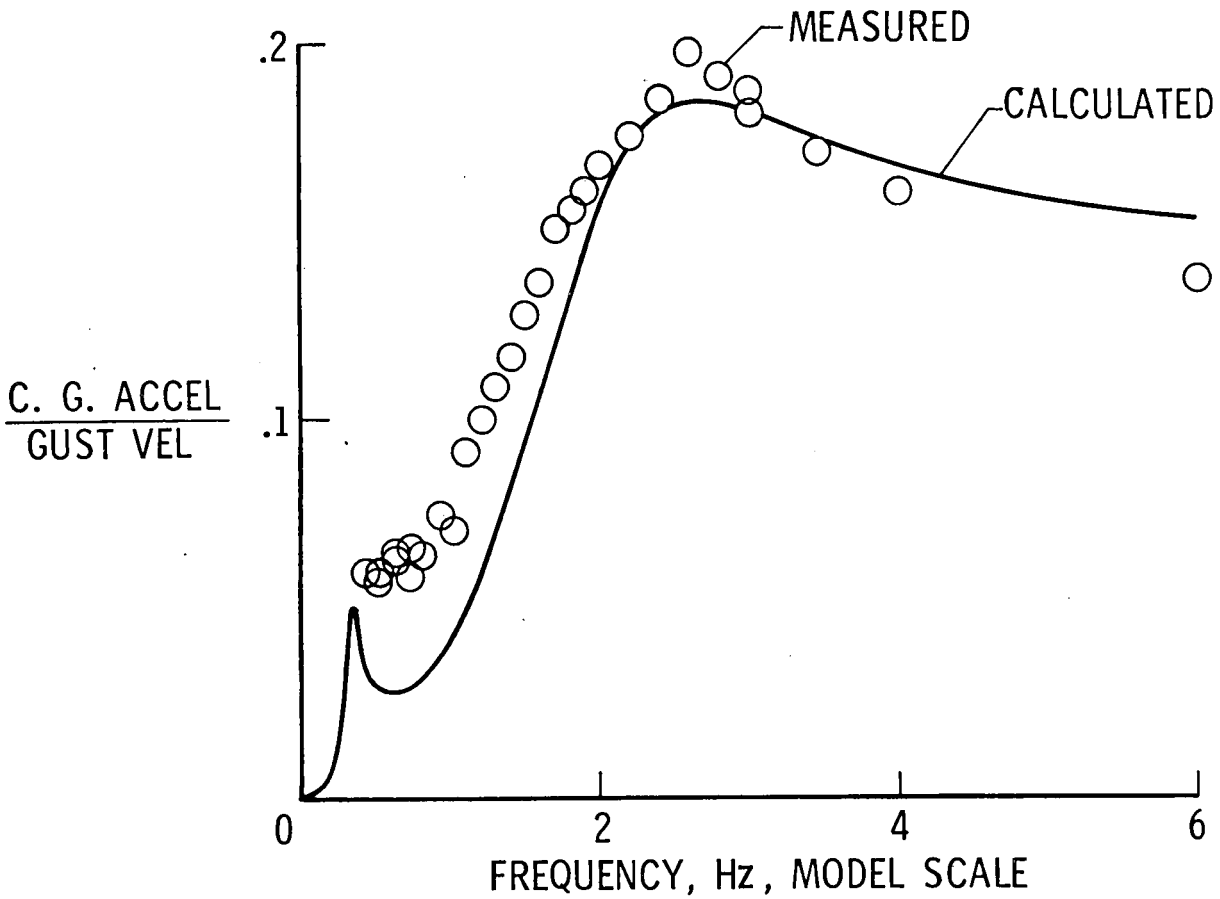


Figure 6. Calculated and measured "Rigid" model response.

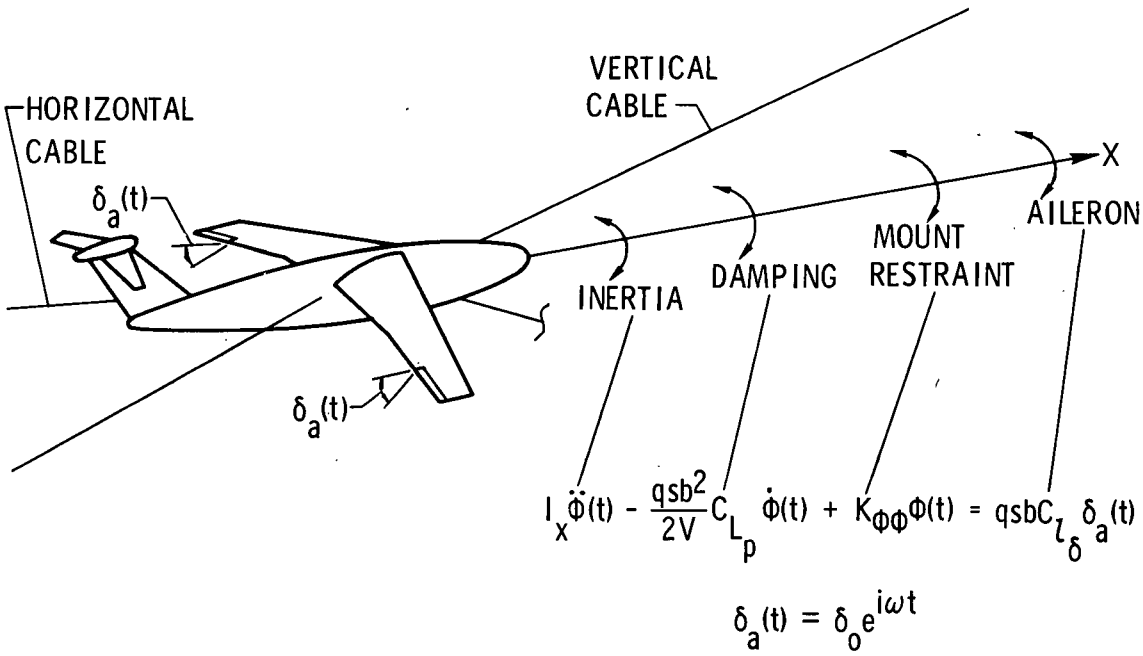


Figure 7. Aileron effectiveness measurements.

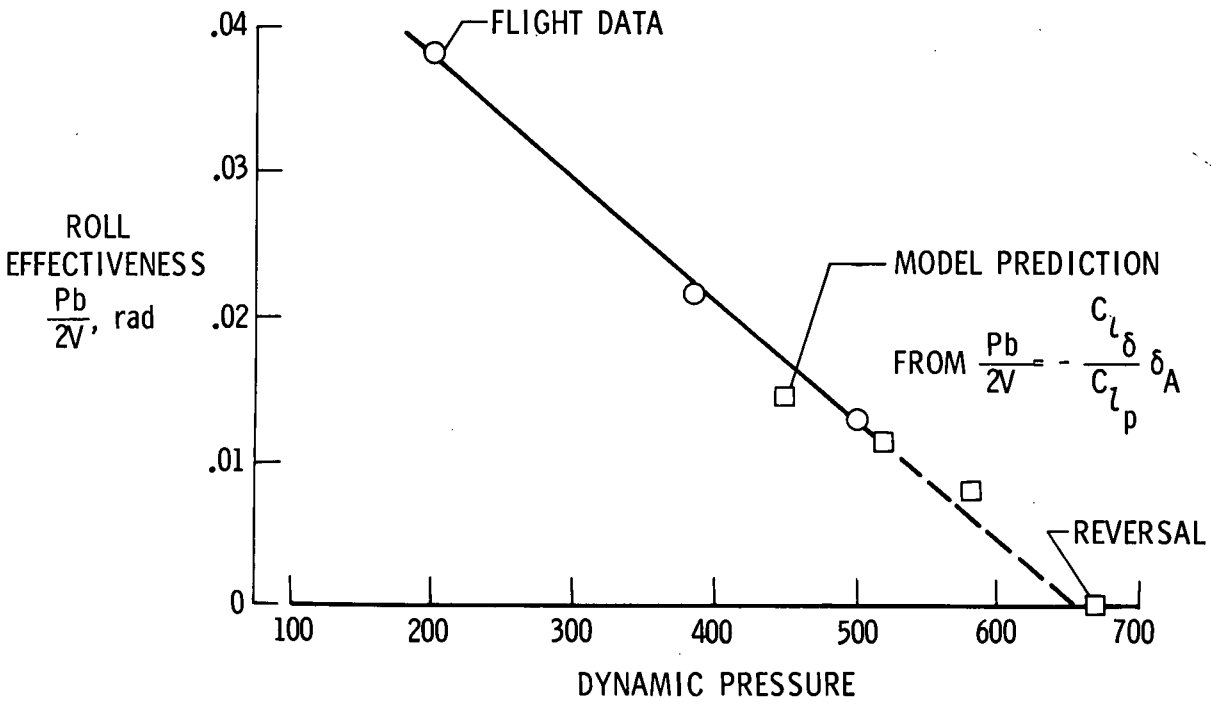


Figure 8. Comparison of flight measurement and model predicted aileron effectiveness.

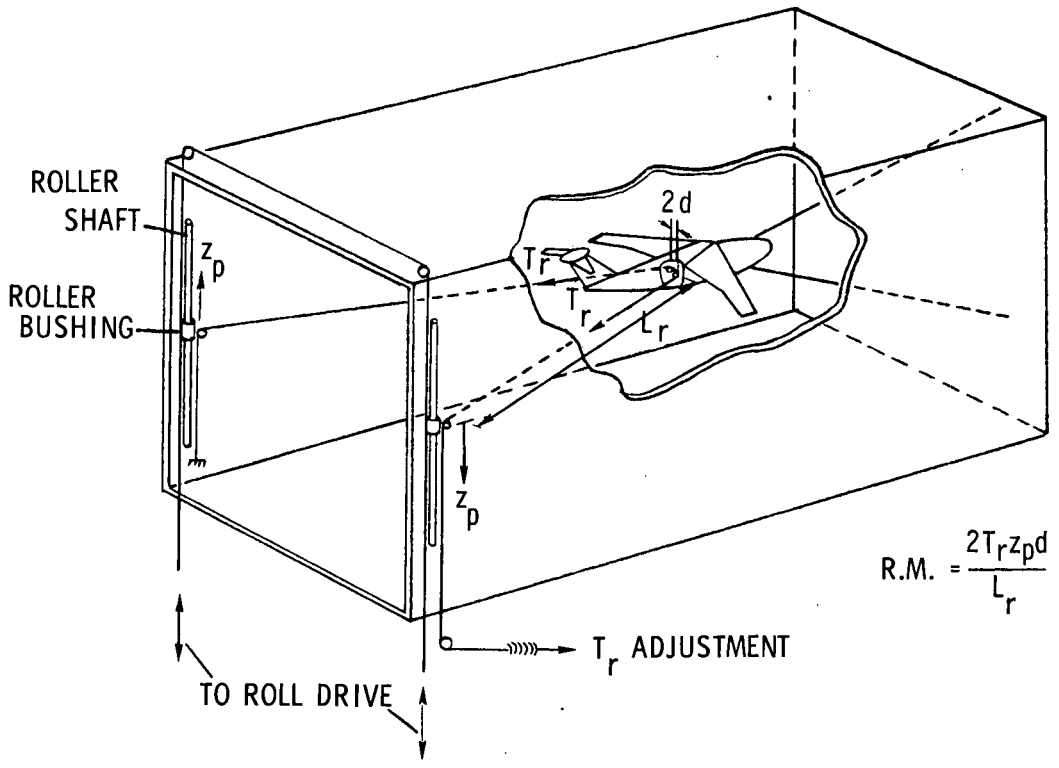


Figure 9. Two-cable-mount with roll control device.

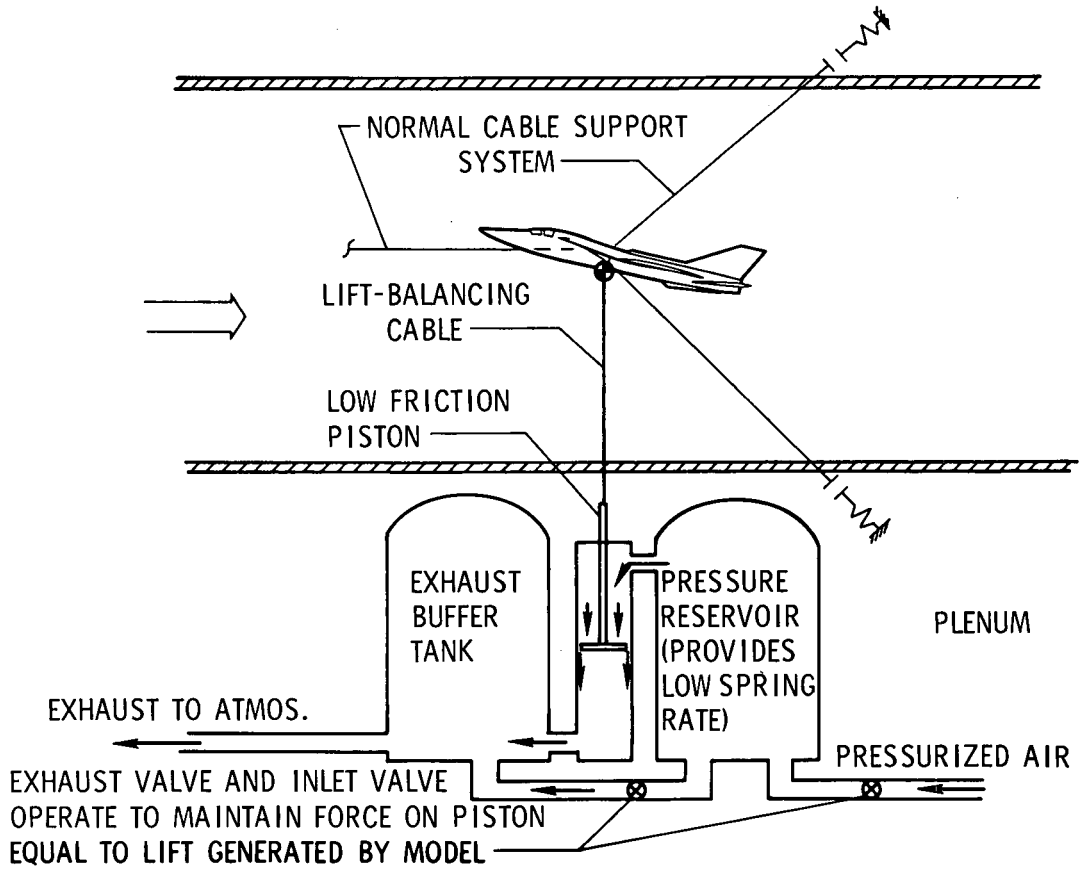


Figure 10. Lift-balancing device for testing models at high-lift coefficient.

FLIGHT AND GROUND LOAD MEASUREMENTS BY STRAIN GAUGES

by

P. B. Hovell

Royal Aircraft Establishment,
Farnborough, Hants.

SUMMARY

The paper discusses the loads which should be measured in structural integrity tests and reviews the techniques available for the interpretation of strain measurements for such purposes. There is a need to measure the overall loads acting on the major components for the study of many loading actions but a knowledge of the local internal loads is required when the environment of flight provides the loading actions. These occur in flight through turbulent air and taxying over a rough runway. Instrumentation problems: recording equipment, strain gauges and adhesives are not discussed.

Sommaire

Le present article est consacré à l'étude des charges qui doivent être mesurées au cours des essais d'intégrité structurale et à l'examen des techniques disponibles pour interpréter les mesures obtenues à cet effet avec les jauges de contrainte. Pour l'étude de nombreux cas de chargement, il y a lieu de mesurer l'ensemble des charges agissant sur les éléments principaux mais, lorsque les chargements sont dus aux conditions ambiantes du vol, il est nécessaire de connaitre les charges internes locales. De tels chargements se manifestent dans le cas de vol en air turbulent et de roulement au sol sur mauvaise piste. On ne traite pas les problèmes d'instrumentation, à savoir les matériels d'enregistrement, les jauges de contrainte et les adhésifs.

1. INTRODUCTION

The trend in airworthiness requirements has been to discard the unrealistic criteria which once formed the basis of the strength and stiffness requirements and to replace them by more rational loading actions in which the appropriate inputs are applied to the flexible aircraft. These refinements have been encouraged by the availability of the computer which allows the investigations to cater for the influences of structural flexibility and mass distribution as well as for the effect of the time element in the disturbance. There must be limitations in such comprehensive calculations and experimental verification of the theoretical conclusions by suitable flight measurements is most desirable. The investigations can be separated into two regimes of interest. Firstly, there is the measurement of the net overall loads, i.e. the algebraic sum of the aerodynamic and inertia loads, acting on a major component when the loading action is initiated by the pilot and when the structural response is of little consequence. Secondly, there is the measurement of the local structural loads when the environment provides the loading action. Typical cases are flight through turbulent air and taxying over a rough runway. In these cases the structural response may dominate the load distributions and the investigations would then establish the magnitudes and frequencies of occurrence of the internal loads and their correlations with the severities of the environments expected during the operational life of the aircraft. This task can best be done with strain gauges attached to selected structural members. The alternative of measuring pressure distributions and accelerations would seem to be precluded because the internal loads would be obtainable only through stressing analyses of the measured overall loads. This would be a formidable task involving the investigation of a multiplicity of flight conditions, each of which may be significant at a particular point in the structure.

The technique to measure overall loads was last discussed by the Fluid Mechanics Panel in 1957 (1). Since then there have been many flight load investigations but little information regarding the techniques required to meet changes in aircraft design and in design philosophy. The bulk of the investigations have been made in America; this brief survey draws on this experience, and also on that obtained in British experiments made during the past few years. Instrumentation problems, recording equipment, strain gauges, and adhesives, are not discussed and the paper is concerned only with the interpretation and use of the measured strains.

2. INTERPRETATION OF FLIGHT MEASURED STRAINS

2.1 Overall Loads

Early attempts to exploit strain measurements in flight investigations used essentially equilibrium methods for their interpretation and, in general, were found to be unsatisfactory. The deficiencies were not in the performance of the strain gauge, nor in the conversion of the response into a stress but arose from the inaccuracies in comparing the measured stresses with those either calculated in the stressing or measured at similar positions on the strength test specimen. The calculated stresses were usually subject to many simplifying assumptions and, as also in the case of the stresses measured on a test specimen, they were known only for a limited number of design cases which did not necessarily match the flight conditions. The derivation of the overall load parameters, bending moment M, torque T and shear V at the particular section introduced further errors from the uncertainties in the effective areas and moment arms to be associated with the measured stresses. The philosophy adopted in British flight programmes was to use strain gauges as transducers for load determination and not for the investigation of stress distributions in the structure. A knowledge of such distributions did not produce good agreement with the known loads applied in major strength tests in which very extensive gauge installations could be used in their determination. The earliest British report (2) emphasised the importance of calibrating the more limited flight installations in order to assess the accuracy of the measuring system.

The difficulties of the equilibrium method were overcome by a statistical technique which was developed by the NACA (3) and, stimulated by the mandatory requirement to measure flight loads on American military aircraft, has been used extensively since the early 1959's. In general, a strain gauge installed in the structure will respond to two or more of the parameters M, T and V. The NACA method uses a sample of gauge responses obtained from the successive application of an individual load at a number of stations on the structure. The gauges are usually installed across a section of the structure to measure the local shear and bending strains in the main structural elements and these quantities are dependent on the position of the calibration load in a simple or complex manner according to the detail design of the structure. It is then assumed that the responses μ_1, μ_2.... of the gauges G_1 G_2.... can be combined such that, for example

$$M = \beta_{11}\,\mu_1 + \beta_{12}\,\mu_2 + \beta_{13}\,\mu_3 + \cdots$$

where M is the overall bending moment at the chosen section and β_{11}, β_{12}, β_{13} etc. are coefficients obtained from the calibration data by regression analysis. Similar equations are obtained for the shear and torque.

There are two possible arguments for the application of these regressions for the estimation of a flight loading:

(a) A statistical argument that the individual load sample is representative of the whole population of loadings and that any flight loading must be a member of that population.

(b) An argument that the flight loading is the summation of proportions of the individual loads. Each of these can be estimated by the regressions and consequently so also can their sum be estimated.

It is extremely difficult to establish the validity of (a) and thus the use of the statistical standard error of the estimate of a distributed loading from the variances and covariances of the regression analysis would be dubious.

The justification for (b) requires the structure to conform with the principle of superposition and the mesh size of the calibration must provide satisfactory representations of the continuously distributed loadings encountered in flight and of the associated gauge responses. Theoretically the regressions can be used over a limitless range of centres of pressure but, in practice, the accuracies of the estimation of any distributed loading will vary with the centre of pressure. Accuracies within $\pm 5\%$ are usually claimed for applications to measure distributed loadings on medium to high aspect ratio structures.

An application of the technique to measure Lightning fin loads (4) illustrate the difficulties of applying it to multi-spar constructions of low aspect ratio. Figure 1 shows the gauge installations and loading pad positions for the measurement of M, T and V at a section 0.69m from the root. Figures 2 and 3 illustrate the variations in the responses of the shear and bending moment gauges on spar 5 with the position of the calibration load. The sensitivity with the location of the load demonstrates that distance is required for reasonable diffusion of the loads into the structure and this is not available for loads inboard of Rib 3. The difficulty, common to all low aspect ratio structures, is reflected in large standard errors of the regressions. The basic NACA method was modified by changing to a mixed load sample comprised of the original individual load calibrations and various distributed loadings appropriate to the flight conditions under investigation. The response data for the latter were obtained by suitable weighting of the individual load data. The centres of pressure of the distributed loadings are shown in Figure 4. The accuracies of the two sets of regressions, one based on the original sample and the other based on the mixed load sample, can be compared in Figures 5 and 6. The acceptance of similar accuracies for a flight loading demands a reasonable matching of the flight responses, suitably scaled, with the appropriate members of the sample as illustrated in Figure 7. Mesh size and the composition of the sample distributed loadings can be important factors in obtaining the agreement.

The Lightning fin investigation did not introduce problems from the supports because the calibration loads were reacted at the main undercarriages. Nevertheless it was necessary to obtain calibration data for loading positions inboard of the measuring section. These data with an associated zero load input were included in the individual load sample and were also taken into account in the superposed loadings. In cases where the gauge responses are affected directly by the reactions of the supports it is necessary to extend the calibrations over the whole of the aircraft. The gauge responses for distributed loadings would then be based on this data and, because the system is in equilibrium, the effects of the supports would disappear. For similar reasons a regression based on the comprehensive individual load calibrations can also be used for the estimation of flight loadings.

In the Lightning investigations the gauge responses were combined mathematically after recording. In earlier applications the gauges were often combined electrically according to the regressions prior to recording. This technique reduced the demands on recording channels but increased the number of gauge installations because usually the gauge stations were required for more than one load parameter. An additional calibration was necessary to check the efficiency of the electrical combinations.

An alternative method assumes that the response of each gauge is a linear function of M, T and V. The coefficients can be obtained from the calibration data and the simultaneous equations for three selected gauges can be used to determine the overall load parameters from the appropriate flight responses. The method has been used in British investigations but the assessment of its accuracy presents some difficulties.

2.2 Local Structural Loads

A most significant design trend during the past decade has been an increasing interest in dynamic loading actions rather than in the quasi-steady flight conditions implicit in the earlier design requirements. This interest has been possible because of the availability of large capacity computers to do the necessary calculations which take into account the static

and dynamic influences of structural flexibility and mass distribution. The introduction of the time element into the response calculations leads to phase differences in the maximum loads in the various structural elements during the loading action. This is particularly so for flight through turbulence and the complexities introduced in the design procedures have been discussed in recent American reports (5) and (6). Flight load investigations under such conditions present similar difficulties. There has also been a greater concern regarding fatigue life assessment which depends on the identification of these regions where local damage may occur and initiate a major structural failure. A successful assessment requires knowledge of the local loads and their frequencies of occurrence during the operational life of the aircraft and the detail design of the structure may be an important factor. For these reasons the emphasis changes from the overall load parameters to the local loads. It is convenient, even if fortuitous, that there has been a general adoption of finite element methods in the stressing procedures. These methods, essential for designing low aspect ratio structures, use computer programmes to calculate the stresses, or loads, in the structural elements of the mathematical model of the structure. These stress distributions will not necessarily be related in a simple manner to the bending moment, torque and shear at a selected section.

Thus in order to assist the designer it is necessary to interpret the flight strain measurements as local structural loads - a proposition which was abandoned in the 1940s. An immediate consequence of the design trends is an increase in the gauge installations. Some guidance, based on technical appraisal or practical experience, is required on the points of measurements and whether the local spanwise or chordwise loads attributable to shear or bending moment, or both, should be measured.

It would be unprofitable, if not impossible, to measure the stresses at a local stress concentration, either for a direct fatigue life assessment or for an extrapolation to ultimate or limit load conditions. At this stage in the art it appears preferable to install the gauges at points where the stress is reasonably uniform and measure the uni-directional stresses in the spar and rib flanges and shear stresses in webs and surfaces rather than the strains induced by the biaxial stresses in the surfaces of the component. This restriction allows the use of multi-gauge installations which will maximise the bridge outputs and also improve temperature compensation. It is important that the flight measurements can be incorporated in the design clearance calculations and Figure 8 illustrates three methods of obtaining the necessary "calibrations" of the gauges, in order that gauge interpretations are compatible with the stressing. Each of these methods have been used in recent British fatigue life substantiation trials. In two experiments the response obtained from a steady symmetric manoeuvre was used to interpret the responses obtained from each gauge during flight through turbulence. This allowed the comparison of the "equivalent c.g. accelerations" at each station with the accelerations at the centre of gravity to be made either by level exeedences or by root-mean squares (rms). These comparisons indicated the degree of "amplificatio" arising from the dynamic response of the aircraft. The internal loads induced by the steady manoeuvre were estimated by normal stressing methods and the gauge responses were thus converted into local loads. In another investigation the flight measurements were used in association with the responses of similarly positioned gauges in the fatigue test specimen. This method eliminated the need to know the load distribution of the steady manoeuvre and to estimate the internal loads for both that distribution and the particular loading applied to the test specimen. It did however introduce some uncertainties of "identical" gauge installations and of possible variations in the dimensions of the flight and test specimens. Such interpretations did not require a load calibration of the test aircraft. When this has been done, as in the case of a Lightning fin investigation, the flight gauge responses can be compared with those for fatigue test conditions by the superposition of the calibration data. The expected operational experiences for these particular aircraft were established from counting accelerometer readings and consequently it was considered sufficient to establish the correlations between the internal loads and c.g. accelerations measured by accelerometer of similar characteristics.

If the gust input had been measured directly it would have been possible to obtain transfer functions at each gauge station from spectral analyses of the gust input and the gauge responses. These transfer functions could then be compared with theoretical calculations and used with a "standard" turbulence spectrum to provide estimates of No. (number of crossings of the mean value per unit time) and A (rms stress or load/rms gust) for analytical studies of fatigue life and limit design conditions. Many structural components are designed by the interaction of direct and shear loads and consequently it would be necessary to obtain the cross spectrum and coherency function to determine whether the two loads are correlated. Incidentally, flight measurements are a direct source of data for these latter analyses. The design of such experiments and the use of spectral techniques are discussed in reference 7.

3. INTERPRETATION OF GROUND MEASURED STRAINS

The gauge installations outlined above could be used for general structural load measurements under landing and ground manoeuvring conditions. There still remains, however, the need to establish the structural integrity of the undercarriage. The landing cases have always been difficult to investigate experimentally - partly because pilots are reluctant to land at vertical velocities near the specified value and partly because of the problems of measurement.

Despite the apparent simplicity of the average undercarriage structure the measurement of the three load parameters - vertical load V, drag load D and side load S - presents many formidable problems, especially for the landing conditions. The three loads do not act through a common point: the vertical load acts through the hub, the side load through the point of tyre contact and the drag load through the hub or the point of tyre contact according to whether the load is from spin-up or from an application of the brakes. In many practical cases the side and drag loads are deduced from bending strain measurements and thus the geometry of the undercarriage, which changes under the action of the various loads, and the attitude of the aircraft relative to the ground must be known before a reliable estimate can be made of the ground loads. The system behaves in a non-linear fashion because of damping and generally at least two of the load parameters use the same load path. The time history of the drag load is dependent on the horizontal speed and the local conditions of friction whereas that of the vertical load depends on the rate of vertical descent and the characteristics of the shock absorber system. Thus the two loads will not usually maximise at the same or related times after touch-down, and the processing of any practical measurements can be most complicated. However, it should be satisfactory to achieve reasonable accuracy only at the maximum load conditions and the appropriate geometries would then be needed for a very limited number of conditions.

The procedure adopted in previous investigations has been to select the more promising positions for the strain gauges and then to calibrate the system for various geometries by the separate application of static loads V, D and S at their appropriate positions. If reference axes in the undercarriage are adopted the calibrations must include moments about the chosen axes as well as loads along them. There is a consequential need for additional gauge stations to cater for the moment determination but some advantage accrues because the need to measure the attitude of the aircraft vanishes. However, this latter measurement is still required if the ground loads are to be established. In some experiments the undercarriage components have been individually calibrated and the relationships between the various parameters and the gauge responses are based on the geometry of the assembly. The use of separate loads or calibrated components can often mask significant interaction effects: for example the estimate of a drag load from a bending strain may be inaccurate because of the additional bending moment induced by a vertical load acting on a structure deflected by the drag load. For such reasons and to allay doubts that the static calibration procedure can cater adequately for dynamic conditions it is recommended that the accuracies of estimation should be checked with gauge response data obtained from drop tests of the undercarriage on a calibrated platform which provides independent measurements of V, D and S.

It is evident from the preceding discussions that the processing of the data could be most time consuming, and as an alternative it might be expedient to introduce statistical methods and to establish relationships between the load parameters and the gauge responses by regression analysis. The sample data could be obtained in one of the following ways:

(a) from a series of drop tests on a calibrated platform in which drag and side load conditions would be simulated by pre-rotation and moving platform techniques (the wedge technique would be unsatisfactory because it produces drag or side loads which are directly correlated with the vertical load throughout the impact cycle);

(b) from a number of static calibrations in which various combinations of V, D and S are applied to an undercarriage;

(c) from the superposition of response data obtained from component calibrations and a knowledge of the geometries of the undercarriage.

It would be most convenient if the regressions could be used universally but it is more likely that acceptable accuracies will be obtained only for a limited range of geometry. Thus samples to match particular ranges would be required.

The preceding discussion has been written with the single-wheel or twin-wheel undercarriage in mind. For these the selection of the critical conditions from the time histories of the load parameters should not be unduly difficult. In the case of bogie undercarriages, either the front or rear wheels contact the ground initially and the bogie beam rotation is controlled by a shock absorber until eventually the other wheels impact with the ground. Thus, in general, the critical ground loads will be deduced from the time histories of three loads and three moments at each end of the beam and from the shock absorber load. A further complication will arise from the fairly large changes in geometry. The loads from ground manoeuvring should be easier to determine because the rates of change of the loads and of the geometries will not be so high.

With uncertainties regarding the points of likely fatigue failure and the nature of the V, D and S loadings it would seem more rational to assemble load spectra for the various components, such as drag strut, shock absorber, brake rods, torque links etc. by direct measurement under typical operating conditions rather than by the inspection of the overall loads.

4. DATUM LEVELS

The relevant flights parameters - speed, altitude, accelerations, pitch, roll and yaw attitudes and rates, control surface positions etc. - must also be measured to identify the particular flight condition. In general it should be necessary to investigate a limited number of flight conditions matching the critical modes of major structural failure and ideally for structural integrity tests it would be desirable to compare directly the flights loads with the unfactored loads of the design conditions. However this may not always be possible and the measured flight loads would then be used to establish confidence in the loading action calculations. The shortcomings arise from two sources. Firstly, it may be physically impossible to match flight and design conditions or it may be too hazardous to simulate an emergency condition specified for the aircraft. Secondly, there are difficulties in the choice of datum levels from which the gauge readings will be interpreted. Recordings taken at ground static conditions do not always correspond to zero load levels in the component and the estimation of the relevant ground loads introduces some uncertainty. In the earliest strain gauge investigations the use of ground zero readings was dubious because of drifts of the gauges and recording equipment. Some improvement is effected by temperature compensated systems such as half or whole bridge installations and further gains accrue from the use of "selective-melt" gauges whose temperature characteristics are matched with those of the structural material. An American technique establishes datum levels of zero stress in flight, but it involves the assumptions that "zero-g and zero-q" conditions produce zero stress throughout the structure and that the corresponding gauge responses can be extrapolated with confidence from measurements taken during roller-coaster manoeuvres at various speeds.

In many of the British investigations only the incremental gauge responses from the 1g level flight conditions have been interpreted as loads, it being assumed that the loading at 1g flight condition is known to reasonable accuracy. This does not preclude the use of ground static levels when there is evidence of the stability of the instrumentation but the increments from these levels may then include thermal loads as well as the usual internal loads. It is envisaged that the gauge installations will be internal and thus protected from any rapid changes in temperature but doubtless the gauges would respond to any self-equilibrating loads induced by differential expansions of the structure. However in the time scale of a manoeuvre or flight through turbulence it is most unlikely that the 1g level flight datum levels will change. Thus there are many advantages to be gained from using incremental strains from flight based zeros for the estimation of the net loads.

CONCLUSIONS

Techniques are available for the interpretation of strain gauge measurements either as overall loads on the major structural components or as local loads in the structure. The former presentation is satisfactory for the study of many loading actions but local load information is more relevant when structural flexibility and mass distribution influence the response of the aircraft to the disturbance. In the particular cases of flight through turbulence and taxying on rough runways, the problems of transferring the measured loads into the design procedures reflect the complexities of the analytical treatment of these loading actions. However there can be little doubt of the need to substantiate the conclusions of theoretical studies by comprehensive flight strain measurements.

The measurement of undercarriage loads present many problems and it seems unlikely that such programmes will be as successful as the measurements to establish the structural integrity of the other major components.

REFERENCES

No.	Author	Title, etc.
1	N. A. Krause	Strain Gauge Calibrations and Flight Loads Testing Techniques AGARD Report 113, May 1957
2	J. Taylor	The investigation of air loads in flight from measurements of strain in the structure ARC R & M 2408, November 1945
3	T. H. Skopinski, W. S. Aiken, Jr. and W. B. Huston	Calibration of strain gauge installations in aircraft structures for the measurement of flight loads NACA Report 1178, 1954
4	P. B. Hovell, D. A. Webber and T. A. Roberts	The use of calibrated strain gauges for flight load determination ARC Current Paper 1041, 1969
5	F. M. Hoblit, N. Pane, J. D. Shelton and F. E. Ashford	Development of a power spectral gust design procedure for civil aircraft FAA-ADS 53, July 1965
6	J. R. Fuller, L. D. Richmond et al	Development of a power spectral gust design procedure for civil aircraft FAA-ADS 54, July 1965
7	E. J. Durbin (ed)	Flight Test Manual, Vol IV AGARD

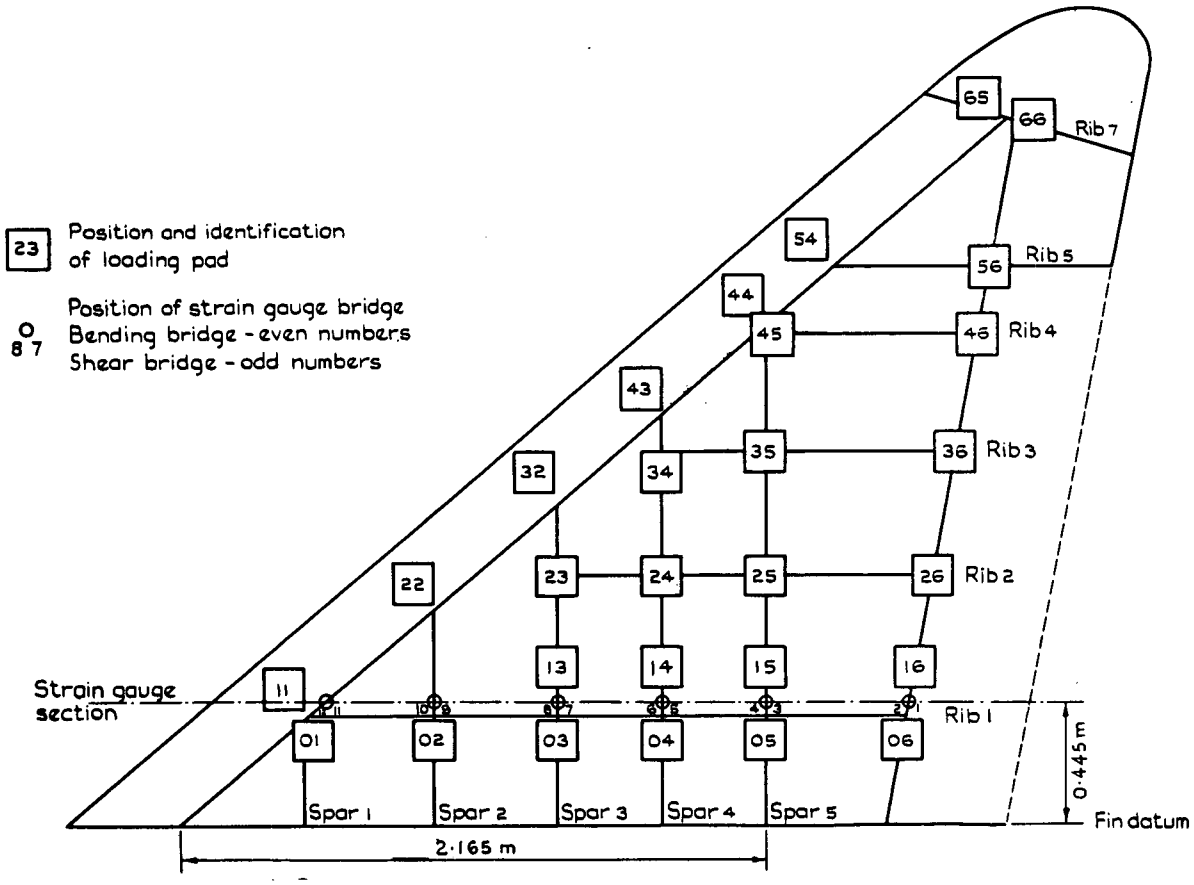


Fig. 1 Strain gauge bridge and loading pad positions

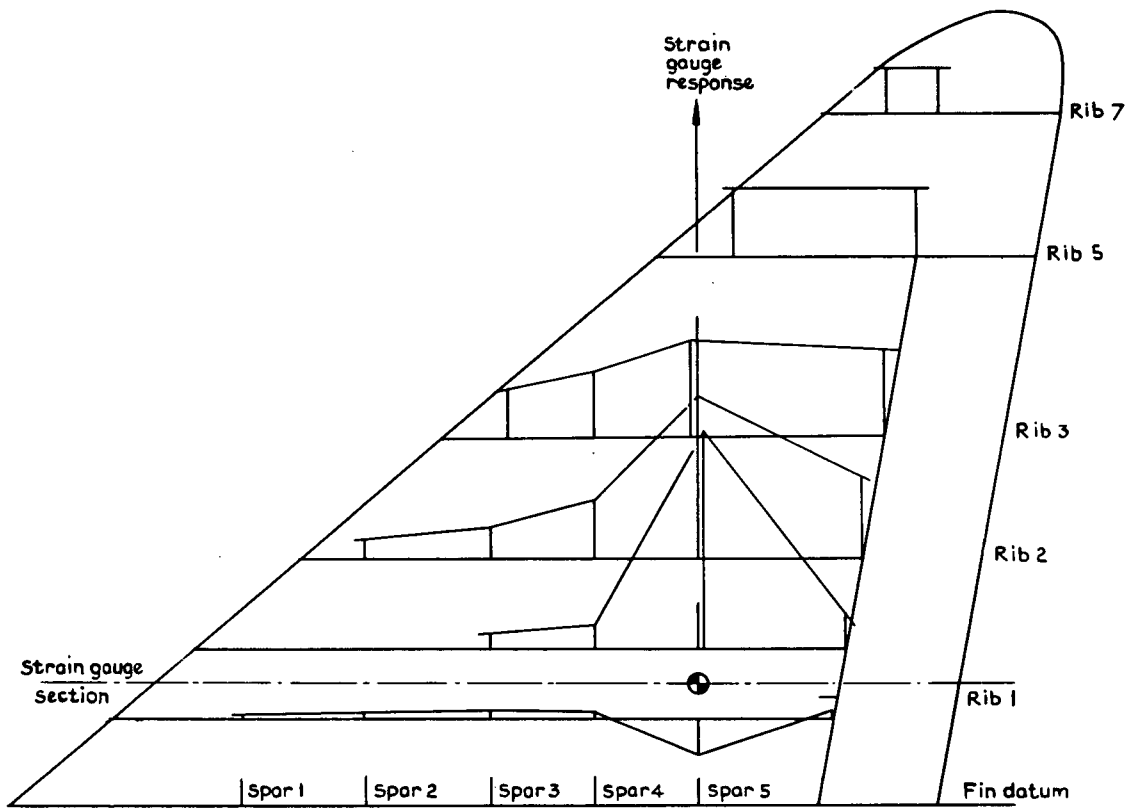


Fig. 2 Response of shear gauge ⊕ on Spar 5 with position of unit load

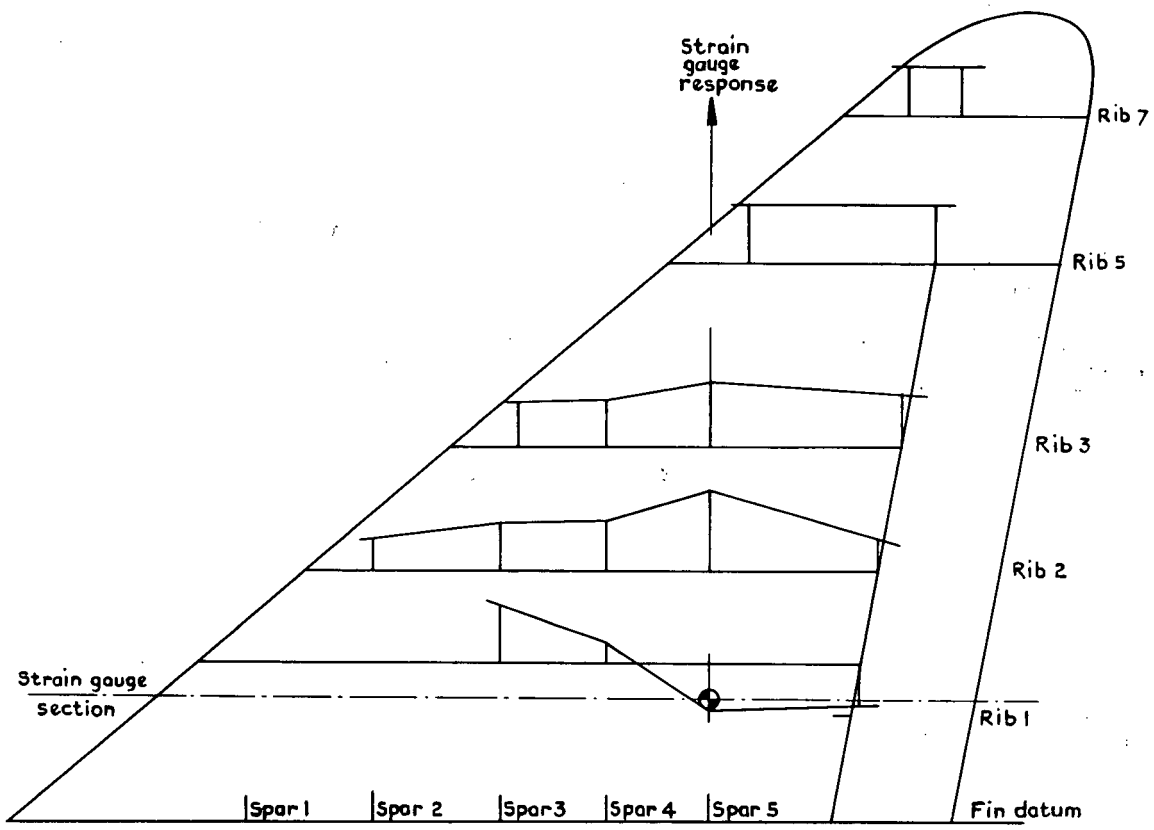


Fig. 3 Response of bending moment gauge ⊕ on Spar 5 with position of load
(Load scaled to produce unit bending moment)

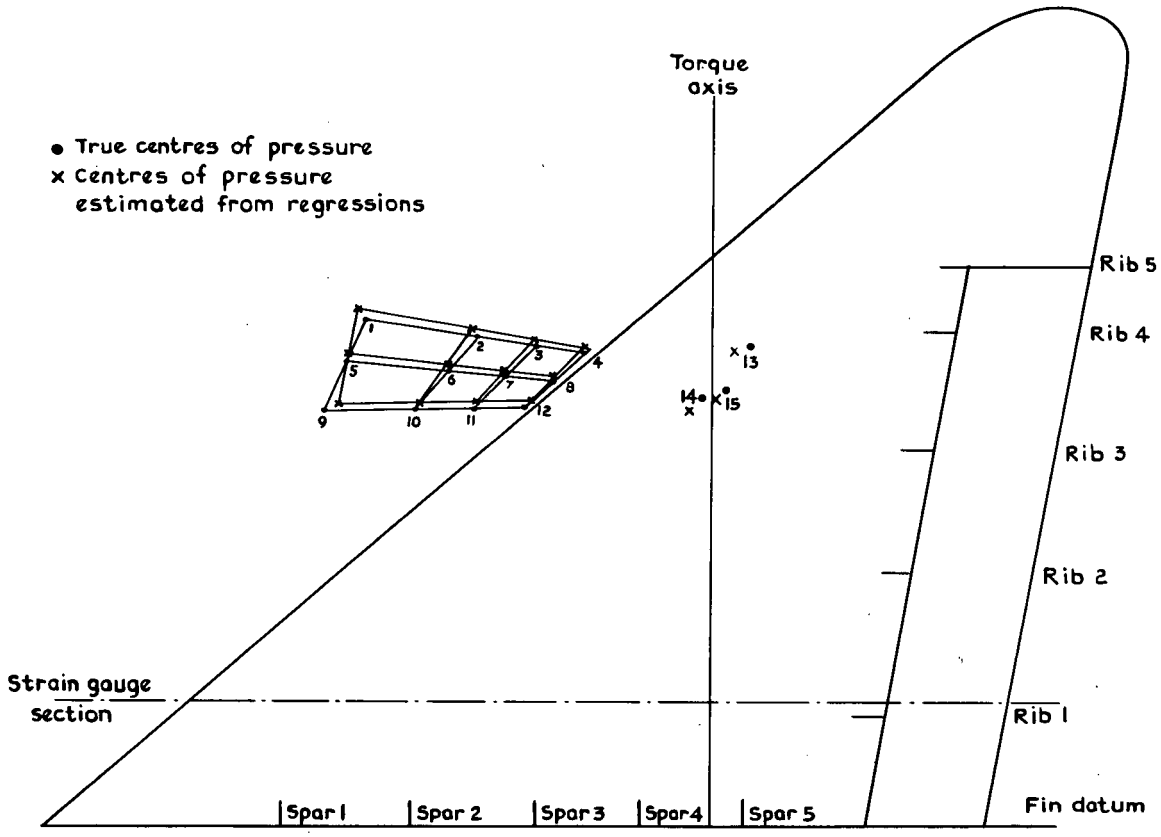


Fig. 4 Centres of pressure of distributed load sample

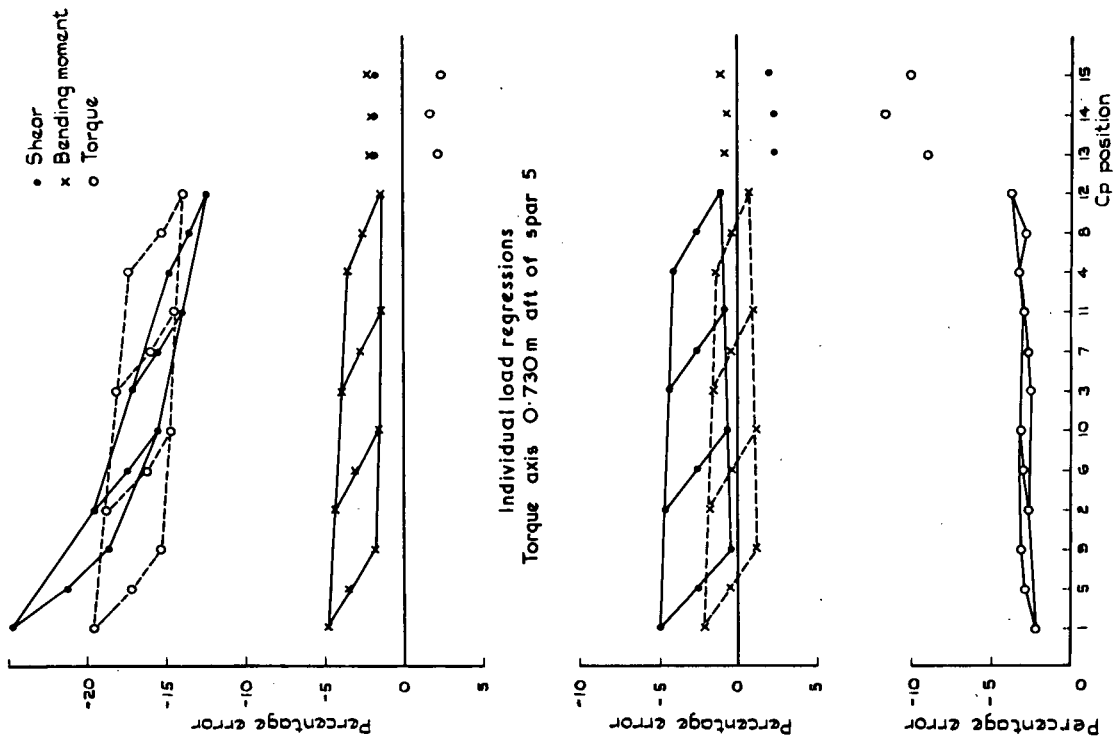


Fig.5 Percentage errors of estimates of sample distributed loads

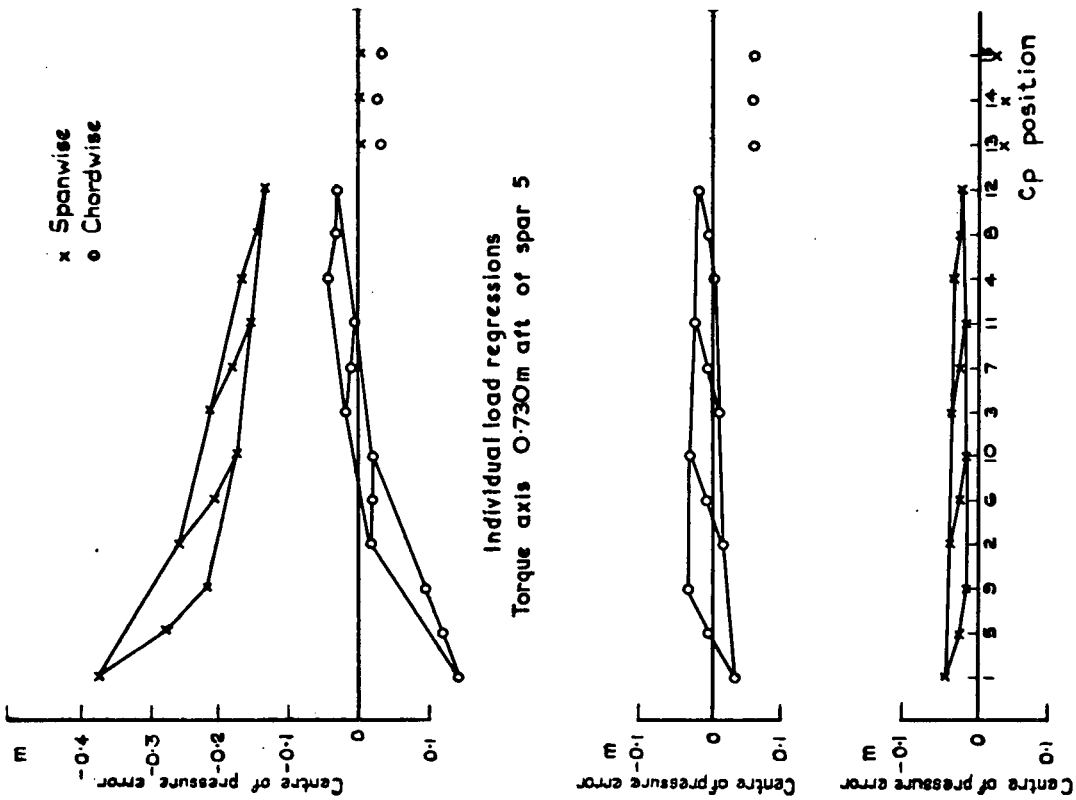
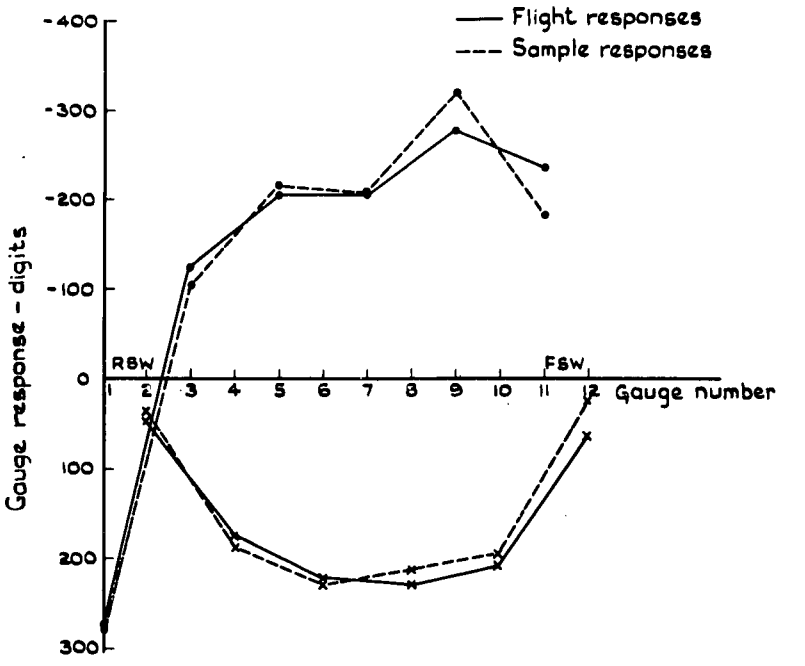


Fig.6 Errors of estimated centres of pressure of sample distributed loads



M = 0·9 Alt = 6350 m Indicated SS = -3·75° Normal accel = 2·1g

Centre of pressure of sample load Spanwise = 1·41 Chordwise = -1·25 m
Estimated centre of pressure of sample load Spanwise = 1·43 Chordwise = -1·20 m
Estimated centre of pressure of flight load Spanwise = 1·42 Chordwise = -1·20 m
Flight load shear estimate = 1179 kg

Fig. 7 Comparison of responses of flight load with sample load. Sideslip to starboard-responses scaled to estimated shear of 606 kg

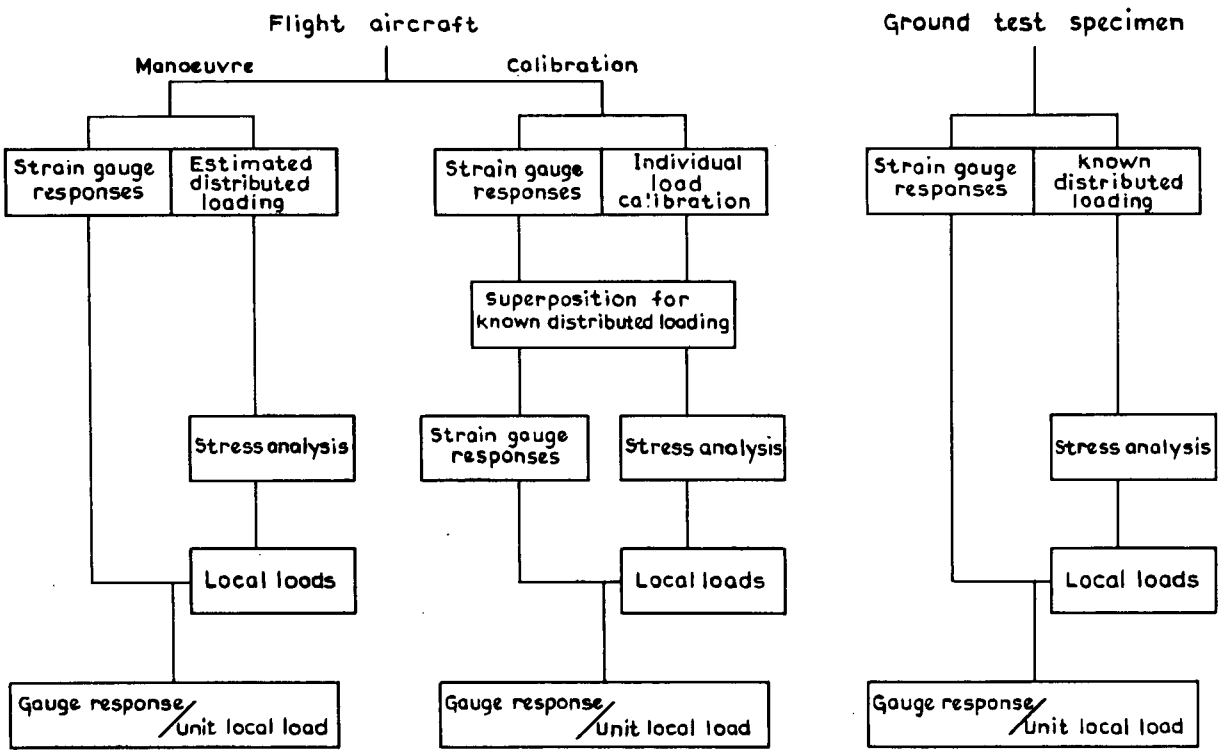


Fig. 8 Calibration of gauge responses as local structural loads

CONSIDERATION OF STABILITY AUGMENTATION SYSTEMS FOR LARGE ELASTIC AIRCRAFT

CLIFFORD F. NEWBERRY

THE BOEING COMPANY
WICHITA, KANSAS

ABSTRACT

Use of stability augmentation systems for control of elastic vibration modes of large flexible aircraft has become a reality. This paper deals with design criteria, development and evaluation of such systems. Examples and illustrations are drawn from three design studies. Two of these studies were for large subsonic aircraft for which the resulting systems have been flight tested. The other study is for a large supersonic airplane currently in the design phase. Analytical methods used to develop stability augmentation system concepts are presented and discussed with examples to show significant aspects of the analysis. Results presented show stability augmentation system performance in terms of mode damping, fatigue damage rates, and ride characteristics in turbulence. Comparisons are made of theoretically predicted and experimental results. Limitations encountered in adapting a Load Alleviation and Mode Stabilization system to an existing airframe configuration are discussed.

This paper was prepared at the request of Mr. William E. Lamar, Deputy Director of the Air Force Flight Dynamics Laboratory, Wright-Patterson Air Force Base, Ohio, for delivery at the Spring 1969 meeting of the Advisory Group for Aviation Research and Development Flight Mechanics Panel on "Aeroelastic Effects from a Flight Mechanics Standpoint", Marseilles University, 21-24 April 1969. The author is indebted to the work conducted by Mr. James I. Arnold and his colleagues for developing the data used in this report. The author is also indebted to the following reviewers of this paper: James I. Arnold, Gerald E. Gergmann, Alfred B. Herren, and Glenn O. Thompson of The Boeing Company.

NOMENCLATURE

Symbol	Description	Units
$\ddot{\delta}$	Control Surface Angular Acceleration	Radians/Second^2
$\dot{\delta}$	Control Surface Angular Velocity	Radians/Second
δ	Control Surface Rotation	Radians
δ_R	Rudder Rotation	Radians
ζ	Damping Ratio	---
θ	Feedback Phase Shift	Degrees
σ	Real Part of Complex Number	---
ϕ	Airplane Roll Rotation	Radians
$\dot{\psi}$	Airplane Yaw Rate	Radians/Second
ψ	Airplane Yaw Rotation	Radians
ω	Frequency	Radians/Second
ω_d	Damped Frequency	Radians/Second
ω_n	Natural Frequency	Radians/Second
BS	Airplane Body Station	Inches
cps	Cycles per Second	---
db	Decibels	---
DOF	Degrees-of-Freedom	---
FT	Feet	---
g	Gravitational Acceleration Constant	Feet/Second^2
$H_1(S)$	Transfer Function for Yaw Rate Feedback Loop	---
$H_2(S)$	Transfer Function for Lateral Acceleration Feedback Loop	---
Hz	Hertz	---
j	$\sqrt{-1}$ Unit Imaginary Number	---
K	Feedback Gain	---
$[K]$	Matrix of Airplane Modal Coefficients	---
KCAS	Calibrated Airspeed	Knots
KEAS	Equivalent Airspeed	Knots
KIPS	Weight	10^3 Pounds
$K_i(X)$	Modal Coefficient for i^{th} Degree-of-Freedom	---
$K_{\ddot{Y}}$	Stability Augmentation Accelerometer Channel Gain	---
$K_{\dot{\psi}}$	Stability Augmentation Yaw Rate Channel Gain	---
LBS	Pounds Weight	---
$[N_2]$	Matrix of Generalized Mass and Aerodynamic Apparent Mass Terms	---
$[N_1]$	Matrix of Generalized Circulatory Aerodynamic Damping Terms	---
$[N_o]$	Matrix of Generalized Structural Stiffness and Non-Circulatory Aerodynamic Stiffness Terms	---
$[n_2]$	Generalized Inertia Force Matrix	---

Symbol	Description	Units
$[n_1]$	Generalized Non-Circulatory Damping Force Matrix	---
$[n_o]$	Generalized Non-Circulatory Spring Force Matrix	---
PSD	Power Spectral Density	---
P_S	Ambient Pressure	---
P_T	Dynamic Pressure	---
$\ddot{q}$	Acceleration of the Generalized Vibration Mode	---
$\dot{q}$	Velocity of the Generalized Vibration Mode	1/Second
q	Displacement of the Generalized Vibration Mode	$1/Second^2$
$[R_3]$	Matrix of Generalized Circulatory Aerodynamic Stiffness Terms	---
$[R_2]$	Matrix of Generalized Circulatory Aerodynamic Damping Terms	---
RAD	Radians	---
RMS	Root Mean Square	---
RPS	Radians per Second	---
$[r_3]$	Generalized Circulatory Spring Force Matrix	---
$[r_2]$	Generalized Circulatory Damping Force Matrix	---
S	Laplace Operator ($S = \sigma + j\omega$)	---
STA	Airplane Station	---
W(t)	Wagner Lift Growth Function	---
WT	Weight	---
$\ddot{Y}$	Airplane Lateral Acceleration	$Feet/Second^2$
Y	Airplane Lateral Translation	Feet

1.0 INTRODUCTION

1.1 A Need for Elastic Mode Control

The continued emphasis on the use of large aircraft with low load factors results in flexible airframes whose elastic modes are approaching the frequencies of the rigid modes of the aircraft. As these elastic mode frequencies become lower, they are more easily excited by atmospheric turbulence and pilot control inputs. The possibilities of the pilot coupling with these elastic modes, or at least exciting them, becomes greater as the frequency separation between elastic and rigid modes of the airplane is reduced. Separation of these modes can be increased by designing a more rigid structure, which may result in added weight, or by stabilizing the modes with an artificial stability augmentation device. Aerodynamic loads imposed upon the airframe by environmental excitation of elastic modes can be alleviated by suitable control functions. Performance of the crew and comfort of the passengers can be directly affected by the elasticity of the airframe. Again, the adverse effects of elasticity can be minimized through the use of stability augmentation devices.

1.2 Purpose of Elastic Augmentation

Artificially stabilizing elastic modes improves certain characteristics of the airframe. Ride characteristics can be improved by increasing the damping or changing the frequency of troublesome elastic modes. A very elastic airframe will deflect in response to a gust which tends initially to reduce loading associated with the disturbance. However, if damping is low, the resulting overshoot in dynamic response will result in higher aerodynamic loads being imposed on the airframe. Therefore, the control system should provide a compromise between resisting the first cycle load and minimizing the overswing. As damping is increased, the number of cycles needed to damp the motion will be reduced, and consequently, fatigue damage will be lessened. The curves shown in Figure 1 illustrate this effect.

Flutter characteristics of an airframe can be improved with the use of augmentation systems wherein the motion of that portion of the airframe tending toward instability can be sensed and a control input generated to damp this instability. Better handling characteristics result from controlling

elastic modes as well as rigid motions of the airplane in a normal environment. Controllability in the presence of large disturbances can also be improved with an artificial stability device.

1.3 Boeing's Involvement in Elastic Mode Control

The United States Air Force sponsored a study conducted by The Boeing Company in 1964 and 1965 to determine whether a stability augmentation system could provide meaningful improvement in the structural life of a large elastic airplane. The design approach used in this study is illustrated in Figure 2, wherein sensor locations, sensor types, and compensation networks are variables. Control surface sizes and locations were constrained to those existing on the aircraft. Since airplane geometry and structure were not significantly altered, basic airplane dynamic properties were also considered to be fixed. The system derived from this study was flight tested and is being incorporated in the fleet.

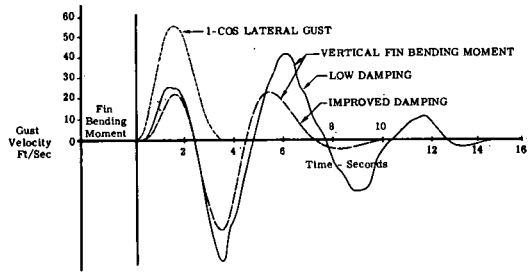


FIG. 1 DAMPING EFFECT ON LOADS

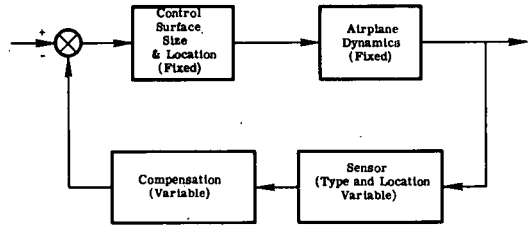


FIG. 2 DESIGN APPROACH

Another Air Force sponsored program used a similar vehicle but allowed control surface modulation on the wings and variable pilot feel characteristics. A programmable analog computer was installed in the airplane to provide the capability to change stability augmentation system parameters in flight. Hardware devised for this study was also demonstrated in flight. In a third program, potential benefits of various control surface locations were assessed. The only remaining block in Figure 2 to be treated as variable is the airplane dynamics. This would be the case if the Load Alleviation and Mode Stabilization concept were applied in the conceptual design stages of an airplane.

Boeing is presently engaged in analytical studies of stability augmentation as applied to a large supersonic airplane. These studies include evaluation of optimum surface and sensor locations, as well as types of sensors. The functional scope of the systems studied includes improved ride qualities, controllability, flutter stability, and reduced structural loads. Research studies are also underway to determine the application of modern control theory to the analysis of these types of control systems.

2.0 TECHNICAL CONSIDERATIONS

2.1 Airplane Mathematical Model

A complete and rigorous elastic airplane mathematical model must be employed for the synthesis of control systems which interact with airplane elasticity. In analysis conducted by Boeing, airplane dynamics are described by a set of coupled, linear, constant coefficient differential equations having linear surface forcing functions and expressible in the following form:

$$\left[N_2\right]\left\{\ddot{q}(t)\right\} + \left[N_1\right]\left\{\dot{q}(t)\right\} + \left[N_o\right]\left\{q(t)\right\} + \left[R_2\right]\left\{W(t) * \ddot{q}(t)\right\} + \left[R_3\right]\left\{W(t) * \dot{q}(t)\right\} = \left[n_2\right]\left\{\ddot{\delta}(t)\right\}$$
$$+ \left[n_1\right]\left\{\dot{\delta}(t)\right\} + \left[n_o\right]\left\{\delta(t)\right\} + \left[r_2\right]\left\{W(t) * \ddot{\delta}(t)\right\} + \left[r_3\right]\left\{W(t) * \dot{\delta}(t)\right\} \qquad \text{Eq. (1)}$$

The square matrices N_2, N_1, etc., and n_2, n_1, etc., are numerical matrices, the elements of which change with flight condition or airplane configuration. Column matrices $q(t)$, $q(t)$, etc., contain dependent variables of the equations of motion in generalized coordinates, and column matrices $\ddot{\delta}(t)$, $\dot{\delta}(t)$, etc., contain the control surface forcing functions. The notation $W(t) * \ddot{q}(t)$ and $W(t) * \dot{q}(t)$ indicates convolution of the Wagner lift growth function with the variable $\ddot{q}(t)$, $\dot{q}(t)$.

In a particular case studied at Boeing the lateral-directional degrees of freedom included three rigid body motions (side displacement, roll rotation, and yaw rotation) together with appropriate structural elastic degrees of freedom. The longitudinal equations contained two rigid body degrees of freedom (pitch rotation and vertical displacement) and the appropriate structural degrees of freedom. The number of structural degrees of freedom varies depending upon the analysis under consideration. Analysis have been conducted using up to 24 degrees of freedom.

Motion at a particular station on the airframe is related to the generalized coordinates through the model coefficients, i.e.,

$$\begin{Bmatrix} y(t) \\ \phi(t) \\ \cdot \\ \cdot \\ \psi(t) \end{Bmatrix} = \left[K\right] \begin{Bmatrix} q_1(t) \\ q_2(t) \\ \cdot \\ \cdot \\ q_n(t) \end{Bmatrix} \qquad \text{Eq. (2)}$$

The K matrix is made up of a numerical array of the modal coefficients, resulting in a 3 x n matrix. For example, yaw rate measured at Body Station $\underline{X}$ with a fixed fuel distribution is described in the following equation:

$$\dot{\psi}(t)_{\text{Sta. X}} \sum_{i=1}^{n} K_i(x)\, \dot{q}_i(t). \qquad \text{Eq. (3)}$$

Plots of typical modal coefficients (commonly called "mode shapes") versus airplane body station are illustrated in Figure 3.

2.2 Problem Identification

A stability augmentation system is normally designed to improve ride qualities, flying qualities, and structural loads. The problem or problems to be addressed within these areas must be identified.

Ride quality is defined as the comfort of the crew and passengers in turbulence. While a rough ride results in physical discomfort and emotional distress for passengers, it can also cause a degradation of flight crew performance. The level of acceleration that the crew and passengers will tolerate is a function of the vibration frequency. Passenger ride quality criteria developed from moving base simulator tests are shown in Figure 4.

Flying qualities include controllability and handling qualities of the aircraft. Controllability is defined here as a property of the integrated system (including airframe, control system, and flight crew) that indicates ability of the system to perform satisfactory in all levels of turbulence. Controllability is primarily concerned with dynamic response of airframe, crew and instruments, controls and accommodations that couple the crew and airframe in the presence of large disturbances. While ride quality is of primary concern in normal turbulence, safety-of-flight aspects during encounters with extreme turbulence may dictate the use of a stability augmentation system to improve airplane controllability. Handling qualities are defined here as a measure of the airplane rigid body stability and response for flight crew inputs in essentially smooth air. Handling qualities, while an integral part of controllability, are more limited in scope and usually require a different control approach than that associated with controllability.

Typically, structural loading and fatigue damage rate are reduced with stability augmentation by reducing peak loads and the number of cycles of loading. An example is discussed later in this paper.

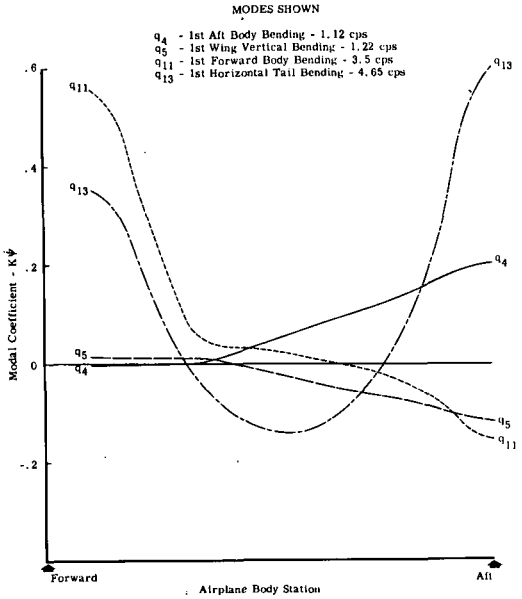


FIG. 3 TYPICAL AIRPLANE ANTISYMMETRIC MODE SHAPES

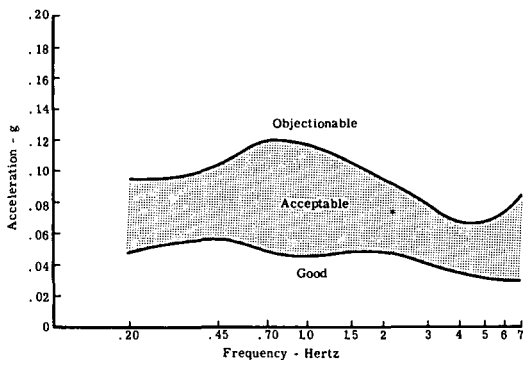


FIG. 4 PASSENGER TOLERANCE TO SINUSOIDAL ACCELERATION

With the airplane simulated on either an analog or digital computer, structural loading resulting from random and discrete gusts can be measured. The magnitude of the induced bending moment compared to bending moment capability provides an indication of the need for load alleviation.

The mathematical simulation can be subjected to a random gust input, and resulting root mean square accelerations along the airframe body can be recorded as shown in Figure 5. The magnitude of the acceleration provides an indication of the ride characteristics of the airframe, and the need for stability augmentation may then be determined from ride quality criteria that indicate acceptable acceleration levels. In this example the forward and aft portions of the aircraft offer the poorest ride.

A review of the modal data (such as that shown in Figure 3) provides insight into the modes causing the largest loads on the airframe. This information is important in determining which modes are to be damped and most effective motion sensor locations. A power spectral density analysis may also be conducted to determine the frequencies at which the greatest amount of energy is being absorbed. Data shown in Figure 6 illustrate how various structural modes in a typical case contribute to lateral acceleration at a particular location.

Root locus methods may be used to identify flutter critical elastic roots. Possible weight savings associated with artificially damping flutter modes, compared to increasing stiffness by adding structure, may be appreciable.

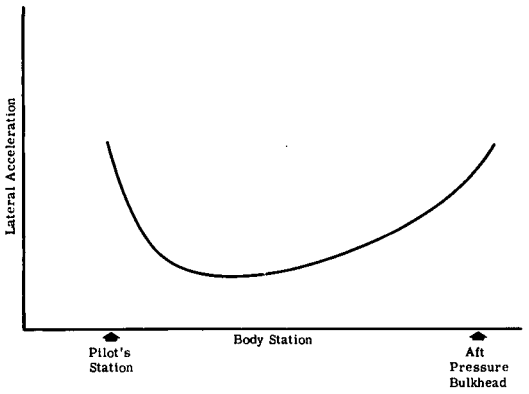


FIG. 5 LATERAL ACCELERATION ENVIRONMENT ALONG FUSELAGE

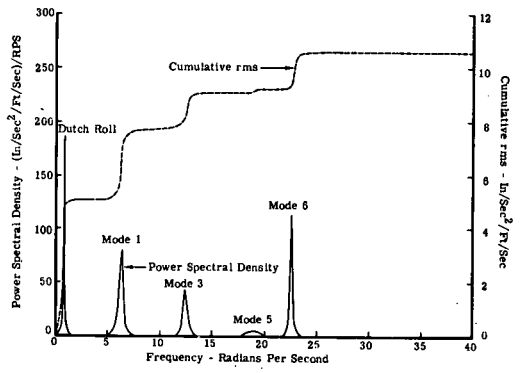


FIG. 6 LATERAL ACCELERATION NEAR PILOT'S STATION

Evaluations of airframe response to random and discrete gusts power spectral density and root locus analyses provides an insight into the need for a stability augmentation system. Such analyses facilitate definition of system performance objectives in terms of improvements in ride qualities, structural loading (both for peak loads and fatigue damage rates), handling qualities, and flutter stability margins.

2.3 Design Considerations

Once the problem is identified and stability augmentation system performance objectives are established, a study to identify candidate systems that offer maximum performance improvements can be conducted. Control surface effectiveness, controllability, and observability of modes, and system hardware requirements must be examined.

Control surface effectiveness is a function of the surface location, size, and travel. The control surface becomes more effective for mode control as it is moved to a location that couples strongly with the structural mode to be controlled. All reasonable control surface locations should be evaluated in terms of effectiveness in controlling troublesome modes. Typical effects of control surface locations on acceleration reductions is shown in Figure 7.

A root locus plot of the airplane transfer function zeroes provides an insight into the best control surface and sensor locations in terms of system stability. If all the zeroes lie in the left hand plane, the potential for a stable system is increased. The distance between zeroes and poles is an indication of the strength of coupling between the control surface and the structural modes. Trade studies can be made to optimize these parameters.

Controllability and observability of modes is evident from root locus plots and modal plots, such as shown in Figure 3. If a sensor can be placed at a position sensitive to the mode to be controlled and insensitive to modes to be ignored, the system is easier to design, and stability compensation networks are generally simpler.

Effects of dynamic response should be evaluated to ensure maximum system performance. A typical plot of acceleration reduction versus actuator bandwidth is shown in Figure 8. Actuator phase shift is also important when controlling structural vibration modes. Experience has indicated that actuator hardware should be built with a higher break frequency than that indicated by Figure 8 in order to achieve reasonable insensitivity to component tolerances. In one system flight tested, the break frequency was increased by a factor of approximately three to assure proper phase shift at the frequency of the structural mode being controlled.

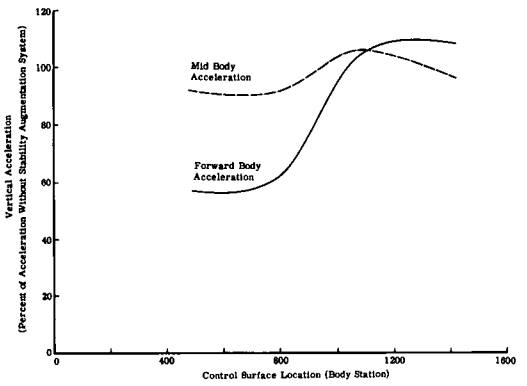


FIG. 7 EFFECT OF CONTROL SURFACE LOCATION

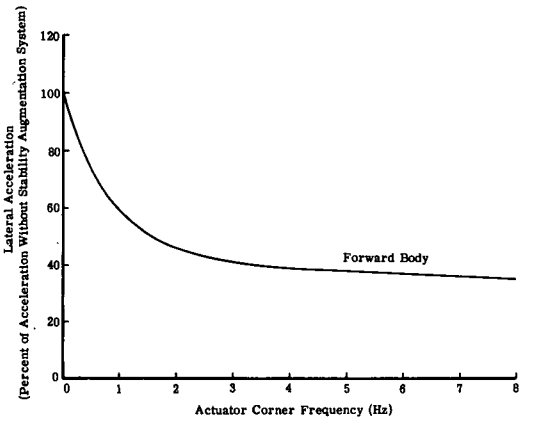


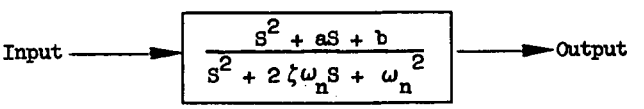
FIG. 8 EFFECTS OF ACTUATOR BANDPASS ON LATERAL ACCELERATION

3.0 AN APPLICATION OF STABILITY AUGMENTATION

Problem identification and feasibility studies reveal areas needing careful examination during subsequent analyses. This section describes analyses conducted at Boeing on one such program. The objectives of this program were to demonstrate the feasibility of reducing fatigue damage rates, peak loads, and improving handling qualities on a large flexible airplane by augmenting the rigid body (Dutch roll) motion and the lower frequency structural vibration modes.

3.1 System Synthesis

To reduce fatigue damage rate and improve airplane handling for gust inputs, the frequency and damping of both the rigid body and structural vibration modes should in general be controlled. To illustrate the problem of determining the phasing required to accomplish this, consider the second-order system shown below:



Each uncoupled degree-of-freedom in the elastic airplane equations of motion is represented by an underdamped second-order system as shown above. The separation of the numerator zeroes and denominator poles is usually maximized for the modes to be controlled through sensor and/or control surface location. The angle at which the root locus departs from the open loop poles (angle of departure for negative feedback) is approximately 90 degrees lead or lag for a transfer function of this type.

The airplane analyzed in this study exhibits 90-degree phase lead at the Dutch roll and lower frequency elastic mode frequencies. Negative rate feedback provides an additional 90-degree phase lead and thus exhibits correct phasing to increase mode damping. Such a feedback has little effect on the natural frequency of the mode. On the other hand, lateral acceleration feedback introduces an additional 180 degrees phase lead, and primarily decreases the natural frequency without affecting mode damping. Therefore, use of acceleration feedback to damp these modes requires approximately 90-degree phase lag in the feedback network. The effect of rate and acceleration feedback on the damping and natural frequency of Dutch roll and first aft body bending modes is illustrated in Figure 9.

Proper selection of sensor types, sensor locations, and feedback networks requires an understanding

of the system and its mathematical model. Several techniques are available to the designer to evaluate effects of various feedback loops on system dynamics and performance. Phase-gain root locus and digital and analog simulations were used during this program. Initial analysis efforts included a survey of various sensor types and locations. As a result of this survey, general areas of sensor locations were selected, and further analyses were conducted with various combinations of loop gains, filters, and perturbations of sensor locations. To design the feedback network, typical sensor and actuator-surface dynamics were included in the stability augmentation system analysis. During the final analysis, transfer functions describing the dynamics of system components were revised to more nearly represent actual hardware.

Studies indicated that yaw rate sensed at any location along the airplane body would provide adquate Dutch roll damping. Therefore, one of the principal considerations in determining the yaw rate sensor location was its effect on structural stability and load reduction performance. Root locus, bode, and mode-shape plots (such as Figure 3) indicated that a rate sensor in the aft body would strongly couple with the aft body structural bending modes. However, yaw rate ($\dot{\psi}$) sensed in the forward body is basically not coupled with the elastic vibration modes except for the 3.5 cps forward body lateral bending mode and the horizontal tail bending mode. It was determined that the amplitude of these modes could be minimized by proper filtering and by proper location of the $\dot{\psi}$ sensor. The initial filter design was primarily intended to attenuate the higher frequency vibration modes. After the $\dot{\psi}$ sensor location was selected, the filter was refined to provide optimum phasing in terms of rigid body motion and elastic mode stability with the sensor and actuator dynamics considered. A washout filter ($S/S + .25$) was included to prevent the stability augmentation system from resisting pilot commands. The root loci shown in Figure 10 illustrates that the $\dot{\psi}$ loop was designed primarily to damp the Dutch roll mode. The composite frequency response of the airframe and yaw rate feedback network shown in Figure 11, shows that the $\dot{\psi}$ loop peaks at the Dutch roll frequency.

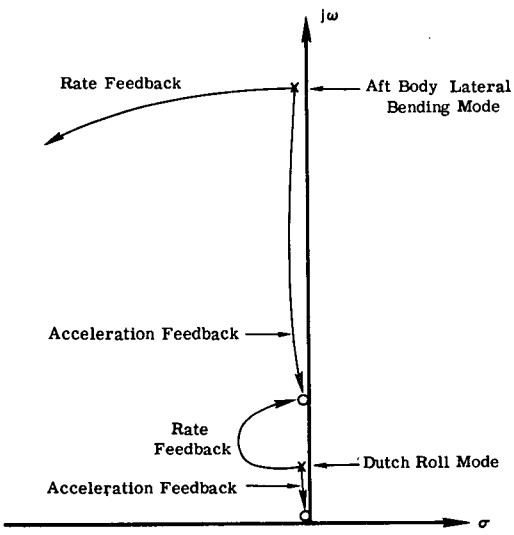


FIG. 9 TYPICAL ROOT LOCUS SHOWING EFFECT OF PHASING BETWEEN AIRPLANE MOTION & RUDDER

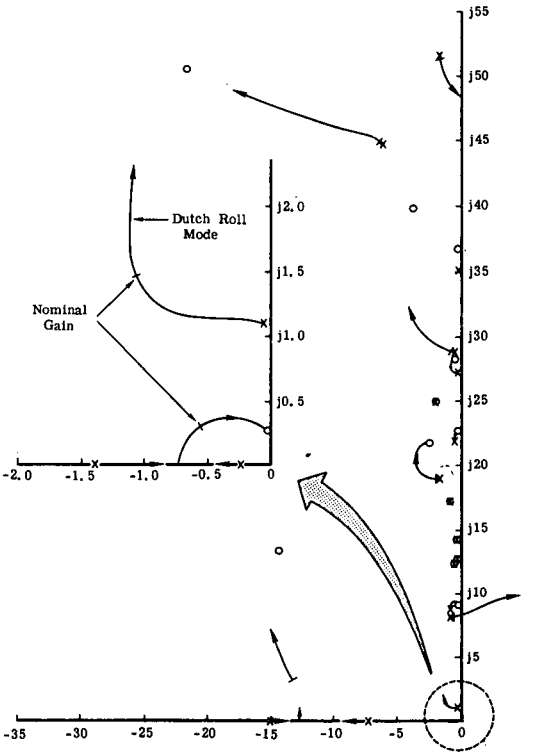


FIG. 10 YAW STABILITY AUGMENTATION SYSTEM GAIN ROOT LOCUS

Lateral acceleration feedback was used to damp the first aft body bending mode (q_1). The acceleration signal was lagged approximately 90 degrees at the mode frequency (1.3 cps). The basis for the 90-degree phase lag requirement is discussed above. The filter design and choice of sensor location was more difficult for the $\ddot{Y}$ loop than for the $\dot{\psi}$ loop, because of stability problems associated with higher frequency elastic vibration modes. Aft body torsion (2.5 - 3.0 cps), forward body bending (3.0 - 3.5 cps), and fin bending (8.0 cps) were the major contributors to the problem. The accelerometer was finally located to minimize the contributions of these modes relative to q_1.

A low-pass filter was used to obtain the desired q_1 phasing and stability. It was difficult to phase q_1 correctly and attenuate the higher frequency modes while maintaining proper phasing at intermediate frequency modes. The accelerometer was located above the fuselage elastic axis to improve torsional mode phasing.

Since the Dutch roll mode also coupled with the rudder for $\ddot{Y}$ feedback, but was not properly phased for damping, a high-pass filter $S/(S + 1.5)$, was included in the lateral acceleration loop. The frequency response of the acceleration channel, shown in Figure 12, illustrates the low frequency attenuation of the washout and the rapid high frequency attenuation of the low-pass filter.

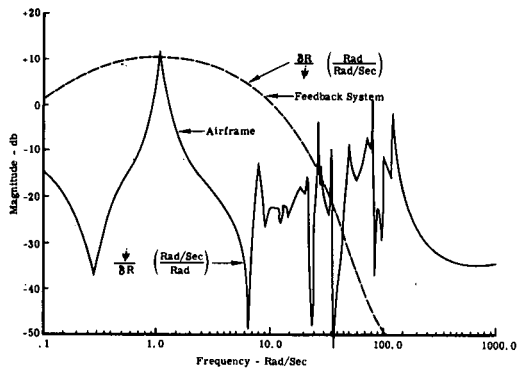


FIG. 11 YAW RATE FREQUENCY RESPONSE

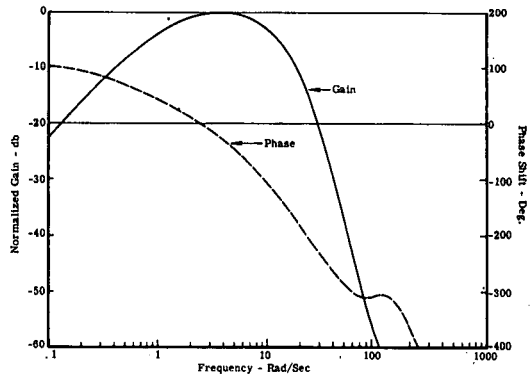


FIG. 12 ACCELERATION CHANNEL FREQUENCY RESPONSE

Equation (4) characterizes the stability augmentation system with both loops closed:

$$1 - \frac{\dot{\psi}}{\delta_R} K_{\dot{\psi}} \; H_1(S) + \frac{\ddot{Y}}{\delta_R} K_{\ddot{Y}} \; H_2(S) = 0 \qquad \text{Eq. (4)}$$

A root locus plot of this equation as a function of $K_{\ddot{Y}}$ for nominal $K_{\dot{\psi}}$ is shown in Figure 13. This plot illustrates the effectiveness of the $\ddot{Y}$ feedback in damping the first aft body lateral bending mode. A block diagram of the final yaw stability augmentation system is shown in Figure 14.

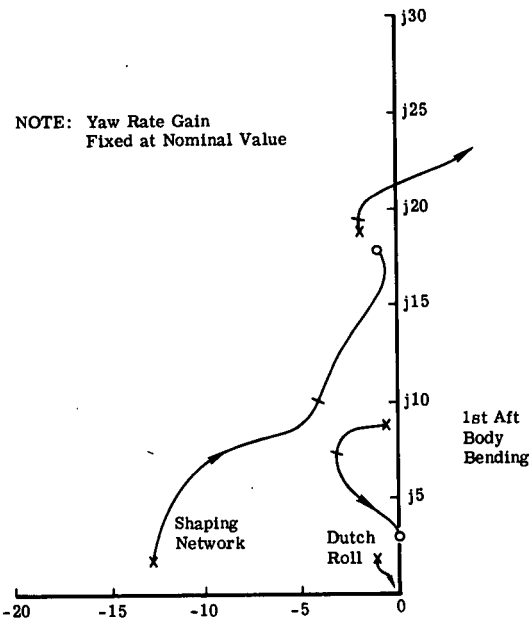


FIG. 13 YAW STABILITY AUGMENTATION SYSTEM GAIN ROOT LOCUS

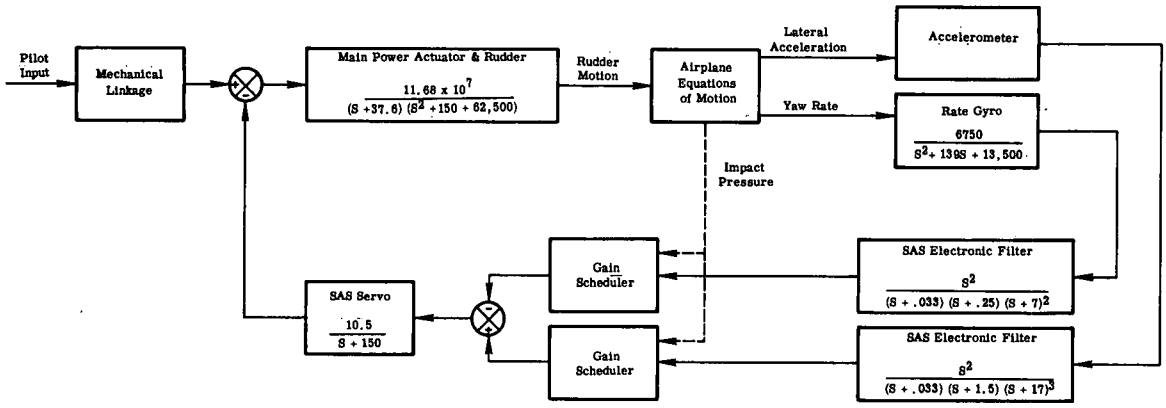


FIG. 14 YAW STABILITY AUGMENTATION SYSTEM BLOCK DIAGRAM

3.2 Analysis of System Performance

Optimum values of yaw rate and lateral acceleration feedback gain were established for each flight condition to provide maximum performance. The yaw rate gain was selected primarily to provide optimum Dutch roll damping and frequency. The acceleration gain was selected to provide maximum damping of the first aft body lateral bending mode. The optimum gain at each flight condition determined a parameter gain schedule for the yaw rate and lateral acceleration feedback variables. A phase-gain root locus plot (for phase and gain variations in both yaw rate and acceleration channels) was used to reveal sensitivity of damping and frequency of Dutch roll and aft body structural vibration modes. A discussion of this technique is contained in Reference 1. Sensitivity analyses were performed with both analog and digital computers to establish allowable tolerance bands for frequency responses of yaw rate and acceleration loops.

3.2.1 System Stability

Stability goals were 10 db gain margin and 60 degrees phase margin for all modes which were actively controlled. Phase margin was defined as the phase shift required in all feedback loops to cause an instability with nominal gains. Gain margin was defined as the minimum gain change required (for any combination of feedback gains) to cause an instability with nominal phase.

Predicted stability boundaries for a typical flight condition, as a function of composite yaw rate and lateral acceleration gain and phase, are presented in Figure 15. The gain in each feedback loop is normalized to the value predicted from the analysis. The stability augmentation system has a gain margin of 9.4 db for the composite yaw rate and lateral acceleration signal. This gain margin is only applicable when both $\dot{\psi}$ and $\ddot{Y}$ gains are varied in the same proportion simultaneously.

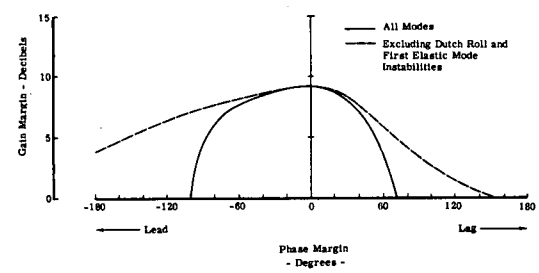


FIG. 15 PREDICTED PHASE-GAIN STABILITY BOUNDARY

Since the purpose of the stability augmentation system is to damp the Dutch roll and lower frequency structural vibration modes, a large phase margin at these modes is not practical. For example, a phase shift of 180 degrees would constitute positive feedback, and any reasonable loop gain would produce a divergent condition. Therefore, it is impractical to specify that these modes be stable independent of phase. However, stability at any phase is desirable for modes above the frequency range to be actively controlled. Accordingly, the dashed line in Figure 15 is drawn to show the stability boundary with the Dutch roll and applicable stability augmented elastic modes omitted.

Phase-gain root locus plots such as shown in Figure 16 were used to compute the phase and gain margins.

3.2.2 System Optimization and Load Response Predictions

An analog computer simulation was used to provide airplane responses for optimization and load response predictions. Bending moments were monitored at three critical points on the airplane structure to evaluate performance of the stability augmentation system. Fatigue damage rate was not evaluated directly, since feasibility investigations had shown fatigue damage rate to be a function of bending moment and bending moment rates. Hence, relative loads performance was examined during the optimization studies, and fatigue damage was explicitly computed after stability augmentation system configuration and gains were finalized. Analog tests consisted of measuring loads and airplane motion response resulting from simulated gust forcing functions. The types of forcing

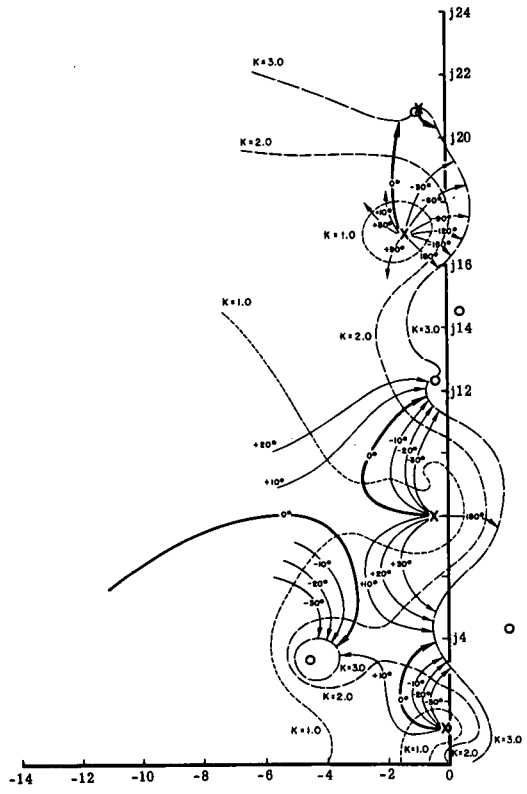


FIG. 16 YAW STABILITY AUGMENTATION SYSTEM PHASE-GAIN ROOT LOCUS

functions used included step inputs, discrete single-cycle sinusoidal pulses (1 - cos ωt), and appropriately filtered white noise.

Step input gust responses were examined to aid in understanding the transient load response characteristics of the multivariable feedback systems. Results indicate that the lateral acceleration loop provides a significant reduction in aft body peak load exceedances as well as a reduction in initial overshoot.

Discrete (1 - cos ωt) gusts were used to evaluate system effectiveness in reducing peak loads. Comparison of bending moment responses with and without the stability augmentation system are shown in Figure 17. Peak lateral bending moment was reduced 33 percent in this particular case.

Random turbulence excitation was used extensively as a basis for examining, comparing, and evaluating stability augmentation system loads performance. Feedback gains were varied until loads and airplane motions approached an approximate minimum within acceptable gain margin constraints.

Yaw rate gain was varied while holding $K\ddot{\psi}$ constant at selected values. A typical result of aft body bending moment is presented in Figure 18. In this case, bending moment is minimized for approximately $K\dot{\psi}$ = 105, which corresponds to the gain selected by root locus stability studies. From the curve for $K\ddot{\psi}$ = 0, it may also be inferred that the system provides approximately 30 percent reduction in bending loads through Dutch roll mode control, and that additional Dutch roll damping would not be expected to significantly reduce loads further.

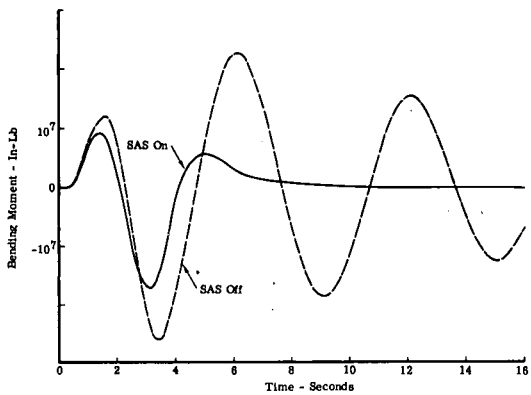


FIG. 17 LATERAL BENDING MOMENT (1 - cos ωt) GUST RESPONSE

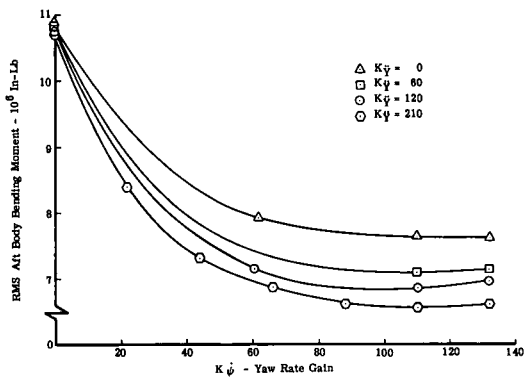


FIG. 18 YAW RATE GAIN OPTIMIZATION

Results of the $K\ddot{\psi}$ gain search, illustrated in Figure 19, shows an additional ten percent reduction was obtained through aft body bending control with $K\dot{\psi}$ set at an optimum value. Although a minimum was not reached, a gain of $K\ddot{\psi}$ = 210 was selected, since higher gains produced insignificant loads reduction at the expense of reduced gain margins. Further gain searches were conducted holding a fixed gain ratio, $K\ddot{\psi}/K\dot{\psi}$ = 2, and incrementing gain downstream of the signal summation. Results, illustrated in Figure 20, again show that gains selected from root locus studies were near optimum for loads reduction. Similar analyses conducted at other flight conditions generally verified this result.

3.3 Flight Test Results

Flight testing of the stability augmentation system was accomplished in several steps as indicated in Figure 21. First, the power actuation system was evaluated during manual flight. Next, the stability augmentation system was turned on at low gains and tested. During this particular test, turbulence was encountered, and Figure 22 shows aft body lateral displacement with the stability augmentation system on and off. The turbulence level was judged to be constant throughout this encounter. The marked improvement obtained with this low gain setting was indicative of improvements to be obtained with this system.

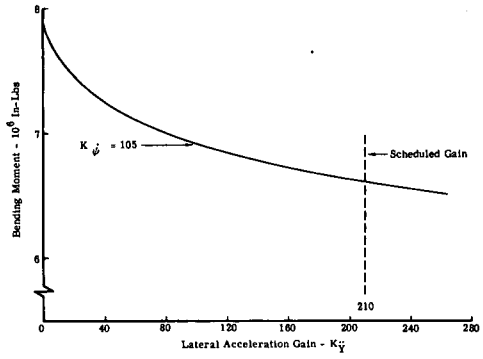


FIG. 19 LATERAL ACCELERATION GAIN OPTIMIZATION

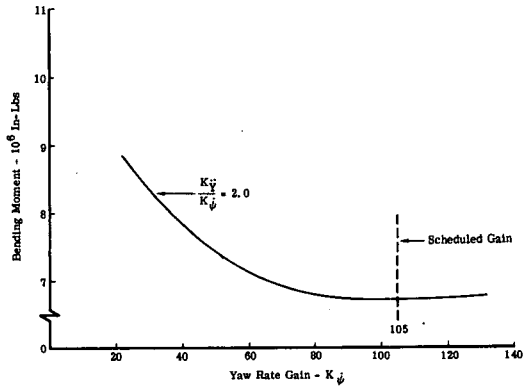


FIG. 20 YAW RATE GAIN OPTIMIZATION

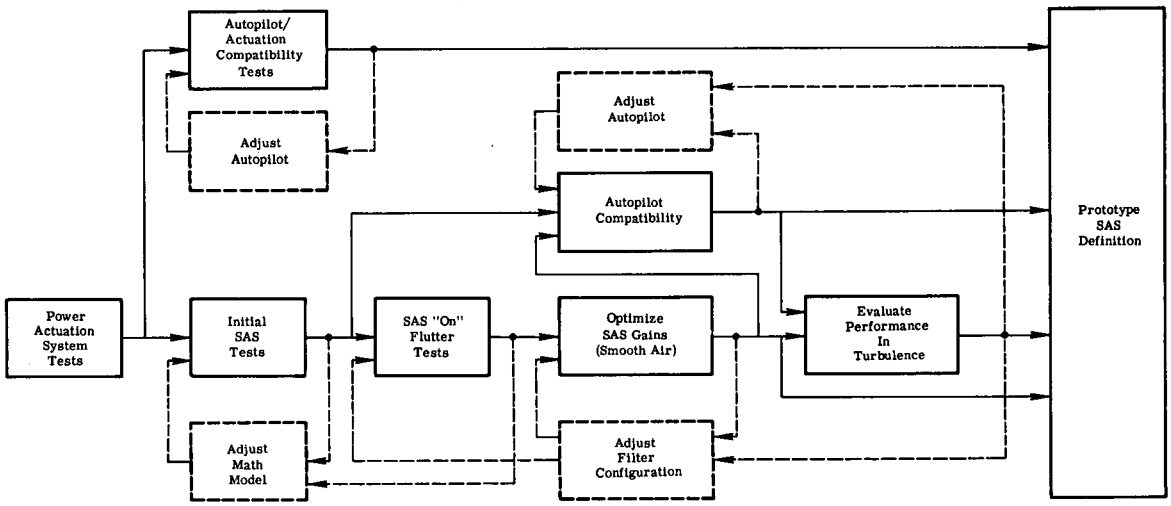


FIG. 21 FLIGHT TEST ACTIVITIES

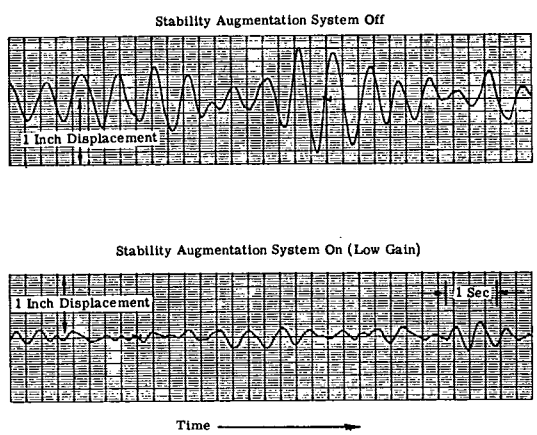


FIG. 22 AFT BODY SIDE DISPLACEMENT IN RANDOM TURBULENCE

Conventional flutter tests were conducted with the stability augmentation system gains varied throughout the desired ranges. Stability criteria were established for testing which required that damping of any structural mode would never be reduced below the following values:

Unaugmented Damping	Damping with SAS
0.1 or greater	.05
0.1 or less	1/2 the original value

During flutter testing, normal flutter excitation techniques (abrupt manual control inputs) were used.

During optimization of the stability augmentation system gains, an electronic signal generator was used to drive the control surfaces with discrete sinusoidal transients. The amplitude, frequency, waveform and number of cycles were precisely controlled. Dutch roll and aft body bending responses measured in flight with the signal generator are shown in Figures 23 and 25.

In Figure 23, the top trace shows rudder transient command, and the middle trace shows the free airplane with the stability augmentation system turned off. In the bottom trace, the stability augmentation system was turned on after the rudder command was set to zero. As can be seen, the Dutch roll mode was quickly damped. Dutch roll damping ratios measured in flight tests are shown in Figure 24 plotted as a function of dynamic pressure. The shaded

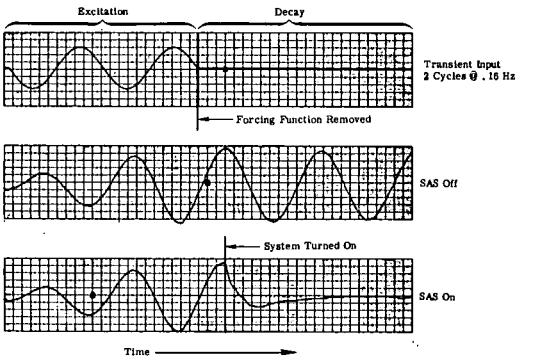


FIG. 23 EFFEKT OF SAS ON DUTCH ROLL OSCILLATION

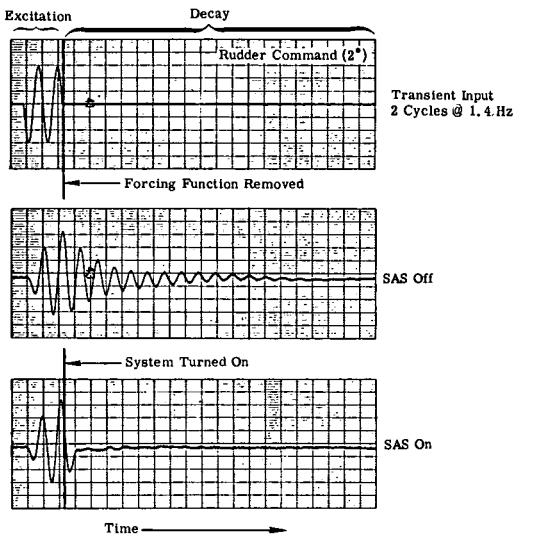


FIG. 25 EFFECT OF STABILITY AUGMENTATION SYSTEM ON LATERAL BENDING OSCILLATION

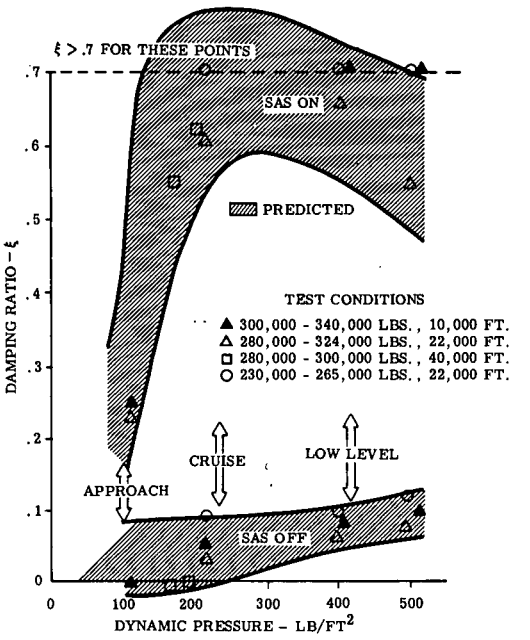


FIG. 24 ANALYSIS AND FLIGHT TEST COMPARISON OF DUTCH ROLL DAMPING RATIO

areas on this figure were predicted from the analysis conducted during the design phase.

Aft body elastic bending mode damping was evaluated in flight by commanding the rudder in an oscillatory manner at the natural frequency of the aft body elastic bending mode. The rudder command was allowed to persist for two cycles and then removed. The three traces shown in Figure 25 are for the rudder command, the aft body bending moment with the stability augmentation system off and with the stability augmentation system on.

As can be seen from these traces the aft body elastic mode has a slow decay with the stability augmentation system off and a very rapid decay with the system turned on. Damping ratios measured in flight tests are shown in Figure 26 and compared with values predicted from the analysis conducted during the design phase.

A major design objective for the stability augmentation system was the reduction in structural fatigue damage rate due to flight through atmospheric turbulence. The experimental responses measured in flight were used with a definition of atmospheric turbulence to calculate stress response statistics. These were then used with fatigue allowables in terms of S-N curves to calculate experimental damage rates. These results are compared with corresponding theoretical data in Figure 27. The results are presented as a ratio with the stability augmentation system on to the damage rate for the basic airplane. These ratios represent the average values for four flight conditions. Good agreement was obtained between theoretical prediction and experimental results.

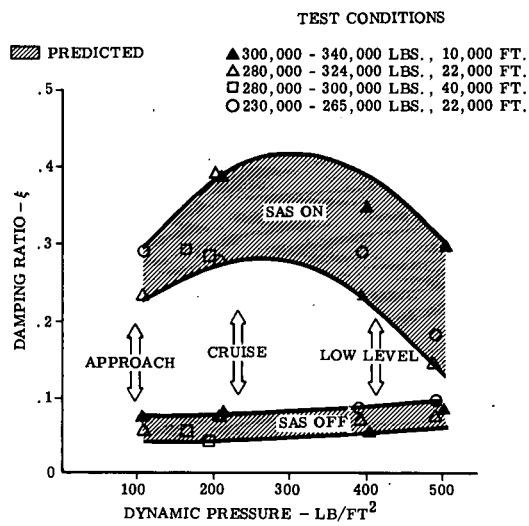


FIG. 26 ANALYSIS AND FLIGHT TEST COMPARISON OF AFT BODY LATERAL BENDING MODE DAMPING RATIO

4.0 STABILITY AUGMENTATION RESEARCH

4.1 Research

The design study discussed in Section 3.0 considered an airplane with a fixed basic configuration. Sensor locations, sensor types, and compensation networks were variable. Performance criteria were reduction of fatigue damage rate

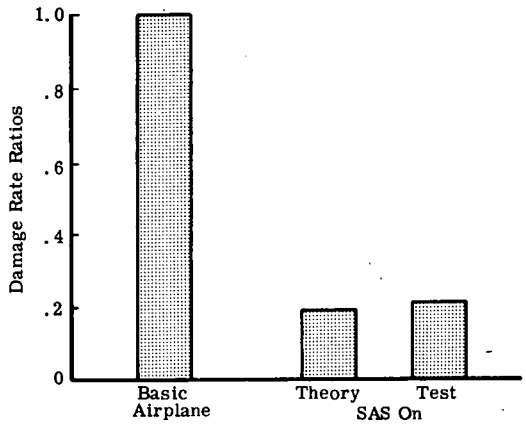


FIG. 27 RELATIVE FATIGUE DAMAGE AFT BODY

and structural peak loads and improvement of handling qualities. This study has been completed, and two research programs are currently underway to extend the state-of-the-art by investigating benefits derivable from:

(1) Relaxing aircraft configuration constraints.

(2) Applying modern control analysis techniques.

(3) Considering other performance criteria.

A large subsonic aircraft and a large supersonic aircraft are being used for these analytical and flight test studies.

4.2 Subsonic Airplane

An Air Force sponsored program has been completed which permitted some variation in control surface characteristics and utilized a programmable onboard computer and variable feel characteristics to the pilots controls. Performance criteria included improvement of ride qualities at the pilot's station and reduction of fatigue damage rate while retaining good handling qualities. Optimal control theory was used to determine theoretical minimums and in selecting practical feedback configuration. This program evolved a stability augmentation system functional concept which was implemented and demonstrated in flight.

4.3 Supersonic Aircraft

Company sponsored programs are in progress which apply both classical and modern control techniques in synthesising stability augmentation systems for a large supersonic aircraft. Using classical methods, stability augmentation systems are being investigated to satisfy requirements for ride qualities and handling qualities criteria and which will, in addition, extend flutter margins. The airframe chosen for study has two elastic modes which become flutter critical as Mach number is held constant and altitude decreased. A root locus of this condition is shown in Figure 28. The third mode becomes unstable at altitudes below 20,000 feet and the fourth mode at altitudes below 18,000 feet. A rate gyro was used to sense these modes and to drive an aileron in a corrective fashion. Figure 29 shows the same root locus with the roots stabilized by a flutter stability augmentation system shown by dashed lines.

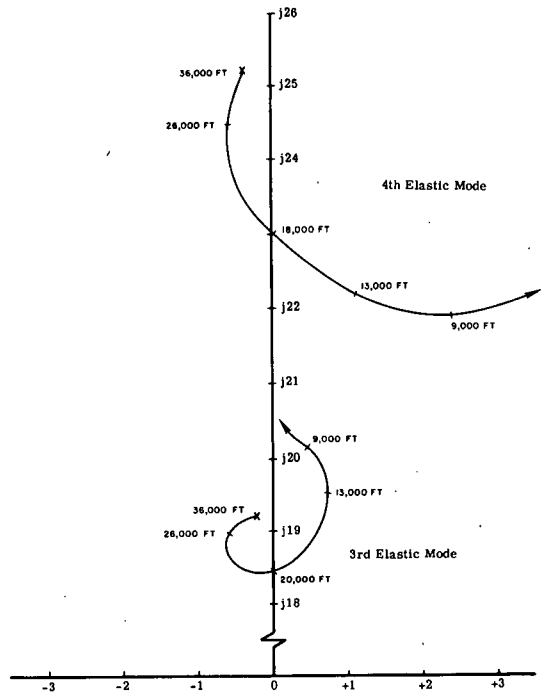


FIG. 28 FREE AIRPLANE SYMMETRIC ROOT LOCUS

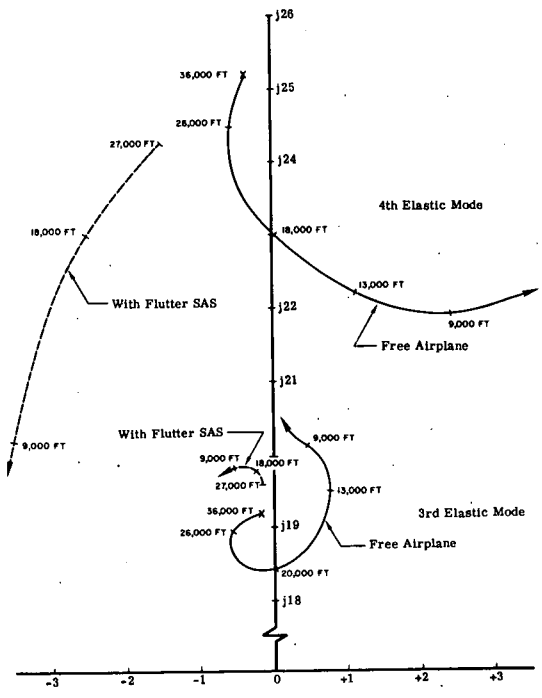


FIG. 29 EFFECT OF FLUTTER SAS ON SYMMETRIC ROOT LOCUS

A related research program employs modern control theory, in particular the root square locus technique, to synthesize stability augmentation systems for a variety of quadratic performance indices.

This study is initially concerned with minimization of structural loads at critical locations. Reduction of accelerations at significant ride quality locations will be considered next. In this effort, particular emphasis is being placed upon the use of realistic feedback variables, sensor types, and locations. The intent is to evolve practical sub-optimal systems using a small number of feedback variables.

5.0 CONCLUSIONS

The work reported in this paper has resulted in a stability augmentation system that damps not only the rigid motions of the airplane but also lower frequency structural modes. The work has verified the utility of analysis tools and has developed new techniques of analyzing complex systems. These techniques have predicted results, and hardware has been built and flight tested on the basis of these predictions. Flight tests conducted under programs sponsored by the United States Air Force have resulted in a verification of the analytical techniques and have opened the way for a wider application of stability augmentation systems. The past few years have seen the flight control system become an even greater integral part of the airframe. Future high performance airplanes will utilize these techniques, and the flight control designer, rather than avoiding system coupling with structural modes will actively control this coupling.

REFERENCES

1. J. I. Arnold, "Automatic Control for Damping Large Aircraft Elastic Vibrations", NAECON Paper, May 1968

2. J. B. Dempster and J. I. Arnold, "Flight Test Evaluation of an Advanced Stability Augmentation System for the B-52 Aircraft", Paper No. 68-10 AIAA 5th Annual Meeting and Technical Display, 21 October 1968

3. Boeing Document D3-6950, "Stability Augmentation System Analysis", G. E. Hodges, O. E. Visor, J. I. Arnold, W. J. Wattman; 29 September 1967

4. AFFDL-TR-68-158, "Aircraft Load Alleviation and Mode Stabilization (LAMS)", December 1968.

INFLUENCE DES EFFETS AEROELASTIQUES SUR L'ETUDE ET LA REALISATION DE L'AMORTISSEUR DE TANGAGE ET DU PILOTE AUTOMATIQUE D'UN AVION DE TRANSPORT SUPERSONIQUE

par

R. DEQUE

SUD-AVIATION - TOULOUSE

SOMMAIRE

Dans un but de simplification de l'étude on peut faire intervenir l'aéroélasticité sous deux aspects suivant que l'on s'intéresse aux problèmes de pilotage $f < 1$ Hz ou à l'influence des stabilisateurs sur les modes vibratoires de l'avion $f > 2$ Hz. On se fixe deux objectifs : améliorer les qualités de vol naturelles de l'avion et ne pas détériorer les caractéristiques d'amortissement des modes structuraux. Ces deux objectifs peuvent être contradictoires avec un système simple et l'on est amené à étudier divers moyens pour les concilier : choix des détecteurs et de leurs emplacements, définition des filtres plus ou moins complexes. La même étude doit être effectuée pour la définition du pilote automatique.

Les problèmes de réalisation des filtres et les conséquences des pannes sont aussi étudiés.

La possibilité d'augmentation artificielle de l'amortissement des modes de structure est brièvement évoquée ainsi que les principales difficultés à vaincre pour y parvenir.

1. - GENERALITES -

L'étude des qualités de vol d'un avion de transport supersonique à voilure du type delta (voir réf. 1) fait rapidement apparaître la nécessité d'une augmentation artificielle de stabilité autour des trois axes. Cette augmentation est nécessaire pour faciliter la tâche du pilote et rendre l'avion plus confortable. De plus sur un avion moderne l'automatisation du pilotage doit être très poussée et l'étude du système de pilotage automatique dans toutes les phases de vol (décollage excepté) est entreprise dès le début du projet.

La recherche de la traînée minimum conduit à la réalisation d'un avion très effilé (le rapport du diamètre du fuselage sur sa longueur est de 1/20 environ, l'épaisseur relative de la voilure est de 2 à 3 %).
On doit donc s'attendre à ce que la flexibilité pose des problèmes de qualités de vol ou du moins intervienne de façon importante dans leur étude.

Nous nous limiterons ici à l'étude des problèmes du contrôle longitudinal. Les problèmes rencontrés en transversal sont en fait assez voisins et les solutions adoptées sont sensiblement les mêmes.

2. - ETUDE DU SYSTEME AUX FREQUENCES DE PILOTAGE -

Les équations du mouvement de l'avion utilisées sont semblables à celles de l'avion supposé rigide. Les coefficients aérodynamiques déterminés par essais en soufflerie sont cependant corrigés des effets de flexibilité. Par exemple l'équation de moment de tangage s'écrit :

$$C_M = C_{M_R}(c_z) + \Delta C_{M_{os.}} + \Delta C_{M_\alpha}\cdot\alpha + \left(C_{M_{qR}} + \Delta C_{M_{qs}}\right)\frac{ql}{V} + C_{M_R}(\delta_q)\times(1+\eta_s) + C_{M_{RS}}\cdot n$$

La détermination des termes correcteurs de flexibilité est exposée dans la réf. 2. L'introduction de la flexibilité ne change donc rien aux méthodes classiques d'études si ce n'est un accroissement de complexité dans la détermination des coefficients des fonctions de transfert. La détermination des caractéristiques du stabilisateur de tangage est donc simplement effectuée par la recherche pour chaque condition de vol des gains maxi et mini acceptables pour satisfaire à un certain critère d'amortissement. Sur la planche 1 on indique pour un certain nombre de cas de vol les gains maxi et mini pour que tous les modes aient un amortissement réduit de 0,6. Le gain maxi correspond à l'amortissement d'un mode à $\sim$ 1 hz qui résulte comme l'on peut le voir sur le lieu des racines de la planche 2 de la combinaison entre un pôle correspondant à la fonction de transfert de servocommande et une racine réelle de l'oscillation d'incidence dégénérée en 2 mouvements apériodiques. On peut se poser le problème de la validité des données quasi statiques utilisées pour ce mode de fréquence élevée (1 Hz). En fait, nous avons vérifié que le gyromètre étant placé dans une zône de l'avion où il est pratiquement soustrait à l'influence des modes structuraux à très basse fréquence (2 à 3 Hz), l'étude des caractéristiques de ce mode à 1 Hz par la méthode de superposition des modes propres donne des résultats sensiblement voisins au point de vue fréquence et amortissement à celle exposée ici.

.../

L'examen de la planche 1 montre qu'une loi simple de variation de gain en fonction du Mach peut être utilisée pour obtenir des performances satisfaisantes dans l'ensemble du domaine de vol et c'est la solution que nous avons retenue. Cette solution est en effet de réalisation beaucoup plus simple que celle d'un système auto adaptable que nous avons aussi considéré au début du projet.

L'étude des lois de pilotage automatique bien que plus complexe relève des mêmes méthodes et nous avons là aussi déterminé des variations de gain en fonction du nombre de Mach.

Les lois ainsi déterminées sont vérifiées et optimisées sur simulateur de vol. Les équations de mécanique du vol utilisées dans le simulateur de vol tiennent compte des effets de flexibilité qui sont introduits de la même façon que pour les études théoriques.

3. - PROBLEMES DE COUPLAGE AVEC LES MODES STRUCTURAUX -

Les capteurs (gyromètres gyroscopes accéléromètres) installés dans l'avion détectent non seulement le mouvement global de l'avion mais aussi les déformations structurales locales correspondant au point où ils sont installés. Les signaux de ces capteurs après avoir été traités dans les calculateurs provoquent des déplacements de gouvernes qui par les charges qu'ils créent entraînent des déformations structurales. On doit donc s'attendre à ce que les systèmes de stabilisation et de pilotage automatique modifient les caractéristiques de vibrations structurales de l'avion.

Nous nous sommes fixés comme objectif que les boucles d'asservissement ainsi créées soient stables avec des marges de stabilité satisfaisantes. Dans le cas de l'amortisseur de tangage le détecteur est un gyromètre. Le premier problème est de choisir son positionnement dans l'avion (Voir planche 3 les déformées de la ligne centrale du fuselage pour les premiers modes de structure). Nous le plaçons dans une zône qui constitue un ventre de déplacement donc un noeud de vitesse angulaire pour le mode 1 (fréquence propre la plus faible). Il sera donc complètement découplé de ce dernier.
Si maintenant nous considérons la fonction de transfert en boucle ouverte de la chaîne de stabilisation, nous observons dans le plan de Nyquist (Pl. 4) que la stabilité de la boucle fermée sera insuffisante.

Nous assurons les marges de stabilité cherchées en mettant en série avec le gyromètre un filtre dit de structure.

Pour l'étude ci-dessus il nous faut connaître la fonction de transfert

$$\frac{\dot{\theta}\ \text{local}}{\delta\ q} = \frac{\text{vitesse de tangage locale}}{\text{braquage gouverne}}$$

Cette fonction de transfert nous est fournie par les spécialistes de vibration. Au début du projet ces fonctions de transfert étaient établies à partir de théories bi-dimentionnelles. Plus tard des méthodes tri-dimensionnelles ont été utilisées et une fois les essais de vibration au sol effectués il a été possible de tenir compte des amortissements dûs à la structure. Ce sont ces dernières informations que nous utilisons

.../

actuellement. Il faut noter que les premières fonctions de transfert fournies étaient très pénalisantes pour le système en raison du peu d'amortissement présenté par certains modes qui nous conduisaient à des filtres relativement complexes. Les problèmes sont beaucoup moins critiques dans le 2e cas.
Le filtre actuellement utilisé est du type coupe-bande et sa fonction de transfert se présente sous la forme de deux polynomes du 2e degré.
On peut voir planche 4 son effet dans un cas de vol subsonique.
Ce filtre a cependant malgré les précautions prises, une influence non négligeable sur les modes d'ensemble avion. En particulier le mode à $\sim$ 1 Hz est assez notablement désamorti par sa présence (Voir planche 1).

La même étude est effectuée en pilotage automatique. Elle est plus complexe en raison d'une part de la présence en plus du gyromètre de la plateforme à inertie qui est installé à un emplacement différent du gyromètre. Le schéma d'étude de la boucle ouverte figure sur la planche 5.

4. - PROTECTION CONTRE LES PANNES -

Deux systèmes de stabilisation sont installés sur l'avion, chacun d'eux étant autosurveillé. En cas de panne du système 1 il est automatiquement déconnecté et le 2e est mis en fonctionnement. Le même type de protection est utilisé pour les pilotes automatiques.

Nous nous intéresserons plus particulièrement aux pannes des filtres de modes structuraux.
Pour cela observons le schéma de principe d'un des deux stabilisateurs de tangage de l'avion (voir planche 6). Les conséquences des diverses pannes envisageables se traduisent par une modification de la fonction de transfert. A une fréquence donnée on peut avoir une modification de la phase de l'amplitude ou des deux. Ces pannes si elles affectent la chaîne de commande peuvent conduire à l'instabilité de la boucle qui en l'absence des comparateurs se traduirait par un cycle limite (pompage de la gouverne) dans la limite d'autorité des stabilisateurs. Cette limite est relativement faible, de l'ordre du degré de gouverne. En fait les comparateurs vont constater une différence entre la chaîne de commande (fautive) et de surveillance (normale) et dès que le seuil du comparateur sera atteint le système sera automatiquement coupé. Compte tenu des caractéristiques des comparateurs la détection s'effectue pour des oscillations dont l'amplitude est nettement inférieure à la limitation d'autorité des stabilisateurs.

5. - AMORTISSEMENT ARTIFICIEL DES MODES DE STRUCTURE -

Le système de stabilisation de tangage défini ci-dessus compte tenu des précautions prises ne modifie pratiquement pas l'amortissement des modes de structures.
Or l'excitation des modes de structure par une forte turbulence par exemple peut être gênante pour le pilotage et le confort des passagers. Des études de simulation de ces phénomènes sont en cours à SUD-AVIATION et dans les laboratoires officiels.
Il paraît séduisant d'amortir artificiellement ces modes. Les moyens à mettre en oeuvre ne sont pas fondamentalement différents de ceux utilisés dans un stabilisateur de tangage

.../

par exemple.

Nous avons effectué quelques études préliminaires pour vérifier s'il était possible de diminuer d'au moins 50 % la réponse en amplitude du 1er mode de structure sans diminuer sensiblement l'amortissement des modes de fréquence plus élevée. Les premiers résultats de ces études bien que très préliminaires paraissent encourageants. Le résultat recherché paraît pouvoir être atteint en installant 2 gyromètres en des endroits particuliers du fuselage, les signaux de ces gyromètres étant convenablement filtrés pour assurer la stabilité des modes de fréquence élevée. Une première conclusion importante de l'étude préliminaire effectuée est qu'il paraît possible d'utiliser les servocommandes de puissance de l'avion malgré leur bande passante limitée.

Des études complémentaires et des essais seraient cependant nécessaires pour la mise au point d'un tel système dans le cas où les essais en vol de l'avion en montreraient la nécessité pour le confort du pilote et des passagers.

6. - CONCLUSION -

Les effets de l'aéroélasticité jouent un très grand rôle dans l'étude des qualités de vol et des systèmes de pilotage d'un avion de transport supersonique. Les méthodes d'études de ces problèmes sont maintenant bien au point et l'on peut envisager leur utilisation pour définir des systèmes capables d'améliorer les caractéristiques de vibration de la structure de l'avion.

LISTE DES REFERENCES -

Réf 1 - Problèmes posés par l'intégration du système de contrôle automatique de vol dans les commandes de vol d'un avion à hautes performances.

R. DEQUE - AGARD Conférence Proceedings N° 17

Réf 2 - Détermination des coefficients aérodynamiques avion souple en vol symétrique

J. WAGNER - Communication à la 34e réunion du Groupe de Travail de Mécanique du Vol de l'AGARD

THE INFLUENCE OF THE ELASTIC DEGREES OF FREEDOM UPON A CONTROL SYSTEM WITH A SMALL STABILITY MARGIN

by

R. Staufenbiel, H. Wald and A. Kanarachos

(V F W, Bremen, Germany)

Lecture: The influence of the elastic degrees of freedom upon a control system with a small stability margin

Authors: R. Staufenbiel, H. Wald and A. Kanarachos
(V F W, Bremen, Germany)

Summary

Flight testing of an automatic flight control system, which was supposed to guide a missile at low altitudes over the open sea, revealed unexpected stability problems. These problems can be explained by the fact that the suspension of the rate gyro introduced an additional coupling moment between vertical acceleration and angular velocity which resulted in a reduction of the stability margin.

1. Introduction

Within the framework of a study on a missile which is to fly at low altitude over the open sea, an AFCS with high-performance altitude-hold was developed. A subsonic drone, model Beech KDB-1, was used as an experimental vehicle in flight testing. It was the development objective to arrive at a solution which would permit flights at altitudes below 10 m above the water level even under adverse weather conditions.

Prior to explaining the stability problems encountered during flight testing in more detail, and subsequent to a brief description of the experimental vehicle, an account will be given of the system design phase up to the point of flight testing. Furthermore, the layout of the control loop and the stability studies conducted prior to flight testing will be discussed.

1.1 Experimental Vehicle

The all-metal drone KDB-1 is a high-wing vehicle with a V-tail. It is propelled by a supercharger-driven 6-cylinder 2-stroke opposed-piston engine of 120 SHP operating an automatic variable-pitch propeller. Figure 1 shows the configuration and the main dimensions.

The maximum take-off weight amounts to approx. 340 kp. At sea level, the drone flies at a speed of 410 km/h, its maximum flying time totals 60 - 80 min.

With its engine running, the KDB-1 is launched by a solid-propellant rocket, and lands by means of a parachute over land or sea. The drone is capable of floating for a limited period of time.

Permissible load factors are + 6.7 and - 3.3 g.

During landing, an impact load of 30 g will be encountered. For this reason, sensitive equipment has to be protected by proper suspension.

1.2 From System Design to Flight Testing

In preparing the analogue computer simulations, all aerodynamic and flight mechanic data of the KDB-1 were evaluated, and an AFCS concept for the specific mission involved was elaborated. The investigations then performed on an analogue computer permitted a general understanding of the influence of the gains employed in the control loop. Among others, investigations were made with regard to the step response of the system due to gusts, altitude change or commanded climbs. The structure of gusts and sea waves, which affect the signals of the radar altimeter, was described by suitable statistical models (power spectra). The effects of the latter were represented by noise generators with filters corresponding to the power spectra. Parallel to the simulations performed on the analogue computer, stability investigations were carried out by way of digital programs using root locus method and Nyquist diagrams. Still another digital program yielded results on the wave contact probability as a function of the flight time at different seas and various wind velocities, whereby it was possible to determine the influence of the gains employed in the control loop.

The work described herein resulted in an optimization of the control loop in accordance with the following requirements:

1. acceptable stability margin
2. low gust sensitivity
3. low wave contact probability

Subsequent to this preliminary optimization, system components were incorporated step by step into the simulation program. This necessitated considerable changes of the AFCS parameters. In the last phase of development, functional tests of the entire system were performed. While only the flight mechanics of the KDB-1 were still simulated on the analogue computer, the following system components were incorporated:

- the servo amplifier with computing networks
- the servo motor with a hinge moment simulation
- the gyros on an analogue computer-controlled flight table
- a radar altitude simulator
- the command transmitter and receiver
- the telemetry system

as well as the ground station, fully equipped for flight testing.

2. Layout and Stability of the Control Loop

The control loop can be devided into a stability augmentation system and a high-performance altitude-hold system, as can be gathered from the general block diagram (fig. 2).

Within the high-performance altitude-hold loop, altitude is measured by a radar altimeter. Deviations from the demanded altitude and the rate of descent result in a vertical acceleration command which is performed by the stability augmentation system.

2.1 Stability Augmentation System (SAS)

In the stability augmentation system, the control surface commands are being computed from the measured pitch rate and vertical acceleration. To reduce the noise level, the measured values are sent through low-pass filters prior to further processing. (This is shown in the block diagram, fig. 3).

Pitch rate signals damped the angle-of-attack oscillation (short-period mode) while the vertical acceleration reduced the missile altitude deviations under gust loads.

Before taking into consideration any of these effects, the dynamic response of the basic missile will be described. For this purpose, the phygoid and short period mode are taken into account:

phygoid	
natural frequency	damping ratio
0.107 $\left[\frac{1}{\text{sec}}\right]$	0.118

short period mode	
natural frequency	damping ratio
5.355 $\left[\frac{1}{\text{sec}}\right]$	0.407

and also the transfer function $\Delta n / \alpha_G$ (fig. 4) which is of particular importance for low-altitude flights, giving the vertical acceleration Δn of the missile with reference to the additional angle of attack $\alpha_G = \frac{W_G}{V_M}$ caused by vertical gusts. From this representation of vertical acceleration under gust loads conclusions can be drawn with regard to the corresponding altitude deviations.

Vertical acceleration signals and the rate of descent during the automatically controlled flight of the missile considerably reduce these altitude deviations (fig. 5 a).

When considering the gust power spectra, the root mean square $\delta\Delta h$ of the altitude deviations decreases (with reference to the root mean square value δW_G of the vertical gust velocity) (fig. 5 b).

Pitch rate signals increase the altitude deviations due to gusts (figs. 5 c and 5 d).

2.2 Altitude-Hold Loop

In the altitude-hold loop, the altitude is measured by a radar altimeter. Since the radar altimeter indicates the true altitude, the waviness of the sea surface has an effect on the flight path.

The altitude errors and their integral are used for forming the corrective signals. In addition, the rate of descent is applied for damping the vertical movement. The rate of descent is obtained by way of an approximated integration of the vertical acceleration. If the rate of descent were generated by differentiating the radar altitudes, the steepness of the waves would be superimposed which, as was shown in study [1], would considerably increase the wave contact probability. By way of the altitude integrating network, it is possible to compensate for the following effects:

- null error of the accelerometers
- acceleration errors in turns due to missile-fixed installation of the accelerometer
- control surface zero position error
- c.g. shifts due to fuel consumption

When adapting the altitude gain, particular attention was paid to the fact that, with the flight direction almost parallel to the wave fronts and the movement of the waves thus being sensed as a low-frequency one, the missile will follow the shape of the waves at a constant height relative to the wave without any substantial phase shift. If the flight direction to the wave front is steeper, however, the altitude changes of the missile should be kept to a minimum in order to avoid any increase of the necessary minimum flight altitude on account of antiphase movements.

Fig. 6 shows the influence of the gain $K_{\Delta h}$ of the altitude on the transfer function $\Delta h/h_w$. It is apparent that, as the value of $K_{\Delta h}$ increases, the missile will continue to follow the movement of the waves at a constant height relative to the waves even at steeper angles (higher frequencies) - $\Delta h/h_w \approx 1$; there is, however, a simultaneous increase in altitude deviation at frequencies leading to antiphase movements.

Fig. 7 shows how the movement of the waves will be followed when the flight direction is almost parallel to the wave crests.

2.3 Stability Investigations

The stability margin of the altitude-hold and the SAS loops was investigated by means of the Nyquist diagrams of $\frac{\Delta n_m}{\Delta n_m^*}$ and $\frac{\Delta h_m}{\Delta h_m^*}$, i.e. the stabilization augmentation loop was assumed to have been "cut open" aft of the accelerometer, and the altitude-hold loop aft of the altimeter (fig. 8).

The Nyquist plots in fig. 9 show that there are sufficient amplitude and phase margins. This result was confirmed by simulations incorporating original components of the control loop.

3. Flight Test Results

The measurements shown in figs. 10 a and 10 b were obtained during flight testing by means of a telemetry station. The values plotted in fig. 10 a were obtained during a commanded horizontal flight, the values in fig. 10 b were recorded during a commanded climb. In both cases, there is merely a slightly damped 2-cps (!) oscillation which is more pronounced, however, during climb.

To continue the flight tests, it became imperative to find out the reasons for this 2-cps oscillation.

4. Interpretation of the Results

The more pronounced 2-cps oscillation during the commanded climb (fig. 10 b) can be explained by the fact that continuous adjustment of the altitude command potentiometer, as required for the climb, was effected by a motor triggered, by a pulse width modulation, at a 2-cps pulse repetition frequency. Consequently, the system was continuously exited within the resonance range of the slightly damped frequency, yielding the larger amplitudes observed during climb.

To find out what had caused the slightly damped 2-cps natural frequency of the system, various influences which might have been responsible for it were investigated:

- overdriving of individual operator amplifiers of the AFCS
- effects of elastic fuselage vibrations
- altimeter disturbance effects etc.

After a thorough investigation, it was obvious that the elastic suspension of the rate gyro had caused the slightly damped frequency of the system. This effect, however, will be explained in more detail below. Even before flight testing, in

the system design phase, the sensor suspensions had been the subject of investigations. Ground tests performed on the KDB-1 with its motor running had revealed that both the accelerometer and the rate gyro, when mounted directly to the fuselage structure, were overdriven on account of the vibrations caused by the motor. Therefore, the elastic sensor suspensions were designed in such a way that all fuselage-transmitted disturbances whose frequencies exceed the effective frequencies of the AFCS will be absorbed by the suspension devices. This was also to eliminate the lowest natural fuselage vibration of approximately 25 cps.

The Nyquist diagram (fig. 11) was used for selecting the cutoff frequency of the elastic suspension of the rate gyro. It is obvious that frequencies above 10 cps may be cut off without decreasing the stability margin, that is near the critical point, the influence of this suspension is slight (fig. 11). The suspension cutoff frequency was, therefore, established at 12 cps.

The elastic suspension was one of the features reviewed after flight testing. It was then, for the first time, that it occoured to us that the off-center arrangement of the rate gyro on the elastically mounted equipment platform might have a bearing on the natural frequency of the system.

For the more detailed investigations that followed, a suspension model, shown in fig. 12, was used. With this model, it was possible to ascertain that the rate of rotation of the gyro platform $\dot{\varphi}$ depends on the pitch rate and the vertical acceleration.

$$\dot{\varphi} = \frac{A(s)}{N(s)} \cdot \dot{\vartheta} + \frac{B(s)}{N(s)} \cdot \frac{g}{l} \cdot \Delta n \qquad (1)$$

whereby the following abbreviations are used:

$$A(s) = \left(1 + 2\frac{\xi_R}{\omega_R} s\right) \cdot \left(1 + 2\frac{\xi_R}{\omega_R} s + \frac{1 - 4\frac{L}{l} \cdot \frac{l_\varrho}{l}}{\omega_T^2} \cdot s^2\right)$$

$$B(s) = 4 \cdot \frac{l_\varrho}{l} \cdot \frac{1}{\omega_T^2} \cdot s \cdot \left(1 + 2\frac{\xi_R}{\omega_R} \cdot s\right) \qquad (2)$$

$$N(s) = \left(1 + 2\frac{\xi_R}{\omega_R} \cdot s\right) \cdot \left[1 + 2\frac{\xi_R}{\omega_R} \cdot s + \left(\frac{1 + \left(\frac{2 l_\varrho^2}{l}\right)}{\omega_T^2} + \frac{1}{\omega_R^2}\right) s^2\right] + \frac{s^4}{\omega_T^2 \cdot \omega_R^2}$$

$\omega_T = \sqrt{\frac{2c}{m}}$ – natural frequency of translatory motion

$\omega_R = \frac{1}{2}\left(\frac{l}{i}\right)\omega_T$ – natural frequency of rotational motion (3)

ξ_R – damping of rotational motion

i radius of inertia of substitute mass

l_e eccentricity of substitute mass relative to platform center

c spring stiffness

b damping factor

Equation (1) reveals the influence of the vertical acceleration on the signal of the rate gyro, this influence being a decisive factor in explaining the 2-cps oscillation. As the eccentricity l_e/l of the rate gyro arrangement increases, the vertical acceleration increasingly affects the rate of rotation of the platform.

By converting equation (1) by means of the transfer function $\Delta n/\dot{\vartheta}$ of the missile, $\dot{\varphi}$ can be shown to be exclusively dependent on $\dot{\vartheta}$:

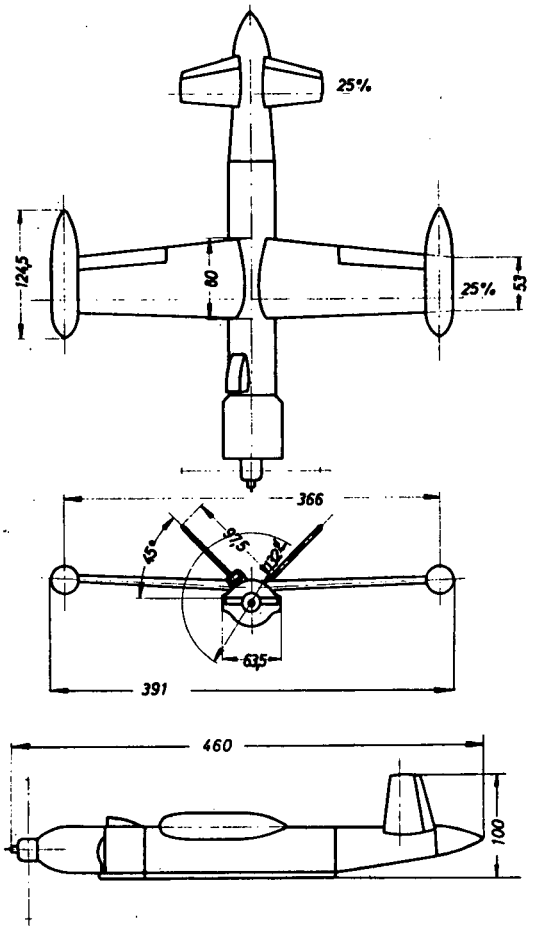
$$\dot{\varphi} = \frac{A(s) + B(s)\frac{\Delta n}{\vartheta}\frac{g}{l}}{N(s)}\,\dot{\vartheta} \qquad (4)$$

In fig. 13, this transfer function $\dot{\varphi}/\dot{\vartheta}$, which can be understood as a multiplier element in the rate gyro path of the control loop, is shown for various eccentricities l_e/l . With increasing eccentricity, a considerable reduction in amplitude is noticeable in the 2-cps range; this means that the large gain margin in the rate gyro path (fig. 11), which is available in the case of a rigid suspension, is reduced. This is apparent from the Nyquist plots $\dot{\vartheta}m/\dot{\vartheta}^*m$ given in fig. 14 for an elastic suspension and different eccentricities. In fig. 15, the root loci of the feedback control loop are plotted for various suspension stiffness values (given by ω_R) and eccentricity values. They reveal that the natural frequencies will shift into the instable range, even at high natural frequencies of the suspension, with slightly increasing eccentricity.

References:

1 "Untersuchung eines Regelsystems zur automatischen Höhenhaltung"
(Kurztitel: Höhenhaltung I)
VFW Bremen, Aug. 1964

General drawing of the drone KDB 1



dimensions in cm

Figure 1

General block diagram of the control system

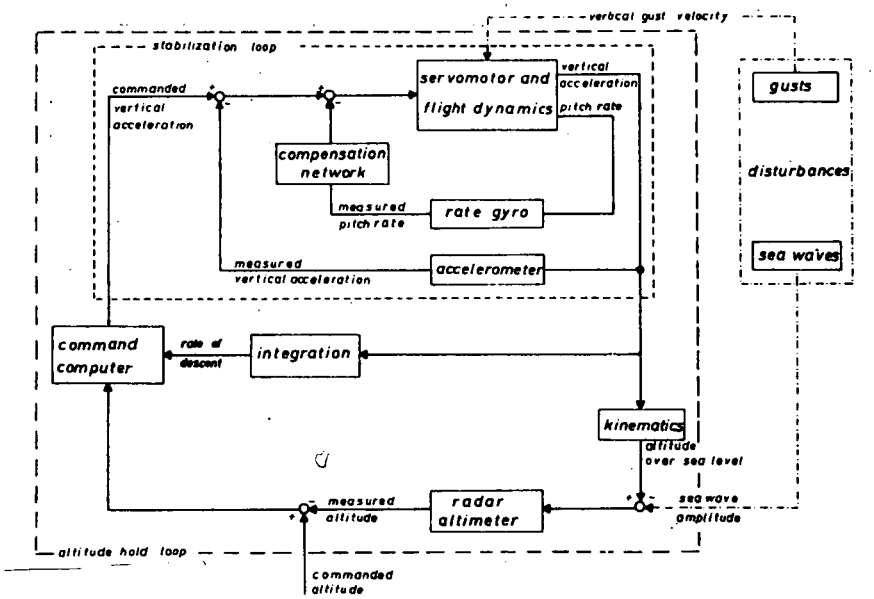


Figure 2

Block diagram of the control system

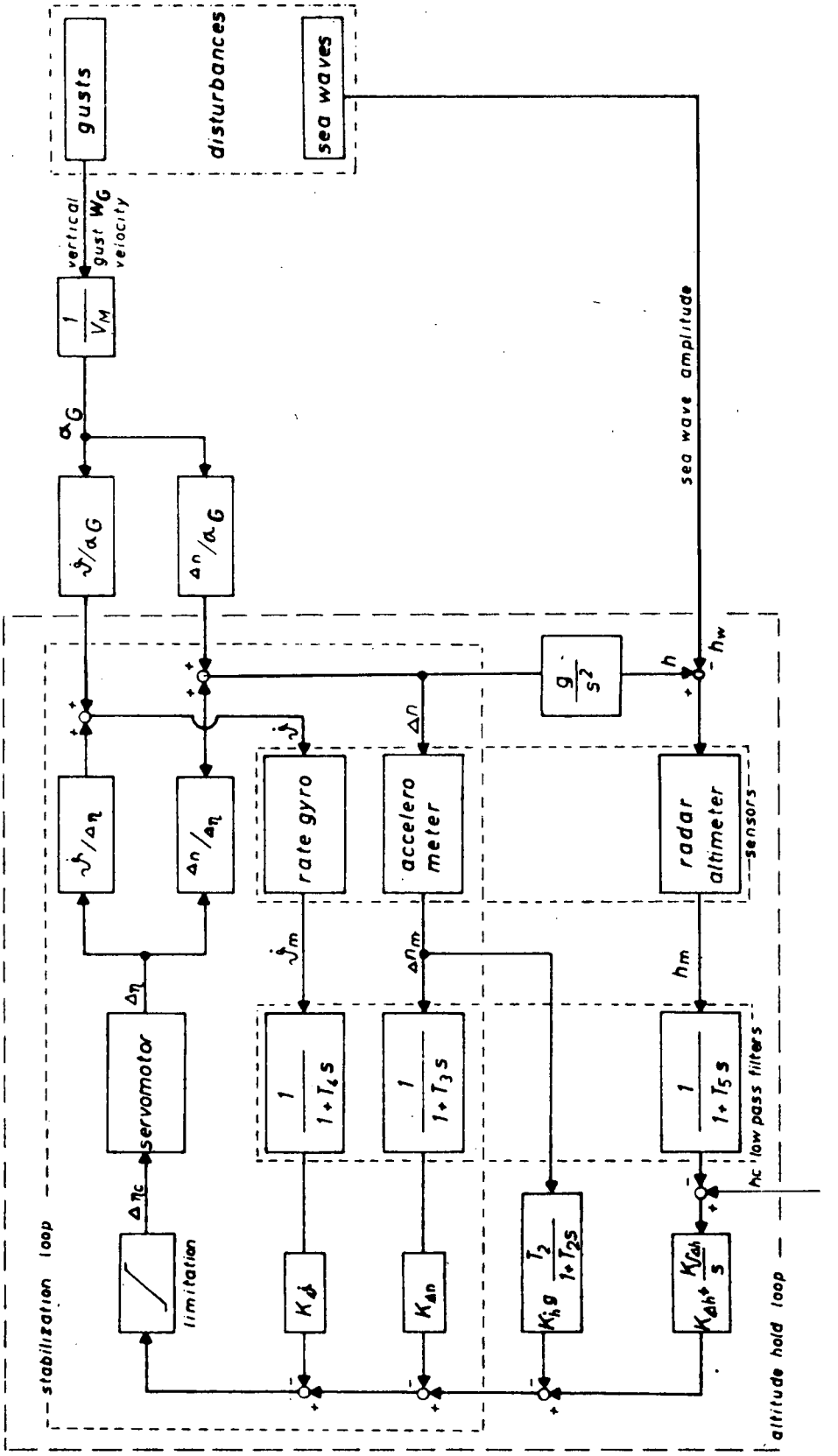


Figure 3

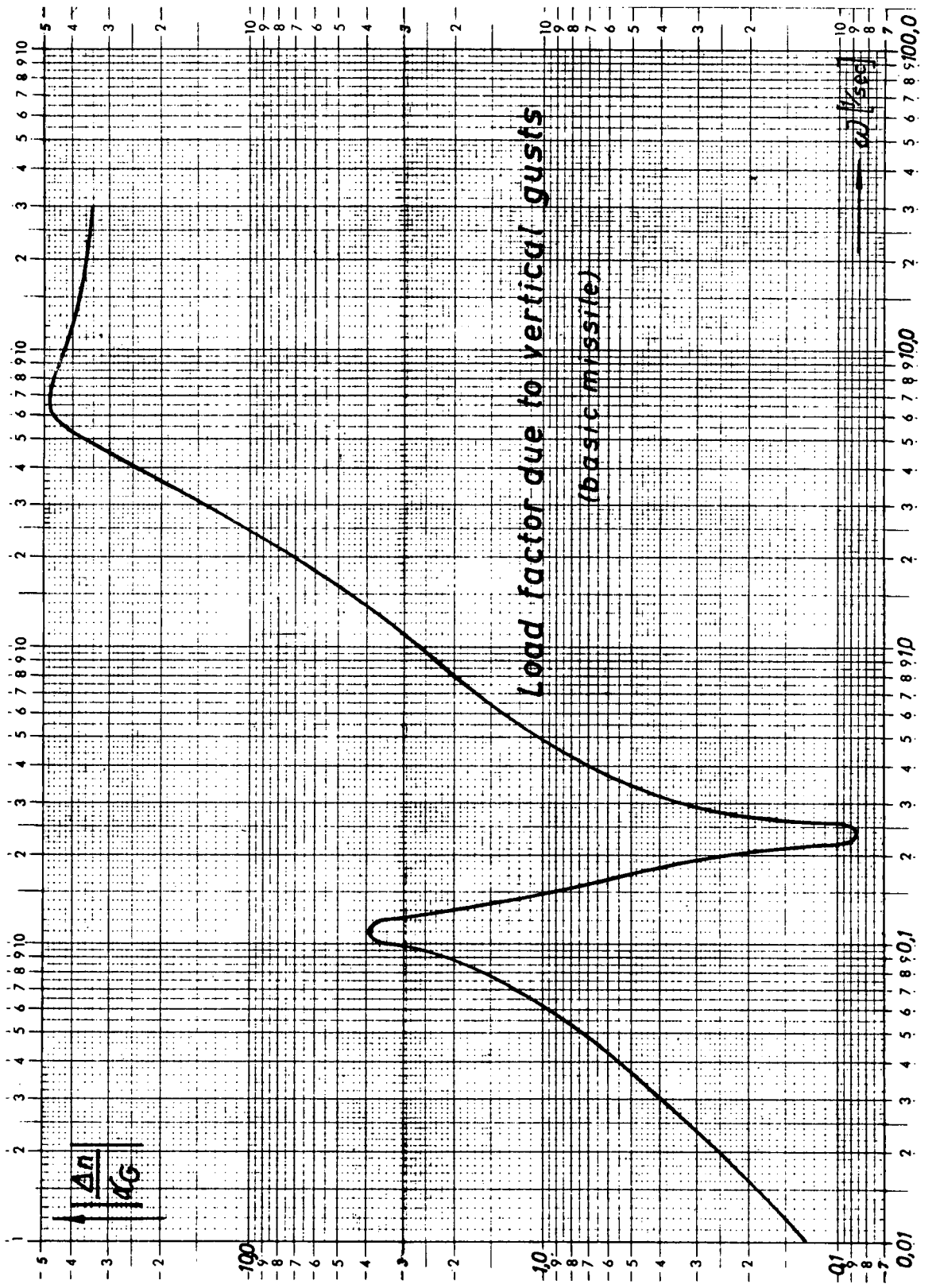

Load factor due to vertical gusts
(basic missile)
$\frac{\Delta n}{\Delta G}$
ω 1/sec

Figure 4

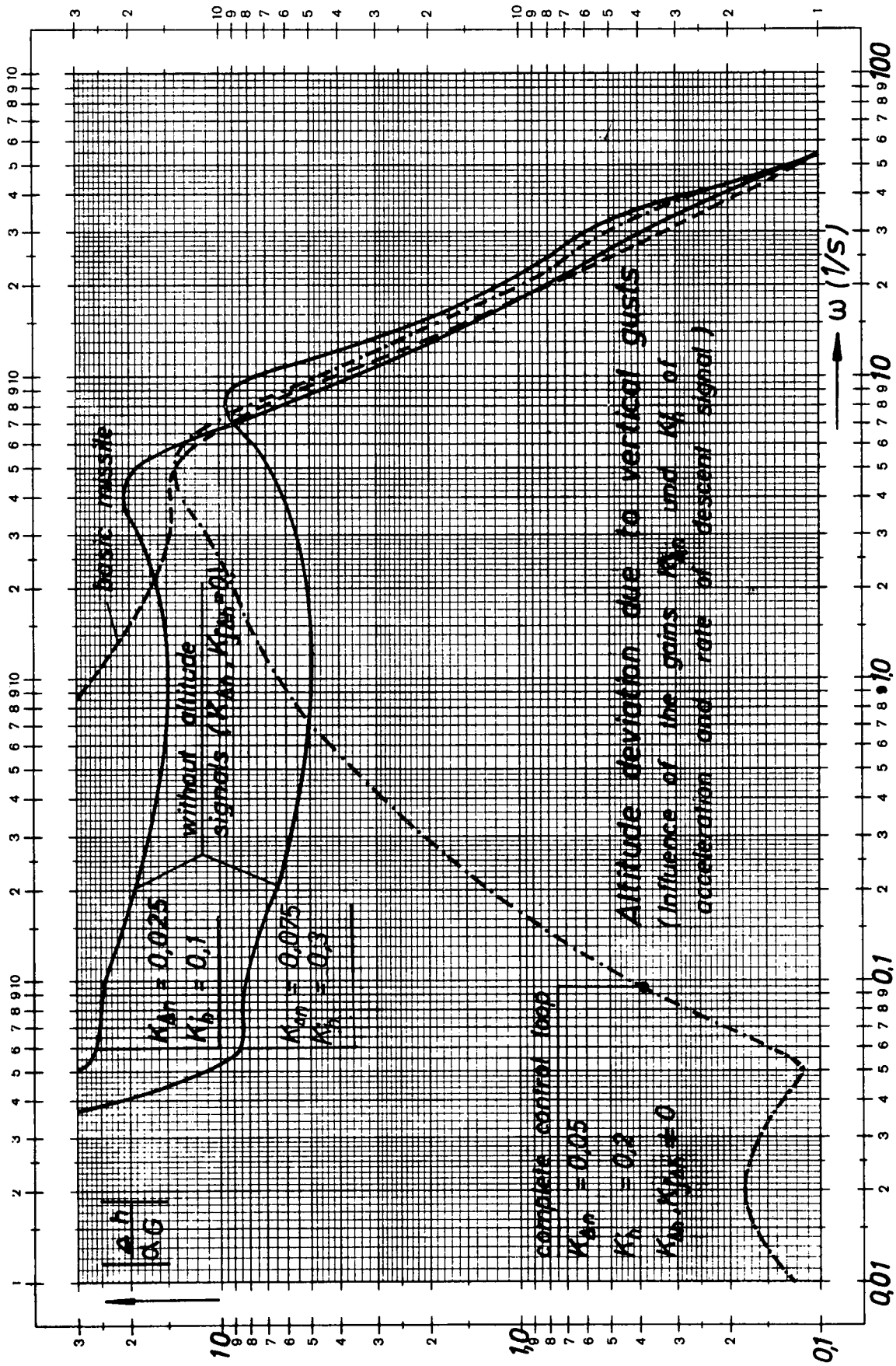

basic pause
without altitude signals (K_{Ah}, K_{Ah}=0)
K_{Ah} = 0,025
K_h = 0,1
K_{Ah} = 0,075
K_h = 0,3
complete control loop
K_{Ah} = 0,05
K_h = 0,2
K_{Ah}, K_{Ah} = 0
Altitude deviation due to vertical gusts
(influence of the gains K_{Ah} und K_h of acceleration and rate of descent signal)
ω (1/s)
$\frac{\Delta h}{\delta_G}$

Figure (5a)

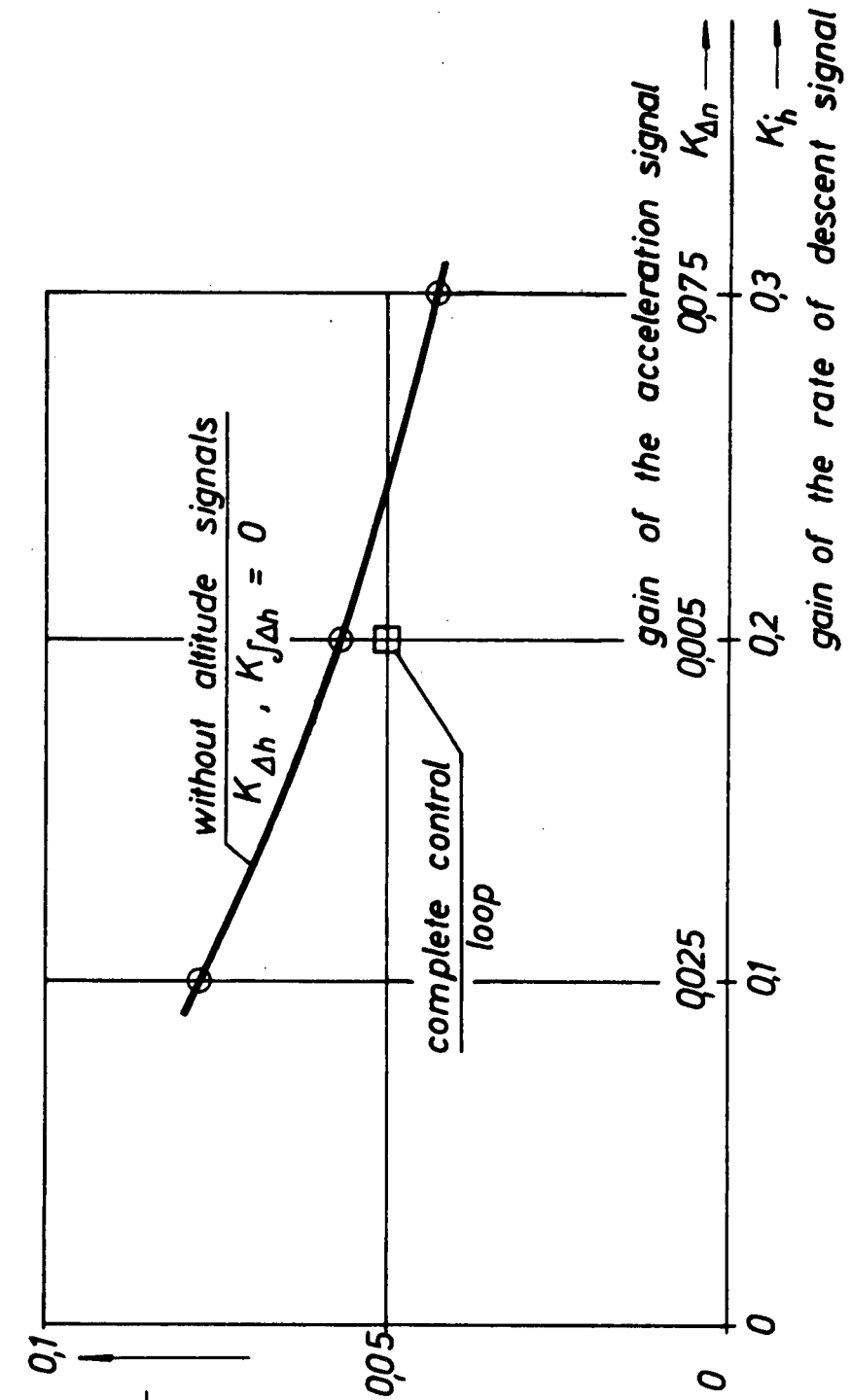

Altitude deviation $\sigma_{\Delta h}$ refered to r.m.s. σ_{wG} of the vertical gust velocity (power spectrum method)
$\frac{\sigma_{\Delta h}}{\sigma_{wG}}$
0,1
0,05
0
without altitude signals
$K_{\Delta h}$, $K_{f\Delta h}$ = 0
complete control loop
0,025
0,05
0,075
gain of the acceleration signal $K_{\Delta n}$
0
0,1
0,2
0,3
gain of the rate of descent signal K_h

Figure 5(b)

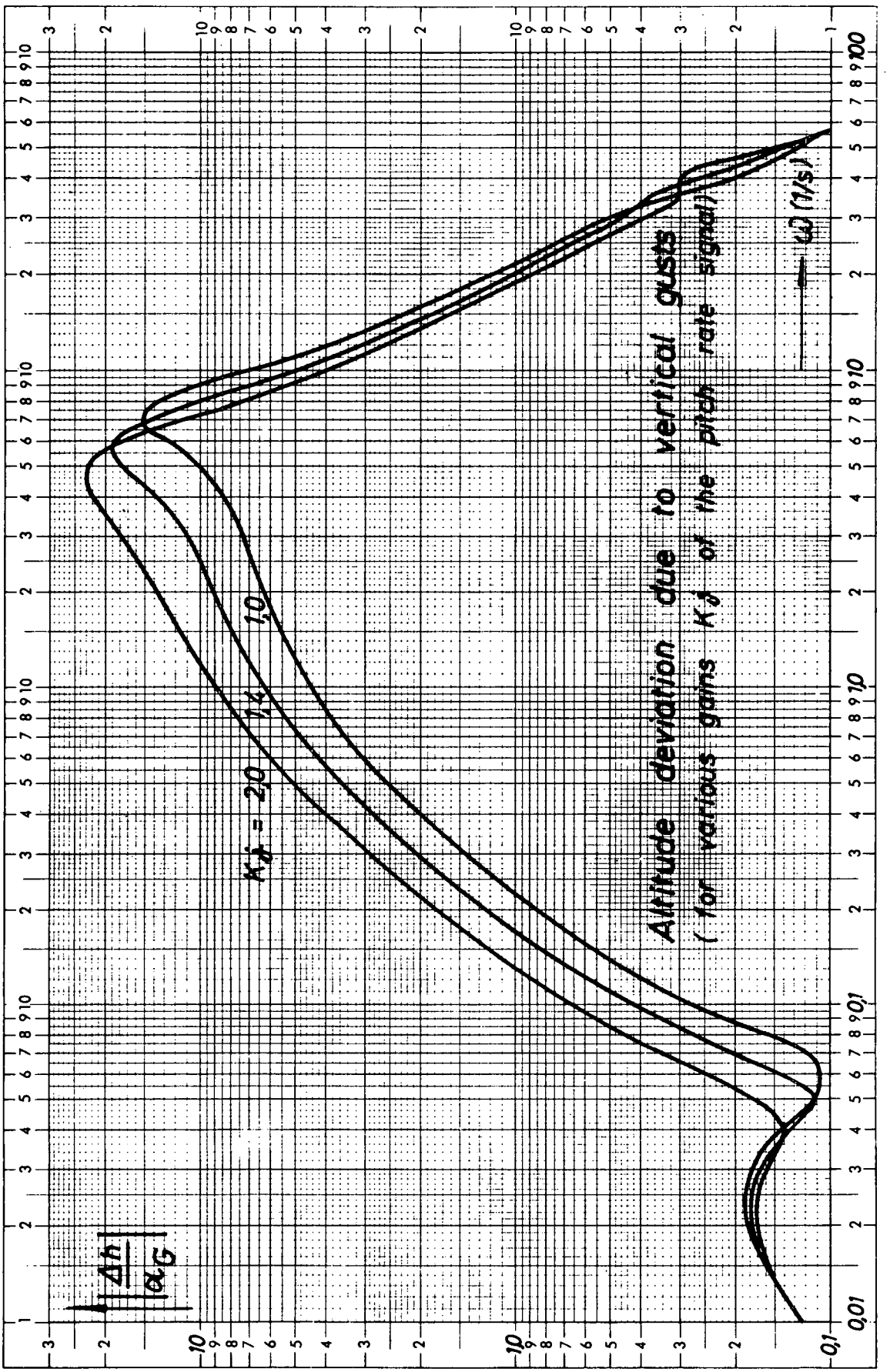

Altitude deviation due to vertical gusts
(for various gains K_ϑ of the pitch rate signal)
K_ϑ = 2,0
1,4
1,0
ω (1/s)
$\left|\frac{\Delta h}{\alpha_G}\right|$

Figure 5(c)

Altitude deviation $\sigma_{\Delta h}$ refered to r.m.s. σ_{WG} of the vertical gust velocity

(power spectrum method)

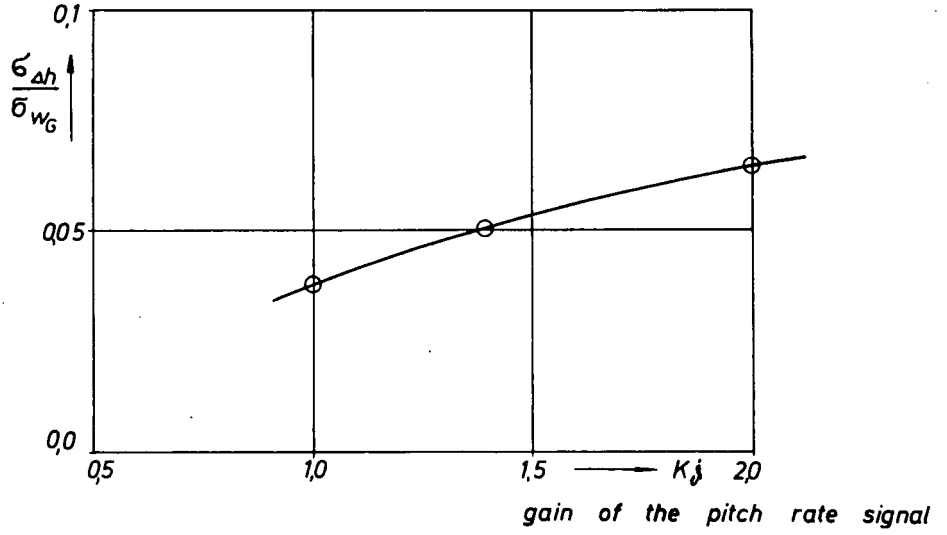


Figure 5(d)

Altitude deviation due to sea waves

(for different gains $K_{\Delta h}$ of the altitude signal)

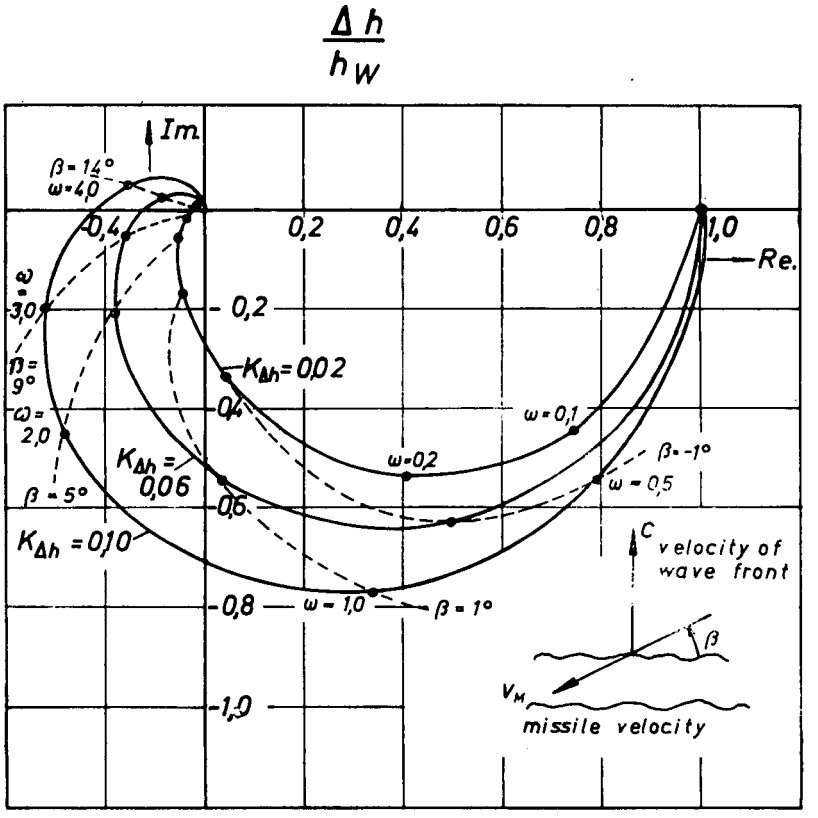


Figure 6

Missile responses due to sea waves

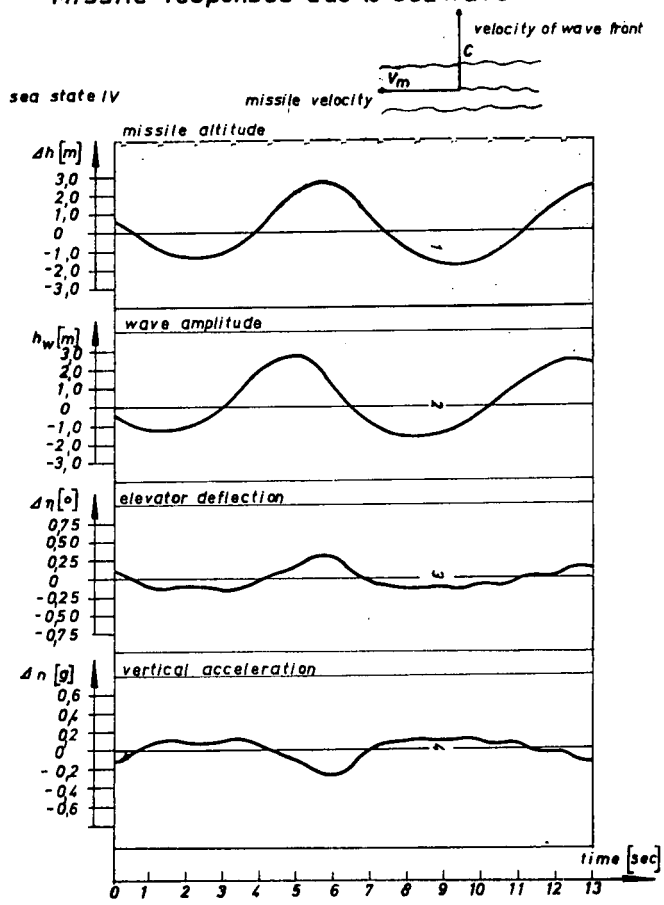


Figure 7

Intersections in the control loop for Nyquist-diagrams

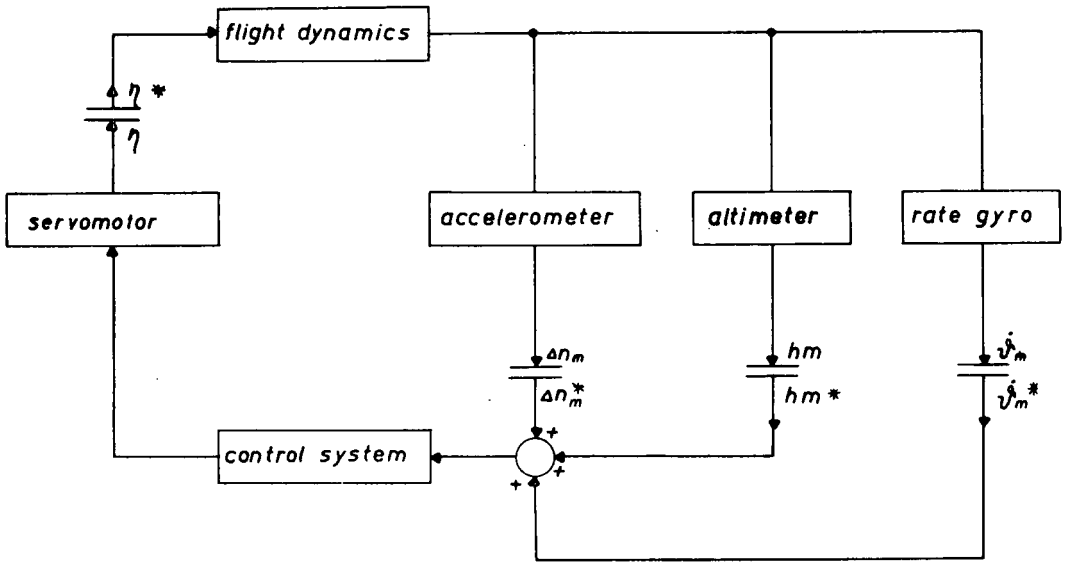


Figure 8

Nyquist-diagrams for accelerometer and altimeter loop

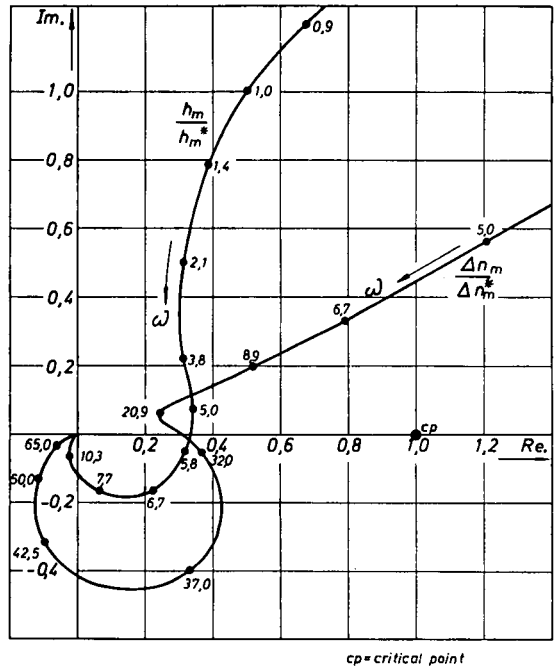


Figure 9

Flight - measurements (horizontal flight)

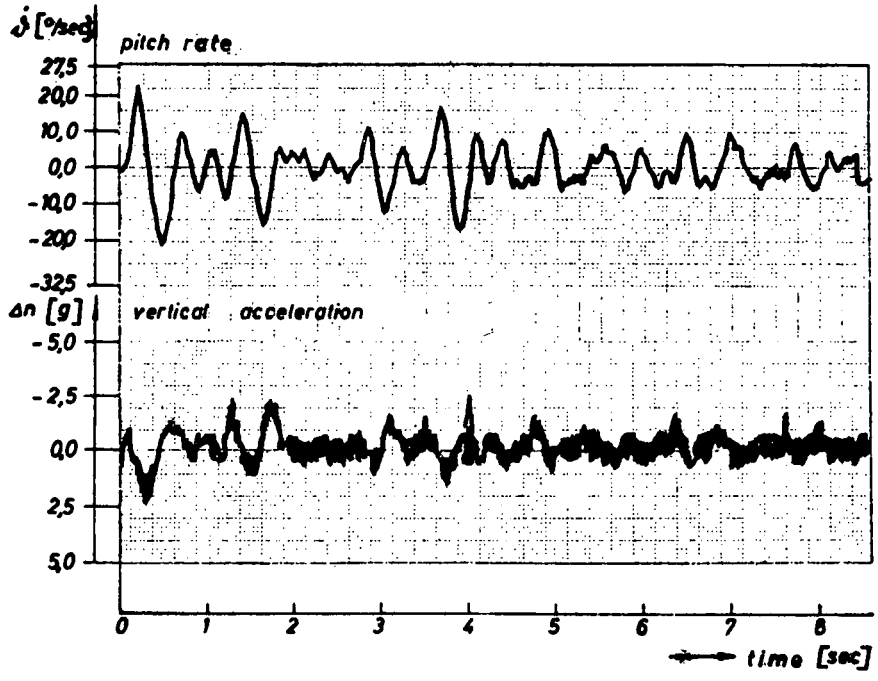


Figure 10(a)

Flight measurements (climb)

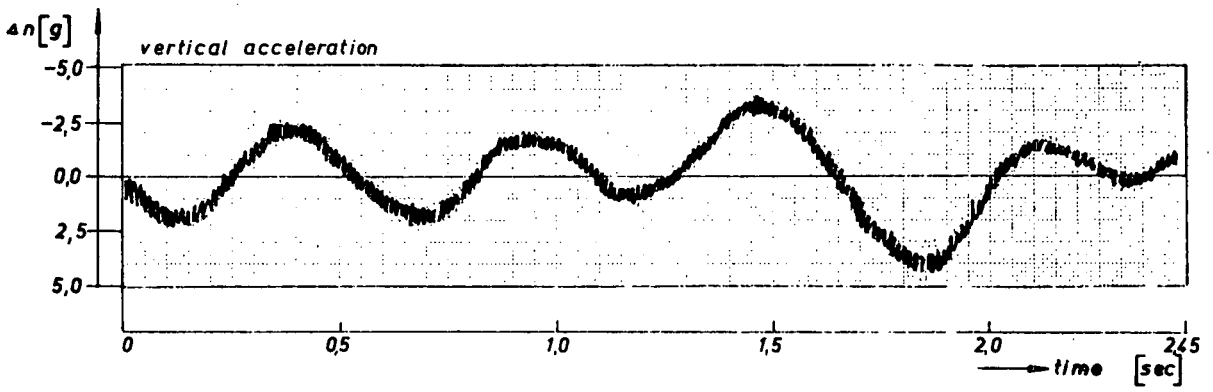
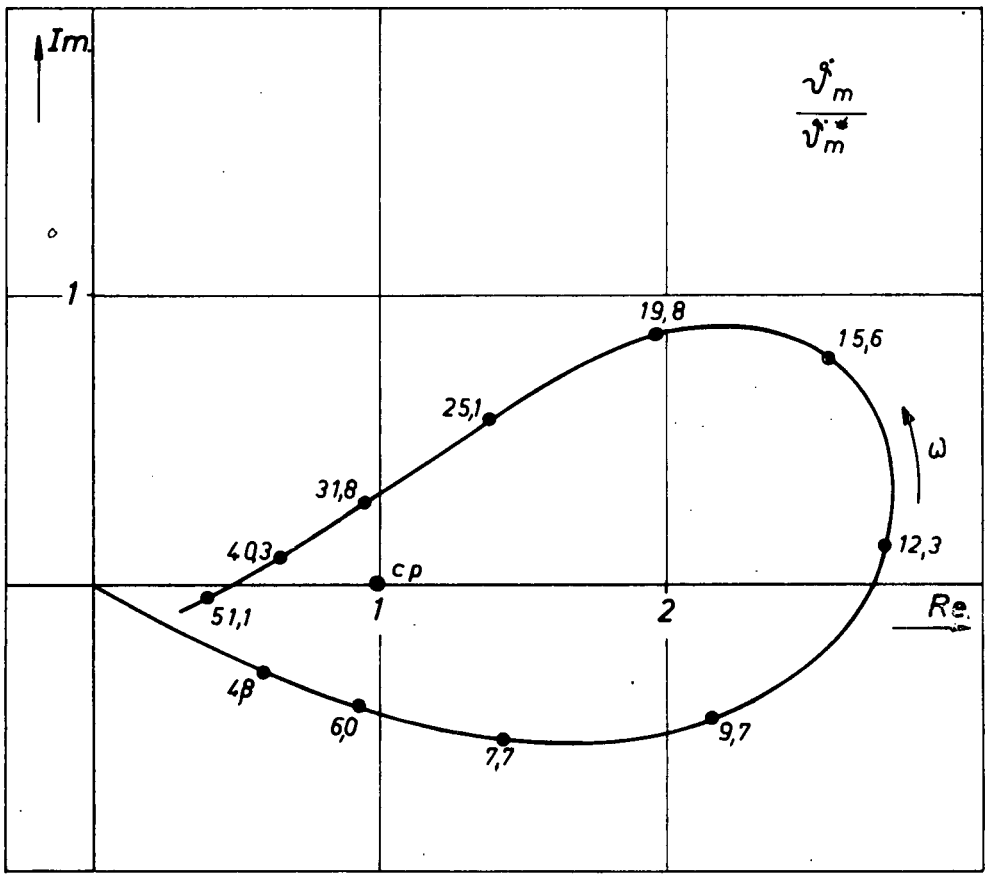


Figure 10(b)

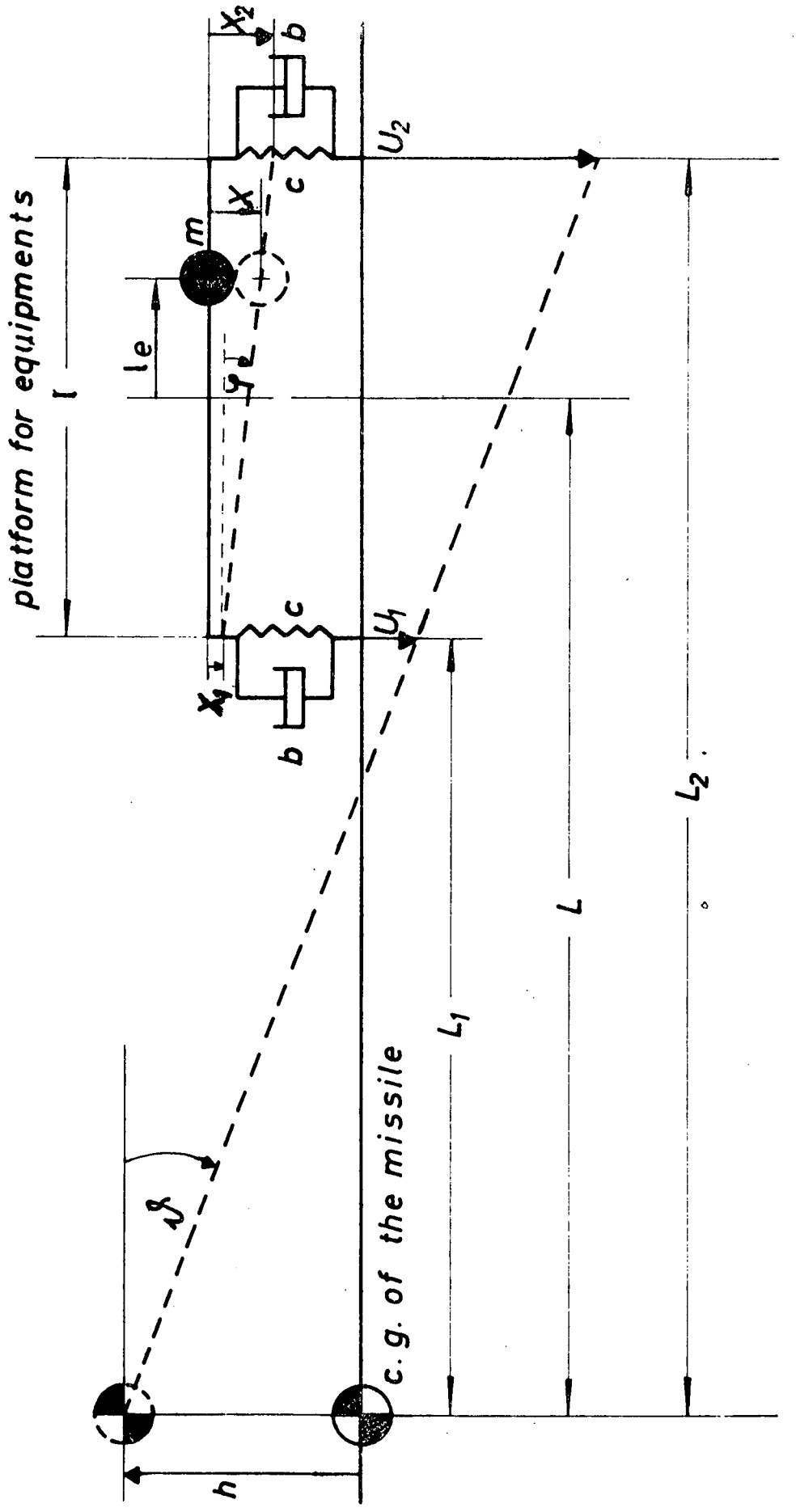
Nyquist-diagram for rate gyro loop

(rigid suspension)



cp = critical point

Figure 11



Model for the elastic suspension of the rate gyro

Figure 12

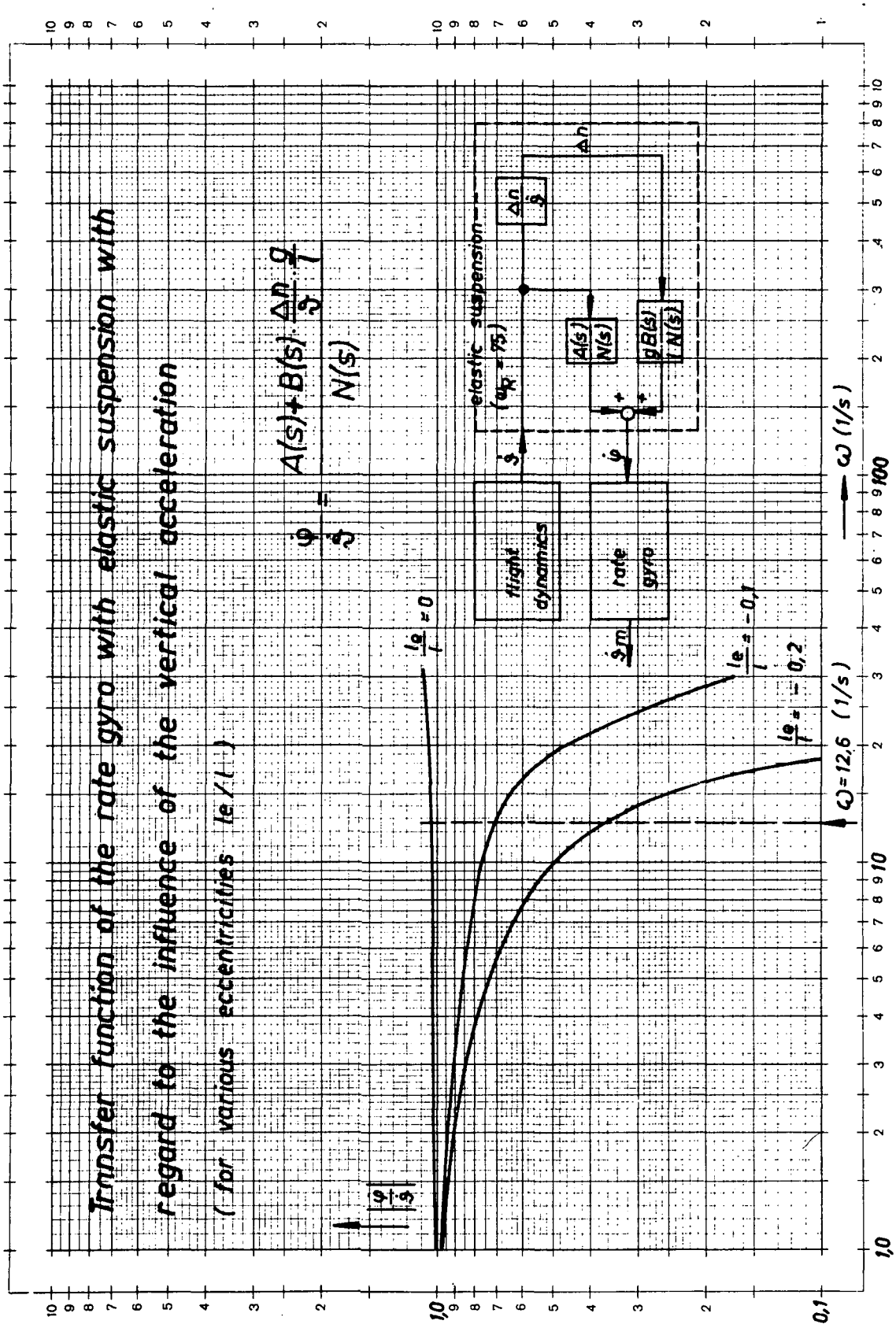

Transfer function of the rate gyro with elastic suspension with regard to the influence of the vertical acceleration
(for various eccentricities le / l)
$\frac{\dot{\varphi}}{\ddot{\vartheta}} = A(s) + B(s) \cdot \frac{\Delta n}{\ddot{\vartheta}} \cdot \frac{g}{l}$
$N(s)$
$\frac{\dot{\varphi}}{\ddot{\vartheta}}$
$\frac{le}{l} = 0$
$\frac{le}{l} = 0,1$
$\frac{le}{l} = 0,2$
$\omega = 12,6$ (1/s)
ω (1/s)
flight dynamics
elastic suspension
(ω_R = 75)
rate gyro
$\ddot{\vartheta}$
$\dot{\vartheta}$
ϑ
$\dot{\varphi}$
φ
Δn
$\frac{\Delta n}{\vartheta}$
A(s)
N(s)
gB(s)
N(s)
1,0
0,1

Figure 13

Influence of the eccentricity $\frac{l_e}{l}$ on the Nyquist-diagram $\frac{\dot{\vartheta}_m}{\dot{\vartheta}_m^*}$

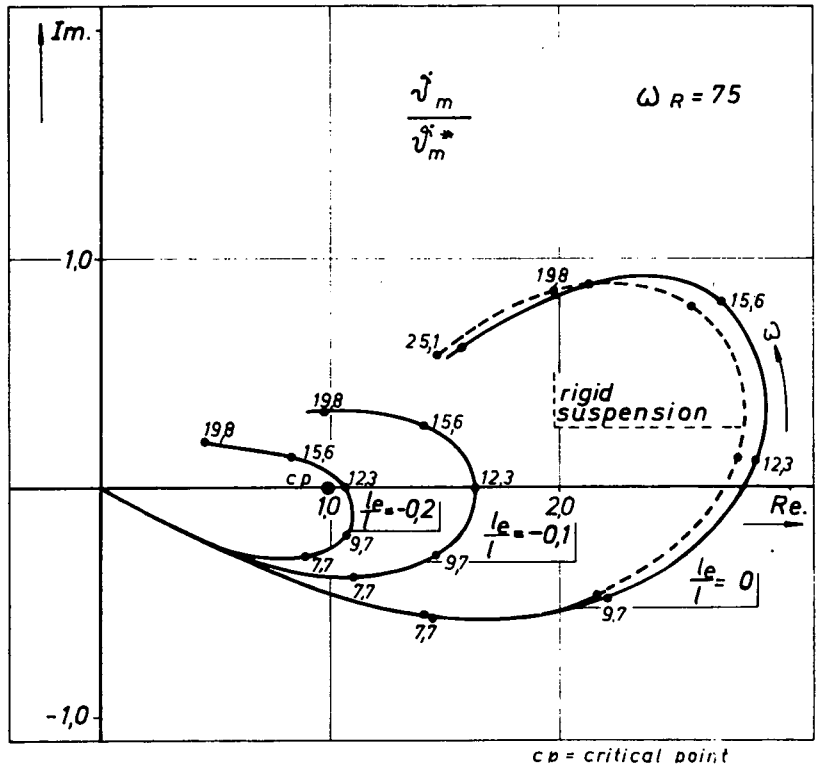


Figure 14

Root loci of the control loop for various suspension stiffness values ω_R and different eccentricities l_e/l

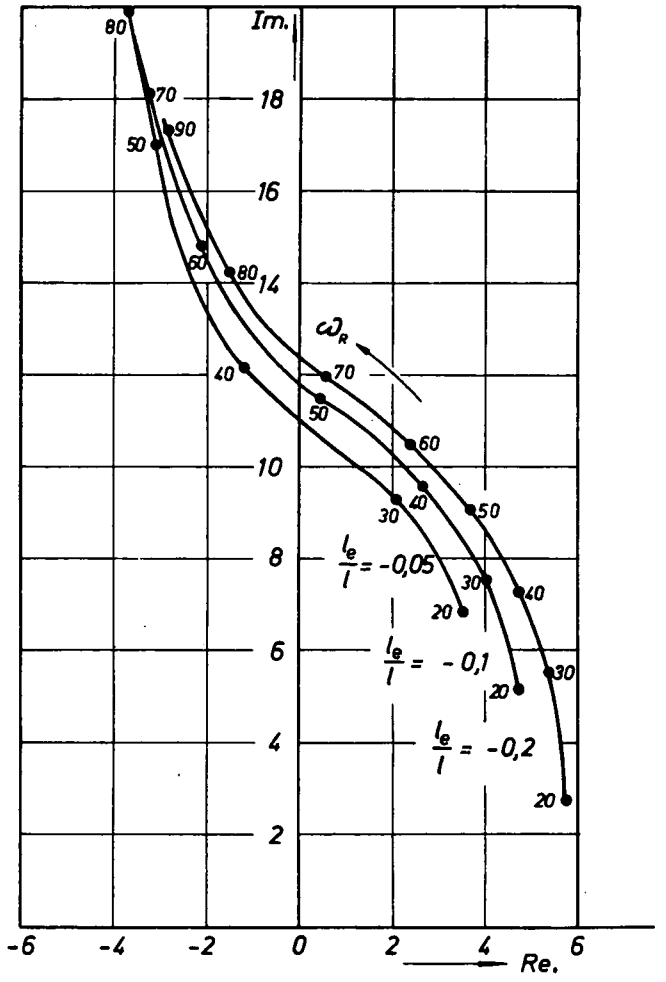


Figure 15

ANALYTICAL DESIGN AND FLIGHT TESTS OF A MODAL SUPPRESSION SYSTEM ON THE XB-70 AIRPLANE

Part I – DESIGN ANALYSIS

John H. Wykes
Staff Scientist
Los Angeles Division
North American Rockwell Corporation

Part II – FLIGHT TESTS

Eldon E. Kordes
Senior Staff Scientist
NASA Flight Research Center
Edwards, California

ANALYTICAL DESIGN AND FLIGHT TESTS OF A MODAL SUPPRESSION SYSTEM ON THE XB-70 AIRPLANE

SUMMARY

A control system designed to damp the structural motion of flexible airframes was flight tested on the XB-70 airplane, a flexible, low-aspect-ratio supersonic configuration. Even though the system—known as ILAF (Identical Location of Accelerometer and Force)—was an exploratory device and was not developed as an optimum system, the flight tests provided valuable information applicable to aircraft of the supersonic-transport type. This paper reviews the design processes and presents some preliminary results obtained from flight tests.

INTRODUCTION

Large aircraft flying through turbulent air experience large structural loads, the pilot and passengers are exposed to a rough ride, and aircraft handling qualities are degraded because of the induced motion of the highly flexible airframe. In recent years, a number of conceptual studies have been conducted on systems designed to suppress the structural motion of flexible airframes(1-6). The study discussed herein and two other studies(5,6) have proceeded also into actual system mechanization and flight test. The Boeing B-52 airplane was used in both of the latter studies. This flexible, subsonic airplane has produced valuable design and performance information on structural mode control systems which might have application to more current, but similar, subsonic aircraft such as the Lockheed C-5A and Boeing 747 transports. Similarly, the North American Rockwell XB-70 airplane presented an opportunity to flight test a structural mode control system in a flexible supersonic configuration, thus providing valuable information applicable to aircraft of the supersonic-transport type.

The structural mode control system implemented on the XB-70 under a program sponsored jointly by the National Aeronautics and Space Administration and the U.S. Air Force was the Identical Location of Accelerometer and Force or ILAF system concept. This concept was explored in previous studies(1-3) and showed attractive potentialities. Since the intent of the program discussed herein was to investigate the concept and not to design a completely operational system, the system designed was required to control only the symmetric structural modes. In addition, the design was constrained to a minimum modification of the existing control system. This paper reviews the design process and presents results from flight tests of the system.

PART I - DESIGN ANALYSIS*

By John H. Wykes

It is impossible within the scope of this paper to discuss all the elements necessary for the successful design of a structural mode control system. Such a design involves the close interplay and coordination of a number of important engineering disciplines. This paper emphasizes those aspects of the design most closely associated with the flight mechanics.

Analytical Design Model

In approaching the design of the structural mode control system for this program, it was decided to use the analytical model of the flexible XB-70 available from previous studies(1). To assemble a new model which reflected all that was known about the actual flight vehicle would have unduly delayed the program. Although this exploratory system was designed in this manner, future design efforts on optimum operational systems will require the use of more rigorous data.

The actual analytical model of this airplane for the longitudinal-symmetric study included the pitch and plunge rigid-body modes and four whole-vehicle structural modes as indicated by the following equations:

Rigid-Body Plunge Mode

$$\dot{\alpha} = q - \left(\frac{q_o S_w}{\bar{m} V_o}\right) \left\{ C_{N_\alpha}\alpha + C_{N_{\dot{\alpha}}}\left(\frac{\dot{\alpha}\bar{c}_w}{2V_o}\right) + C_{N_q}\left(\frac{q\bar{c}_w}{2V_o}\right) + \sum_{i=1\text{ to }4} C_{N_{\eta_i}}\eta_i + \sum_{i=1\text{ to }4} C_{N_{\dot{\eta}_i}}\left(\frac{\dot{\eta}_i}{V_o}\right) \right.$$

$$\left. + C_{N_{\delta_{sv}}}\delta_{sv} + C_{N_{\delta_a}}\delta_a + C_{N_{\delta_e}}\delta_e + C_{N_{w_g}}w_g \right\} - \left(\frac{m_a l_a}{\bar{m} V_o}\right)\ddot{\delta}_a - \left(\frac{m_e l_e}{\bar{m} V_o}\right)\ddot{\delta}_e \qquad (1)$$

---

*Work performed under a research effort jointly sponsored and directed by NASA and the U.S. Air Force under Contract No. NAS4-1175.

Rigid-Body Pitch Mode

$$\dot{q} = \left(\frac{q_o S_w \bar{c}_w}{I_Y}\right)\left\{ C_{m_\alpha}\alpha + C_{m_{\dot{\alpha}}}\left(\frac{\dot{\alpha}\bar{c}_w}{2V_o}\right) + C_{m_q}\left(\frac{q\bar{c}_w}{2V_o}\right) + \sum_{i=1\,\text{to}\,4} C_{m_{\eta_i}}\eta_i + \sum_{i=1\,\text{to}\,4} C_{m_{\dot{\eta}_i}}\left(\frac{\dot{\eta}_i}{V_o}\right) \right.$$

$$\left. + C_{m_{\delta_{sv}}}\delta_{sv} + C_{m_{\delta_a}}\delta_a + C_{m_{\delta_e}}\delta_e + C_{m_{w_g}}w_g \right\} - \left(\frac{\bar{l}_a m_a l_a + I_{H_a}}{I_Y}\right)\ddot{\delta}_a - \left(\frac{\bar{l}_e m_e l_e + I_{H_e}}{I_Y}\right)\ddot{\delta}_e \qquad (2)$$

Structural Modes (Symmetric) (Typical Mode i, i = 1 to 4)

$$\ddot{\eta}_i = -g_{s_i}\omega_i\dot{\eta}_i - \omega_i^2\eta_i + \left(\frac{q_o S_w}{M_i}\right)\left\{ C_{\eta_{i_\alpha}}\alpha + C_{\eta_{i_{\dot{\alpha}}}}\left(\frac{\dot{\alpha}\bar{c}_w}{2V_o}\right) + C_{\eta_{i_q}}\left(\frac{q\bar{c}_w}{2V_o}\right) + \sum_{j=1\,\text{to}\,4} C_{\eta_{i_{\eta_j}}}\eta_j + \sum_{i=1\,\text{to}\,4} C_{\eta_{i_{\dot{\eta}_j}}}\left(\frac{\dot{\eta}_j}{V_o}\right) \right.$$

$$\left. + C_{\eta_{i_{\delta_{sv}}}}\delta_{sv} + C_{\eta_{i_{\delta_a}}}\delta_a + C_{\eta_{i_{\delta_e}}}\delta_e + C_{\eta_{i_{w_g}}}w_g \right\} - \left(\frac{\varphi_i^{a'} m_a l_a - \varphi_i^{a'} I_{H_a}}{M_i}\right)\ddot{\delta}_a - \left(\frac{\varphi_i^{e'} m_e l_e - \varphi_i^{e'} I_{H_e}}{M_i}\right)\ddot{\delta}_e \qquad (3)$$

The aerodynamics due to the vehicle rigid-body and structural-response modes of motion were quasi-steady. The gust-excitation aerodynamics and the elevon control surface aerodynamics also were either quasi-steady or frequency-dependent. In general, the quasi-steady gust and elevon data were used early in the design cycle to obtain answers rapidly, whereas the frequency-dependent data were used in system stability and performance evaluations. The elevon inertia reaction forces into the vehicle's primary structure were also considered. The equations used to calculate the normal load and pitch rate at any point on the vehicle were as follows:

Load Factor

$$(n_z)_{\substack{\text{at any}\\ \text{station}}} = \frac{V_o}{g}(q - \dot{\alpha}) + \frac{l_X}{g}\dot{q} - \sum_{i=1\,\text{to}\,4} \varphi_i^{\text{station X}}\frac{\ddot{\eta}_i}{g} \qquad (4)$$

Rotary Rates

$$(q)_{\substack{\text{at any}\\ \text{station}}} = q - \sum_{i=1\,\text{to}\,4} \varphi_i'^{\text{station X}}\dot{\eta}_i \qquad (5)$$

Equations (1) to (5), together with an analytical description of the control system and sensor dynamics, were used in both calculated and simulator studies of system stability and performance. The simulator included the essentials of the full-scale control-system electronics and hardware. It should be emphasized that the simulator was invaluable in assessing the effects of system nonlinearities, such as rate limiting, hysteresis, deadband, and control-system resonance, not usually handled by analytical techniques.

Before the design was undertaken, it was known that structural modes with higher frequencies than those selected for suppression should be included in the analytical model. There is a practical limit, however, on the number of structural modes that can be considered; this limit is a function of how well the mode characteristics and aerodynamics for the modes can be determined and how conservative, from a stability point of view, the feedback compensation is likely to be.

ILAF Principle

As a starting point for describing the system design, several of the key ideas in the ILAF approach to structural mode suppression will be reviewed. The approach utilizes motion sensing devices rather than gust-velocity sensing vanes mounted on a nose boom. The motion sensing approach is applicable to continuous turbulence as well as to a sharp-edged gust and is used in most modern mode control system design. Another basic feature is that the approach reduces the induced motion by adding damping to each vibration mode.

The principal features of the system are indicated in the coined name—Identical Location of Accelerometer and Force. The name is meant to emphasize the importance of considering the sensing and control-force characteristics concurrently; and, in the specific case considered here, to emphasize that the sensing element (accelerometer) and the control force are located near each other. Such a simple sensor-force arrangement has potential for remaining effective and stable for large changes in the structural mode characteristics and a wide range of flight conditions. This is explained simply in figure 1.

As shown in figure 1, when a point force, F, application to a single structural mode is considered, the control force (generalized force) is $F\varphi_i^F$, where φ_i^F is the normalized mode deflection at the force-application point. Similarly, an accelerometer located at this same force-application point senses the modal

acceleration $\varphi_i^A \ddot{\eta}_i$, where η_i is the time-dependent generalized coordinate for the mode considered. In the presence of normal system lags such as found in the actuators and aerodynamics, the acceleration signal is integrated approximately to obtain a signal at the control surface that is in phase with the modal velocity. Some simple feedback compensation may be required in the integration process. The required structural damping force thus becomes a function of the local structural velocity. If φ_i^F and φ_i^A are at different locations in the structure, it is easy to see that as the mode shape changes with fuel use either φ_i^F or φ_i^A could change sign. Were this to occur, a system instability could result. It would be desirable to keep φ_i^F and φ_i^A always of like sign despite mode shape changes. Obviously, if $\varphi_i^F = \varphi_i^A$, or if the sensor and control force are positioned at the same location, a stable feedback sense can be maintained. This is an extremely simple explanation of the ILAF structural damping technique; considerations of modal coupling and distributed aerodynamics will change the net effect somewhat.

In many practical situations, as on the XB-70 with trailing-edge control surfaces, it is not possible to focus the control force at a single point, as illustrated in figure 2. At subsonic speeds, pressure forces are distributed over the entire chord while still generating most of the load in the vicinity of the elevon. At supersonic speeds, the pressure distribution is confined to the deflected-elevon area. These illustrations show that compliance to the ILAF idea is found at supersonic speeds, whereas the idea is somewhat diluted at subsonic speeds.

Typical Design Considerations

Figure 3 summarizes the key problems inherent in the design of any typical structural mode control system. Illustrated is an ILAF system that uses linear accelerometers as sensors and control surfaces located at the rear of the vehicle as force generators.

Figure 3(a) is a sketch of the frequency response of the sensor (accelerometer) output per unit control-surface deflection displayed as the vector amplitude, $\left|\frac{\Delta n_z}{\delta}\right|$, and the associated phase angle, ψ. The amplitude curve shows some small response at the short-period frequency range and large response in the range of frequencies of the structural modes to be controlled. The amplitude continues to rise at high frequencies as a result of control-surface inertia characteristics. The phase angle is shown to approach -180° at the short-period frequency but returns to oscillate between 0° and -90°.

Figure 3(b) shows the frequency response of the normalized (at $f = 0$) control deflection due to a unit sensor signal input. This frequency response includes sensor dynamics, system compensation, and servo and actuator dynamics. The system compensation is designed to maintain a high amplitude throughout the frequency range of the modes to be controlled and then drop off at higher frequencies.

The relationships $1 + \left|\frac{\Delta n_z}{\delta}\right| \left|\frac{\delta}{\Delta n_z}\right| K = 0$ and $\psi_1 + \psi_2 = -180°$ define an instability in terms of the amplitudes, $\left|\frac{\Delta n_z}{\delta}\right|$ and $\left|\frac{\delta}{\Delta n_z}\right|$, and the corresponding phase angles, ψ_1 and ψ_2, where K is a gain factor associated with the normalized $\left|\frac{\delta}{\Delta n_z}\right|$. Thus, at a particular frequency where the total phase angle just equals -180° and the factor $\left|\frac{\Delta n_z}{\delta}\right| \left|\frac{\delta}{\Delta n_z}\right| K$ has a magnitude greater than -1, the system is unstable at the gain selected. Thus, the crux of the design problem is to maintain high control authority throughout the frequency range of the structural modes to be controlled, but to attenuate it markedly at the higher frequencies. At the same time, the phase-angle magnitude must be minimized throughout the frequency range so that a combined phase angle of -180° occurs at as high a frequency as possible.

Details of Design

ILAF mechanization. – The implementation of the ILAF technique on the XB-70 airplane required the use of the elevons as the mode control force generators, with the primary motion sensing accelerometers located near the hinge line of the second elevon (one of either wing panel). The signal from these accelerometers contained both structural and rigid-body motion components. To obtain as pure a structural motion signal as possible and eliminate most of the whole-vehicle motion component, a secondary acceleration signal is required(1, 3). This secondary signal can be obtained from an accelerometer located near the nominal center of gravity of the airplane, as illustrated in figure 4. This figure also shows the original pitch augmentation sensors to complete the picture of the sensing elements of the integrated Flight Augmentation Control System (FACS) and ILAF structural mode control system.

One of the design ground rules was that the ILAF system would be integrated into the existing XB-70 pitch FACS with a minimum of change. How this was done is illustrated in the block diagram of figure 5. In the original FACS electronic package, the only change, other than the actual ILAF electronics tie-in, was the installation of an electronic limiter (±7°) adjusted to prevent the system from making contact on the existing physical stops. The ILAF electronics tied in just ahead of the existing FACS gain, K_{h_p}, which is an automatic function of Mach number and altitude set by the Central Air Data System (CADS).

In the added-on ILAF electronics the signals from the primary accelerometers on either wing were summed and then halved. This eliminated any whole-vehicle roll motion and antisymmetric structural mode motion signals. The secondary, or midship, accelerometer signal was subtracted from this signal, and the net signal passed through the notch filter. From the notch filter, the signal went to the manual-adjust gain knob in the cockpit, and from there through the compensation. The compensation was designed to magnify the lower frequency mode signals through the lead network and then to attenuate them through the high-frequency lag network. The compensated signal was then fed into the FACS electronics, which drove the servo on the inboard elevon. The outboard elevon panels were actuated by motion from the inboard elevon actuator. This actuator arrangement was one of several sources of significant system lags.

Elevon natural frequency. – One of the important considerations in determining the system feedback elements was the natural frequency of the elevons; the previously mentioned filter was required to eliminate the elevon dynamics from the feedback signal. There was considerable concern that the natural frequency of the elevons would be changed by aerodynamic loading and the in-flight temperature effects on the hydraulic fluid and thus move off the designed notch frequency. Ground tests and analyses were made to establish the magnitude of this effect, since there were no previous flight-test data available to provide any clues.

Ground vibration testing of the airplane in addition to control-system frequency response data revealed that the resonant frequency of the elevon was 20 hertz. The temperature effect on the bulk modulus of the hydraulic fluid was found by calculations to reduce this resonant frequency, whereas the aerodynamic loading was found by calculations to increase it. The net change in the resonant frequency of the elevon was an average increase of 0.6 hertz, which was judged to be small enough to be accommodated by the proposed notch filter designed around the 20-hertz point.

Feedback-element characteristics. – The first compensation network designed for the ILAF system did not provide the proper shaping for satisfactory operation. This was not discovered until flight tests were undertaken. During the first flight, the stability of the ILAF system was investigated by turning up the system gain in small increments and watching the telemetered response for undesirable characteristics. During this operation, a problem of high-frequency feedback was encountered at 26 hertz. The type of response experienced during this feedback is shown in figure 6, in which the power spectral density, $\Phi_{n_{z_A}}$, of one ILAF accelerometer signal is presented for two levels of ILAF gain, K. The solid curve shows the response before the system was turned on (zero gain), and the dashed curve shows the response with the system operating at a gain setting of 20 percent. Above a frequency of 20 hertz, the basic airplane showed two resonances of small magnitude. With the system on, an additional response with a relatively large amplitude, similar to a limit-cycle oscillation, was encountered.

At first, internal accelerometer dynamics and the sensor mountings were suspected, but detailed ground testing revealed that neither was at fault. The trouble was finally traced to a loop in which general aerodynamic excitation of the local wing structure was picked up by the accelerometer and fed through the compensation to activate the servo. This, in turn, produced actuator motion of sufficient magnitude to excite the local structure near the sensor. The limit-cycle oscillation resulted. No elevon-surface motion was evident in the test record of the elevon-position indicator.

One important lesson learned from this experience was that although no reasonable analytical model could have predicted this particular problem, more extensive ground and flight-test data obtained after the system sensors were installed would have been extremely helpful.

The limit-cycle problem dictated a redesign of the compensation network. The redesign provided a greatly reduced signal attenuation at frequencies above 5 hertz. A first attempt was made to design a new linear compensation which would maintain performance through the third-mode frequency (about 5 hertz) yet attenuate the amplitude at the higher frequencies. It was possible to design a filter that had the correct amplitude characteristics, but it could not maintain the required phase lead, and vice-versa. The resulting network in both instances was extremely complex. The final solution required sacrificing some of the desired lead characteristics; thus, some system effectiveness was lost through the third-mode frequency range. Figure 7 compares the characteristics of the original and the modified design which included the notch filter.

Figure 8 shows the calculated performance difference between the modified and the original system. Shown is a frequency response of pilot normal-load factor due to a unit deflection of a small aerodynamic shaker located at the vehicle nose. As expected, the first mode was affected slightly by the change in filter characteristics, whereas the combined second-third mode was adversely affected, as shown by the decrease in damping over that anticipated from the original ILAF design. Even though calculated system performance was degraded for subsonic speeds, it was deemed that performance was good enough to demonstrate the system concept in flight.

PART II - FLIGHT TESTS

By Eldon E. Kordes

The XB-70 program provided the opportunity to carry the study of mode suppression systems into an environment in which operation and performance could be evaluated under actual flight conditions.

The system hardware was installed on the aircraft during the first half of 1968 and was first operated in flight in August 1968. This flight test revealed the limit-cycle problem discussed in Part I. The modified filter was installed, and tests were started in October 1968. At present, not all the tests have been analyzed;

however, enough information has been obtained on the system operation and airplane response so that tentative evaluations and interesting results can be discussed.

Instrumentation

To effectively evaluate the performance of the ILAF mode damper system in flight, the special instrumentation shown in figure 9 was used. A gust boom was installed at the nose of the airplane, with low-inertial balsa-wood vanes to measure the fluctuating velocities associated with turbulence input. Sensors were installed at the base of the boom to measure pitch and roll attitudes, yaw rate, and normal and lateral accelerations. Data from these sensors are used to correct the measured turbulence velocities for airplane motion. Accelerometers to measure airplane normal response were installed at the pilot's station, on the canard, at the center of gravity, in the aft fuselage, on the wing-fold hinges, and near the tip of the left wing. Strain gages on the canard and on the wing hinges were used to measure bending moments. In addition, sensors were installed to measure system behavior and control-surface motions.

Shaker-Vane System

A shaker system was installed on the XB-70 to provide a known and controlled input for tests on the effectiveness of the ILAF system at desired flight conditions. A drawing of the system is shown in figure 10. The system consisted of two 2-square-foot trapezoidal planform surfaces symmetrically mounted at the nose of the airplane just forward of the pilot's station. The amplitude and frequency of oscillation of these vanes were controlled by a servo-hydraulic actuator. The system allowed for trim and both amplitude and frequency control by the co-pilot. The aerodynamic surfaces had amplitude capabilities up to ±12° over the frequency range of 1.4 to 8.0 hertz. Safety and automatic shutdown systems protected the aircraft and the system.

Structural Response

The shaker-vane system was used to excite the XB-70 airframe during flight. Some typical results for subsonic speed are shown in figure 11. The flight data were obtained from a frequency sweep for a constant vane amplitude of ±4° at a Mach number of 0.9 and an altitude of 25,000 feet, for a light weight condition. The circles are the data obtained from flight, and the dashed curve is the calculated airplane response for this flight condition. It should be noted that the flight weight for this test corresponds to approximately 30-percent fuel weight, whereas the calculated response is for a system design condition of 5-percent fuel weight. The calculated response was obtained from the modal solution discussed in Part I; design information on aerodynamics, structural stiffness, and mass distributions was used. For reference, the frequencies obtained from the ground vibration tests with zero-fuel condition and wings folded 25° (corresponding to flight position) are shown for the lowest four symmetric modes. Even though the ground-measured frequencies of the second and third vibration modes are widely separated, the theoretical analysis predicts that the second and third mode frequencies are forced together because of the aerodynamics at this flight condition. The calculated second-third mode response is shown on this plot as the large spike at approximately 4.8 hertz. In general, the calculated results showed less response in the first mode and a significantly greater response in the second-third mode than shown by the response measured in flight.

In order to assess the effect of a more representative description of the airplane dynamic model on the calculated response, the measured ground vibration modes were used to refine the analysis for this flight condition. The ground vibration results were first corrected for the landing-gear strut support conditions used in the ground vibration tests to obtain the airplane free-free modes. These corrected modes were used to calculate the generalized mass associated with each of the structural modes. The analysis made use of the quasi-steady aerodynamics associated with each mode that was calculated for the design mode shapes rather than values recalculated for the modes based on the ground vibration test data.

The results of the modified analysis for the Mach 0.9 light weight condition are shown in comparison with the flight-test results in figure 12. The circles show the flight-test results, and the dashed curve shows the results predicted from the modified ground vibration mode shapes and frequencies. The agreement between measured response and the predicted response is improved over that shown in figure 11 in both amplitude and frequencies for the first three modes, although the damping of the third mode is underestimated. This improvement may be somewhat surprising in light of the rather crude quasi-steady aerodynamics used in the analysis. These results point out the improvement that can be expected when more representative airplane characteristics are used.

ILAF System Performance

Information on the response of the basic airplane to shaker-vane input was used as the reference for evaluating the effectiveness of the ILAF system as a mode damper. In general, the effectiveness of the ILAF system was expected to be better at supersonic conditions than at subsonic conditions. At supersonic speeds the aerodynamic forces generated by control deflections are concentrated at the control surface; hence, the ILAF principle is more nearly satisfied.

Response to shaker-vane input. – Tests for evaluation of the ILAF system were similar to those for the definition of basic airplane response. The ILAF system was turned on and frequency sweeps of the shaker vane were made at the desired flight conditions. The effect of the ILAF system was determined by comparing the response of the airplane with and without the system operating.

Figure 13 shows the effect of ILAF system operation on accelerations at the pilot's station for Mach 0.9 flight with the airplane in the light weight condition. The circles show the response of the basic airplane; and the squares, the response with the ILAF system operating. At this flight condition, the response with the mode damper system on was greater for both the first and third mode than with the system off. In other words, the system was not performing as desired or as predicted. The exact reasons for the poor performance at these conditions are not known; however, major contributing factors are believed to be the effects of nonlinearities, system deadband, loss of lead in the modified filter, and phase and distribution of unsteady aerodynamic forces associated with control-surface deflections. Additional tests are required to define the factors affecting the ILAF system performance at these flight conditions.

In view of the expected better performance at supersonic speeds, the flight-test results obtained at a Mach number of 1.6 are of interest. Figure 14 shows the effect of the ILAF system operation on acceleration at the pilot's station for shaker-vane excitation, in a medium weight condition. The circles are the airplane response with the ILAF system off; the squares, the response measured with the ILAF system on. As can be seen, the system was effective in reducing the amplitude of the first mode; however, no improvement is noted for the higher frequency of the second-third mode. The measured effectiveness of the ILAF system in reducing the response of the first mode was as predicted by analysis. The poor performance in reducing the response of the third mode is not unexpected, because of the increased phase lag in the total system caused by the modified filter (see fig. 7) installed to eliminate the limit-cycle problem. The filter removed the necessary lead and reduced the system effectiveness at the higher frequencies. In addition to the phase-lag problem, other factors such as deadband and nonlinear amplitude effects also tended to degrade system performance.

The response in the first and third modes with and without the ILAF system, measured along the fuselage, is shown in figure 15. The upper curves for the first mode show the acceleration measured at four points along the fuselage, and the lower curves show the results for the third mode. In the first mode, the ILAF system reduced the amplitude proportionately along the entire fuselage. In the third mode, the results showed a slight degrading of the response throughout the airplane with the ILAF system operating.

The demand of the ILAF operation on the airplane mechanical system is shown in figure 16 in which the effects of the ILAF operation on pitch servo motion are presented for the frequency sweep at a Mach 1.6 flight condition. The circles show the response of the servo with the ILAF off, and the squares show the servo motion with the ILAF operating. As can be seen, the ILAF system demanded considerably more servo motion in the first and third modes, with most of the motion called for in the third mode. The system was sensing the third-mode response and driving the servo at this frequency, even though the amplitude of the third mode was not effectively reduced. For these tests, the shaker vane was operating at ±4° amplitude. This information shows the demand of the ILAF system on the servo; however, the actual damping associated with the system operation is dependent on the elevon motion produced by the servo.

The elevon motion during ILAF system operation is shown in figure 17 for the medium weight condition at Mach 1.6 Data are shown for both the inboard and the outboard elevons, since the outboard elevons on each side of the aircraft follow the motion of the inboard elevon and are not driven directly by the servo. The elevon motion was greater at the third-mode frequency than at the first-mode frequency, even though the third airplane mode was not damped effectively. The loss of effectiveness at the higher frequency was probably due to improper phasing in the compensation circuit between the measured motion and applied force. The elevon amplitudes measured during these tests were quite small (on the order of ±1/2°), so that the system deadband and the phase lag between inboard and outboard surfaces would be expected to have large effects. Tests in which the demands by the ILAF system result in larger elevon amplitudes would be expected to minimize these effects and provide improved overall performance. The total effect of the various conditions is being investigated.

Response to turbulence. – The type of test data shown for shaker-vane operation gives some insight into the effectiveness of the system's operation. However, the primary purpose of the system was to reduce the motion resulting from turbulence encounters. Unfortunately, only a small amount of flight-test data was obtained with the ILAF system operating in turbulence. Figure 18 shows the results of a turbulence encounter in which the system was operated for approximately 15 seconds. The circles show the airplane response at the pilot's station with the ILAF system off. The squares are the response with the ILAF system on. Since the turbulence intensity, as measured from the gust vane on the boom, shows that there was a difference in intensity level during these two encounters, the results presented were normalized, for comparison, to a gust input of 1 foot per second root mean square. In general, these results show that the system was effective in reducing response at this flight condition for frequencies up to 5 hertz. Interestingly, during this encounter the pilots reported a noticeable improvement in the airplane vibration response with the ILAF system on.

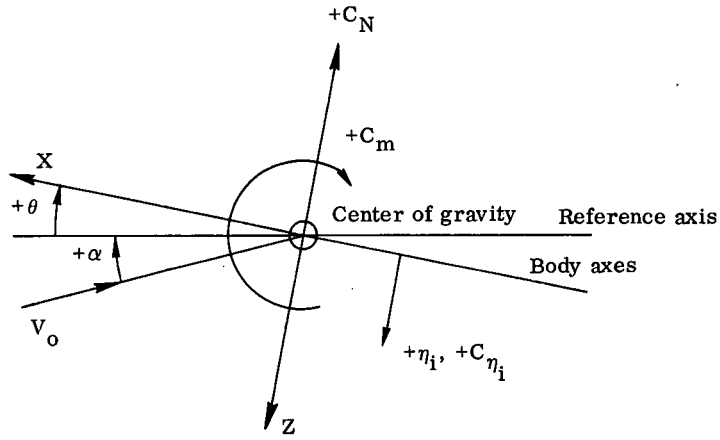
CONCLUDING REMARKS

Significant information was learned from this program, even though the mode damper system did not perform as well as expected for the limited flight condition evaluated. The system installed on the XB-70 airplane was an exploratory device and was not developed as an optimum system. The hardware and technology are probably available to design an operational system for a vehicle like the XB-70 airplane, but the design requires careful attention to the aircraft's vibration response to assure the desired performance without vehicle-systems interaction or instabilities. Even with the best design information, flight tests are required to check and evaluate the systems, since many of the operational problems, such as limit cycles and other nonlinear effects, cannot be predicted.

For the XB-70 flight-test program, an aerodynamic shaker system proved to be a valuable tool for evaluating the system behavior and effectiveness, since turbulence encounters cannot be relied on to provide the inputs for the desired flight-test conditions. Although this exploratory program showed that a mode damper is operationally feasible, additional analytical and flight studies are required to provide a better understanding of the many parameters that control system performance and effectiveness.

SYMBOLS

All aerodynamic, mass, and structural data are in body-axes systems.



C_m pitching-moment coefficient, $\frac{\text{Pitching moment}}{q\bar{c}_w S_w}$

C_{m_q} change in pitching-moment coefficient due to pitching, $\frac{\partial C_m}{\partial \frac{q\bar{c}_w}{2V_o}}$

$C_{m_{w_g}}$ change in pitching-moment coefficient due to gust velocity, $\frac{\partial C_m}{\partial w_g}$

C_{m_α} static longitudinal stability, $\frac{\partial C_m}{\partial \alpha}$

$C_{m_{\dot{\alpha}}}$ change in pitching-moment coefficient due to rate of change of angle of attack, $\frac{\partial C_m}{\partial \frac{\dot{\alpha}\bar{c}_w}{2V_o}}$

C_{m_δ} change in pitching-moment coefficient due to control-surface deflection, $\frac{\partial C_m}{\partial \delta}$

$C_{m_{\eta_i}}$ change in pitching-moment coefficient due to i th mode deflection, $\frac{\partial C_m}{\partial \eta_i}$

$C_{m_{\dot{\eta}_i}}$ change in pitching-moment coefficient due to rate of change of i th mode deflection, $\frac{\partial C_m}{\partial \frac{\dot{\eta}_i}{V_o}}$

C_N normal-force coefficient, $\frac{N}{S_w q_o}$

C_{N_q} change in normal-force coefficient due to pitching, $\frac{\partial C_N}{\partial \frac{q\bar{c}_w}{2V_o}}$

$C_{N_{w_g}}$ change in normal-force coefficient due to gust velocity, $\frac{\partial C_N}{\partial w_g}$

C_{N_α} normal-force curve slope, $\frac{\partial C_N}{\partial \alpha}$

$C_{N_{\dot{\alpha}}}$ change in normal-force coefficient due to rate of change of angle of attack, $\frac{\partial C_N}{\partial \frac{\dot{\alpha}\bar{c}_w}{2V_o}}$

C_{N_δ} change in normal-force coefficient due to control-surface deflection, $\frac{\partial C_N}{\partial \delta}$

$C_{N_{\eta_i}}$ change in normal-force coefficient due to i th mode deflection, $\frac{\partial C_N}{\partial \eta_i}$

$C_{N_{\dot{\eta}_i}}$ change in normal-force coefficient due to rate of change of i th mode deflection, $\frac{\partial C_N}{\partial \frac{\dot{\eta}_i}{V_o}}$

C_{η_i} generalized i th mode force coefficient, $\frac{Q_i}{S_w q_o}$

$C_{\eta_{i_{(\,)}}} = \frac{\partial C_{\eta_i}}{\partial (\,)}$ generalized force coefficient due to variable, $(\,) = \alpha, \left(\frac{\dot{\alpha}\bar{c}_w}{2V_o}\right), \left(\frac{q\bar{c}_v}{2V_o}\right), \delta_{sv}, \delta_a, \delta_e, w_g$

$C_{\eta_{i_{\eta_j}}}$ change in generalized force coefficient due to j th mode deflection, $\frac{\partial C_{\eta_i}}{\partial \eta_j}$

$C_{\eta_{i_{\dot{\eta}_j}}}$ change in generalized force coefficient due to rate of change of j th mode deflection, $\frac{\partial C_{\eta_i}}{\partial \frac{\dot{\eta}_i}{V_o}}$

$\bar{c}_w$ wing mean aerodynamic chord, meters
F force, newtons
f frequency, hertz
g acceleration due to gravity, 9.8 meters/second^2
g_s structural damping coefficient
h_p pressure altitude, meters
I_H moment of inertia of control surface about hinge line, kilograms
I_Y pitching moment of inertia (body Y-axis), kilogram-meter^2
i, j integers
K control-system gain, degree/degree/second
l distance from control-surface hinge line to surface center of gravity, meters
l_X distance from vehicle center of gravity along the body X-axis, meters
$\bar{l}$ distance from control-surface hinge line to vehicle center of gravity, meters
M Mach number
M_i generalized mass of i th mode, $\iint \varphi_i^2(x,y)\,\Delta\bar{m}(x,y)\,dxdy$, kilograms
m control-surface mass, kilograms
$\bar{m}$ airplane total mass, kilograms
N aerodynamic normal force referred to body Z-axis, newtons
n_z normal-load factor, g
Q_i generalized force in i th mode, $\iint -N(x,y)\,\varphi_i(x,y)\,dxdy$
q pitching velocity, degrees/second
q_o dynamic pressure, newtons/meter^2
S_w wing area, meters^2
V_o resultant velocity of center of gravity, meters/second
w_g vertical component of gust velocity, meters/second
X, Z body axes
α angle of attack, degrees
$\Delta\bar{m}$ incremental airplane mass
Δn_z blended ILAF accelerometer signal
$\frac{\Delta P}{q_o}$ pressure coefficient
δ elevon deflection, degrees
δ_s servo displacement, degrees
δ_{sv} shaker-vane deflection, degrees
δ_t wing-tip deflection, degrees
η_i, η_j generalized deflection for i th and j th modes, respectively, meters
θ angle of pitch, degrees
Φ_{n_z} power spectral density of acceleration, g^2/hertz
φ_i normalized mode shape of i th mode
ψ phase angle, degrees
ω_i natural frequency of i th mode, radians/second

Subscripts:
A accelerometer
a inboard elevon panel

e	outboard elevon panels
h_p	altitude
i,j	i th or j th structural mode
n_z	normal acceleration
p	pilot's station
sv	shaker vane
$\dot{\theta}$	pitch rate

Superscripts:

A	location at accelerometer
a	location at inboard elevon
e	location at outboard elevon
F	location at force

A dot over a quantity denotes the derivative with respect to time. A prime denotes differentiation with respect to the independent variable. Vertical bars represent absolute values.

ABBREVIATIONS

BP	buttock plane
CADS	Central Air Data System
FACS	Flight Augmentation Control System
FS	fuselage station
ILAF	Identically Located Accelerometer and Force

REFERENCES

1. Mori, Alva S.; and Wykes, John H.: Control System Aspects of an Analytical Investigation Into Controlling the Structural Modes of Flexible Aircraft. Proceedings of SAE-NASA Aerospace Vehicle Flight Control Conference, Los Angeles, Calif., July 13-15, 1965, pp. 129-140.

2. Wykes, John H.; and Knight, Ronald J.: Progress Report on a Gust Alleviation and Structural Dynamic Stability Augmentation System (GASDSAS) Design Study. Paper No. 66-999, AIAA, 1966.

3. Wykes, John H.: Structural Dynamic Stability Augmentation and Gust Alleviation of Flexible Aircraft. Paper No. 68-1067, AIAA, 1968.

4. Edinger, Lester D.: Design of Elastic Mode Suppression Systems for Ride Quality Improvement and Application to an SST. Paper No. 67-571, AIAA, 1967.

5. Burris, P. M.; Dempster, J. B.; and Johannes, R. P.: Flight Testing Structural Performance of the LAMS Flight Control System. Paper No. 68-244, AIAA, 1968.

6. Dempster, John B.; and Arnold, James I.: Flight Test Evaluation of an Advanced Stability Augmentation System for the B-52 Aircraft. Paper No. 68-1068, AIAA, 1968.

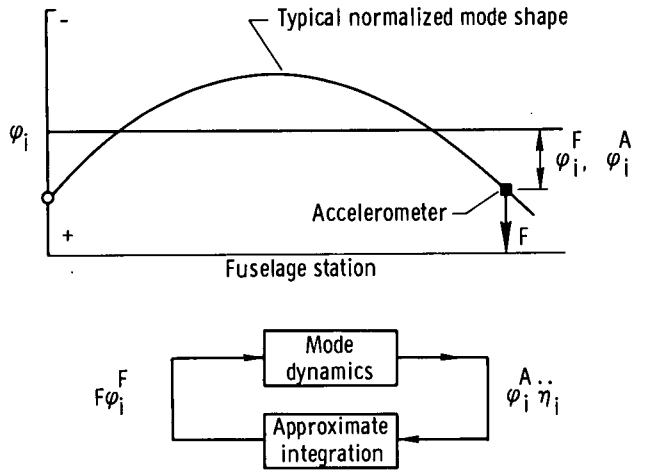


Figure 1.—Simplified explanation of ILAF.

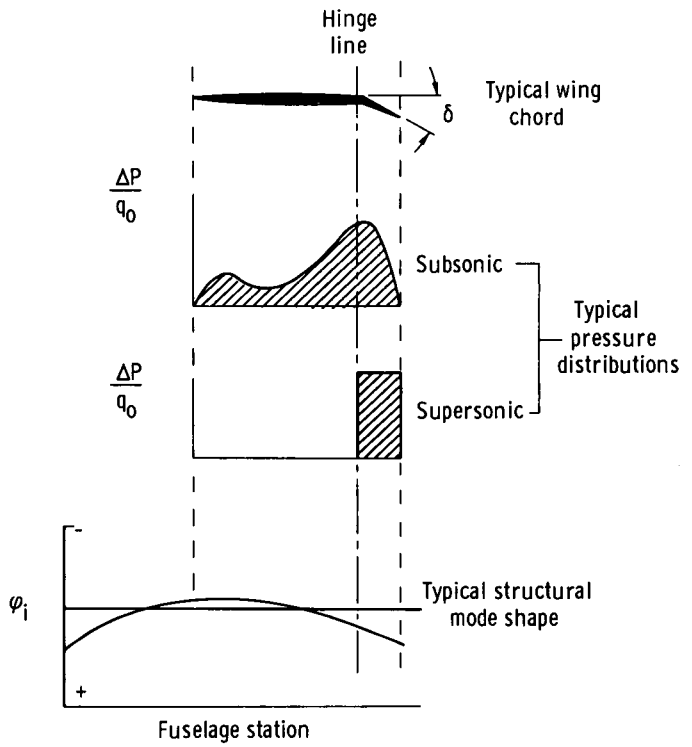
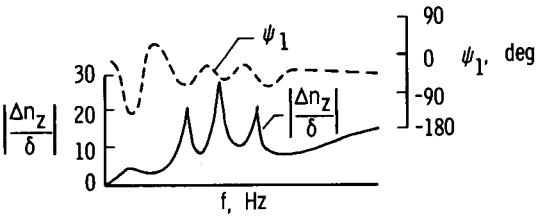
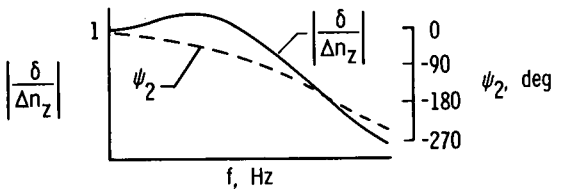


Figure 2.—Realistic airloads induced by trailing-edge control surfaces.



(a) Sensor signal due to control deflection.



(b) Normalized control deflection due to sensor signal.

Figure 3.–Key features of a typical design problem.

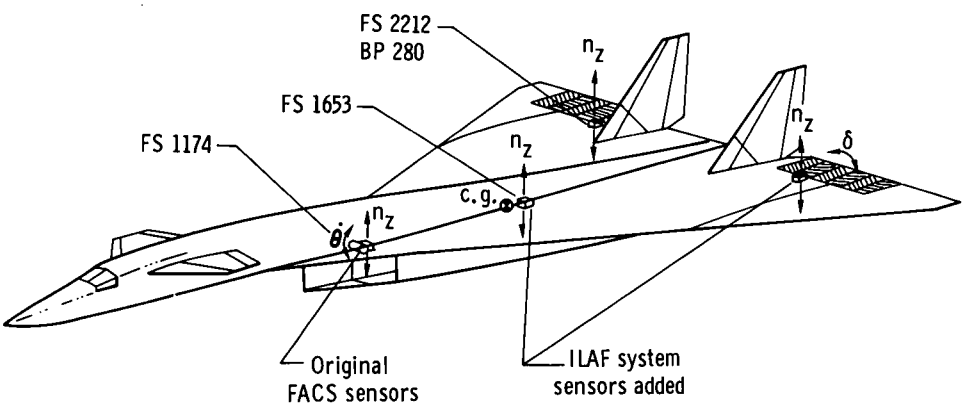


Figure 4.–Location of XB-70 ILAF system sensor and control surfaces for longitudinal-symmetric mode control.

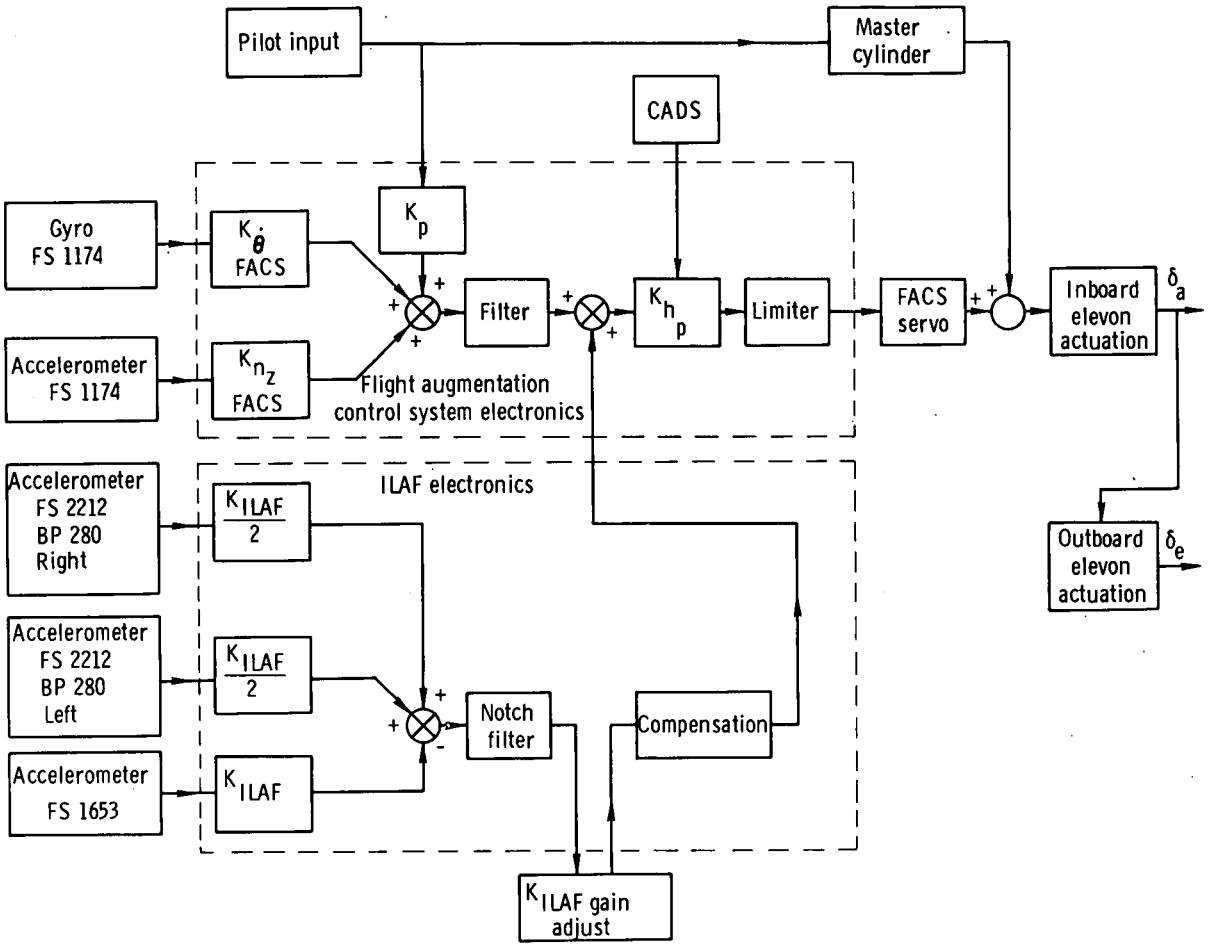


Figure 5.–XB-70 integrated longitudinal symmetric FACS and ILAF system.

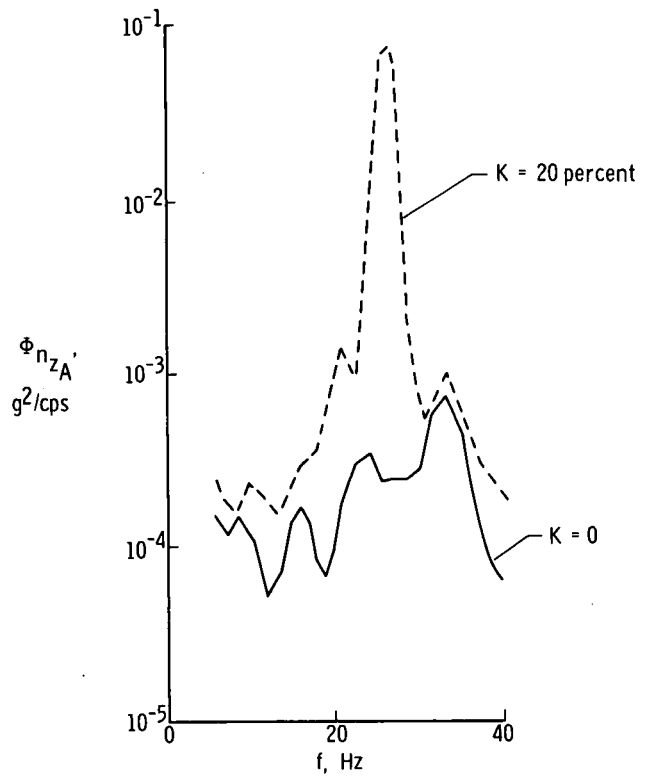


Figure 6.–Illustration of original ILAF system design instability. Right-hand ILAF accelerometer.

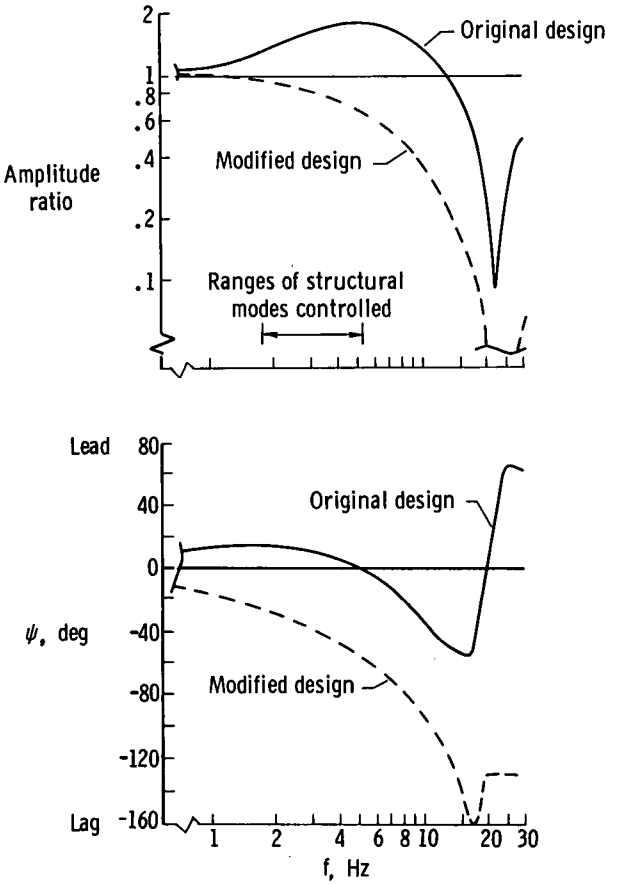


Figure 7.–ILAF system compensation characteristics.

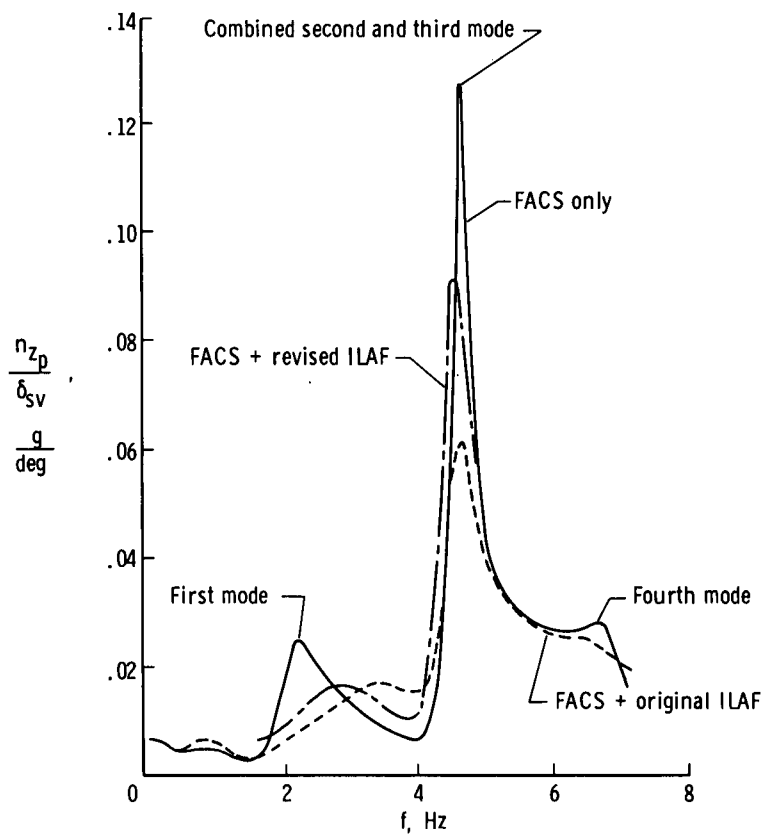


Figure 8.–Calculated typical ILAF structural mode control-system performance. Light weight; $M = 0.9$; $h_p = 25{,}000$ ft; $\delta_t = 25^o$.

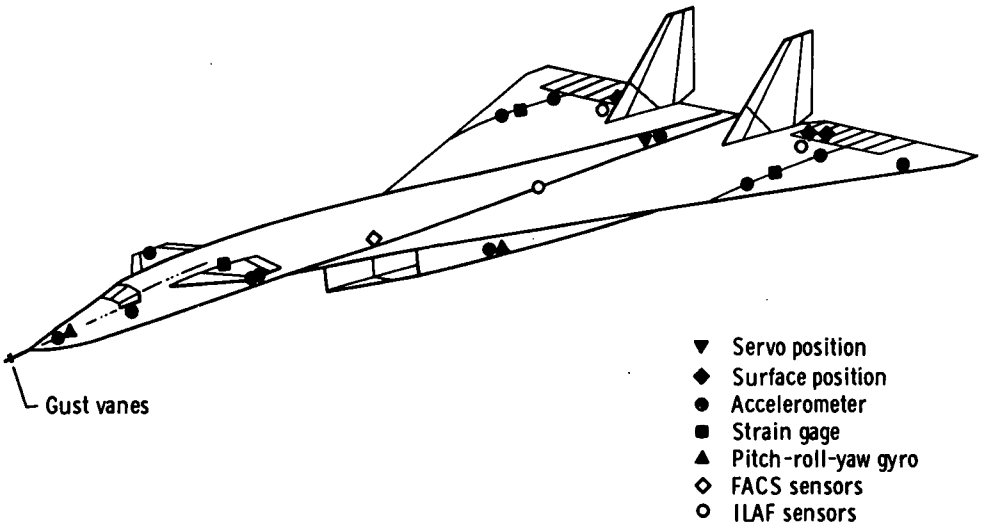


Figure 9.—Instrumentation for measuring atmospheric turbulence and airplane response.

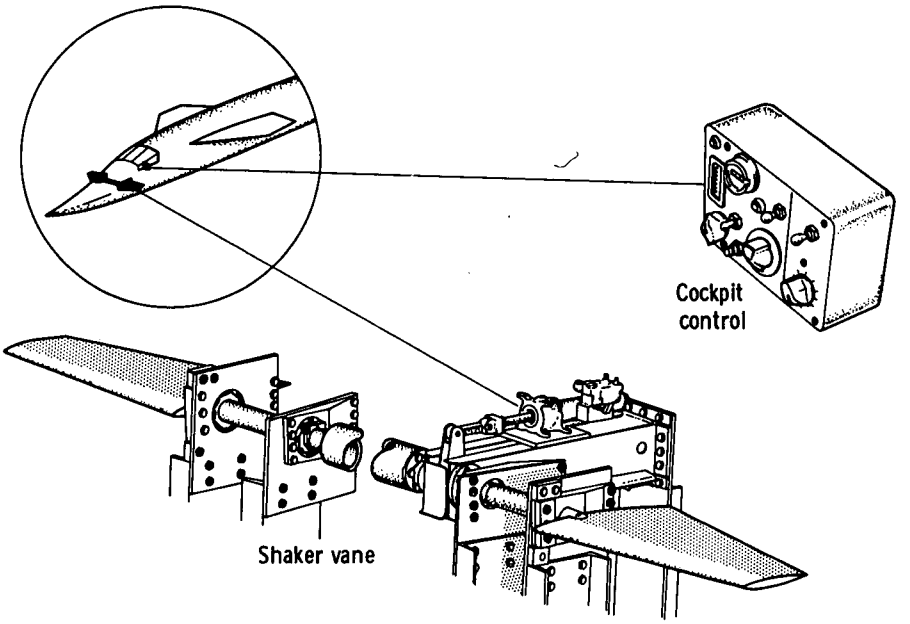


Figure 10.—Shaker-vane system.

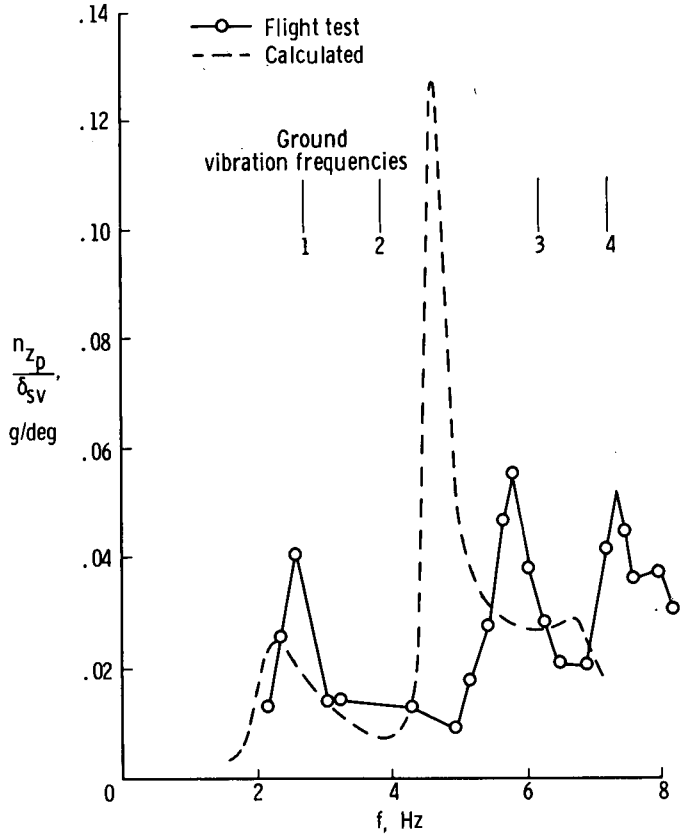


Figure 11.—Comparison of calculated and flight-test acceleration response at the pilot's station due to shaker-vane excitation. Light weight; $M = 0.9$; $h_p = 25{,}000$ ft; FACS on; $\delta_t = 25^o$.

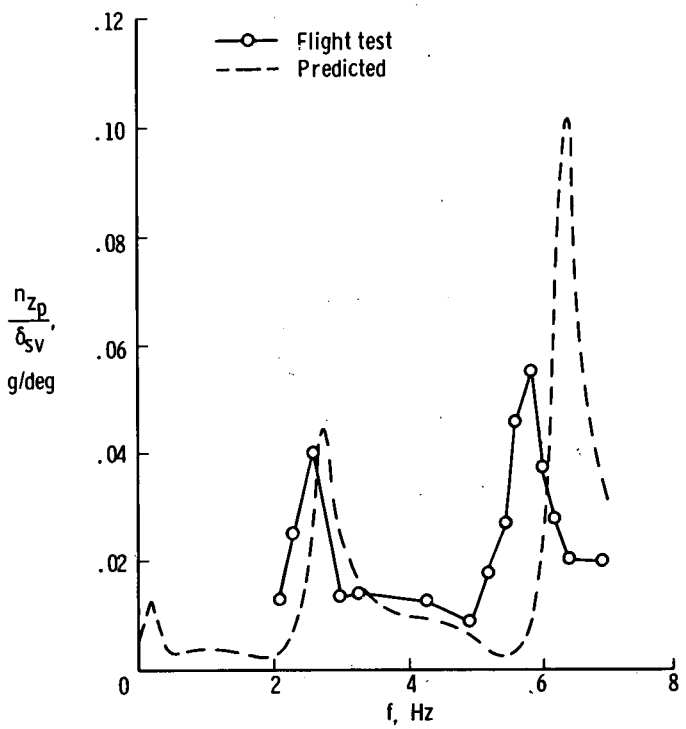


Figure 12.—Comparison of flight-test acceleration response at pilot's station with response predicted on the basis of measured airplane modes. Shaker-vane excitation; light weight; $M = 0.9$; $h_p = 25{,}000$ ft; FACS on; $\delta_t = 25^o$.

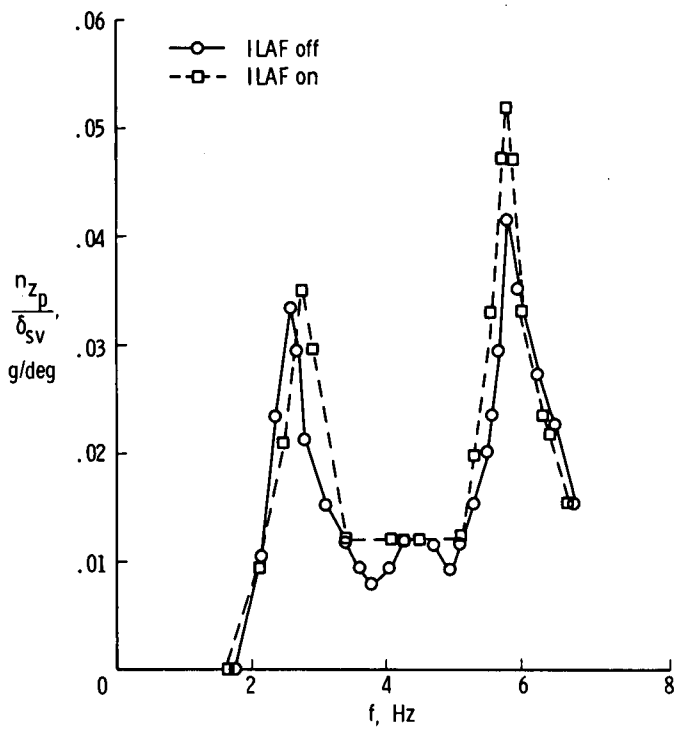


Figure 13.–Effect of ILAF system operation on accelerations measured at the pilot's station for shaker-vane excitation. Light weight; M = 0.9; h_p = 25,000 ft; FACS on; $\delta_t = 25^o$.

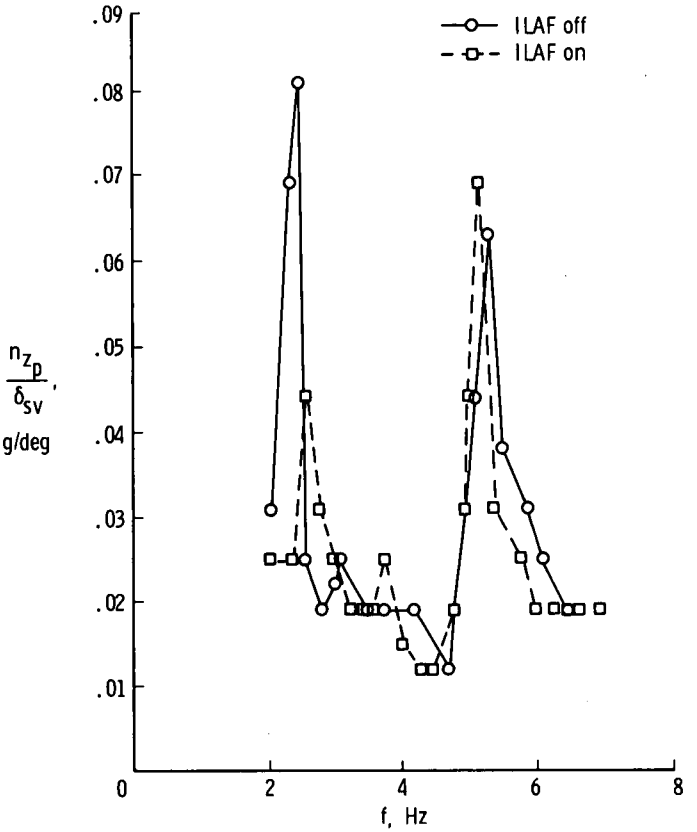
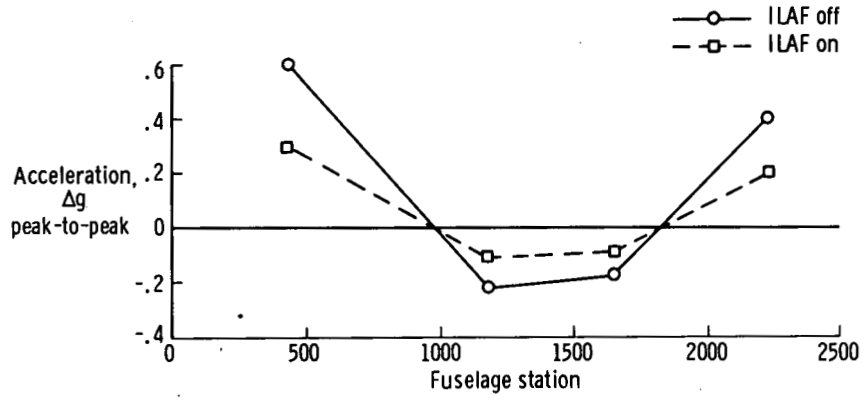
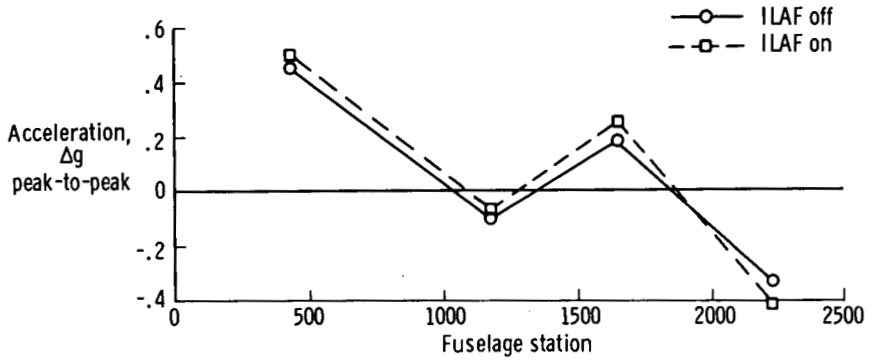


Figure 14.–Effect of ILAF system operation on accelerations measured at the pilot's station for shaker-vane excitation. Light weight; M = 1.6; h_p = 39,000 ft; FACS on; $\delta_t = 65^o$.



(a) First mode.



(b) Third mode.

Figure 15.—Effect of ILAF system operation on accelerations measured along the fuselage for ±4° of shaker-vane excitation. Medium weight; M = 1.6; h_p = 39,000 ft; FACS on; $\delta_t = 65^o$.

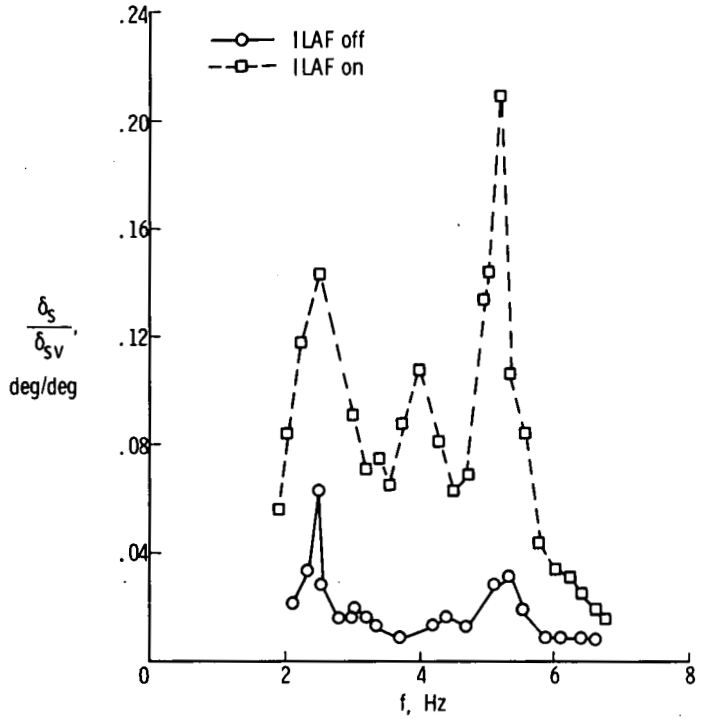


Figure 16.—Effect of ILAF system operation on measured pitch servo motion for shaker-vane excitation. Medium weight; M = 1.6; h_p = 39,000 ft; FACS on; $\delta_t = 65^o$.

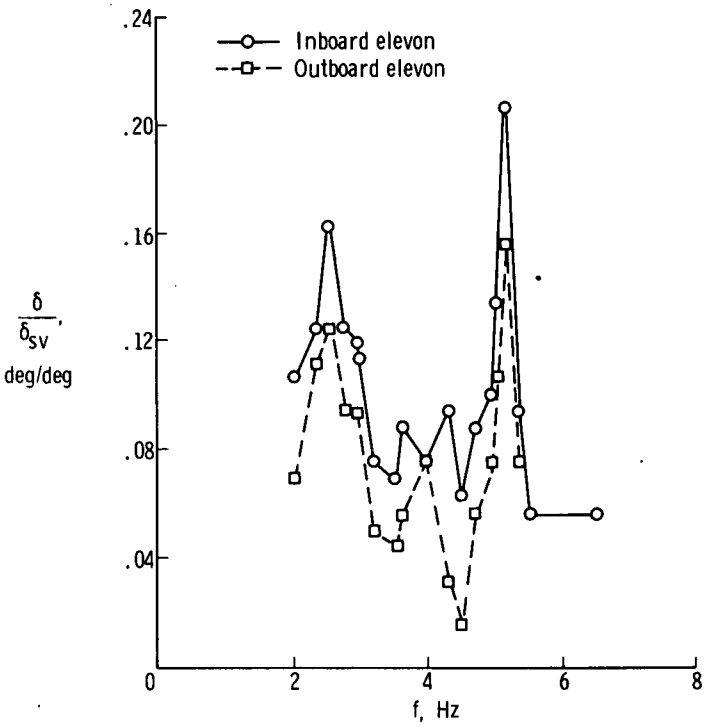


Figure 17.—Measured elevon motion during ILAF system operation for shaker-vane excitation. Medium weight; M = 1.6; h_p = 39,000 ft; FACS on; ILAF on; $\delta_t = 65^o$.

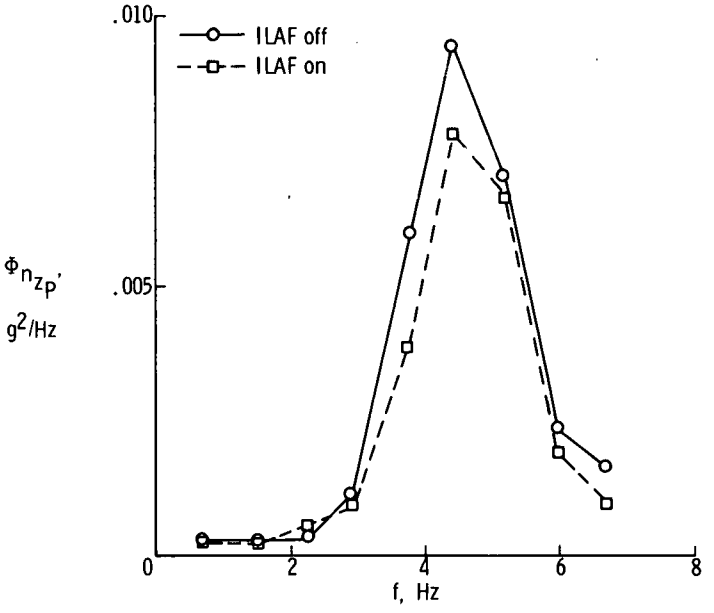


Figure 18.—Effect of ILAF system operation on measured acceleration response to pilot's station during light turbulence. M = 1.19; h_p = 39,000 ft; FACS on; $\delta_t = 25^o$; normalized to 1 ft/sec root mean square gust input.

GUST ALLEVIATION TECHNIQUE ON A LARGE EXPERIMENTAL AIRPLANE

J. A. McKILLOP

ENGINEERING RESEARCH ASSOCIATES

TORONTO CANADA

SUMMARY

The CAMCO V-Liner, or Helevision as it was originally known is a very long special purpose airplane. Because of its length, light weight and flexibility, it can be expected to be sensitive to gusts. To alleviate this gust sensitivity, the wings have been given complete freedom in pitch.

Such an unusual design feature naturally creates problems of dynamic stability. The examination of these problems as well as the gust alleviation effects are the subjects of this paper.

There is little novel theoretical development in this paper. Rather, it is a narrative, reporting the sequence of studies which have been done for this airplane and which have yet to be done. It is presented for the general interest of the panel, even if the conclusions have no great general application.

INTRODUCTION

The CAMCO V-Liner certainly merits the description of a most unusual airplane. If we take overall length as a representative measure of size, it is much the largest airplane ever built--half again the size of the USAF C-5A Galaxie transport.

The other performance/configuration characteristics of the V-Liner are equally unusual, although perhaps not so dramatic. The gross weight at takeoff is under 10,000 lb. The design diving speed if it is reasonable to use such a term, is well under 100 MPH.

The mission for which the airplane has been designed is one of public service information presentation, a mission which has earned the machine the nickname of the "flying billboard." This type of mission has been flown in the past by lighter-than-air machines such as dirigibles or more recently the Goodyear blimp. Similar missions have also been flown by banner towing airplanes or sky writers. But the aircraft used were not primarily designed for this mission, they have been adapted. The distinguishing feature of the V-Liner series is that it has been designed from the outset to perform the airborne information display mission.

The requirements of this mission are these:

1) The information display capacity must have a certain level. In the case of the V-Liner, this was established to be a minimum display of eighteen characters.

2) The display must have a certain level of visibility. For the V-Liner, this was established to be two miles in daylight, and four miles at night. Tests have determined that, aside from illumination requirements, perception or legibility requires that each character have a size of eighteen by twenty feet.

3) The display vehicle must operate at an altitude and speed which permits the display to be most effective. In lay terms, this means that the airplane operates "low and slow." In addition, the mission must be of relatively long duration.

The flight vehicle which has been developed to meet these mission requirements is shown in Figure 1, with detailed specifications given in the table below.

CAMCO V - LINER

DUAL VIDEO SIGN CARRIER

2 PRATT AND WHITNEY PT-6A-20 ENGINES

Dimensions			Weights		Performance	
Length	378	Ft.	Normal Gross	9,300 Lb.	Minimum Speed	40 MPH
Span	69.5	Ft.	Empty	6,670 Lb.	Cruising (Mission Speed)	52 MPH
Wing Area	1,390	Sq.Ft.	Useful Load	2,630 Lb.	Cruising (Ferry Speed)	95 MPH
Wing Loading	6.7	$Lb/ft.^2$	Crew	340 Lb.	Endurance	4 Hrs.
Power Loading	8.4	Lb/hp.	Fuel and Oil	1,160 Lb.	Take-Off Distance	
			Payload	1,130 Lb.	Land	225 Ft.
					Water	330 Ft.
					Ceiling (1 Eng. Out)	12,500 Ft.

We see that the airplane is an extreme form of tandem wing configuration. The fuselage consists of the display section of eighteen bays. Each bay is an equilateral triangle section, twenty feet on a side. Pilots are carried in both the forward and aft hull sections, but the power plants are carried on the forward body only. The airplane is equipped with amphibious floats located at the wing tips so it is capable of operation from either land or water.

The fuselage, or sign carrying structure consists of very light tubular members which are cross braced by pretensioned steel cables. To reduce the drag, the truss members carry swivelling fairings. The display mechanism consists of an array of lamps in lengthwise fairings covering the lower sides of each bay. Messages can be pre-recorded, inserted by the crew, or relayed through a data link system from the ground.

Because of the slow forward speed, the airplane operates at a relatively high lift coefficient in spite of the low wing loading. To avoid stalls due to gusts, a wing capable of achieving a high maximum lift coefficient and a gentle stall is required. With the high parasite drag of the fuselage, the drag of the wing is relatively unimportant. Consequently, the wing section chosen is an eighteen percent thick symmetrical section. To increase its lift effectiveness, the wing is fitted with a fixed leading edge slot.

An intuitive look at the potential flight dynamic problems of this airplane leads us to the conclusion that response to gusts will be one of the principal design considerations. The reaction of the airframe to encounter of a single gust will likely define the structural loads, and the response to excitation from continuous turbulence will probably define the fatigue life, both of the structure and of the crew.

Looking first at the problems of the crew, we must ensure that they will be able to perform their duties properly over an extended flight duration. Tests of the physiological reactions of flight crews have yielded the curves shown in Figure 2. These show that, if we are contemplating flights of over two hours duration, we must limit the incremental accelerations experienced by the pilots to a very low level indeed--of the order of one tenth G.

The airplane has a number of features which are likely to make it sensitive to turbulence. Principal among these are the low wing loading and the flexibility associated with the very long structure. But in addition, the environment is relatively hostile from the turbulence point of view, as we can see from Figure 3.

The turbulence intensity in the low level (1 - 3000 feet) regime is perhaps not large, but we also see that the probability of encountering turbulence of such intensity is virtually unity. So we have an airplane which is likely to be gust-sensitive, must operate all the time in a mildly turbulent environment, yet whose response must be closely controlled in order to permit the flight crew to operate effectively.

These crew reaction problems are further complicated by consideration of the frequency sensitivity of the human pilot. In Figure 4, we see typical curves illustrating subjective response to vibration at varying frequency. These curves show the much discussed heightened awareness of humans in the frequency range near five cycles per second. The exact mechanism of this sensitivity has been argued, being variously ascribed to resonance of the heart in the chest cavity, of the eyeballs in their sockets or of the head on the neck. Whatever these arguments, however, it is agreed that humans are more sensitive to vibration in the five cps. region and we must attempt to suppress modes in this range if we are to have a successful long endurance airplane.

Over the years, there have been many attempts to devise gust alleviation systems for aircraft. Broadly speaking, these fall into two categories.

The first is called active. This type of system uses some sort of feedback control to activate the aircraft's control surfaces. Stability augmentation and artificial damping systems have been in use for some time, but these have usually been incorporated to improve handling characteristics. They reduce pilot fatigue because they make the airplane easier to fly, not because they are particularly effective in reducing gust response.

More recently, interest has become centered on systems which employ more sophisticated sensor arrays and operate over a frequency range which allows artificial damping of the structural modes of the airplane. In this session, we have learned of the latest developments along this approach, in particular the modal suppression system designed for the B-70 which has been described in the previous paper.

The alternative approach to the gust alleviation problem is, naturally enough, called passive. In this category no sensory devices are used; rather an attempt is made to reduce the gust sensitivity by altering the aircraft. To some extent, this can be done by basic design using a high wing loading or a wing planform which has a low lift curve slope. But this approach is usually doomed to failure because it conflicts with the overriding requirements of performance.

Other passive techniques either involve altering the geometry of the airplane in flight, or introducing some flexibility which tends to absorb the gust impact. In the former class, there have been various suggestions for folding wings, telescoping wings, and wings of variable sweeps. The only practical example of this approach is the variable sweep wing fitted to the F-111 and other experimental machines, but this has been done for reasons of improving overall performance as much as for reduction of gust sensitivity.

In the latter class, there have been many proposals for designs which release a portion of the load carrying surface of the wing from its rigid condition and permit it to float freely. The surfaces released can be flaps or ailerons, or a portion of the wing which is deliberately allowed a flexibility either about a spanwise or chordwise hinge axis. This is the technique which has been adopted in an extreme form for the V-Liner, although it has other advantages as we shall see.

The detailed planform of the wing is shown in Figure 5. The wing itself is free to pitch about its quarter chord axis through a thirty degree angular range. Pitch control is provided by servo tabs carried on booms. Each wing is completely independent; pitch control being effected by collective operation of the tab surface, with roll control provided by differential activation.

The principle of operation is to trim each wing to fly at an appropriate lift coefficient. When a gust is encountered, the wing can pivot to maintain its lift coefficient constant, in theory eliminating the effect of the gust. But before we look at the response of the airplane to turbulence, it is in order to study the dynamic stability characteristics to make sure it can be operated satisfactorily in smooth air.

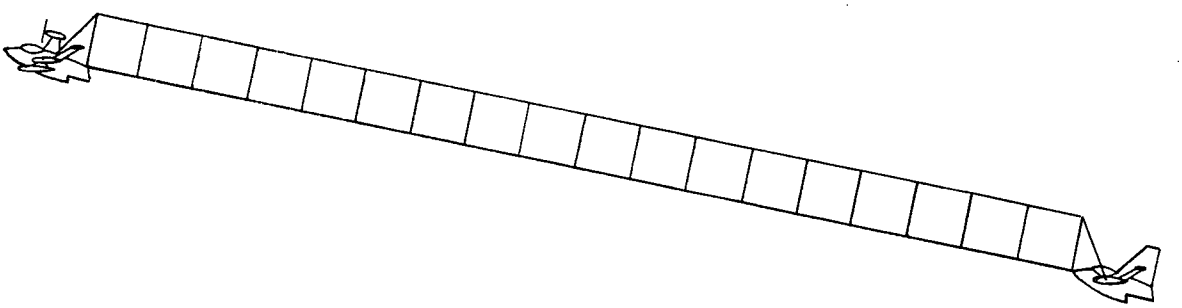
STABILITY ANALYSIS

The stability analyses were begun with a very simplified model. This assumed that the masses of the forward and after bodies were identical, the wings were identical, and the fuselage girder was rigid. Four degrees of freedom were included: vertical translation and pitch of the aircraft, and independent pitch of the two pairs of wings. Variation of forward speed was not included as a variable, so the analysis did not predict the phugoid mode.

The wings were assumed to be statically balanced about their quarter chord pivot axes by the tip floats. The aerodynamic forces on the fuselage girder were neglected.

The solution to this simplified analysis yields two pairs of zero roots corresponding to neutrally stable modes, and two pairs of complex roots representing damped oscillatory modes.

One of the neutrally stable modes is vertical translation, so that the airplane will not return to its original altitude if disturbed, just as is the case with a conventional aircraft. The other neutral mode is a mode of airplane pitch with the wings pitched back in the streamwise direction. The airplane can fly at a constant angle of pitch as illustrated below. Of course, this is an artificial result because the X-force equation has been excluded. The power plant arrangement, plus the fuselage drag will give this mode a positive stability.



The damping of the two oscillatory modes is always positive unless the centre of gravity of a wing is some way aft of its aerodynamic centre, in which case a static divergence results. Unlike a conventional airplane, the stability is not affected by the location of the overall airplane centre of gravity. The two oscillatory roots are very close together and become identical if all the airplane mass is concentrated in the bodies. Then the two ends behave as if they were independent airplanes.

But, in fact the mass distribution is by no means uniform. Because the power plants are located in the forward body, its mass is substantially higher than that of the after body. Therefore, the simplified analysis was repeated with the mass distribution actually calculated for the airplane. The results of this analysis are shown in Figure 8.

We see that we have the two oscillatory roots predicted by the simplified study, but they are by no means identical. However, both are very heavily damped, to the point that the time to half amplitude is of the order of one twentieth of a second.

However encouraging these studies may be we know that the structure is far from rigid and we have only been exploring some of the basic mechanisms of the stability problem. It is necessary to include the influence of the bending degrees of freedom of the girder.

A flexibility analysis of the fuselage girder shows that it may be treated as if it were a simple beam with the properties shown in the Figure 6. It is assumed here, of course, that the crossbracing rods or wires are pre-tensioned so that they remain effective under compression loads. Since the actual longeron tubes are tapered, the effective area A_L is a harmonic mean area. An interesting feature is that the vertical and lateral shear and bending stiffnesses are identical.

The first four vertical bending modes of the airplane are shown in Figure 7. We see that the frequencies are all low and rather close together. One of the primary reasons for the closeness of the frequencies is that, while the girder structure is relatively efficient in bending, it is not so in shear. The effect of the shear flexibility appears even in the first mode, and is quite pronounced in the harmonics. If the shear flexibility is not included, the first three natural frequencies become 1.70, 5.35, and 11.29 cycles per second respectively, quite substantially different from those shown.

When the longitudinal analysis is expanded to include the first two vertical modes, we obtain the results shown in Figure 9. Here we see the same two oscillatory modes with slightly altered frequencies but the same very high damping. The fuselage bending modes are changed very little by forward speed. The dampings are quite low--nearly three cycles to half amplitude for the first mode and over seventeen for the second mode.

These results show that, whilst the airplane is stable, there is little damping in the body bending modes and if they are excited by turbulence, the crew may be in for an unpleasant ride indeed.

The results of a simplified antisymmetric analysis combining airplane roll, girder torsion and the two antisymmetric modes of the wing pairs are shown in Figure 10. We see here the same pair of heavily damped modes of the wings. The torsion mode is much more heavily damped than the vertical modes--of the order of one half cycle to half amplitude. Consequently the problem of a seasickness type of pilot reaction to the antisymmetric modes seems of a much lower order than the problems to be expected from the vertical responses.

GUST RESPONSE STUDY

In this report, we are principally concerned with what might be called "ride quality." This was brought out in the introductory section when we showed that we must limit the incremental acceleration experienced by the pilots to a very low level if they are to fly missions of extended duration without suffering degradation of performance. Therefore in this section, we will examine the longitudinal response to continuous turbulence.

The mathematical techniques used for this analysis have been widely discussed and need no repetition here. The mathematical model of the airplane used to calculate the gust response transfer functions is the same as that used in the stability analyses of the previous section. As in the stability work, both the cases of the airplane with a rigid girder, and the airplane with a flexible girder are considered. Also, as in the previous studies, the aerodynamic forces on the girder are neglected.

The mathematical model of the turbulence spectrum is the Von Karman form recommended by the USAF for the structural fatigue analyses of new aircraft designs. No spanwise distribution of the turbulence was considered. Because we are dealing here with an airplane which is always operating in a low level contour mission, the turbulence scale selected is 500 feet, and the RMS gust intensity to be 3 ft. per second.

The gust response analyses were made for a typical mission speed of 60 MPH. The results, showing the acceleration spectrum at the forward pilot's position are shown in Figure 11. These results are very different from typical response curves which have been obtained for conventional aircraft. In fact, they are almost too good to be true. The RMS acceleration of this response curve is only .0416 G. It is in order to look into the reasons for these favourable results.

When we look back at the stability analyses, we see that the damping of the natural modes is so high that these two modes are practically dead beat and are not likely to contribute to response at these two frequencies. The overall response consists primarily of the response of the vertical translation degree of freedom, a mode which is also shown in the stability analysis to have no damping at all.

When we look at the results for the flexible airplane, that is,when the two girder bending modes are included, the response over the frequency range from 0 to 0.2 cps. is indistinguishable from that in Figure 11. At higher frequencies we find the results shown in Figure 12. Once again, we find the response to be negligible, with no sign of peak responses at the natural frequencies of the structure. The RMS acceleration is actually lower than for the rigid case--only .039 G.

Once again, some searching is in order to discover the reasons for thesemost favourable results. First, as in the rigid case, the two low frequency modes are heavily damped and do not develop resonant responses. But the stability analyses showed the girder bending modes to be poorly damped and one might expect that there ought to be response peaks at these frequencies. But there are two ameliorating factors.

First, if we look at the mode shapes in Figure 8 we see that the pilot is not located at a high deflection point. Because the body masses, particularly that of the forward body, are so much higher than the mass of the girder, the pilot accelerations are not large, even though the response of the mode may be high. Perhaps the responses of these modes may play a greater role in the definition of structural loads throughout the girder than may have been previously suspected.

Second, we find that the low operating speed is a distinct advantage. The turbulence spectrum falls off quite rapidly at a wave number over about 10^{-3}. When the airplane operates at a low forward speed, the wave number ω/V_o becomes relatively large, even for modest values of frequency. In the present case, the wave number of the first girder mode is only 10^{-7} and the input spectrum becomes very small indeed.

So we find that a unique set of circumstances combine to limit the gust sensitivity of the V-Liner, at least from the pilot's viewpoint. The otherwise conventional vertical and pitch modes have no inherent stiffness, so their responses have very low accelerations because of low frequencies. The responses of the otherwise conventional short period modes are extraordinarily heavily damped, so that they do not contribute to overall response. And the wave numbers of the structural modes are so high because of the low forward speed that there is no effective input.

CONCLUSION

The work reported in this paper has illustrated several interesting features of the V-Liner design and points the way for further development.

First, we have demonstrated that the free pitching wing is a very effective gust alleviation mechanism. It also confers exceptional control power since all wing lift is available for control. Providing the control system can be properly arranged, no stability problems arise from gross movements of the overall airplane centre of gravity.

But we must also be aware of the potential influence of the parameters we have neglected in this analysis. Perhaps the most obvious is the deletion of the aerodynamic forces due to the girder and its sign array. Clearly, when some definitive coefficients for fuselage lift and drag are available, these forces must be included. But intuitively, we feel that the fuselage forces should contribute only damping, even if it is only small in some modes.

A more important deletion is the fore - and - aft mode, or X - force equation which suppresses the phugoid mode. For conventional airplanes, this may not be too important, because the gust velocity perturbation is not a high percentage of the free stream velocity, and the steady state drag coefficient is not high. But in the case of the V-Liner, neither of these conditions apply. In our case, the gust velocity perturbation is of the order of five percent of the free stream speed, and the steady state drag coefficient is high. In addition, at the low operating speeds of the airplane there is a relatively large thrust variation with speed from the power plant.

The work reported has also shown that the responses of the girder bending modes, while they do not contribute appreciable pilot acceleration, may nevertheless develop high dynamic stresses in the girder . So it is in order to study the power spectrum of the girder stress to assess its structural fatigue problems.

CAMCO V-LINER

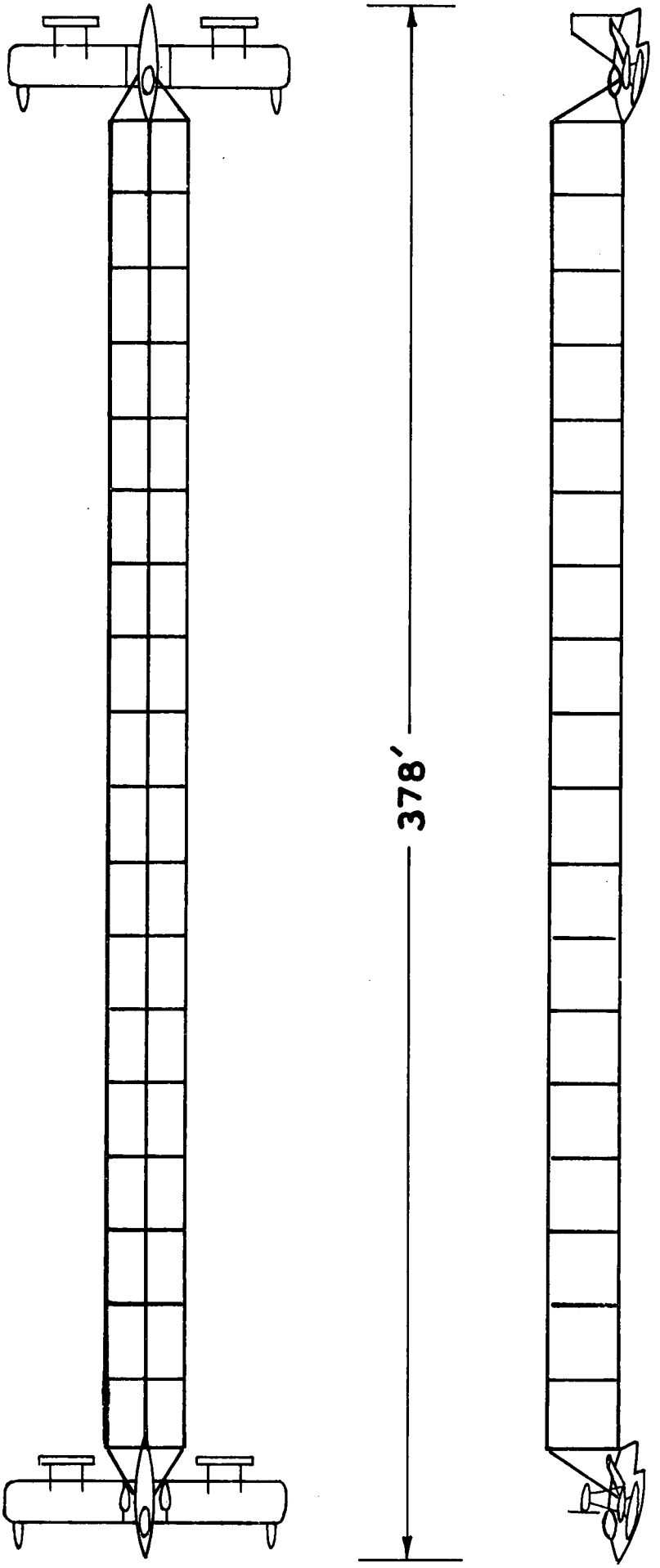


Fig.1 V - Liner general arrangement

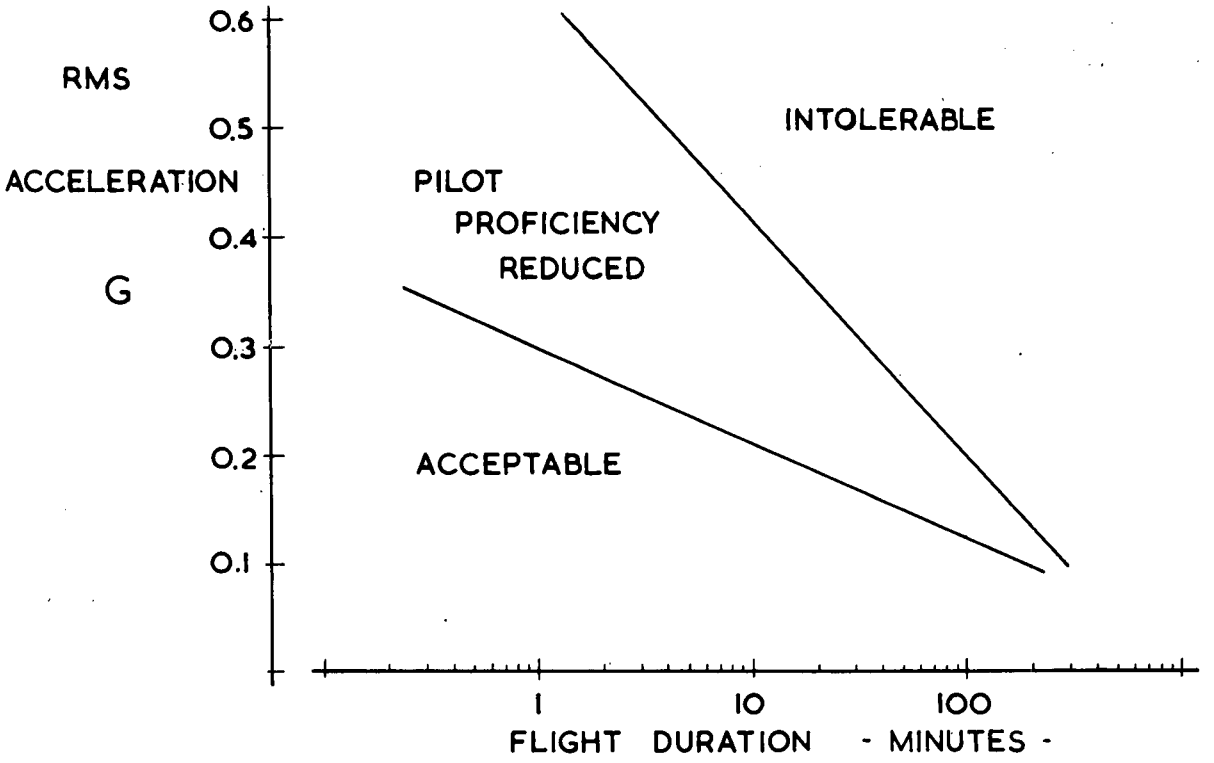


Fig.2 Pilot reaction to vibration

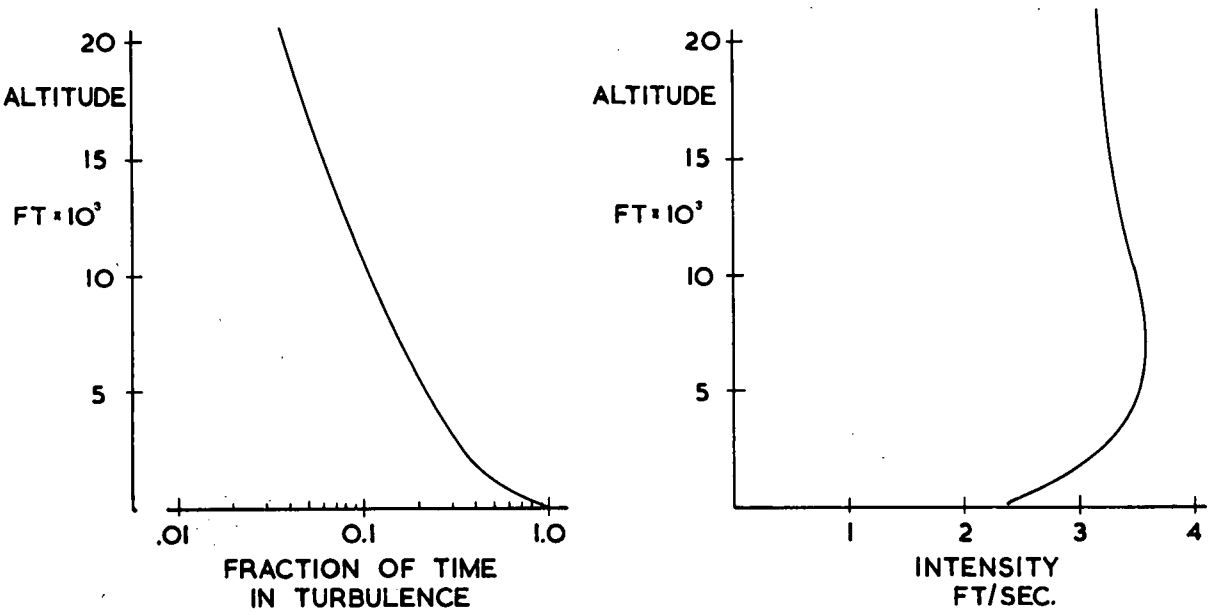


Fig.3 Turbulence field parameters

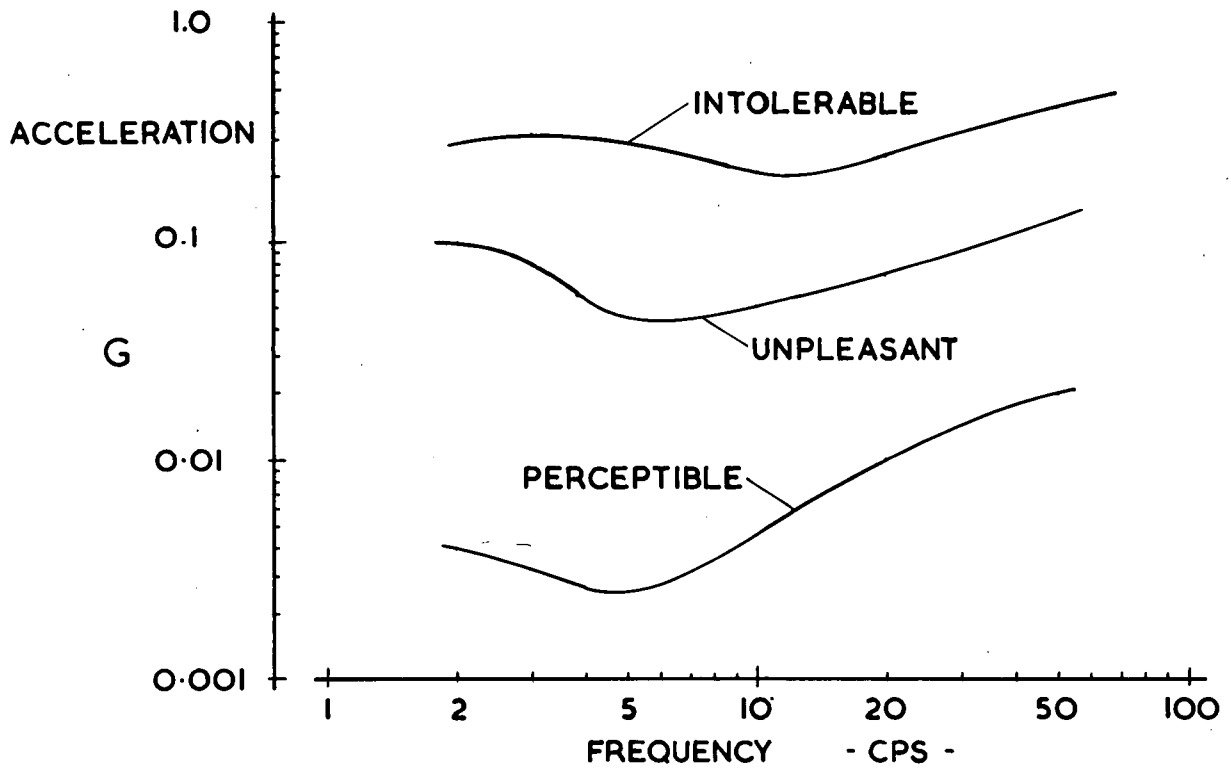


Fig.4 Human frequency sensitivity

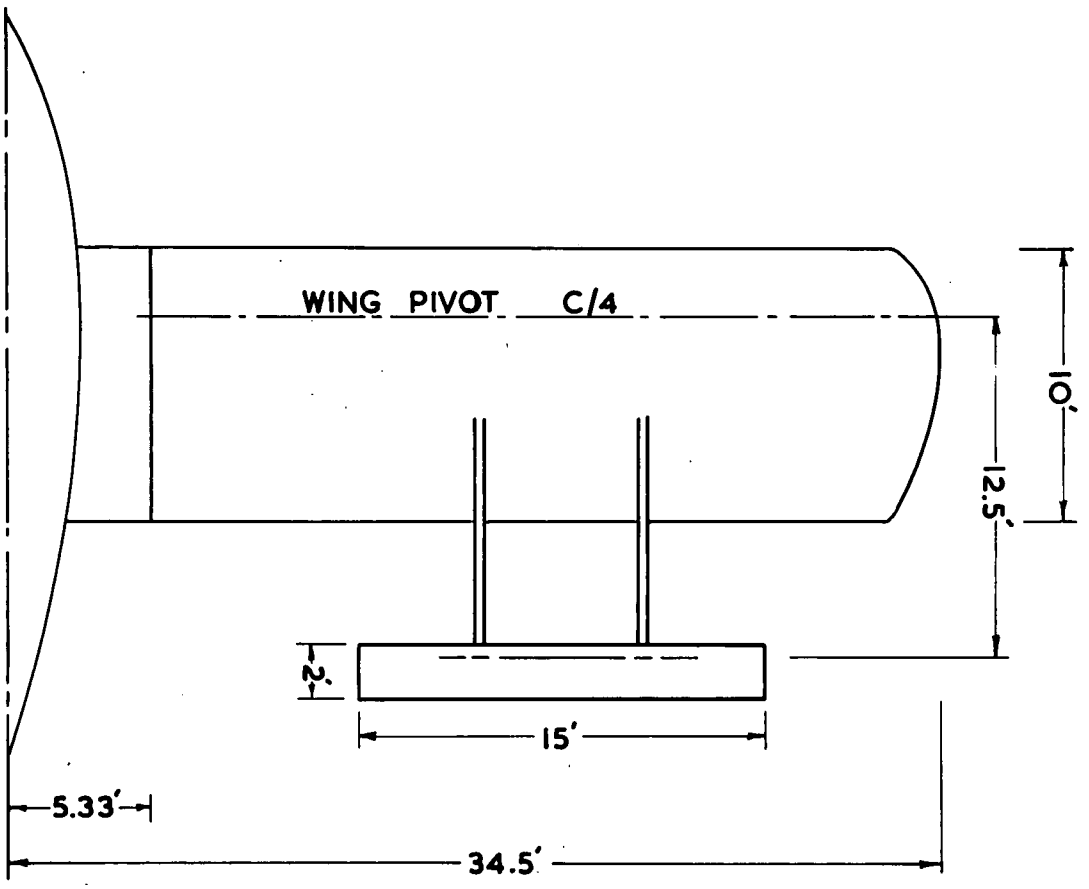
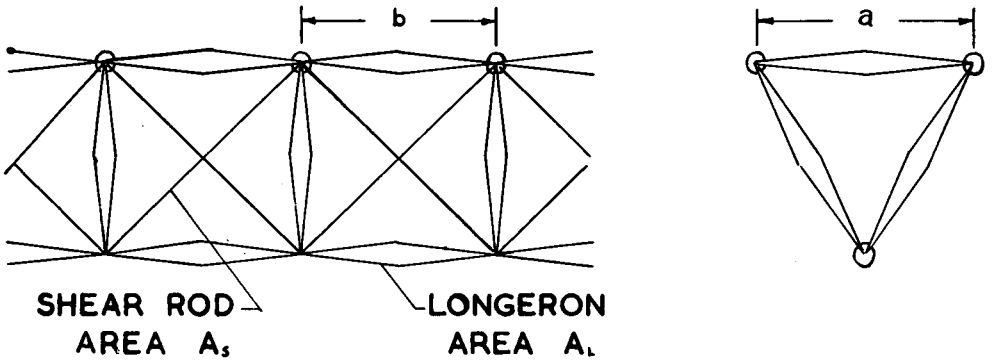


Fig.5 V - Liner wing detail



BENDING STIFFNESS $EI = \frac{EA_L a^2}{2}$

SHEAR STIFFNESS $GAK = \frac{3EA_s a^2 b}{(a^2+b^2)^{3/2}}$

TORSIONAL STIFFNESS $GJ = \frac{EA_s a^4 b}{2(a^2+b^2)^{3/2}}$

Fig.6 Girder flexibility formulae

SYMMETRIC NORMAL MODES

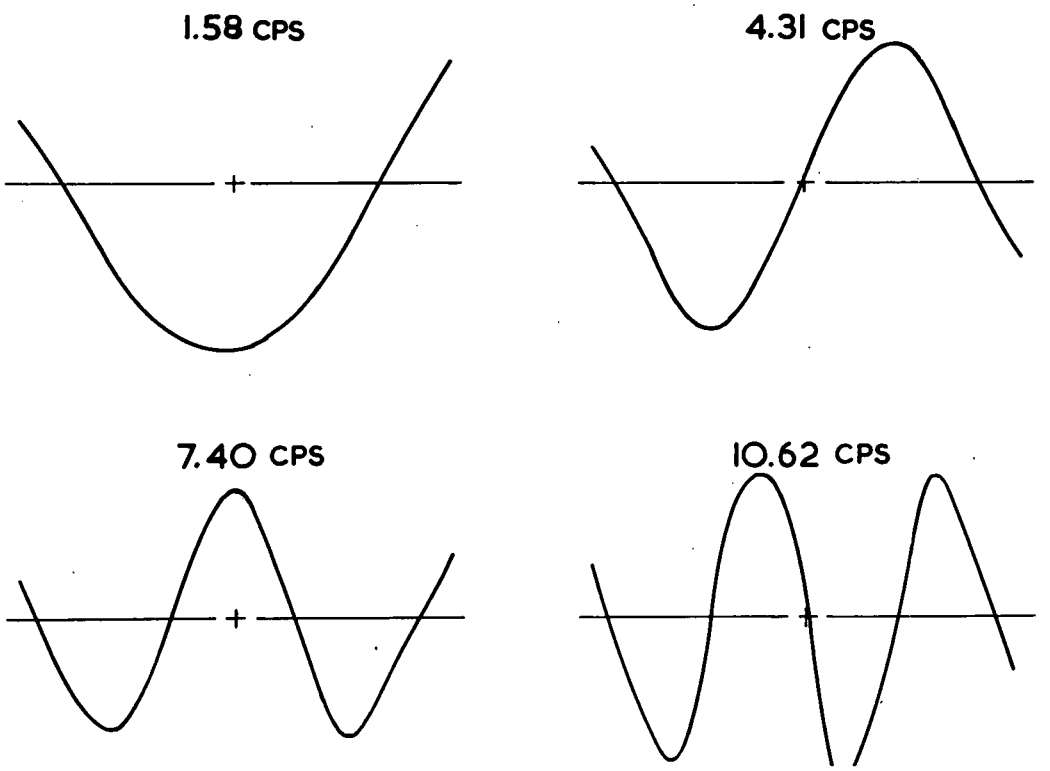


Fig.7 Vertical normal modes

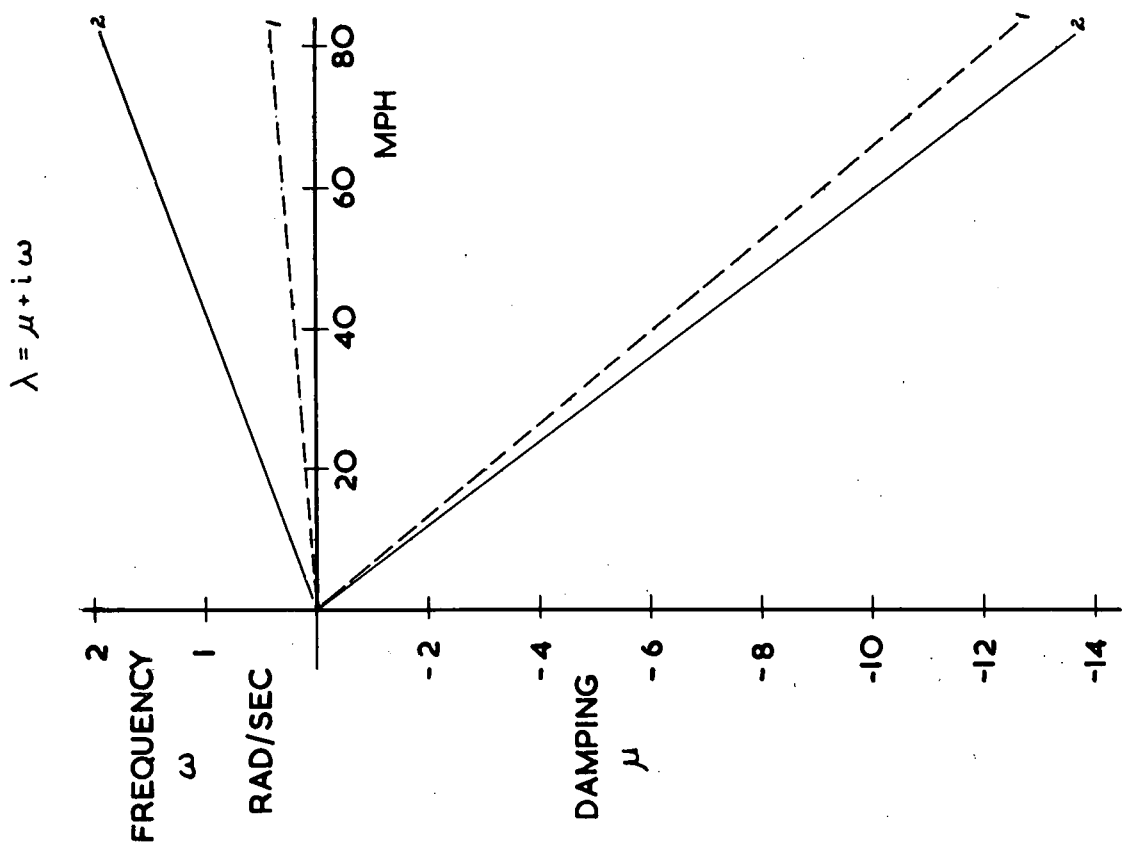


Fig.8 Rigid airplane stability roots

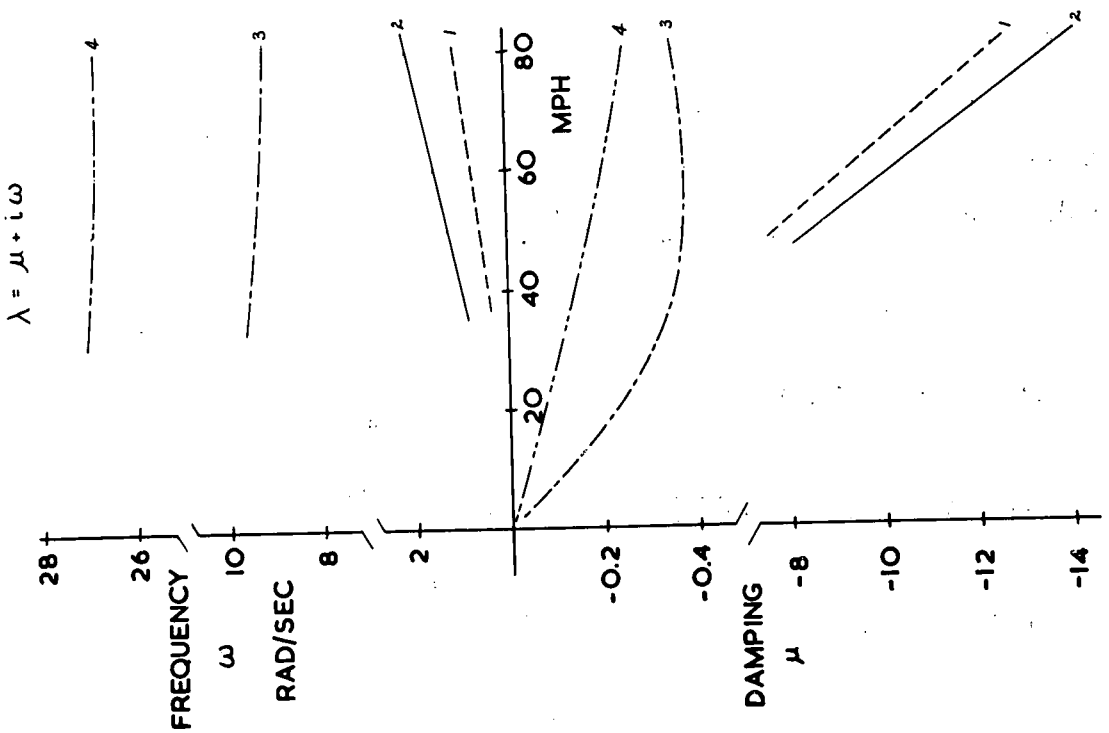


Fig.9 Flexible airplane stability roots

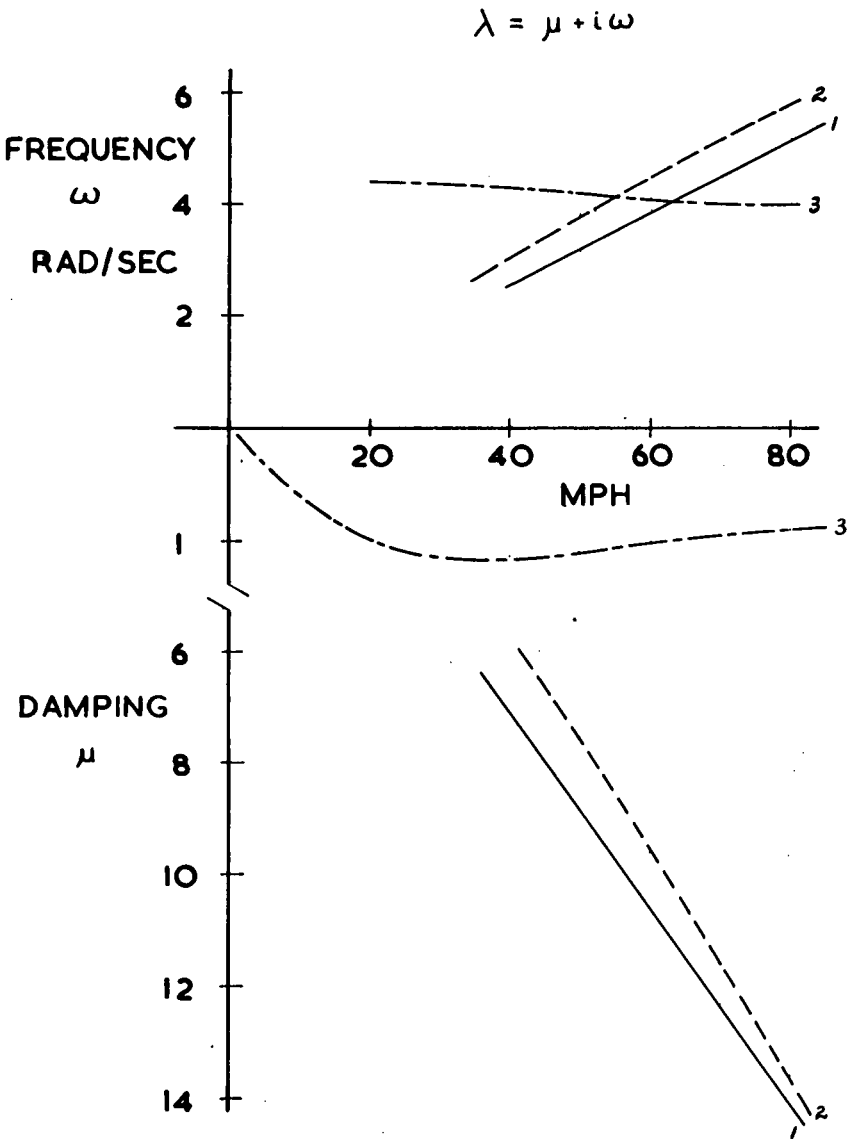


Fig. 10 Antisymmetric stability roots

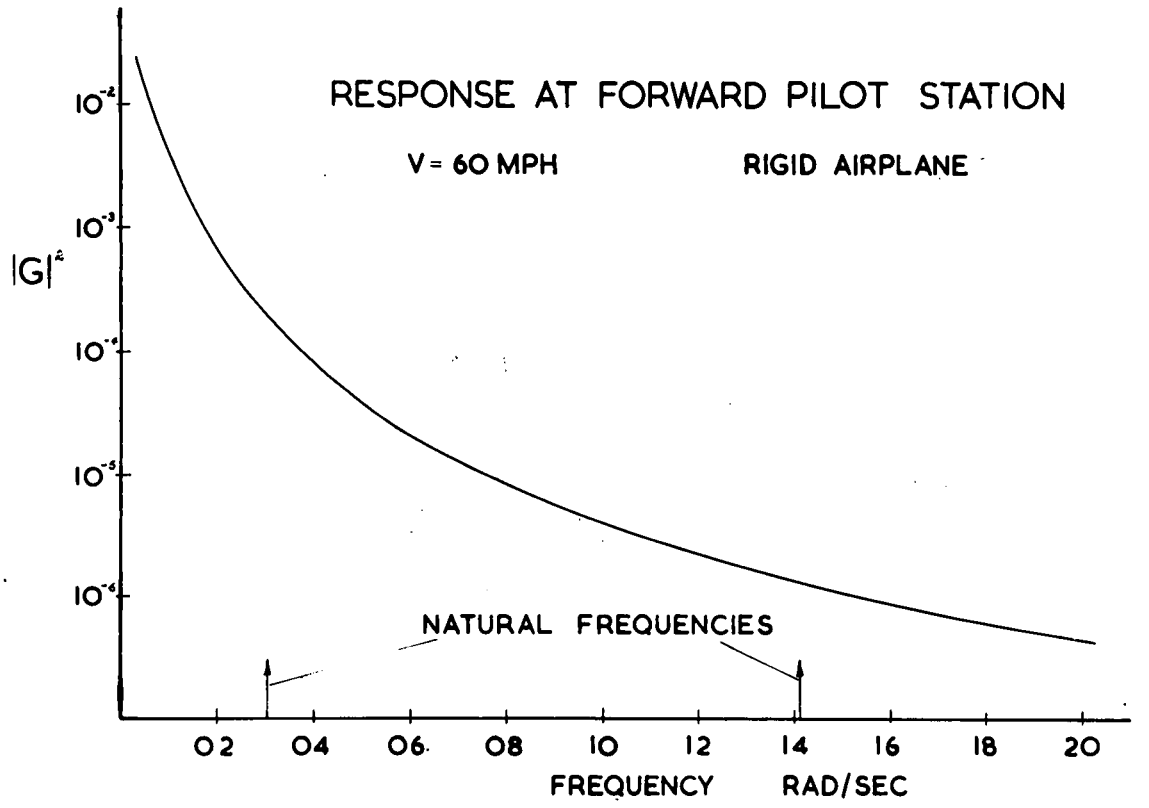


Fig. 11 Low frequency range gust response

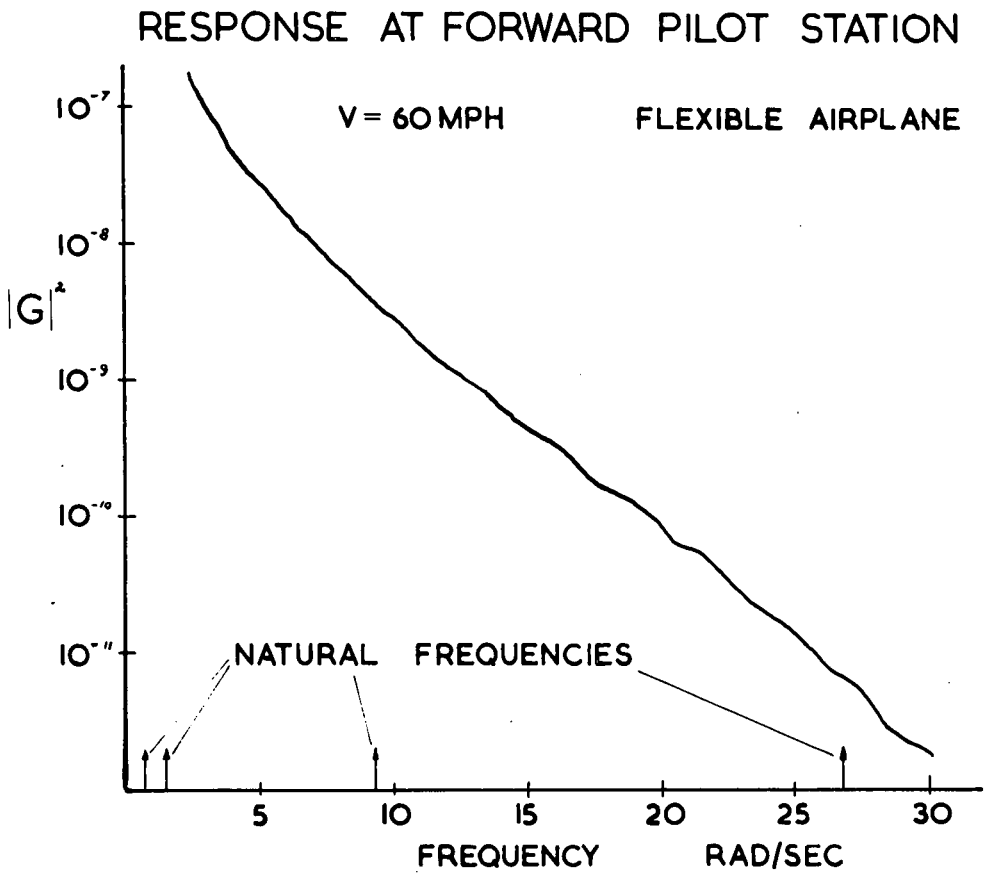


Fig. 12 Full frequency range gust response

ESSAI EN VOL D'UN DISPOSITIF ABSORBEUR DE RAFALES
CONFIGURATION DU SYSTEME-ANALYSE

par Jacqueline BOUJOT

Office National d'Etudes et de Recherches Aérospatiales (O.N.E.R.A.)
(92 - Châtillon - France)

ESSAIS EN VOL D'UN DISPOSITIF ABSORBEUR DE RAFALES
CONFIGURATION DU SYSTEME-ANALYSE

RESUME -

La minimisation des réponses d'un avion à la turbulence atmosphérique est recherchée par un pilotage automatique des gouvernes usuelles, sans modification des qualités de vol de l'appareil.

Les ordres de pilotage sont définis par une convolution de la composante verticale de la turbulence avec une fonction optimale physiquement réalisable.

Appliquée à un avion à aile delta, la théorie conduit à définir un dispositif absorbeur de rafales d'une grande simplicité, susceptible dans l'étape actuelle de réduire l'ensemble des réponses de la structure.

FLIGHT TESTS WITH A GUST ALLEVIATION DEVICE
DESIGN ANALYSIS

ABSTRACT -

Minimizing the response of an aircraft to atmospheric turbulence is attempted through automatic commands of the usual control surfaces without modifying the aircraft flight characteristics.

For this purpose, flight control inputs are defined by a convolution of the vertical component of turbulence with a workable optimum function.

Applied to a delta wing aircraft, the general theory suggests a very simple gust alleviation device. The data obtained indicate that the responses to turbulence are much improved by this device.

1 - INTRODUCTION.-

Les accélérations induites sur un avion du fait de la turbulence atmosphérique qu'il rencontre peuvent s'avérer dangereuses pour la résistance de la structure et désagréables au point de vue du confort de l'équipage ou des passagers. En fait on a besoin actuellement de réaliser des optimisations de vol en turbulence car l'évolution des techniques amène :

- d'une part, à faire voler de gros avions souples pour lesquels les résistances de la structure sont définies par la résistance à la turbulence par les phénomènes de fatigue entre autres ;
- d'autre part, à faire voler des avions près du sol, dans les conditions de turbulence les plus dures que l'on puisse rencontrer.

L'exposé composé de deux parties se propose de définir la configuration d'un dispositif absorbeur de rafales et de présenter les résultats de la vérification en vol de la qualité de ce contrôle optimal.

Analyse.-

Au point de vue théorique le problème relatif au vol longitudinal est abordé sous l'angle du pilotage automatique des gouvernes usuelles par la turbulence, sans modification de la mécanique du vol de l'appareil. La méthode consiste donc à effectuer un pilotage en boucle ouverte représenté par la figure 1.

Ce choix d'un pilotage en boucle ouverte nous a paru nécessaire pour ce qui se rapporte au domaine de la mécanique du vol que le constructeur a déjà cherché à optimiser à l'aide des pilotes automatiques usuels ou par le dessin de l'avion et que, pour des raisons de manoeuvre et de stabilité, on ne peut plus se permettre de toucher.

L'étude générale est faite en partie en utilisant la théorie du contrôle optimal linéaire. Appliquée à l'exemple de l'avion à stabilité variable, avion pratiquement rigide dans la gamme de fréquences considérées, elle permet d'optimiser l'ensemble des réponses de la structure en réduisant en particulier de 55 % la réponse de l'accélération au centre de gravité.

2 - ETUDE THEORIQUE.-

Les résultats de l'étude théorique seront rappelés.

2.1.- Position du problème.-

En vol longitudinal la réponse d'un paramètre $q(t)$ à une excitation par une turbulence $w(t)$ et à un braquage de gouverne $\beta(t)$ s'exprime par l'équation de convolution

$$(1) \qquad \boxed{q(t) = a(t) * w(t) + b(t) * \beta(t)}$$

où $a(t)$ et $b(t)$ sont les réponses impulsionnelles de l'avion à la turbulence et au braquage.

On cherche à effectuer le contrôle de la réponse de l'avion à la turbulence, par une loi de pilotage linéaire

$$(2) \qquad \boxed{\beta(t) = k(t) * w(t)}$$

telle que la variance σ_q^2 de $q(t)$ soit minimisée. Comme il a été mentionné, cette loi permet de réaliser une optimisation du pilotage en turbulence sans modification de la mécanique du vol de l'avion, la réponse en vol de l'avion étant

$$(3) \quad \boxed{q(t) = [a(t) + b(t) * k(t)] * w(t)}$$

La fonction inconnue $k(t)$ n'est acceptable que si elle correspond à un pilotage réel stable c'est-à-dire à un système physiquement réalisable. On a montré qu'une base complète de l'espace $\mathcal{K}$, des fonctions réalisables était formée par les fonctions de Laguerre généralisées $f_p(t)$. Leurs transformées de Laplace

$$(4) \quad \boxed{\mathcal{F}_p(\vartheta) = \left(\frac{1-\vartheta}{1+\vartheta}\right)^p} \qquad p = 0 \ldots \infty$$

représentables facilement avec des amplificateurs opérationnels recurrents forment une base complète de l'ensemble des filtres réalisables.

2.2.- Solution optimale générale.-

Les fonctions de transfert $A(\vartheta)$ et $B(\vartheta)$ ou transformées de Laplace respectives de $a(t)$ et $b(t)$, sont des fractions rationnelles dans le cas de l'étude en quasistationnaire. Dans le cas général, elles peuvent être approchées par des fractions rationnelles. On démontre en utilisant la théorie du contrôle optimal linéaire, que la variance σ_q^2 est minimale pour une fonction $k(t)$ unique, dont on désigne la transformée de Laplace par $K_m(\vartheta)$

Il est important de noter que $K_m(\vartheta)$ est la somme de 2 fractions rationnelles

$$(5) \quad \boxed{K_m(\vartheta) = K_1(\vartheta) + K_2(\vartheta)}$$

Les pôles de $K_1(\vartheta)$ dépendent uniquement de la structure car ils sont les racines de $B^+(\vartheta)\,B^+(-\vartheta)$. Cette quantité indexée de signes signifie qu'au cours de l'étude on a employé la technique de factorisation pour laquelle toute fraction rationnelle telle $B(\vartheta)$ s'écrit sous la forme :

$$(6) \quad \boxed{\begin{array}{lll} B(\vartheta) = B^+(\vartheta)\; B^-(\vartheta) & \text{avec} & \\ B^+(\vartheta) & \text{Analytique et non nulle} & \mathrm{Re}\,\vartheta > 0 \\ B^-(\vartheta) & \text{Analytique et non nulle} & \mathrm{Re}\,\vartheta \leqslant 0 \end{array}}$$

$K_2(\vartheta)$ est uniquement fonction de la turbulence qui intervient dans le calcul, par le modèle spectral de Dryden

$$(7) \quad \Phi_w(\omega) = \sigma_w^2 \; \frac{1 + 3\left(\frac{\omega L}{V}\right)^2}{\left[1 + \left(\frac{\omega L}{V}\right)^2\right]^2}$$

Il faut remarquer que lorsque $B(\vartheta) = B^+(\vartheta)$, la solution optimale

$$(8) \quad \boxed{K'_m(\vartheta) = -\frac{A(\vartheta)}{B(\vartheta)}}$$

est dite triviale et conduit à l'annulation de la variance correspondante.

2.3.- Famille de solutions optimales sur $\mathcal{K}$

La méthode précédente ne peut être exploitée que lorsque les fonctions de transfert sont écrites sous forme explicite simple, application immédiate au cas de l'avion rigide en quasistationnaire. Dans un but de généralité on a été amené à aborder le problème différemment en représentant la fonction inconnue par la série

$$(9)\qquad \boxed{K(\vartheta) = \sum_0^\infty k_\rho \, \mathcal{F}_\rho(\vartheta)} \qquad \sum_0^\infty |k_\rho| < \infty$$

dans laquelle les scalaires K_ρ sont les inconnues à calculer pour réaliser l'optimisation. Ces constantes optimales sont déterminées au rang fini par résolution d'un système linéaire et on démontre que la valeur minimale unique de la variance peut être approchée sur $\mathcal{K}$ par des développements au rang fini.

2.4.- Conséquence - loi optimale approchée.-

Une synthèse des méthodes précédentes conduit, pour des raisons de convergence, à adopter la loi générale simple suivante :

$$(10)\qquad \boxed{\begin{aligned} K(\vartheta) &= K_1(\vartheta) + \sum_\rho c_\rho \, \mathcal{F}_\rho(\vartheta) \\ K_1(\vartheta) &= k + \sum_J \frac{h_J}{\vartheta + |\vartheta_J|} + \sum_I \frac{k_I \vartheta + k'_I}{\vartheta^2 + 2\vartheta|T_I| + (T_I^2 + V_I^2)} \end{aligned}}$$

où ϑ_J et $T_I + j\,VI$ sont les racines de $B^+(\vartheta)B^+(-\vartheta)$ et les constantes h_J, k_I, k'_I, $c_\rho \ldots$ sont déterminées par résolution d'un système linéaire.

On approche ainsi la solution optimale par une suite de fractions rationnelles de pôles connus pour lesquelles un simple calcul des variations permet de déterminer les constantes optimales même pour un modèle de turbulence non analytique - modèle de Karman

(11)

$$\Phi_w(\omega) = \sigma_w^2 \, \frac{1 + 8/3\,(1{,}339\,\frac{\omega L}{V})^2}{\left[1 + (1{,}339\,\frac{\omega L}{V})^2\right]^{11/6}}$$

, plus représentatif de la réalité.

3 - APPLICATION : DEFINITION D'UNE LOI DE PILOTAGE OPTIMAL POUR L'AVION A STABILITE VARIABLE.-

Pour l'étape actuelle du travail l'objectif consiste à optimiser les réponses en accélération le long de l'axe longitudinal de l'avion.

3.1.- Equations.-

On s'intéresse au domaine de la mécanique du vol, pour lequel les équations sont

données en quasistationnaire sans assistance au pilote. On leur adjoint la relation cinématique

$$(12)\quad \alpha = \theta - \frac{\dot{\zeta}}{V} - \frac{w}{V}$$

entre α : incidence locale

w : turbulence normale

θ : angle de tangage

$\dot{\zeta}$: vitesse de pompage

V : vitesse de l'avion

Les calculs sont effectués pour des constantes aérodynamiques déterminées dans les conditions de vol : 1 000', M 0,8, remplissage 1 500 l.

3.2.- Optimisation des accélérations le long de l'axe longitudinal.-

En appliquant les résultats de l'étude théorique, on peut réaliser pour les accélérations le long de l'axe, les optimisations résumées par la figure 2. L'axe des abscisses représente l'axe de l'avion orienté d'avant en arrière, on a porté en ordonnées les rapports $\frac{\sigma_o^2}{\sigma_r^2}$ de la variance du système non piloté à la valeur optimale de la variance au point considéré.

3.3.- Définition de la loi de pilotage optimal.-

Deux points ont été principalement retenus, d'une part le poste piloté, d'autre part le centre de gravité.

La solution ne sera acceptable que :

1°) si elle n'entraîne pas de perturbation importante des autres paramètres

2°) si elle est peu sensible à des paramètres mal connus tels que l'échelle de la turbulence et reste efficace lorsque les coefficients aérodynamiques évoluent.

- Au poste pilote la solution optimale est une solution triviale qui annule la variance de l'accélération, le point considéré devenant centre instantané de rotation. Cette solution séduisante ne peut être retenue car elle pénalise la vitesse de tangage d'une manière physiquement compréhensible.

- Au centre de gravité, la loi optimale calculée dans l'intervalle (0, 10 Hz) s'écrit sous la forme la plus simple c'est-à-dire sans développement complémentaire :

$$(13)\quad K_G(\lambda) = -1{,}49 - \frac{534}{\lambda + 16{,}38} + \frac{597}{\lambda + 17{,}48}$$

pour un coefficient d'échelle de l'ordre de 220 m. Elle réduit la variance de l'accélération dans un rapport de 2,2.

Le tableau et la courbe de la figure 3 résument l'étude de l'influence de l'optimisation en G sur les accélérations en différents points de l'axe. La variance de la vitesse de tangage est en même temps réduite dans un rapport de l'ordre de 3,50.

D'autre part, les gains et les coefficients optimaux restent stationnaires lorsque les coefficients aérodynamiques évoluent ou lorsque l'échelle de turbulence varie.

Ces derniers résultats sont traduits par la figure 4.

On peut ainsi admettre finalement le principe d'une optimisation moyenne et donner pour l'avion, dans les conditions considérées, une loi de la forme

$$(14) \qquad \boxed{\beta(t) = \left[-1{,}43\,\delta(t) - 534\,e^{-16{,}38t} + 597\,e^{-17{,}48t}\right] * \frac{W(t)}{V}}$$

Son introduction dans la chaîne de pilotage réduit de :

- 55 % la variance de l'accélération au centre de gravité
- 42 % la variance de l'accélération au poste pilote
- 72 % la variance de $\theta°$
- 75 % le nombre de dépassements de deux fois l'écart-type, ce qui correspond à une amélioration intéressante de la résistance à la fatigue de l'avion.

REMARQUES.-

Il convient de noter que le problème défini ici est un problème sans contraintes. On s'est contenté de les envisager sous l'aspect final, en vérifiant que les résultats ne présentent pas d'inconvénients pour les autres paramètres. Ultérieurement il sera sans doute nécessaire :

- d'une part, d'introduire des contraintes dans les calculs
- d'autre part, d'utiliser un système autoadaptatif permettant de tenir compte de toutes les conditions de vol de l'avion.

3.4.- Représentation analogique.-

La solution donnée en (14) est facilement réalisable par une série de filtres analogiques qui constituent le dispositif absorbeur de rafales correspondant.

Dans la deuxième partie il sera montré comment les résultats numériques précédents ont été vérifiés au simulateur à partir d'enregistrements de turbulence réelle.

4 - CONCLUSION.-

La solution proposée est simple et générale. Il semble possible de traiter par le même chemin des cas d'optimisation plus complexes, en vol longitudinal ou latéral, suivant une loi de pondération ou avec introduction de contraintes.

De même la méthode s'applique tout au moins pour les basses fréquences, c'est-à-dire dans le domaine de la mécanique du vol, au cas où les modes de déformation de la structure sont introduits dans les calculs.

REFERENCES

[1] BRYSON A.E.
HENRIKSON J.
Estimation using sampled data containing sequentially correlated noise
Journal Spacecraft (June 1968), Vol. 5, N° 6 -

[2] COUPRY G.
Vol en air turbulent
O.N.E.R.A. Note Technique n° 78 1965 -

[3] KALMAN R.E.
BUCY R.S.
New results in linear filtering and Prediction theory
Journal of Basic Engineering - March 1961 -

[4] NASLIN P.
Introduction à la commande optimale - Dunod 1966 -

[5] PALLU de la BARRIERE R.
Cours d'automatique théorique - Dunod 1966 -

[6] PAPOULIS A.
The Fourier Integral and its application
Mc Graw Hill - 1964 -

[7] SAATY
BRAM
Non linear mathematics
Mc Graw Hill - 1964 -

[8] WIENER N.
Time Series - M.I.T. Press 1949 -

[9] BOUJOT J.
Sur l'optimisation du pilotage d'un avion en turbulence
Comptes rendus à l'Académie des Sciences Tome 266 - 1968
Série A p. 360 - 362 -

REPRESENTATION GENERALE DU SYSTEME

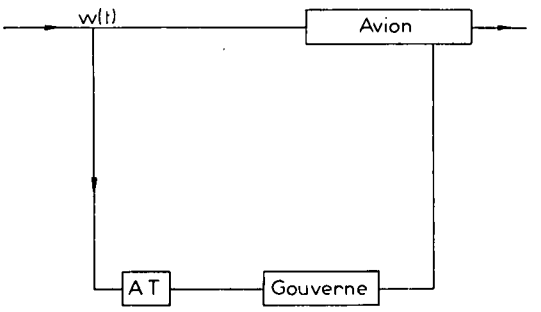


Fig : 1

OPTIMISATION DES ACCELERATIONS LE LONG DE L'AXE LONGITUDINAL
1000' M.0,8

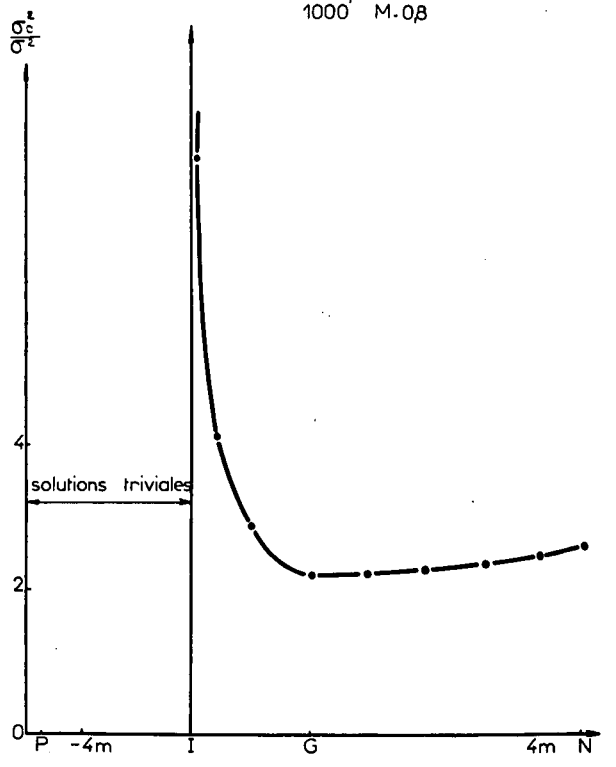


Fig.2

$$K_G(s) = -1{,}49 - \frac{534}{s+16{,}38} + \frac{597}{s+17{,}48}$$

Gains $\frac{\sigma_0^2}{\sigma_i^2}$				
Nombre de termes	3	4	5	6
Poste pilote P	1,694	1,692	1,687	1,687
G optimisation	2,188	2,188	2,188	2,189
Point arrière N	1,702	1,708	1,725	1,729

INFLUENCE DE L OPTIMISATION EN G

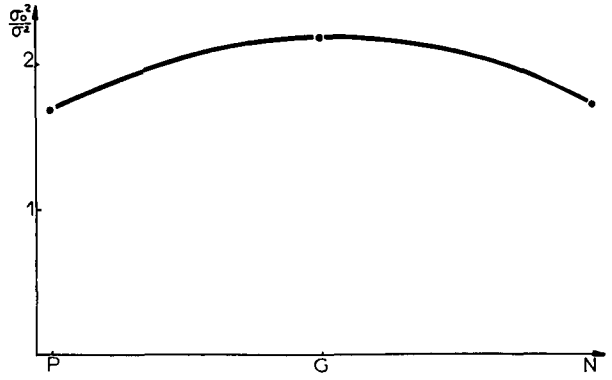


Fig. 3

OPTIMISATION EN G : VARIATION DE L'ECHELLE DE TURBULENCE

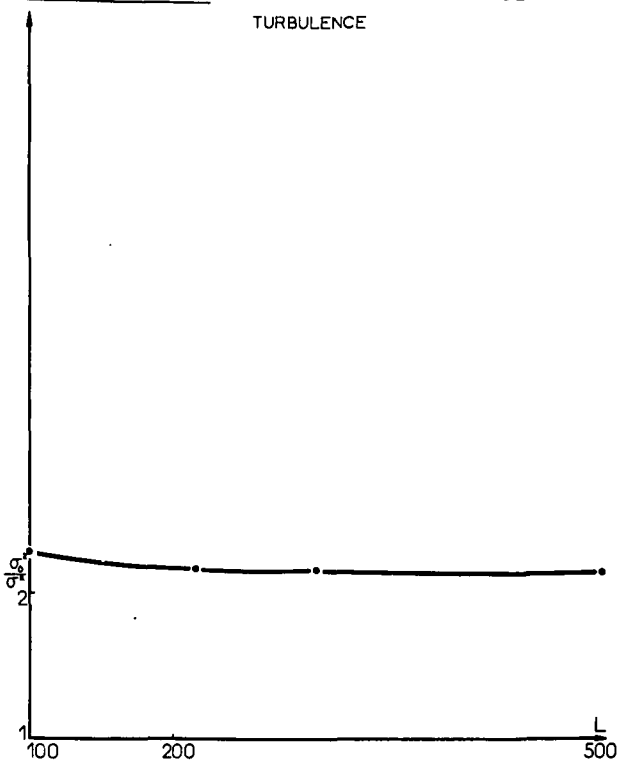


Fig. 4

DISCUSSIONS ON

PAPERS PRESENTED AT THE MEETING

Discussion on the Paper
LES TECHNIQUES UTILISEES EN AEROELASTICITE POUR LA REPRESENTATION DE L'AVION EN VOL
(Paper 2)
presented by
R.Dat and C.Beatrix

Mr. Payne - U.K.

In England and France there is a difference in the usage made of ground resonance test (G.R.T.) results for flutter clearance. In France the GRT results are used directly for flutter clearance. In England the G.R.T. results are compared with calculated modes and then the calculated modes are changed to give good agreement. Final flutter clearance then depends on the modified calculated modes.

Can Mr. Dat say whether similar procedures apply to the calculations of the static aeroelastic effects. Early calculations of these effects are certainly made with the calculated modes. Later in the design are calculations completed with measured G.R.T. modes?

Author's reply

Je pense que la méthode utilisée en Grande Bretagne pour les calculs de flottement est valable aussi pour les calculs statiques. Dans ce cas, la comparaison des modes propres théoriques et expérimentaux conduit à retoucher l'évaluation de la rigidité de certains éléments de structure particulièrement complexes et difficiles à traiter par la théorie prise.

Bien que nous n'utilisions pas cette méthode en France, comme le fait remarquer Mr. Payne, je la trouve intéressante parce qu'elle utilise les informations provenant de l'expérience dans un schéma théorique parfaitement cohérent.

Discussion on the Paper
PRESENT STATUS OF UNSTEADY AERODYNAMICS FOR LIFTING SURFACES
(Paper 3)
presented by
H.Bergh and R.J.Zwaan

Professor Yangos - Greece

Can the authors give an explanation for the generally better correlation between calculated and measured plots in the case of phase as compared to the case of amplitude, especially in subsonic?

Author's reply

In the subsonic case, the differences in amplitudes are caused primarily by boundary layer and thickness effects. This is already present in the steady case, where a well known difference exists between flat plate theory and measurements. The phase angle is primarily dependent on the propagation of disturbances, which is hardly affected by thickness on boundary layer at subsonic speeds. This seems to me the cause of the observed better correlation for the phase.

Discussion on the Paper
ATMOSPHERIC TURBULENCE DESIGN CASES
(Paper 5)
presented by
J.Taylor

Professor Haus - Belgium

1. I believe the relation between gust velocity and recorded acceleration at the C of G. depends on the piloting technique. Is the technique used in the test well defined?

2. An important computing work has been sponsored by the S.M.P., and is carried on in the USA, in order to make use of avoidable acceleration and speed records. There is a lot of them, they represent thousands of flying hours. Is Mr. Taylor connected with that team?

Author's reply

Yes the acceleration does depend on the piloting technique but as all the measurements are on aircraft on normal operations we wish to include such effects as are present due to the piloting. In severe turbulence the action of the pilot in combating the turbulence often increases the acceleration.

We are very much connected with the work being done by the Structures and Materials Panel. The RAE data are enormous as practically every British aircraft carrier is counting accelerometer. We have 600,000 flying hours from the D.H. "Comet" alone.

Professor P.Yangos - Greece

Supplementing the author's reply to Professor Haus's question on the pilot element, I should like to point out that flying in severe turbulence is one of the few cases where one may rely on the uniformity of human element in that pilots will not risk their lives through non observance of the correct technique such as penetration speeds, flying attitude, etc.

Has the author any idea of ICAO's possible reaction regarding the incorporation of his proposed changes on gust envelope in their Appendix 8.

Author's reply

Thank you for your added comments on the value of the pilot.

I expect ICAO will modify their gust requirements and I hope they will take account of this work of mine and all other work on spectral procedures so that they take the best from each.

Discussion on the Paper
UTILISATION D'UN AVION COMME MOYEN DE MESURE DE LA DISTRIBUTION STATISTIQUE DE LA TURBULENCE
(Paper 6)
presented by
G.Coupry et G.Thomasset

Mr. Brisebarre - France

Comment a été déterminée l'échelle de la turbulence L qui intervient en abscisse dans la variation de N_o et A ?

Author's reply

La figure présentée résulte d'une étude théorique de l'influence de l'échelle en utilisant la modèle spectral de Karman.

Professor Haus - Belgium

Comme vous l'avez dit en commençant, vous répondez à la question que j'avais adressée à l'orateur précédent concernant l'effet de l'action du pilote sur l'accélération.

Il me semble que la simulation utilisée pour déterminer cet effet suppose l'avion rigide. En est-il bien ainsi? Les conclusions seraient- elles les mêmes si on introduisait, dans le calcul, un terme tenant compte de la flexibilité de l'avion.

Author's reply

L'étude de l'influence des ordres de profondeur du pilote à partir des équations rigides de l'avion montre que dans tous les cas le pilote n'induit des accélérations qu'à basse fréquence (bien en dessous de la fréquence propre de tangage de l'avion) qui n'atteignent pas la limite supérieure du domaine de fréquence de l'avion rigide.

Discussion on the Paper
AEROELASTIC AND STRUCTURAL DYNAMIC INFLUENCES ON V/STOL HANDLING QUALITIES
(Paper 7)
presented by
Professor R.G.Loewy

D.McGregor - Canada

With reference to the authors reference to collective vs power lever controls for hovering vehicles in my view it has been shown, beyond any doubt, that the power lever is a practical control lever. We at NRC Canada have been flying a variable stability helicopter (Bell 47G-3B1) throughout its complete flight regime (exclusive of slinging) for approximately 4 years and found it much more desirable than a collective. Further proof is provided by the P-1127 and CL-84 experience. The P-1127 has been taken into confined areas many times and the CL-84 has been demonstrated in the rescue role.

Author's reply

It is important that we gather such experience. The degree of assurance that we feel on this subject will depend on the mission, - how much time is to be spent hovering, how confined the spaces are into which the aircraft must be manoeuvred, whether sling loads must be carried, etc. I would tend to feel that jet VTOL operation, such as carried out with the P-1127 is in a different category, say than the air-rescue exercises performed with the CL-84. Before taking decisions in these human factors areas, it is necessary to have the results from flight experience over a wide range of aircraft characteristics, piloting tasks, and pilot backgrounds and skills.

Discussion on the Paper
AEROELASTIC PROBLEMS OF FLEXIBLE V/STOL ROTORS
(Paper 8)
presented by
D.E.Brandt

D.E.Balmford - U.K.

I had two questions concerning mechanical instability:

(1) The difficulties discussed by the author in solving the mechanical instability problems of the tilt wing/tilt rotor type vehicle when using a rotor system employing a blade with a lag plane fundamental natural frequency less than rotational speed appears to me to favour strongly the use of a rotor having a lag plane fundamental natural frequency greater than rotational speed. Why had the author dismissed this solution so rapidly? Successful helicopter tricycle rotors had been built on this principle and this form of solution should be simpler for the tilt wing/tilt rotor type vehicle since the blades tended to be of lower aspect ratio than conventional helicopter blades and hence were comparatively stiffer in the chordwise sense. The fact that the "flopwise" stiffness contribution to lag stiffness in the cruise mode softened the blade in effective lag stiffness was compensated by the fact that the rotor speed in the cruise mode was reduced.

(2) Assuming a "soft" in-plane rotor was adopted, was the picture not quite so black as the author had painted since the high degree of twist inherent in the design of a blade for this type of vehicle meant that blade flap and lag modes were strongly coupled and hence the lag plane damping of the blade was considerably increased by a contribution from the aerodynamic damping of the flopwise component of motion.

Author's reply

(1) We are motivated to address and solve the mechanical instability problem because it appears that a substantial reduction in blade root and control system loads, hence weight, is possible. This comment applies to the "tilt rotor" aircraft which have prop/rotor blades of the same aspect rotor of helicopters. Tilt wing aircraft do utilize the stiff design. Soft in-plane stiffness rotors have also been successfully flown on helicopters like the BO-105 for example.

(2) Yes, I made this point, It must be recognized that aerodynamic damping is not available in all modes of instability. (Rigid body lateral translation is one example), therefore, other means of suppression may be required.

J.B.Scott-Wilson - UK

Could Mr. Brandt say which parameters are correctly scaled in these model tests?

Author's reply

Mass, inertia stiffness, velocity were all properly scaled. Reynolds number and Mach No were not.

Discussion on the Paper
AN ANALYTICAL METHOD FOR PREDICTING THE STABILITY AND CONTROL CHARACTERISTICS OF LARGE ELASTIC AIRPLANES AT SUBSONIC AND SUPERSONIC SPEEDS
(Paper 12)
presented by
A.R.Dusto and H.L.Chevalier

R.J.Zwaan - The Netherlands

You concluded that discrepencies in the stability and control derivatives obtained by the method described by Dr.Dusto, may probably be due to errors inherent in aerodynamic theory. Did you consider the possibility to improve the aerodynamic forces by attributing to the force on each panel a suitable weighting factor. This factor may be derived from experimental results (either steady or unsteady) and may be applied for each deformation mode. Methods to obtain such factors are indicated in the paper of Bergh and Zwaan, and in the references 30 and 31 mentioned in this paper.

Author's reply

Yes, the empirical correction method is under development at Boeing and NASA Ames. But, we would like to be correcting for only those effects which cannot be predicted theoretically. If the basic flow is not adequately represented, the empirical corrections are not very practical.

A.Young - U.K.

1. I am interested by the variation of C_{M_α} with aircraft weight shown on Figure 4 and I wonder if this variation is due to the effect of inertia relief. Were the experimental results obtained during g excursions at constant speed or by varying speed at constant 1g in flight? And does the calculated result for C_{m_α} include the effects of inertia relief?

2. It is possible that the variation arises because of substantially different weight distributions in the wing between flight cases while the aircraft total weight is little changed.

Author's reply

1. The flight test results given in Figure 4 were obtained at constant speed and at 1g conditions. Predicted results do account for inertia relief.

2. It is possible that some of the effects of airplane weight given for C_{m_α} as illustrated in Figure 4 for the flight test results are due to a difference in airplane weight distributions. However there is some question as to the exact weight distributions at the time when the flight test data were recorded. Center of gravity locations were the same in both cases.

Mr. Renaudie - France

1. Does Mr. Dusto think that it is possible to predict the effect of flexibility (magnitude and sense) on the stability cross derivative, for example yawing moment due to aileron deflexion, in the transsonic range on the basis of rigid body wind tunnel aerodynamic results only.

2. Does Mr. Dusto think that a flexible model gives the answer taking account of the scale effect on stability aerodynamic derivatives.

Author's reply

1. It appears, in theory, to be possible to compute lateral directional stability and control derivatives; but, as noted in the written paper, there is a significant effect from the wing which is neglected in the first order aerodynamic theory. A paper to be published by Dr. Paul Rubbert of the Boeing Company will discuss the problem in detail and will present a method of solution which has not as yet been implemented for numerical evaluation.

2. The flexible model cannot give a complete answer to the problems involved in predicting elastic stability derivatives as it is not possible to simulate inertia forces in the wind tunnel. An alternative is to express elastic effects in terms of free-vibration mode shapes which eliminate inertial and gravity effects. However, the costs and technical difficulties involved in constructing and testing a large number of models for adequate quasi-static evaluations may be prohibitive.

Professor H.G.Kuessner - Germany

I would like to ask you, if your influence coefficient method has also been used for flutter calculations. We have found that the restriction of the hundred panel degrees of freedom to a lower number of degrees is not feasible at flutter. We cannot at present solve complex sign value problems of hundred degrees of freedom. Therefore we prefer the orthogonal mode approach.

Author's reply

The influence coefficient method which we are using is based on steady flow theory. It is being extended to predict low frequency unsteady aerodynamic forces by reducing the unsteady flow problem to a problem in steady flow. In neither case is it appropriate to the problem of flutter. The orthogonal mode approach is being used to introduce the structural dynamics into the problem of overall airplane dynamics. In doing this the large number of equations is reduced to a much smaller number by the method of residual flexibility. The numerical difficulty involved in solving the complex sign value problem is thereby avoided. It would appear that the same approach could be used in flutter analysis.

Discussion on the Paper
DETERMINATION DES COEFFICIENTS AERODYNAMIQUES AVION SOUPLE EN VOL SYMETRIQUE
(Paper 15)
presented by
A.Marsan

Mr. Brisebarre - France

1. Pourquoi avez-vous jugé préférable de représenter l'avion souple par une matrice de coefficients d'influence plutôt que par une superposition de modes propres?

2. Vous avez comparé les résultats théoriques de portance et de moment pour l'avion rigide. Avez-vous également les comparaisons pour l'avion souple?

Author's reply

1. Sud-Aviation a toujours préféré utiliser les coefficients d'influence plutôt que les formes propres pour la commodité et la rapidité des calculs. Mais enfin c'est purement subjectif. De toute façon une vérification des coefficients d'influence a été faite à partir des formes mesurées lors des essais au sol. D'autre part la correspondance entre les formes calculées à partir des coefficients d'influence et les formes mesurées est relativement bonne. Nous utilisons les formes propres pour tous les problèmes instationnaires.

2. Je n'ai pas représenté de courbe de gradient de portance avion souple car elle serait fonction de la pression dynamique. Mais il est possible de la tracer pour une pression dynamique particulière à partir de la courbe avion rigide en utilisant les coefficients correcteurs. Rappelons simplement que la correction due à la souplesse avion sur les gradients de portance et de moment de tangage peut atteindre environ 10% de la valeur avion rigide.

Discussion on the Paper
COMBINED EFFECTS OF AEROELASTIC COUPLING AND AERODYNAMIC INTERFERENCE BETWEEN TWO LIFTING SURFACES (WING-TAIL, TANDEM WINGS) ON THE LONGITUDINAL STABILITY
(Paper 16)
presented by
P.G.Hamel

Professor H.G.Küssner - Germany

This lecture comes closest to the procedure used in flutter calculations insofar as it takes in account elasticity and uses correct instationary air forces. There is only a difference in the method. Dr.Hamel used indicial functions, whereas in flutter research we use Laplace transforms. With complex reduced frequencies we can also solve our Lagrange equations for damped or excited oscillations. Only recently we have taken in account the instationary interference of the main wing and the elevator, and we have also found, that this aerodynamic interference has a destabilizing effect.

Author's reply

I appreciate Professor Küssner's statement very much. I only would like to add that the effect of unsteady aerodynamics can be taken into account by either indicial functions or Laplace transforms.

Discussion on the Paper
THEORETICAL INVESTIGATION OF AEROELASTIC INFLUENCES ON THE LIFT DISTRIBUTION AND THE AERODYNAMIC DERIVATIVES OF SWEPT WINGS AT SYMMETRIC AND ANTISYMMETRIC STATIONARY FLIGHT CONDITIONS
(Paper 17)
presented by
W.Schoernack and E.Hassler

P.G.Kafka - Germany

This paper appears to duplicate the work done in NASA TN 3030 69 W.Gray and K.Schenek (1952).

The only difference is the introduction of modes to approximate the wing deflection which in TN 3030 is described by rigorous application of beam theory.

Author's reply

The authors do not know the above mentioned NASA TN 3030. They will look through this paper and give their comments to Mr. Kafka as soon as possible.

Discussion on the Paper
WIND-TUNNEL TECHNIQUES FOR THE STUDY OF AEROELASTIC EFFECTS ON AIRCRAFT STABILITY, CONTROL, AND LOADS
(Paper 18)
presented by
A.G.Rainey and I.Abel

Professor Hafer - Germany

Did you correct your test results with wall effects?

Author's reply

No wall interference corrections were applied to any of the data presented in the paper. Considerable interest in the question of wall interference effects on unsteady aerodynamic data, particularly in ventilated throat wind tunnels, has been generated in the past several years. In fact, Mr. Bergh in his presentation at this meeting presented some recent data pertinent to this question. The state of development of the theory for wind-tunnel wall interference effects is uncertain at this time. H.C.Garner of the National Physical Laboratory, in an informal communication, indicated that his analysis of the wall interference effects for a complete model in our square tunnel with slots in all four walls showed very small unsteady interference corrections. As a result of these and other considerations, we do not, as a matter of practice, attempt to make corrections to dynamic data in the Langley transonic dynamics tunnel.

N. Treinies - Germany

Two questions concerning derivative measurements. First I want to know whether you have had difficulties with wind tunnel turbulence.

Second: which values did you directly measure and in which form. Functions of time are amplitudes and phases relative to a forcing function.

Author's reply

Wind tunnel turbulence has not caused any significant difficulty in the control effectiveness work accomplished so far. Our data processing technique makes use of a special purpose analog computer which calculates the magnitude and phase of the response relative to the input in a manner which has good noise rejection capability. For the aileron effectiveness measurements described in the paper, the aileron displacement was measured with a strain gaged beam transducer located at the aileron and the roll response was measured by integrating the output of a rate gyro.

H. Bergh - The Netherlands

How does your system of derivative measurement compare with that of the Cornell with a swing-sting, especially with regard to accuracy?

Author's reply

The techniques described in the paper for measurement of stability and control derivatives are not directly comparable to the techniques developed at the Cornell Aeronautical Laboratory. At Cornell, a model is forced to move through a motion prescribed by the motion of the support system. In our techniques, only a control surface on the model is given a prescribed motion and the derivatives are then deduced from solving equations of motion very similar to those of the free-flying airplane. Reference 5 of the written version contains a discussion of accuracy considerations for the current technique and the comparison of model predicted and flight measured effectiveness shown in Figure 8 indicates satisfactory accuracy.

Discussion on the Papers

20 :	CONSIDERATION OF STABILITY AUGMENTATION SYSTEMS FOR LARGE ELASTIC AIRCRAFT	by C. Newberry
21 :	INFLUENCE DES EFFETS AEROELASTIQUES SUR L'ETUDE ET LA REALISATION DE L'AMORTISSEUR DE TANGAGE ET DU PILOTE AUTOMATIQUE D'UN AVION DE TRANSPORT SUPERSONIQUE	by R. Deque
23 :	ANALYTICAL DESIGN AND FLIGHT TESTS OF A MODAL SUPPRESSION SYSTEM ON THE XB-70 AIRPLANE	by J.H. Wykes and E.E. Kordes

Questions on Papers 20 and 23:

Professor Doetsch - Germany

We appear to be in a similar position to that of the FMP Meeting at Brussels in 1960 (61 ?), when auto-stabilizers were being introduced to damp rigid aircraft oscillations. I then gave a warning against using black boxes indiscriminately because of the instability danger in case the autostabilizer failed in a critical situation. Now we are coming to the second round in the application of black boxes, this time for the damping of structural vibrations. What is the present attitude or "philosophy" with respect to the same problem of safety in a failure case.

(In particular with respect to the application suggested in Fig. 29 of Mr. Newberry's Paper)

Author's reply

1. **Mr. Wykes:** Fail-safety techniques are on hand for implementing these systems. The XB-70, for instance, had a dual channel mechanization for the ILAF system similar to that which Mr. Bossard mentioned the Concorde has in its stability augmentation system.

2. **Mr. Kordes:** To give you some idea of the reliability of these systems; to my knowledge, neither the basic SAS nor the SAS-ILAF combination ever suffered a dual failure, which would have made the systems inoperative, during any of the XB-70 test flights.

Question on Papers 20, 21 and 23:

P.J.Bramah - UK

Do the authors have any comments to make on the use of the systems described to control helicopter vibration?

Author's reply

I do not know of any current work going on in this area, but it would be a natural for future efforts.

Question on Paper 23:

Mr. Payne - UK

The last figure showed a completely different response picture to the figures showing response to the shaker. Response to the shaker showed peaks at the frequencies at some or all of the first four modal frequencies. Response to turbulence showed just a single peak at 4 HZ. Can one of the speakers suggest the usefulness of a system designed to reduce a type of response which is completely dissimilar from that occurring in practice.

Author's reply

1. **Mr. Kordes:** A major influence on the shape of the power spectral density curve shown is the short interval of time in the gust field available for analysis. To insure accuracy of the amplitudes and reliability of the data we had to limit ourselves to relatively wide frequency bandwidths in the power spectral density analysis. Because of this, we did not have sufficient resolution to separate individual modes.

2. **Mr. Kordes:** Yes. We arbitrarily reduced the frequency bandwidth in the analyses, sacrificing amplitude accuracy, and isolated frequency peaks of the modes similar to those obtained with the shaker vane.

Professor H.G.Kuessner - Germany

If you like to counteract the aerodynamic action of the oscillating vanes near the cockpit, you had to put equal vanes near this place and to operate it in the opposite sense.

If we suppose a given field of atmospheric turbulence or gusts, a very flexible lifting surface could right slip through this field without gust loads like a ray. But since airplanes cannot be built in this way, and because you can only move small parts of the airplane, you cannot expect good gust alleviation by such devices.

Author's reply

Your observations about using the shaker vane in an opposite sense to cancel the excitation from the vane gives me an opportunity to mention the fact that we had begun the process of designing and fabricating the necessary parts to operate the vanes as a structural mode control system. Analytical estimations showed that the system would be fully effective in vertical gust fields having a ft/sec rms intensity. The mechanization was quite simple and was proceeding without difficulty when the XB-70 program was terminated.

AGARD Conference Proceedings No.46 North Atlantic Treaty Organization, Advisory Group for Aerospace Research and Development AEROELASTIC EFFECTS FROM A FLIGHT MECHANICS STANDPOINT Published March 1970 418 pages Twenty-five papers, together with discussions, are contained in this Proceedings. The papers are grouped under the following sessions: I: Preliminary Session Devoted to the State-of-the-art. II: Flight Dynamics of a Flexible VTOL Rotor. III: Flight Dynamics of Flexible Airplanes Theoretical Methods. IV: Experimental Methods for Flight Dynamics of the Flexible Airplane. V: Stability and Control Augmentation Devices. Papers presented at the 34th Meeting of the AGARD Flight Mechanics Panel, held in Marseille, France, 21-25 April 1969.	533.6.013.42	AGARD Conference Proceedings No.46 North Atlantic Treaty Organization, Advisory Group for Aerospace Research and Development AEROELASTIC EFFECTS FROM A FLIGHT MECHANICS STANDPOINT Published March 1970 418 pages Twenty-five papers, together with discussions, are contained in this Proceedings. The papers are grouped under the following sessions: I: Preliminary Session Devoted to the State-of-the-art. II: Flight Dynamics of a Flexible VTOL Rotor. III: Flight Dynamics of Flexible Airplanes Theoretical Methods. IV: Experimental Methods for Flight Dynamics of the Flexible Airplane. V: Stability and Control Augmentation Devices. Papers presented at the 34th Meeting of the AGARD Flight Mechanics Panel, held in Marseille, France, 21-25 April 1969.	533.6.013.42
AGARD Conference Proceedings No.46 North Atlantic Treaty Organization, Advisory Group for Aerospace Research and Development AEROELASTIC EFFECTS FROM A FLIGHT MECHANICS STANDPOINT Published March 1970 418 pages Twenty-five papers, together with discussions, are contained in this Proceedings. The papers are grouped under the following sessions: I: Preliminary Session Devoted to the State-of-the-art. II: Flight Dynamics of a Flexible VTOL Rotor. III: Flight Dynamics of Flexible Airplanes Theoretical Methods. IV: Experimental Methods for Flight Dynamics of the Flexible Airplane. V: Stability and Control Augmentation Devices. Papers presented at the 34th Meeting of the AGARD Flight Mechanics Panel, held in Marseille, France, 21-25 April 1969.	533.6.013.42	AGARD Conference Proceedings No.46 North Atlantic Treaty Organization, Advisory Group for Aerospace Research and Development AEROELASTIC EFFECTS FROM A FLIGHT MECHANICS STANDPOINT Published March 1970 418 pages Twenty-five papers, together with discussions, are contained in this Proceedings. The papers are grouped under the following sessions: I: Preliminary Session Devoted to the State-of-the-art. II: Flight Dynamics of a Flexible VTOL Rotor. III: Flight Dynamics of Flexible Airplanes Theoretical Methods. IV: Experimental Methods for Flight Dynamics of the Flexible Airplane. V: Stability and Control Augmentation Devices. Papers presented at the 34th Meeting of the AGARD Flight Mechanics Panel, held in Marseille, France, 21-25 April 1969.	533.6.013.42

AGARD Conference Proceedings No.46 North Atlantic Treaty Organization, Advisory Group for Aerospace Research and Development AEROELASTIC EFFECTS FROM A FLIGHT MECHANICS STANDPOINT Published March 1970 418 pages Twenty-five papers, together with discussions, are contained in this Proceedings. The papers are grouped under the following sessions: I: Preliminary Session Devoted to the State-of-the-art. II: Flight Dynamics of a Flexible VTOL Rotor. III: Flight Dynamics of Flexible Airplanes Theoretical Methods. IV: Experimental Methods for Flight Dynamics of the Flexible Airplane. V: Stability and Control Augmentation Devices. Papers presented at the 34th Meeting of the AGARD Flight Mechanics Panel, held in Marseille, France, 21-25 April 1969.	533.6.013.42	AGARD Conference Proceedings No.46 North Atlantic Treaty Organization, Advisory Group for Aerospace Research and Development AEROELASTIC EFFECTS FROM A FLIGHT MECHANICS STANDPOINT Published March 1970 418 pages Twenty-five papers, together with discussions, are contained in this Proceedings. The papers are grouped under the following sessions: I: Preliminary Session Devoted to the State-of-the-art. II: Flight Dynamics of a Flexible VTOL Rotor. III: Flight Dynamics of Flexible Airplanes Theoretical Methods. IV: Experimental Methods for Flight Dynamics of the Flexible Airplane. V: Stability and Control Augmentation Devices. Papers presented at the 34th Meeting of the AGARD Flight Mechanics Panel, held in Marseille, France, 21-25 April 1969.	533.6.013.42
AGARD Conference Proceedings No.46 North Atlantic Treaty Organization, Advisory Group for Aerospace Research and Development AEROELASTIC EFFECTS FROM A FLIGHT MECHANICS STANDPOINT Published March 1970 418 pages Twenty-five papers, together with discussions, are contained in this Proceedings. The papers are grouped under the following sessions: I: Preliminary Session Devoted to the State-of-the-art. II: Flight Dynamics of a Flexible VTOL Rotor. III: Flight Dynamics of Flexible Airplanes Theoretical Methods. IV: Experimental Methods for Flight Dynamics of the Flexible Airplane. V: Stability and Control Augmentation Devices. Papers presented at the 34th Meeting of the AGARD Flight Mechanics Panel, held in Marseille, France, 21-25 April 1969.	533.6.013.42	AGARD Conference Proceedings No.46 North Atlantic Treaty Organization, Advisory Group for Aerospace Research and Development AEROELASTIC EFFECTS FROM A FLIGHT MECHANICS STANDPOINT Published March 1970 418 pages Twenty-five papers, together with discussions, are contained in this Proceedings. The papers are grouped under the following sessions: I: Preliminary Session Devoted to the State-of-the-art. II: Flight Dynamics of a Flexible VTOL Rotor. III: Flight Dynamics of Flexible Airplanes Theoretical Methods. IV: Experimental Methods for Flight Dynamics of the Flexible Airplane. V: Stability and Control Augmentation Devices. Papers presented at the 34th Meeting of the AGARD Flight Mechanics Panel, held in Marseille, France, 21-25 April 1969.	533.6.013.42

NATIONAL DISTRIBUTION CENTRES FOR AGARD PUBLICATIONS

AGARD publications are distributed to NATO Member Nations through the National Distribution Centres listed below.

BELGIUM	General J.DELHAYE Coordinateur AGARD - V.S.L. Etat Major Forces Aériennes Caserne Prince Baudouin Place Dailly Bruxelles 3
CANADA	Director of Scientific Information Services Defence Research Board Department of National Defence - 'A' Building Ottawa, Ontario
DENMARK	Danish Defence Research Board Østerbrogades Kaserne Copenhagen Ø
FRANCE	O.N.E.R.A. (Direction) 29, Avenue de la Division Leclerc 92. Châtillon-sous-Bagneux
GERMANY	Zentralstelle für Lüftfahrdokumentation und Information Maria-Theresia Str. 21 8 München 27 Attn: Dr Ing. H.J.RAUTENBERG
GREECE	Greek National Defence Staff D. JSG Athens
ICELAND	Director of Aviation c/o Flugrad Reykjavik
ITALY	Ufficio del Delegato Nazional all' AGARD Ministero Difesa - Aeronautica Roma
LUXEMBOURG	Obtainable through BELGIUM
NETHERLANDS	Netherlands Delegation to AGARD National Aerospace Laboratory, NLR Attn: Mr A.H.GEUDEKER P.O. Box 126 Delft
NORWAY	Norwegian Defense Research Establishment Main Library, c/o Mr P.L.EKERN P.O. Box 25 N-2007 Kjeller
PORTUGAL	Direccao do Servico de Material da Forca Aerea Rua da Escola Politecnica 42 Lisboa Attn: Brig. General Jose de Sousa OLIVEIRA
TURKEY	Turkish General Staff (ARGE) Ankara
UNITED KINGDOM	Ministry of Technology T.I.L. (E) Room 401 Block A, Station Square House St.Mary Cray Orpington, Kent
UNITED STATES	National Aeronautics and Space Administration (NASA) Langley Field, Virginia Attn: Report Distribution and Storage Unit

NATIONAL DISTRIBUTION CENTRES FOR AGARD PUBLICATIONS

AGARD publications are distributed to NATO Member Nations through the National Distribution Centres listed below.

BELGIUM
General J.DELHAYE
Coordinateur AGARD - V.S.L.
Etat Major Forces Aériennes
Caserne Prince Baudouin
Place Dailly, Bruxelles 3

CANADA
Director of Scientific Information Services
Defence Research Board
Department of National Defence - 'A' Building
Ottawa, Ontario

DENMARK
Danish Defence Research Board
Østerbrogades Kaserne
Copenhagen Ø

FRANCE
O.N.E.R.A. (Direction)
29, Avenue de la Division Leclerc
92. Châtillon-sous-Bagneux

GERMANY
Zentralstelle für Lüftfahrdokumentation
und Information
Maria-Theresia Str. 21
8 München 27
Attn: Dr Ing. H.J.RAUTENBERG

GREECE
Hellenic Armed Forces Command
D Branch, Athens

ICELAND
Director of Aviation
c/o Flugrad
Reykjavik

ITALY
Aeronautica Militare
Ufficio del Delegato Nazionale all' AGARD
3, P. le del Turismo
Roma/Eur

LUXEMBOURG
Obtainable through BELGIUM

NETHERLANDS
Netherlands Delegation to AGARD
National Aerospace Laboratory, NLR
Attn: Mr A.H.GEUDEKER
P.O. Box 126
Delft

NORWAY
Norwegian Defense Research Establishment
Main Library, c/o Mr P.L.EKERN
P.O. Box 25
N-2007 Kjeller

PORTUGAL
Direccao do Servico de Material
da Forca Aerea
Rua de Escola Politecnica 42
Lisboa
Attn: Brig. General Jose de Sousa OLIVEIRA

TURKEY
Turkish General Staff (ARGE)
Ankara

UNITED KINGDOM
Ministry of Technology Reports Centre
Station Square House
St. Mary Cray
Orpington, Kent BR5 3RE

UNITED STATES
National Aeronautics and Space Administration (NASA)
Langley Field, Virginia
Attn: Report Distribution and Storage Unit

★ ★ ★

If spare copies are not available at these centres, microfiche or hard copy (printed facsimile, or reproduction from microcopy) may be purchased from:

Clearinghouse for Federal
Scientific and Technical
Information (CFSTI)
Springfield
Virginia 22151, USA

ESRO/ELDO Space
Documentation Service
European Space Research Organization
114, Avenue de Neuilly
92, Neuilly-sur-Seine, France

The request for microfiche or hard copy of an AGARD document should include the AGARD serial number when available, title, author (or editor) and publication date; if known, the NASA Accession Number should also be quoted.

Full bibliographical references and abstracts of the newly issued AGARD publications are given in the following bi-monthly abstract journals with indexes:

Scientific and Technical Aerospace Reports (STAR) published by NASA,
Scientific and Technical Information Facility,
P.O. Box 33, College Park,
Maryland 20740, USA

United States Government Research and Development Report Index (USGDRI), published by the Clearinghouse for Federal Scientific and Technical Information, Springfield,
Virginia 22151, USA

Printed by Technical Editing and Reproduction Ltd
Harford House, 7-9 Charlotte St. London, W1A 1HD